THE USE OF THERMOCOUPLE PSYCHROMETERS TO MEASURE IN SITU SUCTIONS AND WATER CONTENTS IN COMPACTED CLAYS

by

ALAN W. L. WAN

A Thesis
Submitted to the Faculty of Graduate Studies
in Partial Fulfillment of the Requirements for the Degree of

DOCTOR OF PHILOSOPHY

Department of Civil and Geological Engineering
University of Manitoba
Winnipeg, Manitoba

July 1996.

ISBN 0-612-16361-X

Canada

Name _____

Dissertation Abstracts International and *Masters Abstracts International* are arranged by broad, general subject categories. Please select the one subject which most nearly describes the content of your dissertation or thesis. Enter the corresponding four-digit code in the spaces provided.

CIV ENGINEERING
SUBJECT TERM

0543 UMI
SUBJECT CODE

Subject Categories

THE HUMANITIES AND SOCIAL SCIENCES

COMMUNICATIONS AND THE ARTS
Architecture 0729
Art History 0377
Cinema 0900
Dance 0378
Fine Arts 0357
Information Science 0723
Journalism 0391
Library Science 0399
Mass Communications 0708
Music 0413
Speech Communication 0459
Theater 0465

EDUCATION
General 0515
Administration 0514
Adult and Continuing 0516
Agricultural 0517
Art 0273
Bilingual and Multicultural 0282
Business 0688
Community College 0275
Curriculum and Instruction 0727
Early Childhood 0518
Elementary 0524
Finance 0277
Guidance and Counseling 0519
Health 0680
Higher 0745
History of 0520
Home Economics 0278
Industrial 0521
Language and Literature 0279
Mathematics 0280
Music 0522
Philosophy of 0998
Physical 0523
Psychology 0525
Reading 0535
Religious 0527
Sciences 0714
Secondary 0533
Social Sciences 0534
Sociology of 0340
Special 0529
Teacher Training 0530
Technology 0710
Tests and Measurements 0288
Vocational 0747

LANGUAGE, LITERATURE AND LINGUISTICS
Language
- General 0679
- Ancient 0289
- Linguistics 0290
- Modern 0291

Literature
- General 0401
- Classical 0294
- Comparative 0295
- Medieval 0297
- Modern 0298
- African 0316
- American 0591
- Asian 0305
- Canadian (English) 0352
- Canadian (French) 0355
- English 0593
- Germanic 0311
- Latin American 0312
- Middle Eastern 0315
- Romance 0313
- Slavic and East European 0314

PHILOSOPHY, RELIGION AND THEOLOGY
Philosophy 0422
Religion
- General 0318
- Biblical Studies 0321
- Clergy 0319
- History of 0320
- Philosophy of 0322

Theology 0469

SOCIAL SCIENCES
American Studies 0323
Anthropology
- Archaeology 0324
- Cultural 0326
- Physical 0327

Business Administration
- General 0310
- Accounting 0272
- Banking 0770
- Management 0454
- Marketing 0338

Canadian Studies 0385
Economics
- General 0501
- Agricultural 0503
- Commerce-Business 0505
- Finance 0508
- History 0509
- Labor 0510
- Theory 0511

Folklore 0358
Geography 0366
Gerontology 0351
History
- General 0578
- Ancient 0579
- Medieval 0581
- Modern 0582
- Black 0328
- African 0331
- Asia, Australia and Oceania 0332
- Canadian 0334
- European 0335
- Latin American 0336
- Middle Eastern 0333
- United States 0337

History of Science 0585
Law 0398
Political Science
- General 0615
- International Law and Relations 0616
- Public Administration 0617

Recreation 0814
Social Work 0452
Sociology
- General 0626
- Criminology and Penology 0627
- Demography 0938
- Ethnic and Racial Studies 0631
- Individual and Family Studies 0628
- Industrial and Labor Relations 0629
- Public and Social Welfare 0630
- Social Structure and Development 0700
- Theory and Methods 0344

Transportation 0709
Urban and Regional Planning 0999
Women's Studies 0453

THE SCIENCES AND ENGINEERING

BIOLOGICAL SCIENCES
Agriculture
- General 0473
- Agronomy 0285
- Animal Culture and Nutrition 0475
- Animal Pathology 0476
- Food Science and Technology 0359
- Forestry and Wildlife 0478
- Plant Culture 0479
- Plant Pathology 0480
- Plant Physiology 0817
- Range Management 0777
- Wood Technology 0746

Biology
- General 0306
- Anatomy 0287
- Biostatistics 0308
- Botany 0309
- Cell 0379
- Ecology 0329
- Entomology 0353
- Genetics 0369
- Limnology 0793
- Microbiology 0410
- Molecular 0307
- Neuroscience 0317
- Oceanography 0416
- Physiology 0433
- Radiation 0821
- Veterinary Science 0778
- Zoology 0472

Biophysics
- General 0786
- Medical 0760

EARTH SCIENCES
Biogeochemistry 0425
Geochemistry 0996
Geodesy 0370
Geology 0372
Geophysics 0373
Hydrology 0388
Mineralogy 0411
Paleobotany 0345
Paleoecology 0426
Paleontology 0418
Paleozoology 0985
Palynology 0427
Physical Geography 0368
Physical Oceanography 0415

HEALTH AND ENVIRONMENTAL SCIENCES
Environmental Sciences 0768
Health Sciences
- General 0566
- Audiology 0300
- Chemotherapy 0992
- Dentistry 0567
- Education 0350
- Hospital Management 0769
- Human Development 0758
- Immunology 0982
- Medicine and Surgery 0564
- Mental Health 0347
- Nursing 0569
- Nutrition 0570
- Obstetrics and Gynecology 0380
- Occupational Health and Therapy 0354
- Ophthalmology 0381
- Pathology 0571
- Pharmacology 0419
- Pharmacy 0572
- Physical Therapy 0382
- Public Health 0573
- Radiology 0574
- Recreation 0575
- Speech Pathology 0460
- Toxicology 0383

Home Economics 0386

PHYSICAL SCIENCES
Pure Sciences
Chemistry
- General 0485
- Agricultural 0749
- Analytical 0486
- Biochemistry 0487
- Inorganic 0488
- Nuclear 0738
- Organic 0490
- Pharmaceutical 0491
- Physical 0494
- Polymer 0495
- Radiation 0754

Mathematics 0405
Physics
- General 0605
- Acoustics 0986
- Astronomy and Astrophysics 0606
- Atmospheric Science 0608
- Atomic 0748
- Electronics and Electricity 0607
- Elementary Particles and High Energy 0798
- Fluid and Plasma 0759
- Molecular 0609
- Nuclear 0610
- Optics 0752
- Radiation 0756
- Solid State 0611

Statistics 0463

Applied Sciences
Applied Mechanics 0346
Computer Science 0984
Engineering
- General 0537
- Aerospace 0538
- Agricultural 0539
- Automotive 0540
- Biomedical 0541
- Chemical 0542
- Civil 0543
- Electronics and Electrical 0544
- Heat and Thermodynamics 0348
- Hydraulic 0545
- Industrial 0546
- Marine 0547
- Materials Science 0794
- Mechanical 0548
- Metallurgy 0743
- Mining 0551
- Nuclear 0552
- Packaging 0549
- Petroleum 0765
- Sanitary and Municipal 0554
- System Science 0790

Geotechnology 0428
Operations Research 0796
Plastics Technology 0795
Textile Technology 0994

PSYCHOLOGY
General 0621
Behavioral 0384
Clinical 0622
Developmental 0620
Experimental 0623
Industrial 0624
Personality 0625
Physiological 0989
Psychobiology 0349
Psychometrics 0632
Social 0451

THE UNIVERSITY OF MANITOBA

FACULTY OF GRADUATE STUDIES

COPYRIGHT PERMISSION

THE USE OF THERMOCOUPLE PSYCHROMETERS TO MEASURE IN SITU SUCTIONS AND WATER CONTENTS IN COMPACTED CLAYS

BY

ALAN W.L. WAN

A Thesis/Practicum submitted to the Faculty of Graduate Studies of the University of Manitoba in partial fulfillment of the requirements for the degree of

DOCTOR OF PHILOSOPHY

ABSTRACT

This study was carried out to test the hypothesis that thermocouple psychrometers can be used to provide meaningful suction and water content data for the study of the behaviour of unsaturated swelling clays when used as engineered barriers for the disposal of heat-generating radioactive waste.

Calibration tests were carried out to define the precision and accuracy of commercial psychrometers. The suction properties of a sand-bentonite material, sand-illite material, and Boom Clay were measured using the calibrated psychrometers and two other techniques. Previously, uncertainties existed regarding the relationship between soil structure and suction in compacted clays. Mercury intrusion porosimetry studies were carried out to examine the fabric of these soils. It was concluded that total suctions are controlled largely by the micropores in compacted specimens.

The performance of psychrometers as moisture sensors in compacted sand-bentonite material was investigated in the laboratory using triaxial isotropic compression and shear tests. New testing techniques were developed. The usefulness of psychrometers as moisture sensors to measure *in situ* suctions and water contents in compacted sand-bentonite material was examined in a large scale, *in situ*, experiment known as the Buffer/Container Experiment. Results showed that suctions in compacted clays under both well controlled laboratory conditions and more chaotic field conditions can be inferred from the output of psychrometers. Moreover, under the influence of temperature gradients, the outputs of the instruments can be interpreted to provide qualitative and meaningful data on moisture movement in compacted clays.

This study led to a rationale for interpreting psychrometer data from *in situ* measurements on compacted clays. Meaningful information from psychrometers can be attained through the combination of an understanding of the principles of operation of the instruments, an understanding of the constitutive properties of the soil, comprehension of coupled processes that control heat and moisture flow in soils, and total system analysis.

ACKNOWLEDGEMENTS

I would like to thank:

Dr. Malcolm Gray, my supervisor, for his advice, encouragement, and guidance;

Dr. James Graham, for his advice, encouragement and support;

Dr. Nimal Rajapakse, and Dr. Emery Lajtai, for their encouragement and advice;

Dr. Antonio Gens, my external examiner, for his interest in my work;

Ms. Sharon Campbell, Mr. David Hnatiw, Mr. Harold Hume, Mr. Nazeer Khan, Mr. Peter Roach, Mr. Barry Shenton, Ms. Thanh To, and Mr. Bradley Walker, for their technical assistance.

Thanks are extended to my colleagues at Whiteshell Laboratories and the Underground Research Laboratory, Atomic Energy of Canada Limited, and fellow graduate students at the University of Manitoba for their interest and support in my work. In particular, I would like to single out Dr. Bruce Kjartanson and Dr. Neil Chandler, with whom I had many fruitful discussions on instrumentation, and on the complex and difficult topic of heat and moisture flow in unsaturated soils. Many ideas presented in this thesis arose from the discussions with them. I also would like to thank Dr. Norbert Morgenstern, Dr. Krish Radhakrishna, and Dr. K.-C. Lau, for their interest and involvement in my work on psychrometers.

Financial and technical support provided by Atomic Energy of Canada Limited and Ontario Hydro is gratefully acknowledged.

Finally, I am grateful to my family for their support and encouragement during the course of my study.

TABLE OF CONTENTS

LIST OF TABLES

LIST OF FIGURES

LIST OF SYMBOLS AND ABBREVIATIONS

a	Tortuosity factor
a	Coefficient in the temperature correction equation for psychrometer
a_m	Coefficient of soil structure volume change with respect to change in net total stress
a_t	Coefficient of soil structure volume change with respect to change in matric suction
b	Coefficient in the temperature correction equation for psychrometer
b_m	Coefficient of water content change with respect to change in net total stress
b_t	Coefficient of water content change with respect to change in matric suction
C_c	Ionic concentration midway between two parallel clay particles
C_o	Ionic concentration in the free water
C_{pl}	Specific heat capacity of soil liquid water
C_{pv}	Specific heat capacity of soil water vapour
C_{TT}	Coefficient in the governing equation for heat flow
$C_{T\psi}$	Coefficient in the governing equation for heat flow
$C_{\psi T}$	Coefficient in the governing equation for moisture transfer
$C_{\psi\psi}$	Coefficient in the governing equation for moisture transfer
c	Volumetric heat capacity
D_T	Thermal moisture diffusivity
D_w	Diffusion coefficient of water vapour in air
$D_{\theta liq}$	Isothermal liquid diffusivity
$D_{\theta vap}$	Isothermal vapour diffusivity
d	Pore diameter
e	Voids ratio
e_T	Theoretical voids ratio
f	Fractional cross sectional area available for diffusion
G_c	Specific gravity of clay
g	Gravity
i	Hydraulic gradient
K	Hydraulic conductivity or coefficient of permeability
K_{TT}	Coefficient in the governing equation for heat flow
$K_{T\psi}$	Coefficient in the governing equation for heat flow
$K_{\psi T}$	Coefficient in the governing equation for moisture transfer
$K_{\psi\psi}$	Coefficient in the governing equation for moisture transfer
k	Intrinsic permeability
L	Latent heat of water
L_o	Original length of a specimen
M	Molecular mass of water

M	Stress ratio at critical state
N	Location of isotropic compression line in v:lnp' plane
n	Porosity
n_T	Theoretical porosity
P	Swelling pressure
p	Applied pressure in a mercury intrusion porosimetry test
p	Cell pressure
p	Mean total stress
p'	Mean effective stress
p^*	Total stress
p_{at}	Mean total stress with respect to atmospheric pressure
Q	Volumetric water content
q	Deviator stress
R	Molar gas constant
r	Curvature of an air-water meniscus
S	Suction potential
S	Total suction
S_m	Matric suction
S_π	Osmotic suction
s	Matric suction
T	Temperature
T_s	Surface tension of mercury
t	Time
u_a	Pore air pressure
u_w	Pore water pressure
V	Measured output voltage of a psychrometer
V	Volume change
V_p	Vapour pressure
V_{25}	Corrected output voltage of a psychrometer
v	Flow velocity
v	Partial vapour pressure
v	Specific volume
v_o	Saturated vapour pressure of water
w	Water content (by mass)
x	Distance in the x direction
χ	Bishop's Chi factor
ε	Strain
ε_1	Axial strain
ε_3	Lateral strain
ε_s	Shear strain
ε_v	Volume strain

ϕ'	Frictional angle with respect to change in net total stress
ϕ^b	Frictional angle with respect to change in net matric suction
Γ	Location of critical state line in compression plane
γ_b	Bulk density
γ_c	Clay dry density
γ_d	Dry density
γ_w	Density of water
λ	Slope of normal consolidation line or critical state line in v:lnp' plane
λ	Thermal conductivity
μ	Viscosity
ρ	Density
σ	Total stress
σ_1	Major principal total stress
σ_3	Minor principal total stress
σ'	Effective stress
σ_1'	Major principal effective stress
σ_3'	Minor principal effective stress
σ_t	Surface tension of an air-water interface
τ	Shear strength
θ	Contact wetting angle between mercury and soil particles
θ	Water content (by volume)
ψ	Matric suction
ψ_m	Matric potential
ΔL	Change in length of a specimen

CHAPTER 1 INTRODUCTION

1.1 Background

Compacted clays are engineered soil materials which are frequently used in a variety of geotechnical and environmental engineering projects. Examples include highway embankments, earth dams, and landfill liners and covers. In recent years, several countries where nuclear power is used to produce electricity, have been developing methods for the disposal of radioactive wastes. A common approach is the use of compacted clays as engineered barriers in waste repositories to control moisture movement and contaminant transport within and around the disposal sites (AECL, 1994).

Generally, compacted clay barriers are constructed by compacting suitable clay material at a known water content to densities greater than a specified minimum dry density. Normally, pores in the compacted clay will not be saturated with water at the end of construction. That is, the voids between mineral particles are not completely filled with water. Among other factors, the degree of saturation will influence the behaviour of the unsaturated clay. Through an understanding of the constitutive properties of the unsaturated soil in relation to distortion, volume change, and moisture movement, the performance of the clay and the change in performance with changes in degree of saturation can be assessed.

The behaviour of unsaturated compacted clays depends largely on their water contents (Alonso et al., 1987; Thomas, 1992). Water content changes in the soil cause effective stresses, pore air and pore water pressures, and the chemical composition of the pore water to vary. These variations may lead to deformation of the soil. Conversely, deformation alters the fabric and pore size in the soil. In turn these alterations affect the flow paths in the soil through which air and moisture travel. Therefore, thorough

understanding and complete solutions to problems of stability and moisture flow in compacted clays require considerations of coupled processes.

In recent years, several models have been proposed in attempts to rationalize constitutive behaviour and moisture movement in unsaturated soils (Alonso et al., 1990; Thomas, 1992; Fredlund and Rahardjo, 1993; Wheeler and Sivakumar, 1995). Generally, these models are applicable to a limited range of simple soil materials which include cohesionless granular materials and non-swelling clays. Attempts are currently being made to extend these frameworks to more complex engineered materials including dense swelling clays (for example, Gens and Alonso, 1992).

For simple soils, there is a general consensus that the behaviour of an unsaturated soil can be quantitatively described in terms of suction and a limited number of state variables such as void ratio, water content, stress, and temperature (Alonso et al., 1990; Fredlund and Rahardjo, 1993; Wheeler and Sivakumar, 1995). "Suction" is the term used to describe pressures in the water phase that are less than atmospheric. Thus, the use of contemporary models to characterize the behaviour of an unsaturated soil requires the knowledge of relationships between suction and the other state variables. Furthermore, material parameters required for the models must be measurable in laboratory tests in which suctions in the soil can be controlled or measured.

One way of determining suctions in unsaturated soils is the use of the psychrometric technique. This technique relates the suction in an unsaturated soil to the vapour pressure of water in the air in the soil through thermodynamic relationships. Hence, if the vapour pressure in the air in the soil is known, its suction can be determined. A commonly used, commercially available instrument that measures vapour pressures in soils is the thermocouple psychrometer (Richards, 1969). Thermocouple psychrometers have been mostly used in soil science, plant science and agricultural applications (Wiebe et al., 1971; Campbell and Campbell, 1974). Psychrometers also have been used to

measure suctions in natural soils in geotechnical engineering investigations (Richards et al., 1983). However, few attempts have been made to use psychrometers for measuring suctions or as moisture sensors in engineered materials such as the compacted clays used for constructing clay liners and barriers for waste disposal schemes. The aim of the research being reported here was to investigate the usefulness of thermocouple psychrometers for tracking *in situ* suctions and local changes in water content in engineered, compacted clay materials.

1.2 Introduction to thermocouple psychrometry

A typical thermocouple psychrometer is small and simple in design. It consists of a thermocouple circuit protected by a ceramic shield (Briscoe, 1984). Compared with other methods for soil suction measurements, psychrometers can operate successfully in a relatively wide range of suctions from 100 kPa to 7000 kPa (Briscoe, 1984). Because of their small size, psychrometers can be used in both laboratory and field applications (Richards et al., 1983; Edil and Motan, 1984).

The operation of psychrometers is based on principles of thermoelectricity. The outputs of the instruments are related to the vapour pressure in the air in unsaturated soil. The vapour pressure is influenced by several factors including temperature and capillarity (Hillel, 1980). Hence, changes in these factors result in changes in the vapour pressure, which lead to complexities in the interpretation of suction measurements made by the instruments. The principle and operation of thermocouple psychrometers are dealt with more fully in Chapter 3.

In the past, largely, research on psychrometers has been focussed on the effects of temperature on instrument accuracy and performance (Richards, 1969; Brown, 1970; Campbell and Campbell, 1974; Brown and Bartos, 1982). These studies show that temperature fluctuations and temperature gradients lead to temporal and spatial variations

in the vapour pressure in the soil. Attempts to quantify the effects of temperature fluctuations on psychrometer outputs were made by Wiebe et al. (1970) and Brown (1970), who proposed empirical temperature-correction formulae for several commercial psychrometers. However, the effect of temperature gradients on psychrometric measurements remains difficult to quantify (Brown and Bartos, 1982), and little work has been done in this area. It is generally considered that psychrometers cannot be used to provide meaningful data under the influence of temperature gradients. Research described in this thesis has provided data on the effects of temperature gradients on the accuracy of psychrometers. Data from a large scale *in situ* experiment designed to examine a compacted sand-bentonite material as a component of a disposal facility for radioactive waste have been used to examine the role of temperature and vapour pressure gradients on the accuracy and precision of thermocouple psychrometers.

The role of capillarity in controlling vapour pressures, and hence suctions, in dense, compacted clay soils has received little attention in the literature. The use of psychrometers in these soils is complicated by the fact that compacted clays generally develop complex structures characterized by aggregations of clay particles and peds, containing pores with a wide range of diameters which often fall into more than one range of typical pore size. That is, pore size distribution curves are often bi- or tri-modal (Diamond, 1970; Garcia-Bengochea et al., 1979; Juang and Holtz, 1986). The size and distribution of the capillary pores within the soil structure have considerable influence on the vapour pressure in compacted clays.

Moisture movements that accompany stress variations lead to deformations and volume changes in the soil, resulting in changes in porosity and pore size distribution. Because of the complexities associated with soil structure, it is unclear how stress- or strain-induced changes in soil structure will affect suction measurements made by psychrometers. For this reason, there has been uncertainty whether psychrometers can

be used as moisture sensors to measure vapour pressures, suctions and water contents in deforming soils. Before confidence can be gained in measuring material parameters in laboratory tests, and in tracking *in situ* moisture transients in these complex materials, better understanding is needed of the limitations and accuracy of psychrometers.

In summary, there is a need to understand better the stress-strain behaviour of unsaturated compacted soils, particularly plastic clays and the compacted sand-bentonite that has been proposed for nuclear waste disposal (Graham et al., 1992). Psychrometers measure vapour pressure which can be related to total suction. It is known that total suction affects the strength and compressibility of unsaturated soils, but the conditions under which readings of psychrometers are meaningful and useful are unclear. Therefore, research was undertaken to clarify the conditions under which psychrometers can be operated in such a way that their readings contribute usefully to a better understanding of the behaviour of unsaturated clay soils. The improved understanding is mostly needed in connection with various technical questions relating to waste retention and disposal in geo-environmental engineering. Solutions to the technical questions related to nuclear fuel waste disposal would assist the resolution of other questions with respect to the general use of unsaturated, compacted clays in geo-environmental engineering applications.

1.3 Scope of study

The objective of this research was to examine the usefulness of thermocouple psychrometers as moisture sensors in tracking suction and moisture transients in compacted clays. In particular, the effects of stress, deformation, and temperature gradients on suction and vapour pressure measurements in compacted sand-clay materials made by psychrometers were investigated.

A review of literature revealed that past research on psychrometers has been exclusively on temperature effects (Chapter 2). A laboratory testing program was

therefore carried out to investigate the effects of total stress and deformation on suction measurements made in compacted clay soils using commercially available psychrometers. To provide confidence in the measurements by psychrometers, the instruments were first calibrated, and the precision, accuracy, and long term performance of the instruments were defined (Chapter 3). Using psychrometers and two other conventional methods, namely vapour equilibrium and filter paper methods, a series of laboratory tests was carried out to measure the suction-water content relationships of three different soil types under normal atmospheric pressures (Chapter 5). The soils investigated in this study were a sand-bentonite material, a sand-illite material and a reconstituted low-plastic natural clay. The effects of water content, saturation and temperature on suctions in these soils were evaluated.

The possible performance of thermocouple psychrometers as internal sensors in soil masses was investigated in a series of laboratory scale triaxial compression tests (Chapter 6). A new technique for installing a psychrometer inside a test specimen during specimen formation was developed. Triaxial compression tests were carried out on unsaturated compacted sand-bentonite/psychrometer specimens to investigate the effects of stress variation and deformation on suctions measured by psychrometers.

Mercury intrusion porosimetry tests were carried out to determine the pore size distributions of the soils used in this research (Chapter 7). Results from these tests were used to identify the level of complexity of the soil structure and those elements of structure which controls the suction properties in the compacted materials.

The use of psychrometers to measure *in situ* suctions and water contents was investigated in the Buffer/Container Experiment, a large scale *in situ* experiment carried out to examine the performance of a sand-bentonite material used for radioactive waste disposal (Chapter 8).

Based on the findings from suction, triaxial, and mercury intrusion porosimetry tests, a new framework incorporating the concept of soil structure was proposed to explain the effects of stress variations and distortions on suction measurements using thermocouple psychrometers (Chapter 9). The usefulness of the understanding developed through the laboratory studies to field investigation was examined. The roles of temperature-induced vapour pressure gradients, and total stress on the precision and accuracy of psychrometers for tracking *in situ* suction and moisture transients in compacted clays were discussed.

The laboratory and *in situ* investigations reported in this thesis clarify the conditions under which psychrometers can be operated so that they provide meaningful data in the study of the behaviour of unsaturated soils (Chapter 10).

CHAPTER 2 LITERATURE REVIEW

2.1 Background

The research carried out in this study concerns the use of psychrometers for measuring soil suctions and water contents in compacted clays. The literature review presented in this chapter focuses on two main areas: soil suction and properties of compacted clays. A review of the principle of thermocouple psychrometers is given in Chapter 3. The purpose of the review is to clarify what was already known about the performance and operation of psychrometer, and to aid the development of the program of research that has been undertaken.

This chapter divides into five parts. It begins with a review of clay mineralogy. The second part presents theories of soil structure, in particular, the influence of soil structure on the behaviour of compacted clays. The third part of the chapter deals with theories of soil suction. Most compacted clays are unsaturated in nature. A better understanding of their behaviour requires a basic knowledge of theories of unsaturated soil mechanics. To provide this, the fourth part of the chapter reviews theories relating to constitutive modelling of and moisture flow phenomena in unsaturated soils. The fifth and last part presents the conclusions from the literature review, and gives the objectives of the study described in subsequent chapters.

2.2 Clay mineralogy

2.2.1 Clay minerals

It is important to distinguish between clay-size particles and clay minerals. Clay-size particles may have any mineralogical composition but are defined as having an equivalent diameter less than 2μm (Mitchell, 1976). They can contain spherical or

angular particles of primary minerals such as quartz, feldspar or calcite. In contrast, clay minerals are compounds of alumino-silicates derived from chemical weathering of igneous and metamorphic rocks. They are usually curved, flaky or platy in nature (Grim, 1953; Pusch et al., 1990). Clay minerals can exist with sizes larger than 2 μm, though this is relatively unusual. The presence of the only small amount of clay minerals in soils can considerably influence their physical properties.

Clay minerals are crystalline materials formed from sheets of silica and alumina (Figure 2.1). Silica sheets are composed of silicon and oxygen atoms, while alumina sheets are made up of aluminum atoms and hydroxyl groups. The silicon and aluminum atoms in these sheets may be partially replaced by other elements with similar atomic size but different valency in the process known as "isomorphous substitution". Because of imperfections in the lattice structure due to isomorphous substitution, clay minerals generally carry surface charges. Small size, plate-like nature, high specific surface, and the extent of electrochemical unbalance are the major factors that influence the behaviour of clay minerals. For example, they are well known for their affinity for water and in some cases, for their tendency to swell when in contact with water.

There are three common types of clay minerals: kaolinite, illite, and montmorillonite. Their properties are compared in Table 2.1. The basic unit structure of each mineral is shown schematically in Figure 2.1. The differences in the mineral structure and in the bonding between basic structural units lead to differences in size and surface charges of the clay minerals. These latter factors in turn play an important role in influencing the properties of soils. Among clay minerals, particles of montmorillonite are generally smallest and therefore have largest specific surface. Montmorillonite minerals also have the highest density charges. This is reflected by their high values of plastic and liquid limits which are quoted as high as 100% and 800% respectively (Yong and Warkentin, 1975). In contrast, kaolinite minerals generally have the largest particle size

and small specific surfaces. They have low surface density charges, with plastic and liquid limits of 35% and 70% respectively (Yong and Warkentin, 1975).

2.2.2 Clay-water interaction

In a clay-water system, exchangeable cations are attracted to the surfaces of clay particles. Water molecules, being dipolar, are also attracted to clay particles. Under the influence of various types of physico-chemical forces, water exists in three different forms (Mitchell, 1976; Cheung et al., 1987). Surface water is the first 2-3 molecular layers of water tightly attached to the clay particle surface. Its physical properties are strongly influenced by the particle. Next furthest away from the surface water is adsorbed water. This water forms part of a diffuse double layer in which cations dominate and counterbalance the negative charges of the clay particle. The distribution of cations in the diffuse double layer decreases with increasing distance from the clay surface (Yong and Warkentin, 1975; Mitchell, 1976). Because of its close proximity to the clay, the adsorbed water is attracted to the clay particle under a variety of forces including hydrogen bonding and van der Waals forces (Lambe and Whitman, 1969). Surface water and absorbed water are sometimes referred to as immobile water (or structural water) because of their relative immobility and their properties being different from those of ordinary water (Cheung et al., 1987). The third type of water is free water (or interstitial water). This water is not affected by the surface charges on the clay particles and is free to move around in open pores. Montmorillonite is the prime material being investigated in this study and has the highest degree of structuring of soil water.

An important property of montmorillonites, and to a less extent illite, is their ability to swell when given access to water. The mechanism of swelling is complex and is influenced by many factors including mineralogy, soil structure, temperature, and water

chemistry. Theoretically, the swelling pressure in a clay may be estimated using the Van't Hoff equation (Yong and Warkentin, 1975):

$$P = RT(C_C - 2C_O) \qquad [2.1]$$

where P is the swelling pressure, R is the molar gas constant, T is the absolute temperature, C_C is the ionic concentration midway between two parallel particles, and C_O is the ionic concentration in the free water.

Swelling of surface-active clays is often explained by consideration of the physico-chemical interactions between free water and the diffuse double layers surrounding the clay minerals in accordance with the diffuse double layer theory proposed by Guoy (1910) and Chapman (1913). The diffuse double layer theory was originally developed to explain interactions of ions in dilute solutions. While the theory is considered to be applicable to clay-water systems with high water-to-clay ratios (Bolt, 1956; Sridharan and Jayadeva, 1982), the diffuse double layer theory has also been used to help describe swelling phenomena in dense water-saturated clay materials (Graham et al., 1989). According to the theory, when two clay particles are brought close together, their respective diffuse double layers interact with each other. Interaction between the diffuse double layers of two clay particles with similar orientations will result in a higher concentration of cations in the water between the particles than that in the free water. The overlapping diffuse double layers between the clay particles act as a semi-permeable membrane (Mitchell, 1976). This leads to the development of an osmotic potential gradient between the overlapping diffuse double layers and the free water. The consequence is a tendency for free water to move into the space between the particles, leading to the generation of osmotic pressure that tends to force the particles apart. The

mechanical pressure required to oppose this osmotic pressure is known as swelling pressure (Yong and Warkentin, 1975).

2.3 Theory of soil structure

2.3.1 Concepts of soil structure

Soil structure plays an important role in influencing the properties and behaviour of compacted clays (Barden and Sides, 1970; Mitchell, 1976). The development of soil structure is associated with several factors that include clay mineralogy, material preparation, and methods of compaction.

In literature pertinent to the study of compacted clays, the terms "soil structure" and "soil fabric" are often used interchangeably (Collins, 1983). However, the terms have also been specifically defined to reflect their usage in more specific senses as follows. Soil structure is "the physical constitution of a soil material as expressed by the size, shape, and arrangement of the solid particles and associated voids" (Brewer, 1964), and it is intimately related to inter-particles forces (Yong and Warkentin, 1975). In contrast, soil fabric is "the physical constitution of a soil material as expressed by the spatial arrangement of the solid particles and associated voids" (Brewer, 1964). Therefore soil fabric is an element of soil structure that is concerned only with the physical arrangement of the soil particles. These specific definitions will be used in following chapters.

Concepts of soil structure in compacted soils have been significantly advanced by Lambe (1958). His concepts were based on colloidal chemistry and dealt with interactions between individual clay particles. The development of soil structure in compacted clays is a phenomenon associated with material preparation and compaction processes. Compaction improves the mechanical and hydraulic properties of a soil (Lambe and Whitman, 1969). The degree of compaction of a soil is measured against a

dry density - water content curve. This curve is normally obtained from standard laboratory tests carried out in accordance to the American or British standards (American Society of Testing and Materials D 1557; British Standards Institution BS 1377:1975). A characteristic feature of such a curve is that for a given compaction effort, there is a particular water content, known as the optimum water content, at which the highest dry density of the soil is attained. In general, when a soil is compacted to its optimum water content, it tends to exhibit the highest strength and lowest hydraulic conductivity (Lambe and Whitman, 1969) for the selected level of compaction effort.

In Lambe's view, the type of soil structure in a compacted clay is influenced by moulding water content and compaction effort. Soils compacted to the dry side of the optimum water content tend to develop a flocculated, edge-to-face single particle arrangement. In contrast, soils that are formed on the wet side of the optimum, possess a dispersed structure in which clay particles are arranged in a more parallel face-to-face manner. Lambe postulated further that static compaction would produce a more dispersed particle arrangement than dynamic or kneading compaction.

It is now widely recognized that soil structures in compacted clays are much more complex than those proposed in Lambe's concept. Evidence from scanning electron microscopy reveals that interactions between single isolated particles are seldom found in compacted soils (Aylmore and Quirk, 1960; Diamond, 1970; Barden, 1971; Delage and Lefebvre, 1984; Wan, 1987). In contrast to Lambe's concept, clay particles tend to aggregate into distinct groupings consisting of individual particles oriented in similar directions. In turn, these groups, aggregations, or peds, behave as semi-rigid units that interact to give the soil its mechanical properties (Aylmore and Quirk, 1960; Barden and Sides, 1970). The engineering behaviour of compacted clays is not determined by individual particle actions as originally suggested by Lambe but by interactions between particle groupings or aggregates.

2.3.2 Fabric and pore spaces

For clay soils, there are three levels of soil fabric that are recognized: macrofabric, microfabric and ultra-microfabric (Yong and Warkentin, 1975). Macrofabric refers to the level of soil structure that can be seen with the naked eye, whereas microfabric and ultra-microfabric are the soil structures that can be detected only with the aid of an optical microscope and an electron microscope, respectively. The latter two levels are often lumped together and referred simply as microfabric (Collins, 1983).

At the ultra-microscopic level, the fabric units consist of single clay particles, or of *domains* comprised of two or more parallel clay particles acting as a unit (Aylmore and Quirk, 1960). Several domains combine to form a *cluster* which is the name given to the fabric units at microscopic scale. The fabric units at the macroscopic level are called *peds* which are aggregates consisting of clusters of clay particles separated from adjoining peds by surfaces of weaknesses or recognizable voids (Brewer, 1964).

Pores within a ped are called *micropores* or *intra fabric unit pores* whereas those existing between ped units are referred as *macropores* or *inter fabric unit pores* (Yong and Warkentin, 1975). Measurements of pore size distributions in soils are usually obtained using mercury intrusion porosimetry (Diamond, 1970). This technique is based on the principle that mercury, a non-wetting fluid, does not enter a medium containing small pores unless a pressure is applied. The applied pressure (p) is directly related to the pore diameter (d) by the Washburn equation,

$$p = -\frac{4T_s\cos\theta}{d} \qquad [2.2]$$

where T_s is the surface tension of mercury, θ is the contact wetting angle between mercury and the soil particles. The pore size distribution in a soil is the frequency

distribution of the volume of mercury intruded at different applied pressures (from which the diameters are calculated using the Washburn equation).

Results from mercury intrusion porosimetry on compacted clays and sand-clay mixtures show that the pore sizes in these compacted soils are often bimodal, consisting of quite separate distribution of micropores and macropores. The micropores appear to be largely unaffected by either compaction effort or moulding water content (Diamond, 1970; Garcia-Bengochea et al., 1979; Juang and Holtz, 1986). In contrast, increasing compaction effort or increasing water content leads to a reduction in the volume of macropores in the soil. The conclusion derived from this latter observation is that macrostructures in compacted clays are largely the artifacts of material preparation and compaction.

2.3.3 Relationships between soil structure and engineering properties

2.3.3.1 Background

The development of soil structure in compacted clays is a phenomenon associated with material preparation and compaction processes. The soil structure in a compacted clay is largely influenced by the moulding water content and the compaction forces. During material preparation, when water is added to the soil, clay particles tend to coalesce to form peds due to physico-chemical interactions within the clay-water system (Aylmore and Quirk, 1960). The peds behave essentially as individual particles, and so the behaviour and properties of the soil depend largely on the interactions of the peds.

To a large extent, the size and stiffness of the peds in a compacted clay soil, depends on the moulding water content (Wan et al., 1990; Delage and Graham, 1995). At higher water contents, peds are larger and wetter, and they tend to be easily distorted by compaction and shear forces. In contrast, peds formed at lower water contents are

smaller and stiffer. The stiffness of these drier peds is attributable to suctions within the fabric units (Barden and Sides, 1970).

2.3.3.2 Mechanical and swelling behaviour

The stress-strain behaviour of a compacted clay is largely influenced by water content and the confining pressure (Barden and Sides, 1970; Wan et al., 1990). As discussed in section 2.3.3.1, the size of macro-peds tends to increase with increasing moulding water content. At lower confining pressures, the stress-strain behaviour of the soil is influenced by the interactions between macro-peds which behave like semi-rigid individual units. At a given pressure level, soils formed with higher water contents are more dilative in shear than those formed at lower water contents (Wan et al., 1990). As the confining pressure increases, the ped structures tend to deform (Barden and Sides, 1970). At high confining pressures, the stress-strain behaviour and the strength of the soil are essentially dominated by the interactions between individual clay particles.

A common phenomenon observed in unsaturated soils compacted on the dry side of optimum water content is 'collapse' (Matyas and Radhakrishna, 1968; Tadepalli and Fredlund, 1991). Collapse is a phenomenon in which, under the influence of a high applied load, a soil experiences appreciable volume reduction on inundation with water. Barden and Sides (1970) explained that in such a soil, metastable peds exist and their integrities are initially sustained by suctions within the ped units. Upon wetting, the peds lose strength and collapse into neighbouring macropores.

The swelling and consolidation behaviour of a compacted clay is also affected by soil structure (Seed et al., 1962; Brackley, 1975; Wan et al., 1990). Brackley (1975) studied the swelling characteristics of several remoulded montmorillonites and kaolinites, and observed that the free swell in these soils is influenced largely by compaction water content. He explained his observations using a "packet" model. He hypothesized that

the soil structures in these clays may be visualized as consisting of water-saturated packets of clay particles and inter-packet voids filled with air. Upon moisture uptake, the sizes of individual packets increase as a result of physico-chemical interactions between clay particles and pore water within the packets.

2.3.3.3 Suction properties

In analysing problems relating to moisture flow, the relationships of suction with other state variables are required (Fredlund and Rahardjo, 1993). For sands and other cohesionless materials, it is commonly accepted that soil suctions are related to dry density or degree of saturation. In these materials, suctions are attributed to capillary phenomena, and are related to the pore size distribution within the granular soil particle structure. The pore size distribution is in turn affected by the packing of the soil particles and is directly related to the dry density of the soil.

In contrast to cohesionless materials, experimental evidence shows that suctions in compacted clays cannot be singularly related to dry density or degree of saturation (Croney et al., 1958; Olson and Langfelder, 1965; Krahn, 1970; Gray, 1980). Croney et al. (1958) attributed the difference in the suction behaviour between granular materials and compacted clays to the differences in soil structure. They explained that a compacted clay may be considered as a mixture consisting of peds of clay particles which may be water-saturated or unsaturated, and macroscopic inter-ped air voids. The suctions in such a material are largely controlled by the smaller capillary pores within the peds. A change in the density of the soil basically reflects a change in the size of the larger macroscopic voids. Changes in these macroscopic voids have little bearing on the suction in the soil as a whole.

2.3.3.4 Conduction phenomena

Water flow in saturated soils is commonly described by Darcy's law (Yong and Warkentin, 1975),

$$v = - K.i \qquad [2.3]$$

where v is the flow velocity, K is the hydraulic conductivity of the soil medium, and i is the hydraulic gradient. The hydraulic conductivity which is sometimes called the coefficient of permeability, is a function of the porous medium and the permeant. Hydraulic conductivity relates to permeability (also known as specific or intrinsic permeability) by (Freeze and Cherry, 1979),

$$K = \frac{k\rho g}{\mu} \qquad [2.4]$$

where K is the hydraulic conductivity, k is permeability, ρ and μ are density and viscosity, respectively, of the permeant. Because permeability is a characteristic physical property of a porous medium, it relates to certain measurable properties of the soil pore geometry such as porosity and pore size distribution.

The water permeability of a saturated soil compacted dry of optimum is generally higher than the soil formed to the same dry density at wet of optimum. For example, Mitchell et al. (1965) found that the water permeability of a silty clay compacted on the dry side of optimum is almost three orders of magnitude higher than the soil compacted on the wet side of optimum. Lambe (1958) attributed the differences in permeability in compacted soils formed on either side of the optimum to the differences in the clay particle structure. He explained that soils compacted on the dry side tend to have a flocculated open soil structure and therefore have higher porosities. In contrast, soils

formed on the wet side form a closely packed dispersed soil structure with lower porosity. Lambe and Whitman (1969) presented results for several clay soils and showed that, among other factors, the permeability of a soil may be directly related to its void ratio (total porosity). However, these relationships were later found to be inadequate for compacted clays and sand-clay materials (Garcia-Bengochea and Lovell, 1981).

Olsen (1962) postulated that the differences in water permeability between soils compacted on the dry side and the wet side of optimum water content can be explained by means of a cluster model. According to Olsen's model, the permeability of a compacted clay is largely controlled by fluid flow through macropores between clusters of clay particles, rather than through the clusters themselves. Results from later studies by Garcia-Bengochea et al. (1979), Garcia-Bengochea and Lovell (1981), and Juang and Holtz (1986) provided support to Olsen's hypothesis. Using mercury intrusion porosimetry, the researchers investigated relationships between water permeability and pore size distribution in compacted clays and sand-clay mixtures. They showed that for the compacted materials they tested, predictive models based on statistical approaches can be developed to relate the water permeability and the distribution of macropores in the soil. The practical implication of the results by Garcia-Bengochea et al. (1979), Garcia-Bengochea and Lovell (1981), and Juang and Holtz (1986) is that the water permeability in a compacted soil is largely controlled by the inter-ped or inter-cluster porosity, but not by the total porosity in the soil.

The air permeability in an unsaturated soil is also influenced by soil structure and degree of saturation (Matyas, 1967; Barden and Sides, 1970). An important factor that affects the flow of air is the air entry value which is associated with the capillarity in the soil structure. The air entry value in a soil may be defined as the lowest value of suction in the soil that needs to be exceeded before air can be driven through the pores. In an unsaturated compacted clay, because of affinity by the highly-charged particles for water

and capillary actions, the micropores will become water-saturated before the macropores (Brackley, 1975; Gray, 1980). Furthermore, in the micropores, the water can exist under higher suctions than in the macropores. Hence water in the micropores is less easily displaced by air than in the macropores. Air permeabilities in compacted clays are therefore largely controlled by the larger macropores.

The air permeability in an unsaturated soil tends to decrease with increasing saturation. At low saturations, most of the pores in the soil are interconnected, and continuous channels exist for the flow of air. As saturation increases, some of the pores become occluded (or discontinuous) and no longer form part of the passage for air movement. As a result, the air permeability of the soil decreases. At very high saturations, the flow of air is very slow and occurs mainly by means of diffusion in the water-filled pores (Fredlund and Rahardjo, 1993; Kirkham, 1995).

2.3.4 Summary

Soil structure refers to "the physical constitution of a soil material as expressed by the size, shape, and arrangement of the solid particles and associated voids". In compacted clays, due to clay-water interactions, clay particles tend to aggregate to form peds which in turn behave as semi-rigid individual units. The size and stiffness of these peds is largely influenced by moulding water content. Therefore the soil structure in compacted clays may be characterized as a system of aggregations of peds which may be water-saturated or unsaturated, and macro-pores within and between aggregations.

Generally, the soil structure in a compacted clay may be divided into macro- and micro-structures. The two levels refer to, respectively, the soil structures that can and cannot be distinguished with the naked eye. The behaviour of the soil may be influenced by both levels of soil structure. At higher water contents and lower confining pressures, strength and stress-strain behaviour are attributed largely to interactions between macro-

peds. At higher confining pressures, the effects of microstructure within the peds on the mechanical properties of compacted clays become dominant. Air and water permeabilities are governed primarily by the size and distribution of macro-pores within the soil structure. Albeit not conclusively, suction and swelling properties are associated with, respectively, capillary actions and clay-water interactions within the ped structure.

2.4 Theory of soil suction

2.4.1 Background

Generally, it is recognized that moisture flow and deformation in an unsaturated soil are influenced by soil suctions. In recent years, several general frameworks have been proposed in attempts to provide a rational basis for the understanding of moisture movement, volume change and stress-strain behaviour in unsaturated soils (Alonso et al., 1990; Fredlund and Rahardjo, 1993; Wheeler and Sivakumar, 1995). To adopt these frameworks for the study of the behaviour of unsaturated soils, knowledge of suction and its relations with other material parameters and state variables is important and is required. A review of these frameworks is given in Section 2.5. Basic concepts for soil suction and factors influencing this soil property are discussed in Section 2.4, here.

2.4.2 Total suction and components

The suction in an unsaturated clay soil is often referred as total suction and is commonly divided into two major components: matric and osmotic suctions (Richards, 1974). Matric suction is attributed to capillary actions in the soil structure (see Figure 2.2), and is related to surface tension forces in air-water menisci between soil particles and to pore size by:

$$S_m = \frac{2\sigma_t}{r} \qquad [2.5]$$

where S_m is suction, σ_t is the surface tension of an air-water meniscus with radius r.

Osmotic suction is associated with the affinity of clay minerals for water. As shown in Section 2.2.2, clay particles carry negative charges. Dipolar water molecules and cations are adsorbed on to the particle surfaces to form diffuse double layers. The higher concentration of cations in the diffuse double layers surrounding the particles relative to that in the free water in the pores results in the development of osmotic potential gradients between the adsorbed water and the free water. Osmotic suction is the pressure applied to the free water between clay particles to attain an equilibrium with the adsorbed water surrounding the particles. For compacted soils, osmotic suctions are generally insensitive to changes in water content (Fredlund and Rahardjo, 1993). Therefore, variations in the total suction with respect to water content is generally taken as variations in the matric suction.

From a thermodynamic standpoint, the total suction in an unsaturated soil is related to the vapour pressure in the air voids in the soil. Theoretically, the total suction can be calculated using the Kelvin equation (Yong and Warkentin, 1975; Fredlund and Rahardjo, 1993),

$$S = \frac{R.T}{M} \ln\left[\frac{v}{v_o}\right] \qquad [2.6]$$

where S is the total suction, R is the molar gas constant, T is the Kelvin temperature, M is the molecular mass of water, v is the partial vapour pressure, v_o is the saturated vapour pressure, and $\frac{v}{v_o}$ is the relative humidity. The implication of Equation 2.6 is that changes

in vapour pressure in the soil reflect changes in the total suction. Factors which influence vapour pressures in soils are discussed in Section 2.4.3. Note too, that suctions and vapour pressures vary with temperature.

2.4.3 Factors affecting vapour pressures in soils

The vapour pressure and, hence, the total suction in an unsaturated soil are influenced by several factors including chemical composition of the soil water, capillarity, temperature, and external air pressure.

Most soils contain soluble salts. The presence of dissolved salts in the soil water increases its surface tension, thereby lowering the vapour pressure in the soil (Hillel, 1980).

Capillarity is a phenomenon associated with the matric component of total suction (Fredlund and Rahardjo, 1993). In an unsaturated soil, the voids are often represented conceptually as a bundle of capillary tubes. Water is held in these pores by surface tension forces in air-water menisci formed between adjacent soil particles (see Figure 2.2). The vapour pressure in the soil depends on the curvature of the water surface and surface tension of the soil water. The vapour pressure tends to decrease with decreasing radius of curvature of the water surface, or increasing surface tension of the soil water. In turn, the latter factors depend on other geometric and environmental factors.

Water content, grain size, packing of soil particles, and wetability all influence the curvatures of air-water menisci between soil particles (Spangler, 1960). The radius of curvature tends to increase with increasing water content (see Figure 2.3). The vapour pressure in a soil therefore increases with increasing water content. At a given water content, smaller grain size or smaller particle spacing results in a smaller radius of curvature, and hence lower vapour pressure (see Figures 2.4 and 2.5). Figure 2.6 compares two soils with different wetabilities. A soil is said to have low wetability, if

the contact angle between the air-water menisci and the soil particles is greater than zero. An increase in the angle of contact will tend to increase the radius of curvature of the menisci, leading to higher vapour pressure in the soil.

The surface tensions of the air-water menisci are influenced by temperature and external air pressure (Edlefsen and Anderson, 1943; Moore, 1972). The surface tension of water is inversely related to temperature (Edlefsen and Anderson, 1943). Higher temperatures will lead to lower surface tensions in the soil water. Furthermore, increasing temperature will result in an increase in the kinetic energy of the soil water. This will allow more energetic water molecules to overcome the attraction forces from the liquid phase of the soil water and to break away into the open pores within the soil structure, thereby increasing the concentration of water vapour in the soil. Therefore an increase in temperature of the soil will lead to an increase in the vapour pressure (Hillel, 1980).

External air pressure over an air-water meniscus increases the vapour pressures and therefore suctions in three ways. One, the general curvature of the air-water meniscus reduces with increasing pressure, that is, the surface becomes flatter. As the vapour pressure is directly related to the radius of curvature of the air-water meniscus, the flattening of the meniscus (that is, increasing radius of curvature) increases the vapour pressure. Two, an increase in gas pressure over a water surface has an effect of bringing more gaseous molecules into contact with the surface (Osipow, 1962). The attraction of these molecules tends to counteract the tension forces on the water molecules at the air-water interface. Therefore, increasing pressure should generally result in a reduction in the surface tension of water, leading to an increase in vapour pressure above the water surface. Three, Tabor (1969) explained that "external air pressure squeezes extra water molecules out of the liquid", thereby increasing the concentration of water molecules above the water surface, and hence increasing the vapour pressure.

2.4.4 Suction-water content relationships

Soil suction varies with water content (Fredlund and Rahardjo, 1993). Suction values are inversely related to the water content of soils, but the specific relationship varies from one soil to another. The variation between soils are due to a number of factors which notably include the chemical composition of the pore water, surface effects attributed to clay mineral-water interactions, and textural and structural characteristics which affect the pore size distribution in the soil. Generally, for a given range of water content, the water in a clay soil can exist at higher suctions and over a larger suction range than that in a sandy soil (see Figure 2.7).

Because of the insensitivity of osmotic suction to water content variations, changes in the total suction in an unsaturated soil are largely attributed to changes in the matric suction (Fredlund and Rahardjo, 1993), which in turn, is controlled by the capillary pores in the soil. Therefore, using the capillary equation, it is theoretically possible to relate the pore size distribution in a soil with its suction (Corey, 1986). Fredlund and Xing (1994) hypothesized that the suction-water content relationship of any soil can be predicted using the entire range of its pore size distribution. It was shown in Section 2.3 that in compacted clays, capillary pores typically exist as two distinctive ranges of pores commonly referred to as macro- and micro-pores (Garcia-Bengochea et al., 1979; Juang and Holtz, 1986). However, experimental observations show that suctions in these compacted materials are controlled largely by the range of the smallest measurable pores in the pore size distribution, that is, the micropores (Croney et al., 1958; Olson and Langfelder, 1965; Krahn, 1970; Gray, 1980). These observations therefore raise questions on the adequacy of the hypothesis of Fredlund and Xing (1994) to explain the suction behaviour of compacted clay soils. It will be seen later in this thesis that the work carried out in this study clarifies the uncertainty regarding the relation of pore size distribution and soil suction.

2.4.5 Temperature effects on soil suctions

Suctions in soils are influenced by temperature. Observations show that soil suction generally decreases with increasing temperature. The effect of temperature on soil suction is commonly attributed to the dependence of the surface tension of water on temperature (Edlefsen and Anderson , 1943).

2.4.6 Hysteresis

Generally, the suction-water content relationship of a soil may be obtained in two ways: desorption and sorption. In the desorption method, a soil sample is allowed to dry gradually in successive increments of applied suction. The sorption method involves gradually wetting up the soil sample while reducing the suction. Each of these methods produces a continuous curve, but the two curves will not be identical. This hysteresis is observed in both cohesionless granular soils and cohesive soils (Baver et al., 1972; Yong and Warkentin, 1975).

For sands and other cohesionless granular materials, hysteresis is attributed to the "ink-bottle" effect (Yong and Warkentin, 1975; Hillel, 1980). In general, the pores in a granular material are highly variable in size and shape. During desorption, the removal of water from the soil is controlled largely by the smaller pores. The voids in the soil will remain water-saturated until the suctions are high enough to cause the smallest pores to empty. In contrast, during sorption, water uptake by the soil is controlled by the larger pores. The voids in the soil will not fill until the suctions are low enough to fill the largest pores. Therefore, at a given water content, the suction in the soil is higher for desorption than for sorption.

In clays, hysteresis is attributable partly to the "ink-bottle" effect, and partly to changes in the soil fabric and pore size distribution brought about by swelling and shrinking of the soil during the drying and wetting processes (Yong and Warkentin, 1975).

2.4.7 Measurements of soil suctions

This study concerns the use of thermocouple psychrometers to measure suctions in compacted clays. A detailed review of the principle of the method is given in Chapter 3. To provide general background information on current technologies on suction measurements, a brief review of contemporary methods is presented in this section.

Table 2.2 summarizes the methods that are commonly used to determine soil suctions. Largely, the suction range in which they remain functional, and the components of suction that they measure are influenced by the operation principle of each method. The methods listed in Table 2.2 may be broadly grouped in three classes in accordance to the suction components (that is, total, matric, and osmotic suctions) that they determine. Alternatively, these methods may be categorized as those that measure and those that control soil suctions.

Methods that determine total suction in soils include thermocouple psychrometer, filter paper method, and vapour pressure method (Richards, 1967; Campbell and Gee, 1986; Fredlund and Rahardjo, 1993). These methods are based on the premise that the vapour pressure in a soil can be measured or controlled, and that the total suction is thermodynamically related to the vapour pressure via the Kelvin equation (Equation 2.6). Because of the sensitivity of vapour pressure to temperature changes, the accuracy and precision of these methods depend largely on temperature (Campbell and Gee, 1986).

Experimental studies show that the outputs of the psychrometers are strongly influenced by temperature changes and temperature gradients (Wiebe et al., 1977; Brown and Bartos, 1982). Errors in suction measurements due to temperature changes may be corrected using appropriate empirical calibration relationships (Wiebe et al., 1970; Brown, 1970). *In situ* suction measurements using psychrometers are strongly influenced by temperature gradients which lead to spatial and temporal variations in the vapour pressure in the soil (Wiebe et al., 1977; Brown and Bartos, 1982). The effects of

temperature gradients and vapour pressure gradients on the accuracy and precision of psychrometers are difficult to quantify and are presently not well understood. These two factors provide a focus for further research and were investigated in this study.

The filter paper and the pore fluid squeezer methods may be used to measure the osmotic suction in a soil (Fredlund and Rahardjo, 1993). In the latter method, pore fluid is first extracted from the soil using a pore fluid squeezer. The electrical conductivity of the pore fluid is then estimated and converted to soil suction using an osmotic suction-electrical conductivity relationship.

The matric suction in a soil may be determined using tensiometers, hydraulic piezometers, thermal conductivity sensors, or axis translation techniques (Hilf, 1956; Stannard, 1991; Fredlund and Rahardjo, 1993). Tensiometers measure the negative pore water pressures or water tensions in soils. Because of problems associated with cavitation of water, the use of the instruments are generally limited to negative pore water pressures not less than -90 kPa. Thermal conductivity sensors provide indirect measurements of the matric suctions in soils. The outputs of the instruments depend on the thermal conductivities of the soil which can be calibrated to the suction and water content in the soil. In the axis translation technique, matric suction in the soil is controlled during testing by independently regulating the pore air and pore water pressures in the soil. Because of problems associated with cavitation, discontinuity in the air phase in the soil, and limitations of testing equipment, these methods are generally operable in smaller and lower suction ranges, compared with the methods used to measure total and osmotic suctions individually (see Table 2.2).

It was reviewed in Section 2.4.2 that, due to capillarity and the presence of clay minerals, suctions in unsaturated compacted clays are largely total suction, that is, the sum of matric and osmotic suctions. Because of their ability to measure total suction and to function over a wider suction range, the psychrometer, filter paper, and vapour

equilibrium methods were used to measure suctions in the soils tested in this study. Procedures used in the testing program are described in Chapter 4.

2.4.8 Summary

The suction in a soil is generally referred to as total suction, and is assumed to consist of two main components: matric and osmotic suctions. Matric suction is related to capillary phenomena in the soil structure and osmotic suction is associated with physico-chemical interactions in the clay-water system.

From a thermodynamic viewpoint, the total suction in a soil is related to the vapour pressure of the soil water. The vapour pressure is in turn influenced by other material and environmental parameters including water content, chemical composition of soil water, soil fabric, pore size, temperature, and external air pressure. Therefore any variations in these parameters will lead to spatial and temporal changes in the vapour pressure in the soil. In turn, the latter changes could influence the accuracy and precision of suction and water content measurements using thermocouple psychrometers, and other similar methods in which the vapour pressure in the soil is measured or controlled during testing.

Conflicts exist between theories and experimental observations with respect to the relation between suction and soil structure in unsaturated compacted clays. For contemporary theories, it is generally assumed that the suction in a soil is controlled by the whole range of open pores (both macropores and micropores) within the soil structure. In contrast, experimental evidence suggests that for most practical applications and conditions, the suctions in clays with complex soil fabrics and multi-modal pore distributions can be considered to be controlled by a portion of the pore size within the microstructure of the soil. The uncertainty regarding the relationship between soil suction

and pore size distribution formed a subject of focus of this work, which will be presented in Chapter 5.

2.5 Theories of unsaturated soil mechanics

2.5.1 Background

In the last 30 years, much research has been conducted under the topic of unsaturated soil mechanics. Several conceptual models and frameworks have been proposed to describe the various aspects of the behaviour of unsaturated soils, for example, Alonso et al. (1990), Thomas (1992), Fredlund and Rahardjo (1993), Wheeler and Sivakumar (1995). To a large extent, theories of unsaturated soil mechanics derive largely from existing frameworks for saturated soils. In this section, some of the contemporary theories relating to constitutive modelling and moisture flow phenomena in unsaturated soils are reviewed. This review provides the background for the analysis of the data from the triaxial testing program to be presented in Chapter 6.

2.5.2 Constitutive modelling of the behaviour of unsaturated soils

2.5.2.1 Background

Theories of saturated soil mechanics are built upon the concept of effective stress attributed to Terzaghi (1936). The effective stress in a soil cannot be measured directly, but is generally taken as the numerical difference between the external applied total stress and the internal pore water pressure. Terzaghi stated that "all measurable effects of a change in stress such as compression, distortion, and change in shearing resistance are exclusively due to changes in effective stress".

An unsaturated soil is generally considered as a three phase system consisting of solid particles, water and air (Alonso et al., 1990). The presence of the air phase means that the behaviour of the soil cannot simply be described in terms of total stress and pore water pressure. Pore air pressure must be considered. In the early studies on unsaturated soils, attempts were made to relate the strength of and volume change in unsaturated soils with a single effective stress variable which incorporates combinations of total stress, pore water and pore air pressures (Aitchison and Donald 1956; Croney et al., 1958; Bishop, 1959). The most notable effective stress equation was Bishop's (1959) equation, and is given as follows,

$$\sigma' = \sigma - u_a + \chi(u_a - u_w) \qquad [2.7]$$

where σ' is effective stress, σ is total stress, u_a is pore air pressure, u_w is pore water pressure, χ is Bishop's Chi factor which depends on the saturation in the soil.

Later, Jennings and Burland (1962) and others showed that the behaviour of an unsaturated soil cannot simply be expressed in terms of a single effective stress variable. Instead, total stress, pore air pressure and pore water pressure must be combined to form two independent stress state variables, typically chosen as the net total stress (σ-u_a) and the matric suction (u_a-u_w) (Matayas and Radhakrishna, 1968; Fredlund and Morgenstern, 1977; Alonso et al., 1990). This combination of stress state variables is advantageous because in most practical problems, the pore air pressure is atmospheric, and (σ-u_a) reduces to the total stress while (u_a-u_w) reduces to the measured negative pore water pressure (Fredlund and Morgenstern, 1977). Therefore the effects of total stress changes and pore water pressure changes can be separated.

There are two schools of thought in our current understanding of the constitutive behaviour of unsaturated soils. One approach is advocated by Fredlund and his co-

workers at the University of Saskatchewan in Saskatoon (see Fredlund and Rahardjo, 1993). Fredlund's approach is an extension of classical soil mechanics theories on saturated soils. In his approach, deformation and stability of soils are considered separately. The other approach is based on elastic-plastic critical state soil mechanics theories. The general consensus (Delage and Graham, 1995) is that this latter approach provides a more coherent framework which allows both deformation and collapse to be dealt with together (Alonso et al., 1990; Wheeler and Sivakumar, 1995). This is not possible using the classical soil mechanics approach. Furthermore, critical state models can be coupled conceptually with flow models formulated using suctions and pressures as governing variables (Alonso et al., 1987; Thomas, 1992).

2.5.2.2 Classical soil mechanics approach

In classical soil mechanics, two types of analysis are carried out. Limit analysis which is concerned only with the equilibrium of soil masses, requires the knowledge of the stress conditions and strength of the soil. In this type of analysis, displacements in the soil are not considered. On the other hand, deformation analysis deals only with displacements and volume changes in the soil, and the strength of the soil is not required.

In the classical approach to unsaturated soils, the volume change behaviour and strength of an unsaturated soil are described by extended forms of classical soil mechanics equations for saturated soil (Fredlund and Rahardjo, 1993). The volume change in an unsaturated soil is attributed to changes in both the soil structure and the water phase. The change in void ratio in the soil is expressed by,

$$de = a_t.d(\sigma - u_a) + a_m.d(u_a - u_w) \qquad [2.8]$$

and, conversely, the change in water content in the soil is given by,

$$dw = b_t.d(\sigma - u_a) + b_m.d(u_a - u_w) \qquad [2.9]$$

where e is void ratio, w is water content, $(\sigma - u_a)$ is net total stress, $(u_a - u_w)$ is matric suction, and a_t, a_m, b_t, b_m are material parameters determined experimentally.

The shear strength of an unsaturated soil is described by an extended form of the Mohr-Coulomb failure criterion (Fredlund et al., 1978),

$$\tau = c' + (\sigma - u_a).\tan\phi' + (u_a - u_w).\tan\phi^b \qquad [2.10]$$

where τ is the shear strength, $(\sigma - u_a)$ is the net total stress, $(u_a - u_w)$ is the matric suction, ϕ' is the frictional angle with respect to changes in the net total stress, and ϕ^b is the frictional angle with respect to changes in the matric suction. Conceptually an unsaturated soil has the same internal friction angle as a saturated soil, and the contribution of matric suction can be viewed as an increase in the cohesion in the soil (Fredlund, 1979).

2.5.2.3 Critical state soil mechanics approach

Critical state soil mechanics was founded on theories of elasticity and plasticity (Roscoe et al., 1958; Wood, 1990). The critical state approach has the advantages of:

1) coupling volume changes and changes in shear stress in soils,
2) modelling strain-hardening and strain-softening behaviour of soils,
3) linking undrained and drained conditions,
4) accounting for nonlinear behaviour in soils by the specification of an appropriate yield function.

The theory of critical state soil mechanics is based on the concept that under the influence of a certain stress system, a soil will continue to deform, and will eventually approach a critical state, where no further changes in volume or effective stress will occur.

For saturated soils, the state of a soil is fixed by three variables in a 3-dimensional space. The three variables are:

Mean effective stress	$p' = (\sigma'_1 + 2\sigma'_3)/3$
Deviator stress	$q = \sigma'_1 - \sigma'_3$
Specific volume	$v = 1 + e$

Implicit in the general model shown in Figure 2.8 are two important lines: the normal consolidation line and the critical state line. These two lines are typically determined in compression and shear tests using the triaxial apparatus. In these tests, total stresses are applied to the specimens by controlling the axial loads and the confining cell pressures, while the pore water pressures within the specimens are measured. The normal consolidation line is reached by isotropically consolidated specimens after complete water content equilibrium has been reached at any given pressure. The normal consolidation line is described by the relationship,

$$v = \Gamma - \lambda \ln p' \qquad [2.11]$$

where Γ and λ are material constants. The critical state line represents the state of specimens reached after large straining in shear compression. At this state there are no further changes in volume, shear stress, and pore water pressure. The critical state line is described by the relationship,

$$q = Mp' \qquad [2.12]$$

where M is a material constant.

Experimental evidence shows that for a given soil, the normal consolidation and the critical state lines are uniquely fixed in p':q:v space (Wood, 1990). The surface that encompasses the normal consolidation line and the critical state line is the state boundary surface. This surface forms the demarcation between the states where the behaviour is elastic and other states where plastic or failing deformations occur. Tested triaxially, all paths for normally consolidated specimens must lie on the state boundary surface. For overconsolidated specimens, their states initially lie below the state boundary surface and specimens behave elastically. When eventually the specimens are brought to reach the state boundary surface, overconsolidated specimens will follow the state boundary surface and exhibit plastic behaviour as stresses change.

Based on critical state soil mechanics theories for saturated soil, Alonso et al. (1990) proposed a critical state framework for unsaturated soils. Consistent with the assumptions used in models for saturated soils, Alonso et al. (1990) assume that elastic behaviour is observed when the stresses on an unsaturated soil are such that the soil lies within the state boundary surface. Conversely, unsaturated soils will experience plastic deformation if the state of the soil follows the state boundary surface.

In contrast to the requirements for saturated soils described earlier, four state variables are required to represent the state of an unsaturated soil (Alonso et al, 1990; Wheeler and Sivakumar, 1995). These variables are:

Mean total stress	$p = (\sigma_1 + 2\sigma_3)/3 - u_a$
Deviator stress	$q = \sigma_1 - \sigma_3$
Specific volume	$v = 1 + e$

Matric suction $s = u_a - u_w$

Results from triaxial tests on unsaturated kaolin specimens show that the critical state of unsaturated soils depends on the suction in the soil, and unlike saturated soils, cannot be represented by a single critical state line (Wheeler and Sivakumar, 1995). The theoretical expression of the critical state of an unsaturated soil takes the form,

$$q = M(s).p + \mu(s) \qquad [2.13]$$

where M and μ are functions of the matric suction in the soil. The relationship between mean total stress and specific volume also depends on suction, and takes the form,

$$v = N(s) - \lambda(s)\ln(p/p_{at}) \qquad [2.14]$$

where N and λ are functions of the matric suction in the soil, p_{at} is mean total stress with respect to atmospheric pressure.

When the suction in the soil approaches to zero (that is, the saturated condition), Equations 2.13 and 2.14 reduce to a form consistent with Equations 2.12 and 2.11 respectively. As will be seen later in this thesis, the elastic-plastic theories reviewed in this section provide a basis for the discussion of the data from the triaxial tests carried out in this study.

2.5.3 Flow of moisture in unsaturated soils

2.5.3.1 Background

In unsaturated soils, moisture flow takes place in both liquid and vapour phases (Brady, 1974; Hillel, 1980). The movement of moisture in the liquid phase of an unsaturated soil is attributed to driving forces resulting from total head gradients within the soil mass. Total head gradients arise from differences in suction, pressure, water content, and chemical composition of the soil water within the unsaturated soil. Flow takes place in the direction of decreasing total head. The flux which is the flow through unit area per unit time, is proportional to the total head gradient and is affected by the geometric properties of the pore channels through which the flow takes place.

In contrast to liquid flow which depends on the potential difference in the liquid phase, the flow of water vapour in an unsaturated soil is associated with the difference in the kinetic energy of free water molecules in the unsaturated pores (Hausenbuiller, 1972). The kinetic energy of water molecules is expressed in terms of vapour pressure. Water vapour flow occurs when vapour pressure gradients exist. In turn, vapour pressure gradients arise as a result of temperature gradients and chemical gradients associated with the differences in the distribution of solutes in the pore fluid. When liquid continuity in a soil is disrupted, the only form of moisture transport is by means of vapour transfer (Slatyer, 1967).

2.5.3.2 Isothermal liquid flow

It was reviewed in Section 2.3.3.4 that water flow in saturated soils is commonly described by Darcy's law (Yong and Warkentin, 1975). Richards (1931) showed that Darcy's law for saturated flow also applies to moisture flow in unsaturated soils though

now the hydraulic conductivity varies with saturation. The mean one-dimensional flow velocity in an unsaturated soil is expressed mathematically as follows,

$$v = -K(\psi_m)\frac{d\psi_m}{dx} \qquad [2.15]$$

where v is velocity, $K(\psi_m)$ is hydraulic conductivity of the unsaturated soil, ψ_m is matric potential in the soil, and x is the length of the flow path in the x-direction. For unsaturated soils, the hydraulic conductivity varies with water content and suction, and is affected by processes such as hysteresis and temperature (Hillel, 1980; Corey 1986; Neilsen et al. 1986).

2.5.3.3 Vapour flow

The flow of water vapour in an unsaturated soil arises from vapour pressure gradients within the soil, and is generally treated as a diffusion process (Philip and de Vries, 1957; Hillel, 1980). The vapour flux in an unsaturated soil may be expressed by the following differential equation (Slatyer, 1967):

$$q = -a.f.D_w\frac{dV_p}{dx} \qquad [2.16]$$

where q is vapour flux, a is tortuosity factor, f is fractional cross sectional area available for diffusion, D_W is diffusion coefficient of water vapour in air, V_p is vapour pressure, and x is distance.

Philip and de Vries (1957) described a possible mechanism through which water vapour moves within unsaturated soils. They explained that in an unsaturated soil, liquid continuity may not exist, and therefore, liquid water remaining in the system tends to locate almost wholly in small pores or wedges which form necks or islands between the

solid particles. Water vapour moves by condensing on one meniscus of each neck followed by evaporating from the other meniscus of the same neck in such a way that the process proceeds without interruption through regions of vapour and liquid.

2.5.3.4 Coupled heat and moisture flow under the influence of thermal gradients

Moisture flow in unsaturated soils under the influence of thermal gradients is a complex phenomenon. The movement of moisture takes place simultaneously in both liquid and vapour phases (Brady, 1974). In the liquid phase, the flow of moisture occurs largely as a result of total head difference within the soil. In the vapour phase, moisture flows from regions of high vapour pressures to those of lower vapour pressures. In many cases, the liquid and vapour flows occur in the same direction, normally in the direction of decreasing temperature gradient. However, under certain circumstances, competing water content, suction and vapour pressure gradients may co-exist. In these cases, the net flow of moisture depends on the spatial and temporal distributions of temperature, water content and suction within the unsaturated soil. This will be observed later in the Buffer/Container Experiment described in Chapter 8.

A common method of analysing moisture movement under the influence of heat and hydraulic gradients is the mathematical formulation attributed to Philip and de Vries (1957). The Philip and de Vries (1957) model is based on the concept of viscous flow of liquid water under the influence of gravity, capillary and adsorptive forces, and on the concept of vapour movement by diffusion. The model assumes that local thermodynamic equilibrium between liquid and vapour exists at each point within the soil though spatial and time gradients are still present. For one-dimensional flow, the general differential

equations describing the moisture flow and heat transfer under combined temperature and hydraulic gradients are as follows,

Moisture flow:

$$\frac{\partial Q}{\partial t} = \nabla(D_T \nabla T) + \nabla(D_{\Theta_{liq}} \nabla\theta) + \frac{\partial K}{\partial x} \qquad [2.17]$$

Heat flow:

$$c.\frac{\partial T}{\partial t} = \nabla(\lambda \nabla T) - L\nabla(D_{\Theta_{vap}} \nabla T) \qquad [2.18]$$

where ∇T is thermal gradient, $\nabla\theta$ is volumetric water content gradient, D_T is thermal moisture diffusivity, $D_{\Theta liq}$ is isothermal liquid diffusivity, $D_{\Theta vap}$ is isothermal vapour diffusivity, Q is volumetric water content, T is temperature, L is latent heat of water, K is hydraulic conductivity, c is volumetric heat capacity, λ is thermal conductivity, t is time, and x is the length of flow path in the x-direction. The material parameters related to permeability and diffusivity are generally found to be dependent on water content and temperature, and are hysteretic (Radhakrishna et al., 1992).

In the original Philip and de Vries (1957) formulation, volumetric water content (that is, water content determined by volume) is used as a governing variable. In recent years, attempts have been made by others to recast the original formulation using suction and pressure as variables to what is colloquially referred as the "potential" formulation (Milly, 1982; Thomas, 1992). The advantages of the "potential" formulation over the original formulation are discussed by Thomas (1992). Briefly, the use of suction and pressure as variables facilitates coupling of flow models with elastic-plastic stress-strain models such as the critical state model described in Section 2.5.2.3. Furthermore, flow

models based on the "potential" formulation permit the considerations of inhomogeneity in the unsaturated media with respect to material properties and saturation.

Using matric suction and temperature as governing variables, Thomas (1992) developed a mathematical model based on the original Philip and de Vries (1957) formulation to describe the coupled heat and moisture flow in unsaturated soils. His model is shown to be generally applicable to granular materials and non-swelling clays. In his model, the liquid flow and vapour flow are considered separately before combining the two into a conservation of mass equation. Non-isothermal liquid flow is governed by the extension of Darcy's law. The treatment of vapour flow follows the approach proposed by Philip and de Vries (1957). Heat transfer is assumed to take place by means of conduction, latent heat of vaporization and sensible heat transfer. For one-dimensional flow, the governing differential equations for moisture flow and heat transfer are as follows:

Moisture flow:

$$C_{\psi\psi}\frac{\partial \psi}{\partial t} + C_{\psi T}\frac{\partial T}{\partial t} = \frac{\partial}{\partial x}\left(K_{\psi\psi}\frac{\partial \psi}{\partial x}\right) + \frac{\partial}{\partial x}\left(K_{\psi T}\frac{\partial T}{\partial x}\right) + \frac{\partial K}{\partial x} \qquad [2.19]$$

Heat flow:

$$C_{T\psi}\frac{\partial \psi}{\partial t} + C_{TT}\frac{\partial T}{\partial t} = \frac{\partial}{\partial x}\left(K_{T\psi}\frac{\partial \psi}{\partial x}\right) + \frac{\partial}{\partial x}\left(K_{TT}\frac{\partial T}{\partial x}\right) - C_{pl}.u\frac{\partial T}{\partial x} - C_{pv}.v\frac{\partial T}{\partial x} \qquad [2.20]$$

where ψ is matric suction, T is temperature, K is hydraulic conductivity of the unsaturated material, C_{pl} is specific heat capacity of soil water, C_{pv} is specific heat capacity of soil vapour, u is velocity of liquid flow, v is velocity of vapour flow, $C_{\psi\psi}$,

$C_{\psi T}$, $C_{T\psi}$, and C_{TT} are coefficients related to the flow of moisture, and, $K_{\psi\psi}$, $K_{\psi T}$, and $K_{T\psi}$ are coefficients related to heat flow. The material parameters used in this model are generally functions of suction and water content, and are influenced by hysteresis and temperature.

2.6 Synthesis of literature review

It was stated in Chapter 1 that the purpose of this study was to clarify the conditions under which psychrometers can be operated to provide meaning data on *in situ* suctions and water contents in compacted clays. Based on the review given in this chapter, the following conclusions may be drawn.

Certainties

1) The use of contemporary theories of unsaturated soil mechanics to describe moisture flow, strength, and deformation of unsaturated soils requires the knowledge of soil suction and its relationships with other state variables including stress, void ratio, water content, vapour pressure, and temperature.

2) Because of the affinity of clay minerals for water, compacted clays tend to develop complex soil structures. The soil structure in compacted clays may be characterized as a system of aggregations of peds containing micropores which may be water-saturated or unsaturated, and macro-pores within and between aggregations. Stress-strain and strength properties of compacted clays are generally governed by the interactions between peds. Conduction phenomena are primarily controlled by the macropores between peds. In contrast, suction and swelling properties are largely influenced by capillary and clay-water interaction phenomena within the peds.

3) The use of thermocouple psychrometers to measure suctions is based on the premise that the vapour pressure in the soil can be measured or controlled.

4) The vapour pressure in a soil is influenced by several material and environmental factors which include water content, chemical composition of pore water, soil fabric, capillarity, and temperature.

Uncertainties

1) There is little experience on the use of thermocouple psychrometers as a tool to measure suctions in highly compacted clays under laboratory and *in situ* conditions. Particularly, there is little information on the accuracy and precision of the instruments for *in situ* suction measurements at different temperatures and under the influence of temperature gradients. Conditions under which psychrometers can be operated to provide meaningful information for the study of moisture movement in and stress-strain behaviour of unsaturated compacted clays, need to be clarified.

2) Conflicts exist between theories and experimental observations with respect to the relation between suction and soil structure in unsaturated compacted clays. Contemporary theories generally assume that the suction in a soil is controlled by the whole range of open pores (both macropores and micropores) within the soil structure. In contrast, experimental evidence suggest that the suctions in clays with complex soil fabrics and multi-modal pore distributions are largely controlled by a portion of the pore size within the microstructure of the soil.

3) The effects of stress variations and deformations on soil macro- and micro-structure in compacted clays are not clear.

4) Little work has been done to examine the combined effects of stress variation, deformation, and water content on suctions in compacted clays. The effects of these factors on suction measurements using psychrometers are not known.

2.7 Hypothesis

Based on the conclusions from the literature review, the following hypotheses were examined in this thesis.

Hypothesis 1: *The suction in a compacted clay is largely controlled by the soil microstructure.*

Hypothesis 2: *Under normal temperature and atmospheric pressure boundary conditions, thermocouple psychrometers can be used to measure suction in swelling compacted clays.*

Hypothesis 3: *Under constant mass conditions, stress variations and deformations will bring about changes in the soil macro- and micro-structures in a compacted clay. These latter changes in turn will affect the vapour pressure in the soil. Under these conditions, the suction measured by a psychrometer will be different from that suction measured at the same water content by the same instrument under normal atmospheric pressure condition.*

Hypothesis 4: *Spatial and temporal variations in temperature lead to transient non-uniform vapour pressure distributions in a soil. Under these conditions, at a given water content, the suction measured by a calibrated thermocouple psychrometer will be*

different from the suction defined by the suction-water content relationship obtained under constant laboratory conditions.

Confirmation of the hypotheses stated in this section would clarify the conditions under which psychrometers can be used to provide meaningful data in the study of the behaviour of unsaturated soils. In light of the conclusions from the literature review in Section 2.6 and the hypotheses stated in this section (2.7), a series of objectives were developed and are given in Section 2.8. These objectives were achieved by carrying out series of laboratory and *in situ* tests to examine the use of psychrometers to measure suctions and water contents in compacted clays.

2.8 Objectives of study

This study examines the effects of temperature, stress variation, and distortions on suction and water content measurements in compacted clays using thermocouple psychrometers. In particular, the usefulness of psychrometers as moisture sensors in unsaturated dense sand-bentonite material used for the disposal of radioactive waste was investigated. The hypotheses stated in Section 2.7 were examined in this study through a series of objectives given as follows.

1) to clarify the conditions under which psychrometers can be operated to provide meaningful suction and water content data in the study of moisture movement and stress-strain behaviour of unsaturated compacted clays.
2) to clarify the role of soil structure in controlling the vapour pressure, and hence the suction in a soil.
3) To explore the use of contemporary unsaturated soil mechanics frameworks similar to those proposed by Alonso et al. (1990), Gens and Alonso (1992), and Delage and Graham (1995) to describe the inter-relationship of stress, volume

change, and suction of an unsaturated compacted sand-bentonite material proposed for use in the disposal of radioactive waste.

4) To develop a framework to incorporate the effects of stress variations and distortions on suction measurements in compacted clays using thermocouple psychrometers and other psychrometric methods.

5) To establish the bounds of accuracy and precision for thermocouple psychrometers in tracking *in situ* suction and moisture transients under the influence of temperature gradients and stress variations in clay barrier material proposed for use in the disposal of radioactive wastes.

CHAPTER 3 THERMOCOUPLE PSYCHROMETERS

3.1 Background

It was stated in Chapter 1 that the main objective of this study was to clarify the conditions under which thermocouple psychrometers can be operated to provide meaningful suction and water content data in the study of unsaturated compacted clays. Several methods used to measure soil suctions were reviewed in Chapter 2. In this chapter, the psychrometer method is described in greater detail.

To provide confidence in the measurements by psychrometers in the tests which form part of this study, the accuracy and precision of the instruments must be known. In this chapter, the theory of thermocouple psychrometers is reviewed. The type of psychrometer and equipment that have been used in this study are described. Results from a series of laboratory and calibration tests designed and carried out to examine the performance of the psychrometers are discussed.

3.2 Terminology and definitions

This section provides the background on two thermoelectric processes that underlie the operation of thermocouple psychrometers and on the terms commonly used in thermocouple psychrometry.

Peltier effect: When two dissimilar metals are placed in contact, there exists a Peltier electromotive force (*emf*), which depends on the types of metals and the temperature of the junction. When a current is passed across the junction, heat will be either absorbed or liberated. If the current is passed in an opposite direction to the Peltier *emf*, heat is liberated. If the current is forced across the junction in the same direction as the Peltier *emf*, heat is absorbed at the junction.

The latter process is utilized in the cooling of the sensing junction in a psychrometer.

Seebeck effect: This process forms the basis of thermocouples. When two dissimilar metals are joined together to form a closed circuit, two junctions are formed. If these two junctions are maintained at different temperatures, an *emf* is established in the circuit. The magnitude of the *emf* produced is directly proportional to the temperature difference between the two junctions.

Vapour pressure: According to the kinetic theory of liquids and gases, due to kinetic energy, the molecules in a liquid are always in motion. Occasionally, energetic molecules at the surface have enough kinetic energy to break away from the liquid surface. Such molecules overcome attractive forces between themselves and other molecules in the liquid, and they behave like a gas. If the liquid is contained in a sealed container, these water molecules will collide with the wall of the container and the pressure exerted on the wall is known as the vapour pressure. The vapour pressure of a liquid depends on several factors including the chemical composition of the liquid and temperature.

Saturation vapour pressure: This is the maximum possible vapour pressure of a liquid at a given temperature. The relationship between saturation vapour pressure and temperature is shown in Figure 3.1.

Partial vapour pressure: The vapour pressure of a liquid that is lower than the saturation vapour pressure at the same temperature is known as the partial vapour pressure (see Figure 3.1). The magnitude of the partial vapour pressure depends on the chemical composition of the liquid.

Relative humidity: Relative humidity is the ratio of the mass of water vapour per unit volume of air to the mass of water vapour per unit volume of air when the air is saturated with water vapour at the same temperature. Numerically, this is

the same as the ratio of the partial water vapour pressure to the saturation water vapour pressure at the same temperature.

Dew point: The dew point is the temperature to which unsaturated air must be cooled at constant pressure for condensation to occur (see Figure 3.1)

Dry bulb temperature: This is the temperature measured by a dry thermometer placed in a vapour (Figure 3.1).

Wet bulb temperature: If a thermometer with a wetted liner around its bulb is placed in a mass of unsaturated air and allowed to equilibrate with the surrounding air, the thermometer will record a temperature lower than the dry bulb temperature. This is due to liquid evaporating from the liner into the vapour phase and drawing heat from the thermometer through latent heat of evaporation. The temperature recorded on the thermometer is known as the wet bulb temperature (Figure 3.1).

Wet bulb depression: It is the difference between the dry and wet bulb temperatures. The relationship between wet bulb depression, saturation vapour pressure and dew point is depicted in Figure 3.1.

3.3 Description of psychrometer and equipment

3.3.1 Wescor PCT-55 psychrometer

The psychrometers used in this study were Type PCT-55 manufactured by Wescor Inc. in Utah, USA (Figure 3.2). The main part of the instrument is about 25 mm long and about 7 mm in diameter. The instrument consists of two thermocouple junctions protected by a ceramic cup and a Teflon plug (Figure 3.3). Inside the ceramic cup, a chromel wire and a constantan wire are welded together to form the sensing junction, which is used in the measurement of the equilibrium relative humidity. The wires join the

gold pins in the Teflon plug to form the reference junctions for this measurement. Behind the Teflon plug, a third thermocouple junction is formed by joining a copper wire and a constantan wire together. This junction provides the measurement of the ambient (dry bulb) temperature of the soil.

Theory of Operation - Psychrometric Mode

A thermocouple psychrometer can be operated in either the psychrometric (wet bulb) mode or the hygrometric (dew point) mode (Briscoe, 1984). The mode of operation depends on the type of microvoltmeter and data acquisition system used for the measurement. In this study, because of the type of microvoltmeters that were available and used to control the instruments, the psychrometers were operated in the psychrometric mode .

Figure 3.4 shows a typical output of a psychrometer operated in the psychrometric mode. In this mode of operation, using the Peltier effect, a cooling current with sufficient magnitude is passed through the thermocouple circuit for a specified period of time of sufficient length to cause the sensing junction to cool below the dew point of the surrounding air within the ceramic cup. Thus, water vapour is condensed from the air onto the sensing junction. The output of the thermocouple during Peltier cooling is depicted by the part of the curve between *a* and *b*.

At the end of the cooling period (depicted by point *b* on the curve), the cooling current is stopped. At this point, the sensing junction has a lower temperature than either the reference junction or the surrounding atmosphere. Because of the temperature difference between the sensing and reference junctions, an *emf* is set up in the thermocouple due to the Seebeck effect. The magnitude of this *emf* is directly proportional to the temperature gradient between the sensing and reference junctions. The temperature at the sensing junction increases rapidly due to convective heat transfer

between the junction and the surrounding air. Accordingly, the *emf* between the sensing and reference junctions decreases rapidly (points *b* and *c* in Figure 3.4). Eventually the temperature of the sensing junction reaches the wet bulb temperature of the surrounding air at *c*. In this study, the measured *emf* at this temperature is taken as the output of the psychrometer.

The wet bulb temperature is uniquely defined by the partial vapour pressure and the ambient temperature in the soil. Theoretically at this temperature, the cooling caused by the evaporation of water on the junction balances the heat absorbed from the atmosphere. This stage is depicted by the plateau section *c-d* of the output profile shown in Figure 3.4. Theoretically, the line *c-d* should be horizontal. The slope of the plateau is influenced by such factors as the size and shape of the sensing junction, non-uniform coverage of water on the sensing junction during cooling, non-uniform evaporation of the condensed moisture on the junction, and temperature gradients (Savage and Cass, 1984).

Eventually, all of the water on the sensing junction is evaporated, and the temperature of the junction quickly rises to the ambient temperature. Concurrently, the *emf* between the sensing and reference junctions decreases to zero at point *e* on Figure 3.4.

3.3.2 PR-55 and HR-33T microvoltmeters

In this study, two commercial microvoltmeters, namely the PR-55 and the HR-33T, both manufactured by Wescor were used to excite the psychrometers and read their outputs. To facilitate the interpretation, a chart recorder was connected to the microvoltmeters. The PR-55 and HR-33T microvoltmeters provide cooling currents to the psychrometers. Integrated circuits within the microvoltmeters allow the recorded *emf*s to be displayed as temperatures of the reference and sensing junctions, and as temperature gradients across the psychrometer circuit.

The PR-55 can be used in both automatic and manual modes. In the automatic mode, the user specifies a cooling current between 1 to 9 mA and a cooling time up to 99s. The cooling of the sensing junction of the psychrometer is then automatically carried out by the PR-55 in accordance with the specified parameters. In the manual mode, the cooling time is controlled directly by a user-activated switch. The HR-33T can only be operated in the manual mode. The default cooling current is set at 8 mA.

3.4 Cooling parameters: current and time

The magnitude of the cooling current and the duration of its application are important if proper cooling is to be achieved. If the cooling current is too low, or if the cooling time is too short, the temperature of the sensing junction may not reach the dew point temperature. Insufficient cooling may also lead to insufficient volumes of condensed water on the sensing junction. As a consequence, the wet bulb depression will not be clearly defined. Excessive cooling may also undermine the operation of a psychrometer. Too strong a current or too long a cooling time will cause excessive quantities of water vapour from the air to condense on the sensing junction. This could alter the vapour equilibrium of the soil/psychrometer system.

For soils with high water contents (high water potentials or low suctions), the relative humidities in the voids are high. Conversely, drier soils normally have lower water potentials or higher suctions, and have lower relative humidities. Lesser cooling (that is, smaller cooling current and/or shorter cooling time) is required in wetter soils than in drier soils to cause condensation of water vapour from the air on to the sensing junction.

Thus, to a certain extent, the selection of appropriate cooling parameters becomes a matter of judgement and experience that is influenced by the water content and

temperature of the soil (Wiebe et al., 1971). Table 3.1 shows the cooling parameters used in this study.

3.5 Calibration

All the psychrometers used in the study were calibrated prior to use. The calibration provides a relationship between suction potential and instrument output. Each psychrometer calibration was carried out using potassium chloride (KCl) solutions to control the partial vapour pressure surrounding the thermocouple probe of the psychrometer. Figure 3.5 shows the standard relationship between suction potential and molal concentration of KCl solution at 25°C (Young, 1967). Note that 1 molal (m) is defined as 1 mole of solutes per 1 kg of solvent.

The majority of the psychrometers were calibrated at an ambient temperature of 25°C. Several psychrometers were calibrated at 10°C, 25°C, and 50°C to examine the effect of temperature on psychrometer outputs.

Figure 3.6 shows the test arrangement used to calibrate the psychrometers at 25°C. The probe containing the thermocouples was placed inside a sealed polyethylene bottle and suspended above a small quantity of KCl solution of known molal concentration. To maintain constant temperature and minimize the effects of temperature gradients, the sealed bottle containing the psychrometer was partially submerged in a water bath located inside an insulated wooden chamber. The temperature of the inside of the chamber was maintained at an ambient temperature of 25°C by means of circulating the air with a fan unit controlled by an external constant temperature bath. At temperatures lower and higher than the calibration value of 25°C, the sealed bottles containing the KCl solution and the psychrometer were placed in either a temperature controlled commercial refrigerator or an oven.

The psychrometer was first allowed to equilibrate with the partial vapour pressure over the KCl solution for at least 24 hours. At the end of this period, at least three psychrometer output readings were taken and the temperature of the psychrometer was recorded. The bottle was then emptied, rinsed with distilled water, and dried. A different KCl solution was then placed inside the bottle, and the psychrometer was fitted back into the bottle. The procedure for measuring the output from the psychrometer was repeated. Generally, three KCl solutions prepared to concentrations between 0.4 m and 1.0 m were used for each psychrometer calibration. These concentrations correspond to suction potentials of 1.8 MPa to 4.5 MPa respectively at 25°C (see Figure 3.5). A linear regression analysis was then carried out to determine the suction-output relationship for the psychrometer. Figure 3.7 shows the calibration relationship at 25°C for a typical Wescor psychrometer used in this study.

3.6 Psychrometer performance

3.6.1 Precision

The precision of an instrument is defined as "the closeness of approach of each of a number of similar measurements to the arithmetic mean", and is "synonymous with reproducibility and repeatability" (Dunnicliff, 1988). The precision of a thermocouple psychrometer depends on temperature, the type of microvoltmeter and chart recorder used for monitoring, and the interpretation procedures followed by the user.

In this study, three readings of the output of a psychrometer are normally taken for a given suction and temperature suction. The precision of the psychrometer is defined as the difference between the measured instrument output and the average of the three outputs taken under the same conditions. The precision of 40 commercial psychrometers tested in this study are plotted against suction potential in Figure 3.8. From the figure it

can be seen that the instruments are generally precise within ± 0.5μV over the suction range of 1.5 MPa to 5.3 MPa. For this suction range, the average precision of the instruments were determined to be ± 0.25 μV, with a 95% confidence limit of ± 0.22 μV.

In a typical calibration test as described in Section 3.5, the measured psychrometer output varies from 6 μV for 1.4 MPa suction to 25 μV for 5.3 MPa suction. Therefore the margin of error corresponding to the measured precision in the instrument decreases with increasing suction. This conclusion is supported by the data shown in Figure 3.9. An error factor is introduced to quantify the largest difference between the measured output and the average of the three outputs taken by the same psychrometer under the same conditions. The result is expressed as a percentage of the average output. Therefore,

$$\text{Error factor} = \frac{\text{Maximum of (Measured output - Average output)}}{\text{Average output}} \times 100\% \qquad [3.1]$$

In Figure 3.9, the average error factor at each suction represents the average of a group of instruments tested at that suction potential. The number of instruments per group per suction varied between 9 and 30. It can be seen from Figure 3.9 that the average error factor decreases exponentially with increasing suction. Hence the margin of error corresponding to the precision of the instrument decreases with increasing suction.

The effect of temperature on the precision of psychrometers has been examined using the data from a series of tests on unsaturated sand-bentonite material that forms part of this study. All the measurements were carried out using the same psychrometer. Figure 3.10 shows that the precision of the psychrometer is generally independent of temperature. However, the margin of error in the suction measurements tends to increase with decreasing temperature (see Figure 3.11). The error factor at 50°C is generally below 1.5% . In contrast, the error factor is higher at 10°C, about 3% for suctions between

2.5 MPa to 5 MPa, and increases in value with decreasing suction for suctions less than 2.5 MPa.

Based on the results shown in this section, it can be concluded that the precision of the psychrometers used in this study is generally within ± 0.5 μV. For the suction range of 1.5 MPa to 5.3 MPa and temperature from 10°C to 50°C, the maximum difference between the average and measured suctions is restricted to within ± 3%. When the instruments are used in suctions below 1.5 MPa at temperatures less than 25°C, larger differences up to 7% can be expected.

3.6.2 Calibration factors

Information on the calibration of 40 psychrometers tested in this study is tabulated in Table 3.2. The calibration factor (the slope of a statistically fitted straight line through the data and the origin) varies between 188 and 311 kPa/μV. An average global calibration factor for these 40 psychrometers is determined to be 225 kPa/μV, with a standard deviation of 22 kPa/μV. The variability in the calibration factors among the psychrometers is attributed to the inherent differences in the components of the psychrometers such as the sensing junction and the size of the thermocouple circuit. For example, the size of the sensing junction affects the evaporation of the condensed water (Rawlins, 1966), a process which is directly related to the output of the instrument.

Table 3.2 also shows the calibration factors which correspond to the lower 95% and upper 95% confidence levels. The accuracy of each calibration factor is assessed in terms of the standard error of coefficient, that is, the difference between the fitted and the "95%" factors expressed as a percentage of the fitted factor. From Table 3.2, the standard error of coefficient ranges from 1.8% to 12.1%. The average coefficient is determined to be about 6%, which is higher than the average error of 3% attributed to instrument precision as reported in Section 3.6.1.

A deviation parameter was introduced to quantify the difference between the individual psychrometer calibration factor and the average global calibration factor of 225 kPa/μV, expressed as a percentage of the individual factor. The deviation parameter and the standard error of coefficient for each psychrometer are compared in Table 3.2. and Figure 3.12. For 21 of the 40 psychrometers, the deviation parameter is smaller in value than the standard error of coefficient (Table 3.2). Furthermore, the deviation parameters of 30 psychrometers are less than 8% which is the upper 95% confidence limit of the standard error of coefficient (Figure 3.12). Based on the data shown in Table 3.2 and Figure 3.12, it can be concluded that within the bounds of error associated with the accuracy of the calibration relationship, the global factor of 225 kPa/μV could be used in place of individual calibration factors for the same psychrometer type. However, individual calibration factors, and not the global factor, were used to calculate suctions in the remainder of this study.

All the psychrometers had been calibrated by the manufacturer prior to delivery using sodium chloride solution with a suction potential of 2500 kPa at 25°C. The factory calibration was determined by simply dividing the suction potential of 2500 kPa by the measured output. In contrast, the psychrometers used in this study were calibrated above potassium chloride solutions at several suction potentials.

The factory calibration factors are compared with the individual calibration factors determined in this study in Table 3.2. For 35 of the 40 psychrometers, the difference between the factory and this study's calibration factors expressed as a percentage of the latter exceed the standard error of coefficient of 6%. The reason for this discrepancy between the two calibration factors is not clear, but may simply be due to differences in the calibration procedures.

Discrepancies between the factory and user's calibration factors in excess of the error associated with the accuracy and precision of the instrument imply that each

psychrometer should be calibrated before laboratory use. However, when a large number of psychrometers is required for field applications such as monitoring of suction and moisture in clay barriers, instruments may not need to be individually calibrated. Representative instruments can be selected from the group and used to generate a global calibration factor.

3.6.3 Long term drift of psychrometer outputs

Two tests were carried out to examine the possibility of long term drift of psychrometer outputs with time. In one test, a psychrometer was installed in a compacted sand-bentonite specimen formed to a dry density of 1.41 Mg/m^3 at 18.2% water content. In the other test, the specimen was compacted to the same dry density of 1.41 Mg/m^3 at 19.8% water content. Each specimen/psychrometer assembly was wrapped with plastic sheets and sealed in an air tight container to prevent moisture loss during testing. The outputs of the psychrometer were recorded daily for a period of over 500 days. Figure 3.13 shows the trends of the measured suctions in the two specimens. The suctions measured by the psychrometers in the specimens were virtually constant with time. The results from these two tests gives reliance in the results from the longer term tests carried out as part of the studies described in this thesis.

3.6.4 Effect of temperature on psychrometer outputs

The effect of temperature on the type of psychrometer used in this study was examined in the calibration tests. Results of a typical calibration test is shown in Figure 3.14. It can be inferred from the figure that at a given suction potential, the psychrometer output increases with increasing temperature. The dependence of the instrument output on temperature is associated with the increase in the wet bulb

depression at the sensing junction of the psychrometer, that is the difference between the wet- and dry-bulb temperatures.

Figure 3.15 shows the relationship of saturation vapour pressure of water with temperature (Roger and Mayhew, 1981) and the relationship of the partial vapour pressure of 2 m KCl solution with temperature (Campbell and Gardner, 1971). It should be noted that the two curves are not parallel, but deviate from each other as temperature increases. The difference in the saturation vapour pressure and the partial vapour pressure of the KCl solution against temperature is also shown in Figure 3.15. Referring to Figure 3.15, in a typical calibration, the vapour pressure surrounding the probe of the psychrometer is depicted by point v_1 at an initial temperature of t_1. At this temperature and vapour pressure condition, the wet bulb depression to which the output of a psychrometer is directly related is $t_1 - t^o_1$. As the temperature increases to t_2, the vapour pressure of the KCl solution increases to v_2. At this new condition, the wet bulb depression $t_2 - t^o_2$ is larger in value than the wet bulb depression at t_1. Hence, the instrument output increases with increasing temperature.

Due to limitations of the equipment used for controlling temperature, fluctuations up to 5°C were anticipated in tests carried out in part of this study. Savage and Cass (1984) point out that the common practice used to correct for temperature effects is to apply the empirical formula proposed by Wiebe et al. (1970) as follows.

$$V_{25} = \frac{V}{a + b \times T} \qquad [3.2]$$

where V_{25} is the corrected output voltage, V is the measured output voltage, T is the temperature, a and b are parameters which depends on the psychrometer type. According to Wiebe et al. (1970), this empirical formula is suitable for temperatures between 4°C and 25°C. The formula converts the measured psychrometer output to a

value as if it was taken at 25°C. Therefore, suction measurements are standardized to and compared at the same temperature (Wiebe et al., 1971). For the psychrometers used in this study, the parameters a = 0.325 and b = 0.027 $^{o}C^{-1}$ as determined by Brown (1970) are recommended by the manufacturer.

The applicability of Equation [3.2] to the psychrometers used in this study was examined in nine calibration tests in which the instruments were calibrated at 10°C, 25°C, and 50°C. The results of two typical tests are shown in Figures 3.16 and 3.17. Each figure shows the suction-output relationship fitted to the 25°C data, and the 95% confidence envelope. Also shown in the figure are the outputs taken at 10°C and 50°C and converted to V_{25} values using the above empirical formula.

From Figures 3.16 and 3.17, it can be seen that the converted V_{25} values for 50°C generally fall within or close to the 95% confidence envelope. This gives confidence in the use of Equation [3.1] for the temperature range between 25°C to 50°C. In contrast, the converted V_{25} outputs for 10°C are consistently lower than the values defined by the 25°C fitted relationship. The discrepancy is attributed to condensation effects and the inability of the equipment to maintain constant temperature during calibration. At lower temperatures, the absolute humidity, or vapour density, of the air inside the calibration container and within the ceramic shield of the psychrometer decreases. Under the conditions of low temperatures and high relative humidities, condensation can readily take place upon the slightest fluctuation in temperature. The presence of condensed water on the ceramic shield tends to increase the humidity in the localized area around the sensing junction, leading to lower psychrometer outputs. The sensitivity of absolute humidity to temperature fluctuation is illustrated by the following example.

Consider three identical psychrometers being calibrated over 0.5 m KCl solutions at 10°C, 25°C, and 50°C respectively. Applying the Kelvin equation and using steam tables, the partial vapour pressure and the absolute humidity around each psychrometer

can be determined. These are tabulated in Table 3.3. Also included in Table 3.3 is the maximum absolute humidity e_o at each temperature. The air is said to have 100% relative humidity ($RH = v/v_o$) when the maximum absolute humidity is achieved. At this condition, the suction potential is zero according to the Kelvin equation.

Table 3.3 shows that the difference between the absolute humidity and the maximum value at that temperature increases exponentially with increasing temperature. In particular, the difference at 10°C is only 0.15 g/m^3, compared with 1.328 g/m^3 at 50°C. The data in Table 3.3 also demonstrate that a drop in temperature, say from 25°C to 10°C, leads to a decrease in the absolute humidity in the air. In this case, an excess of 13.425 g/m^3 of vapour (that is, 22.673 g/m^3 minus 9.248 g/m^3) becomes available and condenses into liquid as the air cools. This quantity of moisture far exceeds the 0.15 g/m^3 of moisture required to cause an increase in the relative humidity from 98.4% to 100% at 10°C.

The implication of these calculations is twofold. First, temperature plays an important role in affecting the calibration of psychrometers at temperatures lower than 25°C. Precise temperature control within 0.001°C during calibration is essential at these temperatures (Richards, 1969). Second, in the field, precise control of temperature boundary conditions may not be easily effected. Under these conditions, temperature changes may influence the accuracy and precision of psychrometers in measuring *in situ* suctions and water contents. This issue was examined in the Buffer/Container Experiment, and will be discussed in detail in Chapters 8 and 9.

3.7 Summary

In this chapter, the theory of thermocouple psychrometers was reviewed. The type of psychrometer and equipment used in this study have been described and procedures given for calibration and interpretation of instrument outputs.

A series of laboratory and calibration tests were carried out to examine the performance of the Wescor Type PCT-55 psychrometers used in this study. Discrepancy between the factory and users' calibrations in excess of the error associated with the accuracy and precision of the instrument implies that each instrument should be calibrated before use.

Based on the results from the calibration of 40 psychrometers, it is concluded that the accuracy of the instruments is largely governed by the goodness of fit of the suction potential-output relationship on the calibration data. In general, the discrepancies between the predicted and actual suctions are within $\pm 6\%$ of the actual values. The instruments are found to be precise to be ± 0.5 μV for the suction range of 1.4 MPa to 5.3 MPa. Temperature affects the output of an instrument. Providing that temperature fluctuations are limited to $\pm 5^{o}C$, the empirical formula proposed by Wiebe et al. (1970) and Brown (1970) can be used to correct the measured outputs for temperature effects for the range of $25^{o}C$ to $50^{o}C$. At temperatures lower than $25^{o}C$, changes in temperature can affect the calibration and the use of a psychrometer. Precise temperature control therefore needs to be exercised at these temperatures. However, in the field, it is often difficult to maintain constant temperature boundary conditions. Under these circumstances, temperature changes may influence the accuracy and precision of psychrometers in measuring *in situ* suctions and water contents.

CHAPTER 4 LABORATORY TESTING PROGRAM AND METHODS

4.1 Background

One of the objectives of the laboratory investigation was to examine the effects of stress variations and deformations on suction measurements in compacted clays using psychrometers. The testing program was broadly divided into three parts. One, the suction properties of the soil materials used in this study were characterized by the psychrometer method and two other conventional methods. Factors which influence the suction properties of compacted clays were examined. Two, the effects of isotropic and shear compression stresses on suction measurements using psychrometers were investigated in two series of tests on a compacted sand-bentonite material using a triaxial apparatus. Three, relations between soil fabrics, pore size, and stress history for the compacted sand-bentonite material were examined using mercury intrusion porosimetry, scanning electron microscopy, and isotropic compression tests. Results from these tests were used in the development of a conceptual model that describes, in a qualitative manner, the relationship between suctions measured by psychrometers, total stress, and deformation. In the following sections, the soil materials used in this study, and details of the testing program, equipment and test procedures are described.

4.2 Soil materials

It was discussed in Chapter 2 (Literature Review) that mineralogy is one factor that influences suctions in soils. In this study, three soil materials of varying mineralogy were chosen for testing. They were a sand-bentonite material, a sand-illite material, and a reconstituted natural clay soil from Belgium known as Boom Clay. This section reviews the properties of each material, and describes the procedures used for material and specimen preparation.

Sand-bentonite

The sand-bentonite material is a mixture, by dry mass, of 50% silica sand and 50% bentonite. This material is being investigated for use as a barrier material for the disposal of radioactive wastes in Canada (AECL, 1994). The sand component is a well graded fine to medium silica mixture, with 80% of particles within the size range 0.1-1.0 mm (see Figure 4.1). The clay component is a finely ground natural bentonite from Southern Saskatchewan, sold under the tradename Avonseal (Dixon et. al., 1992a). The particle size distribution of the bentonite is shown in Figure 4.2. The clay mineralogy of the bentonite is dominated by montmorillonite and illite (Quigley, 1984). The cation exchange capacity of the bentonite is about 95 meq/100g, with Na^+ (47 meq/100g) and Ca^{2+} (40 meq/100g) as the dominant cations. The clay has a liquid limit of 250% and a plasticity index of 200 (Dixon et al., 1992a). The dry density-water content relationship of the material is shown in Figure 4.3. The lack of a distinct optimum dry density and water content in the compaction curve is attributed to the insufficient energy in the standard dynamic compaction test (ASTM D 1557, 1992) to overcome the shear resistance of the adsorbed water around the bentonite particles (Dixon et al., 1985).

The sand-bentonite material used in this study was the same and excess material used in an underground field-scale clay barrier experiment at the Underground Research Laboratory (URL), near Lac du Bonnet in Manitoba. Relevant details of this experiment will be described in Chapter 8. The material was prepared in 50-kg batches in a Crocker Cumflow RP200 flat pan mixer with a volume capacity of 0.5 m^3 (Dixon et al., 1992a). The material was prepared at a water content of 18%. A natural ground-water recovered from fractures at the 240 level of the URL was used in the mixing. The water has a pH of about 7 to 8, and contains predominantly of Na^+, K^+, Cl^-, and SO_4^{2-} ions. After mixing, the material was kept in sealed plastic bags and stored in barrels to allow water content equalization.

For testing carried out at water contents other than 18%, the water content of the material had to be adjusted. For water contents lower than 18%, a known quantity of the moist soil was removed from the barrel and then dried in an open pan under ambient temperature and humidity condition until the desired water content was achieved. After drying, the soil was manually re-mixed to attain uniform moisture and soil fabric in the material. After mixing, the material was stored in a sealed plastic bag for at least three days before use.

To obtain materials with water contents higher than 18%, a predetermined quantity of ground-water was added to a known amount of moist soil contained in a large pan. The soil-water mixture was then manually re-mixed until the mixture appeared to be homogeneous. After mixing the material was stored in a sealed plastic bag for at least three days before use.

Sand-illite

The sand-illite material also had a 1:1 sand-clay ratio by dry mass. The sand component was identical in gradation and mineralogy to that of the sand-bentonite material. The clay component is an illitic clay shale from Quebec, sold under the tradename Sealbond. Illite, quartz and chlorite are the dominant minerals in the clay (Quigley, 1984). The particle size distribution of the clay is shown in Figure 4.2. The clay has a liquid limit of 30% and a plasticity index of 9, and a cation exchange capacity of 16 meq/100g (Dixon et al., 1985). The dry density-water content relationship of the sand-illite material is shown in Figure 4.3. The material has a maximum dry density of 2.13 Mg/m^3 at a water content of 9%, corresponding to 95% Modified Proctor maximum compaction density at the optimum water content.

The sand-illite material was prepared in a 25-kg batch at a water content of 9%. Mixing was carried out in a Crocker Cumflow RP100 flat pan mixer with a volume

capacity of 0.25 m^3. Distilled water was used in the material preparation. After mixing, the material was stored in plastic bags and kept in air-tight 20 L containers. For testing carried out at water contents other than the optimum, the water content of the material was adjusted in a similar manner as for the sand-bentonite material.

Boom Clay

The natural clay soil tested in this study is Boom Clay from Belgium. Boom Clay deposits are being studied for their suitability to host a repository for heat generating radioactive wastes in Belgium (Pellegrini et al., 1989). The soil arrived at the laboratory in the form of a dry grayish white powder. Based on results from previous studies, the properties of Boom Clay are highly variable (Baldi et al., 1990; Hueckel and Pellegrini, 1992). To characterize the properties of the material used in this study, the following tests were carried out as part of the laboratory testing program:

1) X-ray diffraction analysis
2) Particle size distribution analysis
3) Atterberg limits tests
4) Compaction tests

Results from the X-ray diffraction analysis showed that the mineralogy of the soil was dominated by quartz (83%). The remaining fractions included muscovite (5%), montmorillonite (4%), illite (4%), lizardite (3%), and saponite (1%). The particle size distribution of the soil is shown in Figure 4.2. From the figure, it can be seen that the soil was well graded and contained predominantly clay size particles. The liquid limit and the plasticity index of the soil were measured to be 70% and 35% respectively. Results from compaction tests are shown in Figure 4.3. The optimum dry density of the soil was determined to be 1.91 Mg/m^3 at a water content of 15%.

Distilled water was used in preparing the material. Mixing of the soil and water

was carried out manually in small batches of the order of 500 g. After mixing, the material was kept in sealed plastic bags for at least 3 days before use. Due to the limited amount of Boom Clay available for testing, at the end of each test, the material was dried, crushed up and re-used in future tests.

4.3 Suction test series

The objective of this series was to determine the relationships between suction and other soil parameters including water content, degree of saturation and temperature for the soils used in this study. The soil suctions were measured by psychrometer and two other conventional methods, namely the vapour equilibrium technique and filter paper technique. This section describes the resulting testing program and procedures.

4.3.1 Psychrometer method

Chapter 2 describes how the psychrometer method measures the total soil suction including both the matric and the osmotic components.

4.3.1.1 Single-stage tests

The sand-bentonite material was the prime material investigated in the Buffer/Container Experiment, which will be described in Chapter 8. Because a relatively large number of tests is needed to generate a suction-water content relationship using the single-stage procedure, only the sand-bentonite material was tested using this procedure. Sand-illite material and Boom Clay were tested in the multi-stage tests, which are described in Section 4.3.1.2. Each sand-bentonite specimen used in the single-stage test was formed to a dry density of 1.41 Mg/m^3 or 1.67 Mg/m^3 at water contents from 17% to 24%. Table 4.1 summarizes the initial and final conditions of the specimens.

In a typical test, the sand-bentonite material was compacted statically in a rigid

mould to form a cylindrical specimen measuring 100 mm in diameter and 200 mm long. The specimen was then extruded from the mould, and a 3-mm diameter hole was drilled into the specimen. A calibrated psychrometer was inserted into the hole with the thermocouple component of the instrument located near the centre of the specimen. The remainder of the hole was then backfilled with excess soil. This backfill was lightly compacted using a glass rod. Figure 4.4 shows a compacted sand-bentonite specimen with an embedded psychrometer.

To prevent loss of moisture during testing, the specimen was wrapped with plastic sheeting, and placed in an air tight plastic container. Total suction measurements were carried out at temperatures of 10°C, 25°C, and 50°C. At each temperature, the specimen/psychrometer assembly was allowed to reach thermal and vapour pressure before at least three psychrometer measurements were taken. At the end of the test, the psychrometer was carefully removed from the specimen, and the average water content of the specimen was determined (ASTM D 2216-80, 1992).

4.3.1.2 Multi-stage tests

Two multi-stage tests were carried out: one on sand-illite material and the other on Boom Clay. The specimens used in this test series were nominally 100 mm in diameter with a 1:1 diameter to length ratio. The installation of the psychrometer and sealing of the specimen were carried out in the same manner as for the sand-bentonite specimens tested in the single-stage tests. The initial and final water contents and densities of the sand-illite and Boom Clay specimens are given in Table 4.1. The procedures for a multi-stage test were as follows.

The specimen/psychrometer assembly was first allowed to attain vapour and temperature equilibrium for at least 2 days before three initial psychrometer measurements were taken. The specimen was then allowed to dry to different water

contents in successive stages under ambient temperature and humidity conditions. At the end of each drying stage, the weight of the specimen/psychrometer assembly was measured to determine the moisture loss due to drying. The specimen was then carefully re-wrapped with plastic sheets and was allowed to achieve water content equalization for at least 2 days before three psychrometer readings were taken. The drying process was repeated until the psychrometer was out of its operating range. At the end of the test, the final water content of the specimen was measured by oven drying (ASTM D 2216-80, 1992), and the water content at the end of each drying stage was determined by back-calculation.

4.3.2 Vapour equilibrium technique

The vapour equilibrium technique measures the total suction in a soil (Wilson, 1990). The principle of the method has been described in Chapter 2. In this study, various concentrations of sulphuric acid were used as osmotic agents to provide a range of suction potentials from about 3.5 MPa to 470 MPa. Sulphuric acid was chosen because the relative humidity of the acid is insensitive to temperature change (Young, 1967). Figure 4.5 shows the variation of relative humidity and its corresponding suction potential at 25°C with acid concentration.

Figure 4.6 shows the chamber used in a typical vapour equilibrium test. Tables 4.2 to 4.4 summarize the initial and final conditions of the specimens tested in this series. Both uncompacted and compacted specimens were used. In most tests, they were prepared at the optimum water contents of the respective soil materials. Each compacted specimen which had a nominal diameter of 30 mm and a 10 mm thickness, was formed by statically compacting the soil material in a rigid mould. Both single-stage and multi-stage tests were carried out. The procedures for each test type are explained as follows.

4.3.2.1 Single-stage tests

After formation, the specimen was placed in a petri dish which in turn was placed inside a desiccator over a container of sulphuric acid solution with a known concentration from 1.05 g/ml to 1.70 g/ml (see Figure 4.6). The specimen was then allowed to equilibrate with the vapour pressure of the solution under constant temperatures of 10°C, 25°C or 50°C. At the end of the equalization period, the petri dish containing the specimen was carefully removed from the desiccator. The weight of the specimen was measured to determine the change in moisture during this increment. The petri dish with the specimen was then placed inside the desiccator again and the test was allowed to resume at a different temperature. At the end of the last temperature increment, the specimen was removed from the desiccator, and its final dimensions and water content were measured.

To ensure vapour equilibrium, each desiccator contained no more than 5 specimens. Of major concern was the time required by the compacted specimens to reach thermal and vapour pressure equilibrium within the surrounding environment. At the beginning of this test series, changes in the water content of the specimens were monitored with time. In general, most specimens came to a vapour pressure-water content equilibrium in about ten days. Typical results are shown in Figure 4.7. In this study, an equalization period of at least 4 weeks for each temperature increment was used.

4.3.2.2 Multi-stage tests

The objective of the multi-stage tests was to examine hysteresis in the suction-water content relationship. In a multi-stage test, the specimen first underwent a drying phase and then a wetting phase. During the drying phase, the specimen was dried in a desiccator having progressively drier atmospheres as controlled by the sulphuric acid.

The concentrations of sulphuric acid used in the drying phase were 1.15 g/ml, 1.35 g/ml, 1.50 g/ml, and 1.70 g/ml, corresponding to suctions of 10 MPa, 16 MPa, 100 MPa, and 400 MPa respectively. At the end of each drying stage, the weight of the specimen was measured and the moisture loss was determined. Drying of the specimen was then resumed with the next concentration of sulphuric acid.

When the drying phase was completed, the specimen was allowed to absorb moisture from the atmosphere in the desiccator having progressively higher humidities. The concentrations of sulphuric acid used in the wetting phase were 1.5 g/ml, 1.35 g/ml, 1.15 g/ml, and 1.05 g/ml, corresponding to suctions of 100 MPa, 16 MPa, 10 MPa, and 3 MPa respectively. At the end of the wetting phase, the final water content of the specimen was measured and the water content at the end of each drying or wetting phase was determined by oven drying at 110°C (ASTM D 2216-80, 1992). Water contents at each increment of suction were back-calculated.

4.3.3 Filter paper method

The filter paper technique measures both the total and matric suctions in a soil. The principle of the filter paper technique has been described in Chapter 2.

Whatman Type 42 filter paper was used in the study. While suction-water content relationships for this type of paper are available in the literature (McQueen and Millar, 1968; Al-Khafaf and Hanks, 1974; Chandler and Gutierrez, 1986; Sibley and Williams, 1990), they are only suitable for the suction range from 0.1 MPa to 5.0 MPa. Calibration tests using the vapour equilibrium technique were therefore carried out on the filter paper material used in this study to extend the relationships to the higher suction range of up to about 60 MPa. Figure 4.8 summarizes the results from the calibration tests and the data from the literature. A regression relationship is fitted through the data in Figure 4.8, and is given as follows.

$$\log S = 4.842 - 0.063w \qquad (R^2 = 0.94) \qquad [4.1]$$

where S is the suction potential (kPa) and w is the water content by mass (%) of the filter paper. Equation 4.1 has been used throughout this study for converting filter paper water contents to suctions.

Suction measurements using the filter paper technique were carried out at an ambient temperature of 25°C. The specimens were 100 mm diameter and 50 mm long, and were formed by statically compacting the soil material into a rigid mould to a specified dry density and water content. The initial and final conditions of the specimens tested in this series are summarized in Tables 4.5 to 4.7.

Figure 4.9 shows the equipment used in a typical filter paper test. Three filter paper discs were used on each specimen. The largest disc had the same diameter (100 mm) as the specimen. It was first placed in direct contact with one end of the specimen. Its function was to prevent any contamination of the other two filter paper discs by the specimen. The two remaining discs had slightly smaller diameters of about 97 mm. The second disc was placed in direct contact with the first disc and measured the matric suction in the specimen. The third disc which was separated from the second filter paper by about 2mm, allowed determination of total suction. The separation between the second and third discs was controlled using a thin glass disc with holes which supported the third disc and permitted moisture vapour transfer from the specimen to the disc. To ensure intimate contact between the specimen, and the first and second filter discs, a solid glass disc was placed on top of the third filter paper disc. The specimen/filter paper assembly was then quickly and carefully wrapped with plastic film and placed in a sealed plastic container. The filter paper discs and the specimen were then allowed to equilibrate in a temperature-controlled box with an ambient temperature of 25°C. In general, an equalization time between 4 to 6 weeks was used. In later tests, filter paper

discs were installed on both ends of the specimen to provide two sets of suction measurements from one specimen.

At the end of each test, the specimen and the filter papers were removed quickly from the container, and their water contents determined. Measurements of the weights of the filter papers were carried out using a Mettler AT200 balance with a precision of ± 0.0001g. Once the water contents of the filter papers were determined, they were converted to the total and matric suction using Equation 4.1. The osmotic suction was taken as the numerical difference between the total and matric suctions.

4.4 Triaxial test series

4.4.1 Background

Three series of tests were carried out using a triaxial apparatus. The first two series examined the effects of isotropic and shear compression stresses on psychrometer outputs in compacted sand-bentonite material under constant mass conditions. In the third series of tests, the volume strain-pressure relationships of unsaturated sand-bentonite material were measured under isotropic, constant mass conditions. All triaxial tests were carried out in ambient room temperatures between 20°C to 25°C. Temperature corrections were applied to the psychrometer measurements using Equation 3.2 given in Section 3.6.4.

4.4.2 Equipment

4.4.2.1 Triaxial testing system and instrumentation

Four commercial triaxial cells manufactured by Brainard-Kilman, Georgia, USA were used in this study. Figure 4.10 shows a typical triaxial cell equipped with a lucite

sleeve which gave a cell pressure capability of 1250 kPa. Each cell has an internal diameter of 140 mm and a length of 320 mm. When used with an aluminum sleeve, the cell could be operated to a maximum total pressure of 3500 kPa. The top plate of each triaxial cell was modified to accommodate the use of psychrometers in some of the tests. This required a Conax™ fitting to be fitted in the top plate of each triaxial cell to accommodate the psychrometer cable.

Deaired distilled water was used as cell fluid. Argon gas was used to provide the cell pressure via an air-water interface. Argon was chosen for its low solubility in water. Cell pressures were measured by several types of commercial pressure transducers manufactured by Micro-gage, Sensotec, and Heise respectively. These transducers were calibrated in accordance to the procedures adopted in the Soil Mechanics Laboratories at the University of Manitoba (Saadat, 1989). Strain-controlled shear compression tests were carried out in an ELE 10-ton compression frame. A linear displacement transducer and a dial gauge were used to measured the axial displacements of the specimens in the shear compression tests. Axial load was measured by an external proving ring with a load capacity of 20 kN.

4.4.2.2 Volume change measurement system

Figure 4.11 shows the system that was specifically developed and used in these studies for measuring the volume change of unsaturated sand-bentonite specimens in isotropic compression tests under constant mass conditions. The system consists of a triaxial cell, an air-water interface, a specimen chamber, two pressure-resistant burettes and a conventional glass burette.

The high pressure-resistant burettes used in this study were similar to those used by Saadat (1989) and Oswell (1991). Each burette was essentially a graduated glass burette contained inside a pressure vessel formed by a 500-mm long, thick wall acrylic

tube and two brass caps with Swagelok™ fittings (see Figure 4.12). Pressurization of the burette is carried out through the top brass cap. Drainage of water into and out of the graduated burette is controlled by a pressure-resistant null valve at the bottom cap. Each burette has a maximum operating pressure of 3.5 MPa and a usable volume of about 40 ml. In this study, two pressure-resistant burettes were used in parallel to permit volume change measurements of up to 80 ml.

Two specimen chambers were fabricated. Figure 4.13 shows one of the chambers used in this study. Each chamber is constructed of lucite material and is designed to house a 50-mm diameter and 100-mm long specimen. The chamber consists of three components: a top plate, a sleeve with a flange ring at each end, and a bottom plate with three stabilizers. A 50.5-mm diameter, 3-mm deep recess is machined on the inside face of the bottom plate to provide the restraint to the base cap on which the specimen is seated. Stainless steel screws are used to secure the two end plates on to the flanges of the sleeve. The seal between an end plate and the flange is provided by a sealing O-ring. Swagelok™ fittings are fitted in both the top and bottom plates to provide the connection between the chamber and the burettes.

Referring to Figure 4.11, the specimen chamber fits inside the triaxial cell and is totally submersible in the cell water. The chamber is connected directly to the burettes located outside of the triaxial cell. Therefore, inter-connection is prevented between the inside of the chamber and the remainder of the cell fluid. Volume changes within the specimen chamber are monitored by one of the pressure-resistant burettes. The conventional glass burette is used for flushing the chamber during setup of the specimen, and is isolated from the rest of the system when testing begins. The water in the triaxial cell is supplied and pressurized through an air-water interface.

During operation, the pressures in the air-water interface and the pressure-resistant burettes are supplied by a common argon gas source so that pressure gradients

across the wall of the specimen chamber are negligible. Theoretically, under these conditions, the deformation of the specimen chamber should be zero and the volume change measured by the burette should be exclusively due to deformation of the specimen. In practice, several factors including the compressibilities of the water, latex membranes, rubber O-rings, and the lucite material, and the expansion of exposed drainage lines contribute to the compliance of the measurement system, leading to the possibility of errors in volume change measurements.

To limit the effects of these errors, prior to use, each of the volume measurement systems was calibrated for compliance. In a typical calibration, a dummy brass specimen was used in place of the soil specimen as shown in Figure 4.11. Two latex membranes separated by a thin layer of silicon oil were used to surround the dummy specimen. Several O-rings were used to seal the membranes to the top and bottom caps. Increments of isotropic confining pressure were applied to the specimen up to a total cell pressure of about 3200 kPa. At the end of each increment, the volume change in the measurement system was measured with a pressure-resistant burette.

Figures 4.14 and 4.15 show typical calibration results for two measurement schemes used in this study. The fitted relationship shown in each figure was used to correct the volume change data for system compliance in each test.

4.4.3 Specimen preparation

Depending on the type of test, specimens used in this series were formed by statically compacting the soil material in two or four layers into a rigid mould. Figure 4.16 shows the compaction mould with a removal collar used in this study. Compaction was carried out in a 250 kN MTS compression machine. Three specimen sizes were used.

For tests to measure the effects of isotropic compression stresses on suction

measurements using psychrometers, specimens had a nominal diameter of 100 mm with a 1:1 length to diameter ratio. It was assumed that faster vapour equilibrium within the specimen would be achieved with shorter specimens. In these specimens, the psychrometer was located at the centre of the specimen.

For tests to measure the effects of shear stresses on suction measurements using psychrometer, the specimens measured 100 mm in diameter and 200 mm long, giving the customary 2:1 length to diameter ratio. Because shear stresses were expected to be the greatest at the centre of the specimen, to avoid damaging the psychrometer during shear, the instrument was positioned 10 mm above the centre.

A rigid stainless steel tee-shaped ram was fabricated to facilitate the installation of psychrometers during specimen formation (Figure 4.17). A hole was added in the tee of the ram to permit the psychrometer cable to move independently of the ram during specimen formation. Special compaction procedures had to be developed to allow installation of the psychrometer while retaining good density and water content control. These procedures are explained as follows.

1) The soil material for the bottom layer is added into the mould and is lightly compacted (Figure 4.18a).
2) A cavity is then created by using a blank former between the lightly compacted layer and the ram when the compaction of the layer resumes (Figure 4.18b).
3) A calibrated psychrometer is then inserted into the cavity with the cable of the instrument going through the hole in the compaction ram (Figure 4.18c).
4) The loose material for the top layer is added to the mould covering the psychrometer, and carefully compacted to achieve the length of the specimen needed to achieve the desired dry density (Figure 4.18d).
5) The compacted specimen is then carefully extruded from the mould, and its dimensions and mass are determined.

For isotropic compression tests with volume change measurements, the specimens had a nominal diameter of 50 mm and a nominal length of 100 mm.

4.4.4 Tests to examine the effect of total stress on suction measurements using psychrometers

4.4.4.1 Set up

Procedures used for setting up the specimens were similar to those used by other researchers in the Soil Mechanics Laboratories at the University of Manitoba (see for example, Saadat, 1989). However, two minor changes are noteworthy. First, since pore water and pore air pressures in the specimens were not measured, side drains and filter stones were not used. Second, each top cap was fitted with a Conax™ pressure fitting to accommodate the use of a psychrometer in the test and to prevent the leakage of cell water into the specimen (see Figure 4.19).

Before the specimen was installed in the triaxial cell, the sides of the top cap and the sides of the pedestal of the cell were covered with a thin layer of silicon grease. The specimen was then placed on the pedestal. The top cap was put on top of the specimen with the psychrometer cable going through the Conax™ fitting. Two latex membrane separated by a thin layer of silicon oil were used to surround the specimen. The membranes were sealed onto the pedestal and the top cap with several O-rings. The Conax™ fitting on the top cap was then carefully tightened.

The next step was to re-assemble the triaxial cell. The sleeve was first placed on to the bottom plate of the cell. The remaining psychrometer cable from the specimen was then inserted through the Conax™ fitting in the top plate of the triaxial cell before the plate was fitted on to the sleeve. The tie-rods were then installed and tensioned to hold the top and bottom plates, and the sleeve together. Prior to filling the cell with distilled

water, the ram was securely locked in place. To avoid breakage of the psychrometer cable during testing, sufficient cable length was allowed between the top cap and the top plate of the cell before the Conax^{TM} fitting was tightened.

4.4.4.2 Isotropic compression tests

The objective of this test series was to examine the effect of isotropic compression stresses on suction measurements using psychrometers. To the author's knowledge, this work is an entirely new contribution to the testing of unsaturated soils. Nine isotropic compression tests were carried out under "undrained" constant mass conditions. No attempt was made to measure the air and water pressures inside each specimen during testing. At the time of testing, guidelines on the measurement of pore air and pore water pressures in swelling active soils with complex soil structures were not, and still are not, available in the literature. Therefore "undrained" constant mass tests were carried out to avoid the uncertainties in the interpretation of the pore air and pore water pressures in the dense sand-bentonite material. Technologies in this area are currently being developed in the Soil Mechanics Laboratories at the University of Manitoba. The initial and the final conditions of the specimens tested in this series are summarized in Table 4.8. The general test procedures are described as follows.

After the specimen was set up in the cell, an equalization period of up to 3 days was allowed to attain vapour pressure and temperature equilibrium between the psychrometer and the soil. Three readings of the psychrometer output were then taken to establish the baseline suction in the specimen, that is, the suction under the influence of zero cell pressure.

The specimen was then subjected to cycles of loading-unloading-reloading under "undrained" constant mass conditions. In each stage, the confining pressure was applied to or removed from the specimen in successive increments. In general, increments of

100 kPa to 200 kPa were used during the loading and reloading stages, and about 500 kPa for the unloading stage. Each pressure increment was kept on the specimen for at least 24 hours. At the end of the increment, the total confining pressure and readings of the psychrometer output were recorded. Typically, the equalization times between psychrometer readings were 30 minutes. The maximum confining pressures used in these tests were about 3200 kPa.

At the end of each test, the specimen and its embedded psychrometer were carefully removed from the triaxial cell. The weight and dimensions of the specimen were determined. After the removal of the psychrometer, the water content of the specimen was measured.

4.4.4.3 Shear compression tests

The objective of this test series was to examine the effect of shearing stresses on suction measurements using psychrometers. This work is also a new contribution. Four tests were carried out. The specimens were sheared under strain-controlled conditions in a 10 ton ELE compression machine. Shearing was carried out under "undrained" constant mass conditions for the same reason as the isotropic compression tests described in Section 4.4.4.2. Two shear rates were used in this study. A faster rate of 1.5 %/day was used during daytime and a slower rate of 0.4 %/day overnight and at weekends. Three specimens were sheared to axial strains of more than 10%. The fourth specimen was sheared without lateral confinement. It failed at about 6% axial strain. Table 4.8 summarizes the initial and final conditions of the specimens tested in shear compression. The general test procedures are described as follows.

The specimen was first compressed isotropically, in several successive increments, to the desired confining pressure. After at least 24 hours of vapour pressure and temperature equalization, three readings of the psychrometer output were taken. The

shearing was then initiated. During the shear test, readings of the psychrometer output, axial displacement, proving ring deflection, cell pressure and temperature were taken at intervals of 30 to 60 minutes during the day for the first 2 to 3 days, and then at intervals of 2 to 3 hours thereafter.

Consistent with the procedures used in testing saturated sand-bentonite material (Saadat, 1989), in the first three of the four tests, at the end of shearing, the specimen with the embedded psychrometer was quickly removed from the triaxial cell. The final weight, dimensions and water content of the specimen were then determined. However, in the last test (Specimen SB1880TS4), a slightly modified procedure was followed. This change in procedure was necessitated by the observations in the parallel series of triaxial isotropic compression tests described in Section 4.4.4.2. The new procedure was implemented to allow comparison of the initial and end-of-test suctions in the sheared specimen. At the end of shearing, after the compression machine was turned off, the ram was quickly locked in place to prevent further axial deformation in the specimen. After about six hours, a psychrometer reading was taken. The cell pressure on the specimen was released to zero. The specimen/psychrometer was then allowed to attain vapour pressure-temperature equilibrium for about 18 hours before a final psychrometer reading was taken. The specimen was then removed from the triaxial cell for water content and density measurements.

4.4.5 Isotropic compression tests with volume change measurements

The isotropic compression tests described in Section 4.4.4.2 were carried out without volume change measurements and before the equipment for these measurements were developed. Subsequently, six tests were carried out on unsaturated specimens to measure the compressibility of unsaturated sand-bentonite material under "undrained" constant mass conditions in which there was no net influx of air or water into or out of

the specimen under loading. The initial and final conditions of the specimens are summarized in Table 4.8. The general testing procedures are as follows.

The specimen was first fitted with top and bottom caps. Two membranes separated by a thin layer of silicone oil were then used to surround the specimen and the caps. Two O-rings were used to seal the membranes on each cap. The specimen was then carefully placed on the bottom plate of the specimen chamber (Figure 4.13), ensuring that the bottom cap was properly seated in the recess of the plate. The chamber was then reassembled.

The assembled specimen chamber with the specimen was carefully placed on the bottom plate of triaxial cell. The chamber was then connected to the conventional burette and the pressure-resistant burettes, and was flooded with deaired distilled water with the aid of the burettes. The triaxial cell was then reassembled and flooded with deaired distilled water via the air-water interface. Prior to testing, the water level was adjusted to near the top of each burette such that the volume capacity of the burette was maximized.

The specimen was first isotropically compressed, in successive increments, to a maximum confining pressure up to 3200 kPa, and then incrementally unloaded to zero confining pressure. During this loading phase, pressure increments of 100 kPa to 200 kPa were generally used. Each pressure increment was maintained on the specimen for at least 24 hours. Volume change of the specimen during each pressure increment were monitored by one of the pressure-resistant burettes. Pressure-volume equilibrium generally achieved in the specimen after 24 hours.

For unloading, larger decrements of 400 kPa to 500 kPa were generally used for the confining pressure range from 3200 kPa to 500 kPa. Below 500 kPa, smaller decrements of 100 kPa were used.

At the end of the test, the cell and the specimen chamber were drained of water. The specimen was carefully removed from the chamber. The final dimensions and water

content of the specimen were measured.

4.5 Mercury porosimetry studies

4.5.1 Background

The purpose of the mercury porosimetry studies was to examine the pore size distributions of the sand-bentonite material, sand-illite material, and Boom Clay used in this study. In recent years (for example, Delage and Graham, 1995; Wan at al., 1995), considerable effort has gone into understanding how pore size distribution (PSD), as an appropriate measure of soil microstructure, affects soil suctions. It is increasingly understood (Delage and Graham, 1995) that many compacted plastic clays have bimodal pore size distributions in which the smaller interparticle voids are saturated, and the air phase are seated in the larger voids. To the author's knowledge, no information had previously been obtained about the pore size distributions in sand-bentonite material. It was therefore considered to be important to undertake mercury intrusion porosimetry studies, and relate the results to the macroscopic measurements of compressibility and strength that are reported in later chapters.

The theory of mercury intrusion porosimetry was described briefly in Chapter 2. This section describes the equipment and the general procedures used for specimen preparation and testing. In particular, the influence of specimen preparation on PSD's is discussed.

4.5.2 Equipment

An Autopore II 9220 porosimeter manufactured by Micromeritics, Georgia, USA, was used in this study. The porosimeter is capable of testing two specimens simultaneously up to a maximum operating pressuring of 416 MPa. Depending on the

type of mineral, this pressure corresponds to an equivalent pore diameter of 0.003 μm to 0.004 μm. The operation of the porosimeter is fully automated by a personal computer. Mercury intrusion, and data acquisition, reduction, and plotting are automatically controlled by the commercially supplied software in the computer. No attempt was made to check the codes, which were assumed to be validated by the commercial supplier.

4.5.3 Influence of drying temperature on specimen disturbance

An important prerequisite of conducting a MIP test is that the specimen must be completely removed of free water in the connected pores prior to testing. Methods commonly used for drying specimens include air-drying, oven-drying, freeze-drying and critical-point-drying (Diamond, 1970). Although the latter two methods produce the least disturbance in the specimen, specialized equipment is required and stringent procedures need to be followed. It was therefore decided that the former two methods should be investigated for drying specimens tested in this study. To understand the effect of temperature and drying technique on PSD's, some preliminary tests were carried out.

Figure 4.20 compares the PSD's of two sand-bentonite specimens formed to the same initial dry density of 1.67 Mg/m^3 and 17.6% water content. One specimen was dried at 25°C in controlled humidity over concentrated sulphuric acid solution. The other specimen was dried in an oven at 110°C. It should be emphasized that the data reported in this section can only be used to assess the relative degree of disturbance in the soil structure between different drying methods. Quantitative assessment of the disturbance at different levels of soil structure caused by drying is not possible, as this would require the knowledge of the PSD of an ideal "undisturbed" specimen.

From Figure 4.20, it can be seen that the drying temperature has virtually no effect on the pore size range of 0.004 μm to 0.1 μm. However, there is a measurable difference

in the PSD's over the range of 5 μm to 150 μm. A larger apparent total porosity (taken as the maximum cumulative intrusion in Figure 4.20b) was measured in the specimen dried at the higher temperature of 110°C. It is likely that the difference between the two PSD's is attributed largely to micro-cracking in the specimen dried at 110°C. Based on the data presented in Figure 4.20, it may be concluded that specimen disturbance in relation to drying temperature manifests itself in the larger pore size range of the PSD, and that higher apparent total porosities are measured in specimens dried in the oven at 110°C. It is pointed out that, to facilitate comparison of results, all the specimens used for mercury intrusion porosimetry testing in this study were dried at the same temperature of 25°C.

4.5.4 General procedures for specimen preparation

Each specimen was formed by compacting the soil material into a rigid mould to the desired dry density and water content. The specimens were 30 mm in diameter and 10 mm high. After compaction, the specimen was removed from the mould, and carefully broken up by hand into small samples measuring not more than 5 mm in size. This sample size was chosen because larger samples could not be accommodated in the sample chamber of a penetrometer which is a glass container consisting of a sample chamber and a long stem that supplies the mercury during testing. Each sample was then placed in a small glass container and dried in a desiccator containing concentrated sulphuric acid solution as desiccant for at least two weeks. It should be noted that the samples used in this study were typically larger than the samples for mercury intrusion porosimetry testing used by other researchers (for example, Delage and Lefebvre, 1984; Lapierre et al., 1990).

4.5.5 Test procedures

At the end of the drying period, each sample was carefully placed inside a

penetrometer which fitted inside one of the housings in the porosimeter. The penetrometer was then de-gassed and filled with a known volume of mercury under a vacuum pressure. It should be pointed out that the stem of each penetrometer has a larger volume than the sample chamber, and this ensures sufficient mercury available for the intrusion during a test. To initiate the measurement, increments of positive pressure were applied to the penetrometer, forcing the mercury to intrude into the pores of the sample. At each pressure increment, the applied pressure and the amount of mercury intruded into the sample were automatically recorded by the controlling software in the external computer.

At a given pressure increment, the pore size in a sample is related to the pressure by the Washburn equation,

$$p = -\frac{4T_s\cos\theta}{d} \qquad [2.2 \text{ bis}]$$

where p is the absolute pressure, T_s is the surface tension of mercury, θ is the contact angle between mercury and the soil grain, d is the equilibrium pore diameter (Diamond, 1970). In this study, contact angles between the mercury and the soil grain were taken as 139°, 147°, and 130° for the sand-bentonite material, the sand-illite material, and Boom Clay respectively (Diamond, 1970).

4.5.6 Factors affecting the interpretation of mercury intrusion porosimetry data

Several factors affect the interpretation of the results of mercury intrusion porosimetry tests on compacted clays (Diamond, 1970). These factors are discussed as follows.

Occluded or isolated voids in compacted clay specimens cannot be intruded.

In this study, an Autopore II 9220 porosimeter manufactured by Micromeritics, Georgia, USA, was used for testing. This porosimeter has a maximum pressure capacity of 416 MPa. Depending on the contact angle between the mercury and the clay mineral, the smallest pore diameters that can be measured by the porosimeter varied between 0.003 μm to 0.004 μm. Therefore, pores with mean diameters smaller that these sizes cannot be intruded.

Prior to testing, the specimens need to be dried. The effect of drying temperature on PSD's was discussed in Section 4.5.3. In general, drying leads to shrinkage, resulting in decreased porosities. Results on drying shrinkage will be discussed in Chapter 5.

In a typical MIP test carried out in this study, pressures up to 416 MPa were used. The use of high pressures can affect the accuracy of porosity measurements in two ways. One, elements of the measurement system such as the mercury and the penetrometer may deform under pressure, leading to inaccuracy in the volume measurements of the mercury intruded into the pores. This factor was eliminated by periodic calibrations of the porosimeter. Results from calibration tests were incorporated in the data reduction. Two, high pressures caused compression of the soil structure, leading to the reduction of pore volume. The effect of this factor is difficult to quantify and was not incorporated in the data reduction.

Because of the influence of the factors discussed in this section, quantitative measurements of PSD's and total porosities in compacted clays are difficult. Therefore information provided by mercury intrusion porosimetry is only qualitative. Often scanning electron microscopy is used to provide supplementary information and to aid in the interpretation of data on soil structure (Delage and Lefebvre, 1984; Lapierre et al., 1990). In this study, a limited number of tests using scanning electron microscopy were carried out. Equipment and specimen preparation procedures are described briefly in the next section.

4.6 Scanning electron microscopy

The use of scanning electron microscopy (SEM) to study soil structures is described by Mitchell (1976). In this study, analyses were carried out using an Energy Dispersive JOEL 6300V Spectrometer. Tests were carried out on sand-bentonite material and sand-illite material to allow microscopic examination of the soil structures in the compacted materials. Boom Clay was not tested due to a limited quantity of material for testing.

The samples used for scanning electron microscopy were prepared and dried in the same manner as the samples for mercury intrusion porosimetry. After drying, each SEM sample was plated with a thin layer of gold to expel the electrical charges built up during testing. The sample was then placed inside the spectrometer for examination. The spectrometer projects electrons onto the sample, and measures back electron scatter and secondary electrons emitted from the sample. The measured electron pattern is viewed on a monitor to provide visual representation of the soil structure. The soil structure of each sample is photographed at both low (12 X) and high (5000 X) magnifications. Results from typical tests are presented in Chapter 7.

CHAPTER 5 SUCTION TEST RESULTS

5.1 Background

The laboratory testing program carried out in this study was divided into three parts: suction test series, triaxial test series, and mercury intrusion porosimetry studies. This chapter presents the results from the suction test series. The objective of the suction tests was to measure the suction properties of the three soil materials tested in this study under ambient atmospheric pressure conditions. Relationships between suction and other soil parameters including water content, degree of saturation and temperature were examined. Results from the triaxial test series and the mercury intrusion porosimetry studies will be discussed in Chapters 6 and 7 respectively. Discussion and synthesis of data will be presented in Chapter 9.

5.2 Effects of water content and degree of saturation on total suction

The total suctions in the sand-bentonite material, sand-illite material, and Boom Clay were measured by the psychrometer method, vapour equilibrium technique, and the filter paper technique. For each soil, both uncompacted and compacted specimens were used. Compacted specimens were formed at different degrees of saturation and dry densities corresponding to 80% to 98% of the maximum dry density (see Tables 4.1 to 4.7).

It is customary to relate the suction in a soil to water content and degree of saturation (Yong and Warkentin, 1975; Corey, 1986; Fredlund and Rahardjo, 1993; Fredlund and Xing, 1994). Therefore, results are presented in terms of total suction S - gravimetric water content w relationship; and total suction S - degree of saturation S_r relationship. The gravimetric water content is the ratio of the mass of moisture and the

mass of dry solids, expressed as percentage. Hereafter, unless otherwise stated, the term 'water content' will be used, for brevity, in place of gravimetric water content.

The S - w relationships at 25°C for sand-bentonite material, sand-illite material and Boom Clay are shown on a semi-logarithmic scale in Figures 5.1 to 5.3. The S - S_r relationships for the respective soils are shown in Figures 5.4 to 5.6. Figures 5.1 to 5.3 summarize the data on both uncompacted and compacted specimens, whereas only data on the compacted specimens are given in Figures 5.4 to 5.6. The compacted specimens were formed to different dry densities and degrees of saturation given in Tables 4.1 to 4.7.

From Figures 5.1 to 5.3, it can be seen that the total suction in each soil decreases with increasing w, and that the suction can be broadly related to a singular value of w. This is consistent with general expectations (Krahn and Fredlund, 1972; Yong and Warkentin, 1975; Hillel, 1980). For each soil, the S - w relationship is represented by a bi-linear function as follows, with the suction in MPa expressed in the form log S = A - Bw, (equations [5.1] to [5.6]).

Sand-bentonite material:

w = 1 to 11 %,	log S = 2.729 - 0.142w	$R^2 = 0.99$	[5.1]
w = 11 to 25 %,	log S = 1.983 - 0.074w	$R^2 = 0.91$	[5.2]

Sand-illite material:

w = 0 to 2 %,	log S = 2.647 - 0.892w	$R^2 = 0.97$	[5.3]
w = 2 to 13 %,	log S = 1.415 - 0.175w	$R^2 = 0.91$	[5.4]

Boom Clay:

w = 1 to 8 %,	log S = 2.757 - 0.197w	$R^2 = 0.98$	[5.5]
w = 8 to 17 %,	log S = 1.710 - 0.073w	$R^2 = 0.80$	[5.6]

It can be seen also from Figure 5.1 to 5.3 that for each of the three soil materials tested in this study, the total suctions measured by the psychrometer method, vapour equilibrium technique, and the filter paper technique generally lie within the 95% confidence envelope of all the data. This therefore gives confidence to the use of psychrometers to measure suctions in compacted clays. The lower suction values measured in the sand-illite material by the filter paper method in the 5% to 7% water content range (Figure 5.2) is thought to be attributed to the difficulty in the measurements of water contents of the filter paper discs (see Section 4.3.3).

At a given water content, due to the presence of bentonite, the suction in the sand-bentonite material is higher than that of the sand-illite material (compare Figure 5.1 and 5.2). However, it is interesting to note that the specimens of reconstituted Boom Clay which contained a large quantity of quartz, exhibits a S - w relationship characteristic of soils with high active clay contents such as the sand-bentonite material. The suction properties of Boom Clay may be explained by consideration of the pore size distribution and the size of the capillary pores within the soil structure which relates directly to the matric component of the total suction. The Boom Clay material tested in this study had a particle size distribution similar to those of the bentonite and the illite materials (see Figure 4.2). It may therefore be assumed that the sizes of the capillary pores in the Boom Clay specimens were similar to those in the sand-bentonite and sand-illite specimens. As a result, suctions higher than would be normally be expected from non-swelling clays, were measured in the Boom Clay specimens.

Figures 5.4 to 5.6 show the S - S_r relationships for the sand-bentonite material, sand-illite material, and Boom Clay respectively. The data in the figures show that while the total suction tends to decrease with increasing saturation in the specimen, it cannot be related to a singular value of S_r. Figure 5.7 compares the total suctions in sand-bentonite specimens formed to the same water content but with different degrees of saturation. The

data in this figure confirm that the measured total suction is insensitive to the degree of saturation of the specimen. This behaviour is inconsistent with the theoretical relationships developed in the literature (for example, Yong and Warkentin, 1975; Fredlund and Rahardjo, 1993). This apparent insensitivity of suction to S_r is related to the complexities in the soil structures in the compacted materials. Related results were obtained by Croney et al. (1958), Krahn (1970), Gray (1980) and Musa (1982). This topic will be discussed further in Chapter 9.

5.3 Hysteresis

It was shown in Chapter 2 that the S - w relationship for a soil can be expected to be not unique, and is affected, among other factors, by the paths followed by specimens during testing. The S - w relationship determined by drying or desorption is different from that by wetting or sorption (Hillel, 1980). This phenomenon is known as hysteresis. In this study, the phenomenon of hysteresis was examined on the sand-bentonite material using the multi-stage vapour equilibrium tests. Procedures used in these tests were described in Section 4.3.2.2.

Figures 5.8 to 5.10 show the S - w relationship of three sand-bentonite specimens formed to the same initial water content of 18%, but different dry densities (uncompacted, 1.48 Mg/m^3 and 1.74 Mg/m^3). Each figure compares the S - w relationships of a sand-bentonite specimen measured during drying and wetting phases. The S - w relationship from single-stage tests on specimens formed to different initial water contents are also included in each figure for comparison.

From Figures 5.8 to 5.10, it can be seen that the S - w relationship for the drying phase differs from that for the wetting phase. At a given water content, the total suction in a specimen was higher during drying than wetting. These observations are consistent with those on the behaviour of other soil types reported in the literature (for example,

Yong and Warkentin, 1975; Gray, 1980; Musa, 1982). It can also be seen from the figures that, in general, the S - w relationships for the drying phase are consistent in trend and value with the S - w relationships determined from the single-stage test. The similarity can be explained by the fact that specimens tested in the single-stage tests and the drying phase of the multi-stage tests were subjected to the same test paths, that is, they lost water during testing.

Furthermore, it may be inferred from the data in Figures 5.8 to 5.10 that the difference in S between the wetting and drying paths is largely independent of the dry density and degree of saturation of the specimen. Similar observations were made on kaolinite materials (Musa, 1982). The observations made in this study and in the literature may be taken to imply that total suctions in compacted clays are largely controlled by the micropores within the peds that are part of the compacted soil structure.

5.4 Osmotic suctions

The osmotic suctions S_π in the sand-bentonite material, sand-illite material and Boom Clay were measured using the filter paper technique. Relationships between osmotic suction and water content, and between suction and degree of saturations are given in Figures 5.11 and 5.12 for the sand-bentonite material, Figures 5.13 and 5.14 for the sand-illite material, and Figures 5.15 and 5.16 for Boom Clay. Total suction data for each respective material are also included in these figures for comparison. The osmotic suctions are approximately equal to the total suctions at high $S_r > 85\%$ but significantly lower, as expected, when $S_r < 50\%$.

From Figures 5.11 to 5.16, it can be seen that, in contrast to the total suction, the osmotic suction in each of the soils appears to be independent of the water content or the degree of saturation of the test specimen. It is noted that the scatter in the data are

generally within the range of accuracy of the filter paper technique which is ± 25% of the total suction values (Ridley and Burland, 1994). The results from this study are consistent with the observations made on other clay soils (Krahn and Fredlund, 1972).

Because of the presence of larger quantities of smectite minerals, the osmotic suctions measured in the sand-bentonite material were higher than those in the sand-illite material and Boom Clay. For the sand-bentonite material, the osmotic suction generally varies between 0.5 MPa to 1.5 MPa for water contents of 10% to 24%, with an average value of 0.8 MPa (see Figure 5.11). The measured osmotic suctions are consistent with the range of swelling pressures measured in the same type of sand-bentonite material tested by Dixon et al. (1986). This therefore supports the general hypothesis that the swelling properties of sand-bentonite material are derived from osmotic potential differences (Dixon et al., 1986; Graham et al., 1989).

Figures 5.13 and 5.14 summarize the data on the osmotic suction in the sand-illite material. For the water content range of 5% to 13%, the osmotic suctions lie within a narrow range of 0.2 MPa to 0.5 MPa, with an average of 0.3 MPa. The data for the Boom Clay are given in Figures 5.15 and 5.16. It can be inferred from the data in the figures that for water contents from 11% to 19%, the osmotic suction in Boom Clay also varies generally within a narrow range of 0.2 MPa to 0.5 MPa, averaging at 0.3 MPa.

Based on the data from the filter paper tests, two conclusions can be drawn. One, for the soils tested in this study, the osmotic suctions are generally insensitive to changes in water content. Two, total suctions in these soils are dominated by the matric component. It was shown in Section 5.4 that total suction is largely independent of dry density and degree of saturation, and that it is likely that S is controlled largely by the capillary pores at the microscopic scale. This may be taken to imply that matric suction is controlled by the micropores.

5.5 Temperature effect

Effects of temperature on suctions were examined in the vapour equilibrium tests on all three soil materials and in the single-stage tests using the psychrometer method on the sand-bentonite material. Total suctions measured at 10°C and 50°C in the vapour equilibrium tests are shown in Figures 5.17 to 5.19. Qualitatively, it can be seen from the data in the figures that, at a given water content, the total suctions in each soil tend to decrease with increasing temperature. However the differences are not large.

The suctions in the sand-bentonite material measured at 10°C, 25°C and 50°C by the psychrometer method are shown in Figures 5.7 and 5.20. The data in these figures confirm the results from the vapour equilibrium tests, showing that the total suction at a given water content decreases with increasing temperature. It may be inferred from the data that the effect of temperature on total suction tends to be less at lower temperatures (from 10°C to 25°C) than at higher temperatures (from 25°C to 50°C). It is noted in Figure 5.20 that the suctions for $w > 22\%$ appear to be independent of the water content. The suctions measured in this range of water contents are similar in value to the osmotic suctions measured in the filter paper tests. The implication of this observation, supported by saturation calculations, is that at $w > 22$ %, the micropores within the clay structure are probably water-saturated and the total suction is dominated by the osmotic component.

The influence of temperature on soil suction is commonly explained by consideration of the temperature dependence of the surface tension of the air-water meniscus in the capillary pores in the soil structure (Philip and de Vries, 1957). The surface tension of water decreases with increasing temperature. For water, the relationship between surface tension and temperature is given by,

$$\sigma_t = 1.171 - 0.001516(T + 273.16) \qquad [5.7]$$

where σ_t is surface tension (N/m) and T is temperature (°C) (Edlefsen and Anderson, 1943). The matric suction which is a component of the total suction is directly related to the surface tension of the air-water interface as follows (Fredlund and Rahardjo, 1993),

$$S_m = \frac{4\sigma_t}{d} \qquad [5.8]$$

where S_m is suction, σ_t is surface tension, and d is radius of pore diameter. Hence, an increase in temperature will lead to a decrease in suction.

Comparison between the measured suctions and the suctions predicted by the theory is shown in Figure 5.7. Since all the tests were set up at the ambient temperature of 25°C, the total suctions measured at this temperature were used as the reference suctions for calculating the average pore diameters. For a given water content, the suctions at the temperatures of 10°C and 50°C were calculated as follows.

1) The total suctions measured at 25°C were averaged to give the reference suction. Applying Equations 5.7 and 5.8 and using the reference suction allowed determination of the effective pore diameter, d.
2) Equation 5.7 was then used to calculate the surface tensions at 10°C and 50°C.
3) Applying equation 5.8, the suctions at 10°C and 50°C were computed using the average diameter from step 1) and the surface tension values from step 2).

From Figure 5.7, it can be seen that the total suctions calculated from the theory generally fit the experimental data at the lower temperature of 10°C. At the higher temperature of 50°C, the theory under-predicts the influence of temperature on total suction, That is, the predicted suction is higher than the measured suction. In general therefore, the capillary model cannot adequately explain the effect of temperature on suction. The difference in suction values may be attributed to several factors including

thermal expansion of entrapped air and the effect of dissolved solutes on the surface tension - temperature relation of the soil water (Peck, 1960; Constantz, 1983).

The discrepancy between measurement and theory may be explained by consideration of the effect of temperature on the radius of curvature of the air-water menisci between micropores. Consider the air-water menisci with an initial radius of curvature formed between two curved, flaky clay particles oriented in a similar direction (see Figure 5.21). Thermal expansion of the clay particles and swelling of the clay-water structure reduce the spatial distance between the particles. Furthermore, the mobile free water between the particles tends to increase in volume due to thermal expansion. Under constant mass conditions, the combination of these phenomena causes the free water to migrate towards the edges of the particle assembly, leading to an increase in the radius of curvature of the air-water menisci. As a result, the matric suction decreases according to the capillary equation (Hillel, 1980).

5.6 Shrinkage behaviour

Dry shrinkage of sand-bentonite material, sand-illite material, and Boom Clay were examined using the data from the single-stage vapour equilibrium tests. Test procedures have been described in Section 4.3.2. For each soil type, test specimens were generally formed to a narrow range of water contents at different dry densities (see Tables 4.2 to 4.4). In each test, the specimen was allowed to dry inside a desiccator of constant humidity controlled by sulphuric acid solution. At the end of the drying stage of the test, the final dimensions of the specimen were measured. The total shrinkage is taken as the difference between the initial and the final total volumes expressed as a percentage of the final total volume. Results are summarized in Tables 4.2 to 4.4 and Figures 5.22 to 5.24.

Figures 5.22 to 5.24 show that for each material, the total shrinkage strain is generally independent of the dry density and final water content of the specimen. Similar

observations were made by Dixon et al. (1993). For the sand-bentonite material which was prepared at initial water contents of 16.8% to 18.5%, the total shrinkage strain generally varied between 5% to 7%, averaging at 5.5%. This range of shrinkage is consistent with the shrinkage measurements carried out by Dixon et al. (1993).

The sand-illite material was prepared at initial water contents of 8.5% to 10.0%. The total shrinkage strain generally lay between 0.5% to 2.5%, averaging at 1.2%.

Boom Clay was prepared at initial water contents of 14.8% to 17.7%. The total shrinkage strain generally varied between 2.5% to 5.5%, with an average of 3.9%. The larger shrinkage strains of 5.5% to 6.8% measured in the three driest specimens marked A in Figure 5.24 (final w = 0.4 %) can be attributed to their higher initial water contents of 17.7%. Specimens of compacted clays prepared at higher water contents tend to experience larger shrinkage strains (Dixon et al., 1993).

It is noted that for each soil type, soil materials were generally prepared to a narrow range of water contents, and hence, they had similar peds (Wan et al., 1990). Test specimens were formed by compacting soil materials in a rigid mould to different initial dry densities. Hence the specimens had different macrostructures with different volumes of inter-ped voids (see Figure 5.25). This study and others have shown that dry shrinkage in compacted clays is a function of initial water content and is independent of dry density and final water content. This may be taken to imply that shrinkage in compacted clays is largely controlled by individual ped units which arise from the moulding water content, rather than the macrostructure which is an artifact of specimen preparation.

5.7 Discussion and summary

Suctions were measured in sand-bentonite material, sand-illite material, and Boom Clay by the psychrometer method, vapour equilibrium technique and filter paper

technique. For each of the three soil materials tested in this study, the total suctions measured by the three methods generally lie within the 95% confidence envelope of all the data. This therefore gives confidence to the use of psychrometers to measure suctions in compacted clays under constant temperature, atmospheric pressure conditions.

The results show that total suction is influenced by factors including water content, degree of saturation, temperature, mineralogy, and test path. For the soil types tested in this study, total suction decreases with increasing water content and can be broadly related to a singular value of gravimetric water content. The behaviour is consistent with general expectations. Contrary to some views reported in the literature, no simple relationship between total suction and degree of saturation could be established.

Osmotic suctions were measured in each soil using the filter paper technique. The results show that the osmotic suction is largely independent of water content and degree of saturation. Observations made in this study and reported in the literature led to the conclusion that total suctions in compacted clays such as those tested in this study are dominated by the matric component and are largely controlled by the micropores within the soil structure.

The dependence of total suction on temperature was examined in tests using the psychrometer method and the vapour equilibrium technique. At a constant water content, an increase in temperature leads to small decreases in suction. For sand-bentonite material, the theory under-predicts the effect of temperature on total suction at temperatures higher than the ambient temperature of 25°C. The discrepancy is attributed to several factors including thermal expansion of entrapped air, effect of dissolved solutes on the surface tension-temperature relation of the soil water, and increase in the radius of curvature of the air-water meniscus associated with thermal expansion and swelling of the clay-water structure.

Dry shrinkage behaviour of sand-bentonite material, sand-illite material, and Boom Clay is a function of initial water content, and is independent of dry density and final water content. Shrinkage in these compacted soils is thought to be largely controlled by individual ped units, rather than the macrostructure which comprises of peds and inter-ped voids.

Suction-water content relationships are used in the analysis of problems relating to water movement in unsaturated soils (Thomas, 1992). Results from the suction test series show that the trend of a S - w relationship can be influenced by the test method and the stress paths followed by the specimen during testing. The implication is that, to obtain appropriate S - w relationships for use in design calculations and analyses, methods of measurement must be selected such that the stress paths experienced by the test specimens are representative of those anticipated in the problem considered.

CHAPTER 6 TRIAXIAL TEST RESULTS

6.1 Background

In Chapter 5, it was postulated that suctions in compacted clays are largely governed by the soil microstructure. Stress variations and the resulting deformations will lead to changes in the soil particle arrangement and pore size distribution. Because of the complexities associated with soil structure, it is unclear how these changes will affect suction measurements made by psychrometers.

The primary objective of the triaxial testing program was to examine the effects of total stresses and distortions on suction measurements using thermocouple psychrometers in unsaturated sand-bentonite material. Three series of tests were carried out. The first two series examined the effects of isotropic compression and shear compression stresses on suctions measured by psychrometers. Nine isotropic compression tests and four shear compression tests were carried out. In these tests, due to limitations of the equipment, only changes in the total suction in the specimens during testing were monitored, and volume changes were not measured. The third series of tests was carried out to examine the relationship between volume change and stress in unsaturated sand-bentonite materials. Six isotropic compression tests with volume change measurements were carried out.

6.2 Descriptive parameters

To facilitate presentation and discussion of data in this chapter, the following descriptive parameters are used.

Total suction: $S = S_m + S_\pi$

Total suction is the sum of matric suction S_m and osmotic suction S_π.

Total stress: $p^* = \frac{\sigma_1 + 2\sigma_3}{3}$

Total stress is the numerical average of the axial (σ_1) and lateral (σ_3) principal total stresses on the specimen referenced to atmospheric pressure (p_a), even though the pore air pressure (u_a) was not measured. In triaxial compression tests, the axial stress is the major principal stress, and the lateral stress is the minor principal stress. Compressive stresses are considered positive. It should be noted that this total stress parameter is different from the mean total stress parameter (p) commonly adopted in the study of unsaturated soil mechanics (Alonso et al., 1990; Wheeler and Sivakumar, 1995; Delage and Graham, 1995). The latter parameter is the numerical difference between p* and u_a.

Deviator stress: $q = \sigma_1 - \sigma_3$

Deviator stress is the numerical difference between the axial and lateral principal total stresses on the specimen.

Axial Strain: $\varepsilon_1 = \Delta L/L_o$

Axial strain is the change in length of the specimen (ΔL) divided by the original length (L_o), expressed in percentage. As it is customary in soil mechanics, compressive strains are positive and expansive strains are negative.

Volume Strain: $\varepsilon_v = \varepsilon_1 + 2\,\varepsilon_3$

Volume strain is the sum of the axial strain (ε_1) and lateral strain (ε_3) in the specimen, and is defined as the ratio of volume change to initial volume of the specimen, expressed in percentage. Compressive strains are taken as positive whereas expansive strains are negative.

6.3 Isotropic compression tests with suction measurements using psychrometers

6.3.1 Background

Nine isotropic compression tests with suction measurements were carried out. Six tests were carried out on specimens formed to initial dry densities of 1.41 Mg/m^3 to 1.45 Mg/m^3 at water contents of 17.3% to 22%. The remaining three tests were done on specimens formed to initial dry densities of 1.64 Mg/m^3 to 1.66 Mg/m^3 at water contents of 18.7% to 22.0%. All the tests were carried out under conditions of constant total mass, and therefore constant water content. In each test, a calibrated psychrometer was installed near the middle of the specimen to measure the total suctions in the specimen. Because of limitation of the triaxial equipment used in these tests, volume changes were not measured during the progress of the tests, net volume changes were obtained from the dimensions of the specimens at the end of tests.

The results from the isotropic compression tests are presented in terms of S - p* relationships in Figures 6.1 to 6.9. The initial and final dry densities and water contents of all the specimens tested in this series have been summarized in Table 4.8. The specimens tested in this series had different initial suctions, saturation, and densities; and they generally followed different suction-stress paths during testing. To facilitate discussion, results of each specimen will be presented independently in the following section.

6.3.2 Results

The following pages represent a simple cataloguing of the conditions during the tests. While this represents a rather repetitive presentation of data, it has been felt important to list these conditions carefully since the data are rare, and therefore valuable.

SB1780TX

The S - p* relationship of Specimen SB1780TX is shown in Figure 6.1. This specimen was formed to an initial dry density of 1.41 Mg/m^3 at 17.3% water content, with an average degree of saturation of 50.9%. The initial average total suction measured in the specimen prior to compression was 7830 kPa. The specimen was first isotropically compressed, in successive total stress increments, to a maximum total cell pressure of 3002 kPa. The specimen was then subjected to two unloading-reloading cycles. It was first unloaded, in successive total stress decrements, to 1098 kPa, then reloaded to 3017 kPa, and finally unloaded to 549 kPa.

Figure 6.1 shows that during first-time compression, the total suction tended to decrease non-linearly with increasing total stress for the pressure range of 0 kPa to 3002 kPa. Upon unloading, the total suction tended to increase with decreasing total stress. It can be observed from Figure 6.1 that the rate of suction increase during the unloading phase is less than the rate of suction decrease during first-time compression. At a given total stress, the total suction measured during the unloading phase was consistently lower than that measured during first-time compression.

The paths of the S - p* relationships for the unloading and reloading phases are generally similar. The similarity in the suction paths may be taken as an indication of the existence of pre-yield elasticity in the unsaturated sand-bentonite material (Delage and Graham, 1995).

It should be remembered from Chapter 5 that compacted clays such as the sand-bentonite mixtures tested in this study have complex soil structures characterized by aggregations of clay peds, intra- and inter-ped voids (see also Barden and Sides, 1970; Wan et al., 1990). The difference in suction behaviour of Specimen SB1780TX during loading, unloading, and reloading may be explained by consideration of corresponding changes in the distribution of intra- and inter-ped voids within the specimen. It is

hypothesized that changes in the intra- and inter-ped voids are brought about by the different degrees of elasto-plastic volumetric straining of the individual clay peds and the overall ped structure in the specimen during the two testing phases. The importance of soil structure as a controlling factor on soil suction in compacted clays will be discussed further in Chapter 9.

From measurements at the end of test, the net volume strain of the specimen was compressive and found to be 14.9%. The final dry density and water content were measured to be 1.66 Mg/m^3 and 16.5% respectively, and the final average degree of saturation was determined to be 71.2%. The final total suction at the end of testing, under atmospheric pressure conditions, could not be measured because the psychrometer had ceased functioning.

SB1880TX

The S - p* relationship of Specimen SB1880TX is shown in Figure 6.2. This specimen was formed to an initial dry density of 1.45 Mg/m^3 at 18.0 % water content, with an average degree of saturation of 56.1%. The initial average total suction measured in the specimen prior to compression was 4994 kPa. The specimen was isotropically compressed, in successive total stress increments, to a maximum total cell pressure of 1132 kPa. From Figure 6.2, it can be seen that the total suction in the specimen tended to decrease linearly with increasing total pressure for the pressure range from 0 kPa to 1132 kPa.

The test was aborted prematurely due to leakage through the latex membranes. The net volume strain of the specimen was expansive and was measured to be -2.8%. The final dry density and water content were 1.41 Mg/m^3 and 21.4 % respectively, and the final average degree of saturation was computed to be 63.5%.

SB1980TX

The S - p* relationship of Specimen SB1980TX is shown in Figure 6.3. This specimen was formed to an initial dry density of 1.40 Mg/m^3 at 18.7% water content, with an average degree of saturation of 54.4%. The initial average total suction measured in the specimen prior to compression was 4150 kPa. The specimen was first isotropically compressed, in successive total stress increments, to a maximum total cell pressure of 3105 kPa. The specimen was then unloaded, in successive total stress decrements, to the atmospheric pressure.

The S - p* relationship of this specimen shown in Figure 6.3 is similar in pattern to that of Specimen SB1780TX (see Figure 6.1). From Figure 6.3, it can be seen that during first-time compression, the total suction in Specimen SB1980TX tended to decrease non-linearly with increasing total stress. Upon unloading, the total suction increased with decreasing total stress. The path of the unloading curve is different in position from the first-time compression relationship. At a given total stress, the total suction measured during unloading was consistently lower than that measured during first-time compression. The final total suction at the end of testing was measured to be 4465 kPa.

After the test was completed, the net volume strain of the specimen was found to be 15.8%. The final dry density and water content were 1.67 Mg/m^3 and 18.0% respectively, and the final average degree of saturation was determined to be 78.8%.

SB2080TX

The S - p* relationship of Specimen SB2080TX is shown in Figure 6.4. This specimen was formed to an initial dry density of 1.41 Mg/m^3 at 20.0% water content, with an average degree of saturation of 58.5%. The initial average total suction measured in the specimen prior to compression was 2982 kPa. The specimen was isotropically

compressed, in successive total stress increments, to a maximum total pressure 3018 kPa. From Figure 6.4, it can be seen that the total suction decreased non-linearly with increasing total stress for the pressure range of 0 kPa to 3018 kPa. At the end of the loading phase, the specimen was directly unloaded in one decrement to atmospheric pressure. The final average total suction at the end of test was measured to be 2200 kPa.

The net volume strain of the specimen was found to be 18.8%. The final dry density and water content were 1.74 Mg/m^3 and 19.4% respectively, and the final average degree of saturation was determined to be 94.8%.

SB2180TX

The S - p* relationship of Specimen SB2180TX is shown in Figure 6.5. This specimen was formed to an initial dry density of 1.41 Mg/m^3 at 21.1% water content, with an average degree of saturation of 62.4%. The initial average total suction measured in the specimen prior to compression was 3433 kPa. The specimen was subjected to several loading-unloading-reloading cycles. It was first isotropically compressed, in successive total stress increments, to a total cell pressure of 926 kPa, then unloaded to atmospheric pressure, reloaded to 2038 kPa, unloaded to atmospheric pressure, reloaded to 2953 kPa, and finally unloaded to atmospheric pressure.

From Figure 6.5, it can be seen that during first-time compression, both initially and following the first unload/reload cycle, the total suction decreased non-linearly with increasing total stress for the pressure range of 0 kPa to 2953 kPa. In general, the following unloading and reloading curves are slightly nonlinear, and they follow different paths from the first-time compression curve. At a given total stress, the total suction measured during first-time compression was consistently higher than those measured during unloading and reloading. For the first two unloading and reloading cycles, the unloading and reloading curves in each cycle followed essentially the same paths. The

similarity in the unloading and reloading suction paths observed in the same cycle may be taken as an indication of the existence of pre-yield elasticity in unsaturated sand-bentonite material (Delage and Graham, 1995). A similar observation was made on Specimen SB1780TX reported earlier in this Section. It is interesting to note that the suction path for the final unloading phase of Specimen SB2180TX followed essentially the same path as the second cycle of unloading and reloading (Figure 6.5). The final total suction at the end of testing was measured to be 3077 kPa.

The net volume strain of the specimen was found to be 15.7%. The final dry density and water content were 1.69 Mg/m^3 and 20.0% respectively, and the final average degree of saturation was determined to 89.9%.

SB2280TX

The S - p* relationship of Specimen SB2280TX is shown in Figure 6.6. This specimen was formed to an initial dry density of 1.40 Mg/m^3 at 22.0% water content, with an average degree of saturation of 64.4%. The initial average total suction measured in the specimen prior to compression was 1896 kPa. The specimen was isotropically compressed, in successive total stress increments, to a maximum total cell pressure of 900 kPa. From Figure 6.6, it can be seen that the total suction tended to decrease non-linearly with increasing total stress for the pressure range of 0 kPa to 900 kPa. The final total suction in the specimen was not measured.

The net volume strain of the specimen was found to be 10.1%. The final dry density and water content were 1.57 Mg/m^3 and 21.1% respectively, and the final average degree of saturation was determined to be 78.9%.

SB1895TX

The S - p* relationship of Specimen SB1895TX is shown in Figure 6.7. This specimen was formed to an initial dry density of 1.66 Mg/m^3 at 18.7 % water content, with an average degree of saturation of 80.1%. The initial average total suction measured in the specimen prior to compression was 4458 kPa. The specimen was subjected to several loading-unloading-reloading cycles. It was first isotropically compressed, in successive total stress increments, to a total cell pressure of 1344 kPa, then unloaded to atmospheric pressure, reloaded to 2085 kPa, unloaded to atmospheric pressure, reloaded to 3037 kPa, and finally unloaded to atmospheric pressure.

Consistent with other specimens tested in this series, during first-time compression, the total suction in Specimen SB1895TX decreased with increasing total stress (Figure 6.7). The S - p* relationships for the first unloading/reloading cycle broadly coincide with the first-time compression curve. However, the S - p* relationships for the second unloading/reloading cycle and for the final unloading phase are slightly nonlinear, and they follow a different path from the first-time compression curve. The final average total suction at the end of testing was measured to be 4100 kPa.

The net volume strain of the specimen was measured to be 4.9%. The final dry density and water content were 1.74 Mg/m^3 and 18.3 % respectively. The final average degree of saturation was determined to 90.2%.

SB1995TX

The S - p* relationship of Specimen SB1995TX is shown in Figure 6.8. This specimen was formed to an initial dry density of 1.65 Mg/m^3 at 20.0% water content, with an average degree of saturation of 85.5%. The initial average total suction measured in the specimen prior to compression was 4084 kPa. The specimen was first isotropically compressed, in successive total stress increments, to a maximum total cell

pressure of 2972 kPa. The specimen was then unloaded, in successive total stress decrements, to atmospheric pressure. From Figure 6.8, it can be seen that during first-time compression, the total suction in the specimen decreased with increasing total stress. Conversely upon unloading, the total suction increased with decreasing total stress. The unloading suction curve follows broadly the same path as the first-time compression curve. The final total suction at the end of testing was measured to be 3905 kPa.

The net volume strain of the specimen was measured to be 2.4%. The final dry density and water content were 1.69 Mg/m^3 and 19.5% respectively, and the final degree of saturation was determined to be 88.3%.

SB2295TX

The S - p* relationship of Specimen SB2295TX is shown in Figure 6.9. This specimen was formed to an initial dry density of 1.64 Mg/m^3 at 22.0% water content, with an average degree of saturation of 91.5%. The initial average total suction measured in the specimen prior to compression was 2444 kPa. The specimen was subjected to several loading-unloading-reloading cycles. It was first isotropically compressed, in successive total stress increments, to a total cell pressure of 990 kPa, then unloaded to atmospheric pressure, reloaded to 2126 kPa, unloaded to atmospheric pressure, reloaded to 2348 kPa, and finally unloaded to atmospheric pressure.

Figure 6.9 shows that during first time compression, the total suction in the specimen decreased non-linearly with increasing total stress. The specimen was subjected to two cycles of unloading and reloading. From Figure 6.9, it can be seen that within the scatter of the data, the S - p* relationships for these two cycles follow broadly the same path as the first-time compression curve. It is likely that the scatter in the data was attributed to temperature variations during testing . It is noted that this specimen was formed at a higher moulding water content of 22%. At this water content, the relative

humidities in the pore space were high and were therefore sensitive to temperature fluctuations.

It is interesting to note that during the last total stress increment from 2091 kPa to 2348 kPa, the total suction in the specimen decreased from 574 kPa to 0 kPa (Figure 6.9). Upon final unloading, the total suction in the specimen remained at 0 kPa and did not recover until the total pressure was decreased to less than 1475 kPa. The zero suctions measured during the final unloading phase from 2348 kPa to 1475 kPa imply 100% relative humidity in the soil and inside the ceramic chamber of the psychrometer. It is likely that the high humidity was attributed to the combined effect of temperature fluctuations and total stresses on the specimen. At pressures lower than 1500 kPa, the suction curve for the final unloading phase followed a slightly different path from the first-time compression curve, but the trends of the two curves are broadly similar. The final total suction at the end of testing was measured to be 1320 kPa.

The net volume strain of the specimen was measured to be 3.6%. The final dry density and water content were measured to be 1.71 Mg/m^3, 20.8% respectively, and the final average degree of saturation was determined to be 96.5%.

6.3.3 Total suctions measured under atmospheric pressure conditions

Table 6.1 compares the total suctions in 6 tests measured under atmosphere pressure conditions prior to isotropic compression and at the end of each unloading phase. It can be seen that in 4 of the 6 tests (SB1895TX, SB1980TX, SB1995TX, SB2180TX) reported in the table, the total suction measured at the end of each unloading phase was broadly similar to the initial suction. The percentage difference in suction was generally 7% to 11%. This range of percentage differences is broadly similar in value to the bounds of instrument accuracy of $\pm$ 6% reported in Chapter 3. It was postulated in Chapter 5 that suctions in compacted clays are governed by the soil microstructure. It

may be inferred from the reversal of suction observed in these specimens that the soil microstructure experienced reversible elastic straining. This postulate will be discussed further in Chapter 9.

For Specimens SB2080TX and SB2295TX, differences between the initial suction and the suction measured at the end of the test (Table 6.1) exceed the accuracy of the instruments. It is thought that the larger differences are attributed to two factors. One, insufficient time was given to each specimen to equilibrate at the end of compression before the final suction measurement was carried out. As a consequence, it is likely that the specimens had not attained suction-water content equilibrium. Two, at the end of compression, these two specimens had high average degrees of saturation of 95% and 97% respectively. Therefore, the pores in each specimen were probably water-saturated.

6.3.4 Summary

Nine triaxial isotropic compression tests were carried out to examine the effect of isotropic total stress on suction measurements in unsaturated sand-bentonite material using thermocouple psychrometers. The test specimens were formed at a range of initial dry densities of 1.40 Mg/m^3 to 1.66 Mg/m^3 and water contents of 17.3% to 22.0%. A calibrated thermocouple psychrometer was installed in the middle of each specimen to measure changes in suction during testing. The specimen was isotropically compressed, in successive total stress increments, to a maximum total stress of up to about 3020 kPa. Several specimens were subjected to cycles of unloading and reloading.

The results from these tests show that under constant mass and water content conditions, the total suction in the unsaturated material decreased with increasing total stress. Inversely, the total suction in the unsaturated material increased with decreasing total stress. In general, the suction-stress path followed by a specimen during first-time compression was different from those observed during subsequent unloading/reloading

cycles. The discrepancy reflects the different compression and expansion characteristics of the soil macro- and micro-structures.

Final suctions were measured in several specimens at the end of test. These suctions were broadly similar to the initial suctions in their respective specimens. It was postulated that the reversal of suction was associated with reversible elastic strains in the soil microstructure.

6.4 Shear compression tests with suction measurements using psychrometers

6.4.1 Background

Four shear compression tests were carried out in this study. In each test, a calibrated psychrometer was installed near the centre of the specimen, and was used to measure the total suction in the specimen during shearing. The specimens were formed to similar initial dry densities of 1.40 Mg/m^3 to 1.43 Mg/m^3 at water contents of 18.1% to 19.0%. The average degree of saturation of these specimens varied within a narrow range of 54.8% to 56.2%. One specimen (SB1880TS) was sheared with the confining pressure in the cell remaining atmospheric. The other three specimens were first compressed isotropically, under "undrained" constant mass conditions, to final confining pressures of 515 kPa, 1021 kPa, and 1494 kPa respectively, and then sheared. All four specimens were sheared under strain-controlled, "undrained" constant mass conditions. The procedures used in this test series were described in Chapter 4.

6.4.2 Testing program

SB1880TS1: This specimen was formed to an initial dry density of 1.42 Mg/m^3 at 18.8% water content. The initial average total suction measured in the specimen

prior to shearing was 5156 kPa. The specimen was sheared under atmospheric pressure, at an average strain rate of 1.0 %/day. The test was terminated at an axial strain of 5.6%. The final total suction at the end of shearing was measured to be 5631 kPa.

SB1880TS2: This specimen was formed to an initial dry density of 1.40 Mg/m^3 at 19.0% water content. The specimen was first isotropically compressed, in several successive total stress increments, to a maximum total confining pressure of 1494 kPa (Figure 6.10). The initial total suction measured in the specimen prior to shearing was 2045 kPa. The specimen was then sheared at an average strain rate of 1.26 %/day. The test was terminated at an axial strain of 11.9%. The final total suction at the end of shearing was measured to be 685 kPa. The final dry density and water content were 1.64 Mg/m^3 and 18.3% respectively.

SB1880TS3: This specimen was formed to an initial dry density of 1.41 Mg/m^3 at 18.6% water content. The specimen was first isotropically compressed, in several successive total stress increments, to a maximum total confining pressure of 515 kPa (Figure 6.10). The initial average total suction measured in the specimen prior to shearing was 5208 kPa. The specimen was then sheared at an average strain rate of 0.85 %/day. The test was terminated at an axial strain of 10.8%. The final total suction at the end of shearing was measured to be 4348 kPa. The final dry density and water content were 1.54 Mg/m^3 and 17.3% respectively.

SB1880TS4: This specimen was formed to an initial dry density of 1.43 Mg/m^3 at 18.1% water content. The specimen was first isotropically compressed, in several successive total pressure increments, to a maximum total confining pressure of 1021 kPa (Figure 6.10). The initial average total suction measured in the specimen prior to shearing was 3649 kPa. The specimen was then sheared at an average strain rate of 0.65 %/day. The shearing was terminated at an axial strain of 13.1%.

The final total suction at the end of shearing was measured to be 2382 kPa. The final dry density and water content were 1.67 Mg/m^3 and 17.3% respectively.

6.4.3 Stress-strain characteristics and total stress paths

The deviator stress q - axial strain ε_1 relationships of the four unsaturated sand-bentonite specimens are compared in Figure 6.11. It will be recalled from the Section 6.4.2 that the specimens were formed to similar initial dry densities of 1.40 Mg/m^3 to 1.43 Mg/m^3 at water contents of 18.1% to 19.0%. One specimen was sheared under atmospheric confining pressure, while the other three specimens were isotropically compressed in several pressure increments to 515 kPa, 1021 kPa, and 1494 kPa confining pressure prior to shear.

Figure 6.11 shows that the shapes of the stress-strain curves are not related to confining pressure level, and do not have the same patterns of behaviour that would be seen in saturated soils. Specimen SB1880TS1 which was sheared under atmospheric pressure, behaved in a strongly strain softening, dilative manner. The specimen attained a maximum peak strength of 441 kPa at about 1.7% axial strain. Thereafter, the strength rapidly decreased and reached a steady value of about 70 kPa. The test was terminated at an axial strain of 5.6%.

Specimens SB1880TS2 was sheared under a total confining pressure of 1494 kPa. This specimen reached an essentially constant shearing resistance. A peak deviator stress of 1086 kPa was reached at an axial strain of 9.5%. Thereafter, the deviator stress remained essentially constant with further straining. The test was terminated at an axial strain of 10.9%.

Specimens SB1880TS3 and SB1880TS4 were sheared at intermediate total confining pressures of 515 kPa and 1021 kPa respectively. Both specimens experienced

strain hardening behaviour in shear. Shearing of these specimens was terminated at axial strains of 10.8% and 12.3% respectively.

Figure 6.12 summarizes the stress paths from the shear compression tests plotted in terms of the stress parameters q and p*. As expected, the total stress paths are linear and have the customary gradient of $\Delta q/\Delta p^* = 3$. For Specimen SB1880TS2 which was sheared at the highest confining pressure of 1494 kPa, towards the end of the test, the deviator stress appeared to remain essentially constant with increasing p* and ε_1. This observation may be taken to imply that the specimen was approaching a state where (Wood, 1990),

$$\frac{\partial q}{\partial \varepsilon_s} = \frac{\partial p^*}{\partial \varepsilon_s} = \frac{\partial v}{\partial \varepsilon_s} = 0 .$$

This may be close to a 'critical state' even though the value of $p - u_a$ was not measured.

6.4.4 Total suction responses

Figure 6.10 summarizes the total suction S - total stress p* relationships of the specimens compressed to 515 kPa, 1021 kPa, and 1494 kPa respectively, measured during the isotropic compression phases of the tests. Consistent with the behaviour of the specimens reported in Section 6.3, the total suction in each of three specimens decreased systematically with increasing total stress.

Results from the shearing phases of the tests are summarized in Figures 6.13 to 6.15. Generally, two types of suction response are observed in Figure 6.13. Specimen SB1880TS1 which was sheared under atmospheric pressure showed strain-softening behaviour in shear in Figure 6.11. Its total suction remained relatively constant with an average of 5280 kPa for the first 2% of axial strains, and thereafter, tended to increase with further straining.

Specimens SB1880TS2, SB1880TS3, and SB1880TS4 showed constant or increasing shearing resistance during shearing. They generally showed decreases in total suction with straining (Figure 6.13). The total suction in Specimen SB1880TS2 decreased steadily from 2000 kPa to 900 kPa within the first 5% of axial strains. With further straining, the suction decreased gradually to a constant value approaching 700 kPa. For Specimens SB1880TS3 and SB1880TS4, the total suction in each specimen appeared to remain largely constant in the first 2% of axial strains. With further straining, the suction in the specimen decreased systematically until the end of shear.

The relationships between deviator stress and suction, and between total stress and suction are shown in Figures 6.14 and 6.15 respectively. For Specimen SB1880TS1 which was dilative in shear, the total suction in the specimen remained largely unaffected by q and p* in the early stage of shearing (up to about 2%). After the specimen reached a peak deviator stress of 441 kPa, the total suction in the specimen tended to increase with decreasing q and p*, and with increasing axial strains.

Specimen SB1880TS2 was ductile in shear. The total suction in the specimen tended to decrease with increasing q and p*. Towards the end of the shear test, S, q and p* remained largely constant with further straining, as the specimen approached critical state (Figures 6.14 and 6.15).

Specimens SB1880TS3 and SB1880TS4 were sheared at confining pressures of 515 kPa and 1021 kPa respectively. These two specimens strain-hardened in shear. It may be inferred from the verticality of the initial part of the suction paths (up to q = 400 kPa) in Figure 6.14 that the total suction in each specimen was largely insensitive to the increase in q and p* during the early stages of the shear test. With further straining, the total suction tended to decrease with increasing q and p*.

6.4.5 Total suction response of Specimen SB1880TS4

In the first three tests of this test series (SB1880TS1, SB1880TS2, and SB1880TS3), at the end of shearing, the specimens were quickly removed from the triaxial apparatus for density and water content measurements. However, a slightly different procedure was used in testing Specimen SB1880TS4. At the end of the shearing stage of the triaxial test, the specimen was kept inside the triaxial cell for about 20 hours. During this period, the total suction in the specimen was monitored.

Figure 6.16 compares the total suctions in Specimen SB1880TS4 at the different stages of the triaxial test. The initial total suction of the specimen prior to isotropic compression was measured to be 4897 kPa (point A in Figure 6.16). The specimen was first isotropically compressed in several increments to a confining pressure of 1021 kPa. As expected, the total suction decreased with increasing total pressure during compression. At equilibrium, the total suction in the specimen was measured to be 3649 kPa (point B).

The specimen was then sheared under the influence of a cell pressure of 1021 kPa. Immediately before the shearing machine was turned off, the total suction in the specimen was measured to be 2382 kPa (point C). The shearing was then stopped. The anisotropic loading was removed from the specimen by disconnecting the ram from the top cap, while a nominal isotropic cell pressure of 1006 kPa was maintained on the specimen. The specimen was then allowed to equilibrate at that pressure for about 6 hours. At the end of this dwell period, under a new isotropic loading condition, a slight increase in suction was noted and the total suction was measured to be 2567 kPa (point D).

The total cell pressure was then decreased to atmospheric pressure. The total suctions in the deformed specimen were measured to be 4579 kPa at 2 hours (point E) and 4270 kPa at 20 hours (point F) after the removal of the isotropic cell pressure. These

final suctions measured under atmospheric pressures were broadly similar to the initial suction of 4897 kPa prior to isotropic compression measured under similar atmospheric pressure condition. Similar observations were also made on the isotropically compressed specimens reported in Section 6.3.3. The similarity in suctions before and after testing was thought to be associated with elastic (recoverable) behaviour of the soil microstructure. This postulate will be discussed further in Chapter 9.

6.4.6 Summary

Four triaxial shear compression tests were carried out under constant mass and water content conditions. The objective of these tests was to examine the effect of shear stresses on suction measurements in unsaturated compacted sand-bentonite material using thermocouple psychrometers. The specimens were formed to a narrow range of dry densities of 1.40 Mg/m^3 to 1.43 Mg/m^3 at water contents of 18.1% to 19.0%. Prior to shearing, the specimens were isotropically compressed to different confining pressures of atmospheric pressure, 515 kPa, 1021 kPa, and 1494 kPa respectively. The results of compression was that they all had different initial suctions and degrees of saturation at the beginning of shear.

Because of their different initial conditions, the specimens behaved differently in shear. Specimen SB1880TS1 tested with atmosphere confining pressure was dilative in shear whereas Specimen SB1880TS2 sheared at the highest pressure of 1494 kPa was essentially ductile. In contrast, Specimens SB1880TS3 and SB1880TS4 sheared at intermediate pressures experienced strain-hardening behaviour. This is not the pattern that would be observed in saturated soils. The total suctions in each specimen tended to change with q and p* during shearing. It may be generally stated that for the dilative Specimen SB1880TS1, the suction tended to increase with straining, whereas for the other

specimens which were compressive in shear, the suctions in each specimen tended to decrease with increasing q and p*.

Final suctions in Specimen SB1880TS4 were measured at the end of shearing. Despite distortions in the specimen, the final suctions were broadly similar to the initial suction measured under atmospheric pressure. It is postulated that the reversal of suction was attributed to the elastic behaviour of the soil microstructure.

The observations from this limited number of shear tests are generally compatible with the behaviour that would be predicted by an elastic-plastic conceptual model for the shear and volume change behaviour of unsaturated sand-bentonite material.

6.5 Isotropic compression tests with volume change measurements

6.5.1 Background

It was pointed out in the beginning of this chapter that due to the limitation of the triaxial equipment used in this study, volume change measurements were not carried out in the first two series of triaxial tests. With the development of new volume change equipment, it became possible to undertake a third series of triaxial tests to examine the volume change - stress relationships of compacted sand-bentonite material. Information from this third series of test has been used to assist the interpretation of the results from the isotropic and shear compression tests with suction measurements using psychrometers presented in Sections 6.3 and 6.4.

6.5.2 Testing program

Six tests were carried out in this test series. Four specimens were compacted to a narrow range of initial dry densities of 1.40 Mg/m^3 to 1.45 Mg/m^3 at water contents of

16.4%, 18.7%, 20.3%, and 28.5% respectively. Two specimens were compacted to an initial dry density of 1.66 Mg/m^3 at water contents of 18.7% and 19.3% respectively.

Results from these tests are given in Figures 6.17 to 6.24. The data are presented in terms of volume strain ε_v - total stress p* relationships. The net volume strains of the specimens are summarized in Table 4.8. The stress path used in each test, and the initial and final conditions of the specimen are summarized as follows.

SB2180V1: This specimen was formed to an initial dry density of 1.45 Mg/m^3 at 20.3% water content, with an average degree of saturation of 63.8%. The specimen was subjected to several loading-unloading-reloading cycles, generally in successive total stress increments or decrements (Figure 6.17). It was first isotropically compressed to 1193 kPa, then unloaded to 503 kPa, reloaded to 1007 kPa, unloaded to atmospheric pressure, reloaded to 3137 kPa, and finally unloaded to atmospheric pressure. The final dry density and water content were 1.67 Mg/m^3 and 20.0% respectively. The final average degree of saturation was determined to be 87.9%.

SB1995V2: This specimen was formed to an initial dry density of 1.66 Mg/m^3 at 19.3% water content, with an average degree of saturation of 83.2%. The specimen was first isotropically compressed, in successive total stress increments, to a maximum total cell pressure of 3050 kPa (Figure 6.18). The specimen was then unloaded, in successive total stress decrements, to atmospheric pressure. The final dry density and water content were 1.72 Mg/m^3 and 19.5% respectively. The final average degree of saturation was determined to be 92.7%.

SB1680V3: This specimen was formed to an initial dry density of 1.40 Mg/m^3 at 16.0% water content, with an average degree of saturation of 47.4%. The specimen was first isotropically compressed, in successive total stress increments,

to a maximum total cell pressure of 3023 kPa (Figure 6.19). The specimen was then unloaded, in successive total stress decrements, to atmospheric pressure. The final dry density and water content were 1.63 Mg/m^3 and 17.0% respectively. The final average degree of saturation was determined to be 74.2%.

SB1880V4: This specimen was formed to an initial dry density of 1.40 Mg/m^3 at 18.6% water content, with an average degree of saturation of 54.2%. The specimen was first isotropically compressed, in successive total stress increments, to a maximum total cell pressure of 3075 kPa (Figure 6.20). The specimen was then unloaded, in successive total stress decrements, to atmospheric pressure. The final dry density and water content were 1.66 Mg/m^3 and 18.7% respectively. The final average degree of saturation was determined to be 81.2%.

SB1895V5: This specimen was formed to an initial dry density of 1.66 Mg/m^3 at 18.7% water content, with an average degree of saturation of 80.1%. The specimen was first isotropically compressed, in successive total stress increments, to a maximum total cell pressure of 3054 kPa (Figure 6.21). The specimen was then unloaded, in successive total stress decrements, to atmospheric pressure. The final dry density and water content were 1.72 Mg/m^3 and 18.4% respectively. The final average degree of saturation was determined to be 86.5%.

SB3080V6: This specimen was formed to an initial dry density of 1.42 Mg/m^3 at 28.5% water content, with an average degree of saturation of 85%. The specimen was first isotropically compressed, in successive total stress increments, to a maximum total cell pressure of 3068 kPa (Figure 6.22). The specimen was then unloaded, in successive total stress decrements, to atmospheric pressure. The final dry density and water content were 1.50 Mg/m^3 and 28.8% respectively. The final average degree of saturation was determined to be 97%.

6.5.3 Results

To facilitate discussion, the results from this test series are presented in two sections. Section 6.5.3.1 summarizes the results of Specimens SB2180V1, SB1680V3, SB1880V4, and SB3080V6, which were formed to initial dry densities of 1.41 Mg/m^3 to 1.43 Mg/m^3. Results of Specimens SB1995V2 and SB1895V5 are given in Section 6.5.3.2. These two specimens were formed to higher dry densities of 1.66 Mg/m^3.

6.5.3.1 Specimens SB2180V1, SB1680V3, SB1880V4, and SB3080V6

The ε_v - p* relationships of Specimens SB2180V1, SB1680V3, SB1880V4, and SB3080V6 were shown in Figures 6.17, 6.19, 6.20, and 6.22 respectively. The figures show that the ε_v - p* relationship for each specimen is hysteretic, and may be broadly divided into two parts: a first-time compression curve and an unloading curve. The difference between the loading and unloading paths may be attributable to the different compression and expansion behaviour of the macrostructure and microstructure that comprise the unsaturated compacted soil material. In general, the compression and expansion behaviour of unsaturated compacted sand-bentonite material are consistent with the observations made on natural soils and other compacted soils (Lambe and Whitman, 1969; Musa, 1982; Fredlund and Rahardjo, 1993). Specimen SB3080V6 was formed at a higher water content of 28.2% with an initial degree of saturation of 85%. It can be seen from the data in Figure 6.22 that the specimen became practically incompressible at pressures higher than 800 kPa. Figures 6.23 compares the ε_v - p* relationships of SB1680V3, SB1880V4, and SB2180V1 during first-time compression. From the figure, it can be seen that the first-time compression curves for these three specimens are broadly similar in value and approximately linear for pressures up to 1800 kPa. At total pressures above 1800 kPa, the compressibility of the specimens tended to decrease non-linearly with increasing pressure and with initial water content.

Specimen SB2180V1 which was formed at a higher water content of 21% became less compressible than the drier Specimens SB1880V4 and SB1680V3.

Specimen SB1680V3 was subjected to several cycles of unloading and reloading (see Figure 6.17). As expected, the specimen tended to expand with decreasing total stress. The unloading and reloading curves essentially followed the same path, and were different from the first-time compression curve. These observations of the stress-strain paths may again be taken to imply elastic-plastic behaviour of the unsaturated material. This postulate will be discussed further in Chapter 9.

The final unloading curves of Specimens SB1680V3, SB1880V4, SB2180V1, and SB3080V6 are shown in Figures 6.19, 6.20, 6.17, 6.22 respectively. The behaviour of Specimens SB1680V3, SB1880V4, and SB2180V1 were broadly similar. Generally, each specimen expanded with an expansive volume strain up to -1.5% when the total pressure decreased from the maximum testing pressure to about 100 kPa. When the pressure continued to decrease to atmospheric pressure, larger expansive volume strains up to -10% were recorded. In contrast, Specimen SB3080V6 behaved somewhat differently during unloading. This specimen was formed to a higher water content of 28.2%. This specimen became practically incompressible at pressures higher than 800 kPa (see Figure 6.22), suggesting that it may have become essentially saturated during the application of the cell pressure. During unloading, the volume of the specimen remained essentially constant as the pressure decreased from 3068 kPa to 800 kPa. As the pressure decreased below 800 kPa, the specimen tended to compress slightly with decreasing pressure. This unusual compression behaviour during unloading may be attributed to the possible increase in the effective stress in the soil structure due to the development of negative pore water pressures caused by the unloading process. Eventually, as the pressure decreased to atmospheric pressure, the specimen expanded with an expansive volume strain of -3.5%.

The final net volume strains of SB1680V3, SB1880V4 and SB2180V1 were compressive, and were measured to be 17.6%, 15.8%, and 13.1% respectively. In contrast, Specimen SB3080V6 had a smaller compressive net volume strain of 6.0%.

6.5.3.2 Specimens SB1895V5 and SB1995V2

The ε_v - p* relationships of Specimens SB1895V5 and SB1995V2 for first-time compression are compared in Figure 6.24. These two specimens were compacted to higher initial dry densities of 1.66 Mg/m^3. From the figure, it can be seen that Specimen SB1895V5 which was formed to a lower water content of 18% was less compressible during first time compression than Specimen SB1995V2. This is not the pattern that was observed in the *low density* specimens (see Figure 6.23). It is likely that the difference in the compression behaviour between the *low density* and *high density* specimens was attributed to the different soil structures in the two types of specimens. It is noted that the latter factor is influenced by the initial moulding water content and pressures used in the compaction process.

Consistent with the behaviour observed on the *low density* specimens, it can be seen from Figures 6.18 and 6.21 that Specimens SB1895V5 and SB1995V2 expanded during unloading. The expansive volume strains were generally small, up to -1%, as the total pressure decreased from the maximum testing pressure in each respective test to about 100 kPa. As the total pressure continued to decrease to atmospheric pressure, larger expansive volume strains were measured: -3.6% for Specimen SB1895V5 and -10.0% for Specimen SB1995V2.

The final net volume strains of Specimen SB1895V5 and SB1995V2 specimens were compressive, and were measured to be 3.0% and 3.1% respectively. These volume strains were less than those experienced by the *lower density* specimens reported in Section 6.5.3.1.

6.5.4 Summary

This section has presented results from six triaxial compression tests with volume change measurements. Four specimens were compacted to a narrow range of initial dry densities of 1.40 Mg/m^3 to 1.45 Mg/m^3 at water contents of 16.4%, 18.7%, 20.3%, and 28.5% respectively. Two specimens were compacted to an initial dry density of 1.66 Mg/m^3 at water contents of 18.7% and 19.3% respectively.

The results presented in this section show that the volume change behaviour of unsaturated compacted sand-bentonite material investigated in this study was hysteretic under load-unload cycling. Consistent with observations made on natural soils and other compacted soils, the unsaturated sand-bentonite material was more compressible during first-time compression than during subsequent unloading/reloading cycles. It is postulated here that the different stress-strain paths followed by the unsaturated material during the loading and unloading phases reflect elasto-plasticity in the soil macro- and micro-structures within the compacted material. This postulate will be examined further in Chapter 9.

CHAPTER 7 MERCURY INTRUSION POROSIMETRY STUDIES

7.1 Background

It was hypothesized in Chapter 5 that the suction properties of the sand-bentonite material, sand-illite material and Boom Clay tested in this study are controlled by the soil microstructures. Chapter 6 presented results from triaxial compression tests on unsaturated sand-bentonite material with suction measurements using thermocouple psychrometers. It was postulated that the effects of stress variation and deformation on suction can be explained by consideration of the capillary phenomenon which is related to the soil fabric and associated voids in the unsaturated material. To provide the background information necessary for the interpretation of results from the suction tests and the triaxial tests, series of tests using mercury intrusion porosimetry (MIP) were carried out. The objective of these MIP tests was to measure and compare the pore size distributions (PSD) of the sand-bentonite material, sand-illite material and Boom Clay tested in this study. This chapter presents the results from these tests.

The pore size distributions are presented in terms of incremental intrusion - diameter relationships and cumulative intrusion - diameter relationships. It is noted that the spatial distribution of pores within a specimen cannot be determined from these relationships. The incremental intrusion - diameter relationship provides information on the total volume of pores per unit mass of dry soil at a given pore diameter. This type of relationship allows better assessment of the soil fabric and voids in a specimen (Garcia-Bengochea et al., 1979). The cumulative intrusion - diameter relationship gives the total volume of pores per unit mass of dry soil for a given range of pore diameters. In this chapter, results will be discussed mainly based on incremental intrusion - diameter relationships.

7.2 Relation between clay mineralogy and pore size distribution

Figure 7.1 compares the pore size distributions of typical specimens of the sand-bentonite material, sand-illite material, and Boom Clay during the intrusion stage. The sand-bentonite and sand-illite specimens were formed to 95% maximum dry density at their respective optimum water contents. In contrast, the Boom Clay specimen was compacted to 90% maximum dry density. The dry density and water content at compaction were 1.67 Mg/m^3 and 17.6% for the sand-bentonite material, 2.08 Mg/m^3 and 9.0% for the sand-illite material, and 1.81 Mg/m^3 and 16.8% for Boom Clay.

From Figure 7.1a, it can be seen that the incremental intruded pore volume - diameter relationships of the three specimens are different in shape. The Boom Clay specimen showed a singular distribution with a distinct peak at about 0.06 μm. The pore diameters of this specimen generally fell between 0.004 μm to 0.4 μm. In contrast, the pore size distributions of the compacted sand-illite and sand-bentonite specimens were multi-modal. The sand-illite specimen displayed two distinct modes: a large- and small-pore modes, whereas the sand-bentonite specimen had three distinct modes: large-, intermediate- and small-pore modes. Similar observations on multi-modal PSD's are made on other compacted sand-clay materials (Garcia-Bengochea et al., 1979).

To aid the interpretation of results from the MIP studies, the soil structure of a limited number of sand-illite and sand bentonite specimens were examined using scanning electron microscopy (SEM). Boom Clay was not tested using SEM because only a limited quantity of material was available for testing. Equipment and procedures used in the SEM analyses were described in Section 4.6. Photo micrographs of typical specimens of sand-illite and sand-bentonite materials are shown in Figure 7.2. It can be seen from the observations in the figure that the sand particles in these specimens were not in direct contact with each other. Therefore it can be concluded that the pore size distributions in

the sand-clay materials tested in this study reflected largely the pore structures in the clay phase of the soil.

For the sand-illite specimen, the large pore mode occurred at the pore diameter range of 50 μm to 150 μm, whereas the small pore mode generally lay within 0.04 μm and 0.2 μm (Figure 7.1a). The range of pore diameters in the small pore mode was generally one order of magnitude larger than the thickness of an individual illite particle with a typical thickness of 0.005 μm to 0.03 μm (Yong and Warkentin, 1975; Mitchell, 1976; Hillel, 1980). It may be interpreted from this observation that the small pore mode represents inter-domain pores, that is, pores between groups of parallel clay particles. The bimodal pore size distribution observed in the sand-illite material tested in this study is consistent with the observations made on other non-swelling sand-clay materials (Garcia-Bengochea et al., 1979; Juang and Holtz , 1986).

The sand-bentonite specimen had a trimodal distribution (Figure 7.1a). The three distinct modes occurred at pore diameters of about 20 μm, 2 μm, and 0.01 μm respectively. Both the large and small pore modes of the sand-bentonite material were generally one order of magnitude smaller than the respective pore modes of the sand-illite material (Figure 7.1a). The pore diameters represented by the small pore mode measured in this specimen generally varied from 0.007 μm to 0.025 μm. These pore diameters were similar in size to the range of thickness of bentonite particles which is generally accepted to be 0.001 μm to 0.01 μm (Yong and Warkentin, 1975; Mitchell, 1976; Hillel, 1980). From the observations on this specimen and other sand-bentonite specimens tested in this study, it may be interpreted that the small pore mode represents the pores at the microscopic particle level.

For both the sand-bentonite and sand-illite specimens, the large pore modes are interpreted as inter-ped pores. A ped is a conglomeration of clay particles, domains, and clusters (see Section 2.3.2). These interpretations are supported by observations from

photo micrographs. Figure 7.3 shows the soil structures in typical specimens of compacted sand-bentonite and compacted sand-illite materials. For the sand-bentonite material, the soil structure consists mainly of peds (marked P) with interconnecting voids (marked V). The inter-ped voids are generally larger than 10 μm in size. This size range corresponds to the large pore mode in the pore size distribution. Similarly, the soil structure in the sand-illite specimen is dominated by peds. The inter-ped voids are interconnected and are generally larger than 10 μm in size. These voids are interpreted as the large pore mode in the pore size distribution. It should be noted that due to the limitation of the scanning electron microscope used in this study, features less than 1μm in size could not be examined quantitatively. Therefore, measurements of soil fabric and associated voids using scanning electron microscopy are restricted only to sizes larger than 1 μm.

7.3 Relation between compaction variables and pore size distribution

In this section, the relations between compaction variables (that is, dry density and water content) and pore size distribution in compacted clays are examined. The discussion is based on the results from tests on the sand-bentonite and sand-illite materials used in this study, and the data on an illitic clay reported by Gelmich (1994). It should be noted that the illitic clay used by Gelmich (1994) was mineralogically identical to the clay component of the sand-illite material tested in this study.

The relationships between dry density and PSD are first examined. Data for sand-bentonite material, sand-illite material and illitic clay are presented in Figures 7.4 to 7.7. In each figure, the pore size distributions of specimens formed to the same initial water content but different dry densities are compared. The following general observations are made.

One, for a given water content, the small pore mode remained virtually unchanged irrespective of the dry density of the specimen. Consistent with the data in Figure 7.1, the small pore mode occurred at about 0.01 μm for the sand-bentonite material (Figures 7.4 and 7.5), 0.1 μm for the sand-illite material (Figure 7.6), and 0.15 μm for the illitic clay (Figure 7.7).

Two, the areas under the large and intermediate pore modes tended to decrease with increasing dry density. This observation may be taken to imply that specimens formed at high densities have less volume of inter-ped pores.

Three, it may be inferred from the data in Figures 7.4b and 7.5b that the uncompacted sand-bentonite specimens had lower total porosities than the compacted specimens formed at dry densities of 1.41 M/m^3. Conversely, for the sand-illite material, the uncompacted specimen had the lowest total porosity, compared to the compacted specimens (Figure 7.6b). The smaller pore volumes measured in the uncompacted specimens can be explained by consideration of the testing procedures used in specimen preparation and in the mercury intrusion porosimetry testing. It has been discussed in Section 7.3 that the soil structure in a compacted clay consists of clay peds with interconnected pores. In an uncompacted material, peds tend to exist as individual units. Compaction leads to interactions between individual peds, creating inter-ped voids. The size and distribution of these voids depend largely on the compaction method and forces used in specimen preparation. In a mercury intrusion porosimetry test, the setting-up involves first placing adequate quantity of soil material into the chamber of the penetrometer, followed by the flooding of the chamber with mercury (Figure 7.8). For an uncompacted material, inter-ped voids would be readily filled with mercury (Figure 7.8a). Hence only the intra-ped voids would be intruded during testing. However, low compaction efforts cause peds to bridge over one another, thereby creating additional voids. These inter-ped voids specimen would not be filled during setting-up, and would

become part of the measurable pore structure in the material (Figure 7.8b). The practical implication of the observations in Figures 7.4 to 7.7 is that the large and intermediate pore modes are functions of specimen preparation. The soil structure represented by these two pore modes can be influenced and altered by external forces and processes.

The effect of water content on pore size distribution is examined in Figures 7.9 to 7.11. In each figure, the pore size distributions of specimens formed to the same dry density but different water contents are compared. Figures 7.9 and 7.10 present the data for the sand-bentonite material. The data for illitic clay are compared in Figure 7.11.

From Figures 7.9 and 7.10, it can be seen that for the narrow range of water content from 17.6% to 20.3% used in this study, the pore size distribution of compacted sand-bentonite material was largely unaffected by water content. However, the "wetter" specimens generally showed larger volume of inter-ped pores than the "dryer" specimens. This is inferred from the difference in the total porosities determined from the cumulative intrusion - diameter relationships (Figure 7.9b and 7.10b).

Figure 7.11 compares the pore size distributions of four illitic clay specimens formed to the same initial dry densities of 2.04 Mg/m^3 at different water contents of 10% to 13%. It may be inferred from the data in Figure 7.11 that, with increasing water content, the area under the large pore mode of the PSD decreased while the area under the small pore mode increased. Furthermore, with increasing water content, the large mode pore tended to shift to smaller diameters. At higher water contents, the clay particles were better hydrated, and they tended to form larger and more deformable peds consisting of clay domains, clusters, and intra-ped voids. In general, the data in Figure 7.11 show that increasing water content led to an increase in intra-ped pores, accompanied by a decrease in the inter-ped pores.

Broadly, it can also be seen in Figure 7.11 that the PSD's of the specimens formed at the optimum water content of 12% and at the wet-of-optimum water content of 13%

are broadly similar. That is, the soil structures were similar. Similarities in soil structures in specimens formed at and wet-of-optimum water contents have been observed in other non-swelling clay materials (Garcia-Bengochea et al., 1979; Juang and Holtz, 1986).

7.4 Comparison in pore size distributions between pure clay specimens and sand-clay specimens

The pore size distributions of a sand-bentonite material, natural bentonite, sodium bentonite, and calcium bentonite are compared in Figure 7.12. The sand-bentonite specimen was prepared from a sand-bentonite-water mixture, and was compacted to a dry density of 1.67 Mg/m^3 at 17.6% water content. This dry density corresponds to a clay dry density γ_c of 1.22 Mg/m^3. The clay dry density is defined as the mass of clay divided by the total volume of clay and voids (Sun, 1986). The natural bentonite had the same mineralogical composition as the clay component in the sand-bentonite specimen (Quigley, 1984). Because of its small size and irregular shape, the density of the natural bentonite specimen was not measured. Based on the data reported by Oscarson et al. (1990), it was assumed that the natural bentonite specimen had a clay dry density of 1.2 Mg/m^3. The water content of the bentonite specimen prior to MIP testing was measured to be 5.4%. The sodium bentonite specimen was prepared from dry sodium bentonite powder and compacted to a dry density of 1.3 Mg/m^3 (Choi and Oscarson, 1996). The compacted specimen was then allowed to saturate in a NaCl solution (100 mol/m^3) under low hydraulic head, constant volume conditions for about two weeks. Similar procedures using calcium bentonite powder and $CaCl_2$ solution (50 mol/m^3) were used to prepare the calcium bentonite specimen.

From Figure 7.12, it can be seen that the sand-bentonite specimen has a trimodal pore size distribution, compared to a bimodal distribution for the calcium bentonite

specimen and singular distributions for the sodium bentonite and natural bentonite specimens. The differences in the shape of the pore size distribution of the four bentonite materials may be attributed to two factors. One, the procedures used in specimen preparation were different. Two, the sand particles in the sand-bentonite material influence the soil structure during material and specimen preparation, resulting in multi-modal PSD in the material. It is postulated that the sand particles provided the nuclei for the hydrated clay particles, domains, and peds to coalesce to form larger peds. Lower water contents and the presence of peds gave rise to the development of intra- and inter-ped pores. This postulate is based on limited data and requires further investigation.

Referring again to the data in Figure 7.12, the range of pores represented by the small pore mode in the pore size distribution appeared to be largely independent of the sand content and the type of bentonite. All four bentonite materials showed a peak at a pore diameter of 0.01 μm to 0.02 μm. Based on this observation and on the results reported in Sections 7.2 and 7.3, it may be concluded that the location of the small pore mode in the PSD qualitatively reflects the basic clay minerals in the soil (Garcia-Bengochea et al., 1979).

The data in Figure 7.12 also show that the area under the small pore mode differed between bentonites. It may be inferred from this observation that the natural bentonite specimen had a larger volume of intra-ped voids than the sand-bentonite specimens and the bentonite specimens. The difference in intra-ped voids may be explained by consideration of the availability of moisture for the hydration of the clay particles during specimen formation. The sand-bentonite specimen was formed from a moist sand-clay mixture and had a dry density of 1.67 Mg/m^3 at 17.6%. At this density, the theoretical maximum water content is 23%. Therefore, the sand-bentonite specimen was in a state of moisture deficiency. That is, not all the clay particles were hydrated. Therefore the specimen tended to have lower volume of intra-ped voids.

Low hydraulic gradients were used to saturate the sodium and calcium bentonite specimens in a confined apparatus. Given the short duration of two weeks used for saturation, it is likely that this method of preparation was not effective in producing fully saturated specimens. It may be assumed that the sodium and calcium bentonite specimens were also in the state of moisture deficiency.

The natural bentonite was an intact specimen from the field. Natural bentonitic clays in North America generally derived from geochemical alteration of volcanic ash deposited into shallow marine basins (Dixon et al., 1992b). By considering the environment in which this natural specimen was formed, it is reasonable to assume that the natural bentonite specimen was fully saturated in the field. It is likely that the higher field water content in the natural bentonite led to better hydration of the clay particles, giving rise to a larger volume of intra-ped voids.

The data in Figure 7.12 show that the natural bentonite and the sand-bentonite material contain the same bentonite clay minerals, and have similar micropores as reflected by the range of pores represented by the small pore mode in the PSD's. Therefore suctions which are controlled largely by the micropores, are similar in both materials. However, the areas under the respective small pore modes in the PSD's are different, indicative of different water contents. That means the same suction may exist at different water contents. That is, albeit they have the same clay mineralogy, the soils have different suction-water content relationships. This latter observation has practical implications on the use of psychrometers to measure *in situ* water contents in compacted clays. Knowledge of changes in the water content of soil is a subject of interest in problems of heave and settlement, and heat and moisture flow in unsaturated soils (Fredlund and Rahardjo, 1993; Thomas and He, 1995). Psychrometers measure soil suctions, which in turn can be converted to water contents using a suction-water content relationship (Silvestri, 1994). To obtain accurate water content values, the appropriate

suction-water content relationship of the soil needs to be established and used for the conversion.

7.5 Effect of saturation on pore size distributions in compacted clays

Transport processes in compact soils such as moisture flow, radionuclide migration, gas transport, and microbial activities are influenced by soil fabrics and associated voids (Mitchell, 1976; Pusch et al., 1989; Pusch et al., 1990; Stroes-Gascoyne and West, 1994; Choi and Oscarson, 1996). In particular, it has been shown that water permeability of a compacted soil can be correlated with the large pore mode in the pore size distribution (Garcia-Bengochea et al., 1979; Juang and Holtz, 1986). It is commonly understood that moisture and air movement in a soil generally lead to changes in the effective stress and pore pressures in the soil (Matayas and Radhakrishna, 1968; Fredlund and Rahardjo, 1993). Stress variations are often accompanied by volume change and deformation of the soil structure in processes such as swelling and consolidation. Changes in the soil structure in turn influence the transport properties of the soil. In this section, the effect of water saturation on the PSD's of compacted clays is examined.

Figure 7.13 compares the PSD's of two sand-bentonite specimens which were formed to different saturations prior to drying for MIP testing. One specimen was formed to an initial dry density of 1.67 Mg/m^3 at 17.6% water content, with a initial degree of saturation of 85%. This specimen was dried in an oven at 110°C immediately after formation. The other specimen had an initial dry density of 1.68 Mg/m^3 at 14.9% water content. It was saturated in a permeability apparatus under low hydraulic gradients (Dixon, personal communication). The final water content of the specimen was measured to be 27.4 %. This specimen was also dried in an oven at 110°C prior to MIP testing.

Form Figure 7.13b, it can be seen that the total intrusion of 0.1179 ml/g of the "saturated" specimen was less than the total intrusion of 0.1888 ml/g of the "unsaturated"

specimen. Both specimens showed similar small pore modes. This observations may be taken to imply that the intra-ped pore structures were unaffected by the saturation process. However, water saturation affected the large pore mode. Comparing with the "unsaturated" specimen, the "saturated" specimen showed a broader and "depressed" large pore mode, and its intermediate pore mode was almost eliminated by the saturation process.

Based on the limited data presented in this section, it may be tentatively concluded that the saturation process largely influences the inter-ped pores in compacted clays. The observation has practical implications. Water permeabilities and other transport properties of compacts clays are largely governed by inter-ped pores (Garcia-Bengochea et al., 1979; Juang and Holtz, 1986; Kirkham, 1995). It is tentatively suggested that changes in the pore size distribution at the inter-ped level can affect moisture and gas flow, and other transport phenomena in a compacted clay. However, the data are limited and do not lead to a firm conclusion. To clarify the effect of saturation on PSD's and transport properties in compacted clays, further tests are recommended.

7.6 Effects of isotropic and shear compression stresses on pore size distribution

This section examines the effects of isotropic compression stress and shear stress on pore size distribution in unsaturated sand-bentonite material. The results from the isotropic compression and shear tests were presented in Chapter 6.

Figure 7.14 compares the pore size distributions of four specimens tested in isotropic compression. These specimens were formed to similar initial dry densities of 1.40 Mg/m^3 to 1.45 Mg/m^3 at water contents of 16.4% to 28.5%. They were then isotropically compressed up to a maximum confining total stress of 3100 kPa. The PSD of an intact specimen with a dry density of 1.41 Mg/m^3 and 17.6% water content was

also included in Figure 7.14 for comparison. In Figure 7.15, the PSD's of two specimens formed at initial dry densities of 1.66 Mg/m^3 at 18.7% and 19.3% water contents respectively are compared. These two specimens were also isotropically compressed up to a maximum confining total stress of 3050 kPa. The PSD of an intact specimen with a dry density of 1.67 Mg/m^3 at 17.6% was also included in Figure 7.15 for comparison.

From Figures 7.14 and 7.15, it can be seen that the small pore mode appeared to be unaffected by the isotropic compression stresses. However, the compressed specimens had smaller intermediate and large modes than the intact specimens. It appears that an increase in total stress on a compacted clay leads to a decrease in inter-ped pores in the soil.

Figure 7.16 compares the PSD's of four sand-bentonite specimens which were tested in shear tests. These specimens were formed to similar initial dry densities of 1.40 Mg/m^3 to 1.43 Mg/m^3 at water content of 18.1% to 19.0%. Each specimen was then isotropically compressed to a different confining pressure of 0 kPa, 515 kPa, 1021 kPa, or 1494 kPa, and sheared under constant mass conditions. The PSD of an intact specimen with a dry density of 1.67 Mg/m^3 at 17.6% was also included in Figure 7.16 for comparison. Similar to the observations on the isotropically compressed specimens seen in Figures 7.14 and 7.15, the small pore modes in the sheared specimens appeared to be unaffected by the isotropic compression and shear stresses. However, the areas under the large and intermediate pore modes tended to decrease with increasing total and shear stresses. In particular, it may be inferred from Figure 7.16 that the inter-ped pores in the specimen tested at 1494 kPa was almost completely eliminated by shearing, as indicated by the broad and depressed shape of the large pore mode.

It was discussed in Section 7.5 that the transport properties of a compacted clay are influenced by the large pore mode (that is, inter-ped pores). Results presented in this section (7.6) showed that the large pore mode is affected by mechanical processes such as

compression and shearing. Based on the data presented in this section, it may be concluded that among other factors, the transport properties of a compacted clay can be influenced by stress variations and deformations. The latter factors in turn depend on boundary and loading conditions, and other external and mechanical forces.

The implications of stress-induced changes in soil structures on suction measurements using psychrometers will be discussed in detail in the Chapter 9.

7.7 Comparison between measured and theoretical porosities

The measured and theoretical porosities of compacted specimens of the soils tested in the MIP studies are compared in Figure 7.17. Expressions used to determine the measured porosity n and theoretical porosity n_T are given as follows.

Measured porosity:

$$e = \text{Total Intrusion} \times G_c \times \gamma_w \qquad [7.1]$$

$$n = \frac{e}{1+e} \qquad [7.2]$$

Theoretical porosity:

$$e_T = \frac{G_c \times \gamma_w}{\gamma_c} - 1 \qquad [7.3]$$

$$n_T = \frac{e_T}{1+e_T} \qquad [7.4]$$

where e is the measured porosity, e_T is the theoretical porosity, G_c is the specific gravity of the clay phase, γ_c is the clay dry density, and γ_W is the density of water. It was pointed out in Section 7.2 that mercury intrusion took place in the clay phase of the soil

being tested. Therefore, the clay dry density was used in the calculations, and a specific gravity of 2.75 was assumed for all the soils.

Two observations can be made from the data in Figure 7.17. One, the measured porosities in compacted illite-based materials were consistently lower than the theoretical porosities. Furthermore, the measured values appeared to be largely independent of the clay dry density, varying generally between 0.20 and 0.25. Hence, the lower the clay dry density of the specimen, the larger the difference between the measured and theoretical porosities. Two, the measured porosities in the bentonite-based materials were also consistently lower than the theoretical porosities, by a factor of up to 2. The discrepancy between the measured and theoretical porosities is likely attributed to several factors which include occluded or isolated voids, pressure capacity of the mercury porosimeter, specimen disturbance due to drying, and specimen disturbance during testing (see Section 4.5.6).

7.8 Summary

Mercury intrusion porosimetry tests were carried out to examine the fabric and pore structures in the sand-bentonite material, sand-illite material, and Boom Clay used in this study. Occluded air, porosimeter capacity, and specimen disturbance during drying and testing were identified as potential factors in contributing to the inaccuracy of total porosity measurements in these soils. Because of the influence of these factors, information provided by mercury intrusion porosimetry is only qualitative.

Based on the data presented in this chapter, it can be concluded that the soils used in this study had complex soil structures characterized by conglomerations of clay particles, peds, and voids. These soils had a wide range of pore diameters with bi-modal or tri-modal pore size distribution curves. In general, the pores in these soils may be broadly classified into two main groups. Intra-ped pores are microscopic pores inside

macroscopic peds comprising of clay particles, domains, and clusters. These pores are depicted by the small pore mode in the incremental intrusion - diameter relationship. The small pore mode appears to be uniquely related to the clay mineralogy. Inter-ped pores are macroscopic pores between clay peds. These pores are represented by the large pore mode. External boundary and mechanical forces affect the large pore mode. The implication of the latter observation is that a change in the inter-ped pores may lead to changes in the transport properties of a compacted clay. The implications of stress-induced changes in soil structures on suction measurements using psychrometers will be discussed in detail in Chapter 9.

Comparison of the PSD's of natural bentonite and sand-bentonite material show that while the soils have the same bentonite minerals, their respective suction-water content relationships may be different. To obtain accurate water content values using psychrometers, the appropriate suction-water content relationship of the soil needs to be established and used for converting suctions to water contents.

CHAPTER 8 BUFFER/CONTAINER EXPERIMENT

8.1 Background

It was stated in Chapter 2 that one of the objectives of this study was to investigate the usefulness of thermocouple psychrometers to measure *in situ* suctions and water contents in unsaturated compacted soils under the influence of temperature gradients. This chapter presents results from an *in situ* experiment called the Buffer/Container Experiment that was carried out to examine the performance of an unsaturated compacted sand-bentonite material when used as an engineered barrier for the isolation and disposal of heat generating radioactive waste. In the experiment, the author was responsible for developing the psychrometer technology that was used to track changes in suction and water content in the unsaturated material under the influence of temperature and hydraulic gradients. Discussion of the results in relation to the usefulness and limitations of psychrometers as moisture sensors is given in Chapter 9.

8.2 Canadian Nuclear Fuel Waste Management Program

Atomic Energy of Canada Limited (AECL) is investigating the feasibility of underground disposal of heat generating nuclear fuel waste in granite plutons in the Canadian Shield (AECL, 1994). In the borehole emplacement concept, immobilized waste would be placed in corrosion-resistant containers. These containers would be deposited in boreholes drilled into the floor of rooms in an underground repository located 500 m to 1000 m below ground surface. A sand-bentonite material, known as buffer, would separate the waste container and the host rock. The purpose of the buffer is twofold: to provide structural support to the waste container, and to minimize the release of radionuclides from any breached containers to the biosphere. As a contribution to assessing the borehole emplacement concept, a field scale experiment known as the

Buffer/Container Experiment was carried out at AECL's Underground Research Laboratory (URL), a research facility constructed in a granite pluton near Lac du Bonnet in Manitoba.

8.3 Buffer/Container Experiment

An objective of the Buffer/Container Experiment was to examine the processes of heat and moisture flow in unsaturated buffer under imposed thermal gradients. Figure 8.1 shows a schematic of the Buffer/Container Experiment. The experiment was carried out in a test hole drilled into the floor of a room excavated 240 m beneath the ground surface at AECL's URL. The test-hole was 1.24 m in diameter and 5 m deep. Sand-bentonite buffer was compacted *in situ* into the hole to an average dry density of 1.73 Mg/m^3, at a water content of 18% and an average degree of saturation of 85%. An electrical heater 2.25 m long and 0.64 m in diameter, was buried in the buffer on the vertical axis of the borehole to provide the heat source. The heater has similar dimensions to the containers being proposed for the disposal of Canada's nuclear fuel waste.

Construction of the experiment began in May 1991. Some 500 geotechnical instruments were installed, where appropriate, in the buffer, the host rock and the heater to measure changes in temperature, total and pore pressures, suction and water content (Kjartanson and Keil, 1992). The heater was turned on in November 1991 and provided heat at a constant rate. During the first three weeks of heating, the heater output was maintained at 1000 W. Thereafter the power to the heater was increased to 1200 W and maintained at that value for the following two and a half years. More details of the general aspects of the layout, operation, and results of the experiment are presented by Graham et al. (1996).

8.4 Moisture sensor measurement scheme

To assess moisture distributions during the experiment, commercial moisture sensors were installed in strategic locations within the buffer mass. The water contents in the buffer were measured indirectly using commercially available thermocouple psychrometers and thermal needles. The rationale for the selection of these two types of sensors was discussed by Wan et al. (1992). The moisture sensors were read and recorded using computer based data acquisition systems.

Seventeen psychrometers were installed in the buffer close to the borehole wall where moisture increase was anticipated (Figure 8.2). The instruments were Type PCT-55 manufactured by Wescor Inc. in Logan, Utah, USA. They are the same type of instruments used in the laboratory testing program described in Chapters 4 to 6 of this thesis. The performance and accuracy of the Wescor Type PCT-55 thermocouple psychrometers were discussed in Chapter 3. Slight modifications were done to the psychrometers used in the field experiment. To ensure durability of the instrument, each psychrometer was structurally modified by replacing its vinyl boot with a heat shrink wrapping material and by fitting flexible temperature-resistant tubing over the cable lead (Figure 8.3). The scheme for instrument calibration developed by the author and described in Chapter 3 of this document was used to pre-calibrate the instruments used in the Buffer/Container Experiment.

Twenty one thermal needles were used to measure thermal conductivities in the buffer at selected times during the test. The thermal conductivities were converted to water contents using laboratory defined thermal conductivity-water content relationships (Figure 8.4). The thermal needles were installed in buffer close to the heater where moisture depletion was anticipated (Figure 8.2). The thermal needles were manufactured by Geotherm Inc., Newmarket, Ontario, Canada. Each instrument was 3 mm in diameter, 100 mm long. The instrument is essentially a sealed 304 grade stainless steel tube

containing a high-precision thermistor and a miniature electrical heater. The operation of the instrument is based on the transient probe theory (Blackwell, 1954). The instrument is assumed to be infinitely long and remote from boundaries and other heat sources. It evaluates thermal conductivity from a measured relationship between temperature and time during a constant-power heating pulse lasting several minutes.

8.5 General observations

To provide background information for the discussion of results from the psychrometers used in the Buffer/Container Experiment, this section presents an overview of the general observations in the experiment. It has been shown here through Chapters 1 to 7 that temperature and pressure can influence psychrometer output and hence data interpretation. Thus, particularly, emphasis is given to temperatures and total pressures developed in the unsaturated sand-bentonite buffer during the isothermal and heating phases of the Buffer/Container experiment. A more complete review and synthesis of the results of the experiment are given by Graham et al. (1996).

8.5.1 Temperatures

Some 110 thermocouples and 10 thermistors were installed in the unsaturated buffer, the heater, and the host rock to measure temporal and spatial variations in temperature during the course of the experiment. During the installation phase of the experiment before heating, the ambient air temperature in the room above the experiment generally varied between 15°C and 18°C. The rock temperatures were lower, varying from 12°C to 15°C. The difference in temperature between the air and the rock gave rise to a gradient of 0.5°C/m in the first 5m of the rock and away from the floor of the test room.

The heater was powered on November 20, 1991. This event is denoted as elapsed time = 0 in all the data presented subsequently. The power to the heater was initially maintained at 1000 W. Figure 8.5 shows the evolution of temperature on the heater surface and in the buffer at the mid-height level of the heater. At the onset of the heating phase, the temperature in the system increased rapidly. After about two weeks of heating, the average temperature on the surface of the heater levelled off at about 68°C. The power to the heater was then increased to 1200 W and was maintained at that power for about two and a half years. It can be seen from Figure 8.5 that, in response to the change in power, the temperatures in the system increased quickly in the first 6 weeks. Thereafter, the temperature increase slowed to a steady rate of about 0.05°C/day. At the end of the experiment, the nominal temperature at the heater surface was measured to be 86°C.

The evolution of temperatures within the sand, buffer and backfill along the centreline of the experiment is shown in Figure 8.6. Temporal variations in temperature in the sand and buffer at the mid-height level of the heater are shown in Figure 8.7. From Figures 8.6 and 8.7, it can be seen that temperature gradients quickly developed within the first week of heating. Thereafter, the gradients within the system remained generally stable with time unless the power to the heater was changes. Figures 8.6 and 8.7 show that temperature gradients were about 370°C/m in the silica sand layer surrounding the heater. Temperature gradients of up to 100°C/m were measured in the 25 cm thick buffer annulus and in regions immediately above and below the heater.

8.5.2 Total pressures

The total pressures in the Buffer/Container Experiment were measured by thirteen Geonor vibrating wire type total pressure cells and five Roctest pneumatic pressure cells. The Geonor cells were installed at the buffer/rock interface to measure horizontal total

pressures exerted by the unsaturated buffer on the rock. The vertical pressures were measured by Roctest pneumatic pressure cells embedded within the unsaturated material and one Geonor cell mounted flush with the rock at the bottom of the test hole. The results are presented in Figures 8.8 to 8.16. It should be noted that, for clarity, the vertical scales in Figures 8.8 to 8.13 are different.

Figures 8.8 to 8.11 show the total pressure responses of four paired Geonor cells located above and below the heater, and at the mid-height of the heater. The difference in response between paired cells at the same elevation is attributed to minor difference in the compaction procedures and to local variations in the porosities of the rock (Graham et al., 1996). The latter factor influenced the supply of moisture, and hence the development of pressure in the buffer that was originally unsaturated. Figures 8.12 and 8.13 show the total pressure responses within the buffer measured by the Roctest load cells. Figures 8.14 to 8.16 show the total pressure distributions along the buffer/rock interface and within the buffer at different times of the experiment.

8.5.2.1 Observations before heater activation

The buffer was placed *in situ* by compacting sand-bentonite material in 50-mm lifts, to a target dry density of 1.73 Mg/m^3 (Kjartanson et al., 1992). Locked-in stresses of up to 300 kPa were measured along the buffer rock interface and within the buffer (Figures 8.8 to 8.16). From Figures 8.14 and 8.15, it can be seen that the locked-in stresses are generally higher along the length of the heater in the middle portion of the experiment. It is noted that the psychrometers were installed in vertical cavities drilled into the buffer at the end of each compaction interval. It was assumed that the locked-in stresses in the compacted material had no effect on the initial suction measurements from the psychrometers.

A cavity measuring 0.74 m in diameter and 2.66 m long was created within the buffer mass to house the heater. The cavity was formed by compacting sand-bentonite material in the annular space between a collapsible steel liner and the wall of the test hole. For the cells located in this buffer annulus region, pressures decreases were noted when the collapsible liner was removed (see Figure 8.10, at minus 120 days).

During the pre-heating, installation, phase of the experiments (prior to Day 0), generally, all the Geonor cells located around and below the heater (such as BG7, BG8, BG11, BG12, and BG13), and all the Roctest test cells (BR1 to BR5) registered increases in total pressure with time (Figures 8.10 to 8.13). The rate of increase in total pressure ranged from about 10 to 70 kPa/month. It can be inferred from the gradual pressure increases that moisture was being taken up from the rock by the unsaturated buffer.

The pressure distributions immediately before heater activation are shown in Figures 8.14 to 8.16. The total pressures along the buffer/rock interface and within the buffer generally lay between 50 kPa and 350 kPa These pressures were consistently lower than the maximum swelling pressure of 0.8 MPa to 1.5 MPa measured in saturated specimens from laboratory tests (Dixon et al., 1987).

In general, at the start of the heating phase, the net increases in total pressure with respect to the initial locked-in stresses were small, compared with the swelling pressures in fully saturated material. Values up to 143 kPa were measured at the buffer/rock interface; values up to 137 kPa were measured within the buffer. It was assumed that the changes in total stress during the installation phase had no effect on the suction measurements from psychrometers.

The following conclusions are drawn from the observations made of pressure changes during the pre-heating phase of experiment. First, immediately after emplacement, the unsaturated buffer began to take on moisture from the surrounding rock. Second, the buffer had not reached pressure-water content equilibrium prior to the

activation of the heater. Third, net increases in total pressure along the buffer/rock interface and within the buffer, with respect to the initial locked-in stresses, were small and were assumed to have no effect on the suction measurements from psychrometers.

8.5.2.2 Observations after heater activation

All the cells responded to activation of the heater. Cells which were located in regions above and below the heater (BG1 to BG4, BG11 to BG13, BR1 to BR3) generally showed a rapid increase in total pressure in the first 100 days (Figures 8.8, 8.9, 8.11, and 8.12). Thereafter the total pressures continued to increase, but at a slower rate.

Cells that were around and beside the heater (such as BG7, BG8, BR4 and BR5), all showed strong increases in total pressure at the activation of the heater (Figures 8.10 and 8.13). However, these rapid pressure increases were transient. Generally, after 1 month of heating, the total pressure had decreased quite sharply, and thereafter changes took place more slowly. Four of the eight cells (such as BR4 and BR5) showed systematic pressure increase with time. However, the other four cells (such as BG7 and BG8) which were located beside the heater in the upper region of the buffer annulus showed total decrease with time.

Figures 8.14 and 8.15 show the horizontal total pressures distributions measured by the Geonor cells at the buffer/rock interface at three days after heater activation and at the end of the test. Figure 8.16 shows the five day and end-of-test data for vertical total pressures from the Roctest pressure cells. It can be inferred from these data that total pressures tended to increase with time in regions above and below the heater, whereas pressures in the annulus region beside the heater tended to decrease with time. Variations in total pressure in unsaturated swelling soils such as the sand-bentonite buffer arise from changes in interparticle pressures, pore water pressures and pore air pressures in the unsaturated materials. Changes in the latter pressure components in turn can be linked to

changes in water content and density (Kanno and Wakamatsu, 1992). Therefore, observations made in Figures 8.14 and 8.15 may be taken to suggest that changes in water content and density were occurring within the buffer material during the heating phase of the experiment.

8.6 Psychrometer responses

Seventeen thermocouple psychrometers were installed in the Buffer/Container Experiment to measure vapour pressures and hence suctions in the unsaturated buffer. Estimates of gravimetric water contents were obtained by simple conversion of measured suctions using the suction-water content relationships described in Chapter 5 (Figure 5.1). During the 3 years they were installed, thirteen of the seventeen instruments remained operational. Results from these psychrometers are shown in Figures 8.17 to 8.24. The figures are arranged in sequence from the top of the experiment to the bottom. Results from closely positioned psychrometers or diametrically opposite psychrometers have been plotted together to facilitate discussion. Figures 8.17 to 8.20 present the data in terms of suction-time relationships whereas the water content-time relationships are given in Figures 8.21 to 8.24.

8.6.1 Observations before heater activation

Suction measurements were carried out immediately after the psychrometers were installed. The initial suctions in the unsaturated buffer generally lay between 3200 kPa to 3700 kPa (Figures 8.17 to 8.20). Using the calibration in Figure 5.1, this range of suction corresponds to water contents of 18.2% to 18.8% (Figures 8.21 to 8.24). Therefore the measured water contents were close to the initial target water content of 17.8%.

Installation of the buffer, backfill, instrumentation, and the restraint system took place between June and November 1991. During this pre-heating installation period, the

psychrometers show gradual suction decreases, and, hence, water content increases (see Figures 8.17 to 8.24). In general, the suctions in the buffer just before heater activation varied between 2800 kPa to 3400 kPa, which corresponds to water contents of 18.6% to 19.2%. This range of water content was less than the saturation water content of 22.5%, if no volume changes were experienced. Therefore, the buffer was not at water content or suction equilibrium before heater activation. This observation confirmed the total pressure measurements immediately at the start of the heating phase (Section 8.5.2.1). The lack of saturation in the Buffer/Container Experiment led to the subsequent construction of the Isothermal Test in the URL (without a heater). This test is still in progress at the time of writing.

The Isothermal Test examines how the buffer and rock mass will eventually move towards equilibrium potentials without the added complexity of the heating that was a central feature of the Buffer/Container Experiment (Chandler et al., 1996). In this test, twenty four psychrometers are being used to measure suctions and to indicate moisture movement in the unsaturated buffer. Responses from the instruments used in the Isothermal Test (Chandler, 1993 and 1994) are broadly similar to those of the instruments used in the Buffer/Container Experiment. Combining with those from the installation (pre-heating) phase of the Buffer/Container Experiment, the results of the Isothermal Test add confidence to the continuing use of thermocouple psychrometers as moisture sensors in bentonite-based buffer materials under virtually constant temperature conditions.

8.6.2 Observations after heater activation

The heating phase of the Buffer/Container Experiment began on 20 November 1991. Responses from the psychrometers are also shown in Figures 8.17 to 8.24. In general, all the psychrometers reacted quickly to the activation of the heater. Psychrometers BX1, BX3, and BX5 which were remote from the heater (Figure 8.17 and

Figure 8.21), generally showed suction decreases of up to 500 kPa in the first 50 days of heating. Thereafter, the suctions continued to decrease with time but at slower rates. "Steps" in the suction-time and water content-time relationships are observed at about 200 to 350 days. Thereafter, suctions in the buffer tended to decrease gradually with time. Towards the end of the experiment, the three psychrometers showed virtually similar suctions of 850 kPa to 1000 kPa and water contents of 22.0% to 22.5%. It appeared that the steps observed in these instruments were unique to this instruments group. It is postulated that these steps are associated with changes in total stress. This postulate will be discussed in Chapter 9. It should be pointed out that the perturbations at about 340 days were associated with operator-controlled adjustment of the excitation to the instruments.

Psychrometers BX6 and BX7 (Figures 8.18 and 8.22) were located above and close to the heater. Both instruments showed suction decreases of about 1500 kPa and apparent water content increase of about 2% in the first 50 days of heating. Thereafter the suctions decreased gradually with time. Despite the difference in their initial suctions, the psychrometers showed virtually the same suctions of about 1100 kPa to 1200 kPa, and water contents of 21.5% to 22.0% towards the end of the experiment.

Psychrometers BX8, BX10, BX12 and BX13 were installed next to the heater within the buffer annulus region (Figures 8.19 and 8.23). In general, these psychrometers reacted strongly to the activation of the heater. Psychrometer BX8 located beside the top of the heater showed a significant suction decrease of 3000 kPa and an apparent water content increase of 5% in the first 50 days of heating. The two middle instruments (BX10 and BX12) also showed large suction decreases of up to 2500 kPa and apparent water content increases of up to 4% during the first 150 days of heating. After the initial suction decreases, all three of these psychrometers showed slow and gradual suction increases with time. Hence, it can be suggested that moisture in the buffer annulus region

was moving away from the heater and the buffer was drying. This was later confirmed by water content measurements carried out at the end of the test (see Section 8.8). Psychrometer BX13 was located just below the mid-height of the heater. Initially the instrument showed a large suction decrease of about 1000 kPa in the first 100 days of heater. The suction continued to decrease gradually up to Day 600, but thereafter increased gradually until the end of the experiment.

Psychrometers BX14, BX15, BX16, and BX17 were located below the heater (Figures 8.20 and 8.24). At the onset of the heating phase, three of the four psychrometers (BX14, BX15, and BX17) experienced short term transient perturbations in the first 20 days of heating, and showed suction increases. In particular, BX14 showed a very large suction increase of about 1300 kPa. It is likely that these perturbations were associated with localized transient vapour pressure variations caused by steep temperature gradients near the bottom of the heater (see Figure 8.6). In contrast to the other three psychrometers, BX16 showed a moderate suction decrease of about 500 kPa in the first 50 days of heating. In general, all four psychrometers showed systematic suction decreases and apparent water content increases with time. By the end of the experiment, BX16 and BX17 which were below the heater, were reading lower suctions of 1200 kPa and 900 kPa and higher water contents of 21.5% and 22.5%, respectively. It was encouraging to see that despite the difference in their initial readings, the diametrically paired psychrometers BX14 and BX15 were reading almost the same suctions of about 2000 kPa and water contents of 20.5% by the end of the experiment. This was reassuring with regard to the continuing, long term accuracy and precision of the instruments.

8.7 Responses of thermal needles

To facilitate later discussion and comparison with psychrometer data, this section presents responses from the thermal needles. It was pointed out in Section 8.2 that the

thermal needles measure the thermal conductivity of the unsaturated buffer, which is a function of water content. Results from laboratory tests (Figure 8.4) show that the thermal conductivity of unsaturated sand-bentonite material tends to vary with water content for $w = 3\%$ to 17%, but remains essentially constant at $w > 17\%$. Therefore, thermal needles were installed only in buffer close to the heater where moisture depletion was anticipated. Figures 8.25 and 8.26 show the results of typical thermal needles located above and below the heater, and in the buffer annulus beside the heater. It should be noted that because of problems associated with drying shrinkage and corrosion of the instruments, data from the thermal needles were not available after Day 500.

Unlike the psychrometers, the thermal needles did not show a high level of consistency at the time of placement. From the thermal needle data, the initial water contents were interpreted to be significantly higher than the as-placed water content of 17.8%; values between 21% to 25% were derived. The inconsistency is due to the insensitivity of thermal conductivity to water content at $w > 17\%$ (see Figure 8.4).

In general, all the thermal needles showed little change in thermal conductivity during the pre-heating installation phase and in the first 50 days of the heating phase of the experiment. The water contents in the buffer in which the instruments were located, were equal to or higher than the as-placed water content of 17.8%, and the instruments were insensitive to changes in this region (Figure 8.4).

As heating continued, the instruments that were located remote from and above the heater, showed either small increases or no change in thermal conductivity with time, from which it can be inferred that water contents remained constant or increased above 17.8% (Figure 8.25). However, instruments which were around and beside the heater, generally measured large thermal conductivity decreases, implying drying in the buffer material surrounding the heater (Figures 8.25 and 8.26). It may be inferred from the data

in Figure 8.25 that the drying appeared to slow down at about 400 days after heater activation.

During decommissioning of the experiment, it was revealed that 14 of the 21 thermal needles used in the experiment had corroded. In particular, the stainless steel sheaths of 7 of the 16 thermal needles used in the buffer annulus between the heater and the rock wall were found to be completely corroded, exposing the heater elements and the thermistors. It was reasonable to assume that the use of these instruments was affected by corrosion and lack of contact between the probe and the buffer as a result of temperature-induced drying shrinkage. These latter factors are considered to be acceptable explanation for the scatter in the data such as reflected by the response of BN12 and BN20 seen in Figure 8.26.

8.8 Moisture distributions at the end of experiment

In May 1994, after 897 days of heating, the heater was turned off and the buffer was excavated. During the excavation, the condition of the buffer was inspected visually, and in addition, about 8%, by total mass, of the buffer sampled and tested for water content and density. The details of the carefully controlled procedures used are provided by Roach et al. (1996).

Figure 8.27 shows the water content distribution in the buffer at the end of the experiment. It can be seen that water contents showed strong symmetry in the water content distributions about the central vertical axis of the test hole. In general, significant moisture increases (> 3% increase over the initial average water content of 17.8%) were measured in the narrow zone of buffer immediately adjacent to the rock, and in buffer surrounding the top of the heater. Significant moisture decreases (> 3 % decrease) were detected in buffer immediately adjacent to the heater. In the remaining zones, moderate increases in water content (up to 3% increase) were measured.

The changes in water content were accompanied by changes in dry density (γ_d) within the buffer mass. Figure 8.28 shows the dry density distribution in the buffer. The initial average γ_d of the buffer mass was 1.73 Mg/m^3 at an average water content of 17.8%. In general, the dry density of the buffer above and below the heater, where moisture uptake was measured, decreased to between 1.61 Mg/m^3 and 1.73 Mg/m^3 (that is, the buffer had swelled). In the buffer annulus zones close to the rock where moisture increases were measured, the final dry densities varied between 1.59 Mg/m^3 and 1.66 Mg/m^3. That is, swelling had also taken place in these areas. However, in the annulus region between the heater and the rock, significant drying was observed in the buffer zones closer to the heater. In these zones, the final dry densities were between 1.66 Mg/m^3 to 1.86 Mg/m^3 (that is, the buffer had shrunk and densified).

Based on the measured water contents, it was determined that the buffer as a whole took on about 90 litres of moisture during the experiment. This value is in general agreement with what had been calculated on the basis of the measured inflow from the rock into the test hole prior to the installation of the buffer and heater system (Chandler et al., 1992).

8.9 Comparison of end-of-test psychrometer-measured and actual water contents

Figure 8.29 compares the actual end-of-test water contents of the buffer materials that surrounded the psychrometers and the water contents indicated by the instruments. It can be seen that the psychrometer-measured water contents are consistently higher than the actual values by up to 7% in the extreme case at the top of the heater. The percent error in the measurement generally lies between 8% and 21%, which is larger than the accuracy of $\pm$ 6% determined from the temperature-controlled laboratory tests

reported in Chapter 3. It may be inferred further from the data that the discrepancies tend to be larger for those sensors used in the buffer above the heater. It is suggested here that these discrepancies can be attributable, in part, to water vapour movement from the buffer annulus towards the top of the experiment under the influence of thermal gradients during the early stages of the heating phase, and in part to the total stress effect as postulated in Section 8.6. The implications of vapour pressure gradients and stress effect on the precision and accuracy of suction and water content measurements by psychrometers are discussed in Chapter 9.

8.10 Summary

The Buffer/Container Experiment was carried out to examine the thermal-hydraulic-mechanical interaction between an initially unsaturated sand-bentonite buffer, a heater, and granitic host rock. Commercial thermocouple psychrometers were installed within the unsaturated buffer material to track *in situ* suction and moisture transients in the soil. The instruments were calibrated in accordance with procedures developed by the author and described in Chapter 3 of this thesis. The instruments measured vapour pressures and suctions in the unsaturated soil. Water content values were obtained by simple conversion of suctions using a suction-water content relationship measured under constant laboratory conditions and described in Chapter 5. The end-of-test water contents indicated by the psychrometers predicted water contents that were consistently higher than the actual water contents. The discrepancies are thought to be attributed to a combination of temperature-induced vapour pressure gradients and changes in total stress in the unsaturated buffer. The effects of these observations on the usefulness of psychrometers as moisture sensors to track *in situ* suctions and water contents are discussed in Chapter 9.

CHAPTER 9 DISCUSSION AND SYNTHESIS

9.1 Introduction

The objective of this study was to investigate the usefulness of thermocouple psychrometers to measure *in situ* suctions and water contents in compacted swelling clays. This study arose from the need to clarify conditions under which psychrometers can be operated to provide meaningful data for the study of unsaturated compacted sand-bentonite material for the underground disposal of heat-generating radioactive waste.

The performance of psychrometers as internal sensors in compacted sand-bentonite material, and other compacted clays was examined in series of laboratory tests. These tests were carried out to provide background information for the analysis of psychrometer data from the Buffer/Container Experiment.

In this chapter, results from the suction test series (Chapter 5) and the triaxial test series (Chapter 6) are discussed first to provide a framework for later discussion of the results from the Buffer/Container Experiment. Data from the mercury intrusion porosimetry studies presented in Chapter 7 showed that the sand-bentonite material, sand-illite material, and Boom Clay tested in this study had complex soil fabric and pore structures. Therefore, results from the laboratory tests are analysed on the basis of soil structure theories.

The latter part of this chapter deals with the results from the Buffer/Container Experiment which were presented in Chapter 8. Discussion of the results from the *in situ* experiment is made in light of the framework developed from the laboratory investigations. In particular, the influence of temperature-induced vapour pressure gradients, and total stress effect on the precision and accuracy of *in situ* suction and water content measurements by psychrometers in unsaturated sand-bentonite material are discussed.

A summary of the derived understanding of the usefulness of psychrometers as moisture sensors is given at the end of the chapter.

9.2 Soil structure considerations

The influence of soil structure on the physical and hydraulic properties of compacted soils was discussed in Chapter 2. Recognizing the importance of soil structure in relation to our understanding of the behaviour of compacted clays, tests were carried out on the soils tested in this study using mercury intrusion porosimetry. Results from these tests were presented in Chapter 7.

It was noted in Section 2.2.2 that clay particles carry electrical charges on their surfaces. When water is added to clay particles, water molecules are attracted to the surface of the particles. This is because water is dipolar. That is, a water molecule is electrically neutral, but the centre of action of the two positively charged hydrogen atoms does not spatially coincide with the central negatively charged oxygen atom. Because of clay-water interaction, clay particles tend to aggregate to form domains which are groups of clay particles with similar orientations. Due to forces acting on these small units (Bowles, 1979), domains group together to form clusters, which in turn coalesce to form peds (Yong and Warkentin, 1975). This is clearly supported for the soil studied here by the evidence in photo micrographs in Figure 7.3.

For remoulded and compacted soils, the size and stiffness of peds are largely functions of water content (Musa, 1982; Wan et al., 1990). With higher water content, the peds become larger and softer. It appears that peds behave as discrete units, and that the behaviour of the soil depends greatly on the interaction of the peds. Depending on the moulding water content, peds may be saturated or unsaturated with water. In these circumstances, remoulded and compacted clays have complex fabric structures containing pores with a wide range of diameters and cannot be described as homogeneous. Pore size

distribution curves are often bi-modal or tri-modal. This is reflected in the results from the MIP test presented in Chapter 7 (see for example, Figures 7.4 to 7.7).

9.3 Suction properties

9.3.1 Background

Results from the suction tests have been presented in Chapter 5. Relationships between total suction and water content for sand-bentonite material, sand-illite material, and Boom Clay are shown in Figures 5.1 to 5.3 respectively. Figures 5.4 to 5.6 present the relationships between total suction and degree of saturation for the each of the soils, respectively.

In each of Figures 5.1 to 5.3, the total suctions in the respective soil measured by the psychrometer method, vapour equilibrium technique, and the filter paper technique, generally lie within the 95% confidence envelop of all the data. Therefore, the hypothesis from Chapter 2 '*Under normal temperature and atmospheric pressure boundary conditions, thermocouple psychrometers can be used to measure suction in swelling compacted clays*' is confirmed. This gives confidence to the use of psychrometers to measure suctions in compacted clays under constant temperature conditions.

The data in Figures 5.1 to 5.3 show that, for the soils tested in this study, total suction can be broadly related to a singular value of gravimetric water content. However, contrary to views reported in the literature (Corey, 1986; Fredlund and Rahardjo, 1993), no simple relationship between total suction and degree of saturation can be established as reflected in the data in Figures 5.4 to 5.6. Figures 5.11 to 5.16 show the relationships between osmotic suction and water content, and between osmotic suction and degree of saturation. The data in these figures lead to the broad observation that osmotic suctions

in the three soils were insensitive to changes in water content and degree of saturation. Therefore changes in the total suction were largely controlled by the matric component.

9.3.2 Discussion

In contemporary unsaturated soil mechanics theories (Philip and de Vries, 1957; Fredlund and Rahardjo, 1993), an element of soil is often considered as a simple three phase system consisting of pore air, pore water and granular solid particles (Figure 9.1). Suctions in such a system arise from capillary actions attributed to interactions between air-water menisci and the soil particles. The matric suction (S_m) is related to the curvature of the air-water meniscus (r) by,

$$S_m = \frac{2\sigma_t}{r} \qquad [2.5 \text{ bis}]$$

where σ_t is the surface tension of water. In this simple soil system, dry density reflects the packing of the solid particles. Any changes in dry density therefore lead to changes in the degree of saturation and the volumetric water content. Density change would also result in changes in the packing of the soil particles which in turn influence the curvatures of the air-water menisci, and hence the matric suction in the soil. With this model, singular relationships between suction and volumetric water content, and between suction and degree of saturation can be envisaged.

Observations from photo micrographs and results from the mercury intrusion porosimetry studies presented in Chapter 7 show that the soil structures in the compacted soils tested in this study are more complex than those shown in Figure 9.1. The observed soil structure can be more precisely described as a network of peds which contain domains, clusters, intra-ped and inter-ped voids (Figure 9.2). Each domain is essentially a group of curved and flake-like clay particles. The high affinity of the highly-

charged particles for water and capillary actions cause the smaller intra-ped voids (that is, spaces between adjacent particles) to become water-saturated before the inter-ped voids. Depending on the water content, the matric suctions in these materials can be controlled by the capillary phenomena at the "edges" of the domains and clusters, and are largely influenced by the radius of curvature of the air-water menisci formed between the curved surfaces of adjacent clay particles (Figure 9.2). Under these conditions, changes in density only affect the volume and distribution of the inter-ped voids, but not the intra-ped voids (Croney et al., 1958).

It was hypothesized in Chapter 2 that '*The suction in a compacted clay is largely controlled by the soil microstructure*'. Calculations were carried out to verify this hypothesis. Figure 7.1 compares the PSD's of compacted specimens of sand-bentonite material, sand-illite material, and Boom Clay. Using the capillary equation (Equation 2.5), the suctions that correspond to the different dominant pore modes in Figure 7.1 were calculated. The results are summarized in Table 9.1. From the table, it can be seen that the suctions calculated from the "large pore" diameters are of the order of kilo-Pascals, whereas the suctions from the "small pore" diameters are of the order of mega-Pascals. The range of suction based on the small pore mode is consistent in magnitude with the range of measured matric suctions. These results confirm that matric suctions and intra-ped soil structures are related in compacted clays. That is, the hypothesis stated earlier is confirmed. As a corollary to this hypothesis, it is likely that when the degree of saturation is sufficiently high to partly fill the inter-ped voids with water, then conventional relationships between S and S_r, and between S and θ such as those modelled by Figure 9.1 can be applied to analyses of a soil's behaviour.

It is common to use relationships between suction and degree of saturation, or between suction and volumetric water content in the modelling of moisture movement or deformation in unsaturated soils (Corey, 1986; Fredlund and Rahardjo, 1993). The

findings in this study raise questions concerning the usefulness of volumetric water content and degree of saturation as state variables. The corollary of this observation is that hypotheses regarding the behaviour of unsaturated soils which rely on the use of S-θ or S-S_r relationships may not be suitable or practically applied to model the more complex behaviour of materials such as the engineered, swelling clay barrier being proposed for use in radioactive waste disposal. Suction-gravimetric water content may be more appropriate. This is consistent with the recent observations by Ridley (1995); and Delage and Graham (1995).

9.4 Volume change behaviour of unsaturated sand-bentonite material

9.4.1 Background

Six triaxial isotropic compression tests with volume change measurements were carried out on unsaturated sand-bentonite material to measure the volume change behaviour of the unsaturated material under constant mass and constant water content conditions. The purpose of these tests was to provide background information for the interpretation of data from the triaxial isotropic compression and shear tests with suction measurements using psychrometers.

9.4.2 Volume change behaviour

Figures 6.17, 6.19, 6.20, and 6.22 show the volume strain-total pressure curves for four specimens formed to initial dry densities of 1.40 Mg/m^3 to 1.45 Mg/m^3 at water contents of 16.4% to 28.6%. Figures 6.18 and 6.21 show the volume strain-total pressure curves for two specimens formed to higher initial dry densities of 1.66 Mg/m^3 at water contents of 18.8% and 19.3%.

It was hypothesized in Chapter 6 that differences in the total suction responses during first time isotropic compression and subsequent unload/reload cycling are associated with elastic-plastic behaviour of unsaturated sand-bentonite material. To examine this hypothesis further, the volume strain-total stress relationships given in Chapter 6 are re-presented in Figures 9.3 and 9.4 with stress plotted in $\log_{10}$ scale. To facilitate discussion, data for Specimen SB3080V6 are omitted from the figure. Figure 9.3 re-presents data from materials compacted to 1.40 Mg/m^3 to 1.45 Mg/m^3. Figure 9.4 re-presents data from material compacted to 1.66 Mg/m^3.

From Figures 9.3 and 9.4, it can be seen that the ε_v - log p* relationships are similar in form to conventional e-log p' plots for consolidation data. In the ε_v - log p* space, each specimen shows a change in stiffness with stressing, as indicated by the change in slope of the volume strain-pressure relationship. In saturated soils, such changes in stiffness are commonly taken to represent yield stresses (Wood, 1990). A stiff response is measured when the pressures are below a previous maximum value. The observations in Figures 9.3 and 9.4 may be taken to imply that when the load is below the pre-yield value, the specimen behaves elastically. Once the pressure exceeds the pre-yield value, the specimen compresses plastically with plastic strain hardening.

It may be inferred from the data in Figures 9.3 and 9.4 that the pressures at which yielding first occurred, were similar for the specimens formed to similar lower initial dry densities of 1.40 Mg/m^3 to 1.45 Mg/m^3. As expected, the pressure tended to increase with increasing density. Using the Casagrande (1936) method, the pressures at first-yield were determined from each of the volume strain-log total stress relationships and are summarized in Figure 9.5.

These pressures at first-yield may be related to the compaction pressures used in the formation of the specimens. In the triaxial testing program, specimens were formed by compacting moist sand-bentonite mixture in a rigid mould to a specified dry density

and water content. During compaction, high pressures were required to form the specimens. As a result, locked-in compaction stresses could develop in the specimens and could subsequently affect the compression behaviour of the specimens. Figure 9.5 also shows the relationship between the average compaction pressure, dry density, and water content for unsaturated sand-bentonite material. The data in this figure were obtained from a separate series of compaction tests carried out in this study to examine the correlation between compaction pressures and compaction variables.

Figure 9.5 shows that the average compaction pressures were higher for the *high density* specimens than for the *low density* specimens. For the *low density* specimens, the average pressures are relatively constant for the water content range of 16.5% to 18.6%, measuring between 913 kPa and 931 kPa. A lower compaction pressure of 616 kPa was recorded at a higher water content of 21%. For the *high density* specimens, average compaction pressures of 2544 kPa and 2104 kPa were measured, respectively, in the 16.5% and 21% specimens. A higher average compaction pressure of 3219 kPa was recorded in the 18.6% specimen.

The average compaction pressures presented in Figure 9.5 are generally higher than the pressures at first-yield shown in the same figure. However the relationships between pressure, density, and water content are qualitatively similar for both the compaction and triaxial tests. It is likely that the difference in the pressures can be attributed to varying specimen sizes and test boundary conditions. Smaller, 50mm diameter specimens, were used in the 1-D compaction tests; larger, 100 mm diameter specimens, were tested in the triaxial compression tests.

9.4.3 Discussion

The observations made in the triaxial compression tests with volume change measurements may be explained with the aid of a conceptual model developed by the

author. An unsaturated compacted sand-bentonite specimen may be envisaged as a skeleton of peds with inter-ped voids, or may conceptually be visualized as a stack of loosely organized sponge balls (Figure 9.6a). The sponge balls represent the peds which are aggregations of water-saturated clay domains and clusters, and are often considered to behave as individual units (Barden and Sides, 1970; Collins, 1983). Because of clay-water interactions, peds can become compressible when subjected to high stresses.

When an unsaturated sand-bentonite specimen tested in this study was subjected to isotropic compression stresses above the 'preconsolidation' pressure, it underwent total volume strain which consisted of both plastic and elastic components (Wood, 1990). During first time compression, deformation in the specimen was attributed to the distortion of the skeleton structure, and to localized compression of the peds. This is represented by the tighter packing of the compressed sponge balls in Figure 9.6b. Plastic volume strains in the specimen were caused by changes in the skeleton structure which involved a decrease in the inter-ped voids accompanied by minor re-organization and tighter packing of the individual ped units. This is supported by the results from the MIP tests (Figures 7.16 and 7.17). Elastic strains were attributed to compression of the peds.

During unload-reload cycling, changes in the soil structure were largely attributed to the elastic response of the individual peds. The data in Figures 6.17 to 6.22 show that reversible elastic volume strains were small for the total pressure range of 100 to 3000 kPa. It is likely that for this pressure range, elastic rebound of the peds was lessened by the confinement of the rigid skeleton structure consisting of now much tighter packed and re-organized peds (Figure 9.6c). The integrity of the skeleton structure in turn was maintained by the confining pressure. As the confining pressure decreased to atmospheric pressure, the effect of confining pressure on the skeleton structure and the peds diminished. The peds were free to recover fully to their original shapes and

geometries. This is depicted by the sponge ball model in Figure 9.6c. However permanent plastic deformation was sustained by the skeleton structure. The net volume strains measured at the end of test in Figures 6.17 to 6.22 reflect the changes in inter-ped voids in the deformed specimens.

9.5 Effect of total stress on suction measurements using psychrometers

9.5.1 Background

Figures 6.1 to 6.9 present the total suction-total stress relationships measured in the isotropic triaxial compression tests with suction values from psychrometers embedded in the specimens. Figure 6.10 summarizes the total suction-total stress relationships measured in the pre-shear isotropic compression phase of three triaxial shear compression tests. The data in Figures 6.1 to 6.10 show that under constant mass and constant water content conditions, the psychrometers indicated that suctions decreased with increasing total stress on the specimen during first-time compression. In some of the tests, the specimens were subjected to load-unload cycling. The total suction-total stress relationships in these specimens were hysteretic, that is, the first-time compression and unload-reload paths were different. Table 6.1 compares the total suctions in 6 isotropic compression tests measured under atmospheric pressure conditions prior to isotropic compression and at the end of each unloading phase. The data in the table show that total suctions measured in the distorted specimens under atmospheric pressure conditions were broadly similar to the pre-test total suctions measured in the intact specimens under similar pressure conditions. Similar observation was made in Specimen SB1880TS4 which was first isotropically compressed to a total pressure of 1021 kPa and then sheared. Despite distortions in the specimen, the final total suctions at the end of test

were broadly similar to the initial suction measured under similar atmospheric pressure conditions (Figure 6.16).

9.5.2 Comparison of total suction-total stress relationship between specimens formed to different initial dry densities

In the triaxial compression tests series with suction measurements, six specimens were formed to initial dry densities of 1.41 Mg/m^3 while three specimens were formed to higher dry densities of 1.67 Mg/m^3. Figures 9.7 to 9.9 compare the total suction-total stress relationships of low and high density specimens formed to water content of 18%, 19.5%, and 21% respectively.

It can be seen from the data in Figures 9.7 to 9.9 that for the specimens formed to the same water contents but different initial dry densities, the psychrometers indicated broadly the same total suction-total stress relationships. Therefore the influence of total stress on total suction is independent of dry density and degree of saturation. The relatively large difference between the two relationships of specimens formed to 19.4% to 19.5% water contents (Figure 9.8) is attributed to the poor responses of the psychrometer used in the denser specimen.

When two specimens were formed to the same water contents but different dry densities, they had similar peds and intra-ped voids, but different macroscopic inter-ped voids. This is supported by observations from MIP tests (see Figures 7.4 and 7.5). The similarity in the total suction-total stress relationships may be taken to imply that changes in total suction within respect to total stress change were controlled by the changes in the micropores within the peds and not by the inter-ped macropores. The corollary of this observation is that while changes in macrostructure differed between the two specimens, changes in the microstructures were similar. This latter point is

supported by data from the isotropic compression tests with volume change measurements (see Figures 9.3 and 9.4) and data from MIP tests (Figures 7.16 and 7.17). The results from the triaxial compression tests with suction measurements therefore provide further support to the hypothesis that total suctions in unsaturated sand-bentonite materials are largely controlled by the soil microstructures.

9.5.3 Discussion

At first sight, the results of the triaxial compression tests with suction measurements using psychrometers appeared to contradict the hypothesis discussed in Section 9.3 that total suction in unsaturated compacted sand-bentonite material is related to a singular value of gravimetric water content. However, it can be suggested that under constant mass and water content conditions, the deformation in unsaturated specimens caused by an increase in total compressive stress leads to increases in the degree of saturation in the soil, which correspondingly decreases suction. However, this argument does not adequately explain the similar total suction values measured by the psychrometer in the same specimen before and after testing under atmospheric pressure conditions (see Table 6.1 and Figure 6.16), and the hysteresis in the total suction-total stress relationships. These two observations may only be explained by consideration of the possible influence of soil structures on suction measurements using psychrometers as follows.

9.5.3.1 First time compression

It was hypothesized in Section 9.4 that a typical unsaturated compacted sand-bentonite specimen in this study may be envisaged as a skeleton of peds and inter-ped voids (Figure 9.6a). During first time compression to pressures above an earlier yield stress or the 'preconsolidation' pressure, the skeleton structure of the specimen deformed

plastically, whereas the peds compressed elastically. It was discussed in Section 9.3 that total suction in unsaturated sand-bentonite material is largely governed by the capillary phenomena at the edges of the domains and clusters within peds. Stress-induced compression of the peds led to changes in the air-water menisci (Figure 9.6b). Under constant mass, when the clay particles in the saturated domains and clusters were brought closer together, the radii of curvature, r, of the air-water menisci at the edges of these microstructures increased. As the vapour pressure and total suction in the unsaturated specimen are directly related to r, flatter air-water menisci (that is larger r values) implies higher vapour pressure in the open voids in the soil. The output of a psychrometer is inversely proportional to the vapour pressure. Therefore, under constant mass and water content conditions, the psychrometers used in the compression tests, registered decreasing suctions in the specimens with increasing total stress.

9.5.3.2 Unload-reload cycles

Six specimens tested in the isotropic compression tests were subjected to unload-reload cycling (Figures 6.1, 6.3, 6.6 to 6.9). In general, the unload-reload total suction paths in each specimen were different from the first time compression total suction path. Implications of the rigid skeleton structure and confining pressure on the elastic deformation of the peds were discussed in Section 9.4. Rigid skeleton structure maintained by confining pressure inhibited total elastic recovery of the peds. Since the curvatures of the air-water menisci were largely controlled by the spacings between the clay particles in the water-saturated domains and clusters within the peds, lower total suctions were measured for the total pressure range of 100 kPa to 3000 kPa during unload and reload cycling. When the confining pressure was reduced to atmospheric pressure, the peds expanded freely and elastically to their original shapes (Figure 9.6c). Under these conditions, the air-water menisci at the edges of the peds were similar to those in

the intact specimen prior to compression. As a result, a total suction similar to the initial suction was measured by the psychrometer at the end of test under similar atmospheric pressure conditions.

For Specimens SB1895TX and SB2295TX, the total suction-total stress relationships in each specimen were broadly similar for the first-time compression and the first unload-reload cycling. The similarity in response is associated with the fact that during the first unload-reload cycling of each specimen, the maximum confining pressure applied to the specimen did not exceed the first-yield pressure as discussed in Section 9.4 (see Figure 9.5). As a result, the specimen behaved elastically, with recoverable volume strains, as indicated by the reversibility in the total suction readings.

9.5.4 Conclusions

One of the hypotheses stated in Chapter 2 is that '*Under constant mass conditions, stress variations and deformations will bring about changes in the soil macro- and micro-structures in a compacted clay. These latter changes in turn will affect the vapour pressure in the soil. Under these conditions, the suction measured by a psychrometer will be different from that suction measured at the same water content by the same instrument under normal atmospheric pressure condition'*. In light of the discussions presented in Sections 9.4 and 9.5, it is concluded that this hypothesis is confirmed.

9.6 Elastic-plastic modelling of unsaturated sand-bentonite material: a preliminary investigation

9.6.1 Background

It was stated in Chapter 2 that one of the objectives was to explore the use of contemporary unsaturated soil mechanics frameworks to describe the inter-relationship of stress, volume change, and suction of unsaturated sand-bentonite material proposed for use in the disposal of heat-generating radioactive waste. In this section, a conceptual model based on elastic-plastic theories is proposed. Results from the triaxial shear tests carried out in this studies are discussed within the framework of the proposed model.

9.6.2 Framework for elastic-plastic models

In recent years, various conceptual models based on elastic-plasticity theories have been proposed to rationalize the constitutive behaviour of unsaturated soils (Alonso et al., 1990; Gens and Alonso, 1992; Wheeler and Sivakumar, 1995; Wheeler, 1996). Elastic-plastic modelling of soils requires the knowledge of pre-yield elasticity, yielding, plastic-flow rule, hardening law, and strength law (Atkinson and Bransby, 1978; Wood, 1990). A review of our current understanding of elastic-plastic modelling of unsaturated soils and limitations of existing models is given by Delage and Graham (1995).

A general elastic-plastic model for unsaturated soils was first proposed by Alonso et al. (1990). Later Wheeler and Sivakumar (1995) developed the ideas of hyperlines that describe load-induced and suction-induced yielding into a series of hyper-surfaces that increase with either loading or drying. Figure 9.10 shows the general shape of the yield surface of an unsaturated soil in q:p:S space (Wheeler and Sivakumar, 1995). The model may be used to explain the inter-relationship between yielding due to loading, suction increase, and wetting. Implicit in this model is the assumption that the soil will behave

elastically if its state remains inside the yield surface. However, plastic volume and shear strains will be experienced by the soil if its state traverses the yield surface. Compressive plastic volume strains lead to expansion of the yield surface (that is, volumetric hardening plasticity). A shortcoming of Wheeler and Sivakumar's model is that it does not adequately describe yielding under suction increase at constant p.

Referring to the model in Figure 9.10, for a soil with its initial state at A, isotropic loading inside the surface would lead to yielding at B, followed by plastic hardening to C which lies on an expanded yield surface (not shown in the figure for clarity). Wetting or suction decrease from A would initially produce elastic expansion to F, yielding and plastic compression to G on a new yield surface. Increasing shear stresses from A with constant mean total stress and constant suction would produce yielding at D and plastic hardening towards a critical state at E on a larger yield surface. At critical state, the soil continues to deform without further changes in effective stress, shear stress, and suction (Atkinson and Bransby, 1978; Wood, 1990). Wheeler and Sivakumar (1995) and Zakaria et al. (1995) have presented experimental evidence that strongly support this general approach for isotropic soils.

Figure 9.11 deals with elasticity and yielding of an unsaturated soil in the v:S:log p space (Alonso et al, 1990; Delage and Graham, 1995). Figure 9.11a compares the loading-unloading paths of two unsaturated specimens tested at different constant suctions in v:log p space. The first specimen begins at a lower suction at A, loading through its yield stress B, compressing plastically with volumetric hardening to C, then being unloaded to D. The second specimen is being loaded at a higher suction from L, yielding at M, compressing plastically down its stress hardening line to N, then being unloaded elastically to O. Note the difference in the pre-yield stiffness between the specimens as defined by the κ-line. The current consensus is that pre-yield stiffness during stressing increases with suction (Alonso et al., 1987; Cui and Delage, 1993). Figure 9.11b shows

that plastic volume strains lead to expansion of the yield surface. Points B and M define the initial yield curve LY1 whereas the subsequent yield curve LY2 are linked by points C and N.

9.6.3 A conceptual model for unsaturated sand-bentonite material

The volume strain-total pressure relationships from the isotopic compression tests with volume change measurements were discussed in Section 9.4. The data from these tests show good evidence of yielding (see Figures 9.3 and 9.4), and therefore provide further support for the development of a general elastic-plastic model for unsaturated sand-bentonite material.

Following the ideas of hyper-surfaces developed by Wheeler and Sivakumar (1995), a conceptual model is proposed here to explain the behaviour of unsaturated sand-bentonite material tested in triaxial shear compression. In this model, an associated flow rule is assumed and the yield loci are elliptical in shape. Figure 9.12 presents a schematic of the proposed conceptual model in q:p*:S space, where p* is the total stress variable defined in Section 6.2. This conceptual model is qualitative at this stage, and in part hypothetical. The exact shapes of the yield surfaces, the yield loci, and the tension cut-off line are arbitrarily defined.

The model in Figure 9.12 uses the concept of elastic volume developed by Graham (personal communication). An elastic volume is a 3-D volume in the q:p*:S space bounded by the tension cut-off line, a loading yield line, a suction yield line, and the p* axis. The elastic volume for unsaturated soils is analogous to the pre-yield elastic wall (that is, the κ-line in v:p space) for saturated soils. Depending on the initial water content and, hence, suction, and on previous stress history on the soil, the elastic volume bounds and defines the initial state of the soil. For example, assuming that a soil has an elastic volume of $AB_2D_2C_2$ in Figure 9.12 and that stress conditions place the material

within the elastic volume, then the soil will behave first elastically when stresses change. However when the bounding surface of the elastic volume is reached, the soil will yield and behave plastically with stress changes. If the soil strain hardens, volume hardening is accompanied by enlargement of the elastic volume. The current state of the soil is now represented by an expanded elastic volume as depicted by $AB_3D_3C_3$. Conversely, if the soil strain softens, a reduced elastic volume given by $AB_1D_1C_1$ determines its current state.

One assumption of the conceptual model in Figure 9.12 is that the model is "capped" at high suctions. That is, for a given elastic volume, its boundary is terminated by a fixed constant suction wall, such as the constant suction wall D_1C_1 for the elastic volume $AB_1D_1C_1$. This feature allows the modelling of yield when the soil is subjected to constant p* loading with suction increase. At this stage, the detailed shape of constant suction walls is unknown. It has been assumed elliptical and vertical in q:p* planes at constant S.

9.6.4 Modelling of elastic-plastic behaviour of unsaturated sand-bentonite material in shear

In this section, the stress paths of four hypothetical specimens (SP1 to SP4) in shear are examined within the framework of the proposed conceptual model. These stress paths have been chosen to allow comparison between the predicted behaviour and actual behaviour measured in the four triaxial shear tests described in Section 6.4.

It is recalled that the triaxial shear specimens tested in this study were formed to similar initial conditions with dry densities of 1.40 Mg/m^3 to 1.43 Mg/m^3 and a water content of 18%. The specimens were then isotropically compressed to 0 kPa, 515 kPa,

1021 kPa, and 1494 kPa. Therefore, these specimens were at different v:S:p* states prior to shear with initial conditions represented by different elastic volumes.

It is assumed that the respective hypothetical specimens SP1 to SP4 have the same initial densities and pressure-volume states as the triaxial shear specimens; and they are sheared under the same stress paths as the sheared specimens, that is, "undrained" constant mass conditions with a total stress path of a gradient of 3.

SP1

Referring to Figure 9.13, SP1 is sheared with zero (atmospheric) confining pressure, and has an initial state at point A1. This point must lie on the constant suction ellipse SY5a inside the elastic volume arbitrarily shown in the figure as EV5. Because the specimen is sheared under "undrained" constant mass conditions, its stress path in the q:p* space has a 3v:1h gradient. The triaxial compression stress path intersects the original p*:q:S yield surface (SY5a) at B1 to the 'dry' side of the critical state hyperline (Figure 9.13). Assuming an associated flow rule, the normal to the local yield locus at this point has a negative $d\varepsilon^{v}_{p}$ component. That is, the plastic strain increment vector perpendicular to the yield surface has a negative slope. The model therefore suggests that, upon yielding, the specimen will expand plastically and strain-soften, producing a smaller elastic volume of reduced shearing resistance. At the same time, expansions lead to small increases in suction as the state of the specimen approaches critical state near C1 on the constant suction ellipse SY1a defined by an elastic volume EV1 which is smaller than the initial elastic volume EV5. This agrees qualitatively with the observed behaviour of Specimen SB1880TS1 which showed dilative, strain softening behaviour in shear (Figures 6.11 and 6.12).

SP2

Figure 9.14 shows a suggested stress path for SP2 which is sheared under a moderate confining pressure. It is assumed that the state of SP2 is still bounded within the elastic volume EV5. The state of SP2 is represented by point A2 on the same constant suction ellipse SY5a as SP1. Hypothetically sheared under "undrained" constant mass conditions, the total stress path has a gradient of 3. Increasing the shear stresses on SP2 causes the specimen to yield at B2 which is just on the 'wet' of the critical state hyperline (Figure 9.14). The normal to the local yield locus at this point has a positive $d\varepsilon^v_p$ component. Volumetric hardening is accompanied by enlargement of the elastic volume. This specimen therefore strain hardens, compresses, and experiences suction decreases until it approaches critical state near C2 on the constant suction ellipse SY7a defined by an elastic volume EV7 which is larger than the initial elastic volume EV5. This agrees qualitatively with the observed strain hardening behaviour of Specimen SB1880TS3 which was isotropically confined at 515 kPa prior to shear (Figures 6.11 and 6.12).

SP3

Figure 9.15 shows the hypothetical stress paths of SP3 which is isotropically compressed to a higher confining pressure than SP2. It therefore has a lower initial suction at the beginning of shearing than either SP1 or SP2. Because the maximum isotropic compression pressure on SP3 exceeds the pressure at first yield, it is assumed that the initial condition of the specimen is represented by a larger elastic volume EV9 than that of SP2 (EV5 in Figure 9.14). The state of the specimen is depicted by point A3 lying inside the constant suction ellipse SY9a in EV9. Assuming a 3v:1h total stress path, yielding occurs at a stress state on the original yield locus at B3 with a positive $d\varepsilon^v_p$ component. The specimen compresses plastically with suction decreases, and

experiences volumetric hardening. The specimen continues to strain harden until its stress path moves towards critical state near C3 on the constant suction ellipse SY13a defined by a larger elastic volume EV13. This agrees qualitatively with the observed strain hardening behaviour of Specimen SB1880TS4 which was isotropically compressed to 1021 kPa prior to shear (Figures 6.11 and 6.12). The pressure of first yield of Specimen SB1880TS4 was about 500 kPa.

SP4

SP4 is sheared under the highest isotropic confining pressure which is assumed to far exceed the pressure at first yield. Therefore, the initial condition of the specimen is assumed to be represented by A4 lying inside the constant suction ellipse SY13a in the elastic volume EV13 (Figure 9.16) which is, again, larger than SY9a, the post isotropic compression condition of SP3. With a 3v:1h total stress path, the specimen first yields on the original yield locus at B4 with a positive $d\varepsilon^{v}_{p}$ component. It then compresses plastically, producing a suction decrease, and its stress path moves towards critical state at C4 on the constant suction ellipse SY18a defined by a larger elastic volume EV18. This agrees qualitatively with the observed behaviour of Specimen SB1880TS2 which was isotropically compressed to 1494 kPa prior to shear and for which the pressure at first yield was again about 500 kPa (Figures 6.11 and 6.12). Specimen SB1880TS2 showed an increase in strength with shearing, and lightly overconsolidated behaviour in shear.

9.6.5 Discussion

The conceptual model presented in this section is the first attempt to use an elastic-plastic framework to synthesize triaxial data on unsaturated sand-bentonite material in a useful and coherent manner. The model only deals with the shear behaviour in the q:p*:S space and is therefore incomplete. It is recommended that future work

should be extended to examine the shape of the yield hypersurfaces, and the volumetric behaviour in the v:S:p* space.

While the model is qualitative and hypothetical in part, it has been shown that the model can be used to explain the strain softening and strain hardening behaviour experienced by the specimens tested in shear. It is also encouraging to see that the model qualitatively shows that for the specimens tested at confining pressures up to 1000 kPa, the magnitude of the shear strength near critical state reached by the specimen tended to increase with increasing confining pressure. However, the model does not predict lower shear strengths at critical state for the specimens tested at confining pressures higher than 1000 kPa, as indicated by the behaviour of SB1880TS2 (see Figure 6.12). This inadequacy may be associated with the use of the total stress variable p* in presenting the data, and may be explained by consideration of the soil structures as follows.

The importance of soil structure in influencing the behaviour of compacted soils has long been recognized. Gens and Alonso (1992) were the first researchers to identify the need to consider the role of soil micro- and macro-structures in constitutive modelling of unsaturated swelling clays. Work is now in progress by Gens, Alonso, their colleagues and others (for example, Ridley, 1995; Wheeler, 1996) to develop usable constitutive elastic-plastic models for unsaturated swelling soils. It was discussed in Section 9.2 that compacted sand-bentonite material has complex soil structures with tri-modal pore size distributions. A compacted sand-bentonite specimen may be envisaged as a skeleton structure consisting of peds and inter-ped macrovoids that contain some air. The peds are largely saturated and behave essentially as single units with elastic properties. Therefore the actual S_r of the soil micro- and macro-structures can be quite different from the average S_r of the whole specimen. For the specimens tested in shear tests, the average S_r was measured to be 80% to 85%.

When an unsaturated specimen is subjected to shear stresses, plastic deformation largely takes place in the partially saturated skeleton structure while the saturated peds experience elastic compression (see Section 9.4). The integrity of the peds is maintained by the suction forces attributed to the capillary effects at the edges of the peds. The suctions are in turn influenced by the magnitude of the compression stresses on the peds. Earlier chapters showed that suction changes can be measured by psychrometers. At low confining pressures and correspondingly lower saturations, deformation in the specimen has little effect on the air and water pressures in the inter-ped macrovoids (Lambe and Whitman, 1969). Volume change and strength of the unsaturated soil are largely the result of changes in effective stresses at the contacts between peds units. Therefore the total stress paths may be taken essentially as the effective stress paths. For specimens tested at higher confining pressures (such as Specimen SB1880TS2), the saturation S_r is higher. As the load on the specimen is increased sufficiently to cause the pore air to go into solution, the specimen approaches saturation. This is supported by the data in Figure 6.13 that at axial strains of more than 4%, the total suction in the specimen remained largely constant at about 800 kPa. This value is similar to the range of osmotic suctions reported in Chapter 5, indicative of saturation in the specimen. Further load increase leads to positive pore water pressures in the macrovoids. While positive pore water pressure has no effect on the shear stress, the effective stresses at the contacts between the peds decrease. In this case, the total stress path does not represent the actual stress path experienced by the specimen. Referring to Figure 9.16, assuming positive water pressures, the actual effective stress path will start at A4, but move to the left of the total stress path and reach critical state at a lower q value at C4'.

The implication of the foregoing discussion is that while the suction properties of an unsaturated sand-bentonite material are governed by the micropores, the strength and stress-strain behaviour of the unsaturated material are influenced by the interaction of the

peds at the macroscopic level. Suction indirectly affects the strength and deformation characteristics of the soil insofar as maintaining the integrity of the ped units during shearing. The suction in the unsaturated soil is in turn influenced by the initial moulding water content and subsequent changes in water content as may occur in a drained test. Therefore, the conceptual model presented here implicitly considers the effects of micro- and macro-structures on the constitutive behaviour of unsaturated sand-bentonite material.

As a corollary to the foregoing discussion, qualitative agreement between the trends of suction paths measured by thermocouple psychrometers and those predicted by the conceptual elastic-plastic model shows that the instruments can be successfully used in unsaturated sand-bentonite to provide meaningful data. This adds confidence to the continuing use of psychrometers to measure suctions and water contents in unsaturated compacted swelling clays under well-controlled laboratory conditions.

9.7 Buffer/Container Experiment

9.7.1 Background

It was stated in Chapter 1 that an objective of this study was to examine the usefulness of thermocouple psychrometers in measuring *in situ* suctions and water contents in compacted sand-bentonite material. Results from the Buffer/Container Experiment were presented in Chapter 8. It was hypothesized in Section 8.9 that the discrepancy between the actual water contents and the values measured by psychrometers at the end of the experiment were attributed to vapour pressure and total stress effects. In this section, these two factors are examined in detail. Discussion of the results from the *in situ* experiment is made within the context of the discussions on the laboratory studies presented in Sections 9.3 to 9.6.

9.7.2 End-of-test water content distribution

The end-of-test water content distribution in the buffer was shown in Figure 8.27. The distribution showed good symmetry about the vertical axis of the experiment. To a large extent, the moisture distribution was influenced largely by the temperatures in the system, and otherwise by hydrogeological condition in the surrounding rock, and the geometry of the test. Examination of the temperature data presented in Chapter 8 reveals steep temperature gradients; the temperatures and temperature gradients changes quickly in the buffer close to the heater when the heater was first powered (see Figures 8.5 and 8.7). Subsequently the temperature regime became quite stable. As expected, there was considerable drying in the buffer around the heater. Heating also affected the pore water pressures in the rock. Figure 9.17 shows the influence of temperature on the pore water pressures in the rock measured by hydraulic packers and piezometers (Graham et al., 1996). Due to spatial and temporal variations in temperature and hydraulic potential, competing gradients existed between the annular buffer and the surrounding rock. Elevated pore pressures in the rock caused water to move towards the buffer, whereas elevated temperatures in the buffer tended to drive moisture towards the buffer-rock interface. It is likely that during the initial stage of the heating phase of the experiment the latter condition prevailed, whereas during the latter stage when steady state condition was approached, the former process dominated. This hypothesis is partly confirmed by the increased water contents in regions close to the rock walls of the hole. Furthermore, results from moisture mass balance calculations indicate that there was a small net increase in water content at the end of the test (see Section 8.8). It can be inferred from this observation that the water content distribution shown in Figure 8.27 was not simply a redistribution of moisture under the influence of temperature gradients. Inflows from the surrounding rock also contributed to the changes in water content in the compacted material. The former phenomenon of temperature effects was dominant.

For the top 1 m of buffer remote from the heater, temperature changes were slow and gradual (see Figure 8.6). Therefore the buffer was under approximately isothermal temperature conditions. Temperature had little impact on the pore pressure gradients in the rock (see Figure 9.17). In this region, moisture uptake by the unsaturated buffer was largely controlled by the hydraulic gradients in the surrounding rock. This hypothesis is partly confirmed by the end-of-test water content data. The end-of-test water content distribution for the top 1-m of buffer in Figure 8.27 shows good axial symmetry with an outer region of saturated buffer encompassing an inner core of unsaturated buffer. It may be inferred from the figure that the measured transverse water content gradients were essentially uniform throughout the top 1m of buffer, from which it can be inferred that water supply was largely attributed to the hydraulic flows from the granite rock.

The ability of psychrometers (such as BX8, BX10, BX12, and BX13) located close to the heater to measure suctions and water contents was greatly influenced by temperature and temperature-induced vapour pressure gradients. In contrast, instruments remote from the heater (such as BX1, BX3, and BX5) were influenced less by temperature changes. Under these latter conditions, swelling pressure development and total stress effect played an important role in affecting the precision and accuracy of the psychrometers and the ability to effectively interpret the data.

9.7.3 Temperature effect on suction and water content measurements by psychrometers

It is recognized that in field applications, psychrometer data can be subject to errors induced by temperature effects (Richards, 1969; Brown, 1970). Inaccuracies in the measurement may arise as a result of

a) temperature fluctuations during the course of the measurement,

b) thermally-induced vapour pressure gradients.

The former factor may be minimized by limiting temperature fluctuations to less than 0.001°C during the measurement (Richards, 1969). In the transient heating phase of the Buffer/Container Experiment, a 30-second cooling time was used to cool the sensing junction of the instrument. During this 30-second measurement period, maximum temperature increases in the buffer around the instrument were recorded to be 0.0005°C.

With respect to the latter factor, control of water vapour movement within the buffer mass was not possible. However, the importance of water vapour movement on suction and water content measurements using psychrometers can be qualitatively examined by comparing the responses of two paired instruments: thermal needle BN4 and psychrometer BX8. The instruments were located near the top of the buffer annulus, where temperature gradients were steeper than in other areas of the buffer. They were on the same horizontal level at radial distances of 0.42 m and 0.60 m respectively from the vertical axis of the heater. Figure 9.18 compares the apparent water content changes measured by the two instruments. Positive changes normally indicate moisture increase and vice versa. It can be seen from Figure 9.18 that during the first 50 days of heating, the psychrometer indicated an apparent water content increase of about 4% whereas the thermal needle indicates a net water content decrease of about 1%. Thus it may be inferred that the quantity of moisture taken in by the larger outer buffer zone is larger than the amount of moisture leaving the smaller inner zone. Considering moisture mass balance, this explanation is impermissible. The discrepancy is explained by consideration of the effects of temperature-induced water vapour gradients on the suction measurements made by the psychrometer as follows.

It was pointed out in Section 8.5 that during the first 50 days of heating, temperatures were increasing rapidly in the buffer region that surrounded the heater. In particular, steep temperature gradients were observed in the buffer annulus region

between the heater and the rock. Higher temperatures of up to 55°C were measured in the buffer closer to the heater whereas cooler temperatures of up to 35°C were observed in the buffer beside the rock. These temperature differences led to the development of localized transient vapour pressure gradients within the buffer annulus. Therefore, water vapour tended to move from the inner buffer zone in which the thermal needles were used to the outer buffer zone next to the rock where the psychrometers were located.

It is recalled that psychrometers measure vapour pressures in the void spaces in an unsaturated soil. Thermodynamically, the vapour pressure in the soil can be related to total suction via the Kelvin equation (Hillel, 1980). The water contents measured in the buffer by the psychrometers were determined by simple conversion of the suction data via the suction-water content relationship (Equation 5.2) presented in Chapter 5. This relationship was determined under constant equilibrium laboratory conditions without transients. This simple conversion procedure does not take into consideration thermally-induced vapour pressure effects.

Calculations were carried out to examine the sensitivity of suction and water content to the addition of water vapour associated with vapour pressure gradients. Theoretically, an increase of less than 1 g/m^3 of water vapour is sufficient to cause a reduction in apparent suction in a cubic metre of buffer from 4000 kPa to 0 kPa. However, this quantity of moisture does not significantly change the gravimetric water content. As a corollary to the results of the theoretical calculations, under the influence of temperature-induced vapour pressure gradients, at a given water content, the suction measured by a calibrated psychrometer can be expected to be less than the suction defined by the suction-water content relationship obtained under constant laboratory conditions. Therefore *Hypothesis 4* stated in Chapter 2 is confirmed.

The results of these calculations have practical implications. Refer again to the annular buffer zone in which psychrometer BX8 and thermal needle BN4 were used

(Figure 9.18). Under the influence of transient temperature-induced vapour pressure gradients, a small amount of water vapour was sufficient to cause the vapour pressure to approach saturation vapour pressure in the cooler outer buffer region where the psychrometer was used. Hence, the relative humidity approached 100%, and the measured suction tended to decrease to zero. With the commonly used and simple suction-water content conversion technique adopted for analysing the psychrometer data, the suction changes were interpreted to give changes in the total gravimetric water content, that is, changes in both the vapour and liquid component of the water content. Under these conditions, the psychrometer over-predicted the water content in the unsaturated soil.

Based on observations during the experiment and on results conducted after the test, the following conclusions can be made as to the usefulness of psychrometers to measured *in situ* suctions and water contents in buffer and similar materials under the influence of temperature. Provided that temperature fluctuations are restricted to $\pm 5^{o}C$ and changes in total stress are small such as the conditions encountered during the pre-heating phase of the Buffer/Container Experiment, the instruments can be used to measure suctions, and the simple conversion technique can be used to provide water content values. The effect of total stress on suction measurements using psychrometers is discussed in the next section. However, in field conditions in which large temperature variations exist, transient thermally-induced vapour pressure gradients develop. Because the simple conversion technique does not account for the effect of vapour pressure gradient, the use of such technique leads to over-estimated water content values when full equilibrium is attained. Even with the preceding limitations, it is likely that the instruments can still be used to infer suctions.

While the commercial psychrometers and thermal needles could not precisely indicate the water contents in the unsaturated buffer in the Buffer/Container Experiment

during the heating phase of the experiment, the data from the instruments could be interpreted to indicate the patterns of moisture transfer in the clay under heating. In particular, the psychrometer data clearly demonstrated that under the influence of changing temperature gradients, moisture movement is largely dominated by the vapour phase. This observation therefore confirms the need to incorporate the mechanism of water vapour transfer in the modelling of processes that control heat and moisture flows in compacted clay barriers for the disposal of heat-generating radioactive waste (Thomas and He, 1995).

9.7.4 Total stress effect on suction and water content measurements by psychrometers

Figures 8.17 shows the suction-time relationship of psychrometers BX1, BX3, and BX5. From the figure, it can be seen that 'steps' were measured in the suction-time relationships between 170 and 250 days after the heating began. These steps appeared to be unique to this group of instruments which was remote from the heater. It was discussed in Section 9.7.2 that during the period of 170 and 250 days, changes in temperature and temperature gradient were small (see Figures 8.5 to 8.7). Therefore it is assumed that these 'steps' could not have been caused by temperature-induced vapour pressure gradients. Similar observations were made in the Isothermal Test where no heating was used (Chandler, 1994). In light of the results from the triaxial compression tested presented in Section 6.3, the 'steps' observed in the suction-time and water content-relationships are explained by consideration of total stress effects on suction measurements using psychrometers.

During the isothermal phase of the experiment, the changes in suction were gradual. Based on the similarity in the shape of the suction-time curves in Figure 8.17

(Hillel, 1980), it was reasonable to assume that moisture movement in this isothermal phase was dominated largely by vapour transport. At the beginning of the heating phase, temperatures were changing quickly. It is likely that moisture movement was dominated by transient temperature-induced vapour pressure and water content gradients in the axial direction. The suction decreased relatively quickly over a short period of time (Figure 8.17). As the temperature approached steady state, the suction continued to decrease gradually by virtue of the hydraulic gradients between the rock and the buffer.

As the moisture front moved inward, the buffer closest to the rock became saturated first, and on saturation, developed maximum swelling pressures as controlled by the clay dry density (Dixon et al., 1991). Because of low hydraulic conductivies (Dixon et al. 1993), it is likely that the development of swelling pressure in the saturated buffer led to stress-induced compression of the adjoining unsaturated buffer under a partially undrained condition (see Figure 9.19). Results from triaxial tests presented in Chapter 6 show that when an unsaturated sand-bentonite specimen was compressed at constant mass, the total suction in the specimen tended to decrease with increasing total stress. Therefore, it may be assumed that under the influence of compressive stresses, psychrometers located in the compressed unsaturated buffer would indicate lower total suctions even though the water contents had remained virtually constant. As the moisture front moved toward the compressed buffer, the suction in the buffer continued to decrease (Figure 8.17). When the buffer became saturated, the measured total suction would ultimately move to a value close to the osmotic suction of 0.5 MPa to 1.5 MPa (see Chapter 5).

In Section 8.9, the end-of-test actual water contents were compared with the values measured by the psychrometers. Larger differences in the water content values were noted for the psychrometers used in the top 2 m of the experiment. The larger discrepancies were due in part to vapour pressure effect discussed in Section 9.7.3 and in

part to the total stress effect discussed in this section. Figure 8.21 shows the water content-time relationships for psychrometers BX1, BX3, and BX5. These relationships were obtained by simple conversion of the suctions to water content values using the suction-water content relationship measured under constant atmospheric conditions. As discussed earlier, the 'steps' in the suction-time curves are attributed to total stress effects on the unsaturated buffer brought on by the swelling pressure of the adjoining saturated buffer near the rock. Therefore the observed changes in suction did not truly reflect the changes in the water content in the unsaturated soil. The simple conversion procedure did not incorporate the effect of total stress on the suction measurements using psychrometers, and therefore led to over-estimated water content values.

In the Buffer/Container Experiment, total pressure cells were not installed close to the psychrometers. Therefore the stress conditions at the points of suction measurements were not known. Under *in situ* conditions, the stress-strain and hydraulic boundary conditions in the buffer were changing with time. It may be assumed that stress-induced volume changes in the unsaturated buffer took place under partially drained conditions. Therefore, the suction-water content relationships from 'undrained' constant mass tests presented in Chapter 6 are too idealistic and do not give precise water content values. It is likely that conceptual models such as the one described in Section 9.6, and an understanding of both the stress and hydraulic boundary conditions need to be developed further to quantitatively and accurately define the suction and water content state of the buffer.

9.7.5 Comparison of responses of psychrometers, thermal needles and total pressure cells

Results from the psychrometers and thermal needles were presented in Sections 8.6 and 8.7 respectively. It was shown in Section 9.7.3 that temperature-induced vapour pressure gradients affected the ability of the psychrometers to provide absolute water content values, particularly, during the transient heating phase of the experiment. The effect of total stress on the use of psychrometers to infer water contents was examined in Section 9.7.4. In the case of thermal needles, several factors contributed to the inaccuracy of the instruments in measuring water contents (see Section 8.7). These factors include insensitivity of thermal conductivity to water content at $w > 17\%$, temperature-induced drying shrinkage, and corrosion.

While the values of absolute water contents and water content changes measured by the psychrometers and thermal needles may be in error, the trends of moisture variations, dw, are noteworthy. The term "moisture variation" is defined as the difference between the inferred water content and the initial water content. It is used to determine possible changes in the vapour pressure in the unsaturated buffer at the point of measurement. The latter factors are in turn influenced by both the vapour and liquid components of the soil water in the unsaturated soil (Hillel, 1980; Briscoe, 1984). To facilitate presentation of the data, moisture variation is simply taken as the water content change with respect to the initial water content expressed in % water content. Figure 9.20 presents the best interpretation of the patterns of moisture variations in the unsaturated buffer at Days 0, 50, 100, 200, 400, and 525 respectively since heater activation. Positive values are moisture increases and vice versa.

Several observations can be made from the data in Figure 9.20. One, in the first 50 days of heating, a wetting zone ($2\% < dw < 4\%$) developed beside the rock in the

buffer annulus at a depth of 1.5 m to 3 m (Figure 9.20b). Two, after Day 100, the extent of the wet zone at 1.5 m to 3 m diminished with time as the heating continued (Figure 9.20c). However, the wet zone at 1.25 m to 1.5 m continued to spread upward and laterally as moisture was drawn from the rock and driven from the drying buffer that surrounded the heater into the buffer above and remote from the heater. Three, a dry zone ($-2\% < dw < 0$) began to develop in the buffer annulus at a depth of 2 m to 4 m between Day 50 and Day 100. With time, the zone appeared to extend outward toward the rock, and to the buffer below the heater (Figure 9.20d). Thereafter the extended zone generally remained at a constant range of water content for the period up to Day 525. Four, after Day 400, the buffer above and below the heater was wetting up slowly under virtually isothermal condition (Figures 9.20e and 9.20f).

Based on the observations and data from the psychrometers beyond 525 days as shown in Figures 8.17 to 8.24, it may be assumed that only small, but finite, changes in the water content continued to take place in the buffer after Day 525 until the end of test at Day 897. This assumption is qualitatively supported by the broad similarity in moisture pattern between the moisture sensor data at Day 525 (Figure 9.20f) and actual water content measurements at the end of test (Figure 8.27). However, it should be pointed out that one notable difference exists between the two moisture patterns. The dry buffer zone immediately above the heater as observed at the end of the test (Figure 8.27) is clearly absent from the moisture sensor data (Figure 9.20). This discrepancy arises from the shortage of instrumentation in the buffer mass above the heater.

In general, the responses of the moisture sensors correlated qualitatively with those of the total pressure cells. Figure 9.21 compares the responses of the psychrometers and Geonor total pressure cells. It can be seen from the figure that the total pressures in the buffer zone above and below the heater systematically increased

with time, implying moisture uptake in these areas. The psychrometers showed a steady decrease in the total suction after the initial drop during the transient heating phase. The pressure and psychrometer data are consistent. Similarly, in the buffer annulus, thermal expansion of the heater led to an initial increase in the total pressure (see Section 8.5.2.2). This was followed by subsequent pressure decreases in the buffer due to drying of the material. Correspondingly, as pressures decreased, the psychrometers showed a steady increase in suction with time during the latter part of the experiment.

9.7.6 Total system analysis

The discussions presented in this section identified the importance of total system analysis when dealing with complex swelling clays such as the buffer. Because of the complexities associated with clay-water interactions in compacted sand-bentonite buffer, stress-strain behaviour, deformation and moisture flow are intimately linked. Limited and sometimes confusing information was gained when the data from each individual group of instruments were analysed in isolation. Only when the data from the different groups of instruments (namely, the psychrometers, thermal needles, total pressure cells, hydraulic packers, and piezometers) were considered as a whole, could clearer patterns and trends with respect to moisture movement and pressure development be detected. Processes such as temperature-induced vapour pressure gradients, total stress effects, and dry shrinkage effects were identified and incorporated in the analyses of the data from the commercial moisture sensors.

9.8 Summary

The objective of this study was to investigate the usefulness of thermocouple psychrometers to measure *in situ* suctions and water contents in compacted swelling clays. This study arose from the need to clarify conditions under which psychrometers

can be used to provide meaningful data for the study of unsaturated compacted sand-bentonite material for the underground disposal of heat-generating radioactive waste.

Laboratory and calibration tests were carried out to define the precision and accuracy of commercial psychrometers used in this study. The performance of psychrometers as internal sensors in compacted sand-bentonite material was examined in triaxial isotropic compression and shear tests. The usefulness of psychrometers as moisture sensors in tracking *in situ* suctions and water contents in compacted clays was investigated in the Buffer/Container Experiment.

Based on the results from these laboratory and *in situ* tests, the following understanding has been derived. Under well-controlled laboratory conditions, psychrometers can be used to measure suctions in compacted clays, as supported by the results from suction tests (Chapter 5) and triaxial tests (Chapter 6). In the field, stress and temperature boundary conditions cannot be properly controlled. When temperature fluctuations and total stress changes are small such as the conditions encountered in the pre-heating phase of the Buffer/Container Experiment, the instruments can be successfully used to infer suctions and water contents. However, under the influence of temperature and vapour pressure gradients, and the effect of stress-induced compression, psychrometers may be limited to provide useful information on suctions, but not water contents. Under these latter conditions, while precise water content values are uncertain, the instruments are useful in providing qualitative but meaningful data on the trends of moisture movement under the influence of temperature and hydraulic gradients (see Section 9.7).

Geotechnical instruments are widely used in various civil, geotechnical, and environmental projects for monitoring the performance of engineered structures under field conditions. Interpretation of measurements from the instruments is often difficult. This is because the precision and accuracy of the measurements are sometimes influenced

by the intrusion of the instruments and by other external and environmental factors such as temperature (Dunnicliff, 1988). An example is the use of embedment total pressure cells to measure total pressures in soils. Difference in stiffness between the instruments and the soil may lead to over-estimated or under-estimated values of total soil pressures.

This study showed that the interpretation of *in situ* suctions and water contents using psychrometers is not straightforward. Because of the complexities in the suction-water content relationships of compacted swelling clays, readings from the psychrometers cannot be simply converted to suctions or water contents using simple relationships obtained under constant laboratory conditions. Meaningful and useful information from the instruments can only be gained through combination of an understanding of the principles of operation of the instruments, an understanding of the constitutive relationship of the soil, and comprehension of the coupled processes that control heat and moisture movement. Results from this study also highlighted the importance of total system analysis in field investigations of heat-moisture flow phenomena in compacted swelling clays.

In light of the conclusions from this study, instrumentation schemes in future sealing experiments for the disposal of radioactive waste, need to be planned and designed such that information provided by the instruments is maximized to permit proper interpretation of the data. For example, total pressure cells should be installed in close proximity to psychrometers to facilitate proper interpretation of *in situ* suction and water content measurements. If several types of moisture sensors are used, the instruments should be installed in overlapped zones to allow cross checking of measurements.

CHAPTER 10 CONCLUSIONS AND RECOMMENDATIONS

10.1 Background

The general purpose of this study was to investigate the usefulness of thermocouple psychrometers as moisture sensors to track *in situ* suctions and water contents in compacted clays. The specific objectives of this study identified in Chapter 2 were as follows:

1) to clarify the conditions under which psychrometers can be operated to provide meaningful readings and data in the study of moisture movement and stress-strain behaviour of unsaturated compacted clays.

2) to clarify the role of soil structure in controlling the vapour pressure, and hence the suction in a soil.

3) To explore the use of contemporary unsaturated soil mechanics frameworks similar to those proposed by Alonso et al. (1990), Gens and Alonso (1992), and Delage and Graham (1995) to describe the inter-relationship of stress, volume change, and suction of an unsaturated compacted sand-bentonite material proposed for use in the disposal of heat-generating radioactive waste.

4) To develop a framework to incorporate the effects of stress variations and distortions on suction measurements in compacted clays using thermocouple psychrometers and other psychrometric methods.

5) To establish the bounds of accuracy and precision for thermocouple psychrometers in tracking *in situ* suction and moisture transients under the influence of temperature gradients and stress variations in clay barrier material proposed for use in the disposal of radioactive wastes.

The results of the laboratory and *in situ* tests presented in this thesis indicate that the above objectives have been met.

10.2 Conclusions

The following conclusions are drawn from the studies.

1) Under constant temperature and pressure conditions, commercial thermocouple psychrometers used in this study were accurate to be within ± 6% of the actual suction. They had a precision of ± 0.5μV for the suction range of 1.4 MPa to 5.3 MPa.

2) Providing that the temperature does not vary by ± 5°C, the empirical formula proposed by Wiebe et al. (1970) and Brown (1970) can be used for the psychrometers used in this study to correct the measured outputs against temperature effects for the range of 25°C to 50°C.

3) Suction tests at constant temperatures were carried out on a sand-bentonite material, sand-illite material and Boom Clay using the psychrometer method, vapour equilibrium technique, and filter paper technique. The suction-water content relationships measured by the three methods were statistically indistinguishable. This adds confidence in the use of psychrometers to measure suctions under controlled laboratory conditions.

4) Based on the results from the suction and mercury intrusion porosimetry tests, the total suctions in the sand-bentonite material, sand-illite material and Boom Clay are controlled largely by clay-water interactions in the micropores.

5) Generally, osmotic suctions in the sand-bentonite material, sand-illite material and Boom Clay are largely independent of water content and degree of saturation. Changes in total suctions in these soils can be attributed to the changes in the matric suction.

6) Triaxial isotropic compression tests were carried out to examine the effects of total stress and volume change on suction measurements in compacted sand-bentonite material using psychrometers. Under 'undrained' constant mass

conditions, the total suction in an initially unsaturated specimen tended to decrease with increasing total stress. Hysteresis in the suction paths was generally observed during load-unloading cycling. The difference in suction paths is associated with the different elasto-plasticty characteristics of the soil micro- and macro-structures.

7) A qualitative conceptual elastic-plastic model was proposed to deal with the behaviour of unsaturated sand-bentonite in q:p*:S space. This model adequately explains the results of triaxial tests, and adds further confidence in the use of psychrometers in measuring *in situ* suctions in compacted clays.

8) Under well-controlled laboratory conditions, psychrometers can be used to derive values for the suctions in compacted clays of the type examined in these studies.

9) In the field, provided that temperature fluctuations and total stress changes are small such as conditions encountered in the pre-heating phase of the Buffer/Container Experiment, the instruments can be used successfully to derive values for suctions and water contents.

10) Under the influence of temperature and vapour pressure gradients, and the effect of stress-induced compression, psychrometers may be only useful to derive values for suction but not water content. However, while the instruments cannot indicate water contents precisely, given a total system analysis, the instruments are useful in providing qualitative and meaningful data on the trends of moisture movement.

11) Data from the psychrometers used in the Buffer/Container Experiment showed that under the influence of changing temperature gradients such as the conditions encountered in the annular region of the experiment during the heat phase, moisture movement is dominated largely by the vapour phase. The mechanisms

of vapour transfer need to be incorporated in conceptual and computer models for the design of clay barriers for the disposal of radioactive waste.

12) Because of the complexities in the suction-water content relationships of compacted swelling clays, readings from the psychrometers cannot be converted to suctions or water contents using simple relationships obtained under constant laboratory conditions. Psychrometer data are best applied in combination with observations from other instrument types.

13) This study has provided a rationale for interpreting psychrometer data in compacted clays. Meaningful and useful information from the instruments can be attained through a combination of an understanding of the principles of the operation of the instruments, an understanding of constitutive properties of the soil, comprehension of the coupled processes that control heat and moisture flow in soils, and total system analysis.

10.3 Recommendations

The more important recommendations arising from this work regarding both research to clarify remaining uncertainties and the application and use of psychrometers are as follows.

10.3.1 Laboratory studies

1) Triaxial tests should be carried out to define the exact shape of the yield hyper-surfaces of the conceptual elastic-plastic model proposed in this study. This model should also be extended to include the behaviour of unsaturated sand-bentonite material in the v:S:p* space.

2) In this study, triaxial compression tests with suction measurements using psychrometers were carried out under "undrained" constant mass conditions.

However, these tests did not simulate the partially drained conditions encountered in the Buffer/Container Experiment. Controlled water uptake tests carried out in a triaxial apparatus are recommended to better understand the suction-stress-water content relationship measured under partially drained conditions.

3) Laboratory scale tests should be carried out to better quantify the effect of temperature-induced vapour pressure gradients on the accuracy and precision of psychrometers. Tests can be carried out on 0.5m long column-specimens of compacted sand-bentonite material. In each specimen, psychrometers can be installed in the compacted material at equal spacings along the length of the specimen. Temperature gradients can be set up across the length of the specimen. Changes in psychrometer outputs can be measured and correlated with the vapour pressure gradients under different test boundary conditions.

10.3.2 *In situ* measurements

In future *in situ* experiments designed to study the behaviour of compacted clays, instrumentation schemes should be planned and implemented such that information from the instruments are maximized to allow proper interpretation of the data. The following recommendations concern *in situ* suction and water content measurements on compacted clays in future in situ experiments.

1) Total pressure cells should be used in conjunction with and installed in close proximity to psychrometers to facilitate proper interpretation of *in situ* suction and water content measurements. In this regard, a combined psychrometer/total stress cell could be developed for this purpose.

2) If several types of moisture sensors are used, the instruments should be installed in overlapped zones to allow cross checking of measurements.

3) Total suction measurements should be supplemented by pore air and pore water pressure measurements using piezometers to provide information on pore pressure conditions in the soil near or at full saturation.

4) Moisture sensors capable of measuring total suctions of up to 1500 kPa have been developed at Imperial College, UK, by Ridley and Burland (1993). This type of instruments may be used to infer suctions in the buffer near and at saturation. The usefulness of the Imperial College moisture sensors to track *in situ* suction and moisture transients in compacted sand-bentonite material should be investigated.

5) The moisture sensor scheme for the Buffer/Container Experiment was designed with the expectation that the instruments would provide usable information throughout the experiment. Therefore, thermal needles were used in the dryer buffer close to the heater where temperature gradients were steep; psychrometers were installed in the wetter buffer next to the rock where temporal changes in temperature were gradual. While psychrometers are influenced by the transient effects of temperature, this study shows that the instruments can provide useful information under constant temperature and pressure conditions. In future clay barrier experiments in which heating is incorporated, psychrometers should be installed in the soil near the heat source to provide information on the long term suctions and water contents in the soil at steady state.

REFERENCES

Aitchison, G.D., and Donald, I.B. 1956. Effective stresses in unsaturated soils. Proceedings of the 2nd Australian-New Zealand Conference Soil Mechanics Foundation Engineering, pp. 192-199.

Al-Khafaf, S., and Hanks, R.J. 1974. Evaluation of the filter paper method for estimating soil water potential. Soil Science, **117**, pp. 194-199.

Alonso, E.E., Gens, A., and Hight, D.W. 1987. General Report. Proceedings of the 9th European Conference on Soil Mechanics and Foundation Engineering, Dublin.

Alonso, E.E., Gens, A., and Josa, A. 1990. The constitutive model for partially saturated soils. Géotechnique, **40**, pp. 405-430.

American Society of Testing and Materials 1992. Test Designation D 422, 'Standard methods for particle-size analysis of soils'. ASTM, Philadelphia.

American Society of Testing and Materials 1992. Test Designation D 1557, 'Standard methods for moisture-density relations of soils and soil-aggregate mixtures using 10-lb (4.54-kg) rammer and 18-in. (457-mm) drop'. ASTM, Philadelphia.

American Society of Testing and Materials 1992. Test Designation D 2216-80, 'Standard method for laboratory determination of water (moisture) content of soil, rock, and soil-aggregate mixtures'. ASTM, Philadelphia.

Anderson, M.G. 1984. Prediction of soil suction for slopes in Hong Kong. GCO Publication No. 1/84, Geotechnical Control Office, Engineering Development Department, Hong Kong.

Atkinson, J.H., and Bransby, P.L. 1978. "The Mechanics of Soils: An Introduction to Critical State Soil Mechanics". McGraw-Hill Book Company (UK) Limited, Maidenhead, Berkshire, England.

Atomic Energy of Canada Limited. 1994. The Environmental Impact Statement on the Concept for Disposal of Canada's Nuclear Fuel Waste. AECL-10721.

Aylmore, L.A.G., and Quirk, J.P. 1960. Domain or turbostratic structure in clays. Nature, London, **187**, pp. 1046-1048.

BS1377:1975. 'Methods of test for soils for civil engineering purposes'. British Standards Institution, London.

Balasubramonian, B.I. 1972. Swelling of compaction shale. Ph.D. thesis, University of Alberta, Edmonton, Canada.

Baldi, G., Hueckel, T., Peano, A., and Pellegini, R. 1990. Development in modelling of thermo-hydro-geomechanical behaviour of Boom Clay and clay based buffer materials. ISMES Final Report to CEC, Volume I.

Barden, L. 1971. Examples of clay structure and its influence on engineering behaviour. Roscoe Memorial Symposium, Cambridge.

Barden, L., and Sides, G.R. 1970. Engineering behaviour and structure of compacted clay, Journal of the Soil Mechanics and Foundations Division, Proceedings of the American Society of Civil Engineers, **96**, pp. 1171-1200.

Baver, L.D., Gardner, W.H., and Gardner, W.R. 1972. "Soil Physics". John Wiley & Sons, New York.

Bishop, A.W. 1959. The principle of effective stress. Teknisk Ukeblad, **39**, pp. 859-863.

Blackwell, J.H. 1954. A transient-flow method for determination of thermal constants of insulating materials in bulk. Journal of Applied Physics, **25**, N2.

Bolt, G.H. 1956. Physico-chemical analysis of the compressibility of pure clays. Géotechnique, **6**, pp. 86-93.

Bowles, J.E. 1979. "Physical and Geotechnical Properties of Soils". McGraw-Hill Book Company, New York.

Brackley, I.J.A. 1975. A model of unsaturated clay structure and its application to swell behaviour. Proceedings of the 6th Regional Conference for Africa on Soil Mechanics and Foundation Engineering, Durban, South Africa, September 1975, pp. 71-79.

Brady, N.C. 1974. "The Nature and Properties of Soils". MacMillan Publishing Co., Inc., New York.

Brewer, R. 1964. "Fabric and Mineral Analysis of Soils". John Wiley & Sons, Inc., New York.

Briscoe, R.D. 1984. Thermocouple psychrometers for water potential measurements, Proceedings of the NATO Advanced study Institute on 'Advanced Agricultural Instrumentation', Il Ciocco (Pisa), Italy, May 27-June 9, 1984.

Brown, R.W. 1970. Measurement of water potential with thermocouple psychrometers: construction and application. USDA For. Serv. Res. Pap. INT-80, Intermt. For. and Range Exp. Stn., Ogden, Utah.

Brown, R.W., and Bartos, D.L. 1982. A calibration model for screen-caged Peltier thermocouple psychrometers, Research paper INT-293, Forest Service, United States of Department of Agriculture.

Campbell, G.S., and Campbell, M.D. 1974. Evaluation of a thermocouple hygrometer for measuring leaf water potential *in situ*. Agronomy Journal, **66**, pp. 24-27.

Campbell, G.S., and Gardner, W.H. 1971. Psychrometric measurement of soil water potential: temperature and bulk density effects. Proceedings, Soil Science Society of America, **35**, pp. 8-12.

Campbell, G.S., and Gee, G.W. 1986. Chapter 25, Water Potential: Miscellaneous Methods, in "Methods of Soil Analysis. Part I. Physical and Mineralogical Methods". Agronomy Monograph No. 9, American Society of Agronomy-Soil Science Society of America, Madison, Wisconsin, USA.

Casagrande, A. 1936. The determination of the pre-consolidation load and its practical significance. Discussion D-34. Proceedings of the 1st International Conference on Soil Mechanics and Foundation Engineering, Cambridge, MA, Vol. III, pp. 60-64.

Chandler, N.A. 1993. Buffer/Container Experiment Coordination Meeting No. 10, Atomic Energy of Canada Limited, July 1993.

Chandler, N.A. 1994. Buffer/Container Experiment Coordination Meeting No. 11, Atomic Energy of Canada Limited, April 1994.

Chandler, N.A., Kjartanson, B.H., Kozak, E.T., Martin, C.D., and Thompson, P.M. 1992. Monitoring the geomechanical and hydrogeological response in granite for AECL Research's Buffer/Container Experiment. Proceedings of the 33rd US Symposium on Rock Mechanics, Santa Fe, CA., pp. 161-170.

Chandler, N.A., Gray, M.N., Wan, A.W.L., and Kozak, E.T. 1996. Large-scale sealing experiments in granite. Proceedings of the 2nd North American Rock Mechanics Symposium, Montreal, June 19-21, pp. 1463-1470.

Chandler, R.J., and Gutierrez, C.I. 1986. The filter-paper method of suction measurement, Géotechnique, **36**, pp. 265-268.

Chapman, D.C. 1913. A contribution to the theory of electro-capillarity. Philosophical Magazine, **25**, pp. 475-481.

Cheung, S.C.H., Gray, M.N., and Dixon, D.A. 1987. Hydraulic and ionic diffusion properties of bentonite-sand buffer materials. Coupled Processes Associated with Nuclear Waste Repositories, pp. 393-407.

Choi, J.-W. and Oscarson, D.W. 1996. Diffusive transport through compacted Na- and Ca-bentonite. Journal of Contaminant Hydrogeology, 22, pp. 189-202.

Collins, K. 1983. Scanning electron microscopy of engineering soils. Geoderma, **30**, pp. 243-252.

Constantz, J. 1983. Laboratory analysis of water retention in unsaturated materials at high temperature. in Role of the Unsaturated Zone in Radioactive and Hazardous Waste Disposal, J.W. Mercier et al., (eds.), Ann Arbor Science, Ann Arbor, MI, pp. 147-164.

Corey, A.T. 1986. "Mechanics of Immiscible Fluids in Porous Media". Water Resources Publications, Littleton, Colorado.

Croney, D., Coleman, J.D., and Black, W.P.M. 1958. Studies of the movement and distribution of water in soil in relation to highway design and performance, HRB Special Report 40, Washington DC, pp. 226-252.

Cui, Y.J., and Delage, P. 1993. On the elastic-plastic behaviour of an unsaturated silt. ASCE Special Publication No. 39, pp. 115-126.

Cui, Y.J., Delage, P., and Sultan, N. 1995. An elastic-plastic model for compacted soils. Unsaturated Soils. Proceedings of the 1st International Conference on Unsaturated Soils, Paris, France, 6-8 September 1995, pp. 703-709.

Delage, P., and Graham, J. 1995. Understanding the behaviour of unsaturated soils requires reliable conceptual model. State of the Art Report. Proceedings of the 1st International Conference on Unsaturated Soils, Paris, France, 6-8 September 1995.

Delage, P., and Lefebvre, G. 1984. Study of the structure of a sensitive Champlain clay and of its evolution during consolidation. Canadian Geotechnical Journal, **21**, pp. 21-35.

Diamond, S. 1970. Pore size distribution in clays. Clay and Clay Minerals, **18**, pp. 7-23.

Dixon, D.A., Wan, A.W.L., Graham, J., and, Campbell, S.L. 1993. Assessment of self-sealing and self-healing abilities of dense, high-bentonite-content sealing materials. Proceedings of the 1993 Joint CSCE-ASCE National Conference on Environmental Engineering, July 12-14, 1993, Montreal, Quebec.

Dixon, D.A., Wan, A.W.L., Graham, J., and Kjartanson, B.H. 1991. Assessing pressure-volume equilibrium in bentonite-based materials. Proceedings of the 44th Canadian Geotechnical Conference, September 29-October 2, 1991, Calgary, Alberta.

Dixon, D.A., Gray, M.N., and Thomas, A.W. 1985. A study of the compaction properties of potential clay-sand buffer mixtures for use in nuclear fuel waste disposal, Engineering Geology, **21**, pp. 247-255.

Dixon, D.A., Gray, M.N., Baumgartner, P., and Rigby, G.L. 1986. Pressure acting on waste containers in bentonite-based materials. Proceedings of the 2nd International Conference on Radioactive Waste Management, Winnipeg, Manitoba, September 7-11, 1986.

Dixon, D.A., Hnatiw, D.S.J., and Kohle, C.L. 1992a. Preparation and quality control of materials used in the reference buffer material. Atomic Energy of Canada Limited, Technical Record, TR-575.

Dixon, D.A., Hnatiw, D.S.J., and Walker, B.T. 1992b. The bentonite industry in North America: suppliers, reserves, processing capacity and products. Atomic Energy of Canada Limited, Report, AECL-10587, COG-92-80.

Dunnicliff, J. 1988. "Geotechnical Instrumentation For Monitoring Field Performance". John Wiley & Sons, New York.

Edil, T.B., and Motan, S.E. 1984. Laboratory evaluation of soil suction components. Geotechnical Testing Journal, **7**, pp. 173-181.

Edlefsen, N.E., and Anderson, A.B.C. 1943. Thermodynamics of soil moisture. Hilgardia, **15**, pp. 31-298.

Fredlund, D.G. 1979. Second Canadian Geotechnical Colloquium: Appropriate concepts and technology for unsaturated soils. Canadian Geotechnical Journal, **16**, pp. 121-131.

Fredlund, D.G. and Morgenstern, N.R. 1977. Stress state variables for unsaturated soils. Journal of the Geotechnical Engineering Division, ASCE, **103**, pp. 447-466.

Fredlund, D.G., Morgenstern, N. R., and Widger, R.A. 1978. The shear strength of unsaturated soils. Canadian Geotechnical Journal, **15**, pp. 313-321.

Fredlund, D.G. and Rahardjo, H. 1993. "Soil Mechanics for Unsaturated Soils". John Wiley & Sons, Inc., New York.

Fredlund, D.G., and Xing, A. 1994. Equations for the soil-water characteristic curve. Canadian Geotechnical Journal, **31**, pp. 521-532.

Freeze, R.A., and Cherry, J.A. 1979. "Groundwater". Prentice-Hall, Inc., Englewood Cliffs, New Jersey.

Garcia-Bengochea, I., and Lovell, C.W. 1981. Correlative measurements of pore size distribution and permeability in soils. In "Permeability and Groundwater Contaminant Transport", ASTM STP 746, T.F. Zimmie and C.O. Riggs, eds., American Society for Testing and Materials, 1981, pp. 137-150.

Garcia-Bengochea, I., Lovell, C.W., and Altschaeffl, A.G. 1979. Pore size distribution and permeability of silty clays. Journal of Geotechnical Engineering Division, Proceedings of the American Society of Civil Engineers, **105**, pp. 839-856.

Gelmich, K.S. 1994. Gas breakthrough and mercury intrusion porosimetry testing on illite. Report, Department of Civil and Geological Engineering, University of Manitoba, Winnipeg, Manitoba.

Gens, A., and Alonso, E.E. 1992. A framework for the behaviour of unsaturated expansive clays. Canadian Geotechnical Journal, **29**, pp. 1013-1032.

Gouy, G. 1910. Sur la constitution de la charge électrique à la surface d'un électrolyte. Annales de Physique (Paris) Série 4, **9**, pp. 457-468.

Graham, J., Saadat, F., Gray, M.N., Dixon, D.A., and Zhang, Q.Y. 1989. Strength and volume change behaviour of a sand-bentonite mixture. Canadian Geotechnical Journal, **26**, pp. 292-305.

Graham, J., Oswell, J.M., and Gary, M.N. 1992. The effective stress concept in saturated sand-clay buffer. Canadian Geotechnical Journal, **29**, pp. 1033-1043.

Graham, J., Chandler, N.A., Dixon, D.A., Roach, P.J., To, T., and Wan, A.W.L. 1996. The Buffer/Container Experiment: Volume 4 - Results, Synthesis, Issues. Report, Atomic Energy of Canada Limited.

Gray, M.N. 1980. The behaviour of a granite soil in shear. Materials Division Report No. 14, Geotechnical Control Office, Public Works Department, Hong Kong.

Grim, R.E. 1953. "Clay mineralogy". McGraw Hill Book Company, Inc., New York.

Hausenbuiller, R.L. 1972. "Soil Science: Principles and Practices". Wm. C. Brown Company Publishers, Dubuque, Iowa.

Hilf, J.W. 1956. An investigation of pore water pressure in compacted cohesive soils. Tech. Memo. No. 654, U.S. Department of the Interior, Bureau of Reclamation, Design and Construction Division, Denver, Colorado.

Hillel, D. 1980. "Fundamentals of Soil Physics". Academic Press, New York.

Hueckel, T., and Pellegrini, R. 1992. Effective stress and water pressure in saturated clays during heating-cooling cycles, Canadian Geotechnical Journal, **29**, pp. 1095-1102.

Jennings, J.E., and Burland, J.B. 1962. Limitations to the use of effective stresses in partly saturated soils. Géotechnique, **12**, pp. 125-144.

Juang, C.H., and Holtz, R.D. 1986. Fabric, pore size distribution, and permeability of sandy soils. Journal of Geotechnical Engineering Division, ASCE, **112**, pp. 855-868.

Kanno, T., and Wakamatsu, H. 1992. Water uptake and swelling properties of unsaturated bentonite buffer materials. Canadian Geotechnical Journal, **29**, pp. 1102-1107.

Kirkham, T.L. 1995. Development of test equipment and procedures for determination of the gas-breakthrough pressure of compacted clay materials with preliminary results. M.Sc. Thesis. University of Manitoba, Winnipeg, Manitoba, Canada.

Kjartanson, B.H., and Keil, L.D. 1992. Buffer/Container Experiment: detailed design report. Atomic Energy of Canada Limited, Unpublished report.

Kjartanson, B.H., Chandler, N.A., Wan, A.W.L., Kohle, C.L., and Roach, P.J. 1992. Use of a method specification for in situ compaction of clay-based barrier materials. Proceedings of the 3rd International Conference on High-Level Radioactive Waste Management, April 12-16, 1992, Las Vegas, Nevada, pp. 1129-1136.

Krahn, J. 1970. Comparison of soil pore water potential components. M.Sc. thesis, University of Saskatchewan, Saskatoon, Canada.

Krahn, J., and Fredlund, D.G. 1972. On total, matric and osmotic suction. Soil Science, **114**, pp. 339-348.

Lambe, T.W. 1958. The engineering behaviour of compacted clay. Journal of Soil Mechanics and Foundation Engineering, American Society of Civil Engineers, **84**, pp. 1-35.

Lambe, T.W., and Whitman, R.V. 1969. "Soil Mechanics". John Wiley & Sons, Inc., New York.

Lapierre, C., Leroueil, S., and Locat, J. 1990. Mercury intrusion and permeability of Louiseville clay. Canadian Geotechnical Journal, **27**, pp. 761-773.

Matyas, E. L. 1967. Air and water permeability of compacted soils. Permeability and Capillarity of Soils, ASTM STP 417, American Society of Testing and Materials, pp. 160-173.

Matyas, E.L., and Radhakrishna, H.S. 1968. Volume change characteristics of partially saturated soils. Géotechnique, **18**, pp. 432-448.

McQueen, I.S., and Millar, R.F. 1968. Calibration and evaluation of a wide-range gravimetric method for measuring moisture stress. Soil Science, **106**, pp. 225-231.

Milly, P.C.D. 1982. Moisture and heat transport in hysteretic, inhomogeneous porous media: a matric head-based formulation and numerical solution, Water Resources Research, **18**, pp. 489-498.

Mitchell, J.K. 1976. "Fundamental of Soil Behaviour". Wiley & Sons, New York.

Mitchell, J.K., Hooper, D.R., and Campanella, R.G. 1965. Permeability of compacted clay. Journal of the Soil Mechanics and Foundations Division, Proceedings of the American Society of Civil Engineers, **91**, pp. 41-65.

Monteith, J.L. 1973. "Principles of Environmental Physics". American Elsevier Publishing Company, Inc., New York.

Moore, W.J. 1972. "Physical Chemistry". Prentice-Hall, Inc., Englewood Cliffs, New Jersey.

Musa, A.M. 1982. On the yield of a compacted soil. M.Sc. Thesis, University of Wales, Cardiff, UK.

Nielsen, D. R., Van Genuchten, M. Th. and Biggar, J. W. 1986. Water flow and solute transport processes in the unsaturated zone. Water Resources Research, **22**, pp. 89S-108S.

Olsen, H.W. 1962. Hydraulic flow through saturated clays. Clays and Clay Mineralogy, **11**, pp. 131-161.

Olson, R.E., and Langfelder L.J. 1965. Pore water pressures in unsaturated soils. Journal of the Soil Mechanics and Foundations Division, Proceedings of the American Society of Civil Engineers, **91**, pp. 127-150.

Oscarson, D.W., Dixon, D.A., and Gray, M.N. 1990. Swelling capacity and permeability of an unprocessed and a processed bentonitic clay. Engineering Geology, **28**, pp. 281-289.

Osipow, L.I. 1962. "Surface Chemistry: Theory and Industrial Applications", American Chemical Society Monograph Series, Reinhold Publishing Corporation, New York.

Oswell, J.M. 1991. Elastic plastic behaviour of a sand-bentonite mixture. Ph.D. thesis, University of Manitoba, Winnipeg, Manitoba, Canada.

Peck, A.J. 1960. Change of moisture tension with temperature and air pressure: theoretical. Soil Science, **89**, pp. 303-310.

Pellegrini, R., Borsetto, M., Peano, A., and Tassoni, E. 1989. Factors affecting the thermo-hydro-mechanical response of clay in the safety assessment of nuclear waste repositories. In "Excavation responses in deep radioactive waste repositories-implications for engineering design and safety performance". Proceedings, OECD (Paris) Nuclear Energy Agency Workshop, Winnipeg, Manitoba, 1988, pp. 501-514.

Phene, C.J., Hoffman, G.J., and Rawlins, S.L. 1971. Measuring soil matric potential in situ by sensing heat dissipation with a porous body: theory and sensor construction. Proceedings, Soil Science Society of America, **35**, pp. 27-32.

Philip, J.R., and de Vries, D.A. 1957. Moisture movement in porous materials under temperature gradients. Transactions, American Geophysical Union, **38**, pp. 222-232.

Pusch, R., Karnland, O., Muurinen, A. 1989. Transport and microstructural phenomena in bentonite clay with respect to the behaviour and influence of Na, Cu and U. Technical Report, TR 89-34, SKB, Stockholm, Sweden.

Pusch, R., Karnland, O., Hökmark, H. 1990. GMM - A general microstructural model for qualitative and quantitative studies of smectite. Technical Report, TR 90-43, SKB, Stockholm, Sweden.

Quigley, R.M. 1984. Quantitative mineralogy and preliminary pore-water chemistry of candidate buffer and backfill materials for a nuclear fuel waste disposal vault. Atomic Energy of Canada Limited, Report, AECL-7827.

Radhakrishna, H.S., Lau, K.-C., Kjartanson, B.H., and Crawford, A.M. 1992. Numerical modelling of heat and moisture transport through bentonite-sand buffer. Canadian Geotechnical Journal, **29**, pp. 1044-1059.

Rawlins, S.L. 1966. Theory for thermocouple psychrometers used to measure water potential in soil and plant samples, Agricultural Meteorology, **3**, pp. 293-310.

Richards, B.G. 1967. A review of methods for the determination of the moisture flow properties of unsaturated soils. Tech. Memo. No. 5, Commonwealth Science and Industrial Research Organisation, Australia.

Richards, B.G. 1969. Psychrometric techniques for measuring soil water potential. Division of Soil Mechanics Technical Report No. 9, Commonwealth Scientific and Industrial Research Organization, Australia.

Richards, B.G. 1974. Behaviour of unsaturated soils. In "Soil Mechanics-New Horizons", I.K. Lee (ed.), Newnes-Butterworths, London, 1974, pp. 113-157.

Richards, B.G., Peter, P., and Emerson, W.W. 1983. The effects of vegetation on the swelling and shrinkage of soils in Australia. Géotechnique, **33**, pp. 127-139.

Richards, L.A. 1931. Capillary conduction of liquids through porous mediums. Physics, **1**, pp. 318-333.

Ridley, A.M. 1995. Strength-suction-moisture content relationships for kaolin under normal atmospheric conditions. Proceedings of the 1st International Conference on Unsaturated Soils, Paris, France, 6-8 September 1995, pp. 645-651.

Ridley, A.M., and Burland, J.B. 1993. A new instrument for the measurement of soil moisture suction. Géotechnique, **43**, pp. 321-324.

Ridley, A.M., and Burland, J.B. 1994. Reply to a discussion on "A new instrument for the measurement of soil moisture suction" by Ridley and Burland. Géotechnique, **44**, pp. 551-556.

Roach, P.J., Hampshire, R.A., Keith, S.G., Kohle, C.L., Rolleston, L.A., and Steiner, V.P. 1996. The design, construction, testing, and use of equipment for decommissioning the Buffer/Container Experiment. Atomic Energy of Canada Limited, Technical record.

Roger, G.F.C., and Mayhew, Y.R. 1981. "Thermodynamics and Transport Properties of Fluids". Basil Blackwell, Oxford.

Roscoe, K.H., Schofield, A.N., and Wroth, C.P. 1958. On the yielding of soils. Géotechnique, **8**, pp. 22-53.

Saadat, F. 1989. Constitutive modelling of the behaviour of a sand-bentonite mixture. Ph.D. thesis, University of Manitoba, Winnipeg, Manitoba, Canada.

Savage, M.J., and Cass, A. 1984. Measurement of water potential using *in situ* thermocouple hygrometer. Advances in Agronomy, **37**, pp. 73-126.

Seed, H.B., Mitchell, J.K., and Chan, C.K. 1962. Studies of swell and swell pressure characteristics of compacted clays. US Highway Research Board, Bulletin 313.

Sibley, J.W. and Williams, D.J. 1990. A new filter material for measuring soil suction. Geotechnical Testing Journal, **13**, pp. 381-384.

Silvestri, V. 1994. Water content relationships of a sensitive clay subjected to cycles of capillary pressures. Geotechnical Testing Journal, **17**, pp. 57-64.

Slatyer, R.O. 1967. "Plant-Water Relationships". Academic Press, London.

Spangler, M.G. 1960. "Soil Engineering". Internal Textbook Company, Scranton, Pennsylvania.

Sridharan, A., and Jayadeva, M.S. 1982. Double layer theory and compressibility of clays. Géotechnique, **32**, pp. 133-144.

Stannard, D.I. 1992. Tensiometer - theory, construction, and use. Geotechnical Testing Journal, **15**, pp. 48-58.

Stroes-Gascoyne, S., and West, J.M. 1994. Microbial issues pertaining to the Canadian concept for the disposal of nuclear fuel waste. Atomic Energy of Canada Limited Report, AECL-10808, COG-93-54.

Sun, B.C.-C. 1986. Stress-strain properties in sand-clay buffer materials. M.Sc. thesis, University of Manitoba, Winnipeg, Manitoba, Canada.

Tabor, D. 1969. "Gases, Liquids and Solids". Cambridge University Press, Cambridge.

Tadepalli, R. and Fredlund, D. G. 1991. The collapse behavior of a compacted soil during inundation. Canadian Geotechnical Journal, **28**, pp. 477-488.

Terzaghi, K. 1936. The shearing resistance of saturated soils. Proceedings of the 1st International Conference on Soil Mechanics and Foundation Engineering, Cambridge, MA, Vol. I, pp. 54-56.

Thomas, H.R. 1992. On the development of a model of coupled heat and transfer in unsaturated soil. Canadian Geotechnical Journal, **29**, pp. 1107-1112.

Thomas, H.R., and He, Y. 1995. Analysis of coupled heat, moisture and air transfer in a deformable unsaturated soil. Géotechnique, **45**, pp. 677-689.

Wan, A.W.L. 1987. Compaction and strength characteristics of sand-clay buffer material formed at swelling pressure-water content equilibrium. M.Sc. thesis, Department of Civil Engineering, University of Manitoba, Winnipeg, Canada.

Wan, A.W.L., Graham, J., and Gray, M.N. 1990. Influence of soil structure on the stress-strain behaviour of sand-bentonite mixtures. Geotechnical Testing Journal, **13**, pp. 179-187.

Wan, A.W.L., Kjartanson, B.H., Spinney, M.H., Radhakrishna, H.S., and Lau, K.-C. 1992. A system for measuring moisture transients in clay-based barrier materials. Proceedings of the 3rd International Conference on High-Level Radioactive Waste Management, April 12-16, 1992, Las Vegas, Nevada, pp. 1122-1128.

Wan, A.W.L., Gray, M.N., and Graham, J. 1995. On the relations of suction, moisture content, and soil structure in compacted clays. Proceedings of the 1st International Conference on Unsaturated Soils, Paris, 6-8 June 1995, pp. 215-222.

Wheeler, S.J. 1996. Inclusion of specific water volume within an elasto-plastic model for unsaturated soil. Canadian Geotechnical Journal, **33**, pp. 42-57.

Wheeler, S.J., and Sivakumar, V. 1995. An elasto-plastic critical state framework for unsaturated soil. Géotechnique, **45**, pp. 35-53.

Wiebe, H.H., Brown, R.W., and Barker, J. 1977. Temperature gradient effects on in situ hygrometer measurements of water potential. Agronomy Journal, **69**.

Wiebe, H.H., Brown, R.W., Daniel, T.W., and Campbell, E. 1970. Water potential measurements in trees. BioScience, **20**, pp. 225-226.

Wiebe, H.H., Campbell, G.S., Gardner, W.H., Rawlins, S.L., Cary, J.W., and Brown, R.W. 1971. Measurement of plant and soil water status. Utah Agricultural Experiment Station, Bulletin 484.

Wilson, G.W. 1990. Soil evaporative fluxes for geotechnical engineering problems. Ph.D. thesis, University of Saskatchewan, Saskatoon, Saskatchewan, Canada.

Wood, D.M. 1990. "Soil Behaviour and Critical State Soil Mechanics". Cambridge University Press, Cambridge.

Yong, R.N., and Warkentin, B.P. 1975. "Introduction to Soil Behaviour". The Macmillan Company, New York.

Young, J.F. 1967. Humidity control in the laboratory using salt solutions - a review. Journal of Applied Chemistry, **17**, pp. 241-245.

Zakaria, L., Wheeler, S.J., and Anderson, W.F. 1995. Yielding of unsaturated compacted kaolin. Proceedings of the 1st International Conference on Unsaturated Soils, Paris, 6-8 June 1995, pp. 223-228.

Properties	Kaolinite	Illite	Montmorillonite
Planar diameter (μm)	0.1-4	0.1-2	0.01-1
Basic layer thickness (μm)	0.00072	0.001	0.001
Particle thickness (μm)	0.05	0.005-0.03	0.001-0.01
Specific surface (m^2/g)	5-20	8-120	700-800
Cation exchange capacity (meq/100g)	3-15	15-40	80-100
Plastic limit (%)	25-35	35-40	100
Liquid limit (%)	50-70	60-90	300-800

Table 2.1 Properties of common clay minerals (after Yong and Warkentin, 1975; Hillel, 1980).

Methods	Suction Range	Suction Components	Principle	References
Thermocouple psychrometer	100 to 7000 kPa	Total	Measure vapour pressure	Richards (1967); Briscoe (1984)
Filter paper method	Entire range	Total, matric, osmotic	Measure vapour pressure	Chandler and Gutierrez (1986); Fredlund and Rahardjo (1993)
Vapour equilibrium method	Entire range	Total	Control vapour pressure	Campbell and Gee, (1986); Wilson (1990)
Pore fluid squeezer	Entire range	Osmotic	Measure thermal conductivity of pore fluid	Balasubramonian (1972); Krahn and Fredlund (1972)
Tensiometer and hydraulic piezometer	< 90 kPa	Matric	Measure water tension	Anderson (1984); Stannard (1991)
Thermal conductivity sensor	< 300 kPa	Matric	Measure thermal conductivity	Phene et al. (1971); Fredlund and Rahardjo (1993)
Axis translation technique	< 1500 kPa	Matric	Control air and water pressures	Hilf (1956); Fredlund and Rahardjo (1993)

Table 2.2 Comparison of methods for measuring soil suctions.

Microvoltmeter	Cooling Current (mA)	Cooling Time (s)
PR-55	6 to 9	20 to 40
HR-33T	8	20 to 40

Table 3.1 Cooling parameters used in this study.

Psychrometer	Calibration Factor [This Study] (kPa/μV)	R^2	Calibration Factor [Lower 95%] (kPa/μV)	Calibration Factor [Upper 95%] (kPa/μV)	Standard Error Of Coefficient (%)	Deviation Parameter (%)	Calibration Factor [Factory] (kPa/μV)	Difference Between This Study & Factory (%)
33913	245	1.00	239	250	2.2	8.1	284	39.4
35466	236	0.98	226	247	4.3	4.9	189	46.9
36001	208	1.00	205	212	1.8	7.8	227	18.8
36003	219	0.97	208	230	4.9	2.7	212	7.1
36006	198	0.85	174	222	12.1	13.7	214	16.0
36009	201	0.87	178	224	11.4	11.9	223	22.3
36021	228	0.93	217	239	5.0	1.4	N/A	N/A
36262	215	0.90	202	229	6.4	4.4	223	7.8
36263	209	0.91	196	222	6.1	7.5	240	31.2
36264	219	0.90	205	232	6.2	2.8	234	15.0
36265	225	0.90	211	240	6.5	0.1	269	43.7
36266	208	0.89	194	222	6.9	8.1	236	27.9
36267	208	0.89	195	221	6.4	8.1	278	69.8
36268	215	0.89	200	229	6.6	4.8	234	19.1
36269	218	0.96	207	230	5.3	2.9	245	26.6
36270	221	0.89	203	239	8.3	1.7	219	1.8
36271	236	0.95	226	245	4.0	4.7	250	14.1
36272	192	0.98	184	199	4.0	17.2	240	48.6
36273	218	0.92	206	230	5.7	3.2	269	50.9
36274	214	0.91	201	227	6.0	4.9	243	28.4
36276	193	0.93	177	209	8.3	16.5	255	62.1
36277	247	0.96	238	255	3.5	8.9	N/A	N/A
36279	213	0.98	205	222	4.1	5.5	243	29.6
36282	223	0.94	208	238	6.6	0.8	227	4.3
36284	188	0.99	181	194	3.6	19.9	219	31.7
36285	232	0.98	222	242	4.2	3.1	219	12.8
36286	231	0.98	223	240	3.8	2.9	217	14.0
36287	242	0.98	234	250	3.4	7.1	238	3.9
36293	311	0.95	293	330	6.0	27.8	243	68.6
36436	233	0.98	224	242	3.8	3.4	210	22.7
36437	224	0.96	213	235	4.7	0.4	192	31.7
36438	234	0.96	223	246	5.0	4.1	200	34.4
36439	225	0.93	209	241	7.0	0.2	205	20.3
36441	255	0.95	242	268	5.1	11.9	207	48.7
36443	212	0.99	205	220	3.5	5.9	205	7.4
36446	229	0.88	209	249	8.9	1.8	223	5.7
36450	267	0.92	250	284	6.4	15.7	217	49.2
36454	225	0.97	215	235	4.3	0.1	221	3.9
36458	228	0.80	201	255	11.7	1.5	217	10.8
36467	246	0.85	221	271	10.0	8.6	N/A	N/A
Average	225	0.93	212	238	5.8	6.7	229	27.0
Maximum	311	1.00	293	330	12.1	27.8	284	69.8
Minimum	188	0.80	174	194	1.8	0.1	189	1.8
Stand. Dev.	22	0.05	22	23	2.4	6.0	22	18.6
Count	40	40	40	40	40	40	37	37

N/A: Not available

Table 3.2 Comparison of psychrometer calibration factors.

Psychrometer	A	B	C
ψ (kPa)	2158	2280	2411
T (°C)	10	25	50
RH (%)	98.4	98.4	98.4
v_o (kPa)	1.227	3.166	12.330
v (kPa)	1.207	3.114	12.133
e_o (g/m^3)	9.398	23.041	83.056
e (g/m^3)	9.248	22.673	81.728
Δe (g/m^3)	0.150	0.368	1.328

where ψ is suction potential, T is temperature, RH is relative humidity, v_o is saturated water vapour pressure, v is partial vapour pressure, e_o is saturated absolute humidity, and e is absolute humidity.

Table 3.3 Comparison of vapour pressures and absolute humidities at different temperatures.

Specimen Number	Material	Test Type	Initial Water Content (%)	Initial Bulk Density (Mg/m^3)	Initial Dry Density (Mg/m^3)	Final Water Content (%)	Final Bulk Density (Mg/m^3)	Final Dry Density (Mg/m^3)
P-18-80	S/B	Single-stage	17.6	1.64	1.40	17.7	1.63	1.38
P-18-95	S/B	Single-stage	17.6	1.99	1.69	17.8	1.97	1.68
P-20-80	S/B	Single-stage	19.6	1.69	1.41	19.5	1.69	1.42
P-20-95	S/B	Single-stage	19.6	2.00	1.68	19.0	2.00	1.68
P-22-80	S/B	Single-stage	21.5	1.68	1.38	20.8	1.66	1.38
P-22-95	S/B	Single-stage	21.3	1.98	1.63	20.5	1.98	1.64
P-24-80	S/B	Single-stage	23.2	1.72	1.39	21.9	1.71	1.40
P-26-80	S/B	Single-stage	25.6	1.79	1.42	25.0	1.79	1.43
P-26-95	S/B	Single-stage	25.6	1.96	1.56	25.0	1.93	1.55
SI-PSY-INC	S/I	Multi-stage	9.6	2.09	1.90	2.3	1.96	1.91
BC-PSY-INC	BC	Multi-stage	17.5	1.86	1.59	13.0	1.84	1.63

S/B Sand-bentonite
S/I Sand-illite
BC Boom clay

Table 4.1 Summary of conditions of specimens tested by the psychrometer method.

Specimen Number	Test Type	H_2SO_4 Concentration (g/ml)	Total Suction at 25°C (MPa)	Initial Water Content (%)	Initial Bulk Density (Mg/m^3)	Initial Dry Density (Mg/m^3)	Final Water Content (%)	Final Bulk Density (Mg/m^3)	Final Dry Density (Mg/m^3)	Total Shrinkage Strain (%)
SB-L1-1.05	Single-stage	1.05	3.5	18.0	Uncompacted	Uncompacted	18.0	Uncompacted	Uncompacted	N/A
SB-L2-1.05	Single-stage	1.05	3.5	18.0	Uncompacted	Uncompacted	17.2	Uncompacted	Uncompacted	N/A
SB-L-1.10	Single-stage	1.10	8.6	18.0	Uncompacted	Uncompacted	12.0	Uncompacted	Uncompacted	N/A
SB-80-1.10	Single-stage	1.10	8.6	18.0	1.65	1.40	11.9	1.68	1.50	7.12
SB-95-1.10	Single-stage	1.10	8.6	18.0	1.88	1.60	12.2	1.91	1.70	6.51
SB-98-1.10	Single-stage	1.10	8.6	18.0	2.09	1.77	11.0	2.09	1.88	6.17
SB-L-1.15	Single-stage	1.15	16.2	16.8	Uncompacted	Uncompacted	11.5	Uncompacted	Uncompacted	N/A
SB-80-1.15	Single-stage	1.15	16.2	16.8	1.64	1.40	10.6	1.63	1.48	5.26
SB-95-1.15	Single-stage	1.15	16.2	16.8	1.90	1.63	10.4	1.89	1.71	5.13
SB-98-1.15	Single-stage	1.15	16.2	16.8	2.00	1.72	9.8	1.90	1.73	0.72
SB-L-1.25	Single-stage	1.25	47.9	18.0	Uncompacted	Uncompacted	7.0	Uncompacted	Uncompacted	N/A
SB-80-1.25	Single-stage	1.25	47.9	18.0	1.64	1.39	6.9	1.60	1.49	7.09
SB-95-1.25	Single-stage	1.25	47.9	18.0	1.93	1.63	7.1	1.86	1.73	6.20
SB-98-1.25	Single-stage	1.25	47.9	18.0	1.98	1.68	7.0	1.90	1.77	5.64
SB-L-1.35	Single-stage	1.35	102.4	16.8	Uncompacted	Uncompacted	4.7	Uncompacted	Uncompacted	N/A
SB-80-1.35	Single-stage	1.35	102.4	16.8	1.62	1.39	4.7	1.53	1.46	5.31
SB-95-1.35	Single-stage	1.35	102.4	16.8	1.91	1.63	5.3	1.81	1.71	5.12
SB-98-1.35	Single-stage	1.35	102.4	16.8	1.98	1.70	5.1	1.85	1.76	3.67
SB-L-1.50	Single-stage	1.50	227.9	18.5	Uncompacted	Uncompacted	2.1	Uncompacted	Uncompacted	N/A
SB-80-1.50	Single-stage	1.50	227.9	18.5	1.60	1.35	2.2	N/A	N/A	N/A
SB-95-1.50	Single-stage	1.50	227.9	18.5	1.84	1.55	2.1	N/A	N/A	N/A
SB-98-1.50	Single-stage	1.50	227.9	18.5	1.86	1.57	2.0	N/A	N/A	N/A
SB-L-1.70	Single-stage	1.70	469.3	16.8	Uncompacted	Uncompacted	0.6	N/A	N/A	N/A
SB-80-1.70	Single-stage	1.70	469.3	16.8	1.63	1.39	0.6	1.50	1.49	6.90
SB-95-1.70	Single-stage	1.70	469.3	16.8	1.91	1.63	0.7	1.74	1.73	5.61
SB-98-1.70	Single-stage	1.70	469.3	16.8	1.94	1.66	0.6	1.77	1.76	5.93
SB1-L-INC	Multi-stage	N/A	N/A	18.0	Uncompacted	Uncompacted	8.7	Uncompacted	Uncompacted	N/A
SB2-90-INC	Multi-stage	N/A	N/A	18.0	1.90	1.61	8.9	1.90	1.74	7.99
SB3-85-INC	Multi-stage	N/A	N/A	18.0	1.83	1.55	9.1	1.84	1.69	8.79
SB4-73-INC	Multi-stage	N/A	N/A	18.0	1.57	1.33	9.1	1.62	1.48	11.43
SB5-80-INC	Multi-stage	N/A	N/A	18.0	1.60	1.35	9.0	1.61	1.48	9.38

N/A: not available

Table 4.2 Summary of conditions of sand-bentonite specimens in the vapour equilibrium test series.

Specimen Number	H_2SO_4 Concentration (g/ml)	Total Suction at 25°C (MPa)	Initial Water Content (%)	Initial Bulk Density (Mg/m^3)	Initial Dry Density (Mg/m^3)	Final Water Content (%)	Final Bulk Density (Mg/m^3)	Final Dry Density (Mg/m^3)	Total Shrinkage Strain (%)
SI-L1-1.05	1.05	3.5	10.0	Uncompacted	Uncompacted	5.0	Uncompacted	Uncompacted	N/A
SI-L2-1.05	1.05	3.5	10.0	Uncompacted	Uncompacted	4.9	Uncompacted	Uncompacted	N/A
SI-L-1.10	1.10	8.6	8.6	Uncompacted	Uncompacted	2.3	Uncompacted	Uncompacted	N/A
SI-80-1.10	1.10	8.6	8.6	1.86	1.72	2.2	1.77	1.73	0.64
SI-95-1.10	1.10	8.6	8.6	2.29	2.11	2.2	2.16	2.11	0.39
SI-98-1.10	1.10	8.6	8.6	2.30	2.12	2.2	2.19	2.14	0.92
SI-L-1.15	1.15	16.2	10.0	Uncompacted	Uncompacted	1.5	Uncompacted	Uncompacted	N/A
SI-80-1.15	1.15	16.2	10.0	1.88	1.71	1.6	1.75	1.72	0.79
SI-95-1.15	1.15	16.2	10.0	2.20	2.00	1.4	2.08	2.05	2.37
SI-98-1.15	1.15	16.2	10.0	2.32	2.11	1.5	2.16	2.12	0.82
SI-L-1.25	1.25	47.9	8.5	Uncompacted	Uncompacted	1.0	Uncompacted	Uncompacted	N/A
SI-80-1.25	1.25	47.9	8.5	1.88	1.74	0.9	1.75	1.73	-0.05
SI-95-1.25	1.25	47.9	8.5	2.17	2.00	0.9	2.03	2.01	0.38
SI-98-1.25	1.25	47.9	8.5	2.23	2.06	0.8	2.15	2.13	3.72
SI-L-1.35	1.35	102.4	10.0	Uncompacted	Uncompacted	0.5	Uncompacted	Uncompacted	N/A
SI-80-1.35	1.35	102.4	10.0	1.88	1.71	0.5	1.73	1.72	0.80
SI-95-1.35	1.35	102.4	10.0	2.11	1.92	0.6	1.96	1.95	1.86
SI-98-1.35	1.35	102.4	10.0	2.24	2.04	0.6	2.06	2.05	0.45
SI-L-1.50	1.50	227.9	10.0	Uncompacted	Uncompacted	0.2	Uncompacted	Uncompacted	N/A
SI-80-1.50	1.50	227.9	10.0	1.84	1.67	0.3	1.69	1.68	0.89
SI-95-1.50	1.50	227.9	10.0	2.18	1.98	0.3	2.02	2.01	1.45
SI-98-1.50	1.50	227.9	10.0	2.24	2.03	0.3	2.09	2.08	2.52
SI-L-1.70	1.70	469.3	10.0	Uncompacted	Uncompacted	0.1	Uncompacted	Uncompacted	N/A
SI-80-1.70	1.70	469.3	10.0	1.85	1.68	0.1	1.70	1.70	1.36
SI-95-1.70	1.70	469.3	10.0	2.21	2.01	0.1	2.02	2.02	0.51
SI-98-1.70	1.70	469.3	10.0	2.25	2.04	0.1	2.07	2.07	1.41

N/A: not applicable

Table 4.3 Summary of conditions of sand-illite specimens in the vapour equilibrium test series.

Specimen Number	H_2SO_4 Concentration (g/ml)	Total Suction at 25°C (MPa)	Initial Water Content (%)	Initial Bulk Density (Mg/m^3)	Initial Dry Density (Mg/m^3)	Final Water Content (%)	Final Bulk Density (Mg/m^3)	Final Dry Density (Mg/m^3)	Total Dry Shrinkage Strain (%)
BC-L1-1.05	1.05	3.5	15.0	Uncompacted	Uncompacted	14.3	Uncompacted	Uncompacted	N/A
BC-L2-1.05	1.05	3.5	15.0	Uncompacted	Uncompacted	14.3	Uncompacted	Uncompacted	N/A
BC-L-1.1	1.10	8.6	15.8	Uncompacted	Uncompacted	10.0	Uncompacted	Uncompacted	N/A
BC-80-1.1	1.10	8.6	15.8	1.72	1.49	10.2	1.68	1.53	2.57
BC-95-1.1	1.10	8.6	15.8	2.06	1.78	10.3	2.01	1.82	2.44
BC-98-1.1	1.10	8.6	15.8	2.09	1.80	10.4	2.07	1.87	3.80
BC-L-S2-1.15	1.15	16.2	2.0	Uncompacted	Uncompacted	6.9	Uncompacted	Uncompacted	N/A
BC-S3-1.15	1.15	16.2	15.4	2.02	1.75	7.5	1.96	1.82	3.97
BC-S4-1.15	1.15	16.2	15.4	2.03	1.76	7.6	1.96	1.82	3.51
BC-L-1.15	1.15	16.2	2.1	Uncompacted	Uncompacted	6.8	Uncompacted	Uncompacted	N/A
BC-95-1.15	1.15	16.2	15.7	2.04	1.76	7.4	1.94	1.80	2.34
BC-L-1.25	1.25	47.9	14.8	Uncompacted	Uncompacted	5.6	Uncompacted	Uncompacted	N/A
BC-80-1.25	1.25	47.9	14.8	1.73	1.51	5.7	1.68	1.59	5.29
BC-95-1.25	1.25	47.9	14.8	1.97	1.72	5.7	1.91	1.81	5.07
BC-98-1.25	1.25	47.9	14.8	2.14	1.87	5.7	2.04	1.93	3.54
BC-L-1.35	1.35	102.4	15.3	Uncompacted	Uncompacted	3.5	Uncompacted	Uncompacted	N/A
BC-80-1.35	1.35	102.4	14.3	1.71	1.50	3.4	1.61	1.56	3.68
BC-95-1.35	1.35	102.4	14.3	2.01	1.76	3.4	1.90	1.84	4.47
BC-98-1.35	1.35	102.4	14.3	2.04	1.78	3.4	1.90	1.83	2.85
BC-L-1.5	1.50	227.9	14.3	Uncompacted	Uncompacted	1.9	Uncompacted	Uncompacted	N/A
BC-80-1.5	1.50	227.9	14.3	1.75	1.53	1.9	1.63	1.60	4.43
BC-95-1.5	1.50	227.9	14.3	2.03	1.77	4.3	1.91	1.83	3.17
BC-98-1.5	1.50	227.9	14.3	2.08	1.82	1.8	1.88	1.85	1.49
BC-L-1.7	1.70	469.3	17.7	Uncompacted	Uncompacted	0.3	Uncompacted	Uncompacted	N/A
BC-80-1.7	1.70	469.3	17.7	1.77	1.51	0.4	1.59	1.59	5.47
BC-95-1.7	1.70	469.3	17.7	2.00	1.70	0.4	1.81	1.80	5.81
BC-98-1.7	1.70	469.3	17.7	2.06	1.75	0.4	1.88	1.87	6.80

N/A: not applicable

Table 4.4 Summary of conditions of Boom clay specimens in the vapour equilibrium test series.

Specimen Number	Initial Water Content (%)	Initial Bulk Density (Mg/m^3)	Initial Dry Density (Mg/m^3)	Final Water Content (%)	Final Bulk Density (Mg/m^3)	Final Dry Density (Mg/m^3)
SB1080-FP	10.2	1.55	1.40	9.7	1.52	1.39
SB1090-FP	10.2	1.73	1.57	9.4	1.72	1.57
SB1095-FP	9.5	1.81	1.65	9.1	1.79	1.64
SB1280-FP	12.0	1.58	1.41	11.0	1.56	1.40
SB1290-FP	12.0	1.77	1.58	11.5	1.75	1.57
SB1295-FP	12.0	1.85	1.65	11.0	1.83	1.65
SB1480-FP	13.6	1.60	1.41	13.1	1.58	1.40
SB1490-FP	13.6	1.78	1.57	13.2	1.77	1.56
SB1495-FP	13.6	1.88	1.65	13.3	1.84	1.63
SB1680-FP	16.3	1.62	1.40	15.0	1.61	1.40
SB1680-FP2	16.4	1.63	1.40	14.8	1.62	1.41
SB1690-FP	16.3	1.84	1.59	15.0	1.85	1.61
SB1695-FP	15.7	1.93	1.67	14.9	1.92	1.67
SB1695-FP2	16.4	1.91	1.64	15.2	1.91	1.66
SB1880-FP	18.1	1.67	1.41	16.9	1.67	1.43
SB1880-FP2	17.6	1.65	1.40	16.9	1.65	1.41
SB1890-FP	17.0	1.84	1.57	16.3	1.83	1.57
SB1895-FP	17.0	1.94	1.66	16.5	1.94	1.66
SB1895-FP2	17.6	1.97	1.68	17.0	1.97	1.69
SB2080-FP	20.0	1.68	1.40	18.9	1.67	1.41
SB2090-FP	20.0	1.86	1.55	19.8	1.86	1.55
SB2095-FP	20.0	2.00	1.67	19.7	2.01	1.68
SB2280-FP	22.1	1.71	1.40	20.1	1.71	1.42
SB2280-FP2	21.8	1.71	1.41	17.2	1.71	1.46
SB2290-FP	22.1	1.92	1.57	20.9	1.94	1.61
SB2295-FP	22.0	2.04	1.67	21.7	2.01	1.65
SB2295-FP2	21.8	2.02	1.65	16.9	2.01	1.72
SB2480-FP	24.0	1.74	1.40	22.9	1.73	1.41
SB2490-FP	24.0	1.96	1.58	22.8	1.98	1.61
SB2495-FP	24.0	2.00	1.61	22.4	1.98	1.62
SB2680-FP	25.3	1.77	1.41	24.0	1.77	1.42
SB2690-FP	25.3	1.96	1.57	22.7	1.93	1.58
SB2695-FP	25.3	1.93	1.54	24.5	1.91	1.53

Table 4.5 Summary of conditions of sand-bentonite specimens in the filter paper test series.

Specimen Number	Initial Water Content (%)	Initial Bulk Density (Mg/m^3)	Initial Dry Density (Mg/m^3)	Final Water Content (%)	Final Bulk Density (Mg/m^3)	Final Dry Density (Mg/m^3)
SI0580-FP	5.0	1.79	1.71	5.0	1.77	1.69
SI0780-FP	6.4	1.83	1.72	6.5	1.82	1.71
SI0980-FP	9.3	1.85	1.69	8.9	1.84	1.69
SI1180-FP	11.1	1.94	1.75	10.9	1.90	1.71
SI1380-FP	13.2	2.09	1.85	12.4	2.08	1.85
SI0590-FP	5.3	2.01	1.90	5.1	2.01	1.91
SI0790-FP	7.2	2.04	1.90	6.9	2.04	1.91
SI0990-FP	9.2	2.08	1.91	9.1	2.10	1.92
SI1190-FP	10.9	2.15	1.94	10.7	2.15	1.94
SI1390-FP	13.3	2.16	1.91	12.6	2.18	1.94
SI0595-FP	5.3	2.12	2.01	5.3	2.11	2.00
SI0795-FP	7.2	2.16	2.01	6.8	2.18	2.04
SI0995-FP	9.2	2.19	2.00	8.9	2.21	2.03
SI1195-FP	10.9	2.24	2.02	10.8	2.22	2.01
SI1395-FP	13.3	2.28	2.01	12.4	2.23	1.98

Table 4.6 Summary of conditions of sand-illite specimens in the filter paper test series.

Specimen Number	Initial Water Content (%)	Initial Bulk Density (Mg/m^3)	Initial Dry Density (Mg/m^3)	Final Water Content (%)	Final Bulk Density (Mg/m^3)	Final Dry Density (Mg/m^3)
BC1180-FP	10.7	1.70	1.53	10.7	1.69	1.53
BC1380-FP	13.3	1.76	1.55	13.1	1.75	1.55
BC1580-FP	17.4	1.81	1.54	16.9	1.79	1.54
BC1780-FP	19.5	1.83	1.53	18.8	1.83	1.54
BC1190-FP	12.7	1.99	1.77	12.0	1.98	1.77
BC1390-FP	12.9	2.05	1.81	12.2	2.02	1.80
BC1590-FP	14.1	2.06	1.80	13.7	2.04	1.79
BC1790-FP	16.6	2.09	1.79	15.9	2.09	1.80
BC1790-FP2	17.0	2.16	1.85	16.8	2.11	1.81

Table 4.7 Summary of conditions of Boom clay specimens in the filter paper test series.

Specimen Number	Test type	Psychrometer	Volume Change Measurement	Initial Moisture Content (%)	Initial Bulk Density (Mg/m^3)	Initial Dry Density (Mg/m^3)	Final Moisture Content (%)	Final Bulk Density (Mg/m^3)	Final Dry Density (Mg/m^3)	Total Volume Strain (%)
SB1780TX	Isotropic compression	Yes	No	17.3	1.65	1.41	16.5	1.93	1.66	14.90
SB1880TX	Isotropic compression	Yes	No	18.0	1.71	1.45	21.4	1.72	1.41	-2.80 *
SB1895TX	Isotropic compression	Yes	No	18.7	1.97	1.66	18.3	2.06	1.74	4.86
SB1980TX	Isotropic compression	Yes	No	18.7	1.66	1.40	18.0	1.97	1.67	15.81
SB1995TX	Isotropic compression	Yes	No	20.0	1.99	1.65	19.5	2.02	1.69	2.42
SB2080TX	Isotropic compression	Yes	No	20.0	1.69	1.41	19.4	2.08	1.74	18.76
SB2180TX	Isotropic compression	Yes	No	21.1	1.71	1.41	20.0	2.02	1.69	15.65
SB2280TX	Isotropic compression	Yes	No	22.0	1.71	1.40	21.1	1.90	1.57	10.13
SB2295TX	Isotropic compression	Yes	No	22.0	2.00	1.64	20.8	2.06	1.71	3.60
SB1880TS1	Shear compression	Yes	No	18.8	1.68	1.42	18.0	N/A	N/A	N/A
SB1880TS2	Shear compression	Yes	No	19.0	1.67	1.40	18.3	1.94	1.64	13.73
SB1880TS3	Shear compression	Yes	No	18.6	1.67	1.41	17.3	1.81	1.54	7.72
SB1880TS4	Shear compression	Yes	No	18.1	1.69	1.43	17.3	1.96	1.67	13.65
SB2180V1	Isotropic compression	No	Yes	20.3	1.75	1.45	20.0	2.01	1.67	13.10
SB1995V2	Isotropic compression	No	Yes	19.3	1.98	1.66	19.5	2.06	1.72	3.29
SB1680V3	Isotropic compression	No	Yes	16.4	1.62	1.40	16.3	1.97	1.70	17.63
SB1880V4	Isotropic compression	No	Yes	18.6	1.66	1.40	18.7	1.98	1.66	15.85
SB1895V5	Isotropic compression	No	Yes	18.7	1.97	1.66	18.4	2.03	1.72	3.02
SB3080V6	Isotropic compression	No	Yes	28.5	1.82	1.42	28.8	1.93	1.50	5.99

N/A: not available
* Leakage problem

Table 4.8 Summary of sand-bentonite specimens in the triaxial test series.

Specimen	Final water content (%)	Final dry density (Mg/m^3)	Total suction at the start of compression (kPa)	Total suction at the end of 1st unloading cycle (kPa)	Total suction at the end of 2nd unloading cycle (kPa)	Total suction at the end of test (kPa)
SB1895TX	18.3	1.74	4460	4130	3960	4100
SB1980TX	18.0	1.67	4160	N/A	N/A	4465
SB1995TX	19.5	1.69	4085	N/A	N/A	3905
SB2080TX	19.4	1.74	2980	N/A	N/A	2170
SB2180TX	20.0	1.69	3430	3090	2950	3080
SB2295TX	20.8	1.71	2445	2270	1840	1320

N/A: not applicable

Table 6.1 Comparison of measured total suctions at ambient atmospheric pressures.

Material	Calculated		Measured	
	Suction from large pore mode (MPa)	Suction from small pore mode (MPa)	Suction (MPa)	Water Content (%)
Sand-bentonite	0.002 to 0.048	2.9 to 72.0	1 to 500	25 to 1
Sand-illite	0.002 to 0.041	0.6 to 72.0	0.5 to 500	13 to 1
Boom clay	N/A	0.3 to 72.0	1 to 500	20 to 1

N/A: not available

Table 9.1 Comparison of calculated and measured suctions in compacted clays.

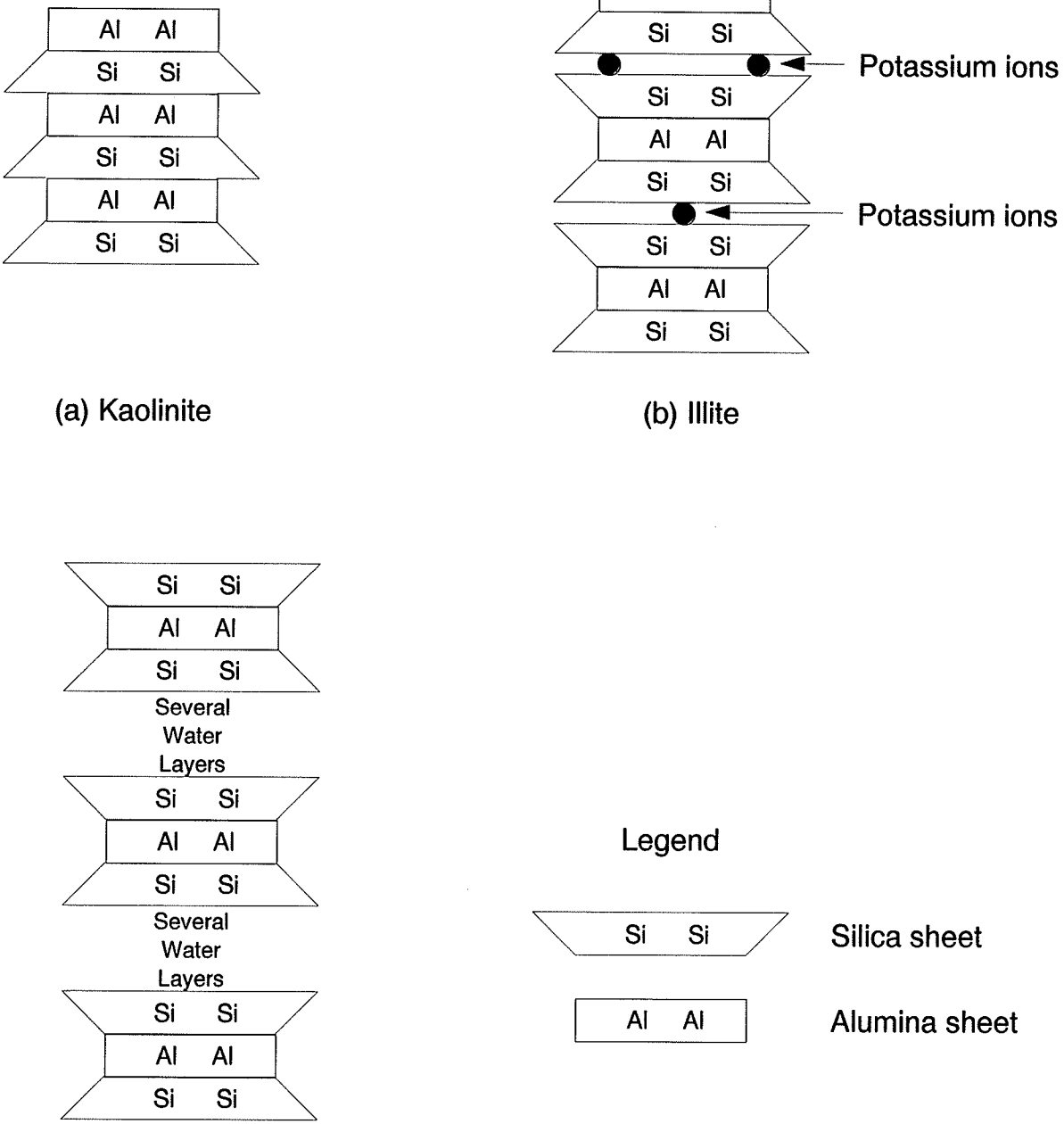

Figure 2.1 Structure of (a) kaolinite, (b) illite, (c) montmorillonite (after Yong and Warkentin, 1975).

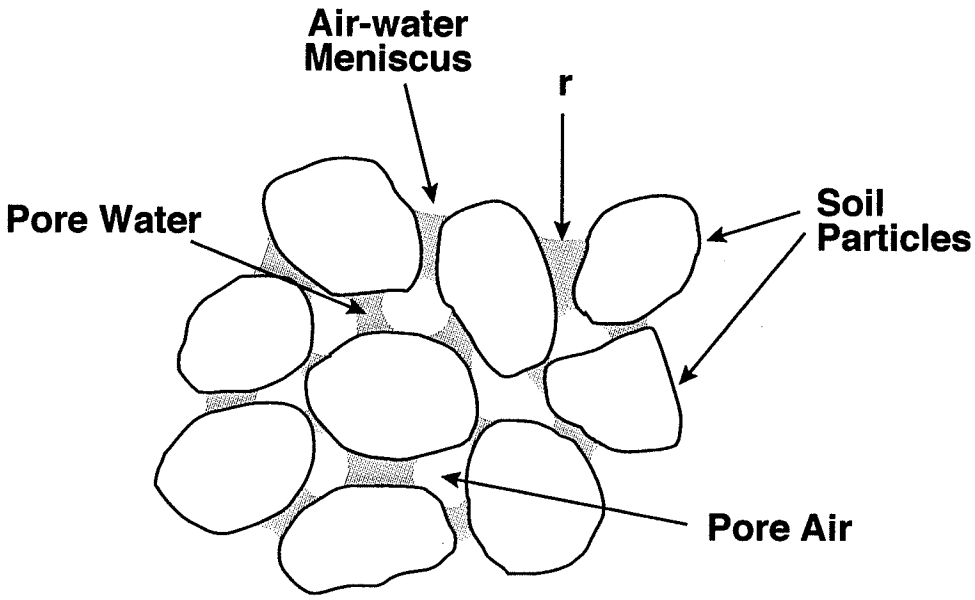

Figure 2.2 A simple unsaturated soil system.

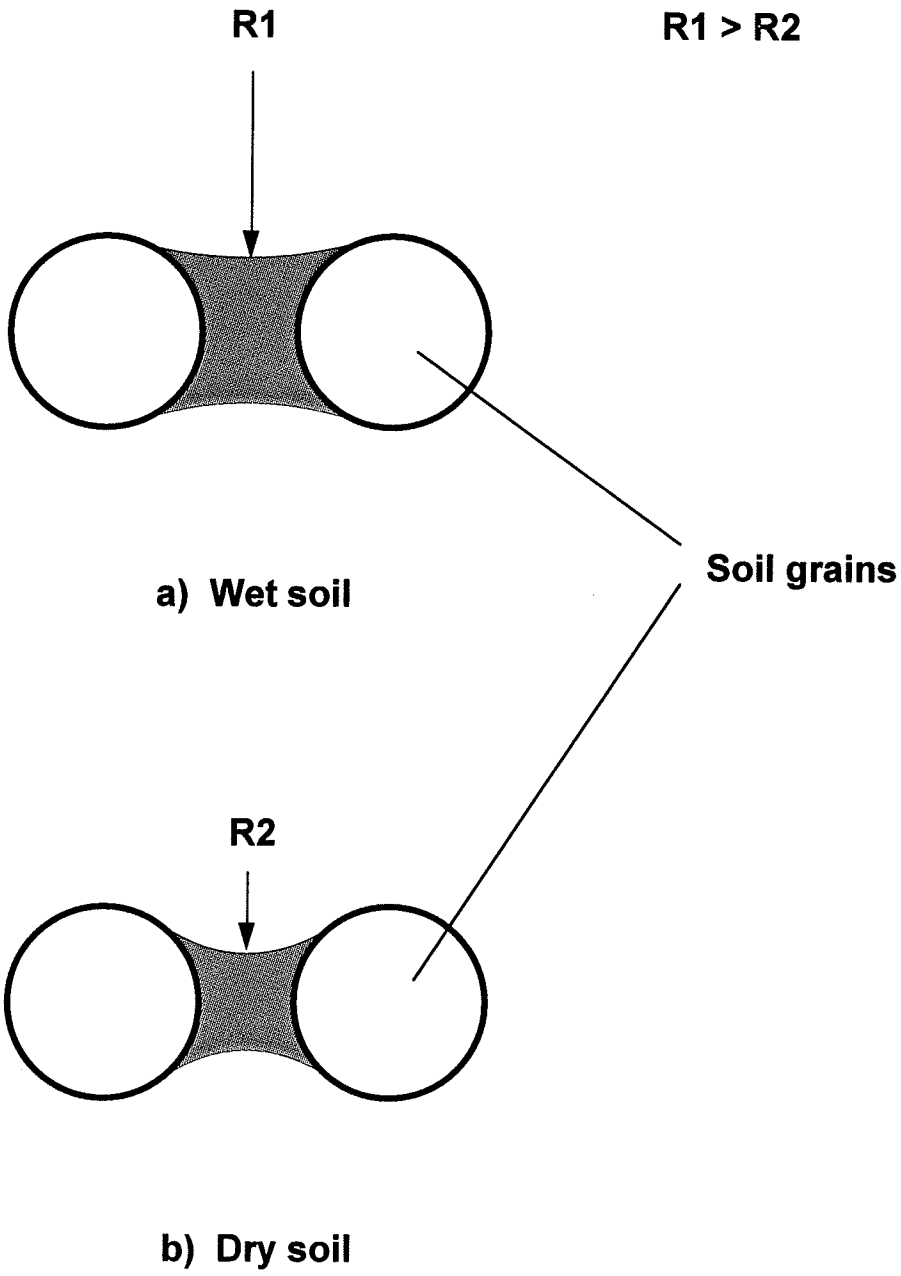

Figure 2.3 Effect of water content on curvature of air-water interface (after Spangler, 1960).

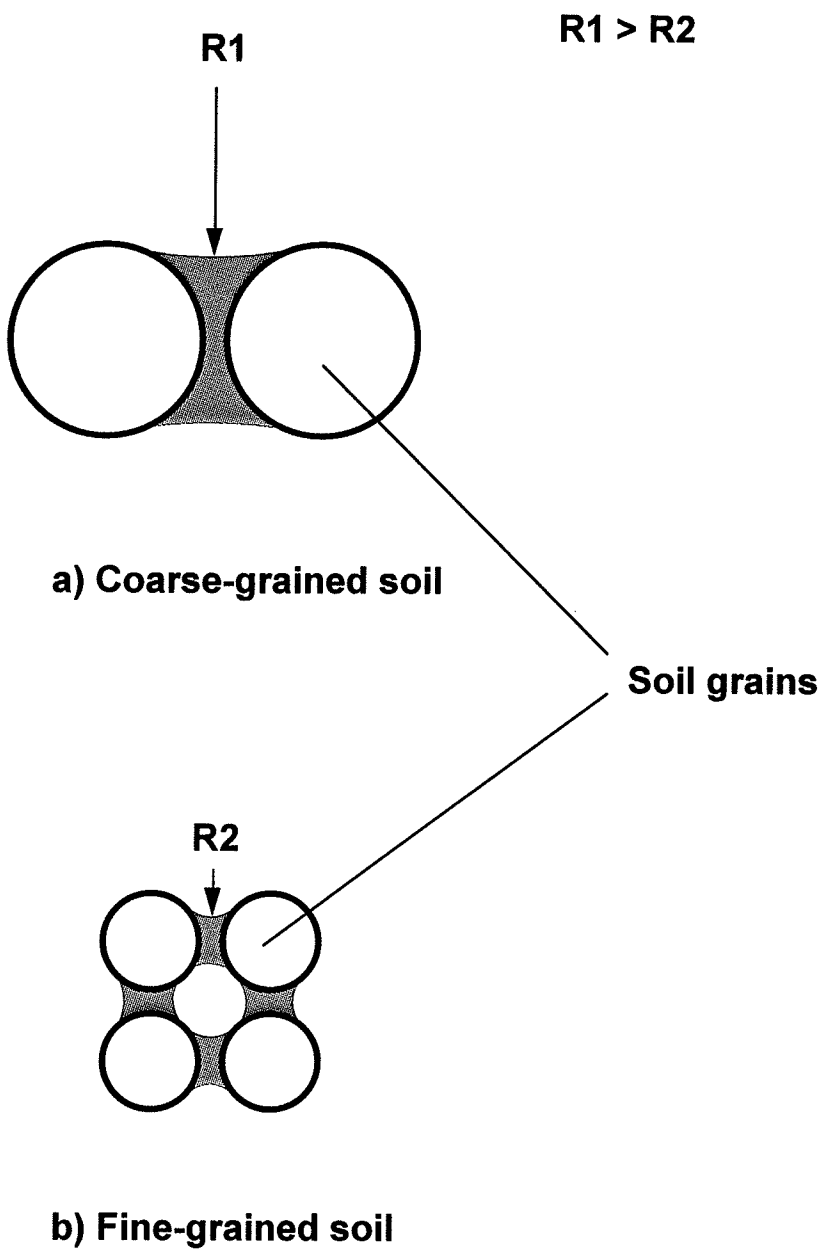

Figure 2.4 Effect of particle size on curvature of air-water interface (after Spangler, 1960).

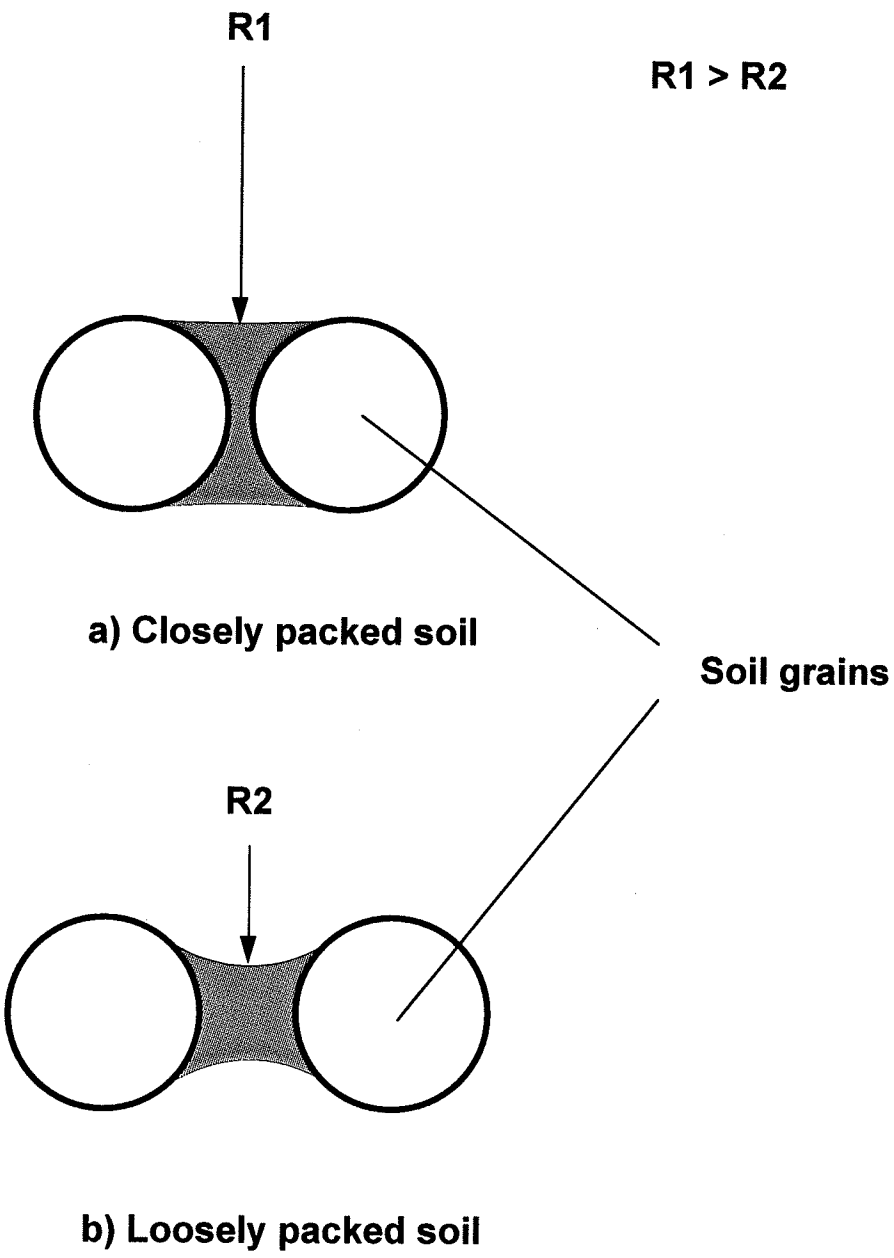

Figure 2.5 Influence of state of packing of soil on curvature of air-water interface (after Spangler, 1960).

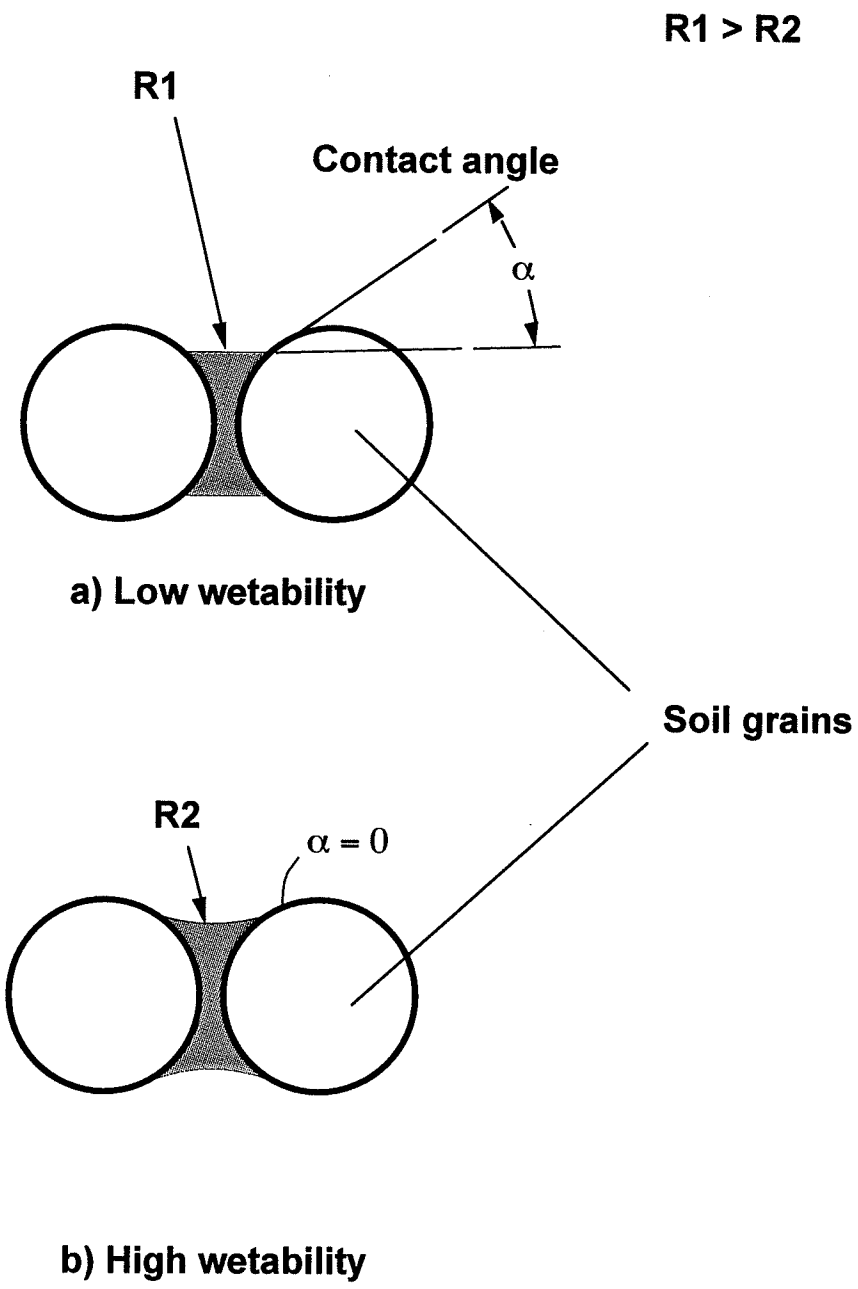

Figure 2.6 Influence of wetability of soil grains on curvarture of air-water interface (after Spangler, 1960).

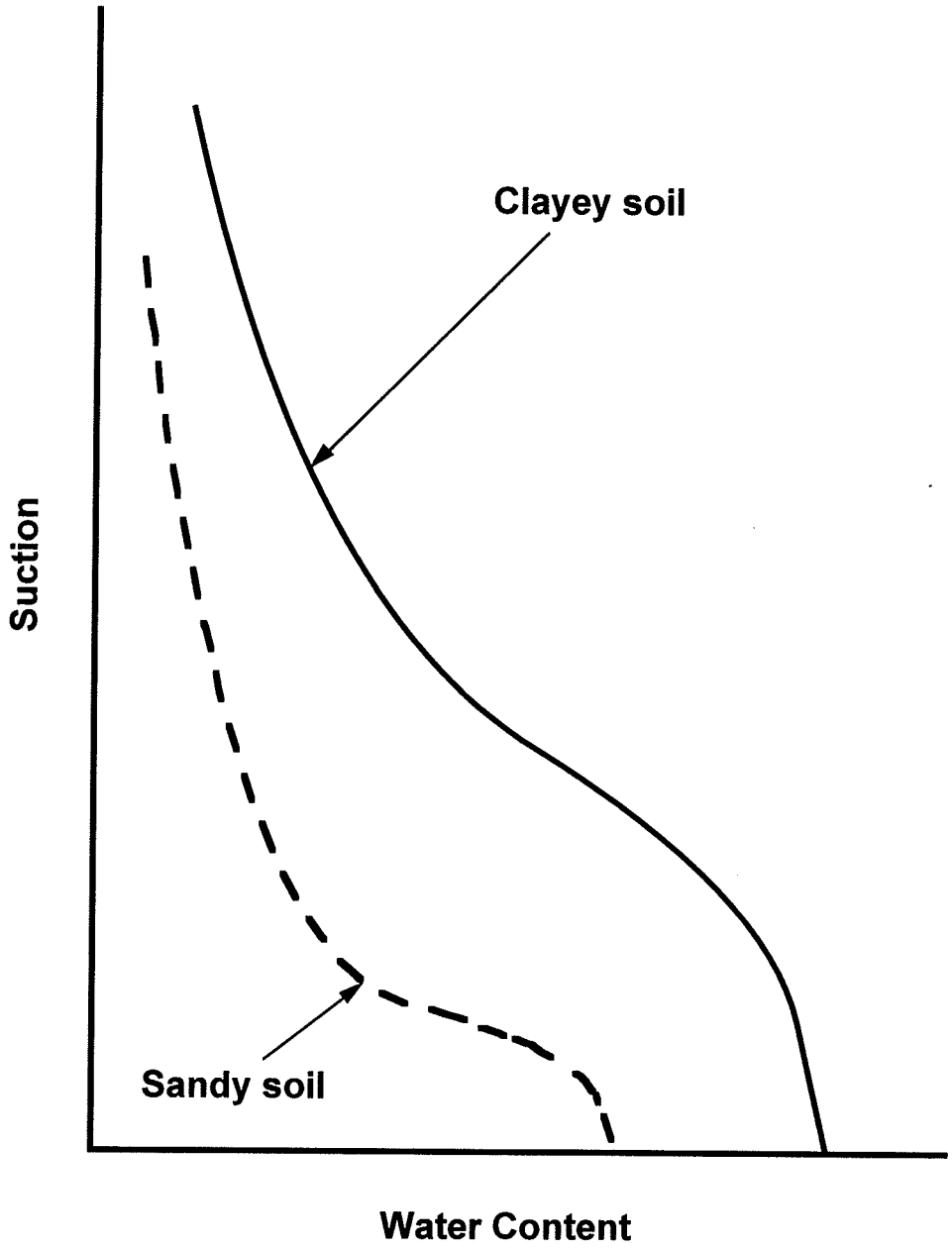

Figure 2.7 Comparison of suction-moisture content relationships between a clayey soil and a sandy soil.

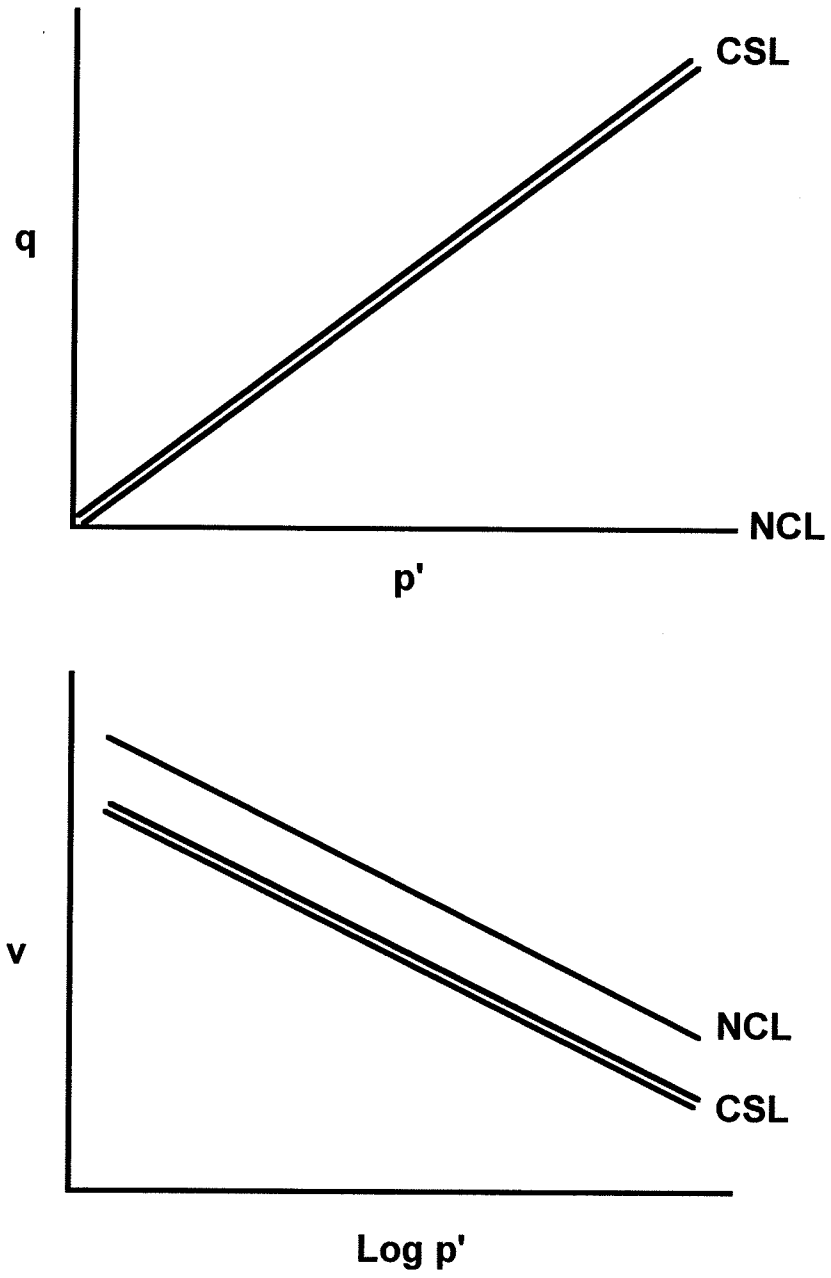

Figure 2.8 A schematicof the normal consolidation line (NCL) and critical state line (CSL) of a saturated soil.

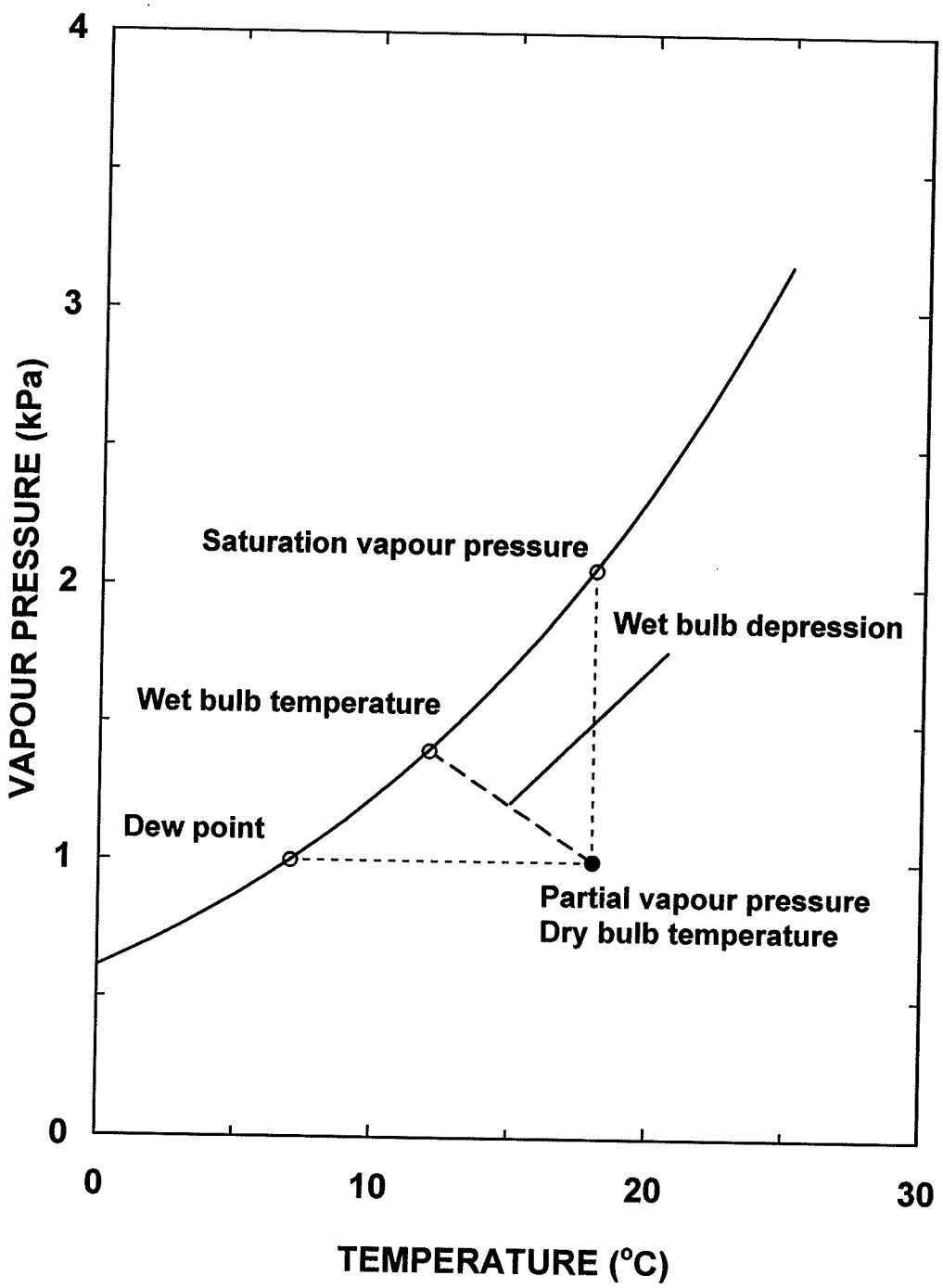

Figure 3.1 Relation between saturated vapour pressure of water, dew point, and wet bulb depression (after Monteith, 1973).

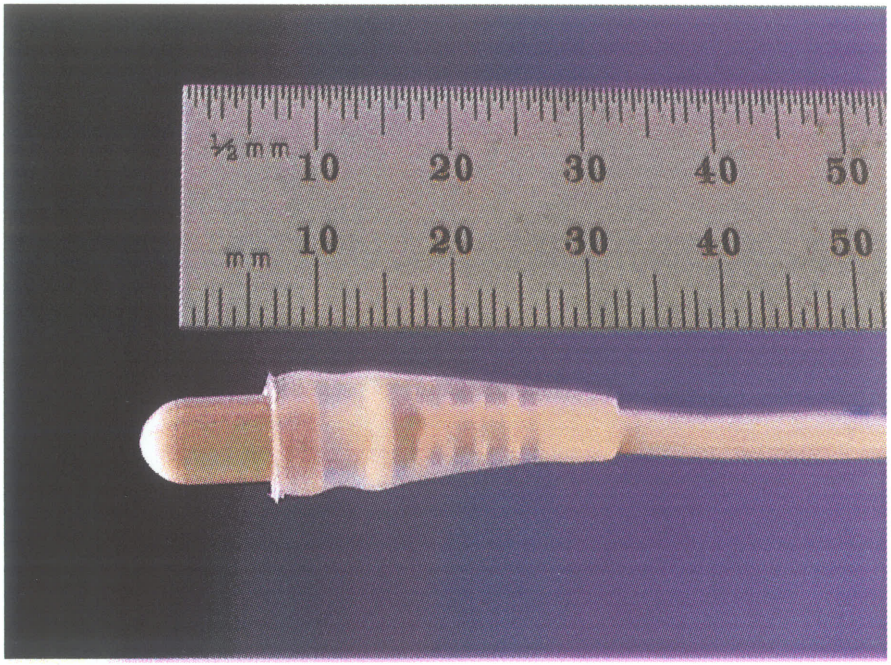

Figure 3.2 Thermocouple psychrometer: Wescor Type PCT-55.

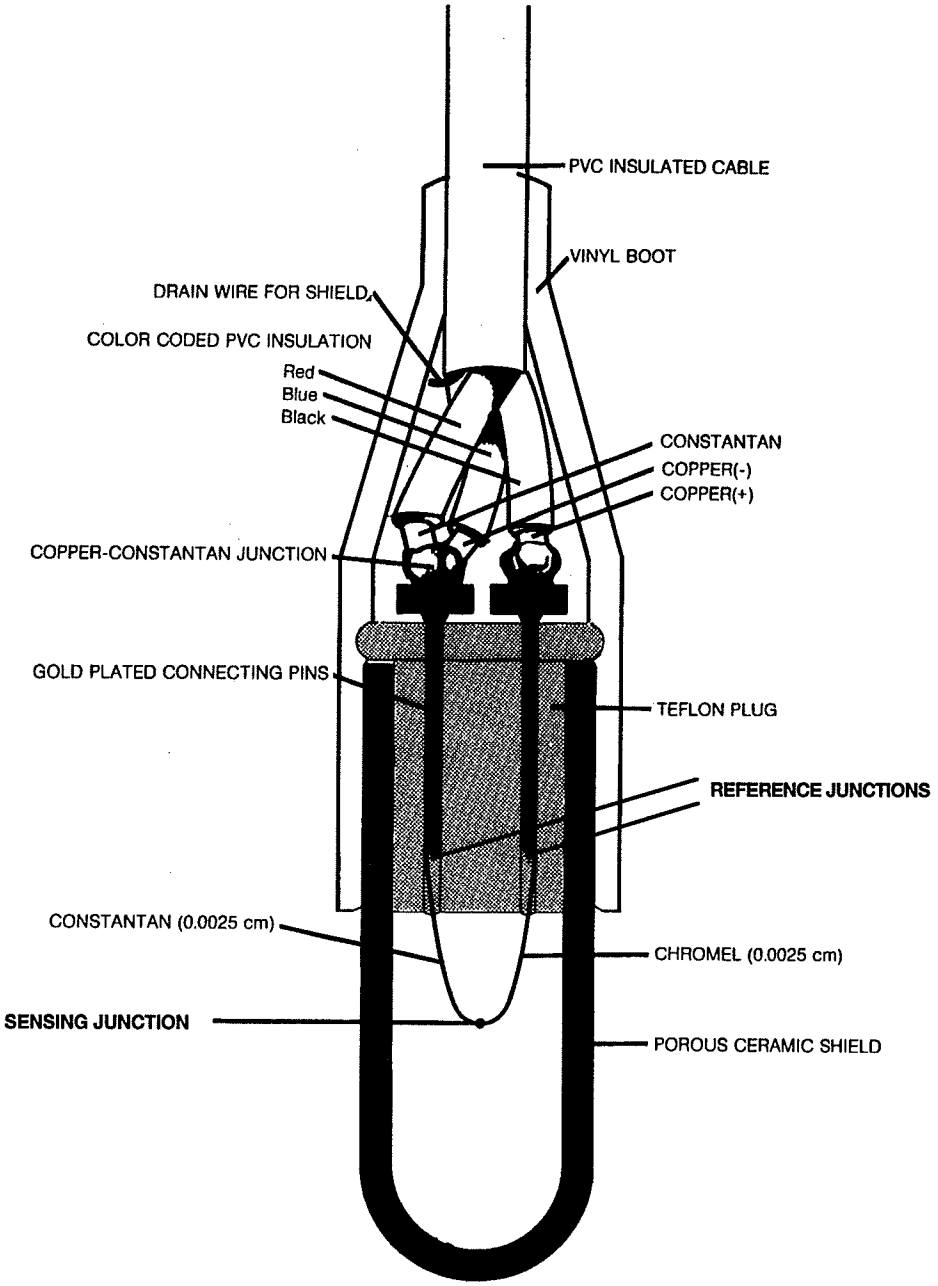

Figure 3.3 A schematic of a Wescor Type PCT-55 psychrometer (after Briscoe, 1984).

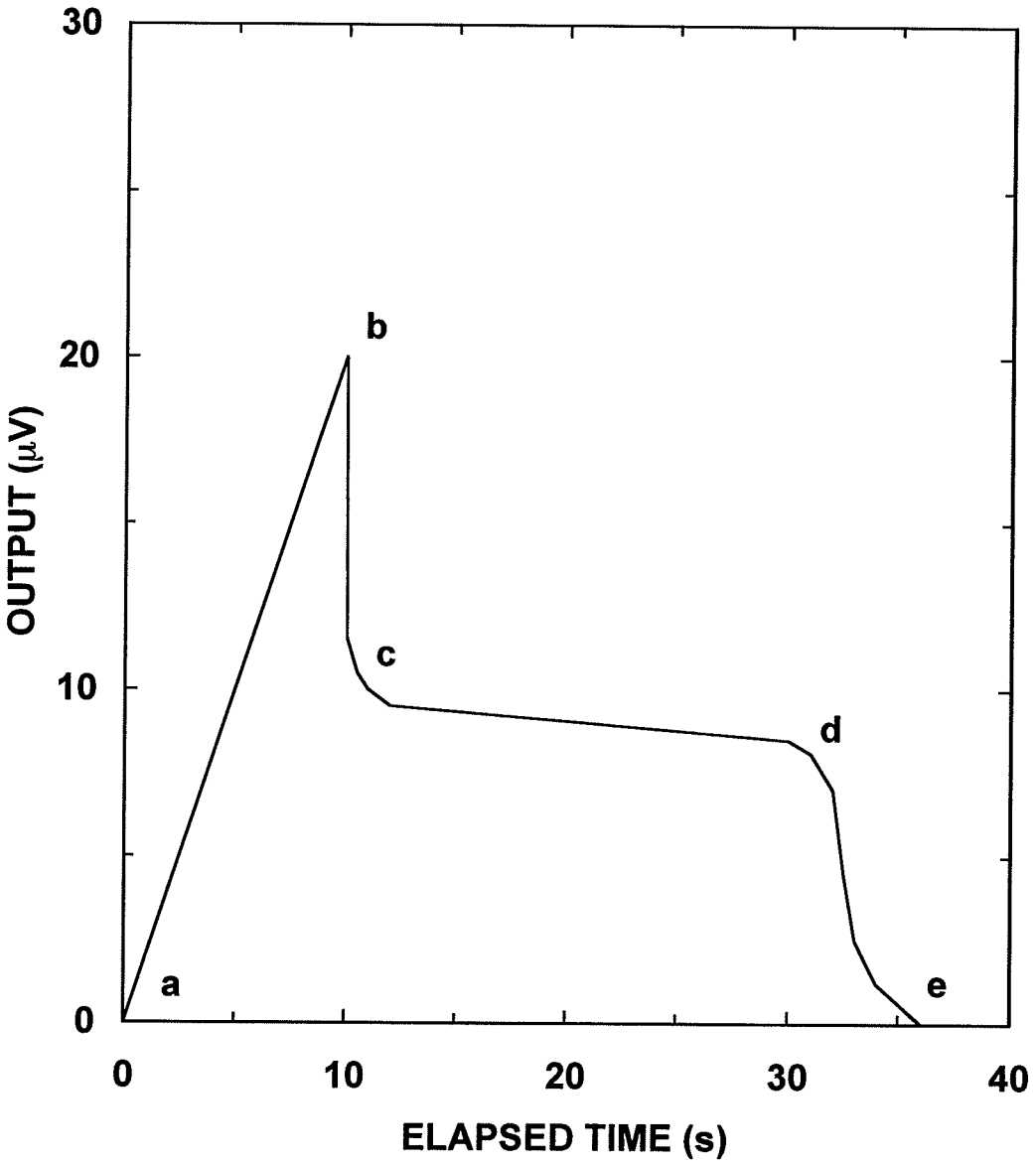

Figure 3.4 An output of a psychrometer used in the psychrometric mode.

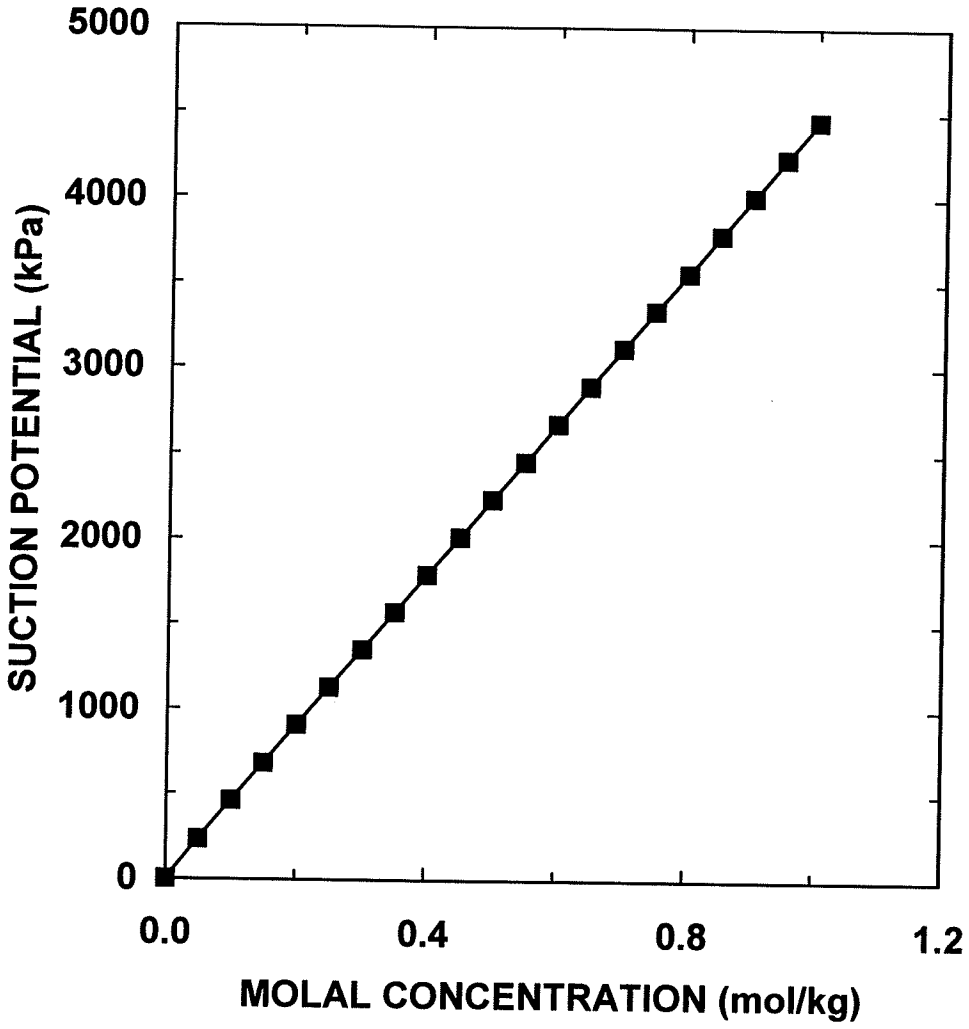

Figure 3.5 Suction potential-molal concentration relationship for KCl at 25°C.

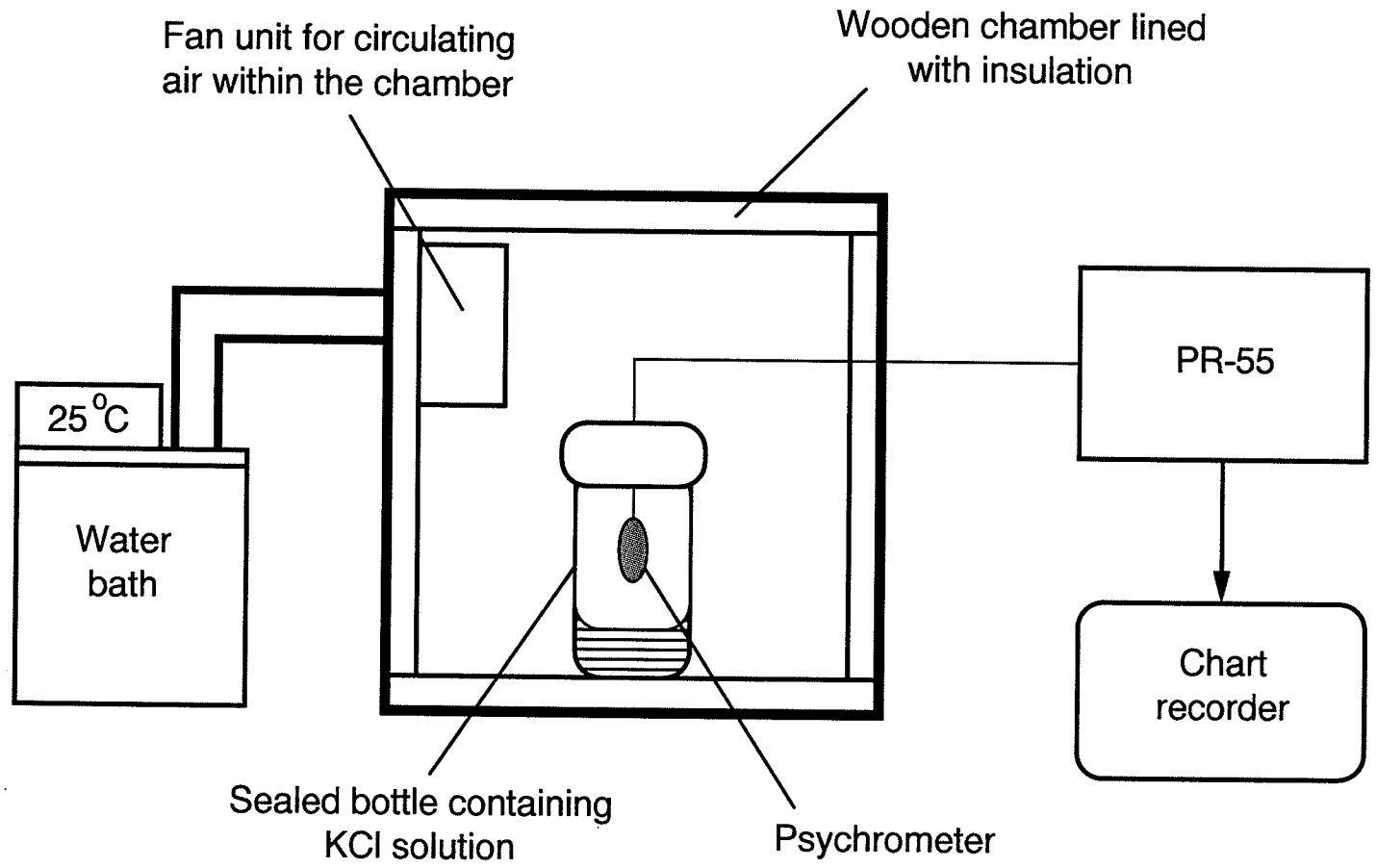

Figure 3.6 Psychrometer calibration scheme.

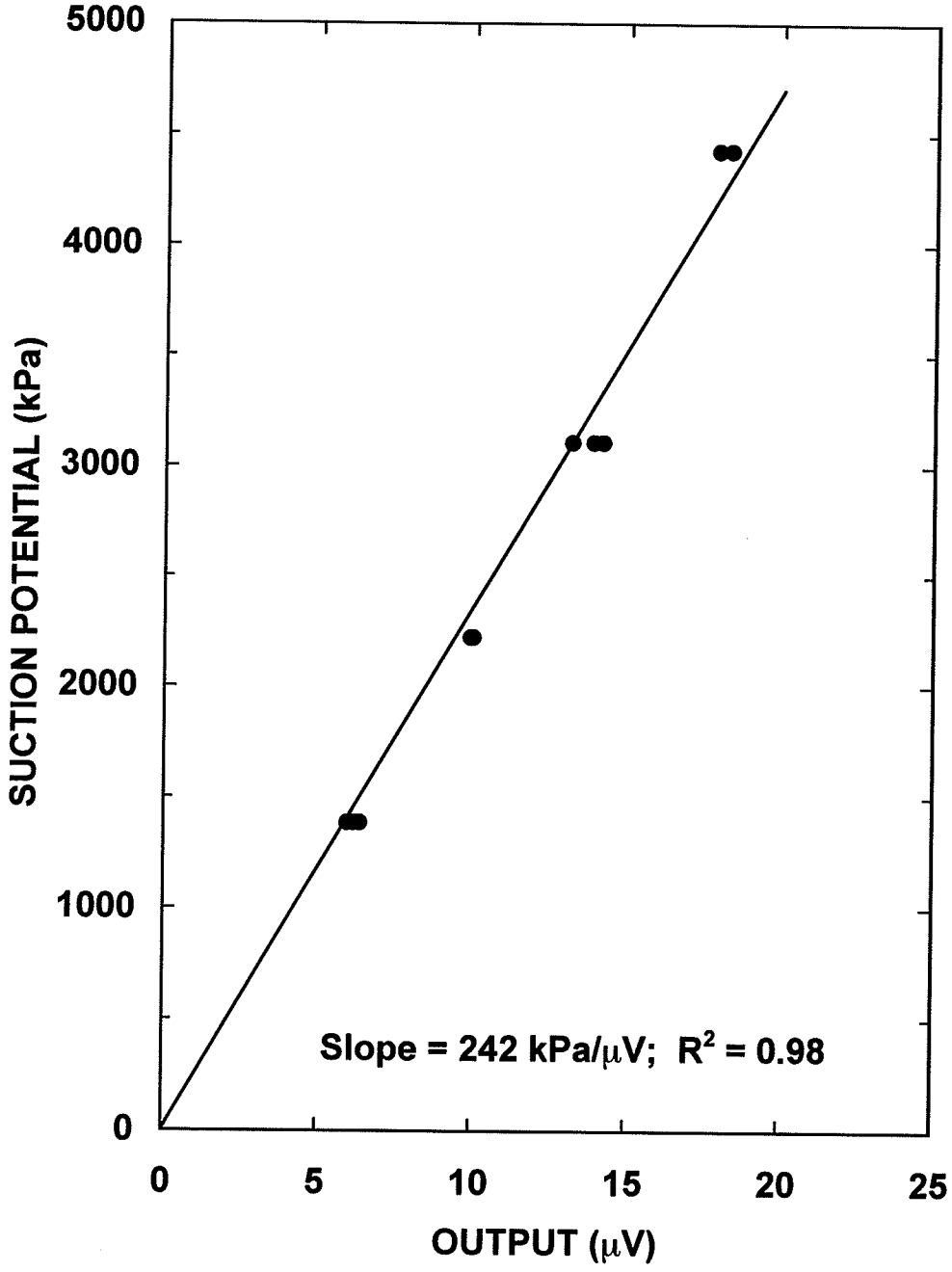

Figure 3.7 Suction potential-output relationship: Psychrometer # 36287.

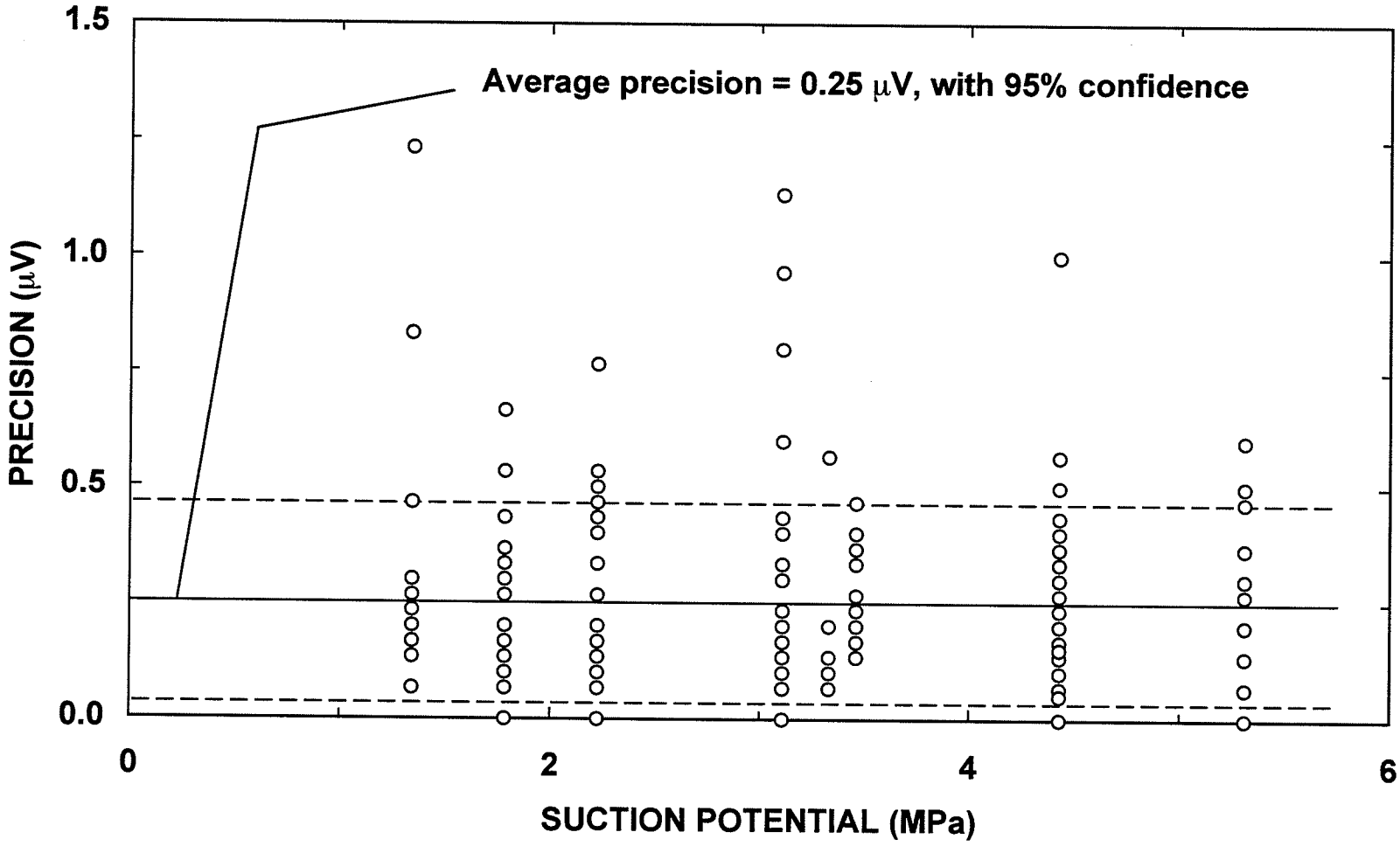

Figure 3.8 Precision of Wescor psychrometers.

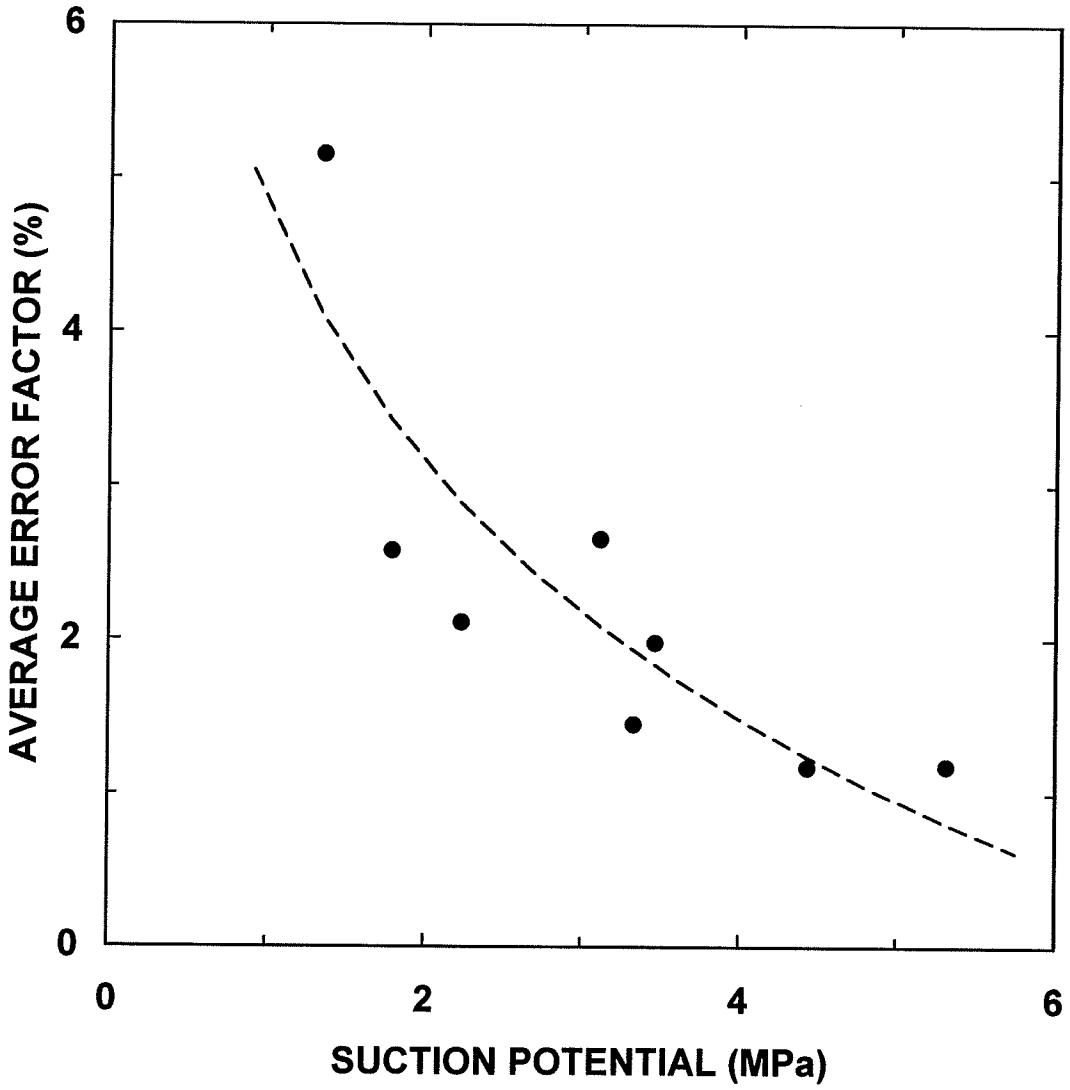

Figure 3.9 Variation of average error factor with suction potential.

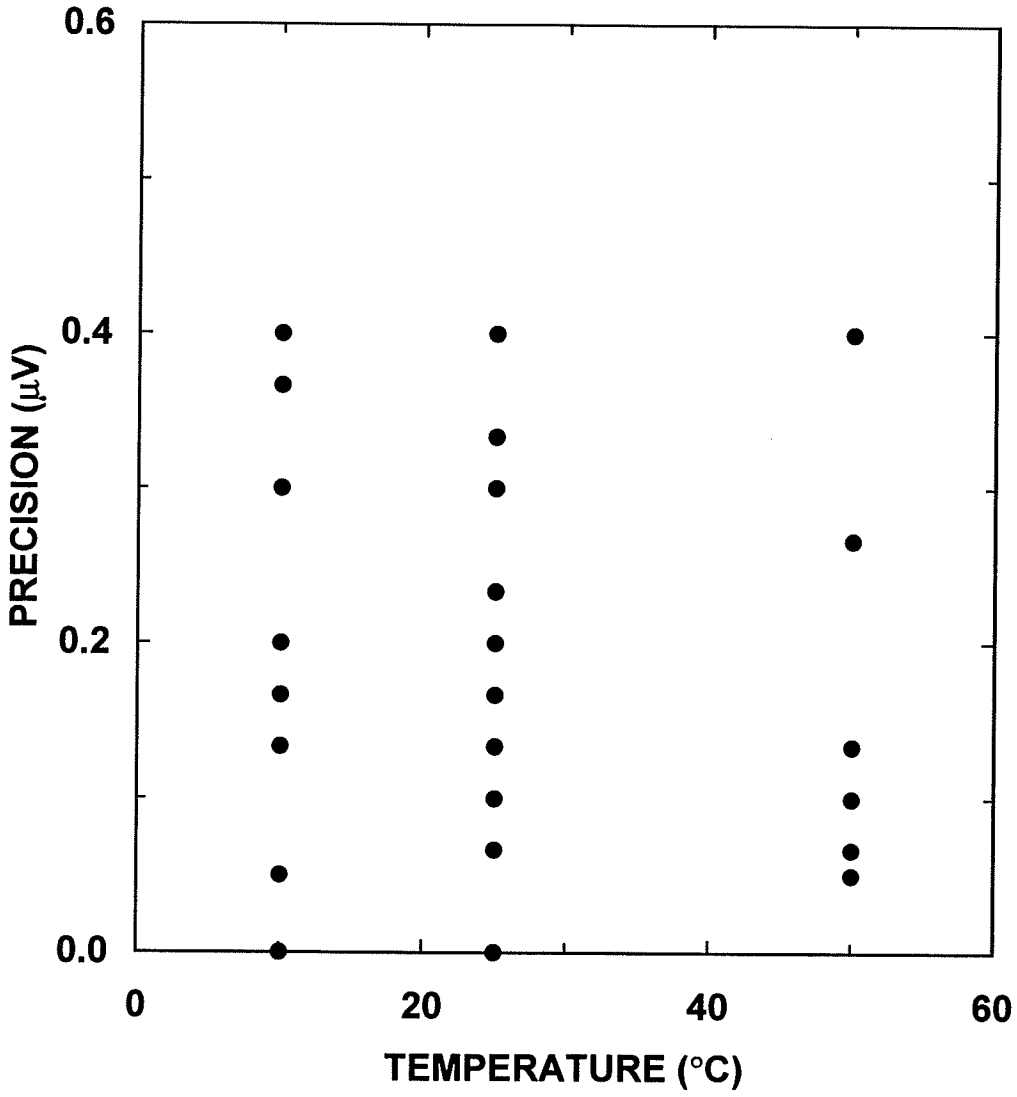

Figure 3.10 Influence of temperature on psychrometer precision.

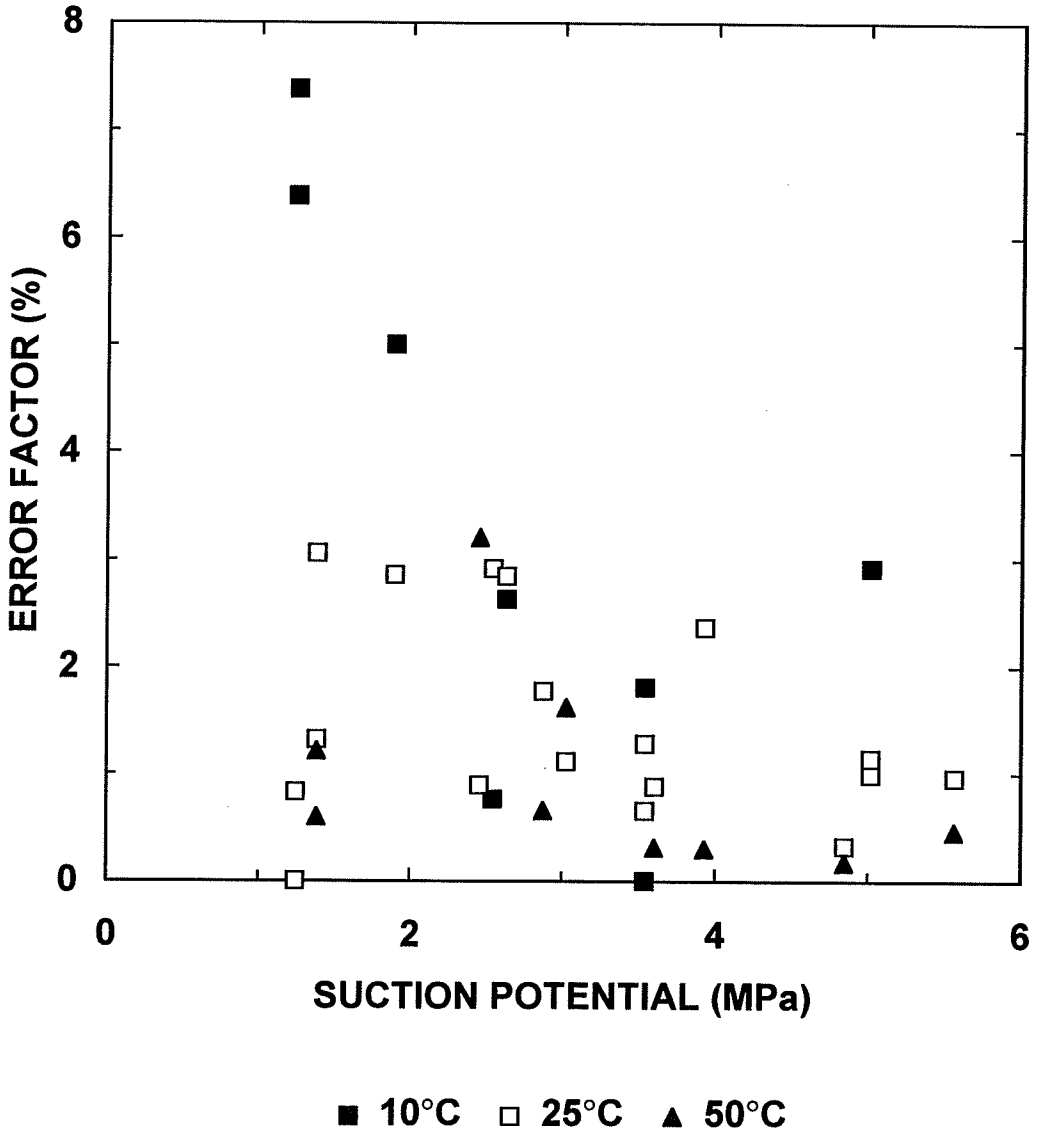

Figure 3.11 Variation of error factor with suction potential and temperature.

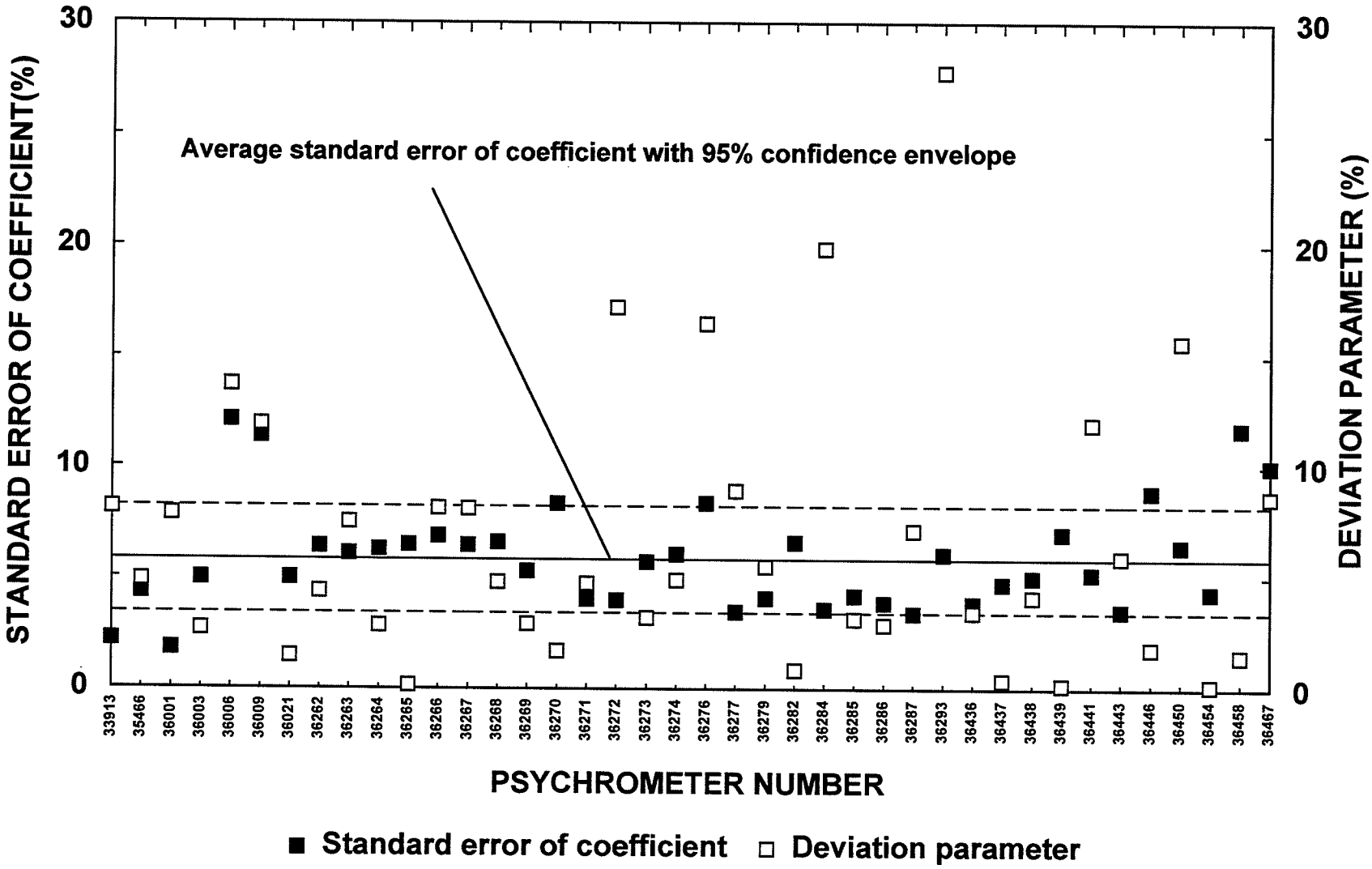

Figure 3.12 Comparison between standard error of coefficient and deviation parameter.

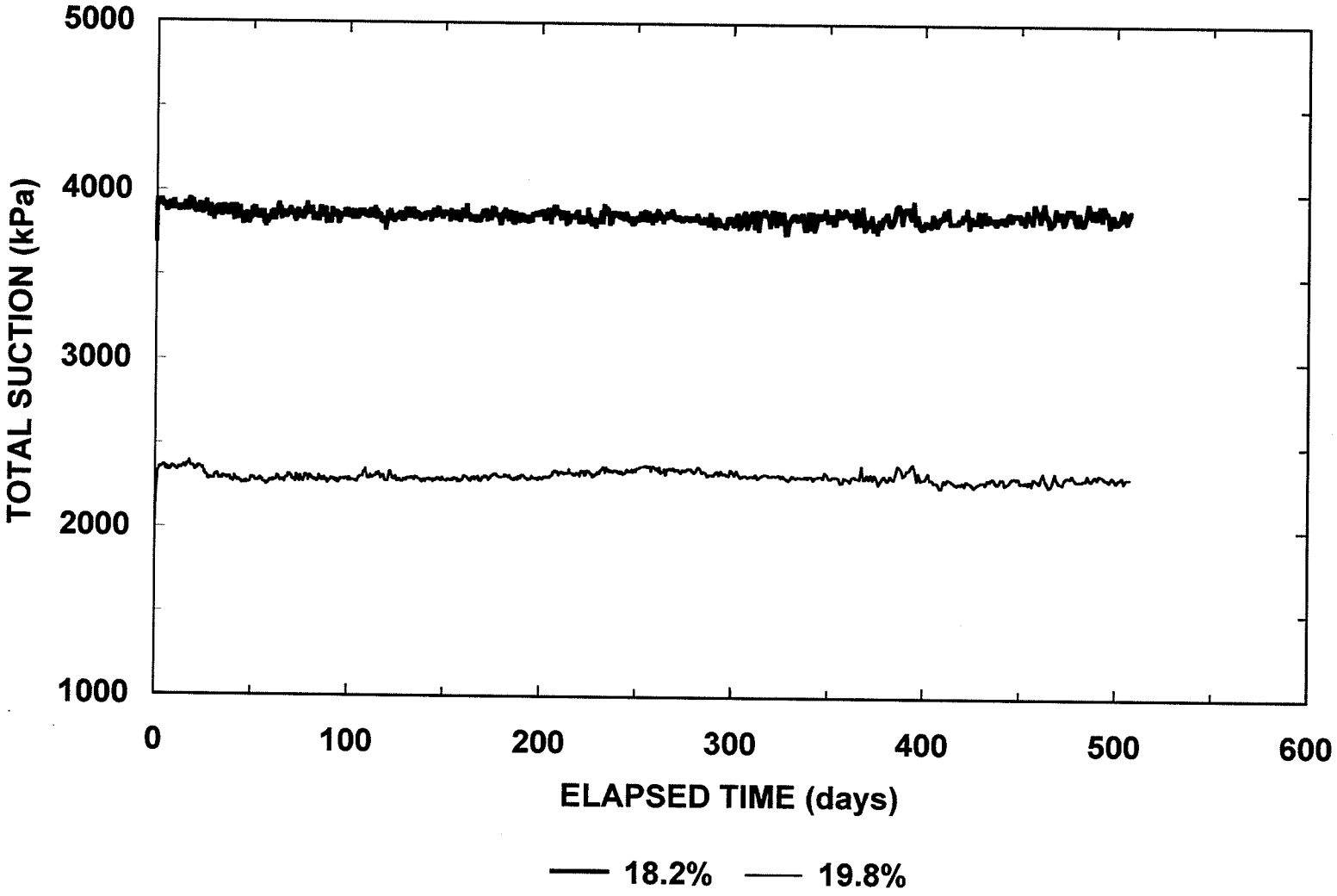

Figure 3.13 Results from tests to examine long term drift of psychrometer outputs in sand-bentonite materials at specified water contents.

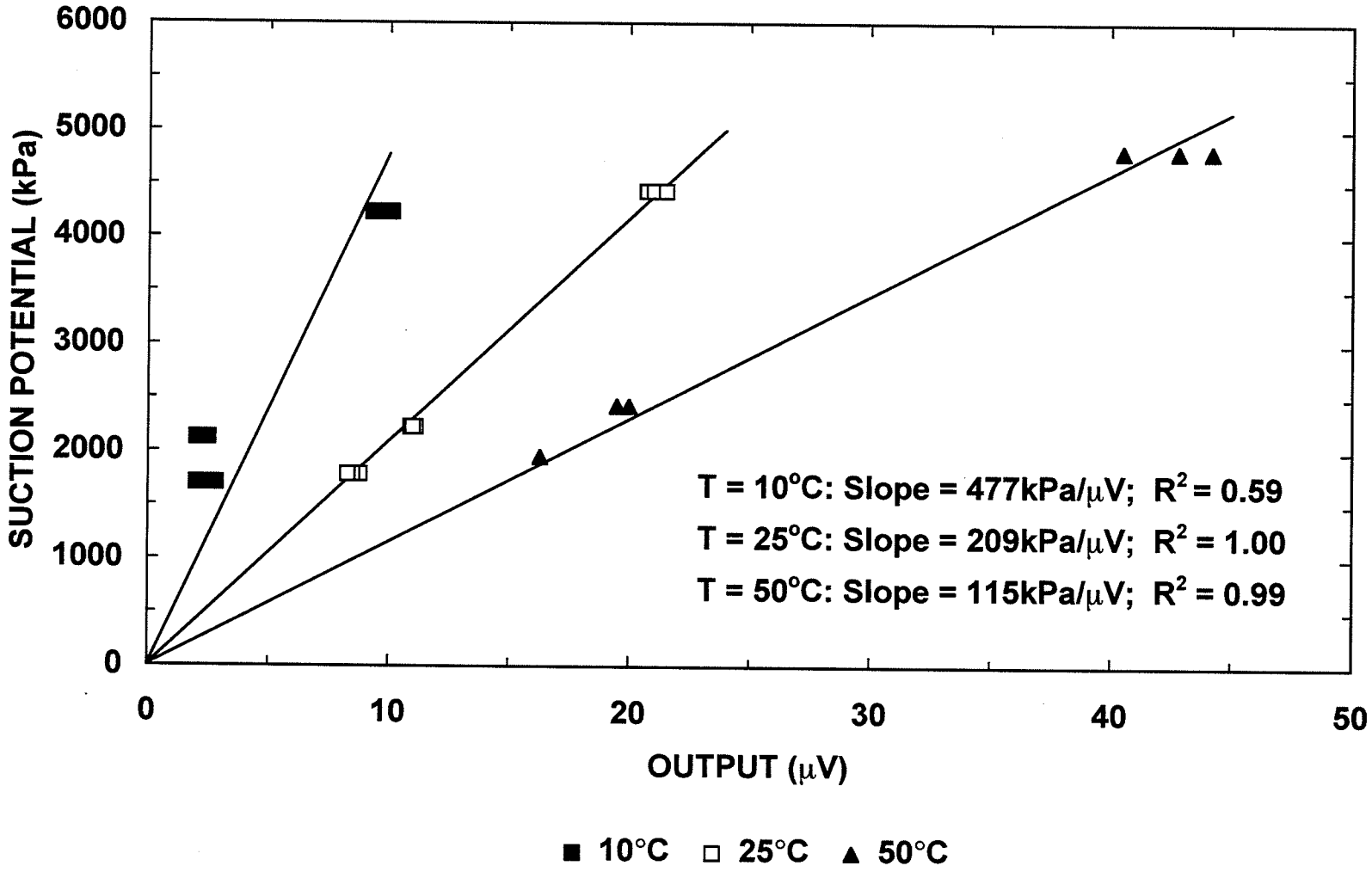

Figure 3.14 Calibration relationships for Psychrometer # 36001 at different temperatures.

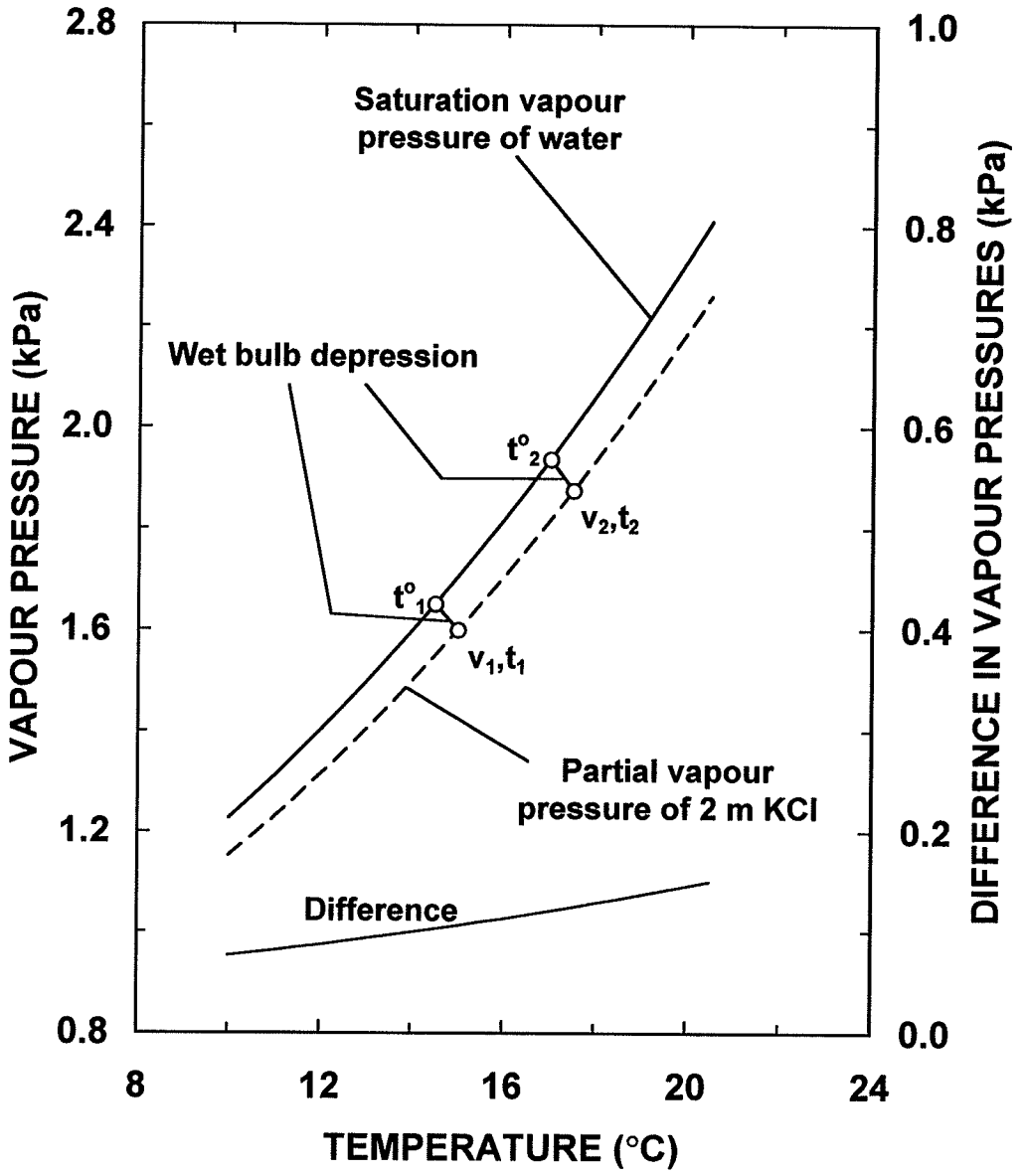

Figure 3.15 Vapour pressures of water and 2 m KCl solution.

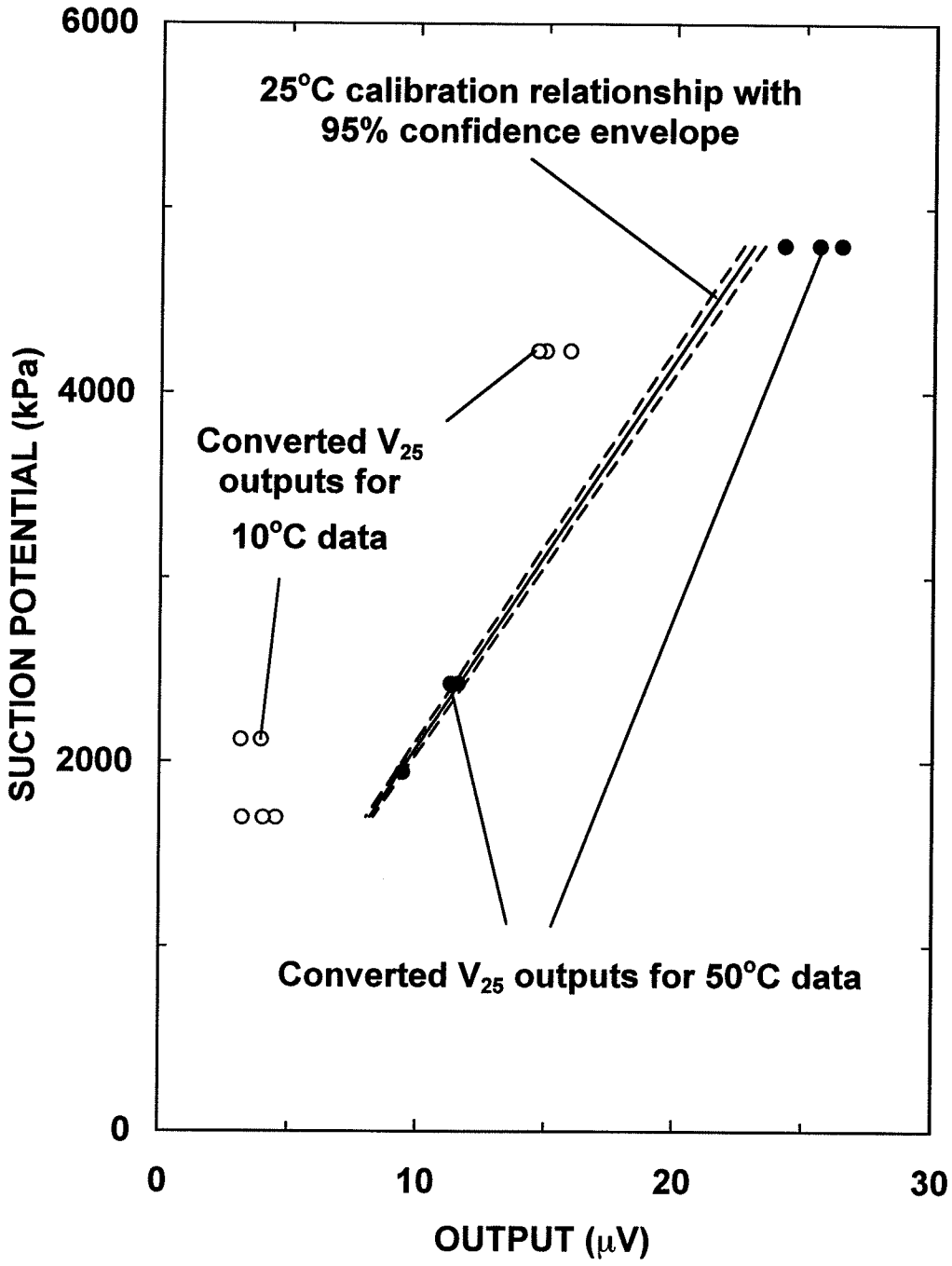

Figure 3.16 Comparison between converted V25 outputs and outputs predicted by the 25°C calibration relationship: Psychrometer # 36001.

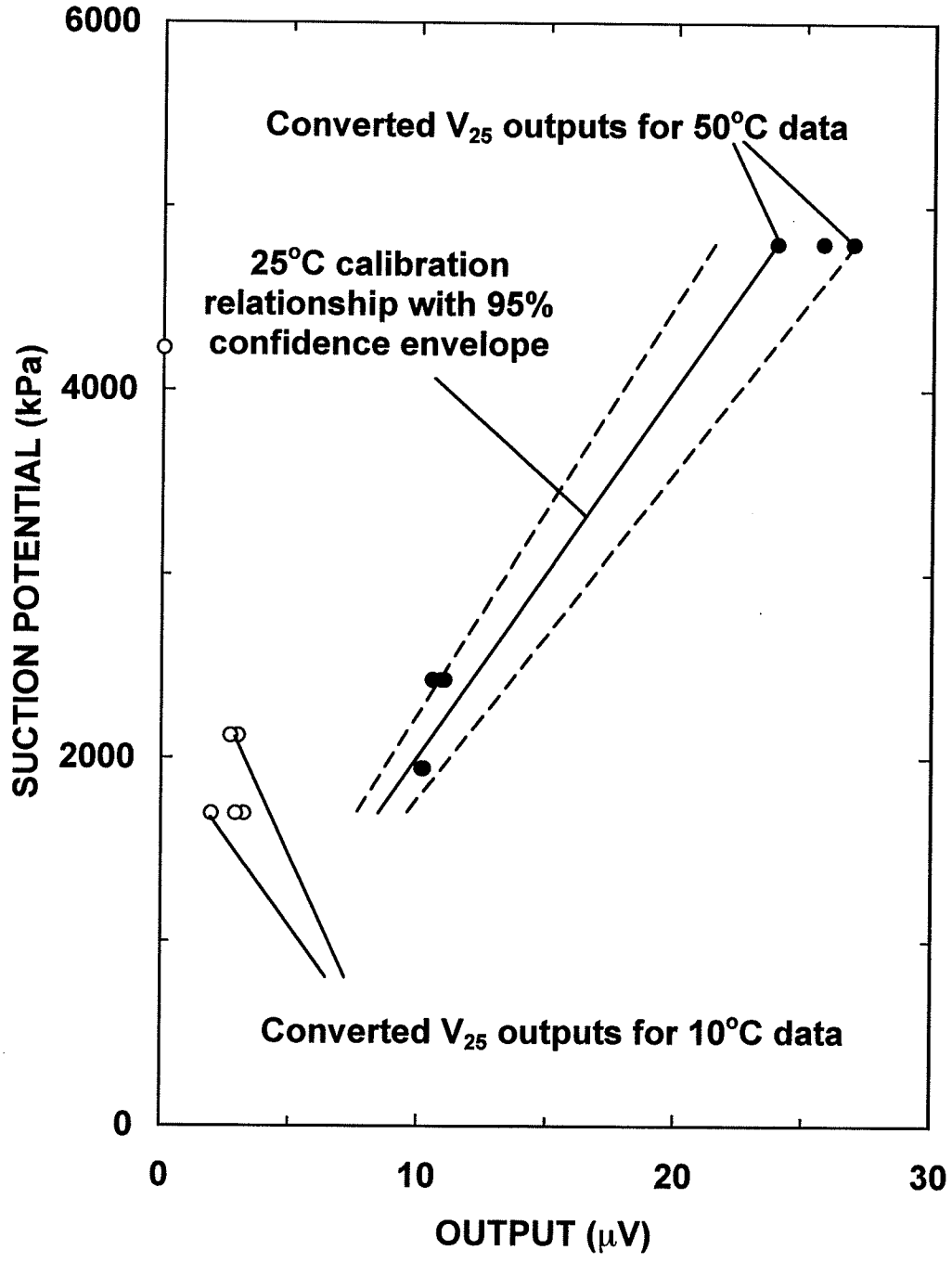

Figure 3.17 Comparison between converted V25 outputs and outputs predicted by the 25°C calibration relationship: Psychrometer # 36009.

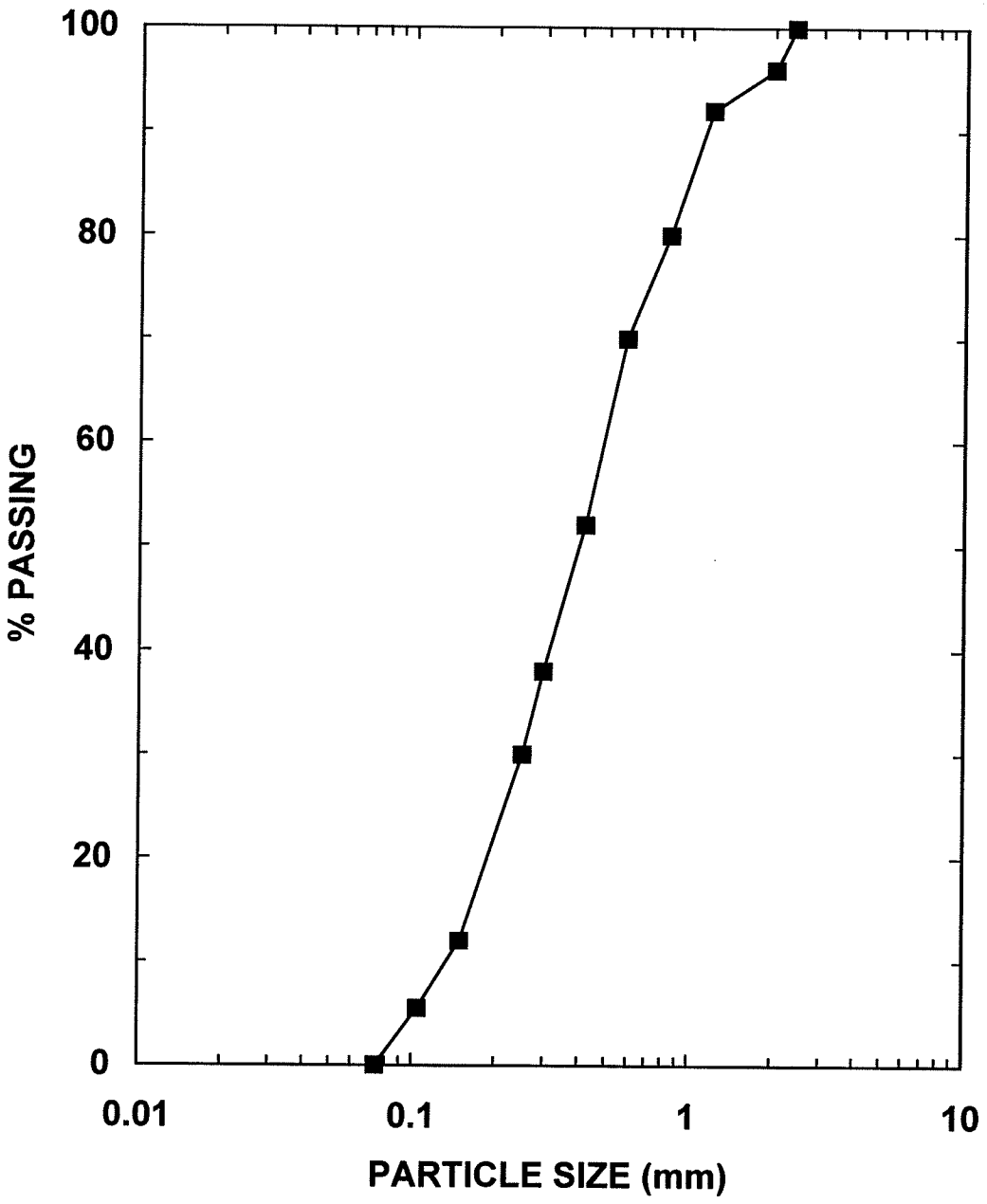

Figure 4.1 Particle size distribution of graded silica sand (determined by ASTM Test Designation: D 422).

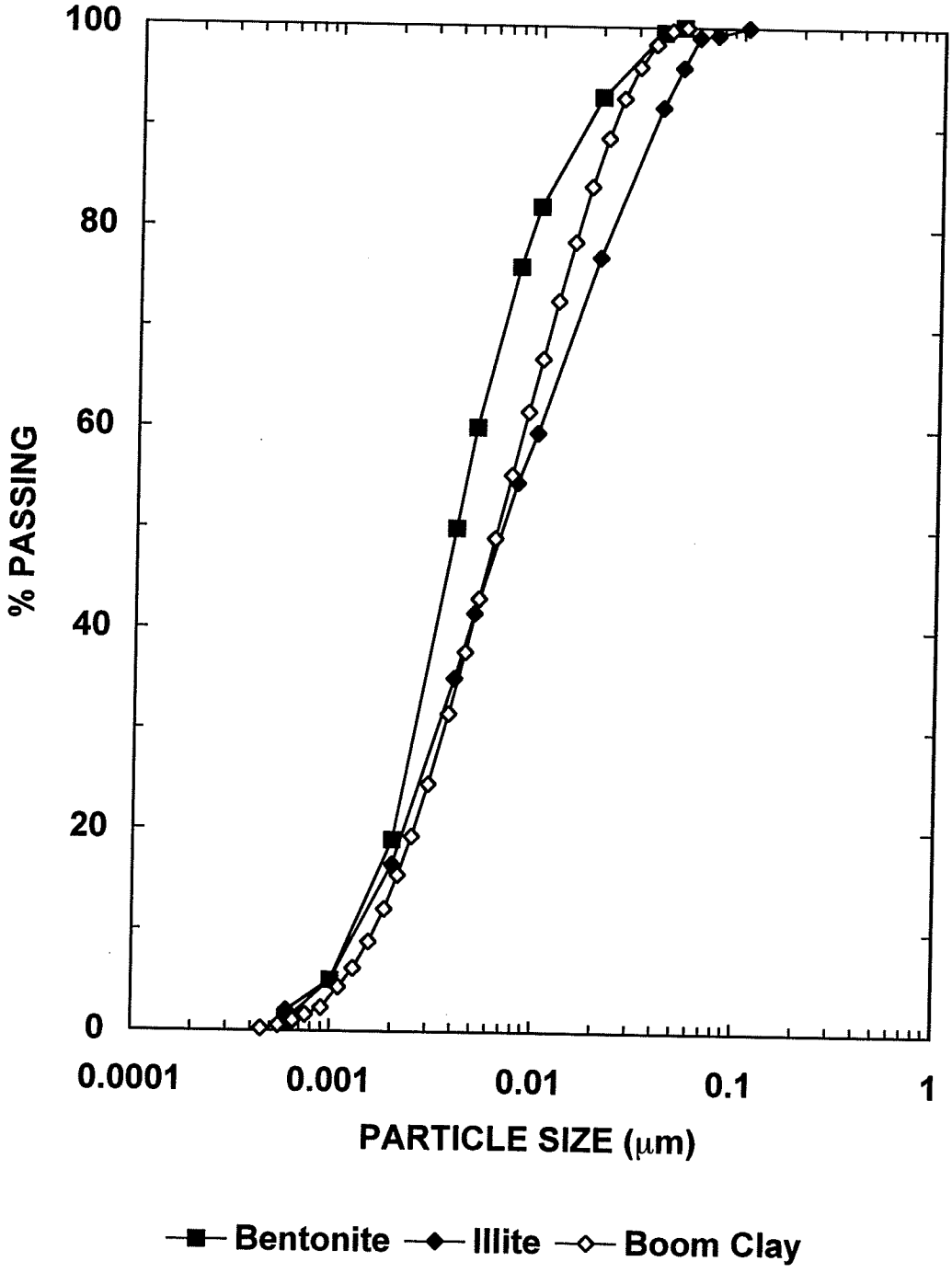

Figure 4.2 Particle size distributions of bentonite, illite and Boom Clay (determined by ASTM Test Designation: D 422).

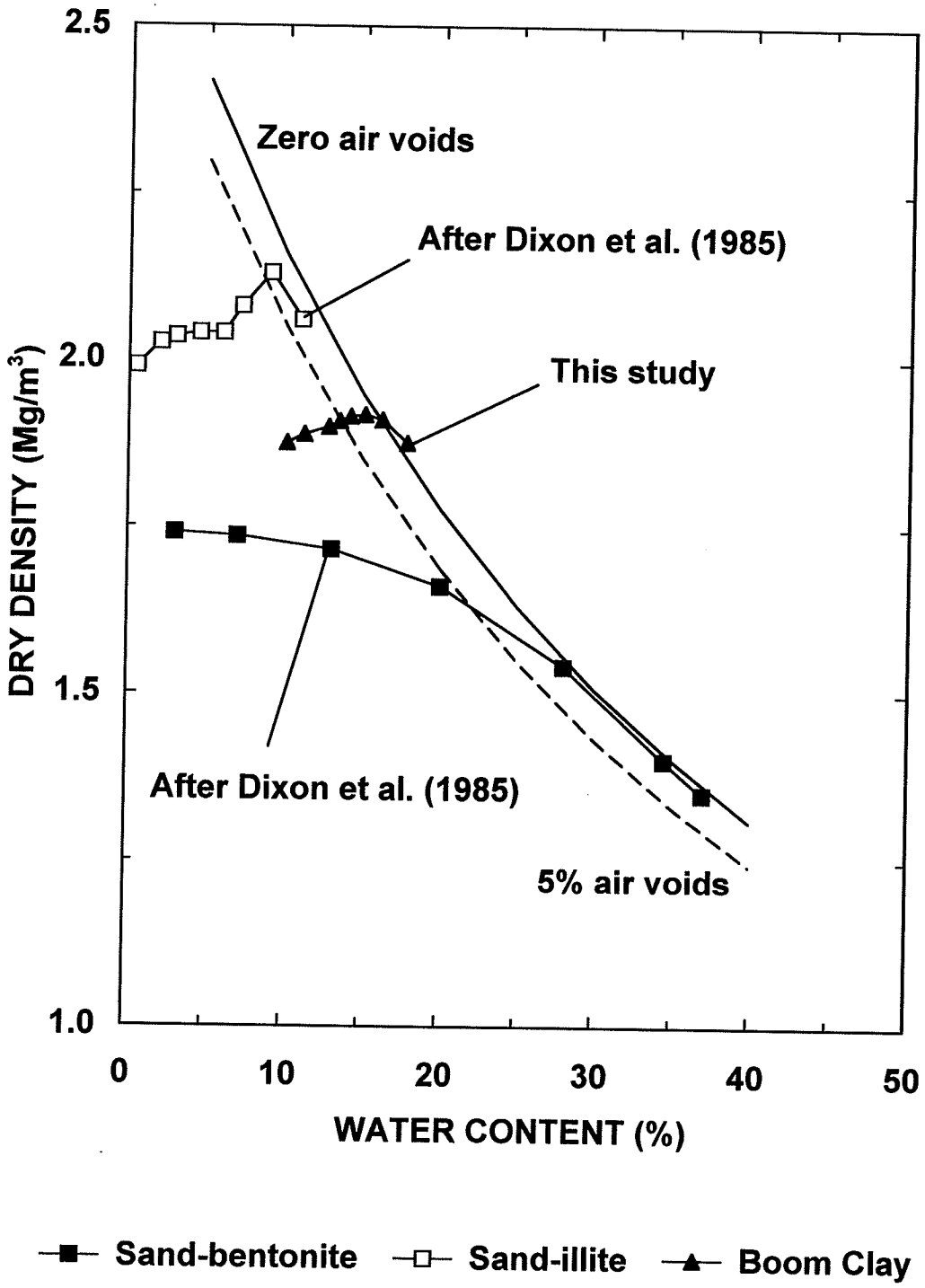

Figure 4.3 Dry density - water content relationships of sand-bentonite material, sand-illite material, and Boom Clay.

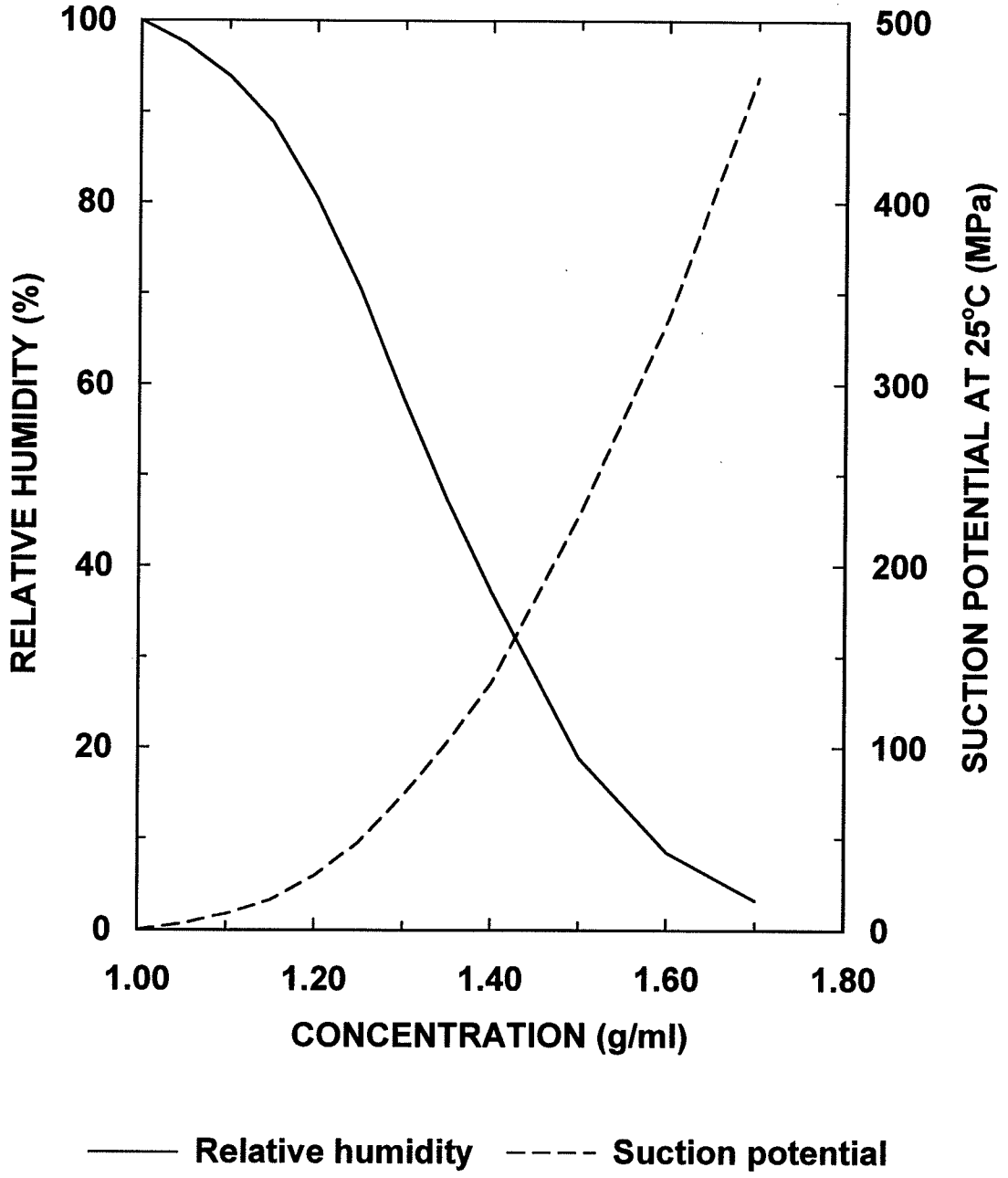

Figure 4.5 Relative humidity and suction potential of sulphuric acid.

Figure 4.6 Vapour equilibrium test.

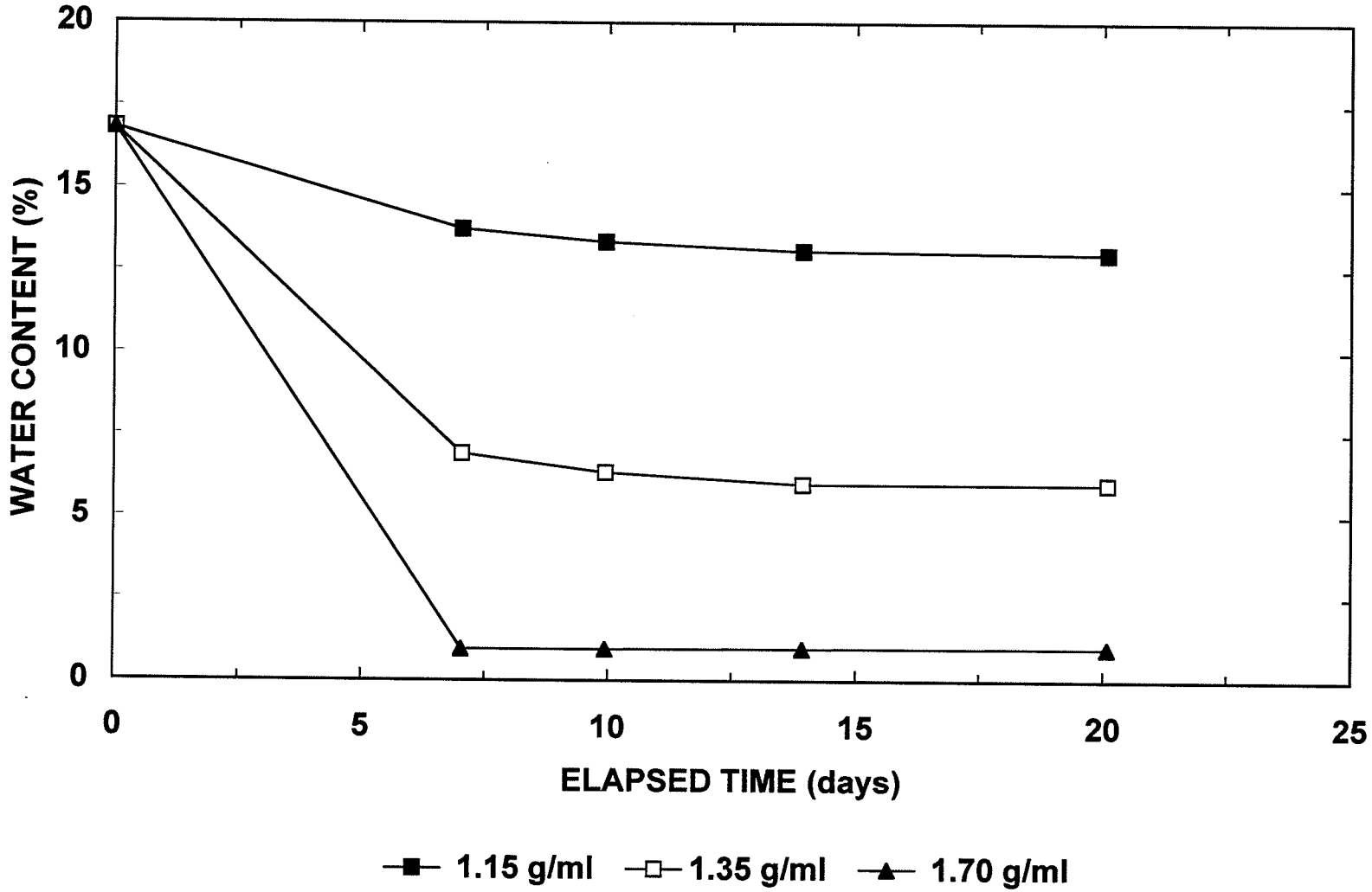

Figure 4.7 Time to equilibrium in vapour equilibrium tests: sand-bentonite specimens over sulphuric acids at specified concentrations.

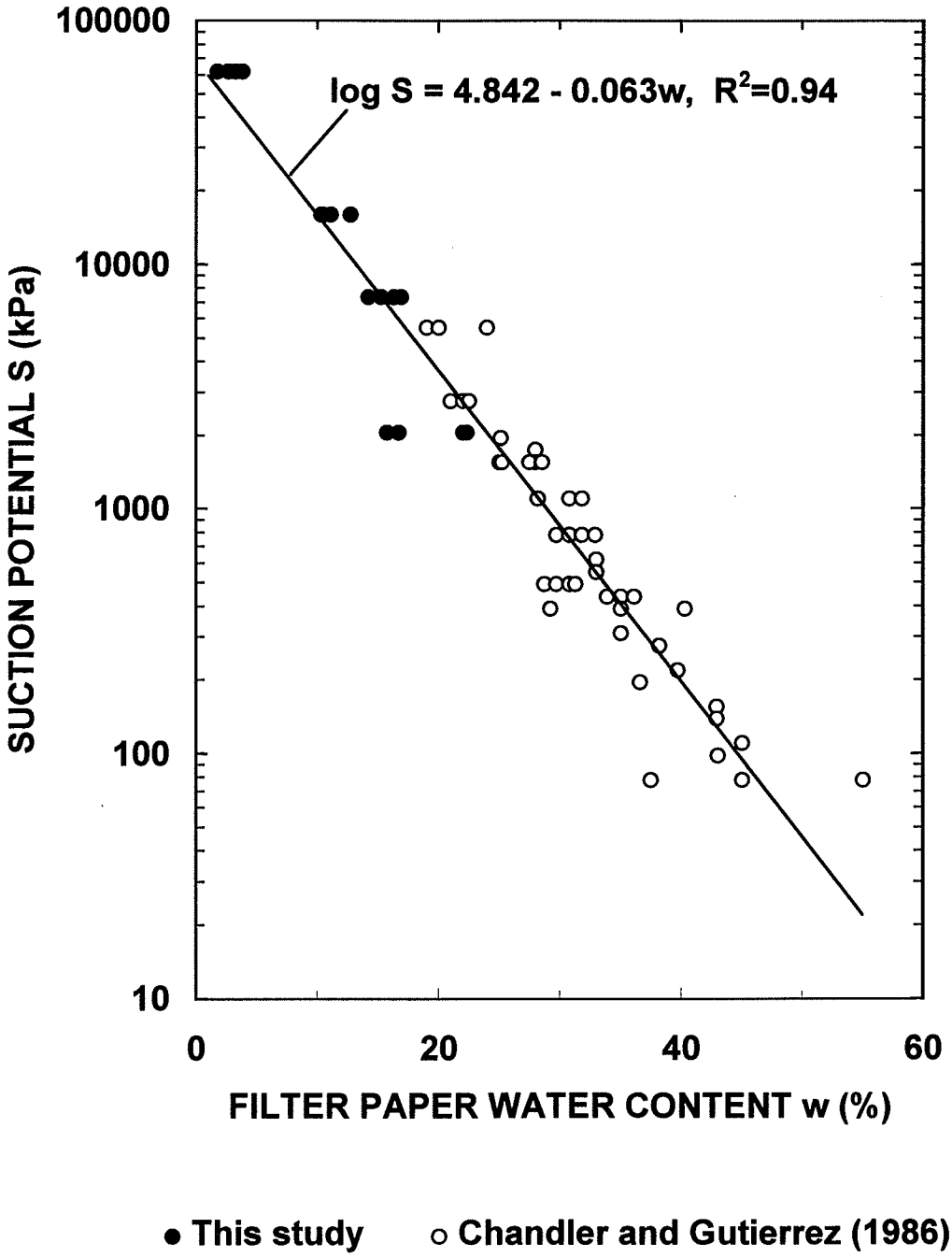

Figure 4.8 Suction potential-water content relationship for Whatman Type 42 filter paper.

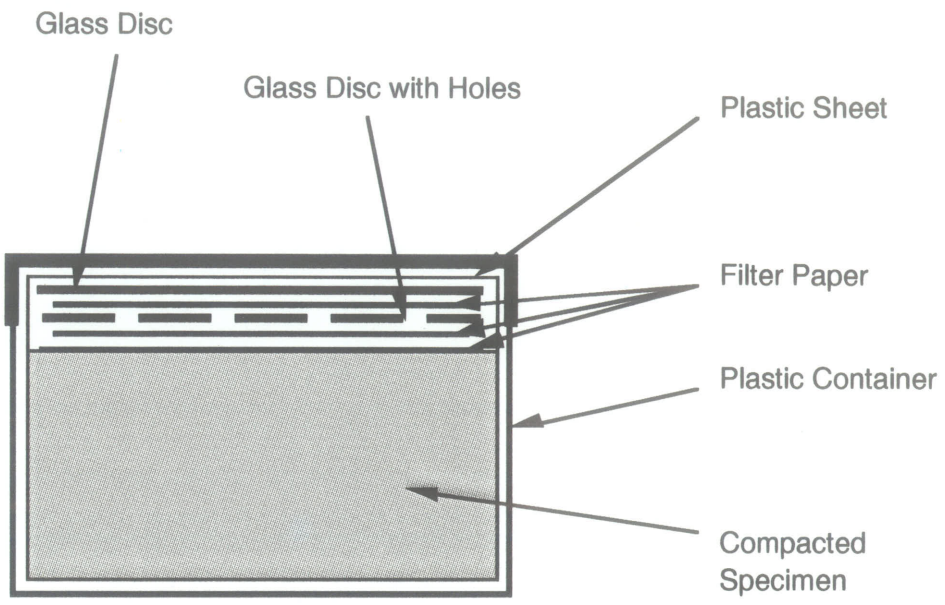

a) Test setup

b) Equipment

Figure 4.9 Filter paper test.

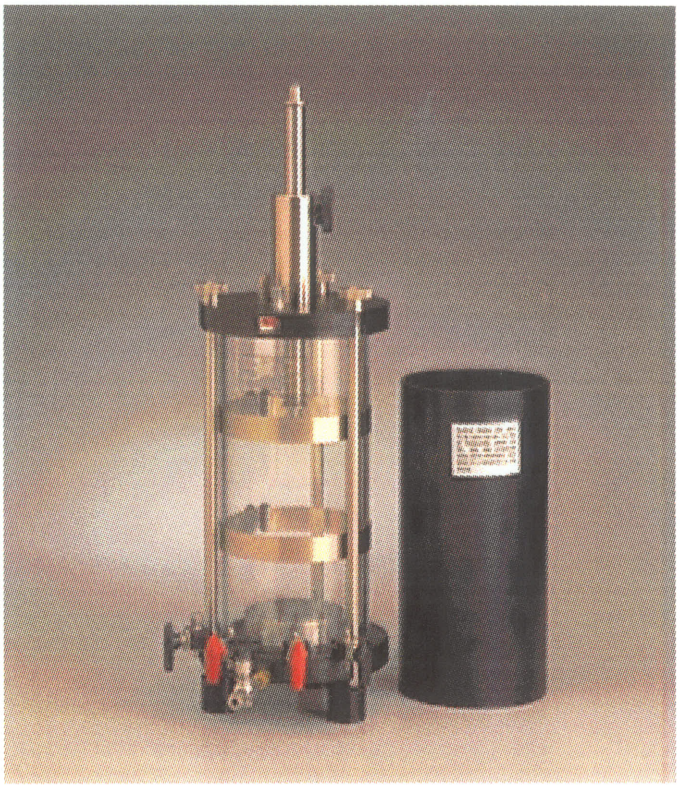

Figure 4.10 Triaxial cell with lucite and aluminum sleeves.

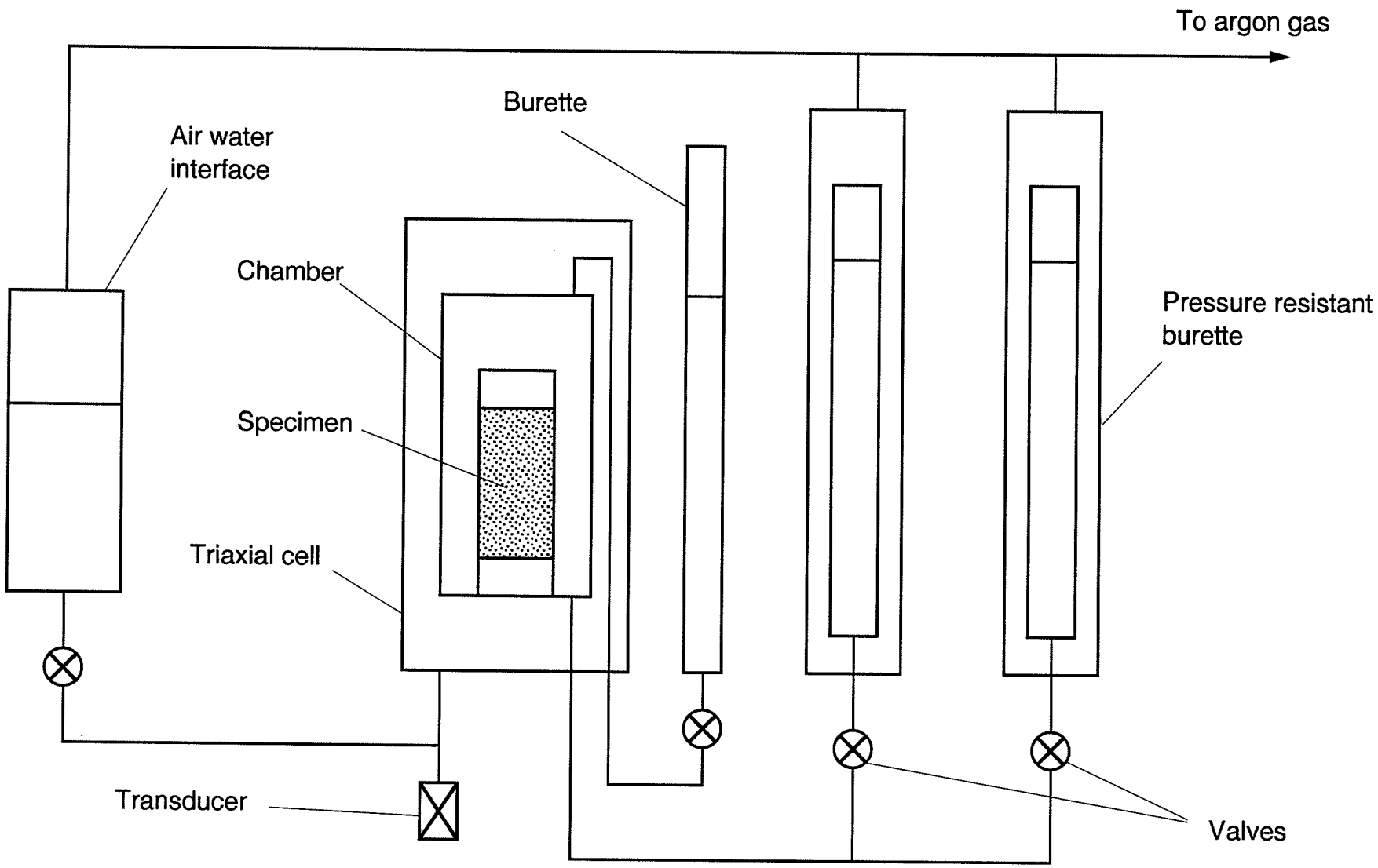

Figure 4.11 Volume change measurement scheme.

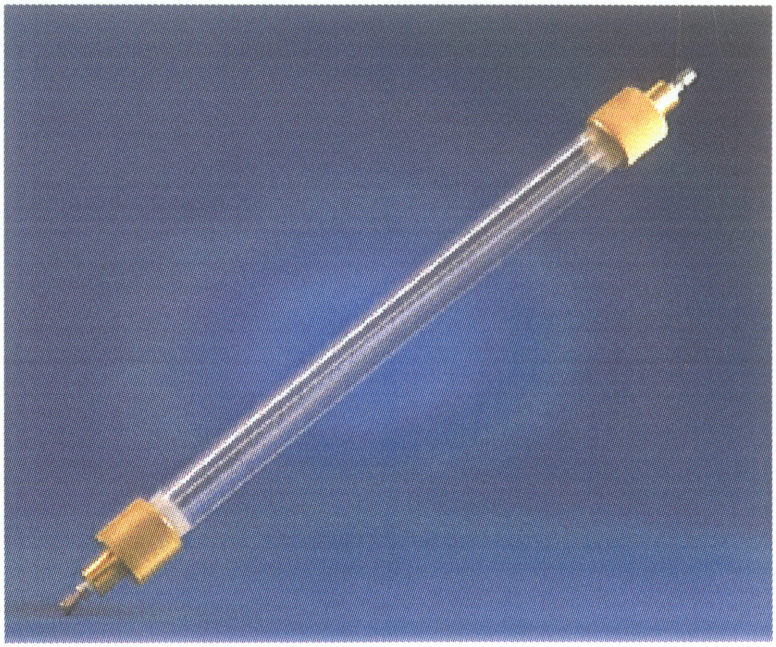

Figure 4.12 High pressure resistant burette.

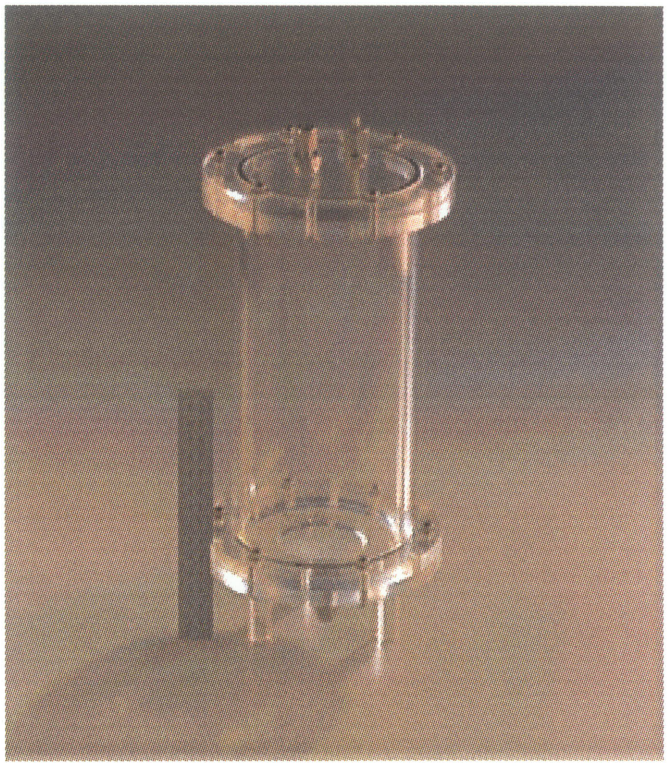

Figure 4.13 Specimen chamber used in volume change measurement scheme.

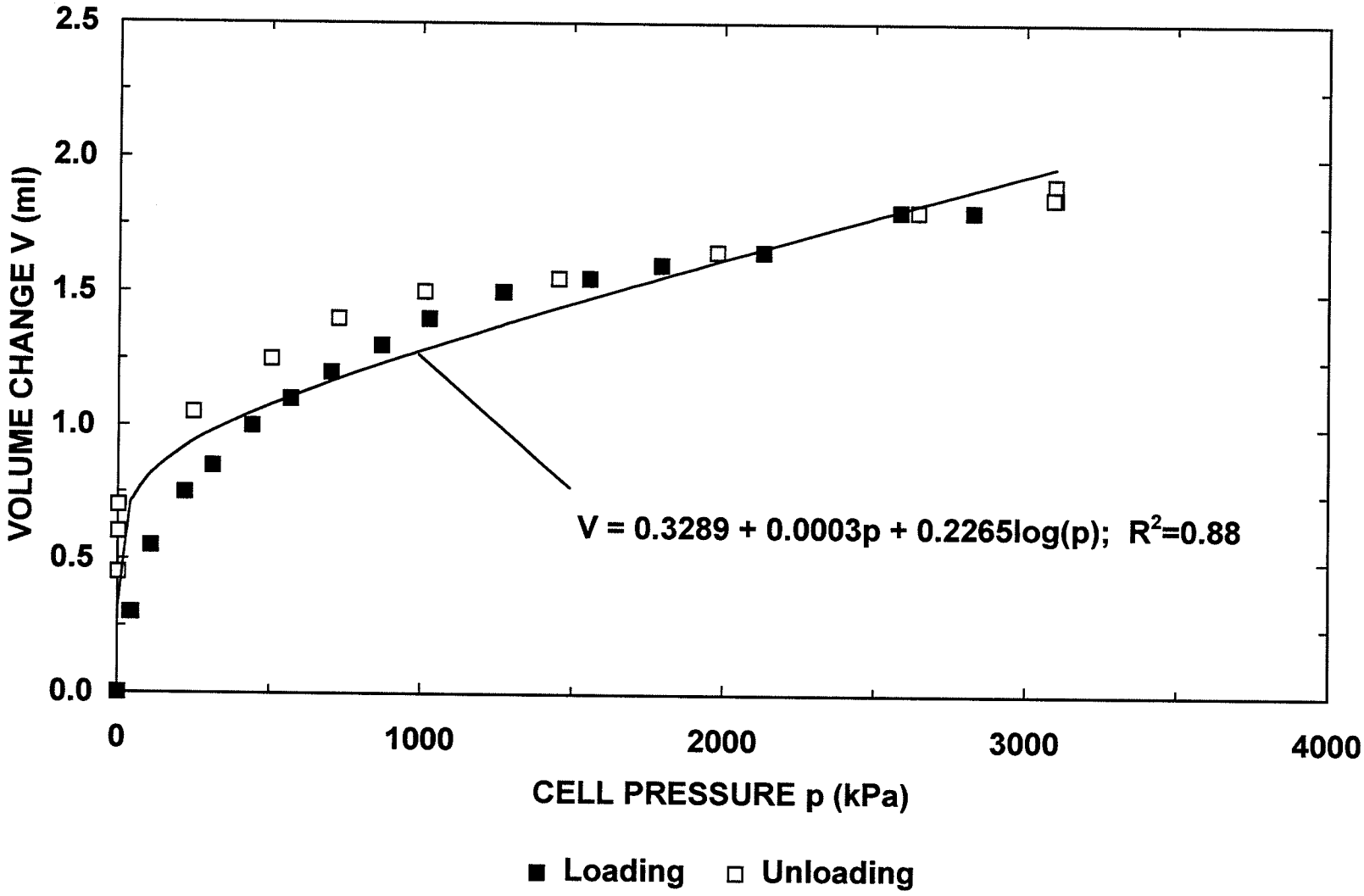

Figure 4.14 Volume change-cell pressure relationship for Buret 2/System 1.

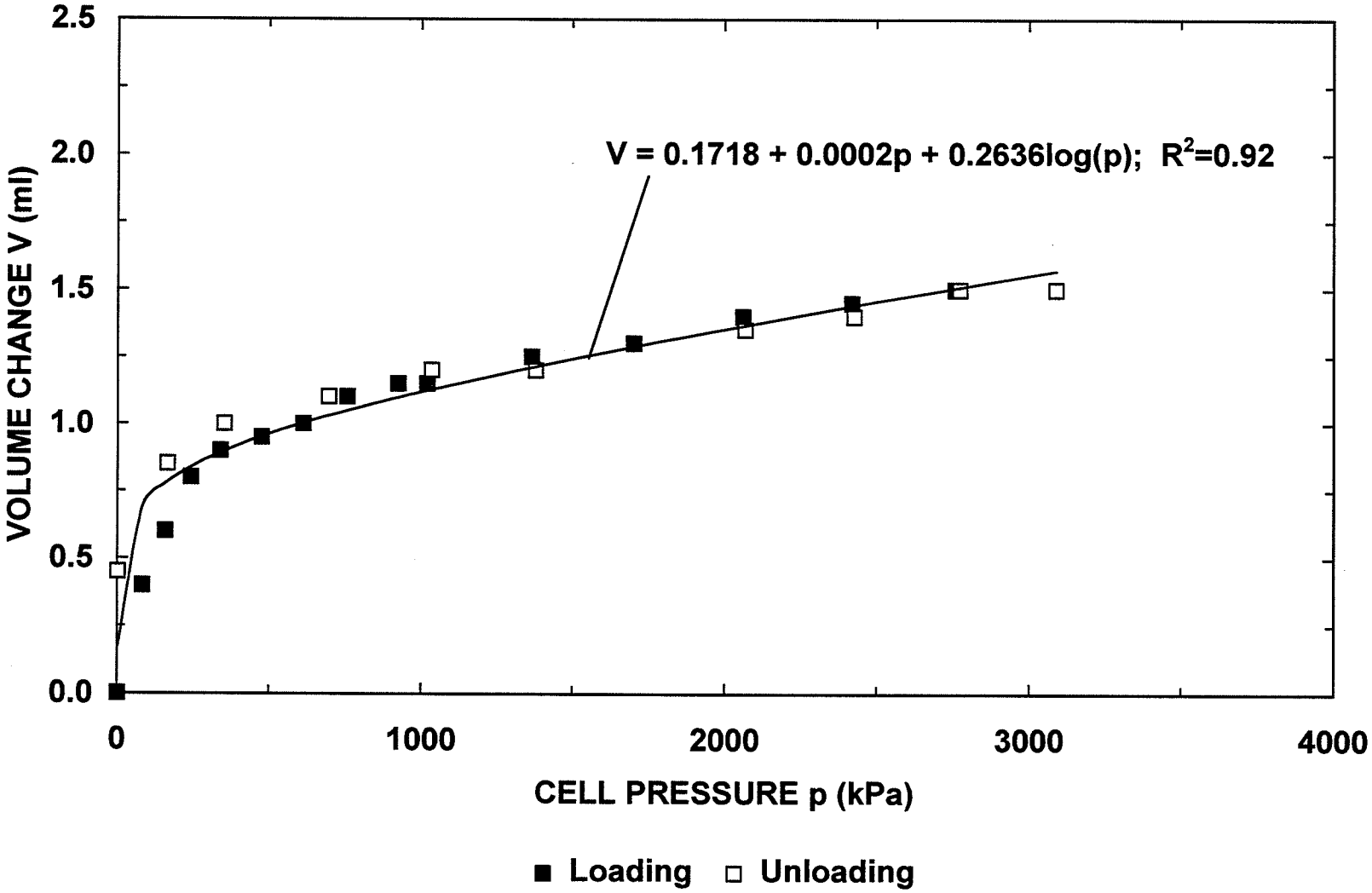

Figure 4.15 Volume change-cell pressure relationship for Buret 5/System 2.

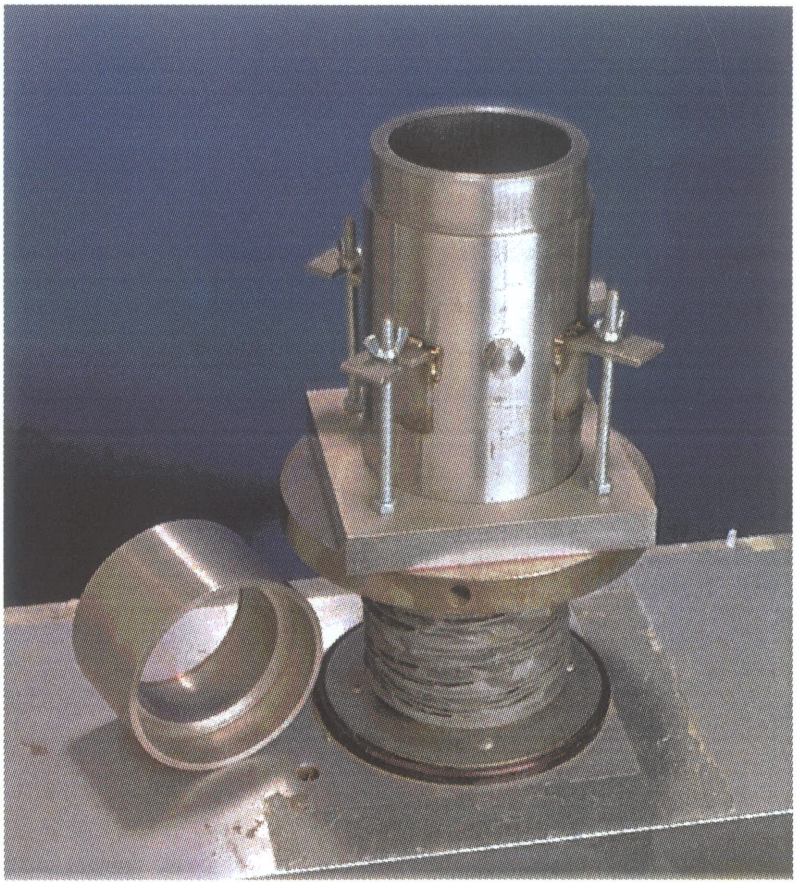

Figure 4.16 Compaction mould with removable collar.

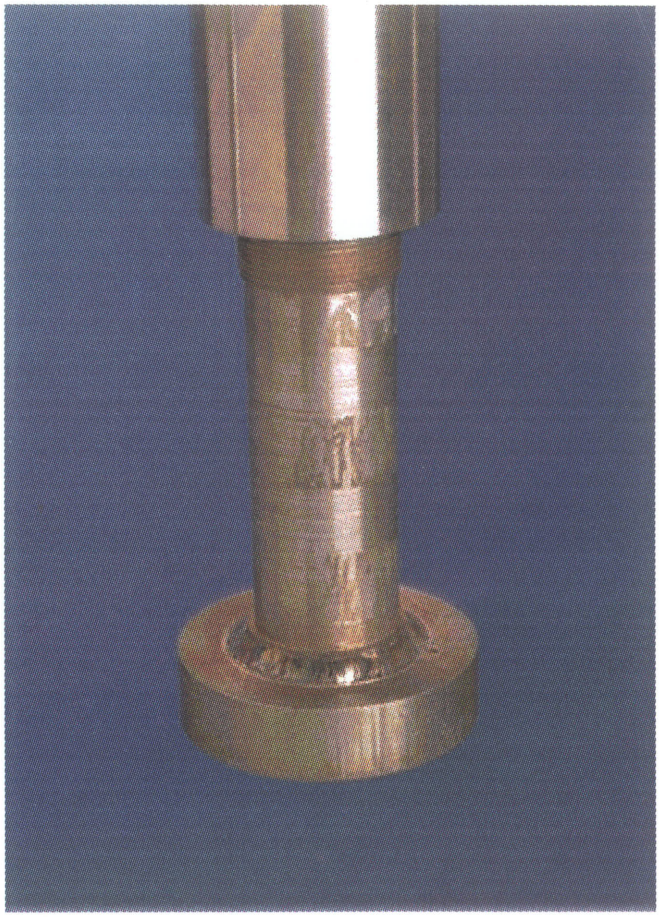

Figure 4.17 Stainless steel tee-shaped ram.

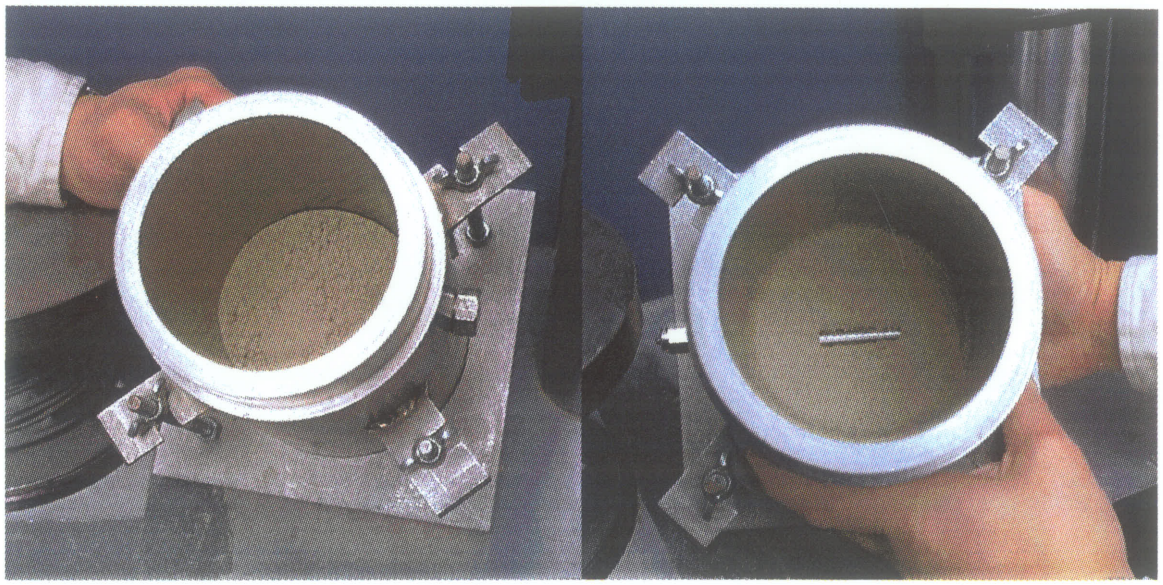

(a) (b)

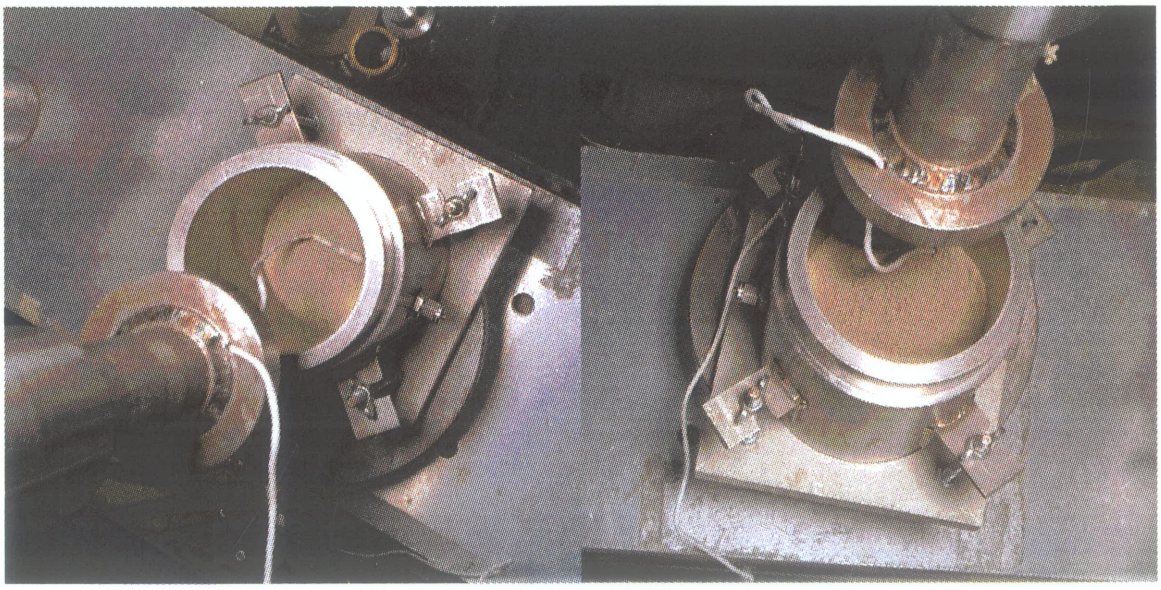

(c) (d)

Figure 4.18 Specimen preparation and psychrometer installation.

Figure 4.19 Top cap fitted with a Conax™ fitting.

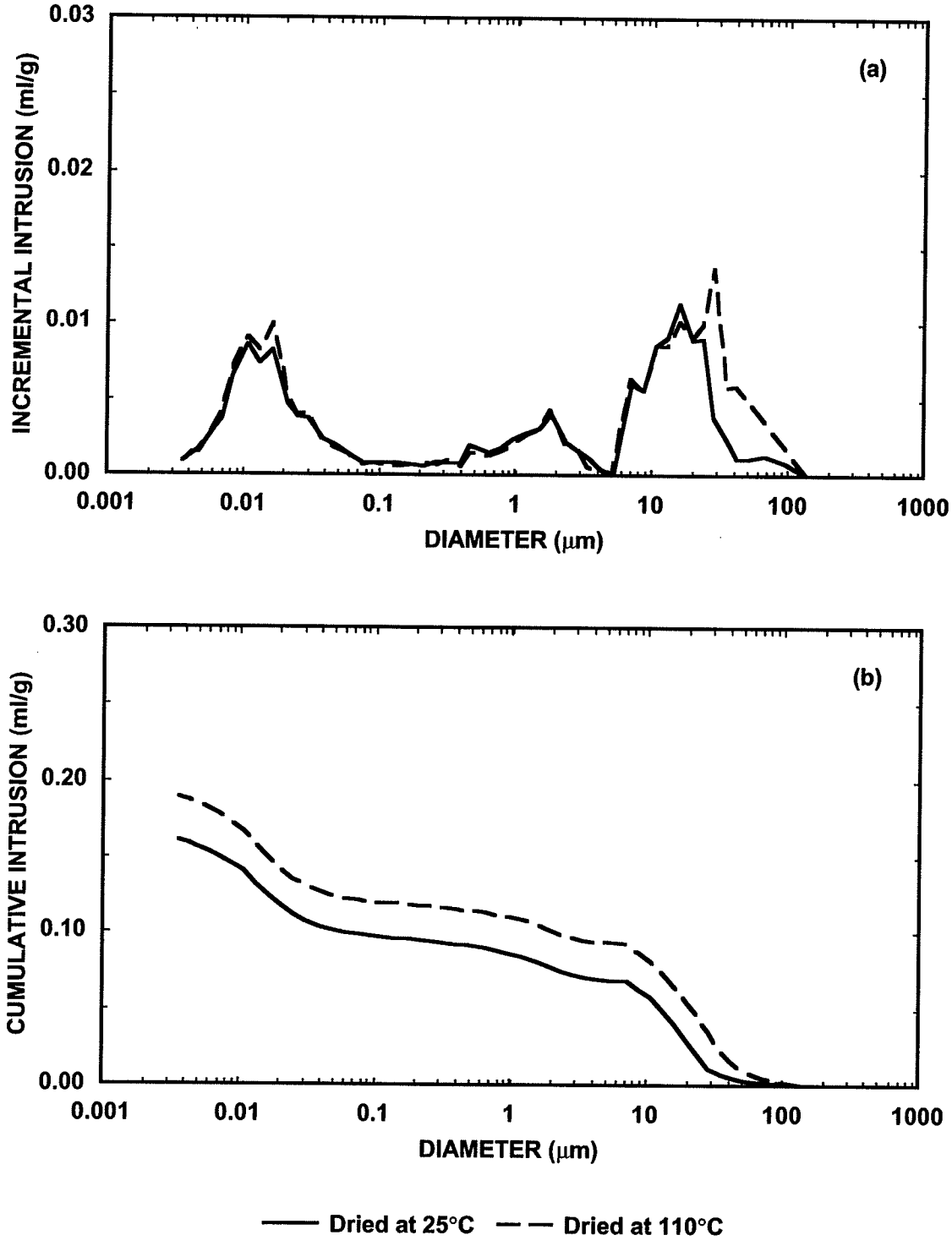

Figure 4.20 Comparison of pore size distributions in sand-bentonite specimens dried at different temperatures.

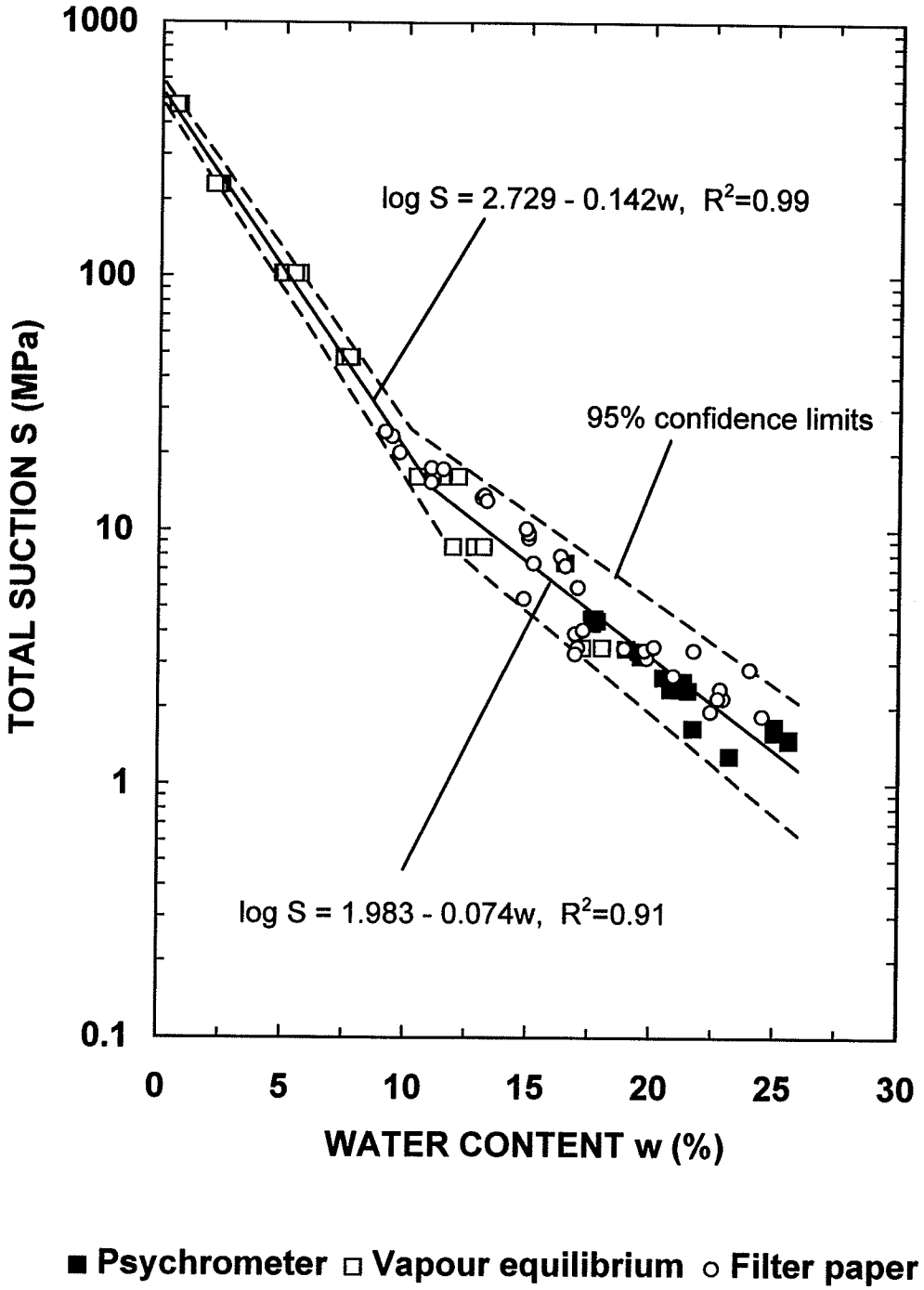

Figure 5.1 Suction-water content relationship of sand-bentonite material.

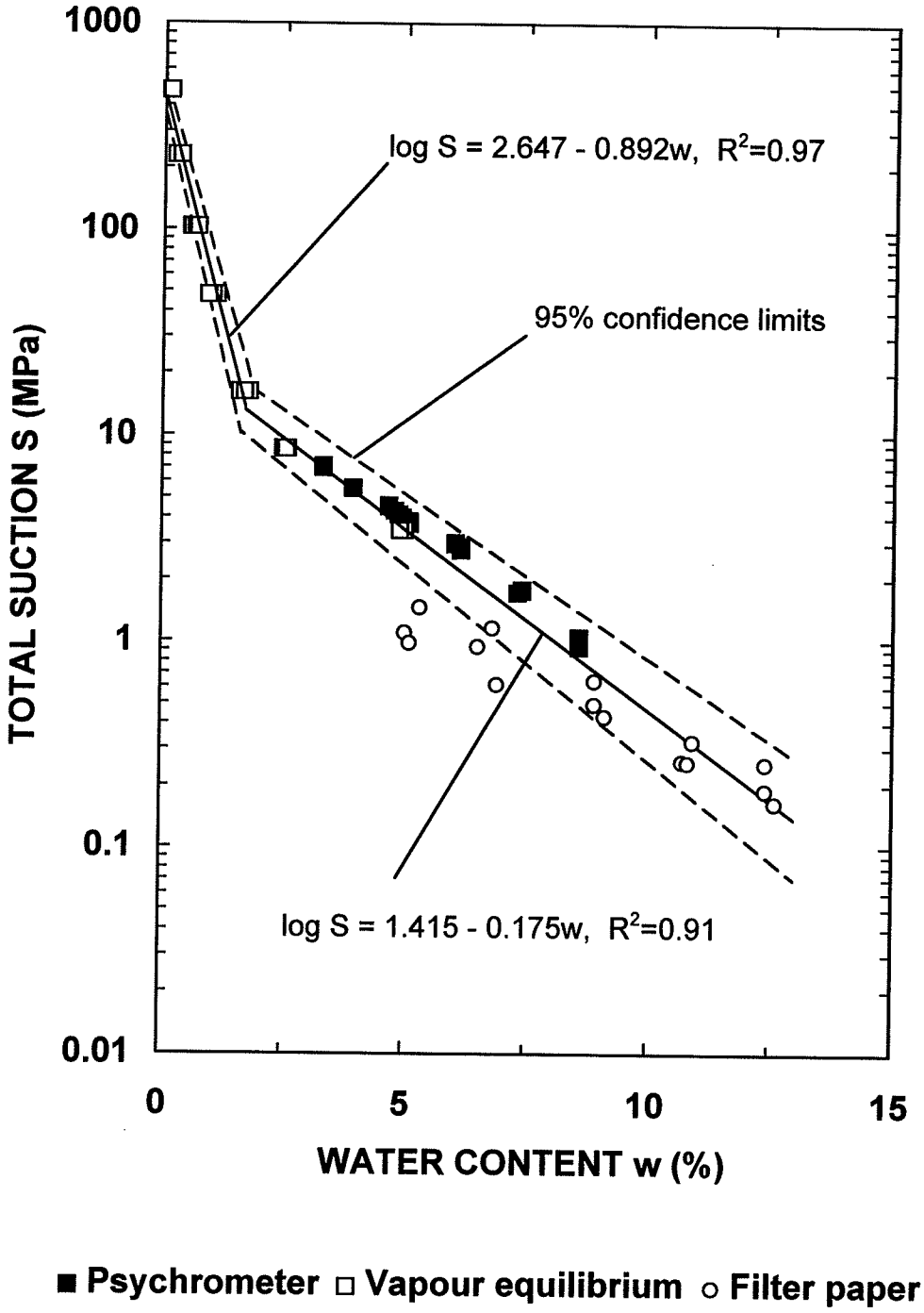

Figure 5.2 Suction-water content relationship of sand-illite material.

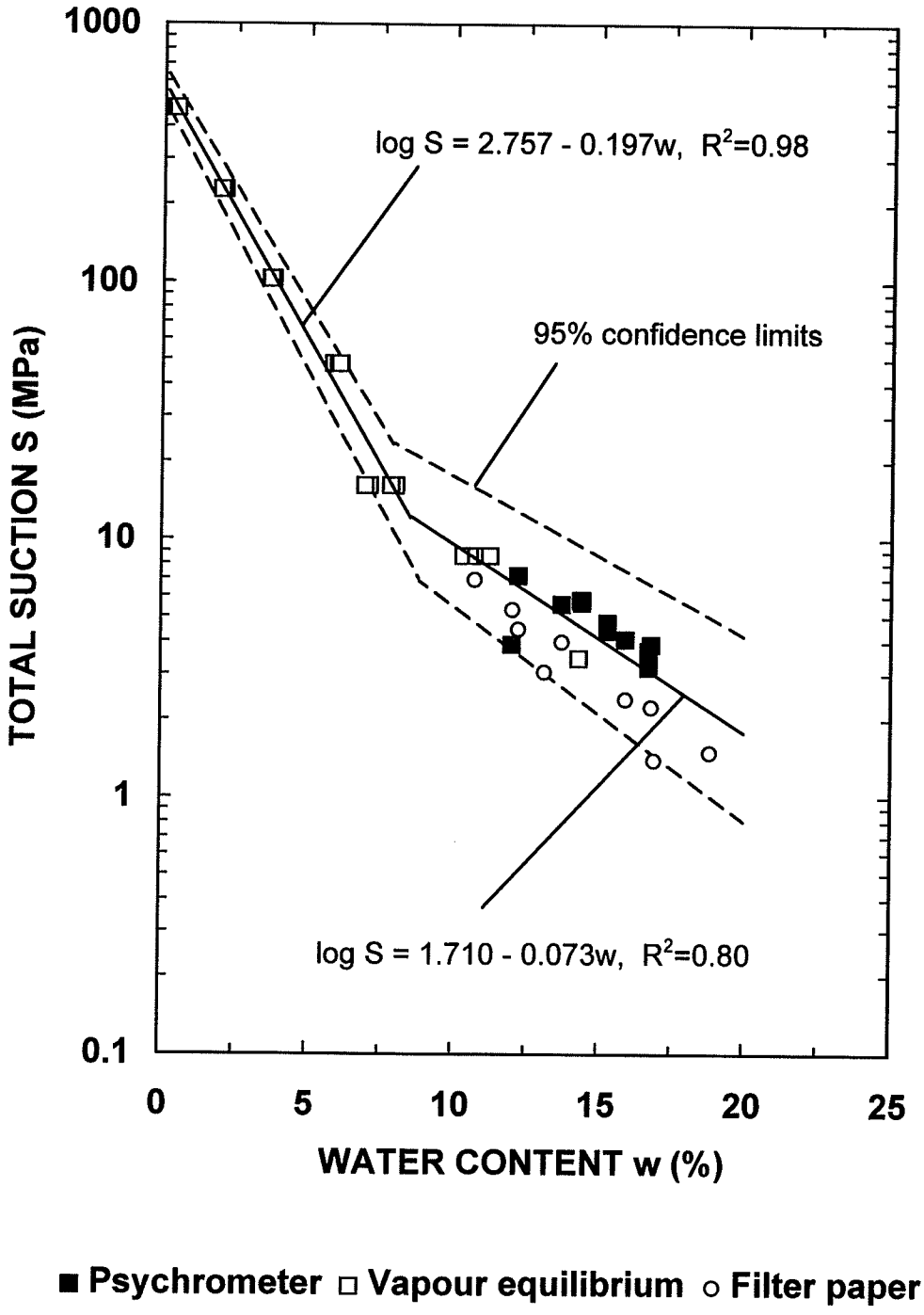

Figure 5.3 Suction-water content relationship of Boom Clay.

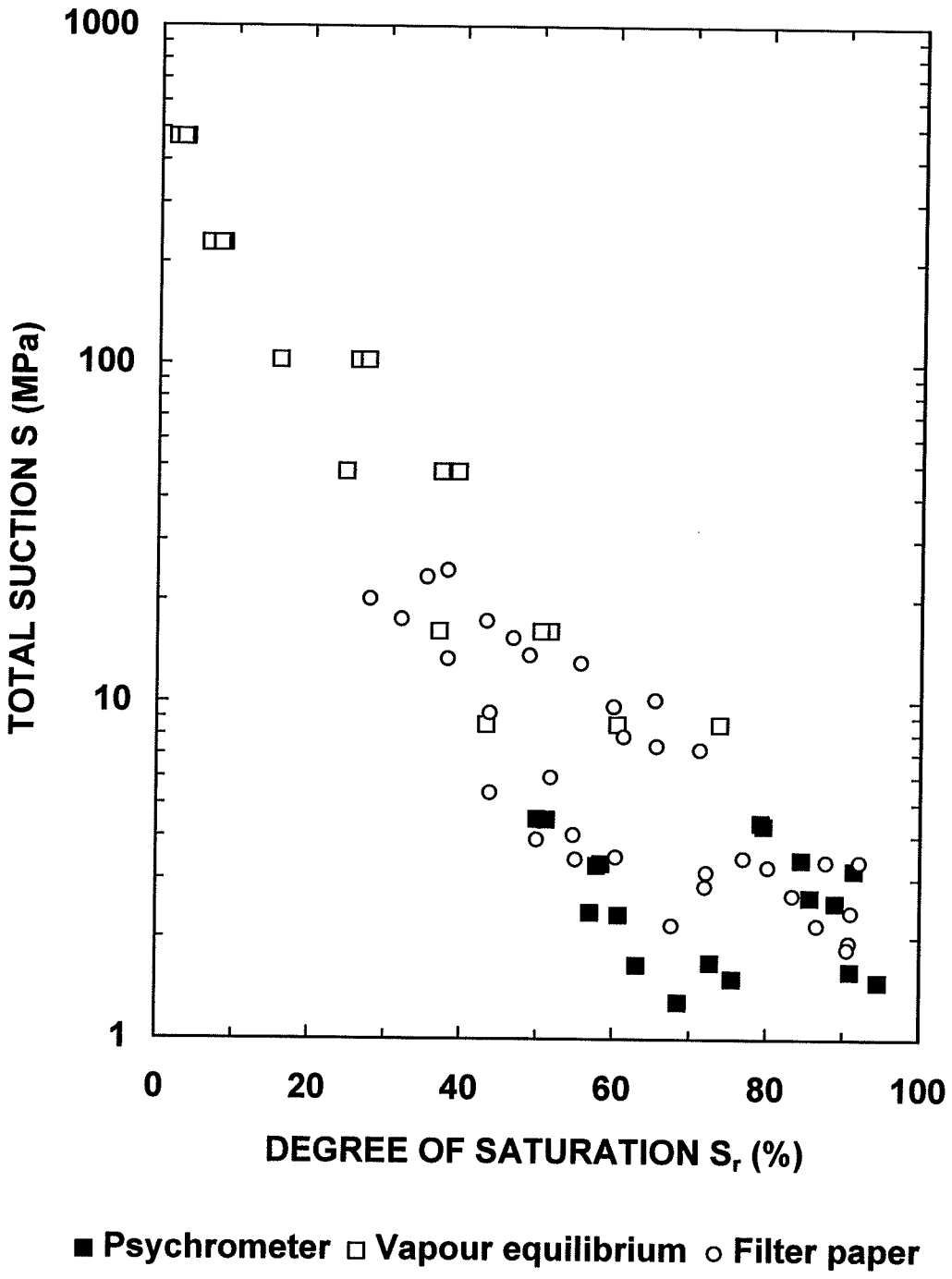

Figure 5.4 Suction-saturation relationship of sand-bentonite material.

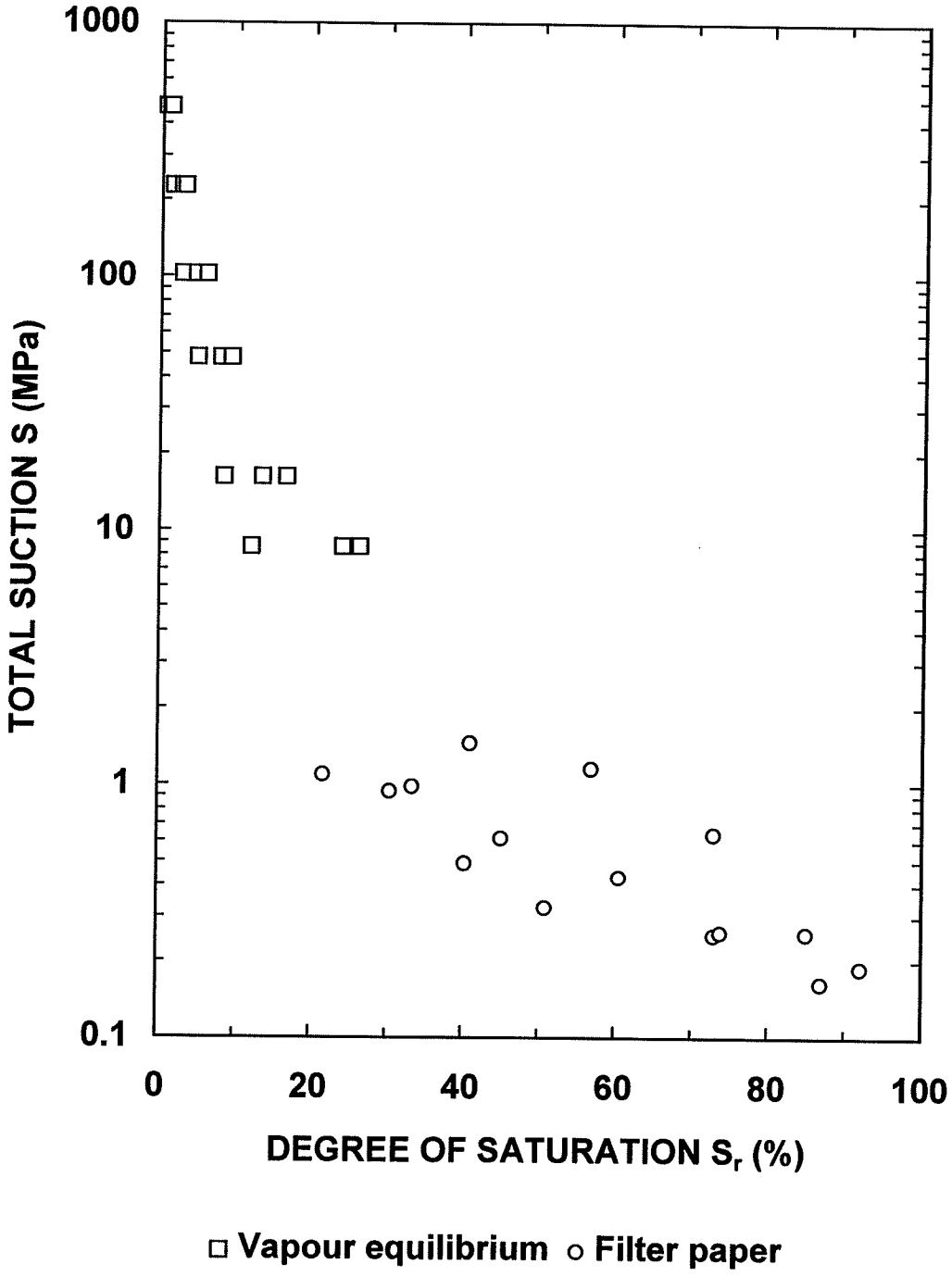

Figure 5.5 Suction-saturation relationship of sand-illite material.

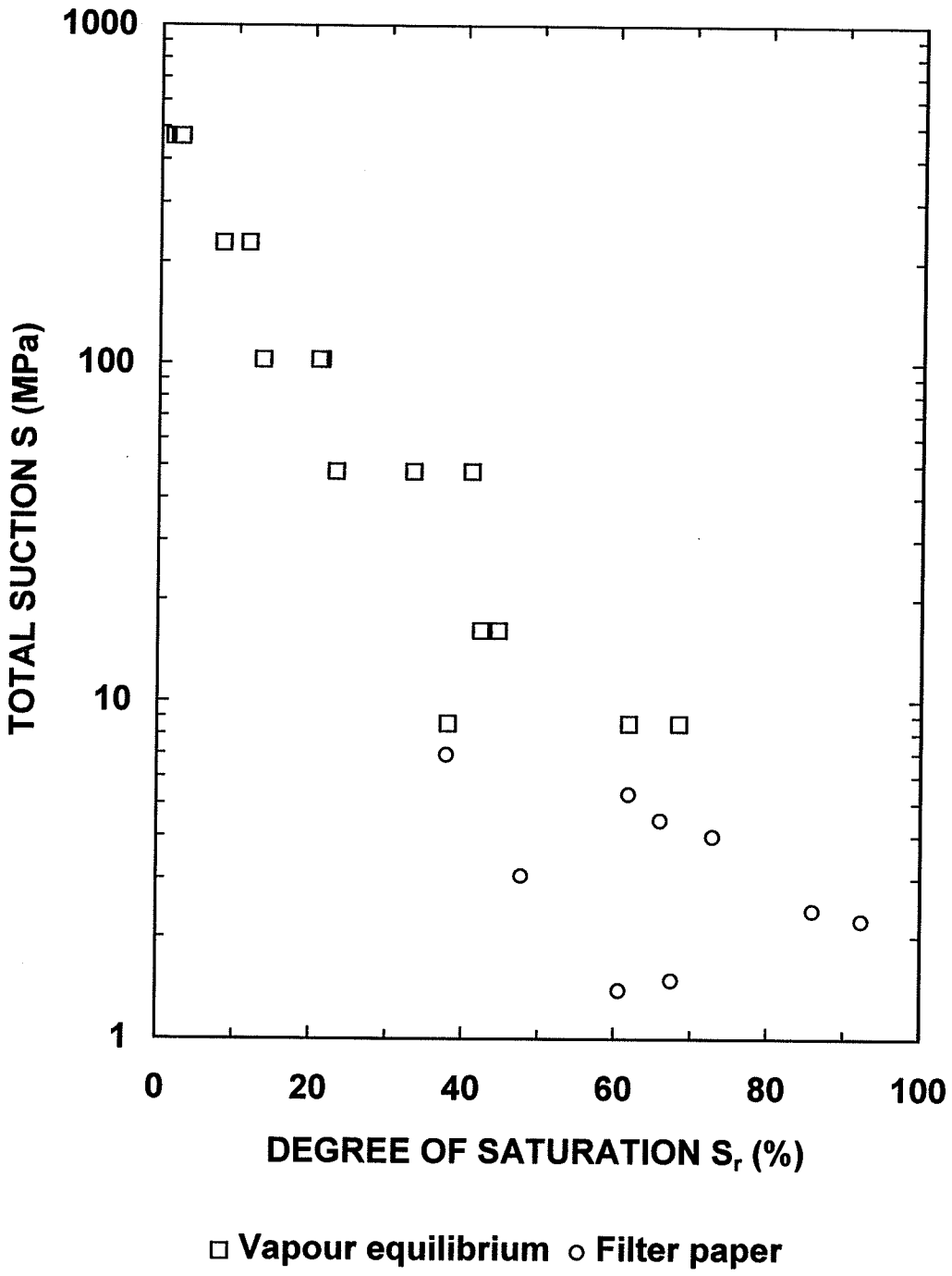

Figure 5.6 Suction-saturation relationship of Boom Clay.

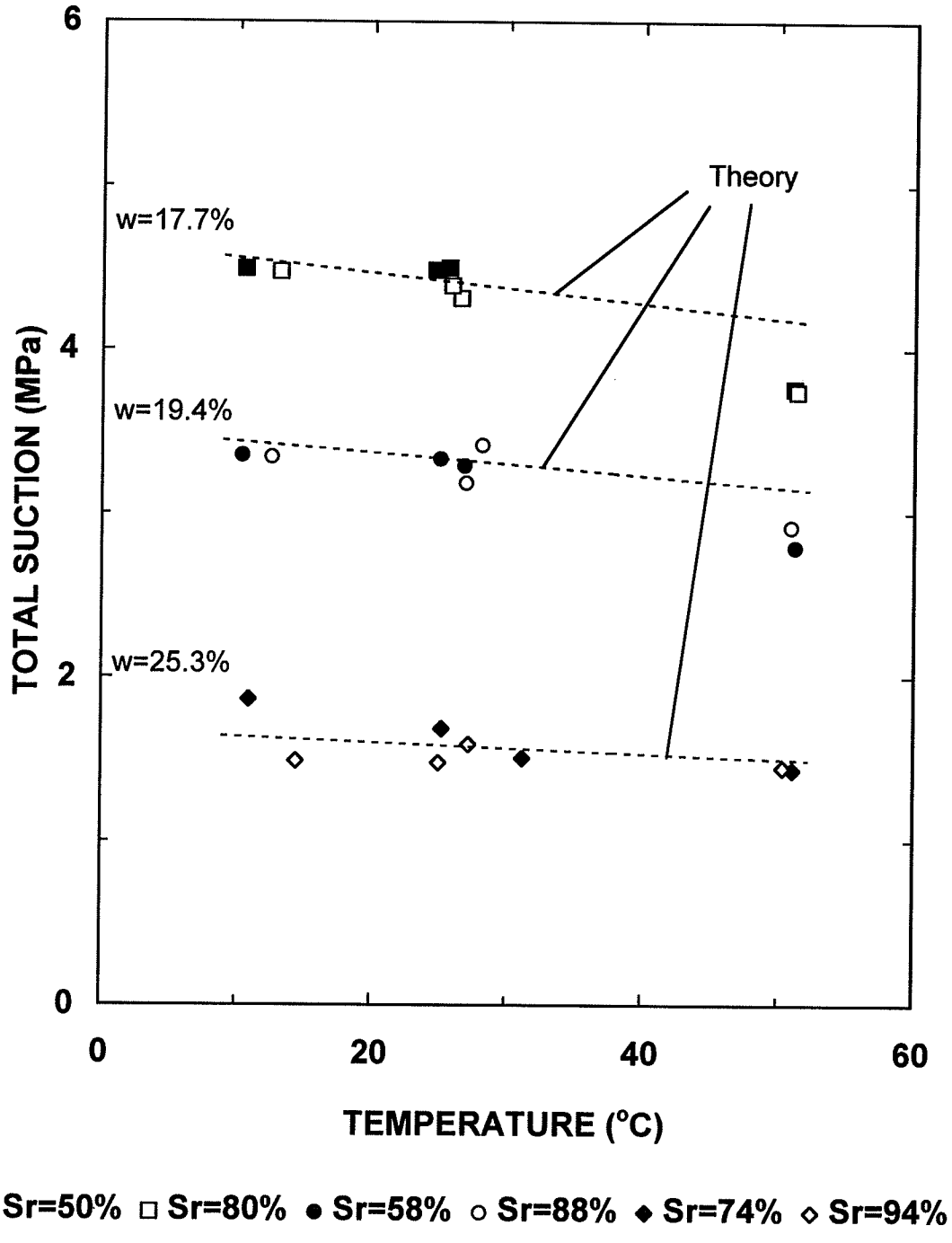

Figure 5.7 Effects of saturation and temperature on total suction in sand-bentonite material.

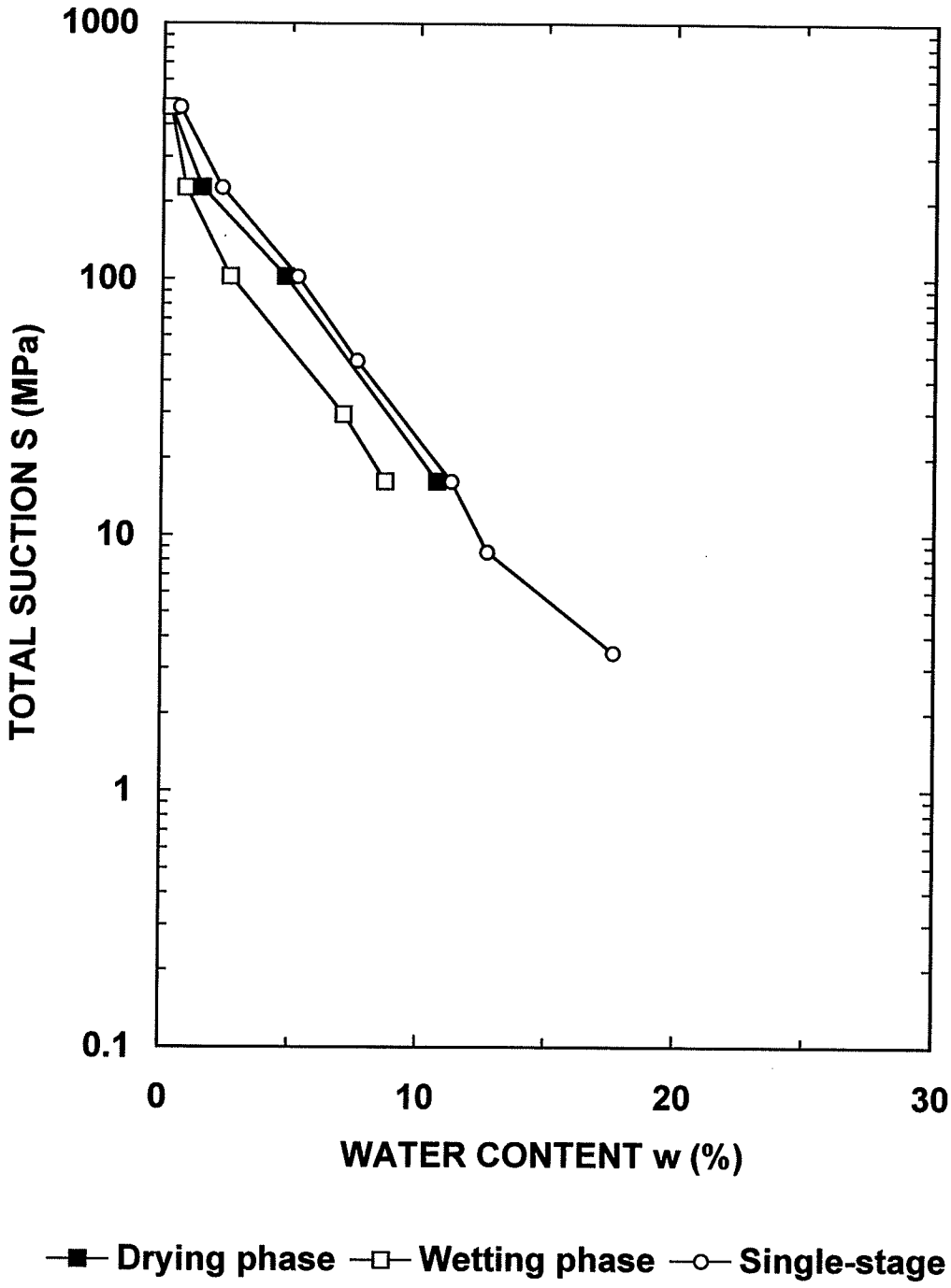

Figure 5.8 Suction-water content relationships of uncompacted sand-bentonite material.

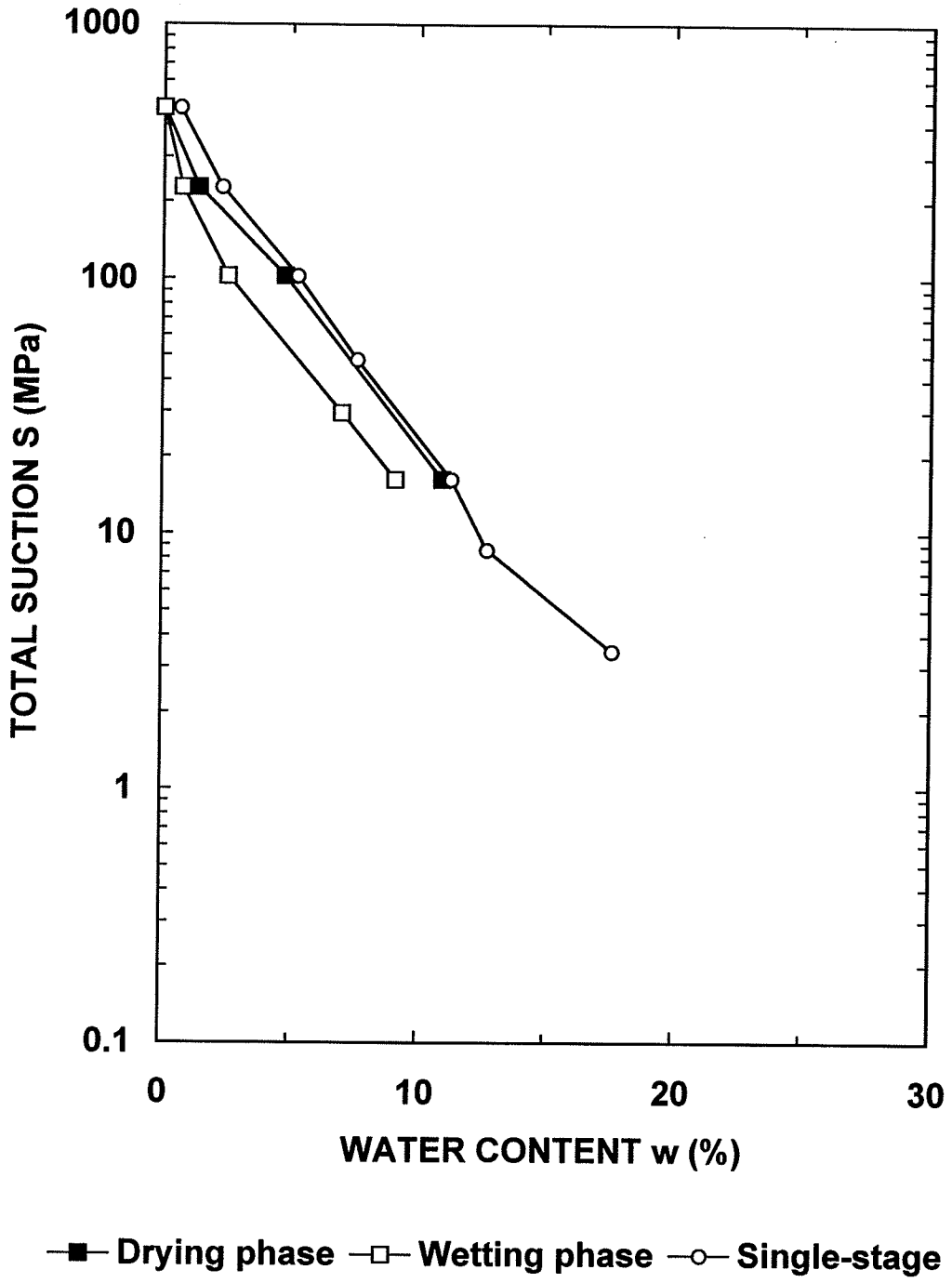

Figure 5.9 Suction-water content relationships of compacted sand-bentonite material: 5 mm thick, γd=1.48Mg/m3.

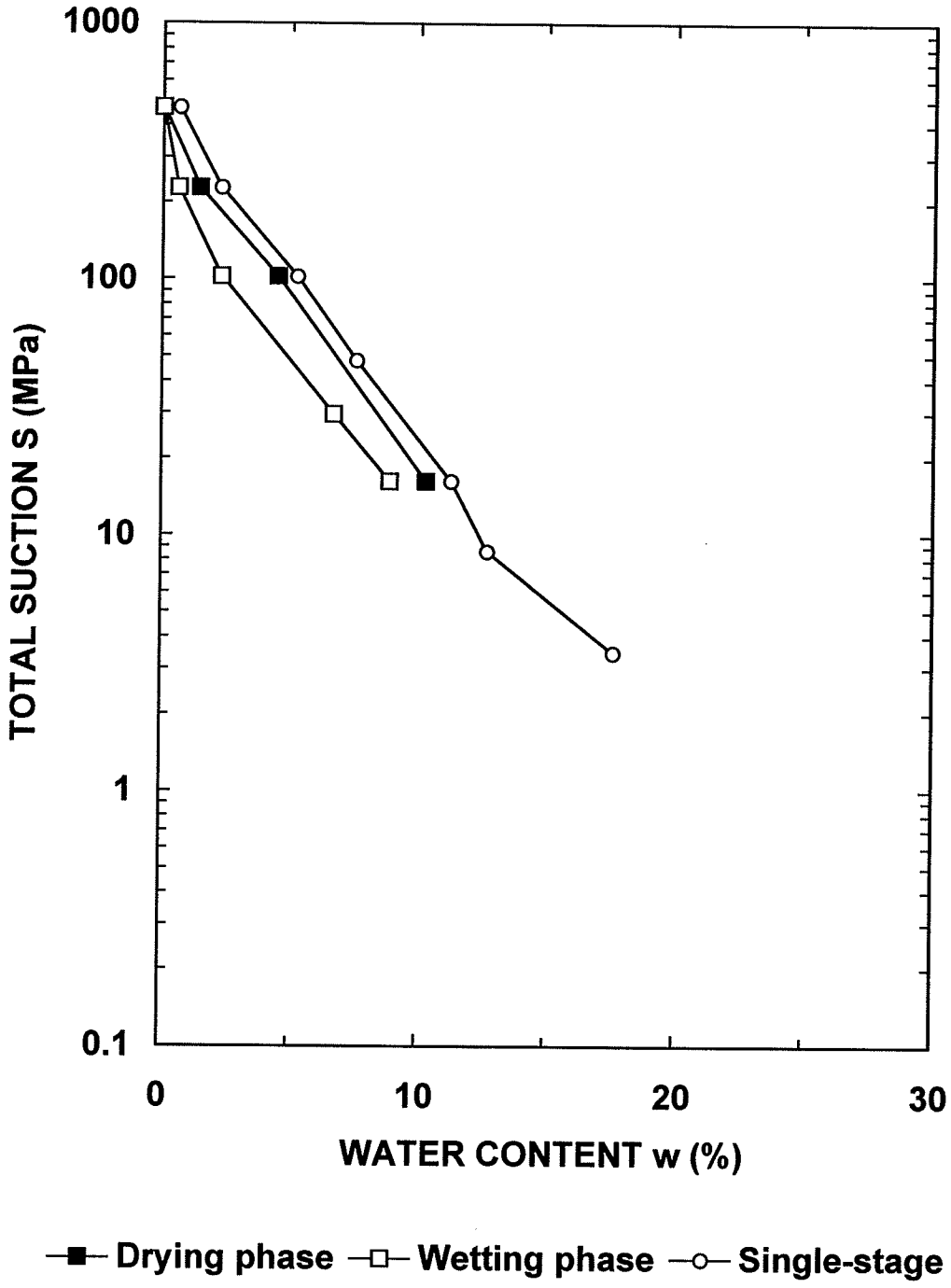

Figure 5.10 Suction-water content relationships of compacted sand-bentonite material: 10 mm thick, γd=1.74Mg/m3.

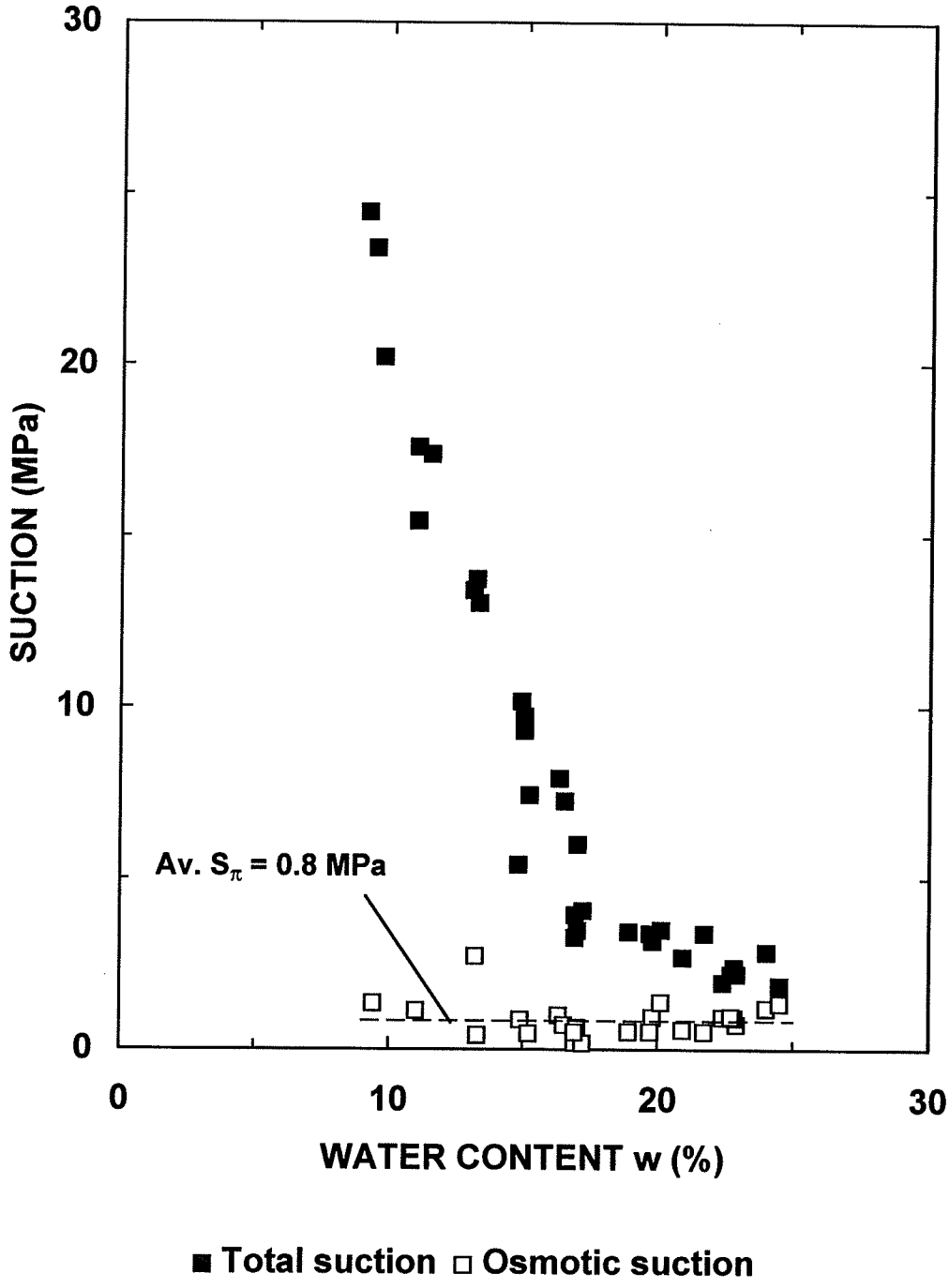

Figure 5.11 Influence of water content on total and osmotic suctions in sand-bentonite material.

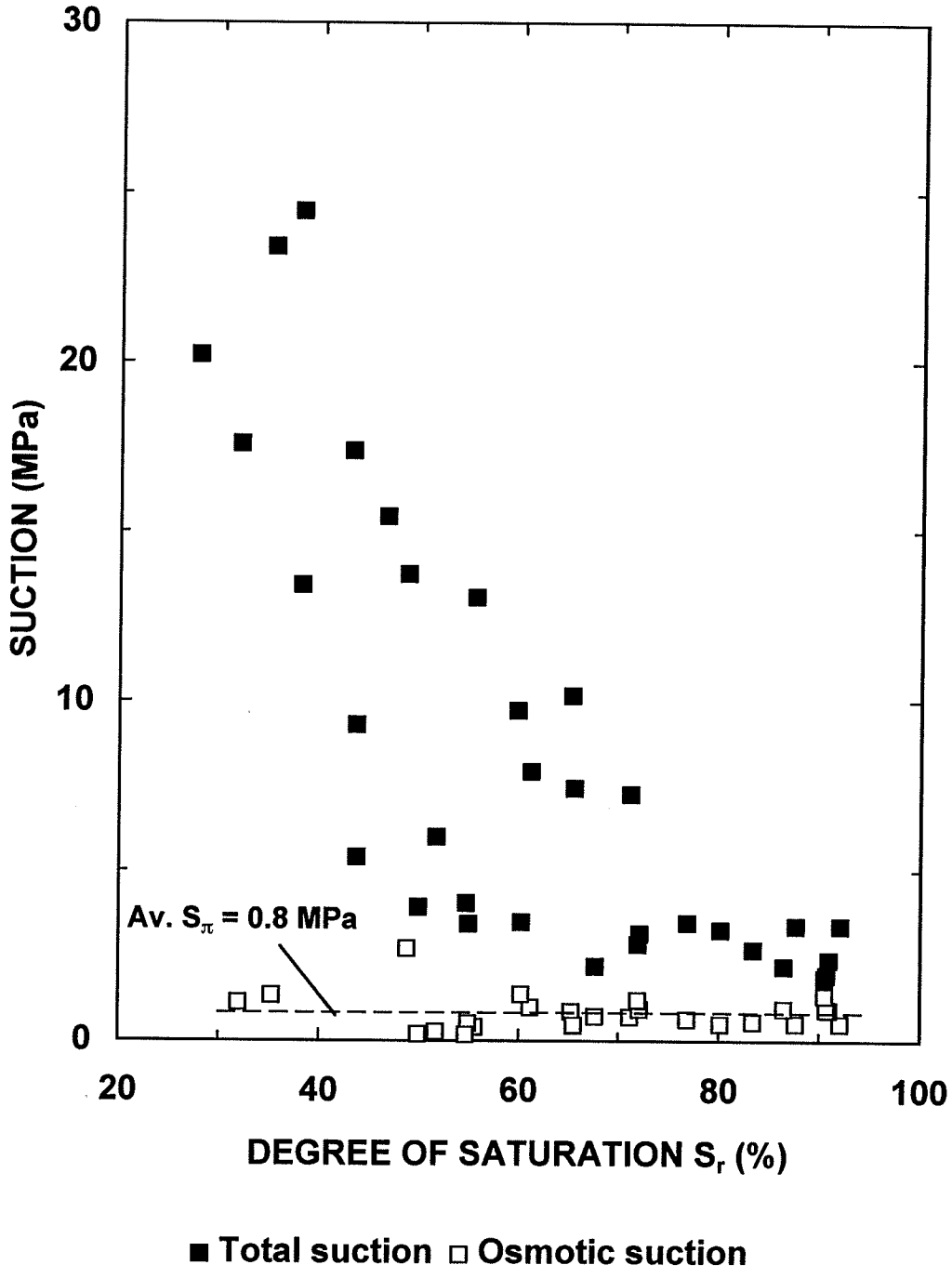

Figure 5.12 Influence of saturation on total and osmotic suctions in sand-bentonite material.

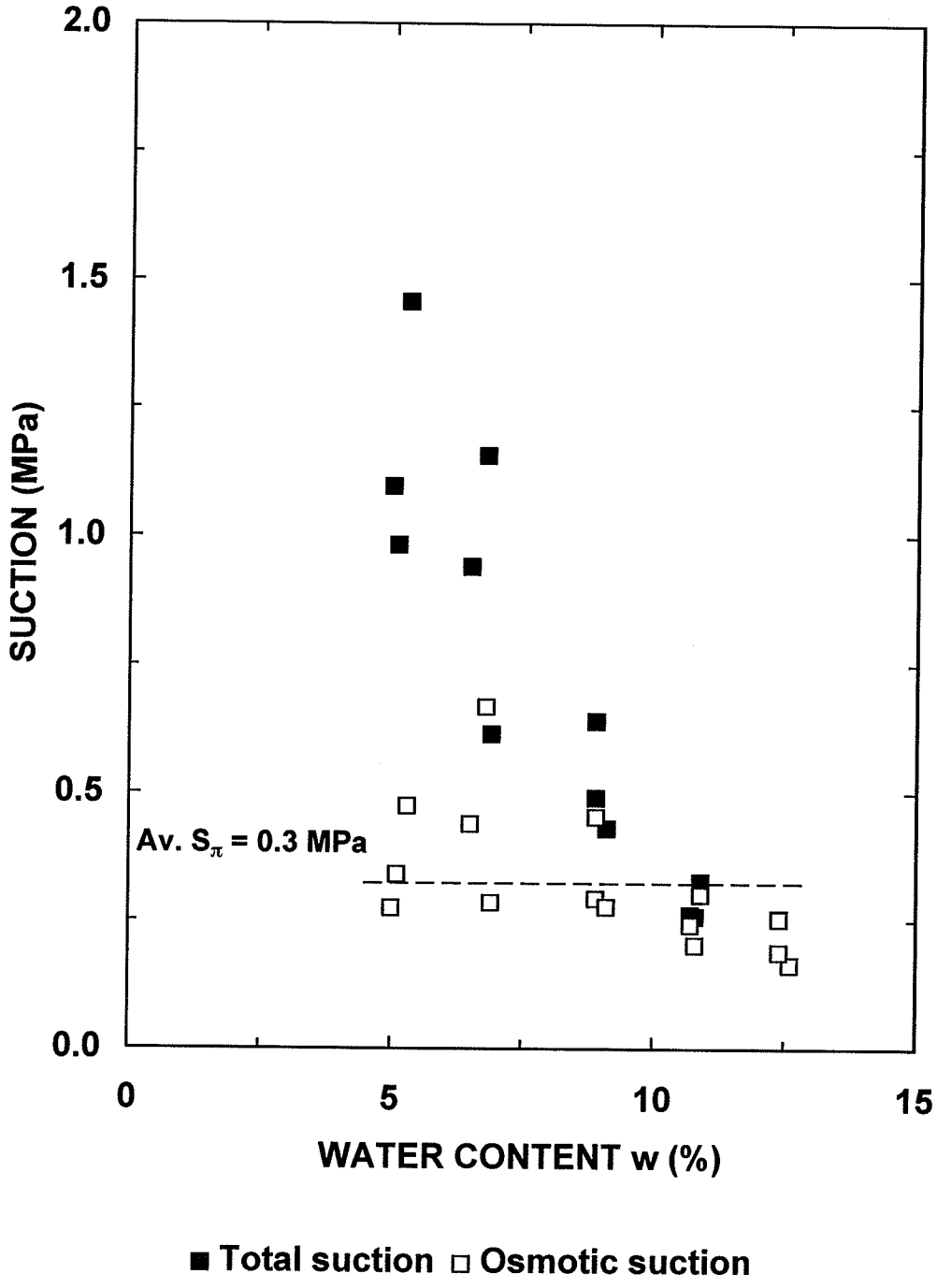

Figure 5.13 Influence of water content on total and osmotic suctions in sand-illite material.

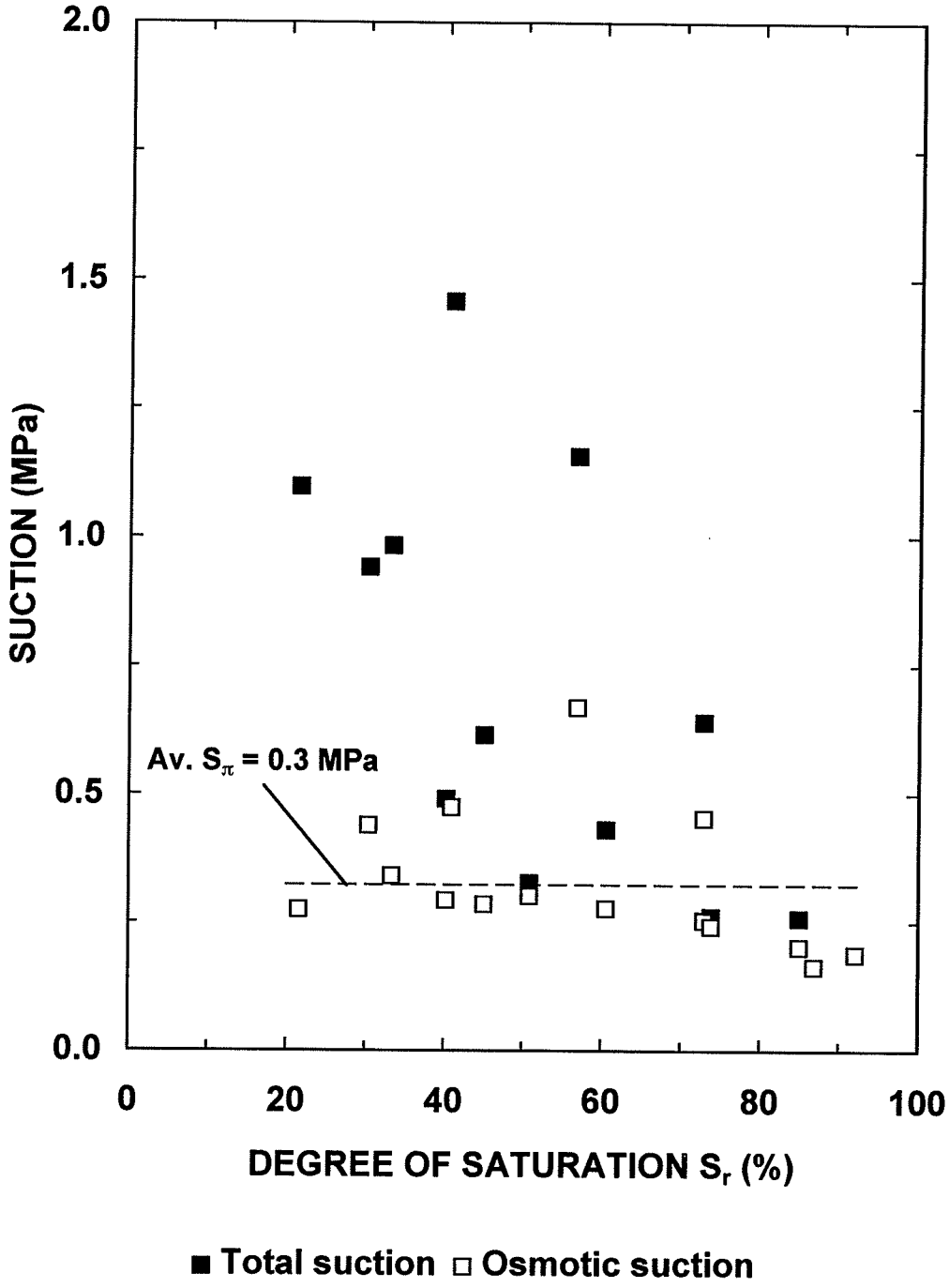

Figure 5.14 Influence of saturation on total and osmotic suctions in sand-illite material.

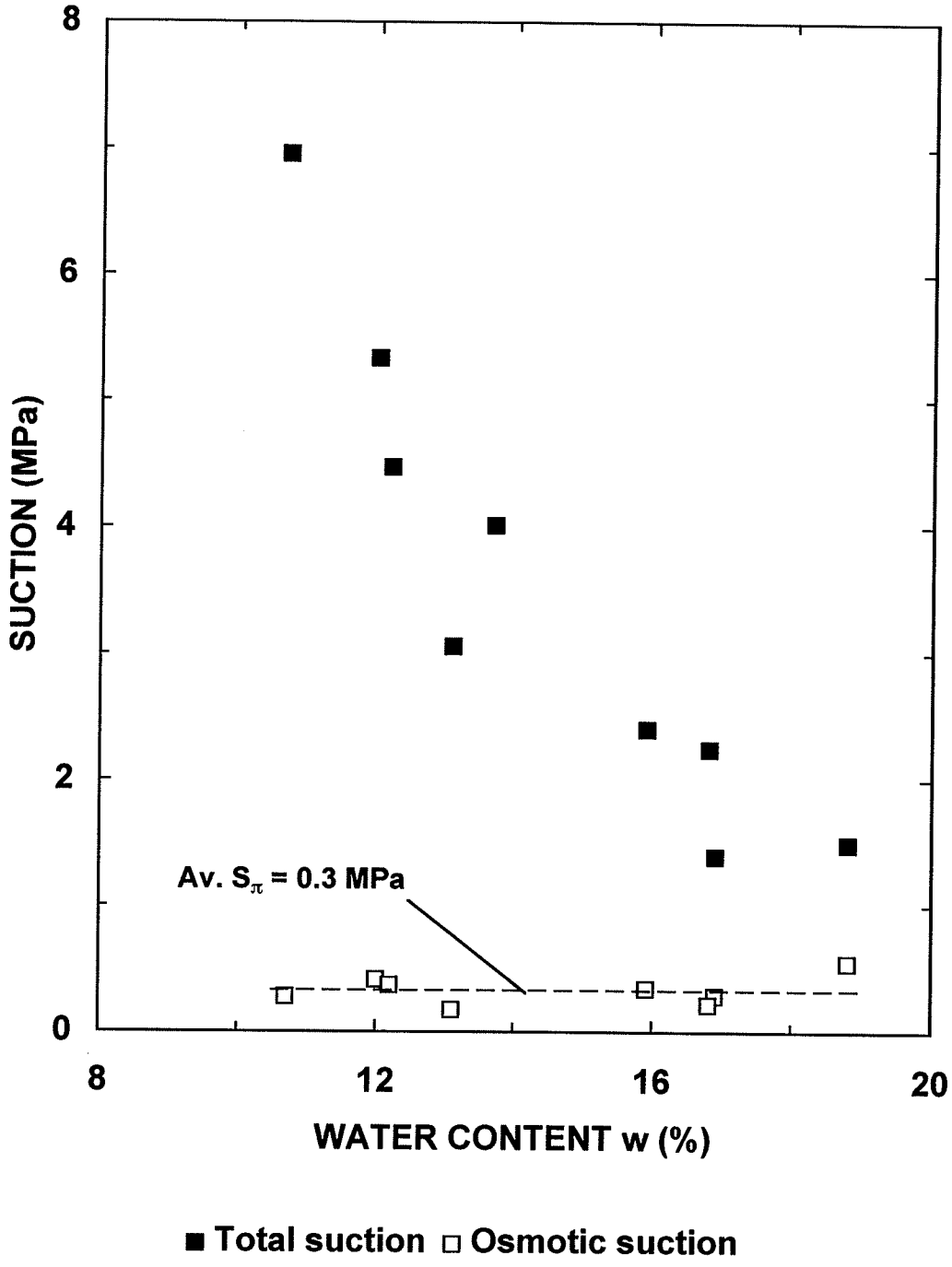

Figure 5.15 Influence of water content on total and osmotic suctions in Boom Clay.

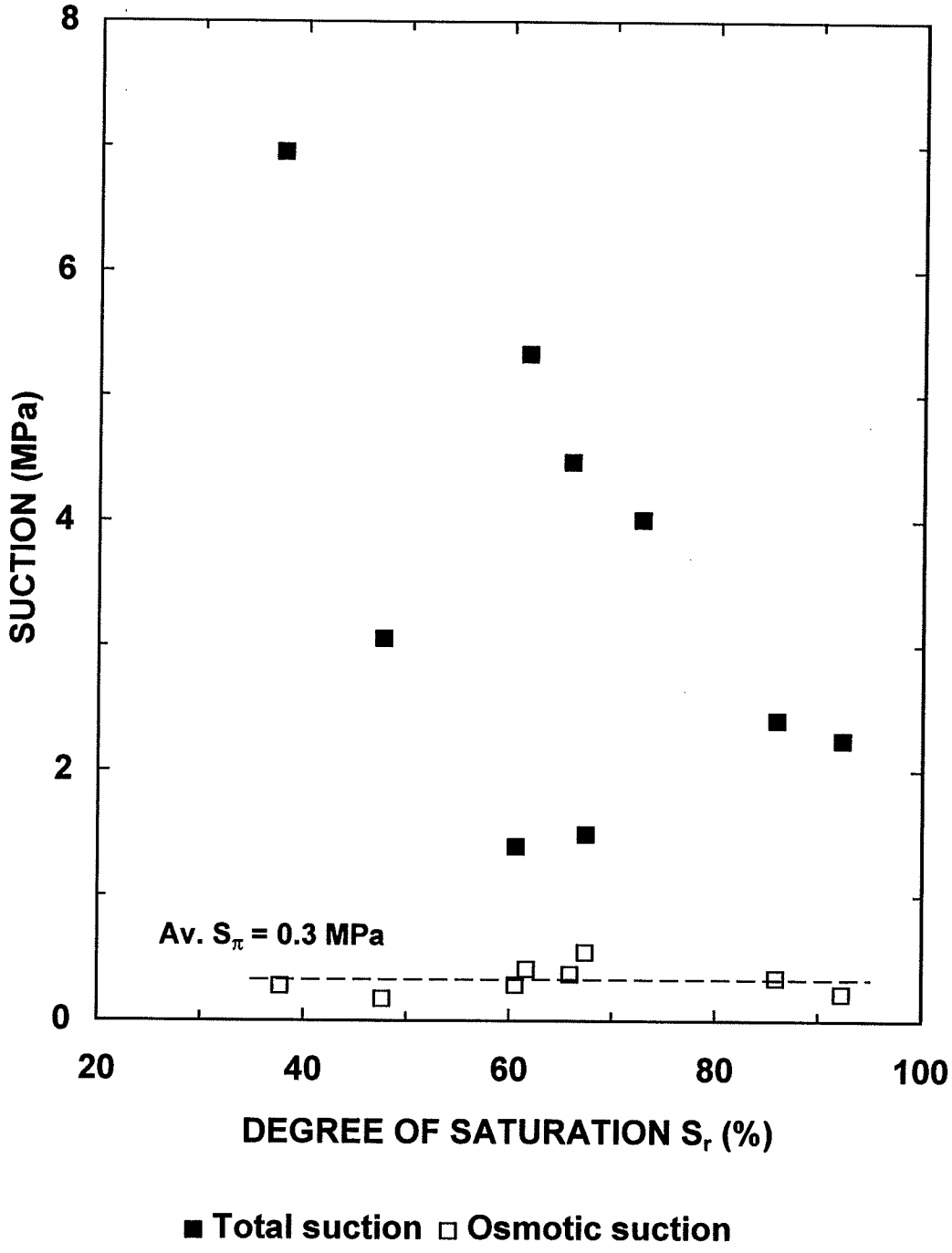

Figure 5.16 Influence of saturation on total and osmotic suctions in Boom Clay.

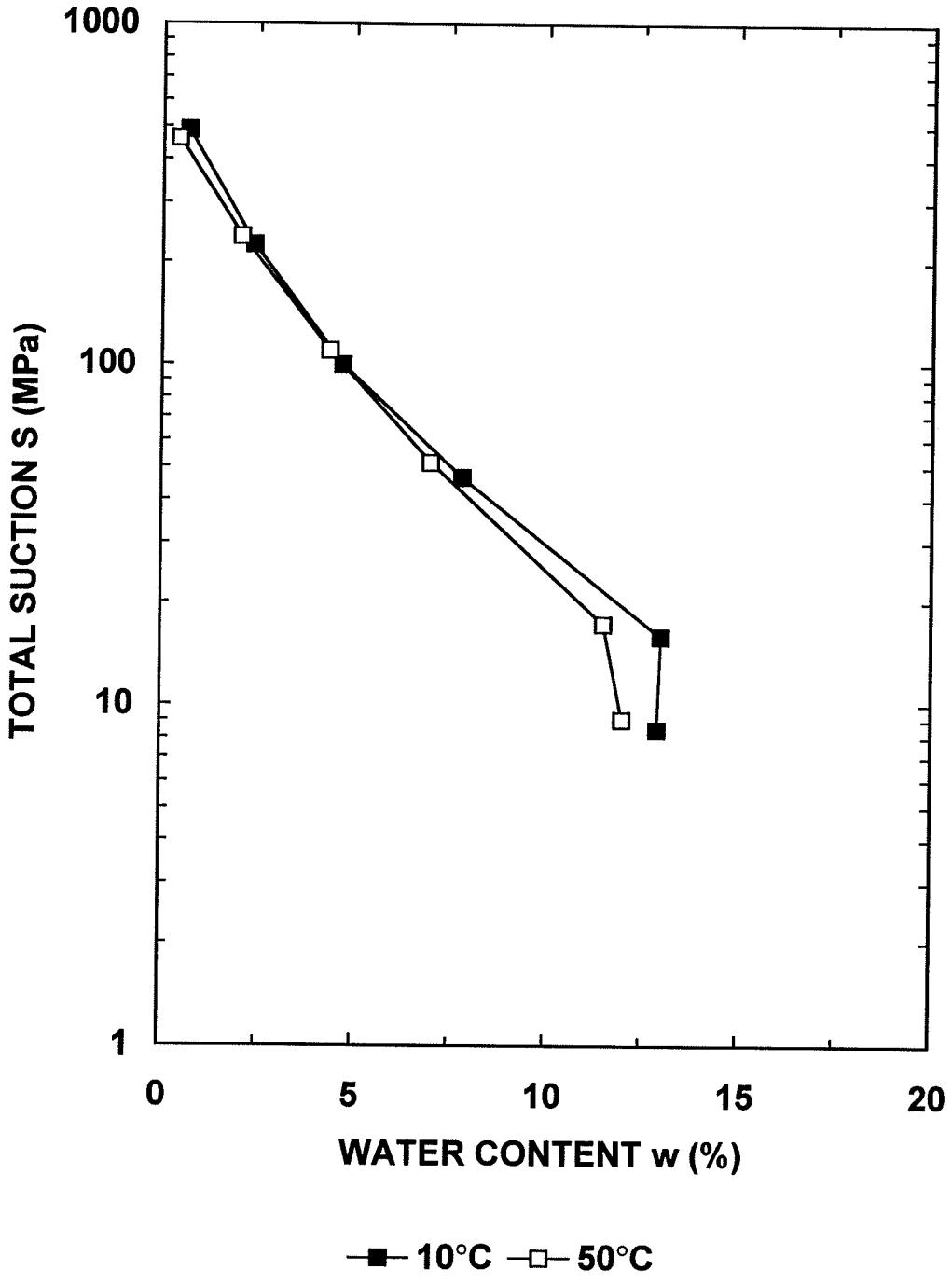

Figure 5.17 Influence of temperature on total suction in sand-bentonite material.

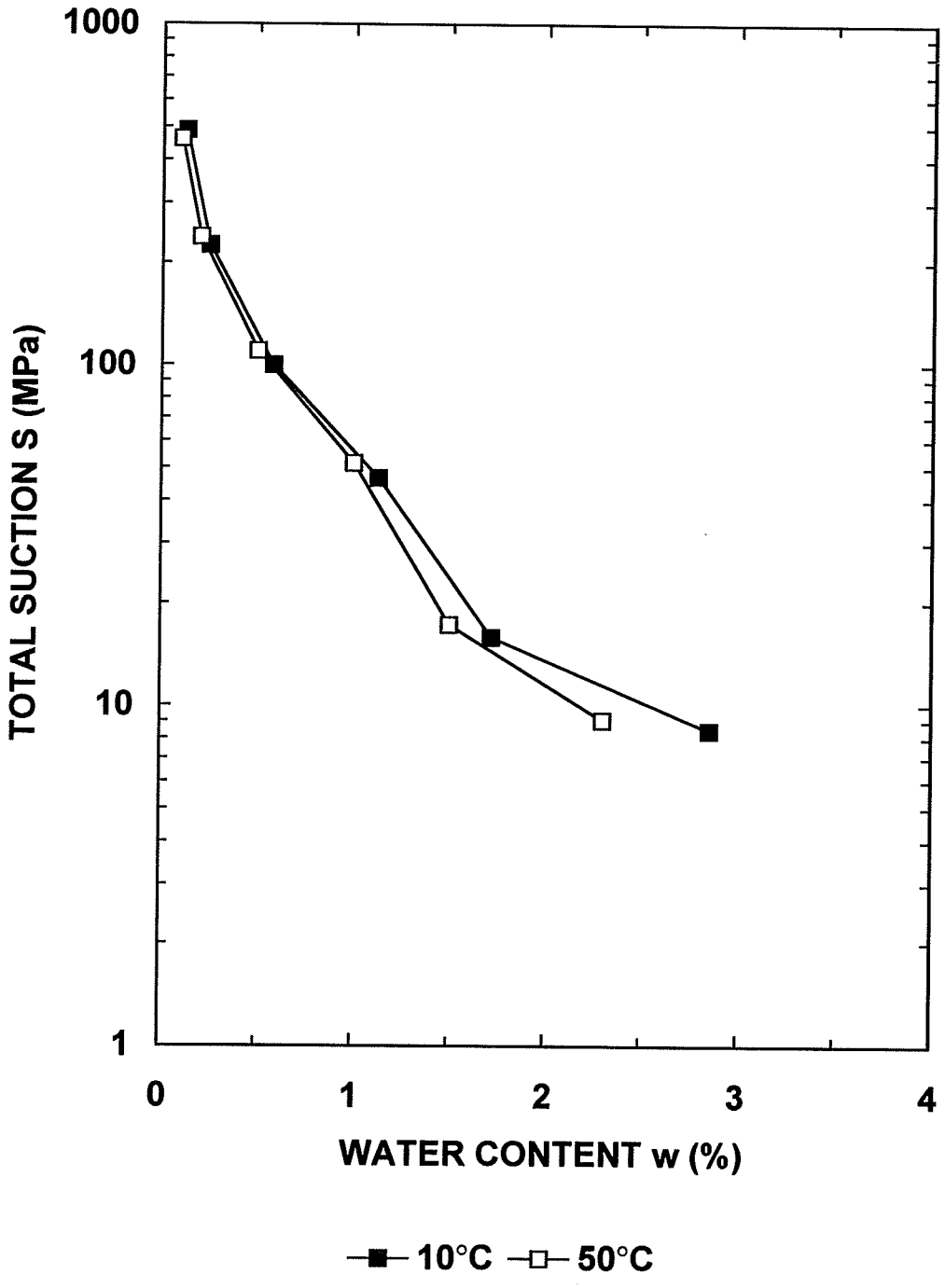

Figure 5.18 Influence of temperature on total suction in sand-illite material.

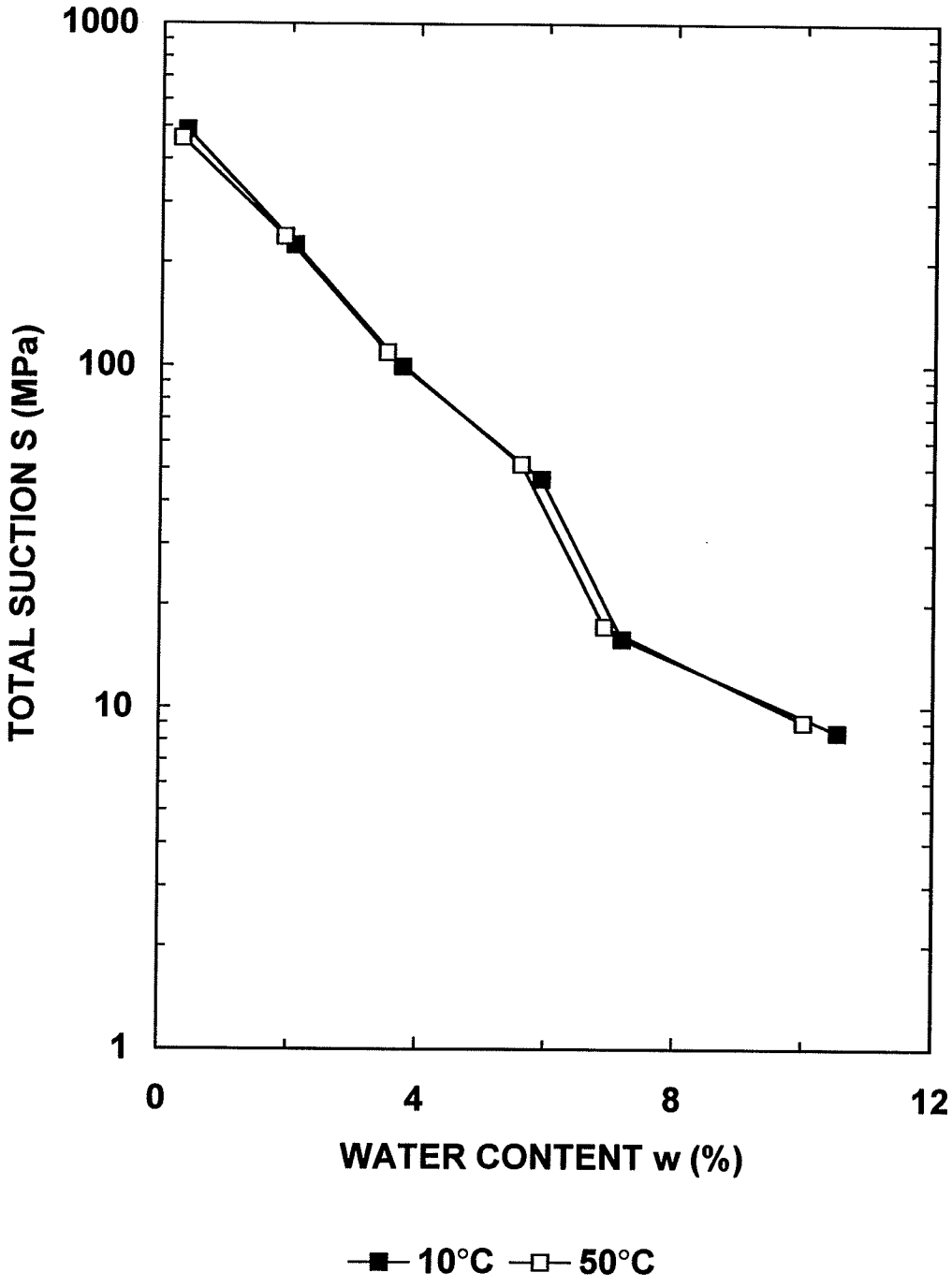

Figure 5.19 Influence of temperature on total suction in Boom Clay.

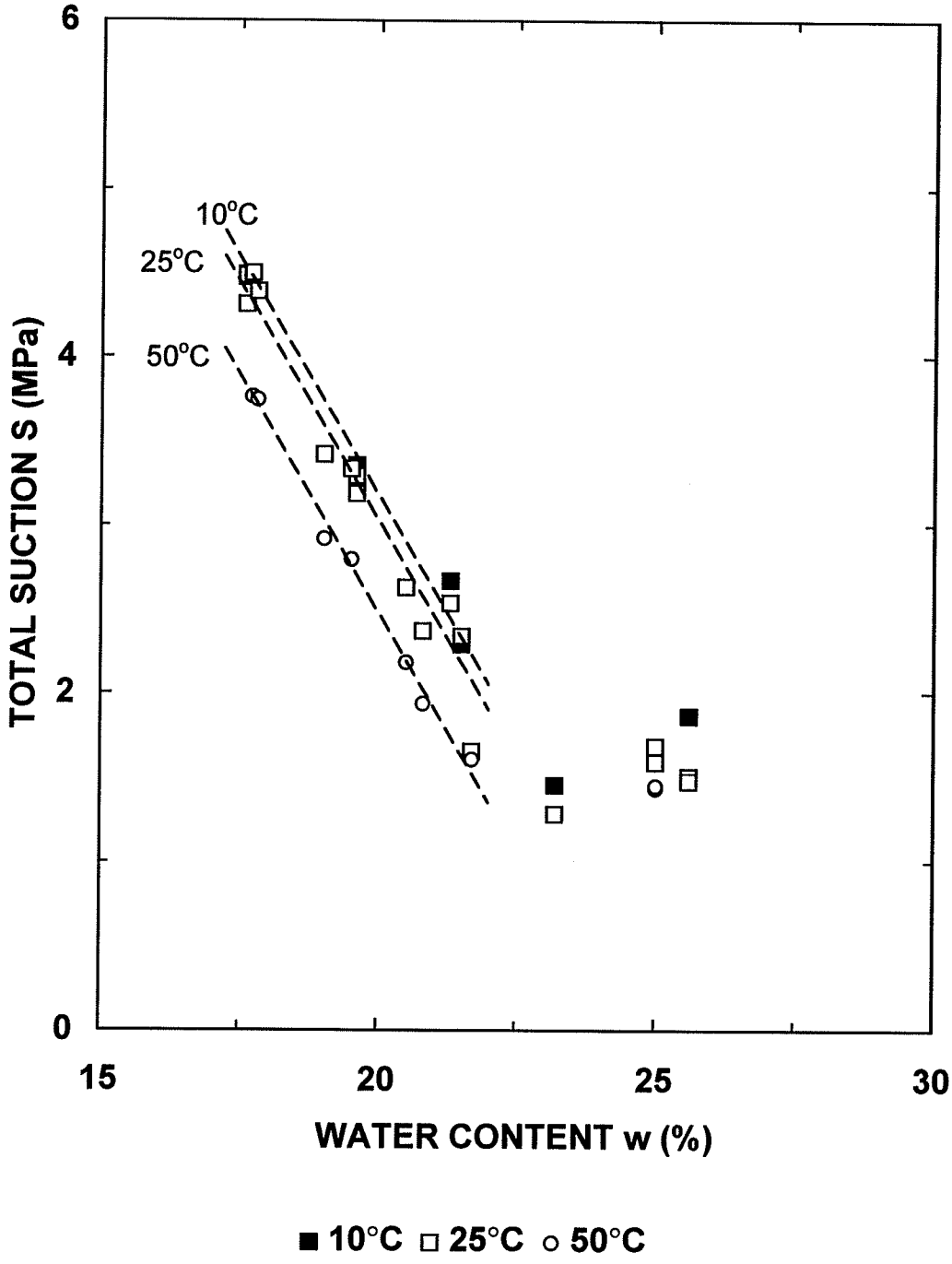

Figure 5.20 Influence of temperature on total suction in sand-bentonite material.

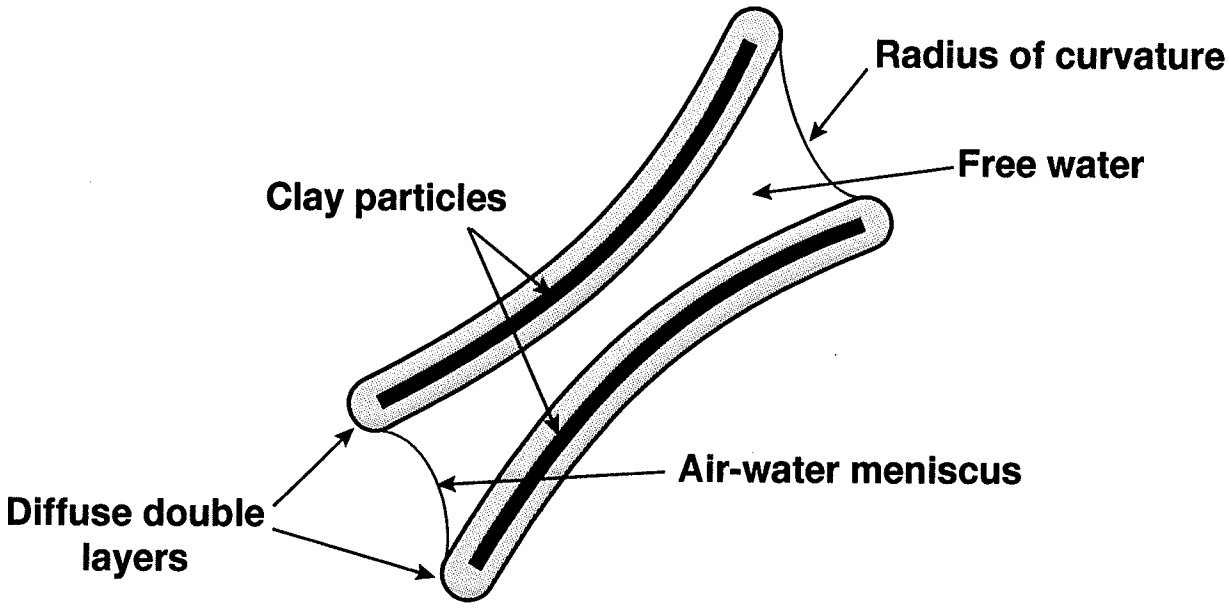

Figure 5.21 Interaction between clay particles, diffuse double layers, and free water.

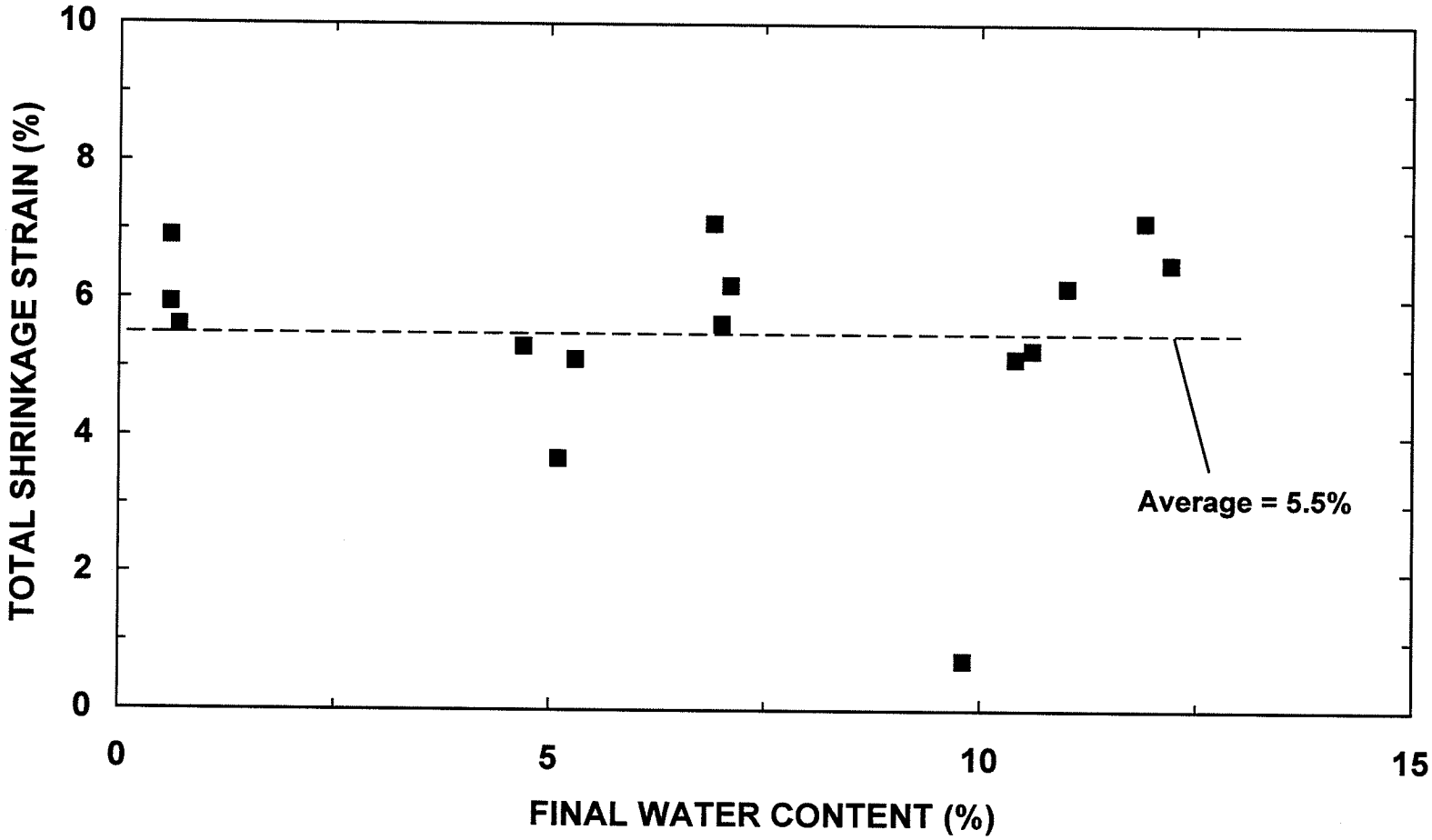

Figure 5.22 Shrinkage behaviour of sand-bentonite material prepared at initial water contents of 16.8% to 18.5%.

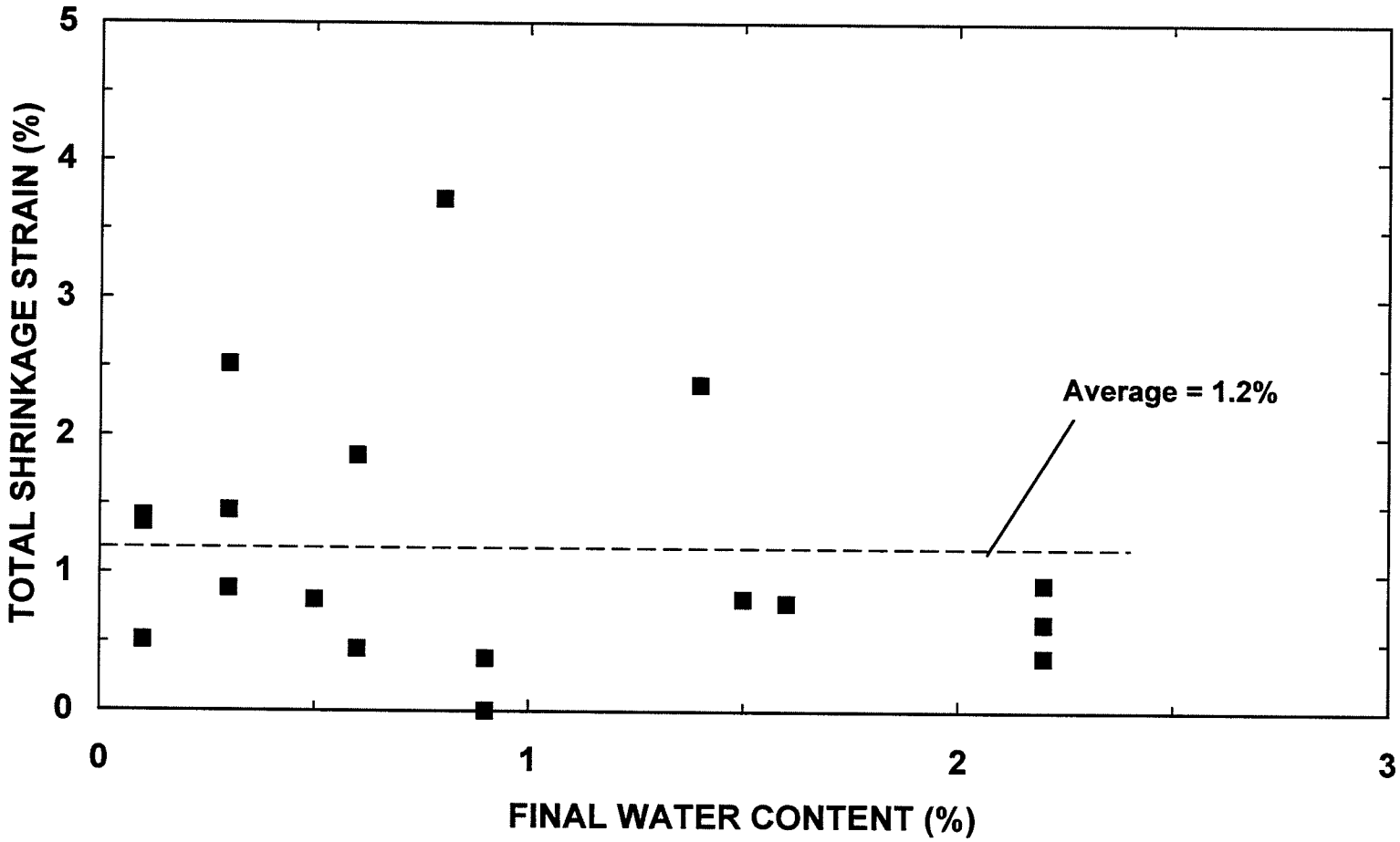

Figure 5.23 Shrinkage behaviour of sand-illite material prepared at initial water contents of 8.5% to 10.0%.

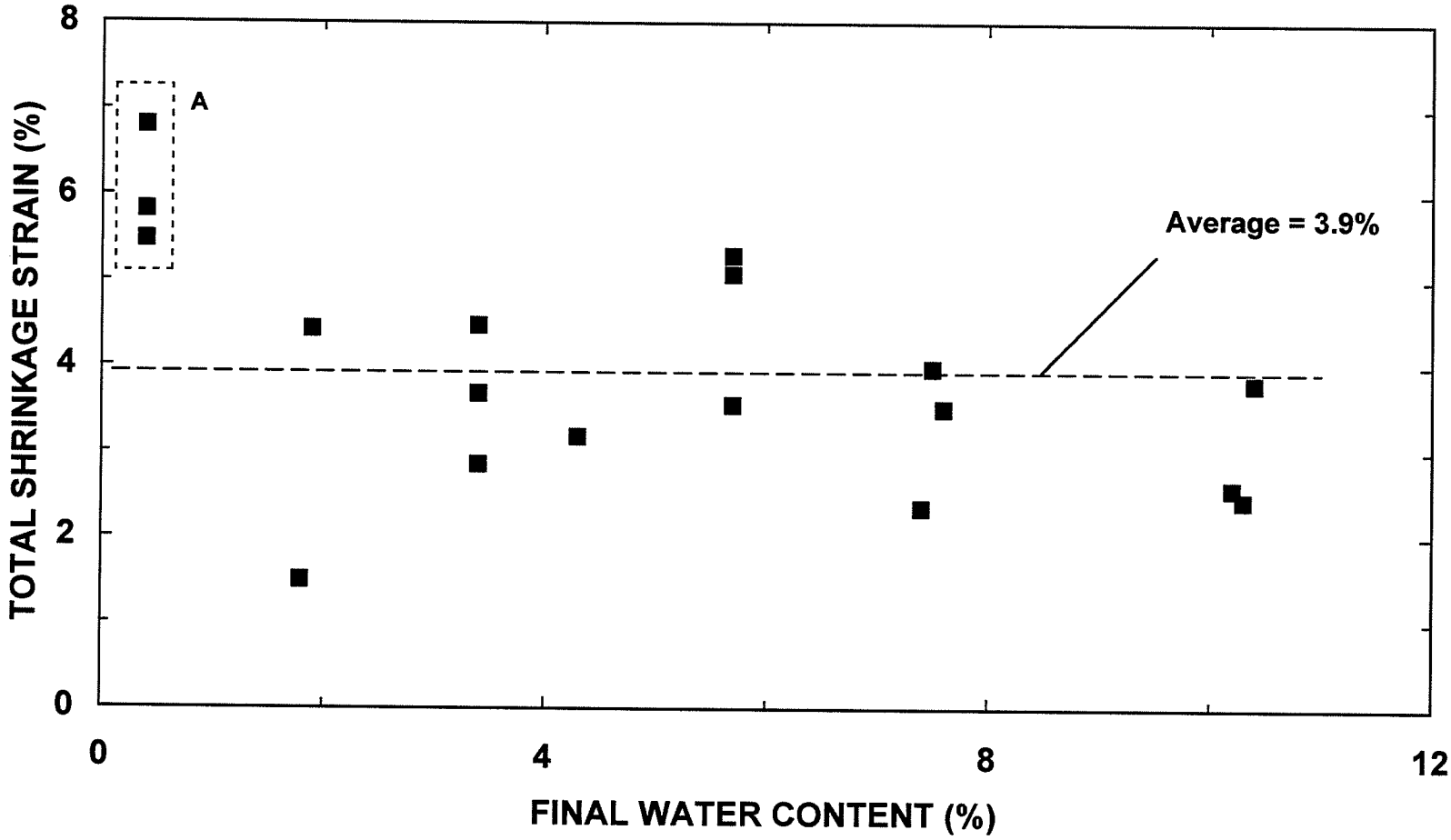

Figure 5.24 Shrinkage behaviour of Boom Clay prepared at initial water contents of 14.8% to 17.7%.

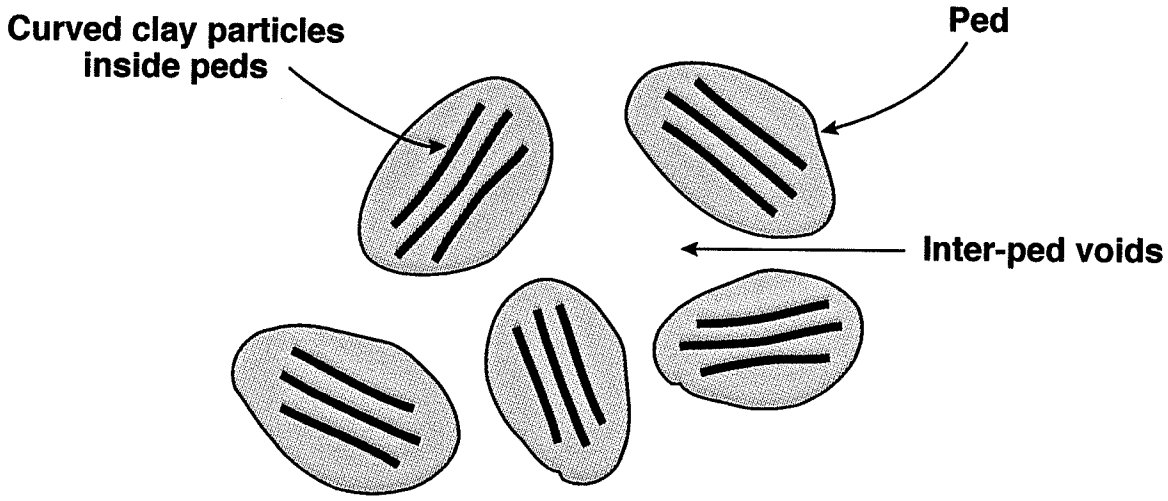

(a) Loosely-compacted specimen

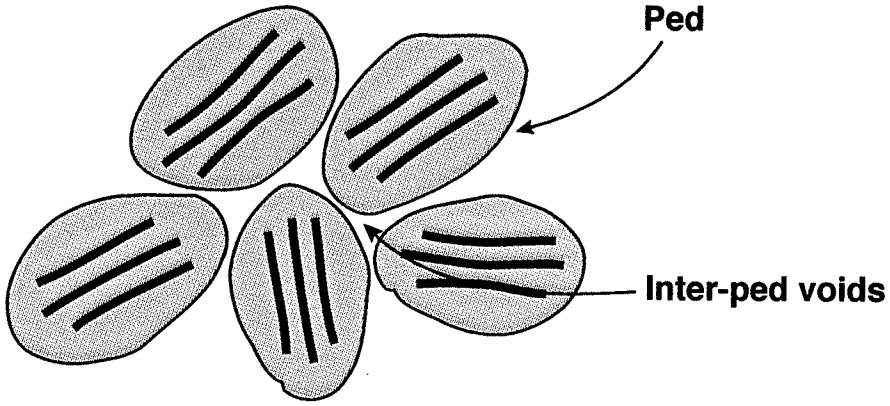

(b) Densely-compacted specimen

Figure 5.25 Soil structures of loosely-compacted and densely-compacted specimens.

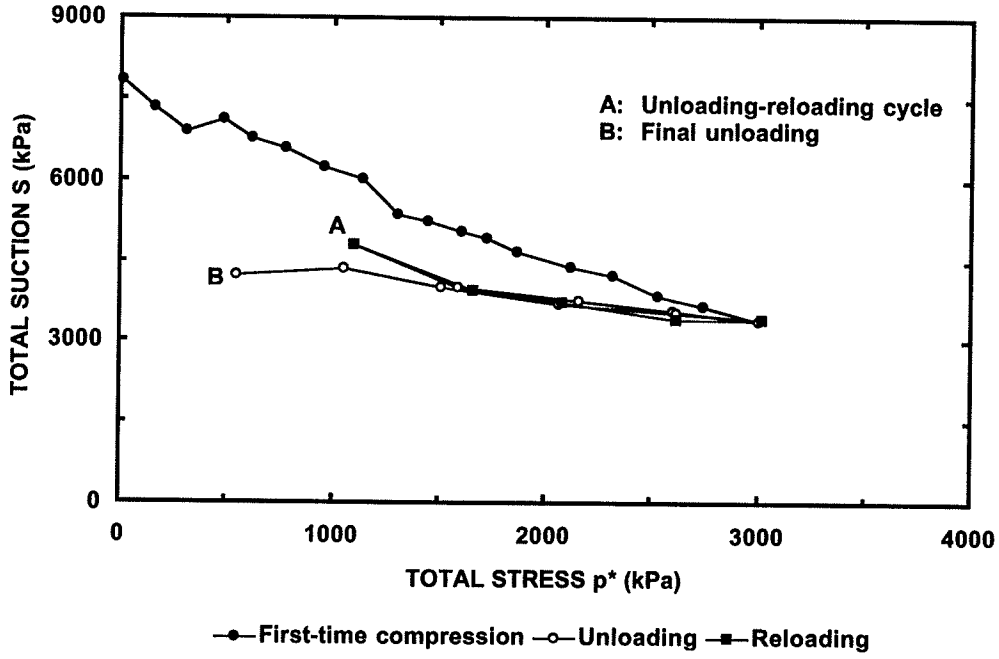

Figure 6.1 Total suction-total stress relationship: Specimen SB1780TX.

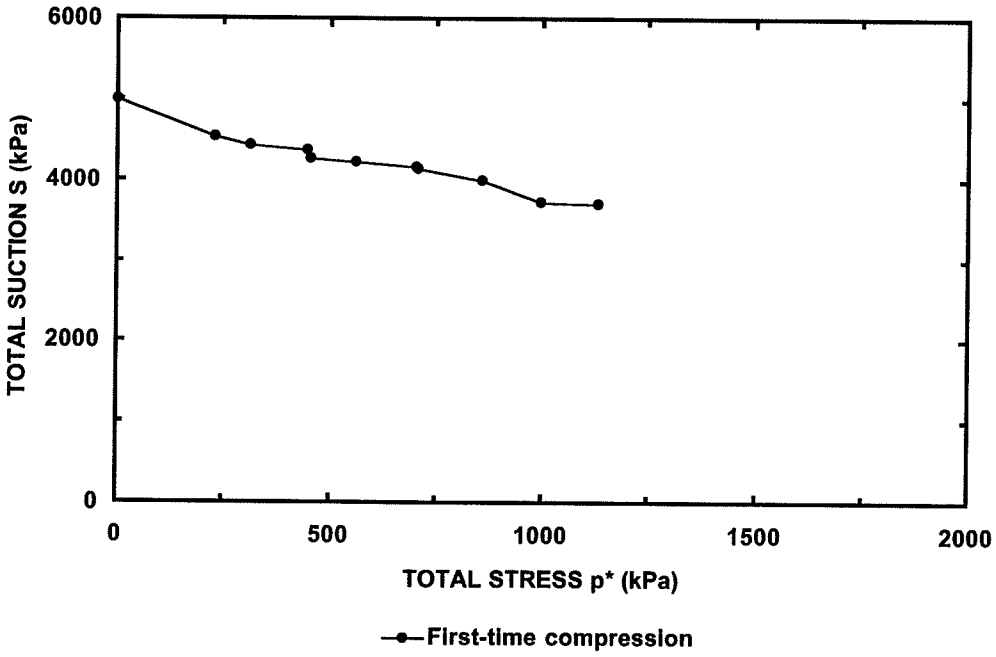

Figure 6.2 Total suction-total stress relationship: Specimen SB1880TX.

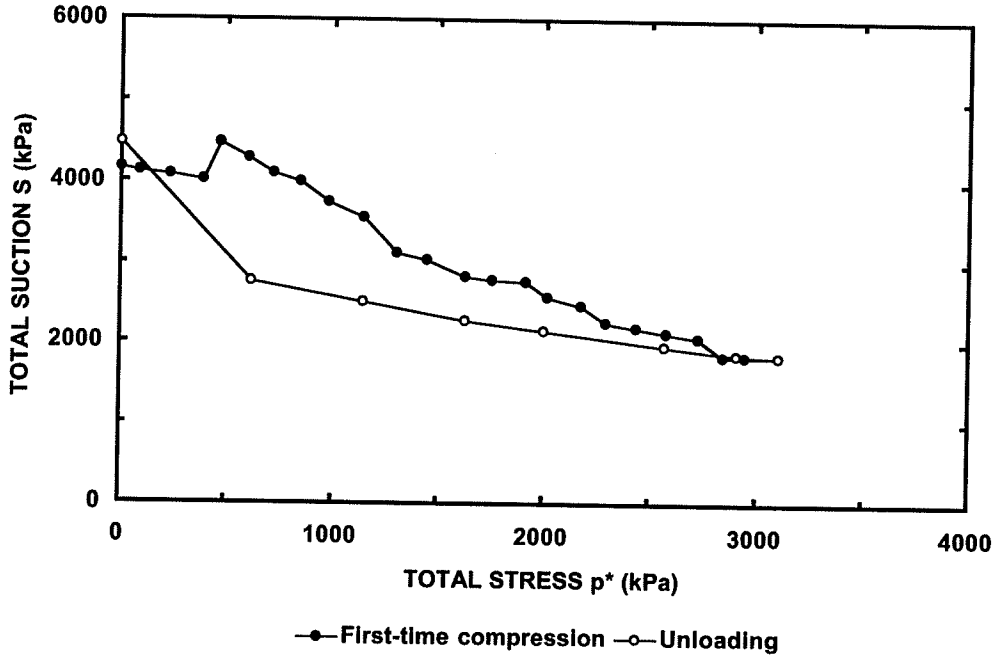

Figure 6.3 Total suction-total stress relationship: Specimen SB1980TX.

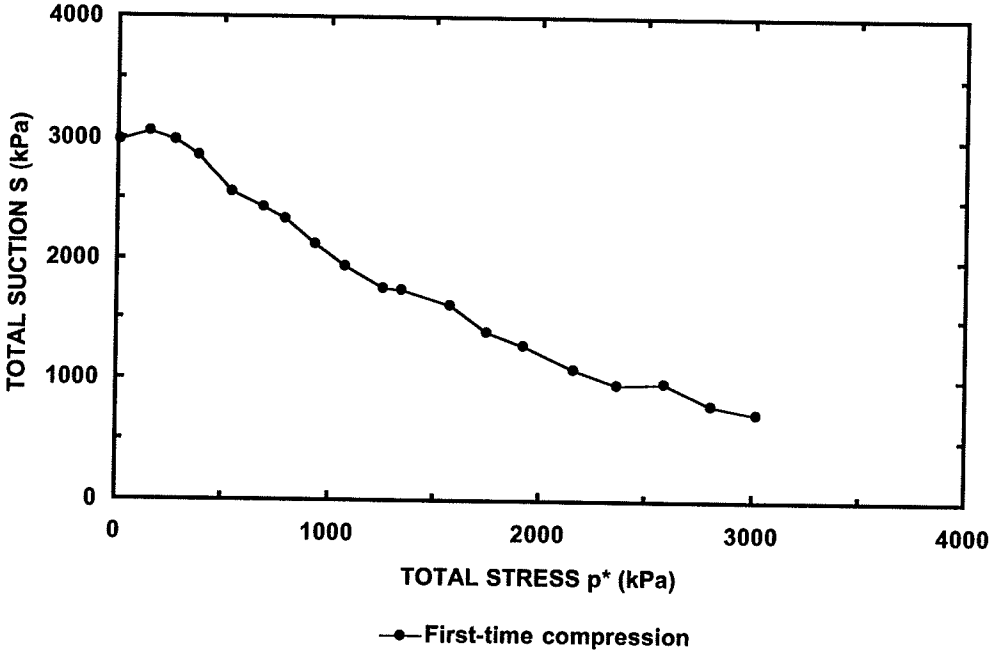

Figure 6.4 Total suction-total stress relationship: Specimen SB2080TX.

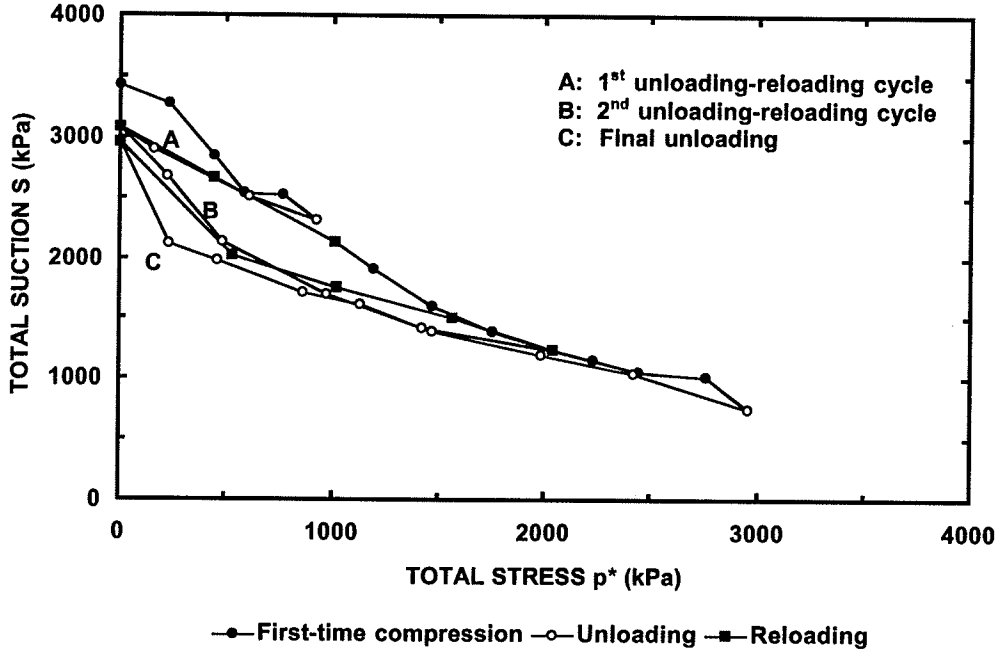

Figure 6.5 Total suction-total stress relationship: Specimen SB2180TX.

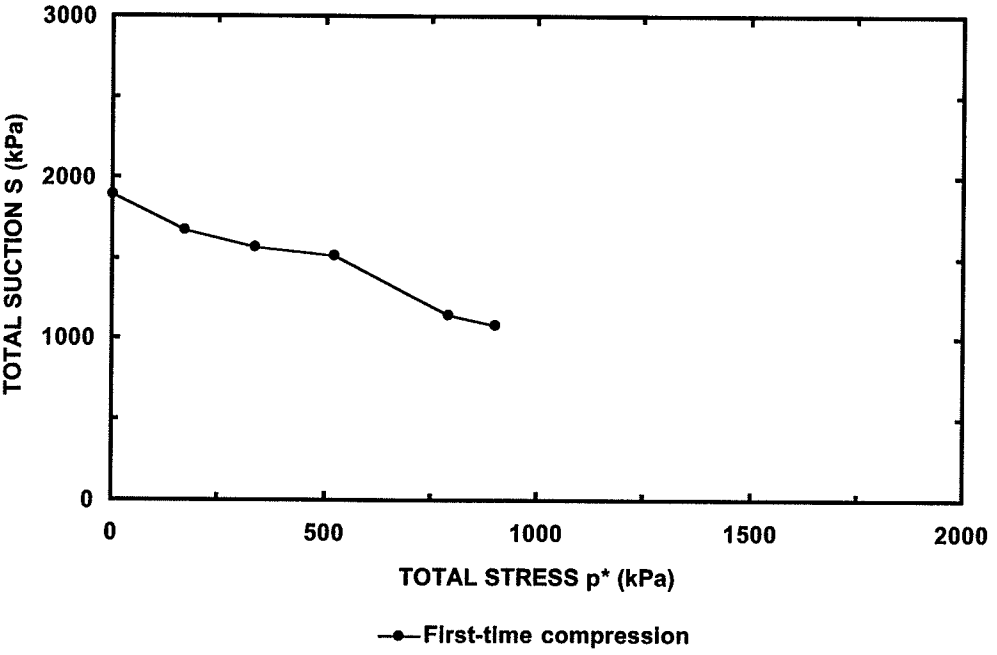

Figure 6.6 Total suction-total stress relationship: Specimen SB2280TX.

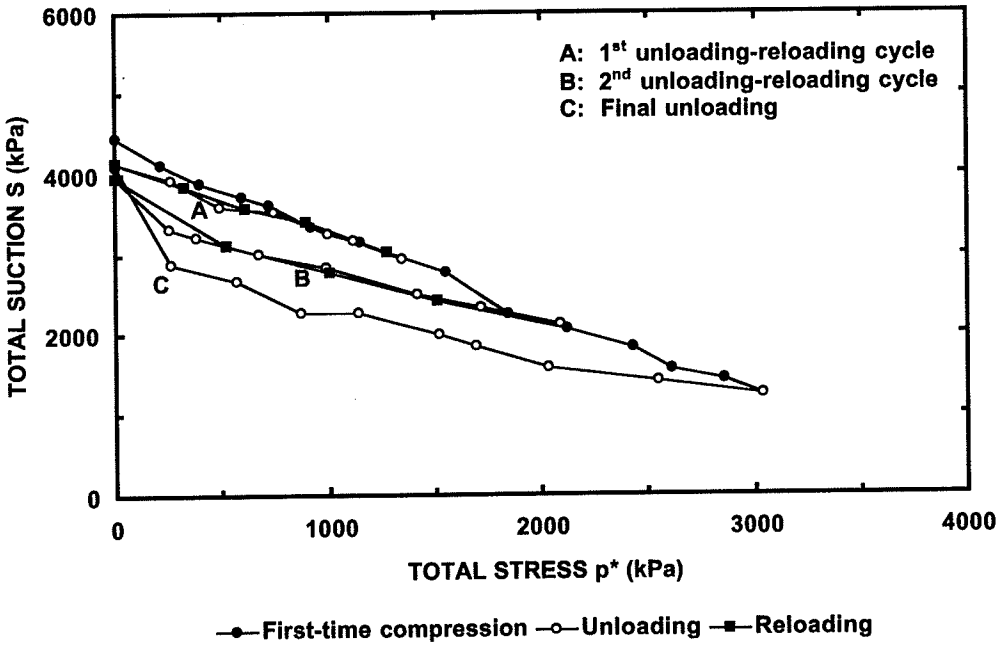

Figure 6.7 Total suction-total stress relationship: Specimen SB1895TX.

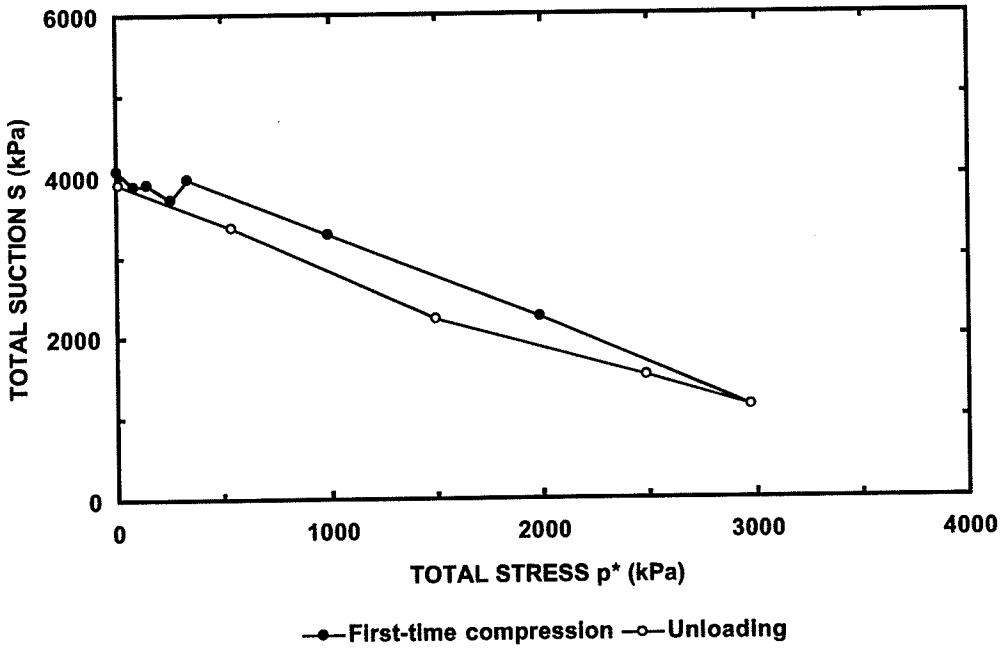

Figure 6.8 Total suction-total stress relationship: Specimen SB1995TX.

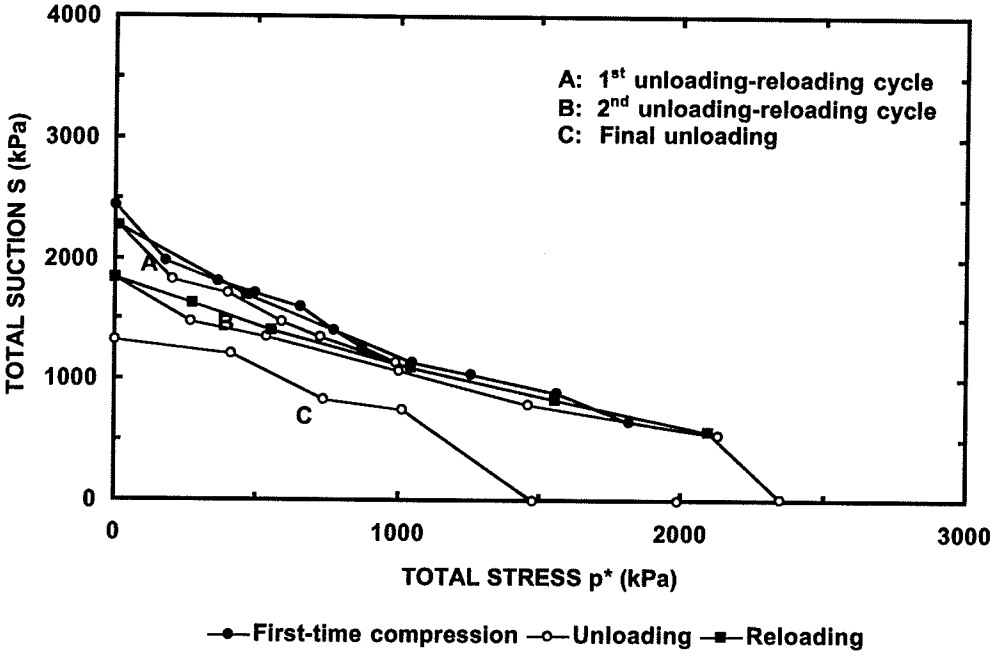

Figure 6.9 Total suction-total stress relationship: Specimen SB2295TX.

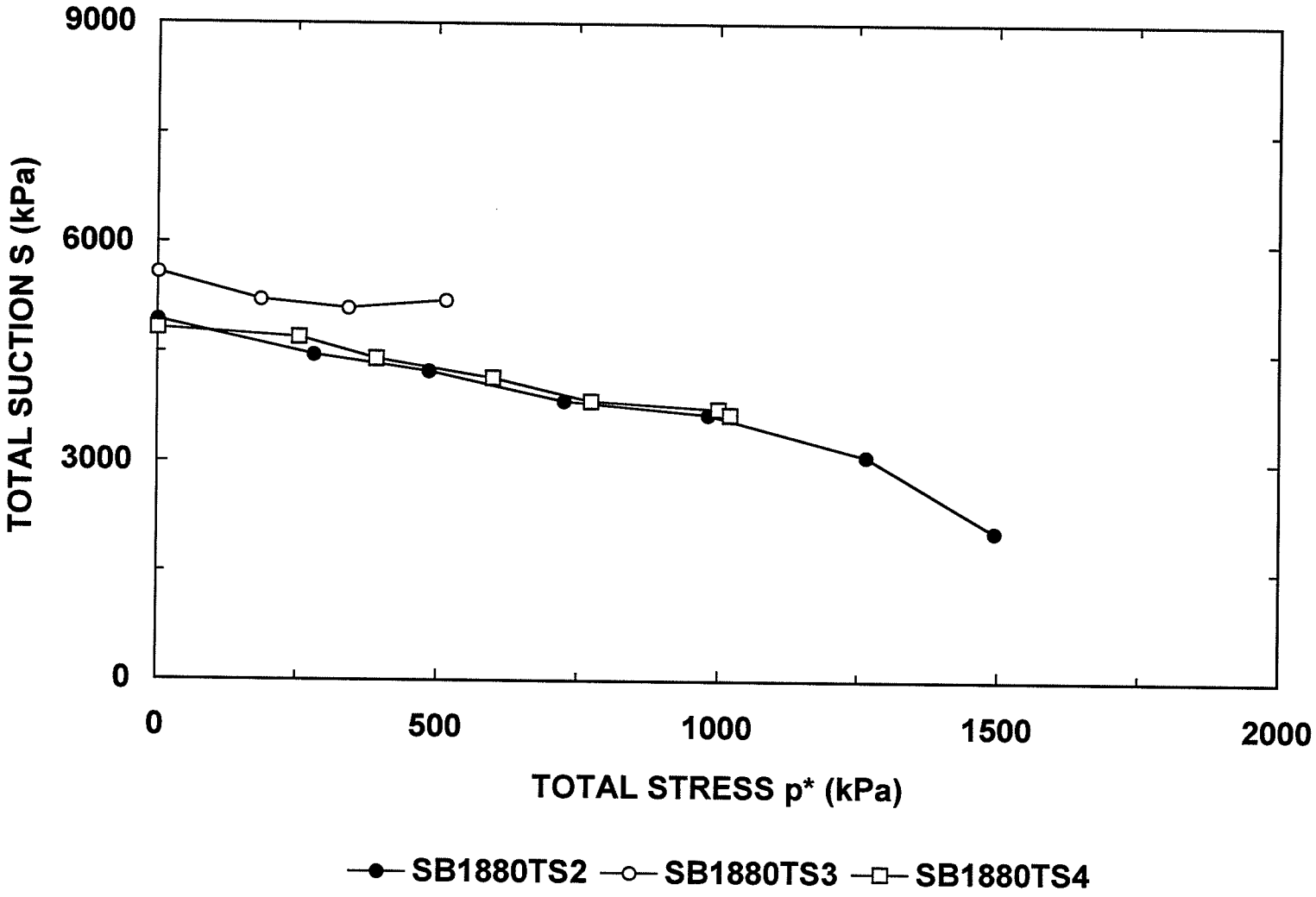

Figure 6.10 Total suction-total stress relationships: SB1880TS2, SB1880TS3, and SB1880TS4.

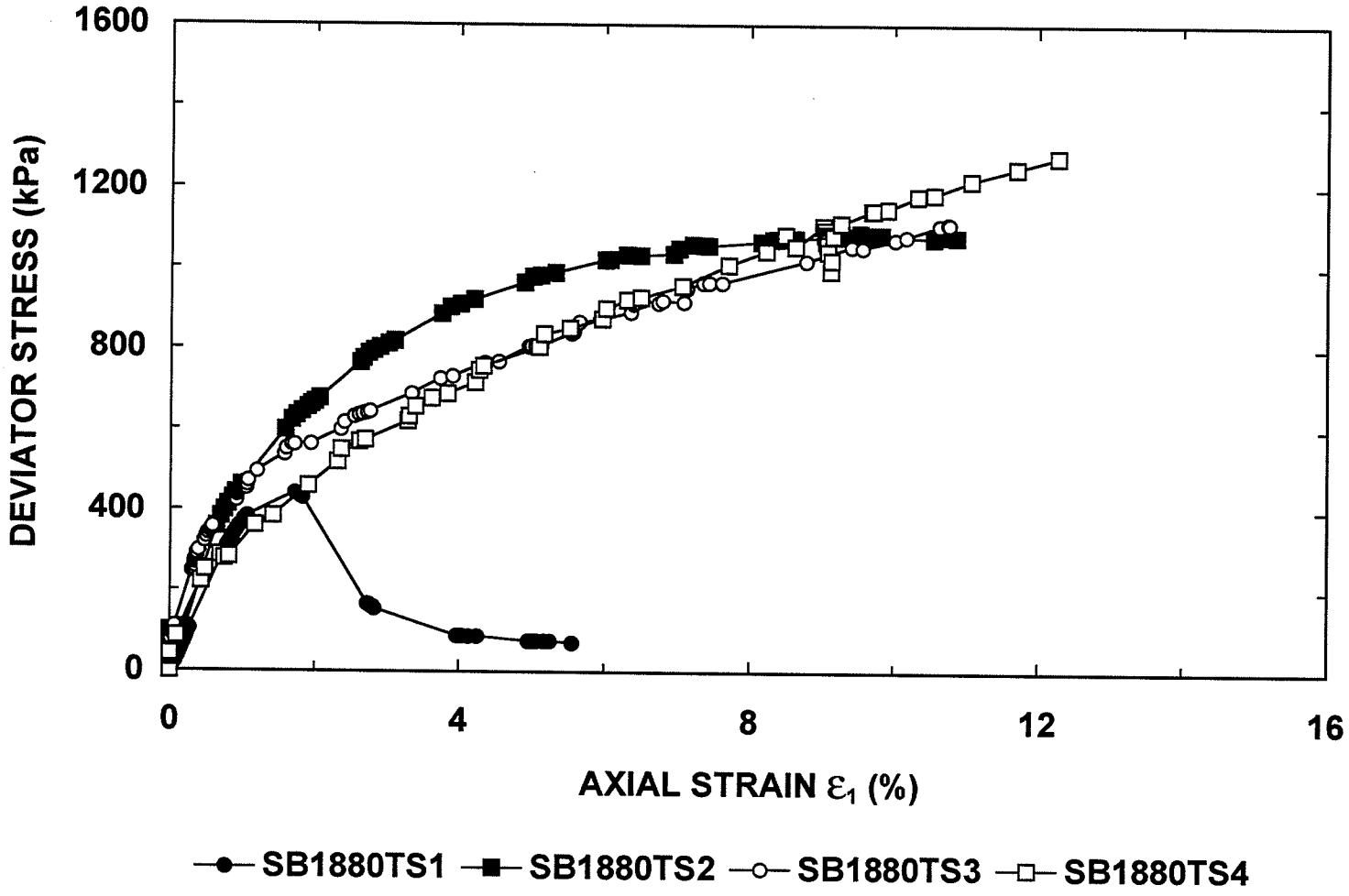

Figure 6.11 Stress-strain behaviour of unsaturated sand-bentonite material.

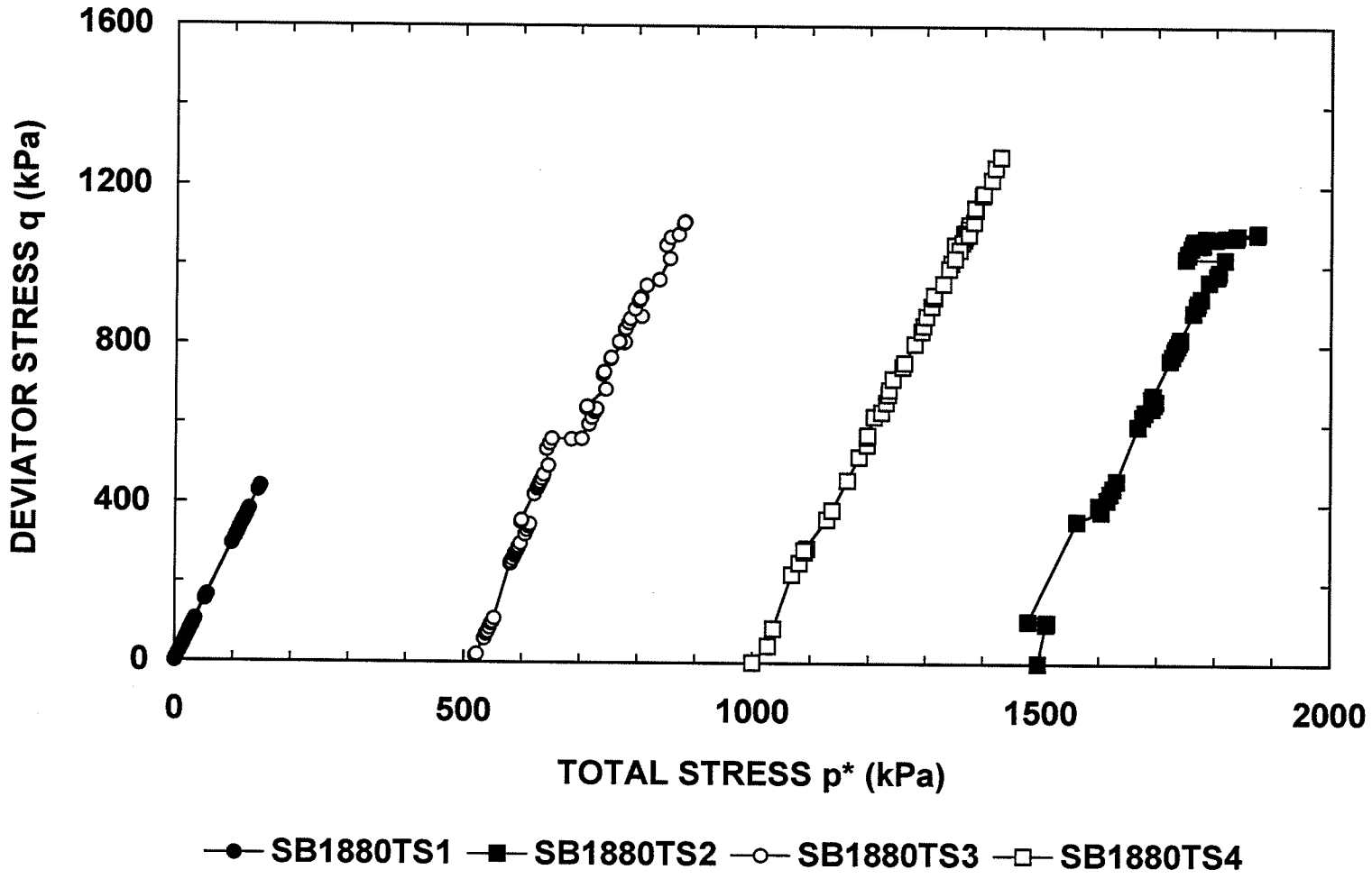

Figure 6.12 Total stress paths of sand-bentonite specimens tested in shear compression tests.

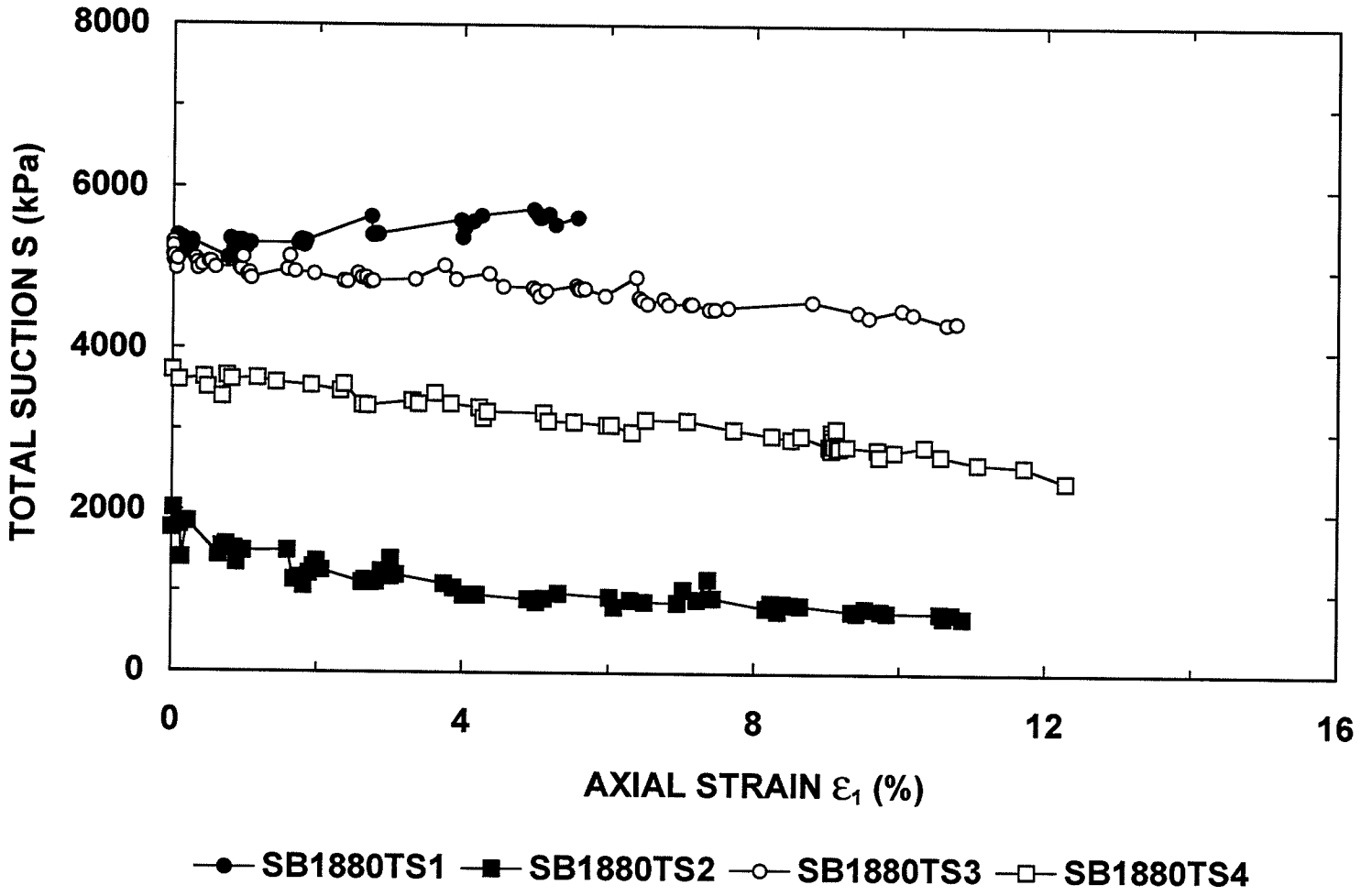

Figure 6.13 Total suction-axial strain relationships of unsaturated sand-bentonite material.

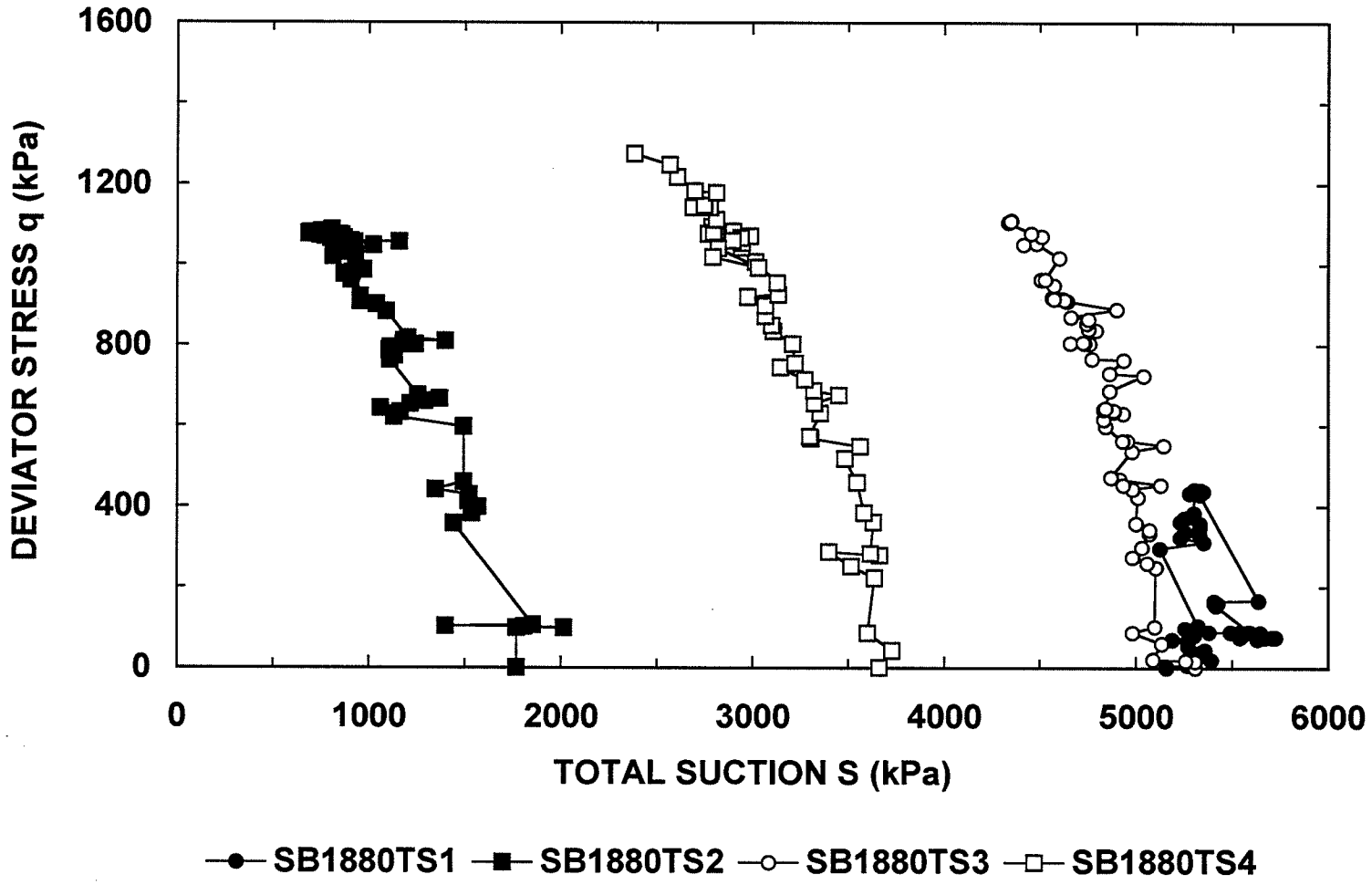

Figure 6.14 Deviator stress-total suction relationships of unsaturated sand-bentonite material.

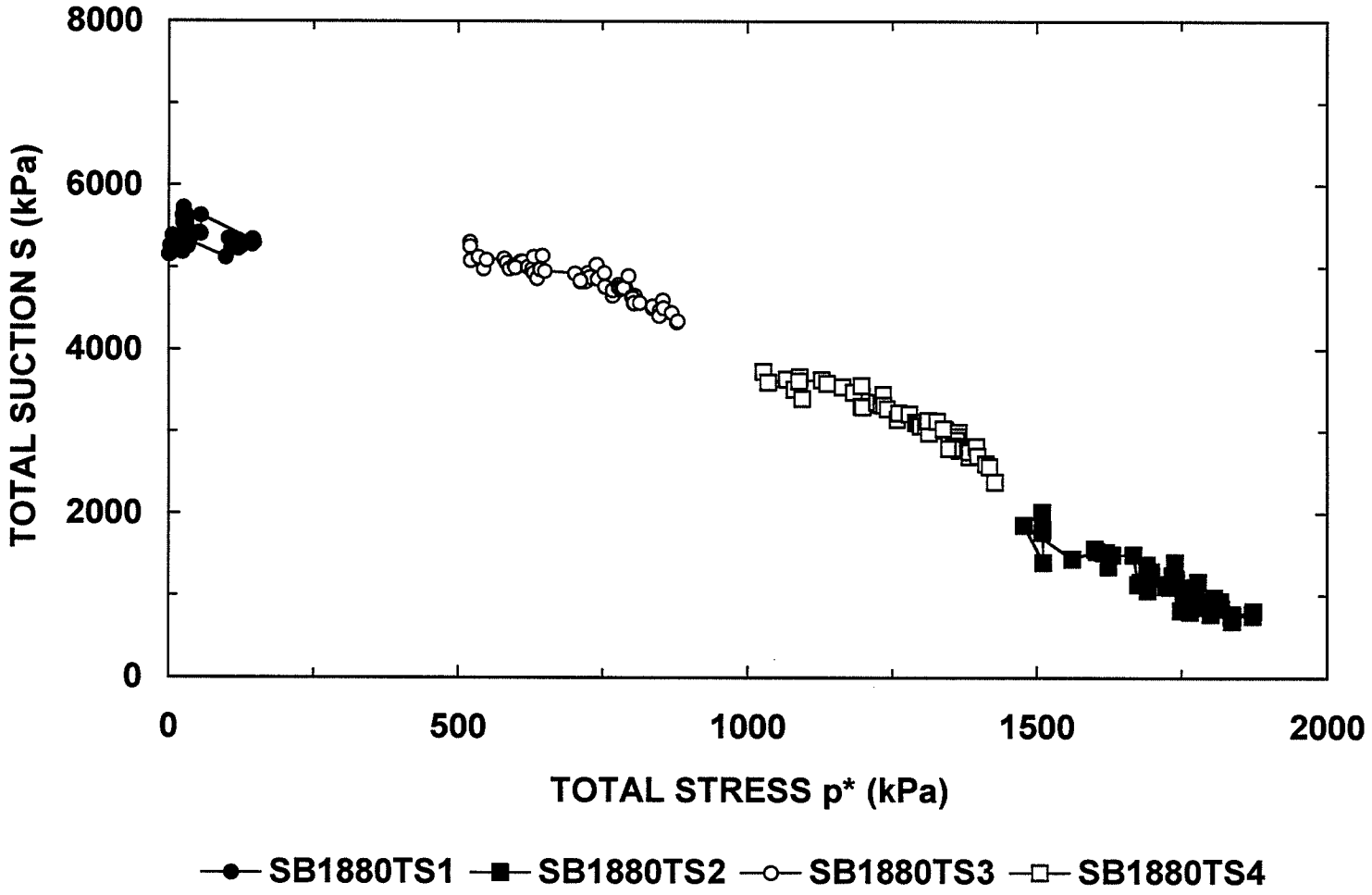

Figure 6.15 Total suction-total stress relatioships of unsaturated sand-bentonite material.

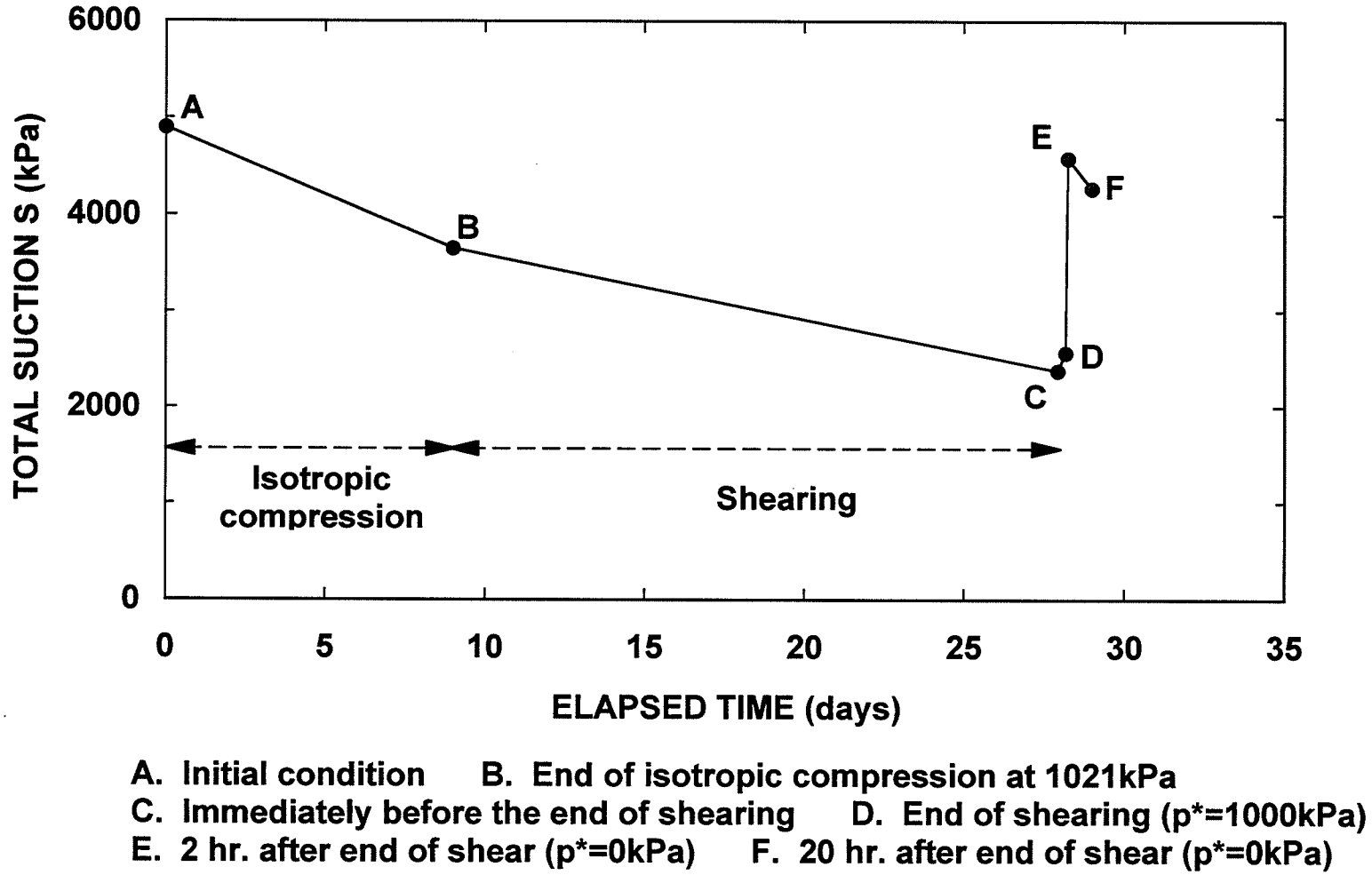

Figure 6.16 Variation of total suction with time in Specimen SB1880TS4.

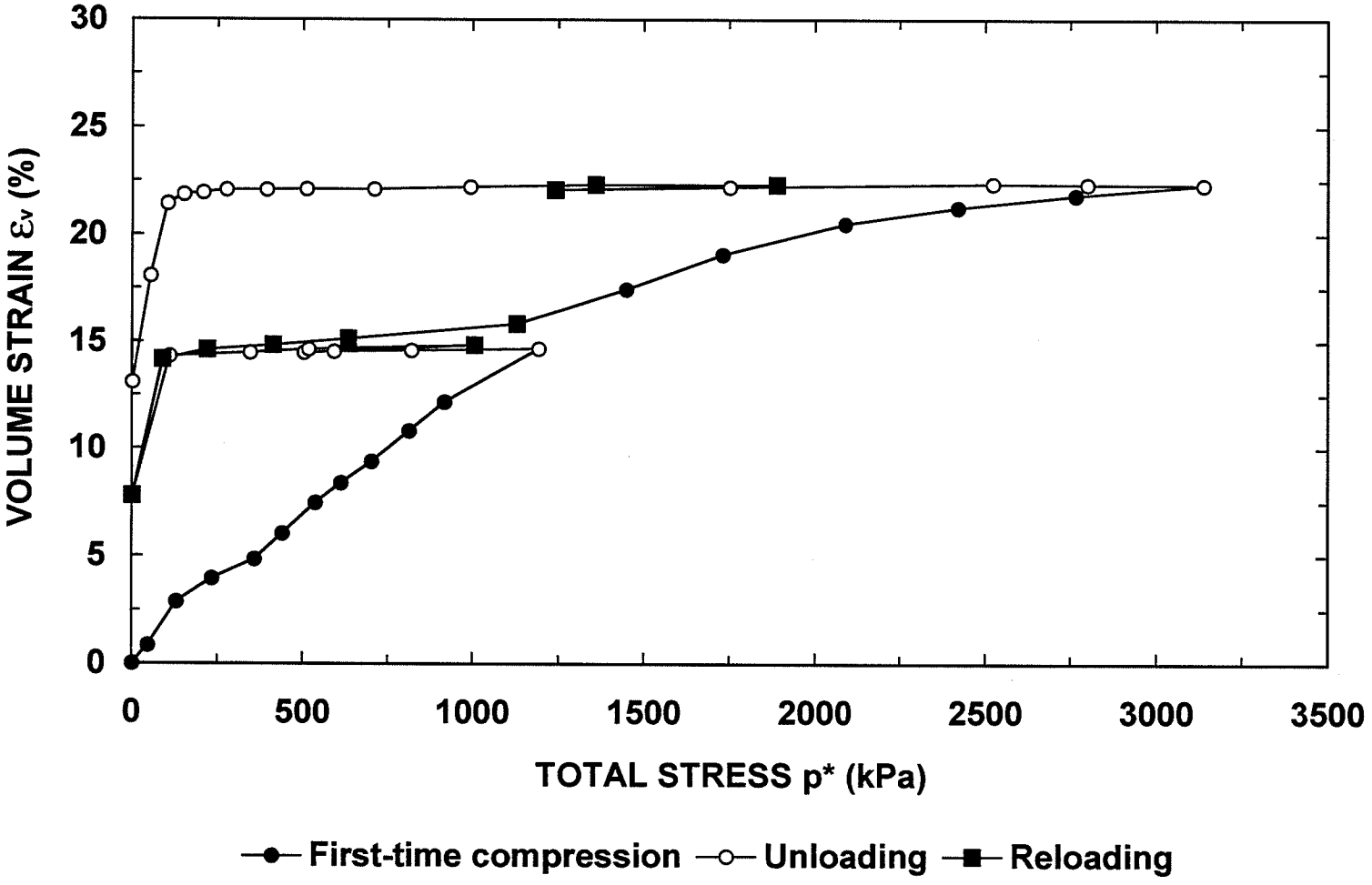

Figure 6.17 Volume strain-total stress relationship of Specimen SB2180V1.

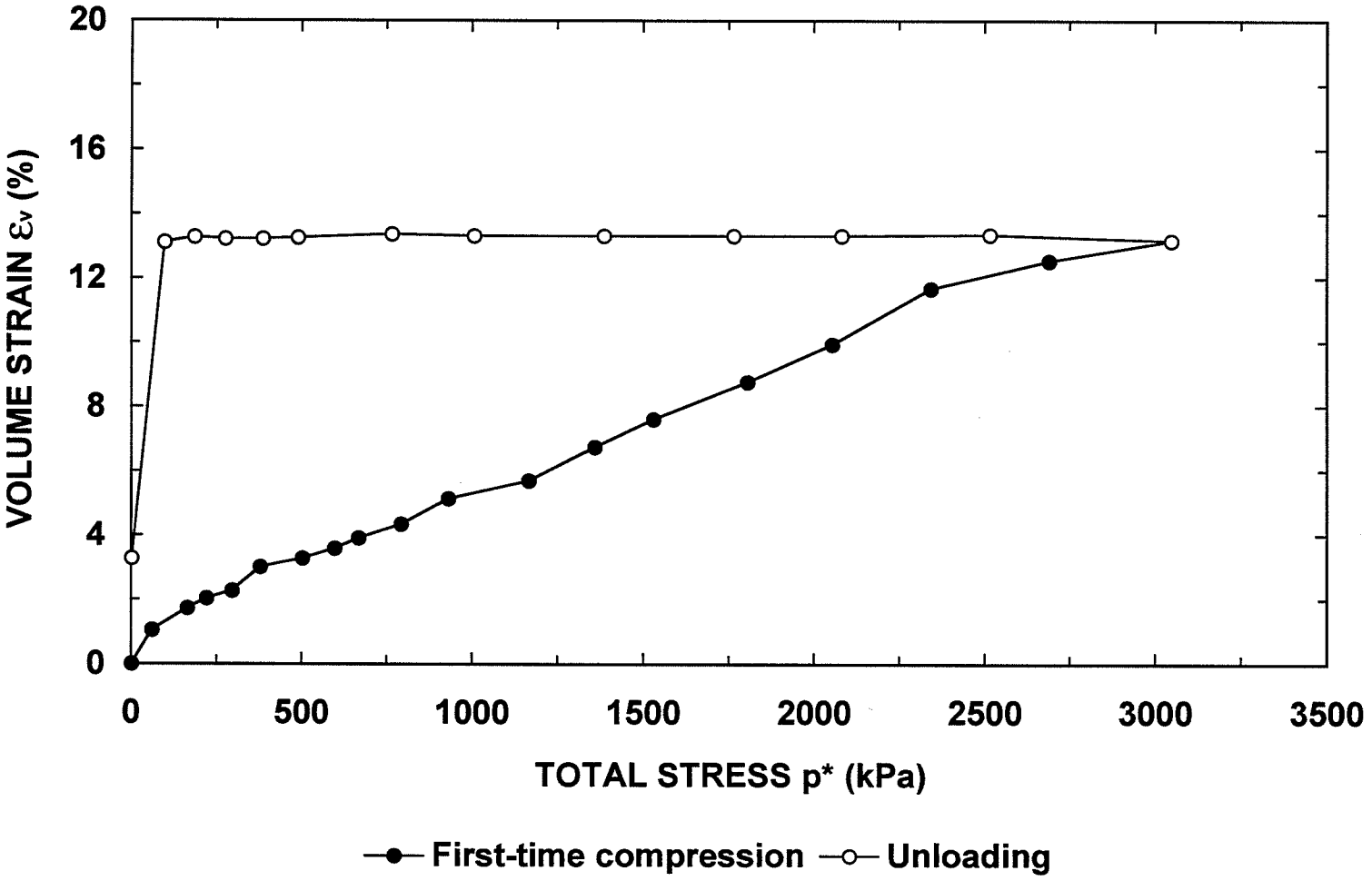

Figure 6.18 Volume strain-total stress relationship of Specimen SB1995V2.

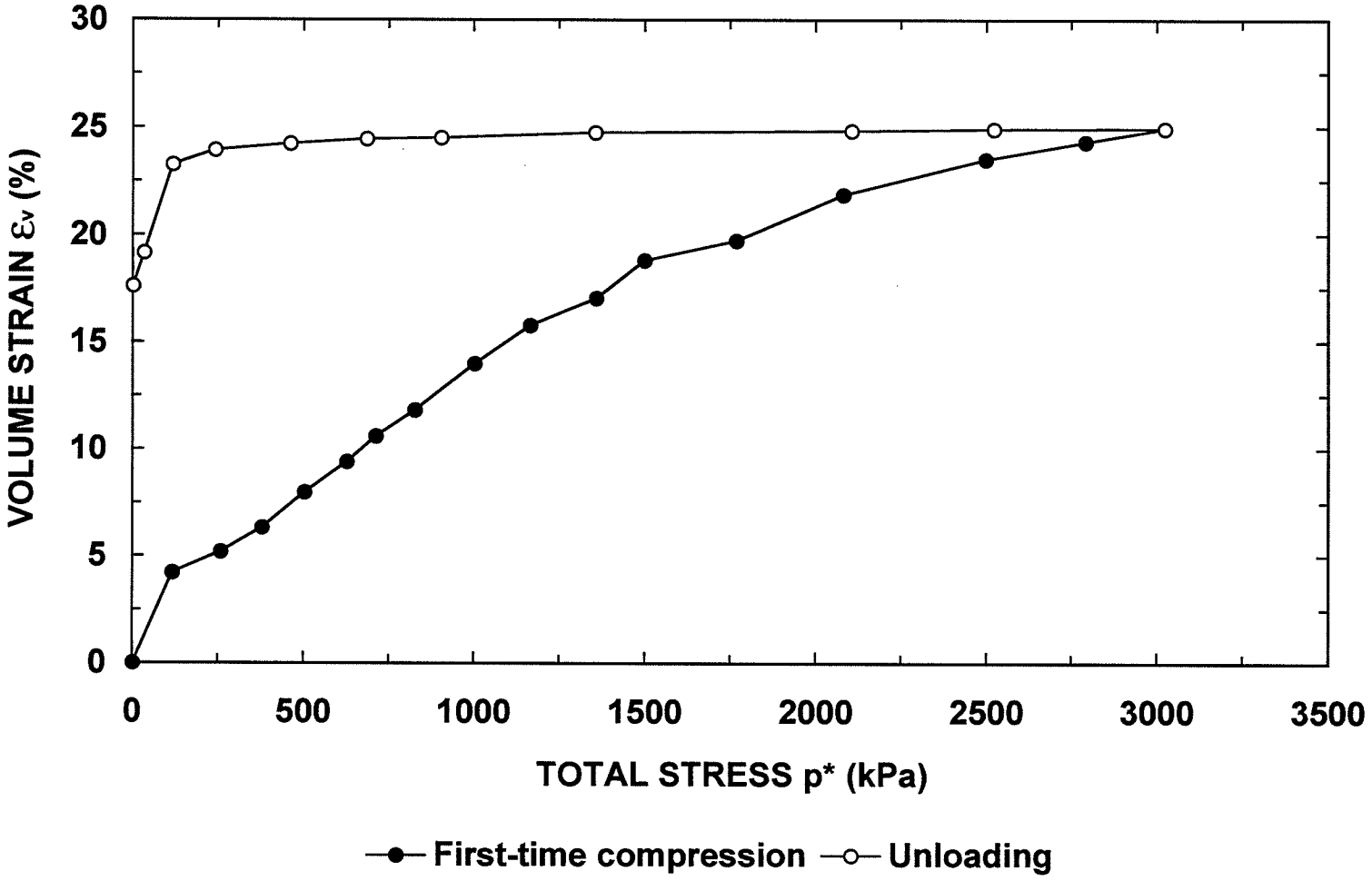

Figure 6.19 Volume strain-total stress relationship of Specimen SB1680V3.

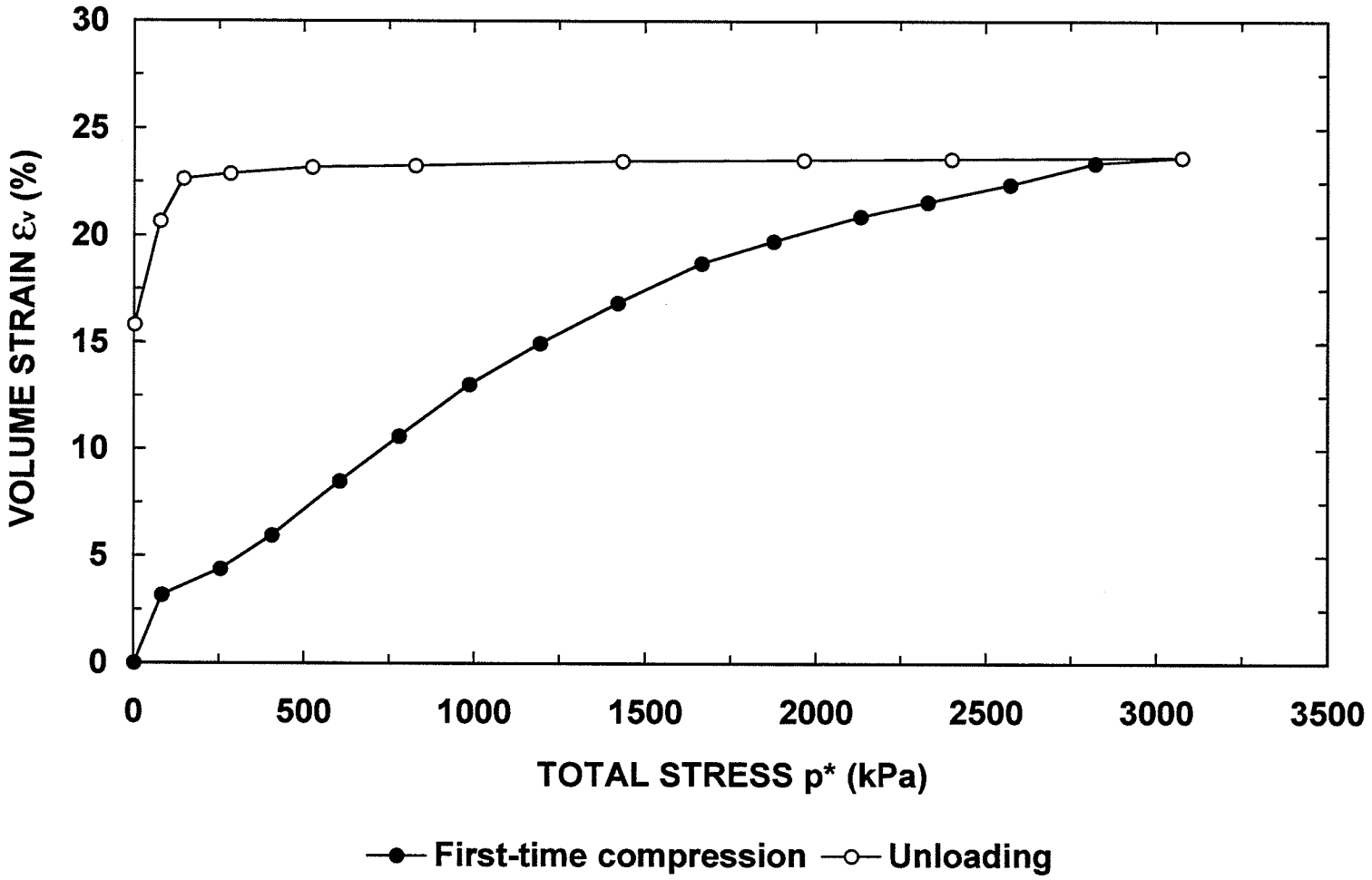

Figure 6.20 Volume strain-total stress relationship of Specimen SB1880V4.

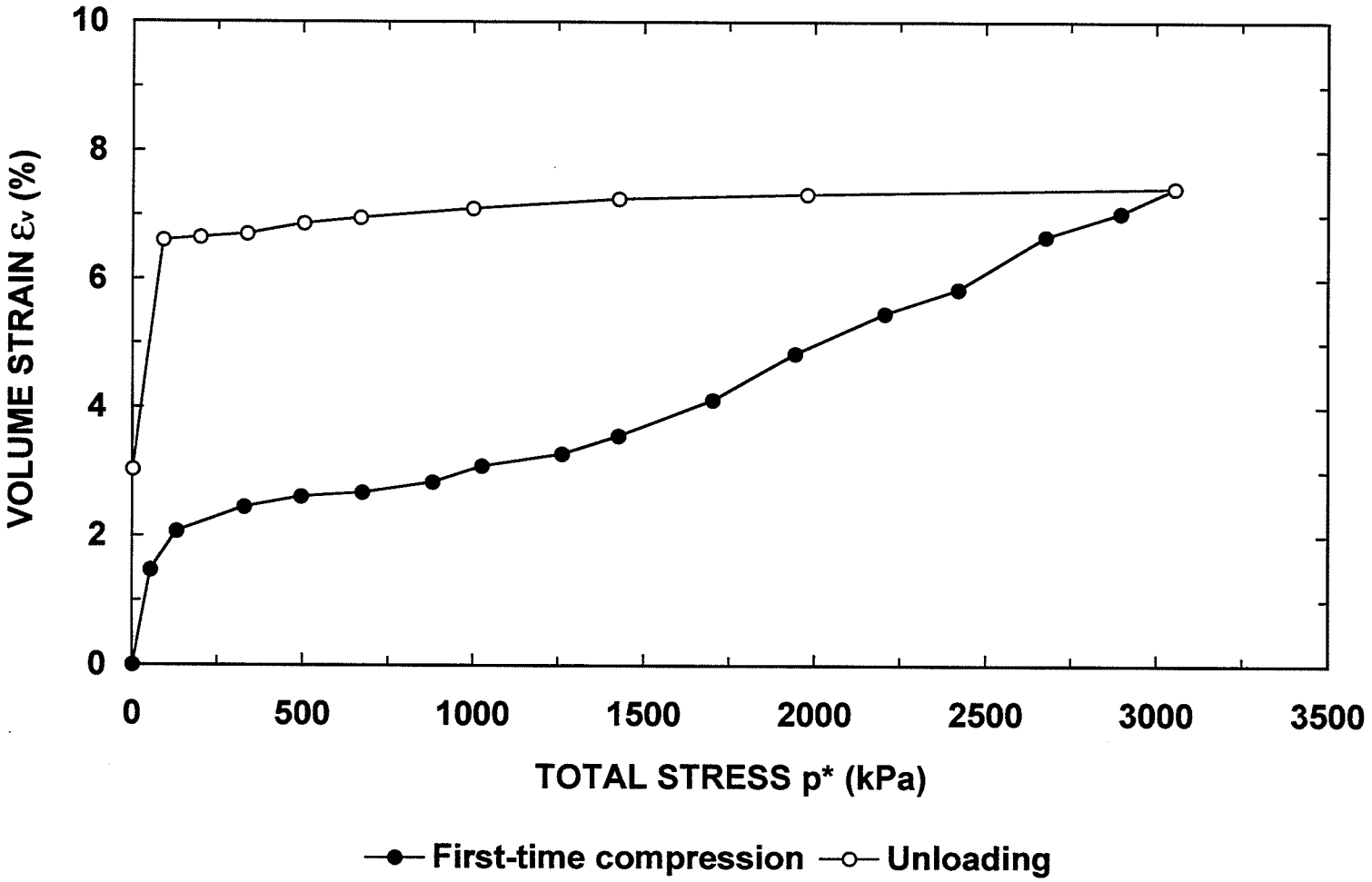

Figure 6.21 Volume strain-total stress relationship of Specimen SB1895V5.

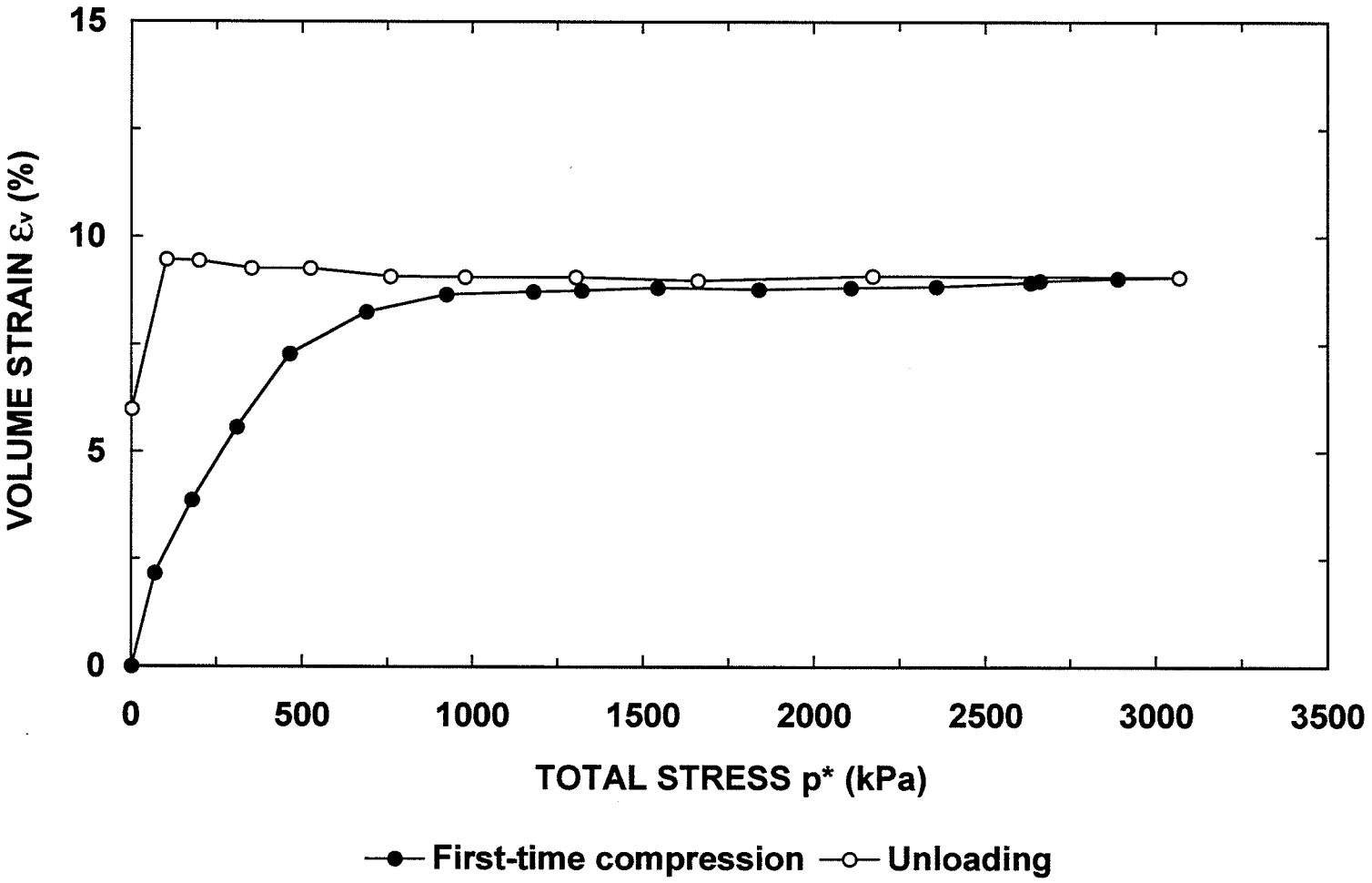

Figure 6.22 Volume strain-total stress relationship of Specimen SB3080V6.

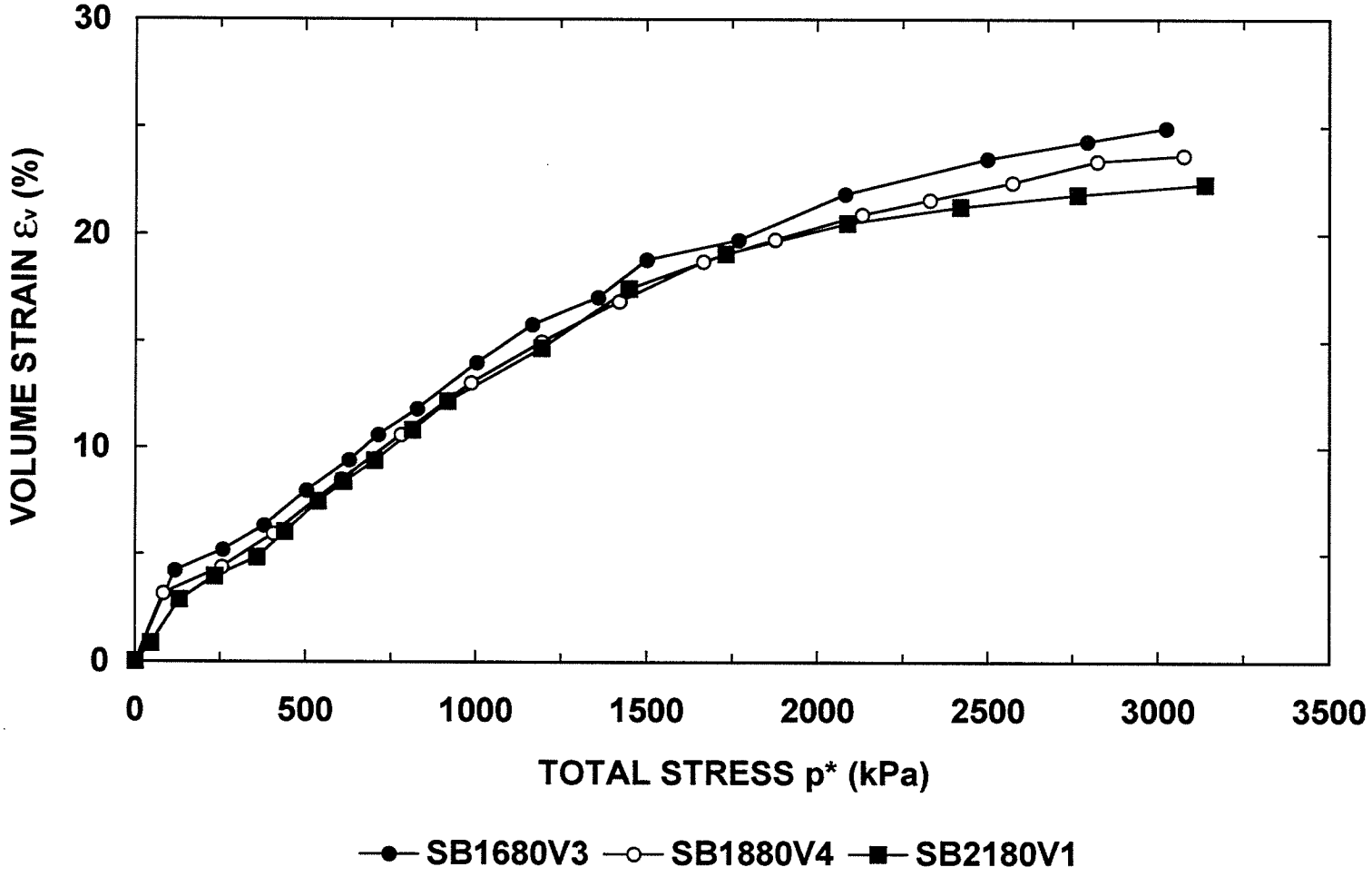

Figure 6.23 Comparison of volume strain-total stress relationships of "low density" sand-bentonite specimens.

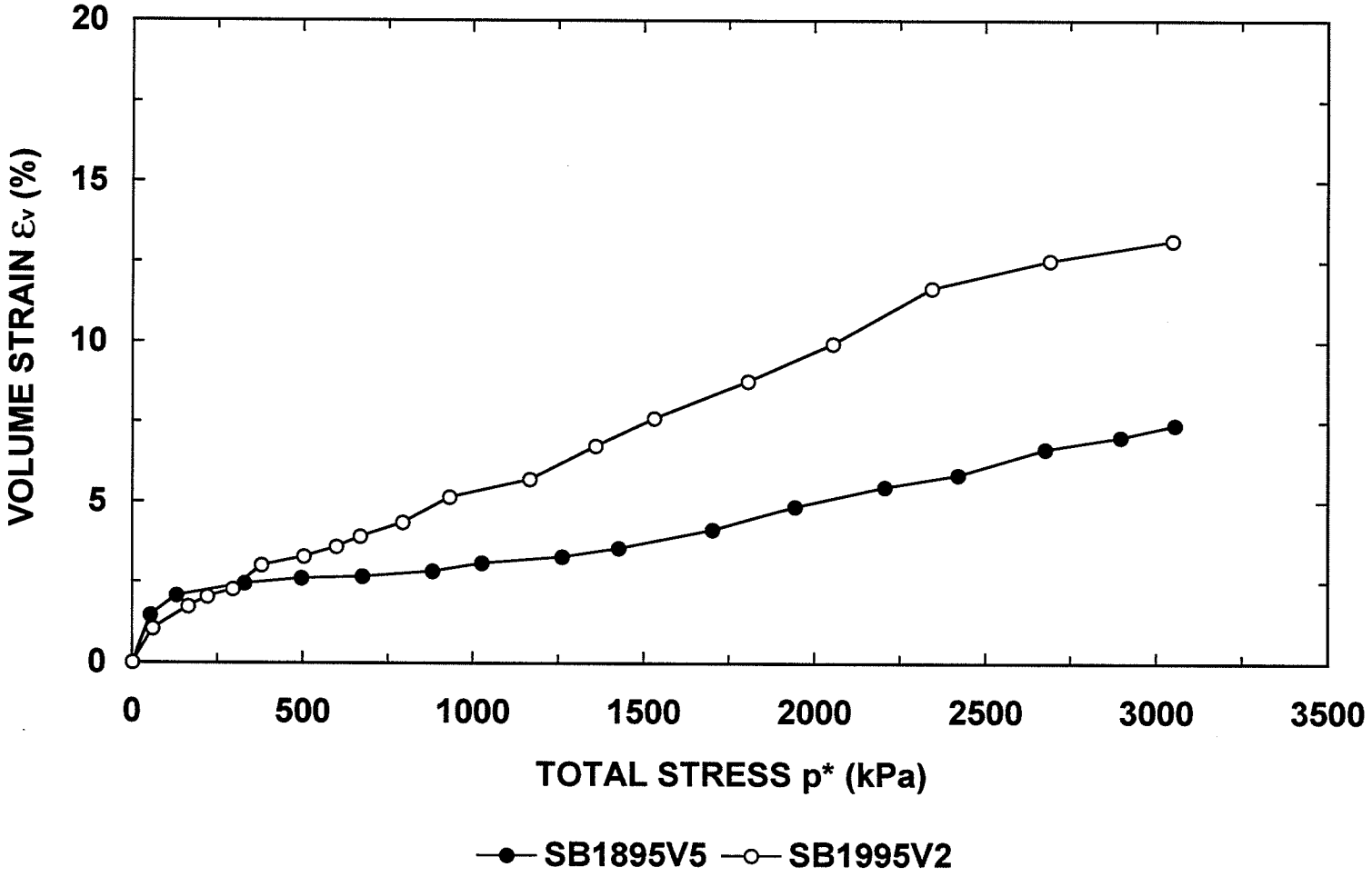

Figure 6.24 Comparison of volume strain-total stress relationships of "high density" sand-bentonite specimens.

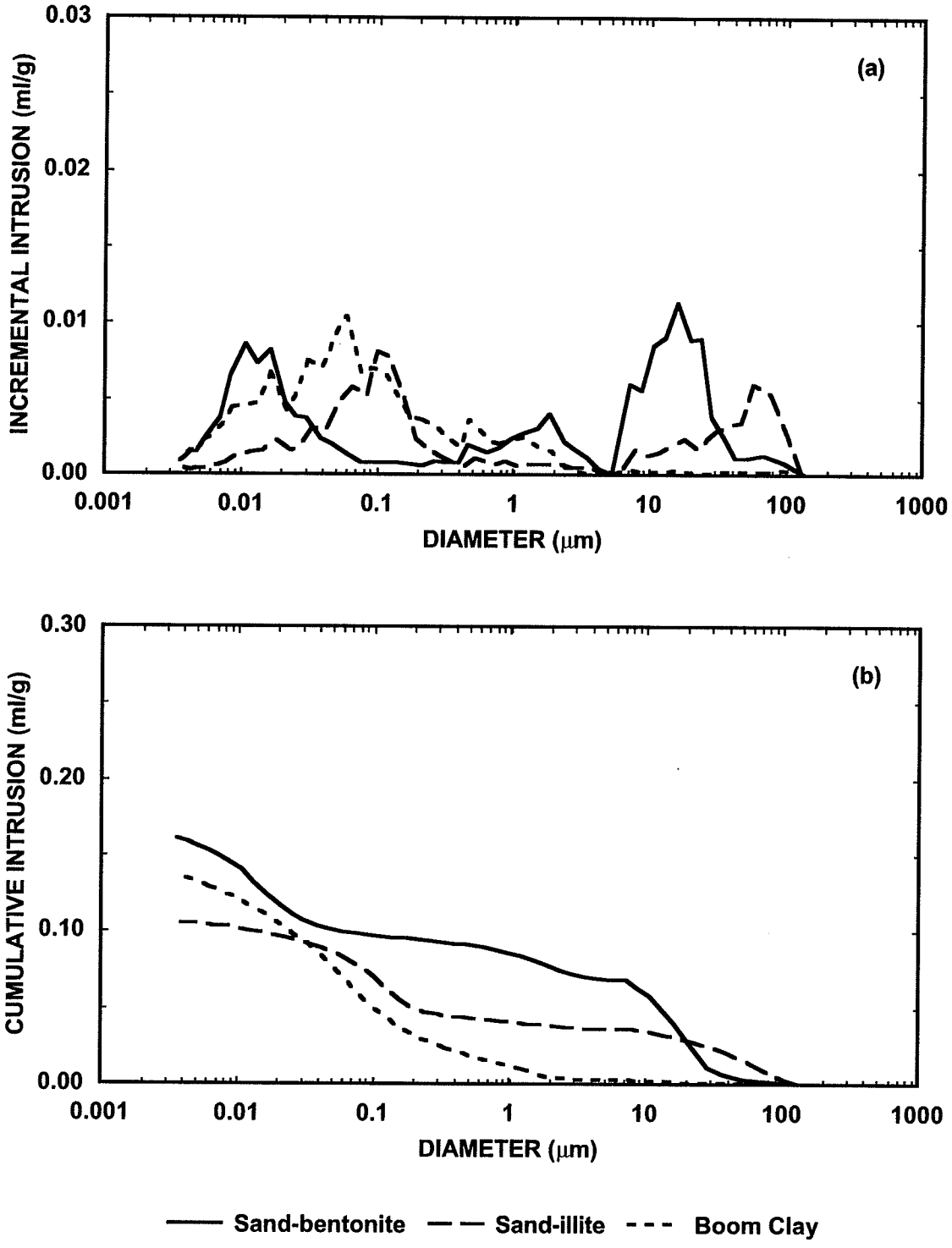

Figure 7.1 Comparison of pore size distributions in sand-bentonite material, sand-illite material, and Boom Clay.

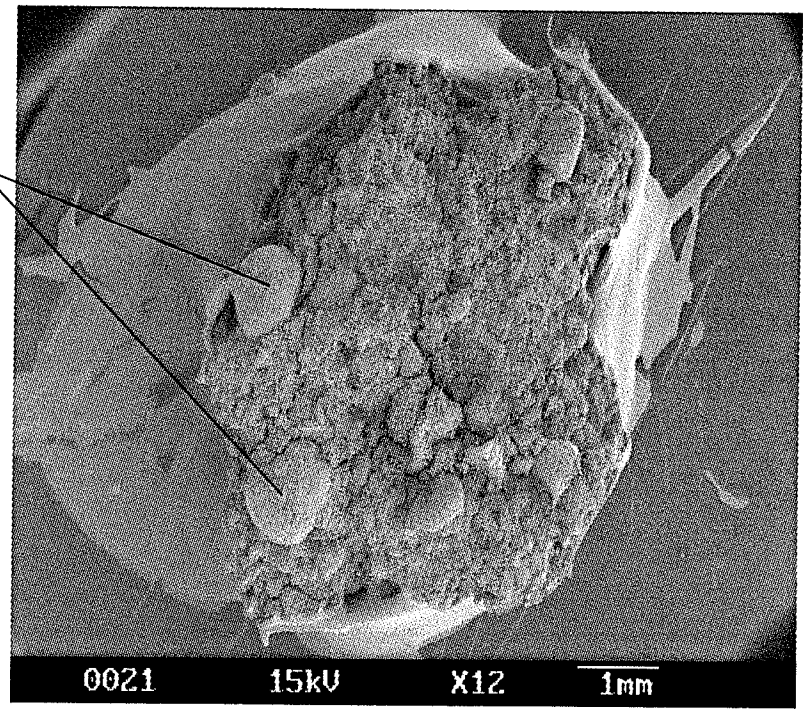

Sand-bentonite material

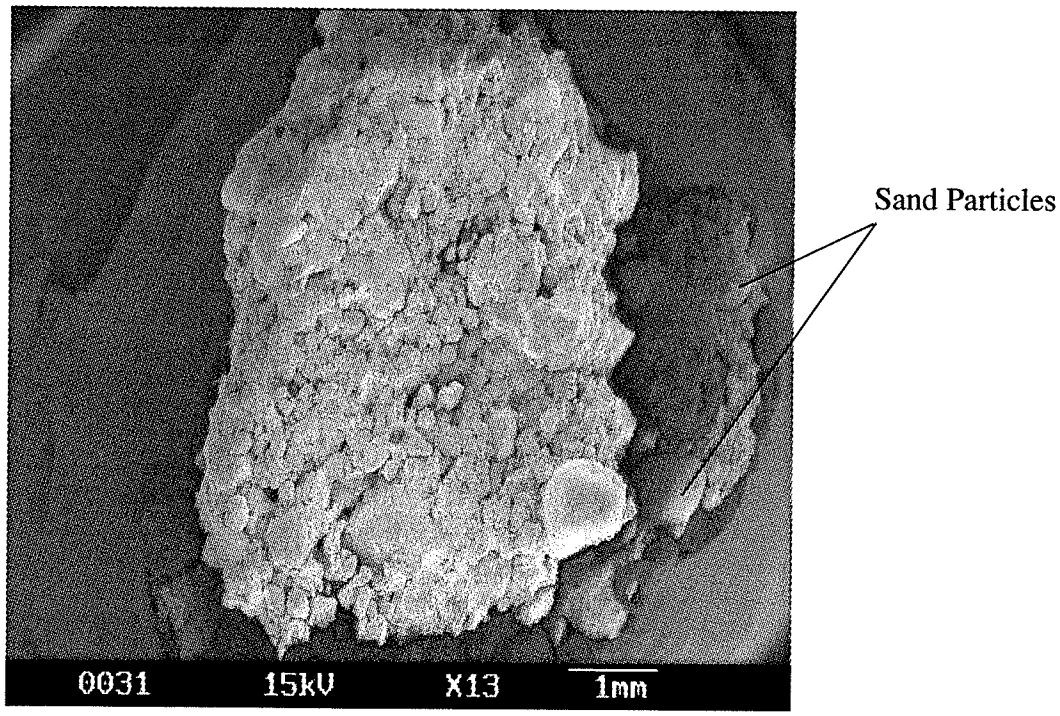

Sand-illite material

Figure 7.2 SEM micrographs of the soil structure in compacted sand-clay materials (low magnifications X12 & X13).

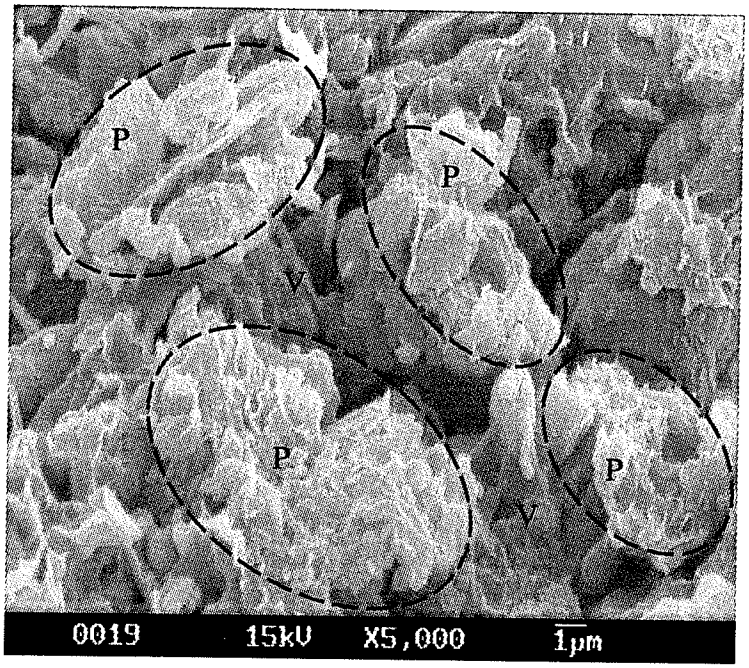

Sand-bentonite material

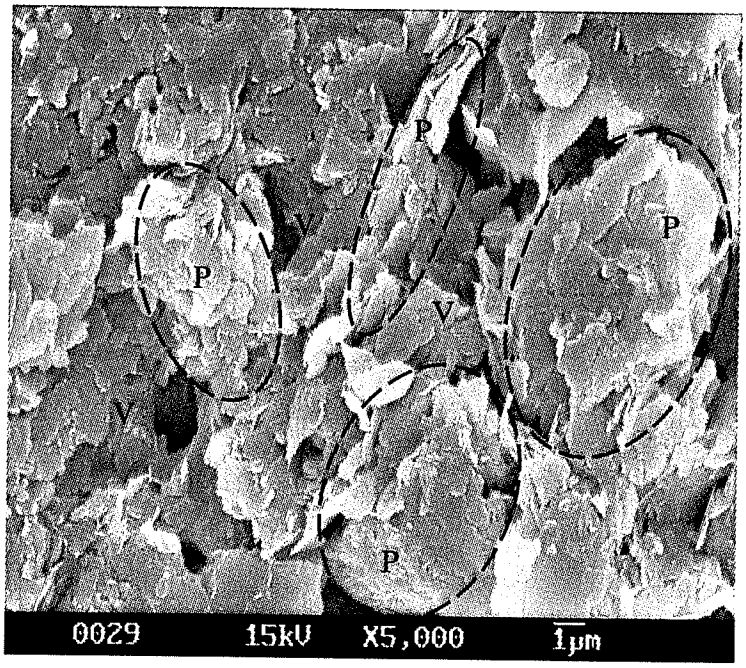

Sand-illite material

P: peds; V: inter-ped voids

Figure 7.3 SEM micrographs of the soil structure in compacted sand-clay materials (high magnifications X5000).

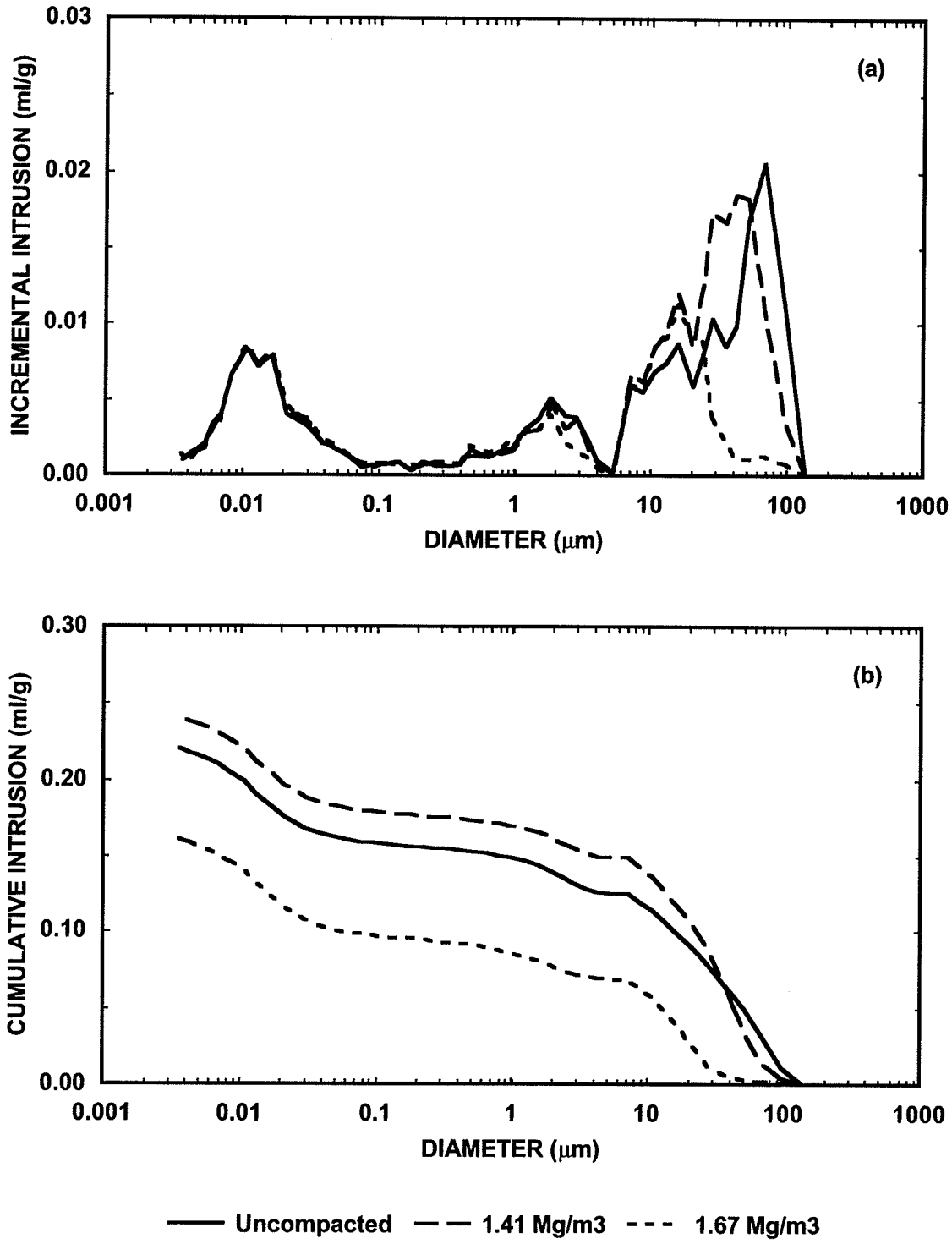

Figure 7.4 Comparison of pores size distributions in sand-bentonite specimens formed to w = 17.6% at different dry densities.

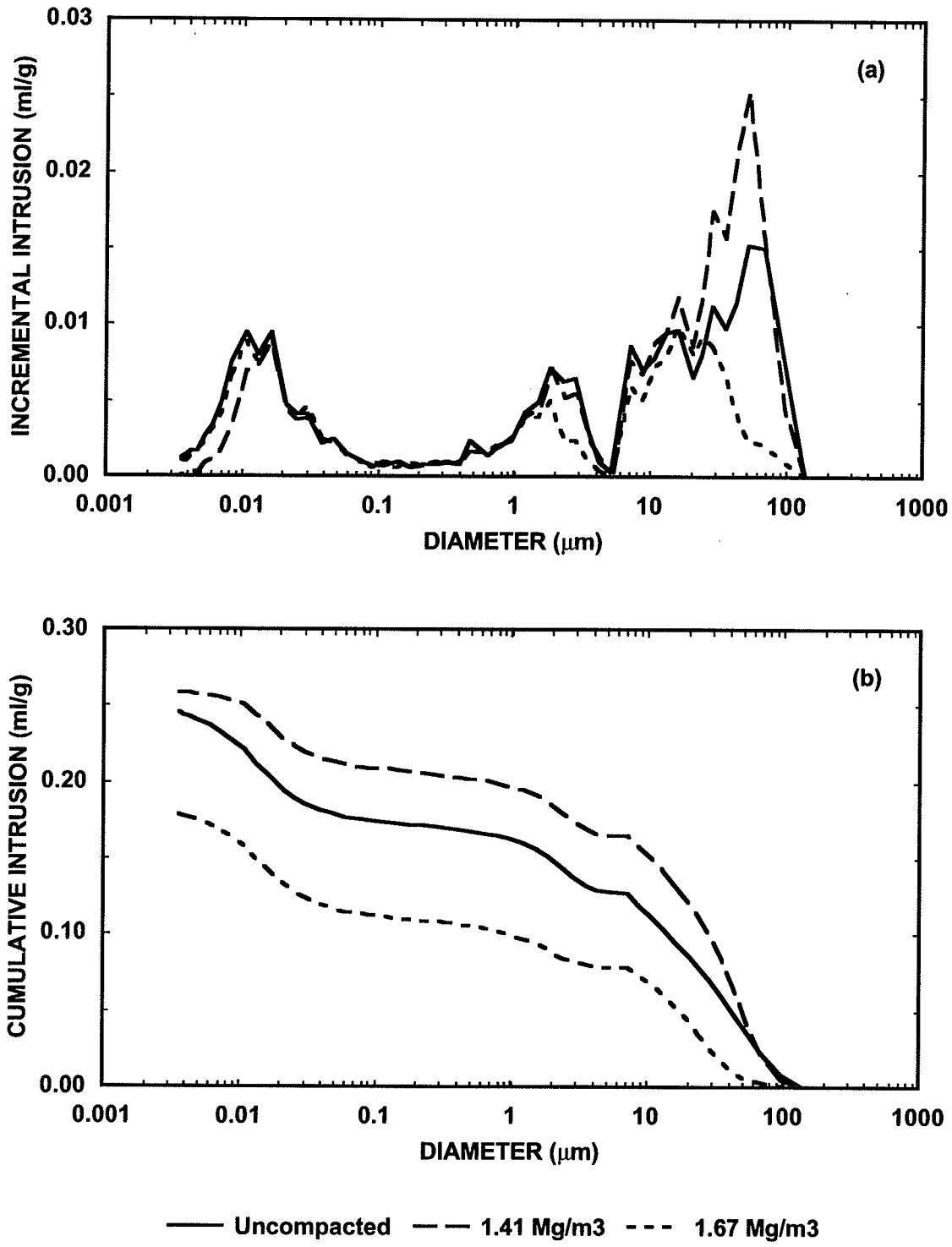

Figure 7.5 Comparison of pore size distributions in sand-bentonite specimens formed to w = 20.3% at different dry densities.

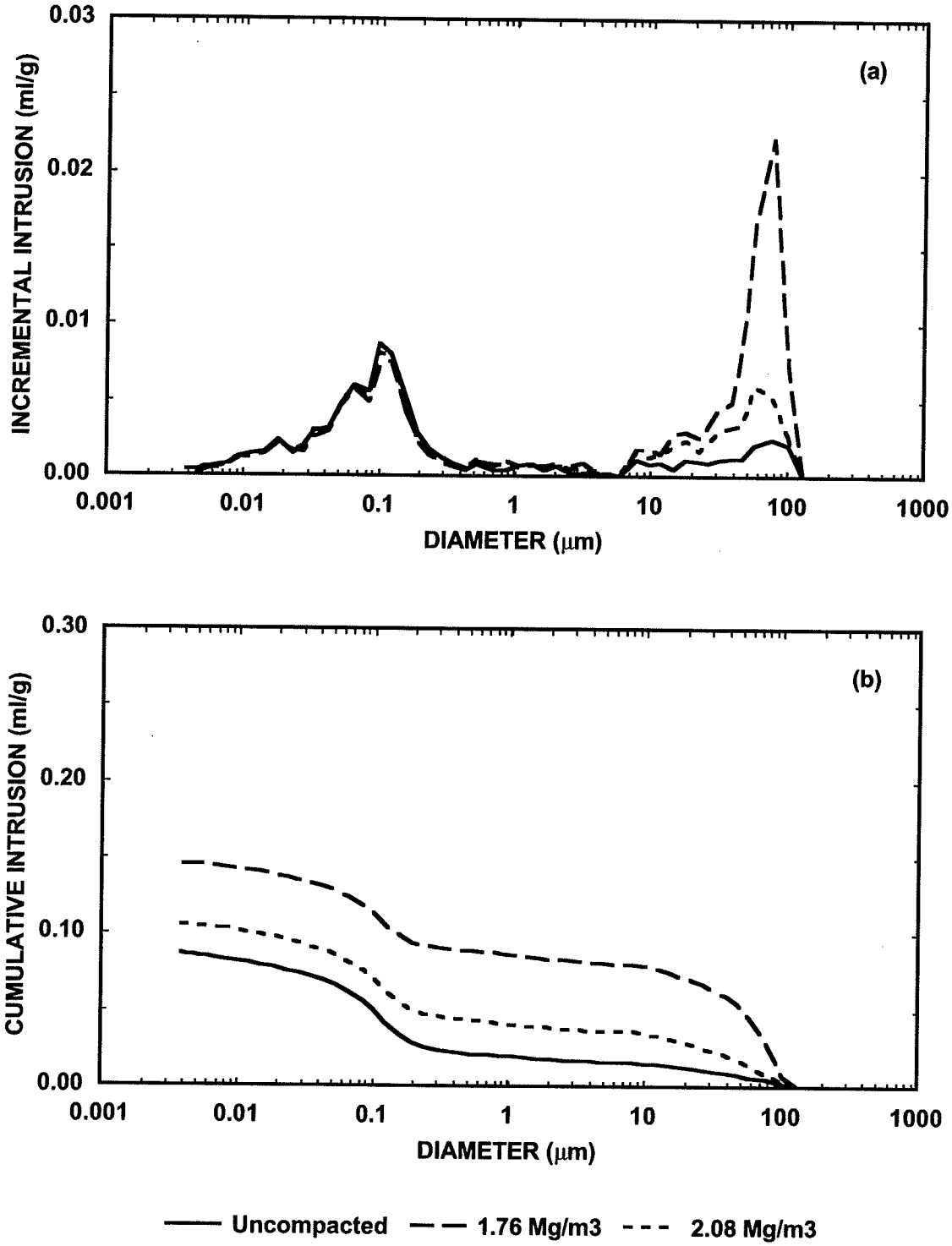

Figure 7.6 Comparison of pore size distributions in sand-illite specimens formed to w = 9% at different dry densities.

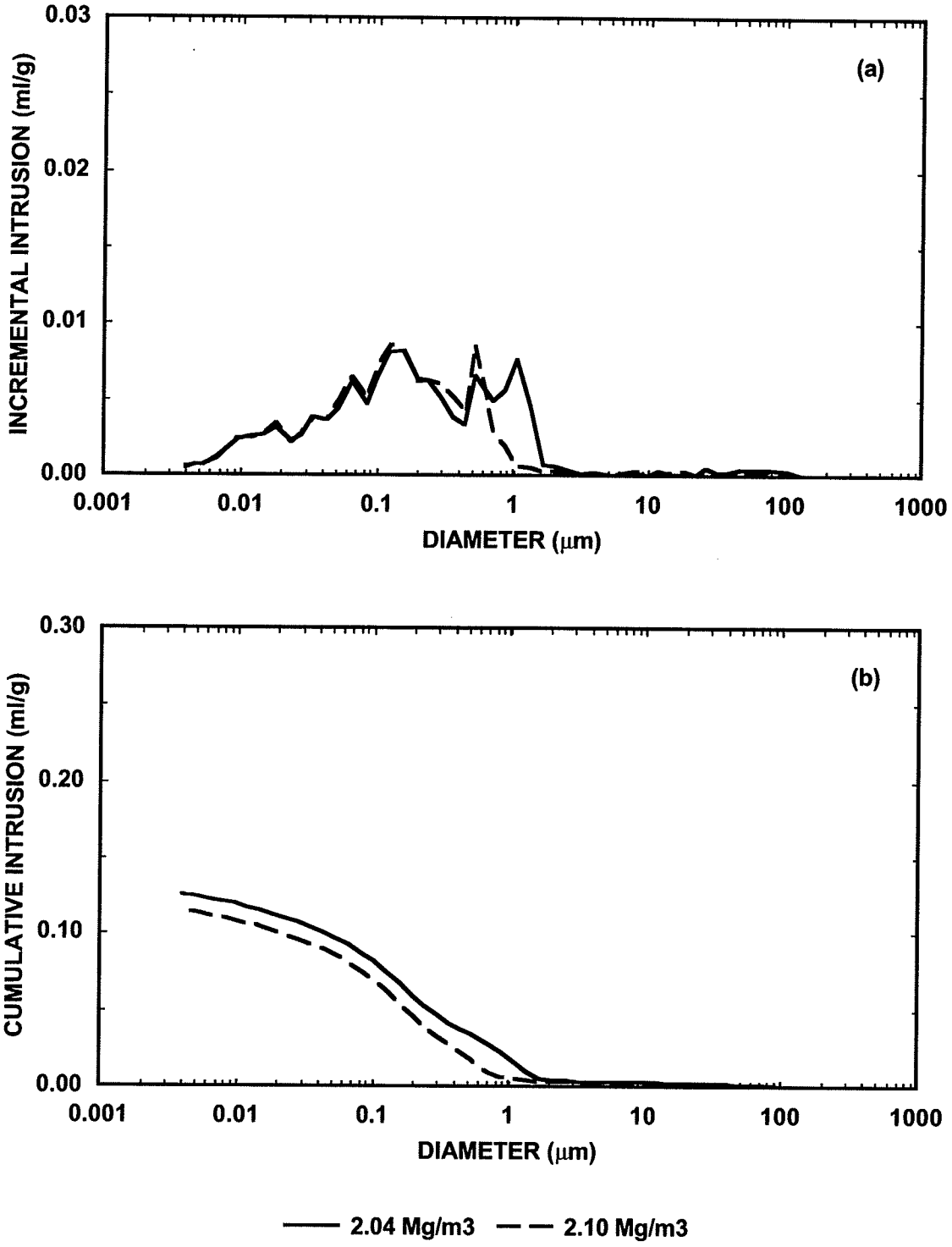

Figure 7.7 Comparison of pore size distributions in illitic clay specimens formed to w = 11% at different dry densities.

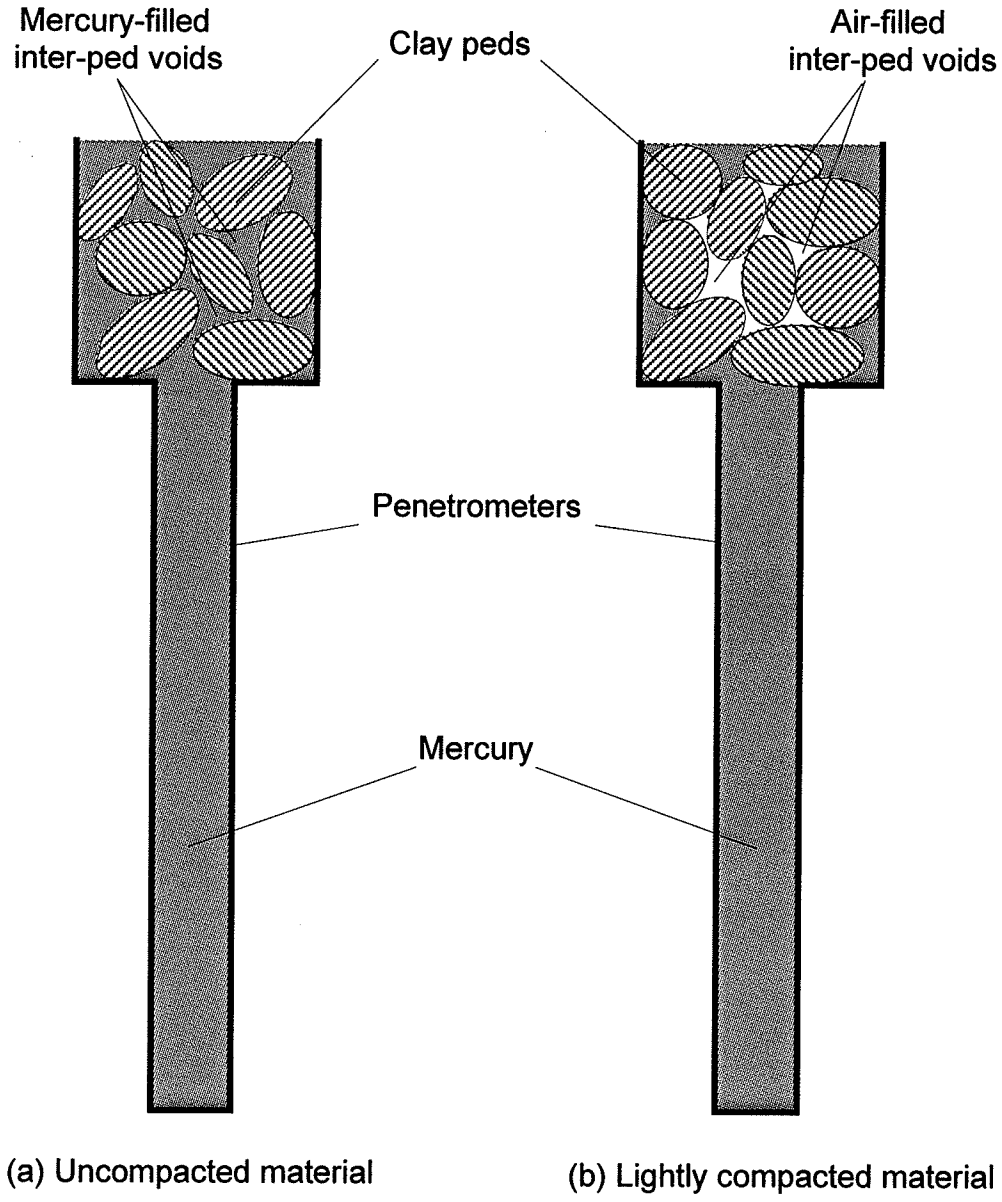

Figure 7.8 Conditions of penetrometer-specimen assembley after mercury filling.

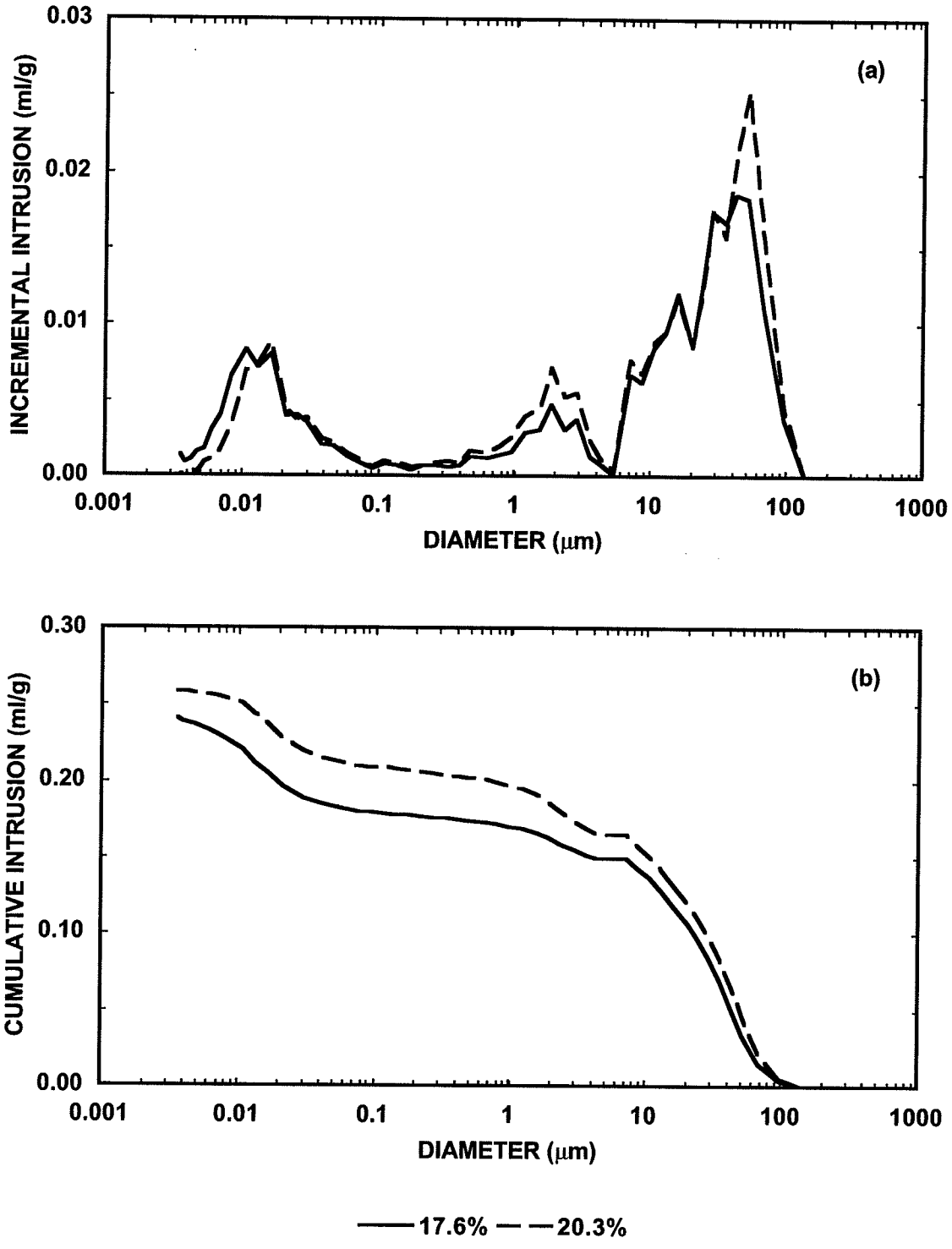

Figure 7.9 Comparison of pore size distributions in sand-bentonite specimens formed at γ_d = 1.41 Mg/m^3 to different water contents.

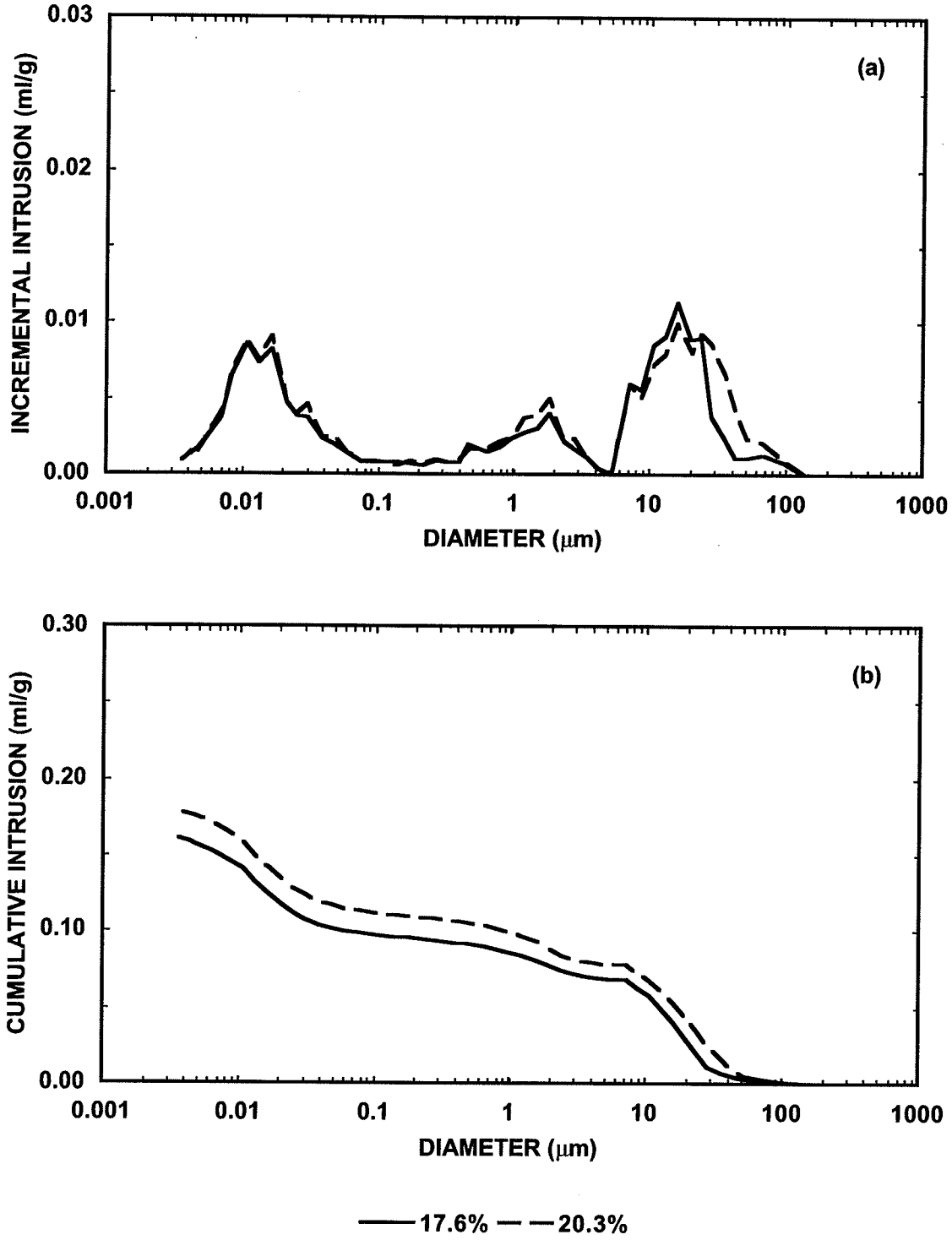

Figure 7.10 Comparison of pore size distributions in sand-bentonite specimens formed at γ_d = 1.67 Mg/m^3 to different water contents.

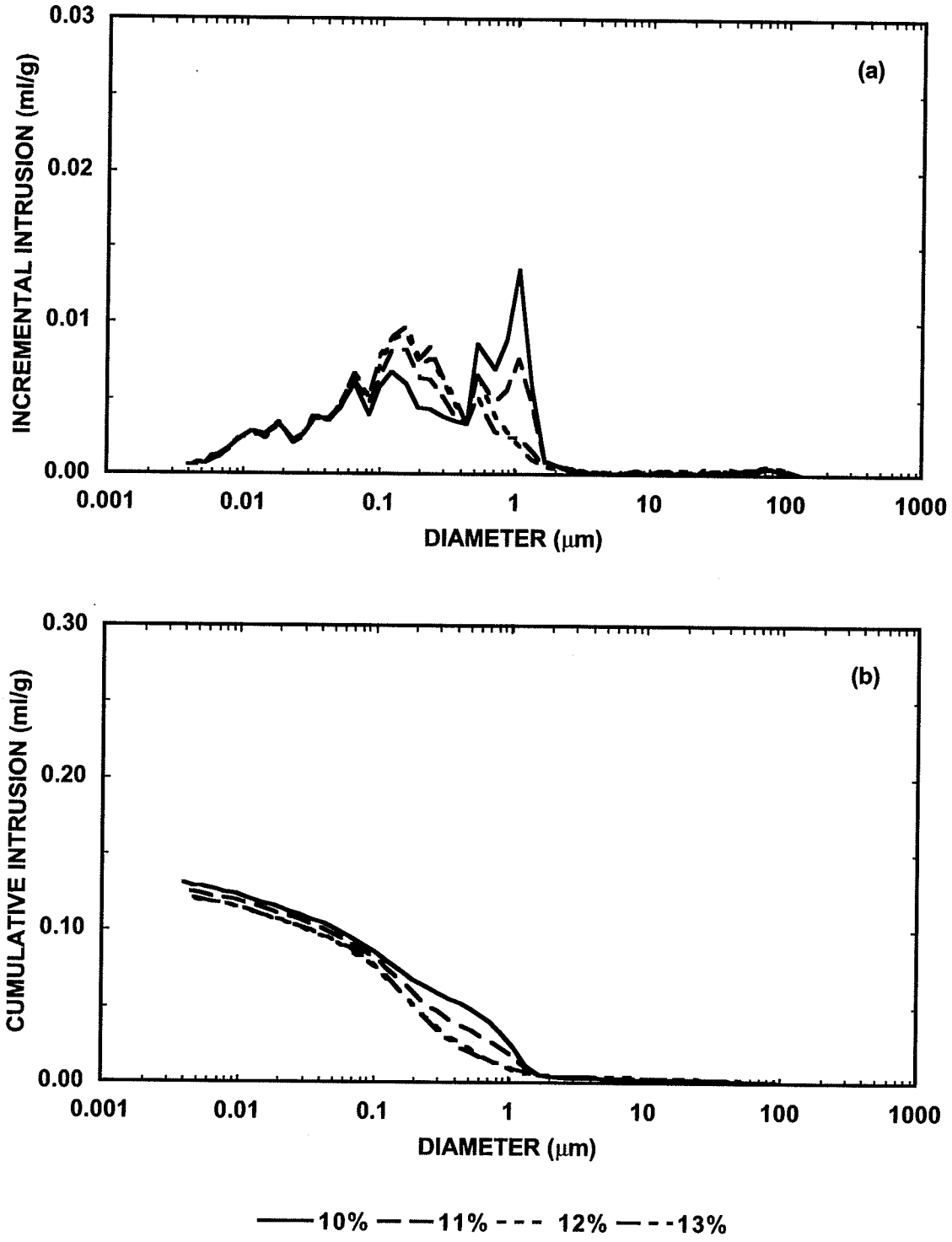

Figure 7.11 Comparison of pore size distributions in illitic clay specimens formed at γ_d = 2.04 Mg/m^3 to different water contents.

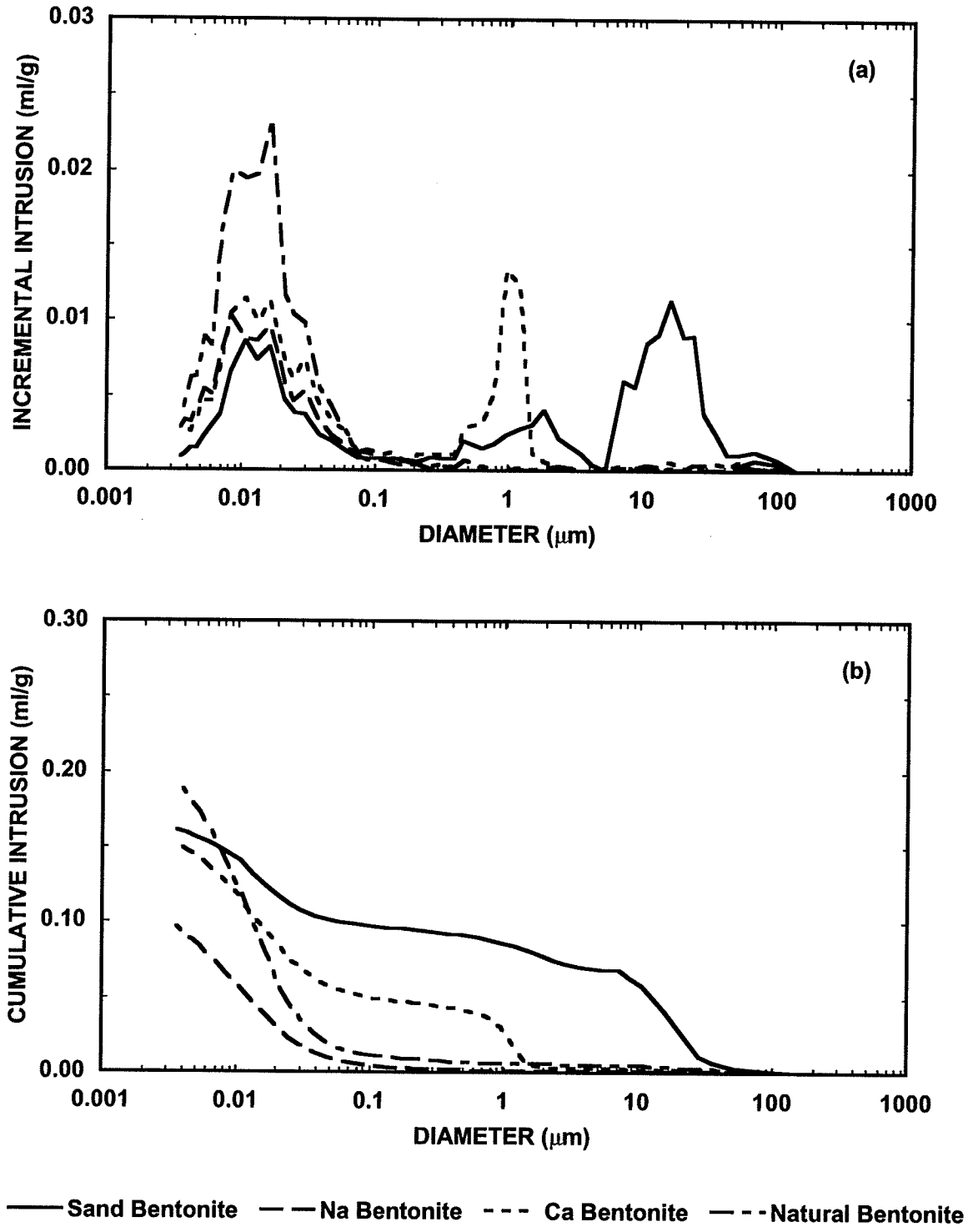

Figure 7.12 Comparison of pore size distributions in sand-bentonite material, sodium bentonite, calcium bentonite, and natural bentonite.

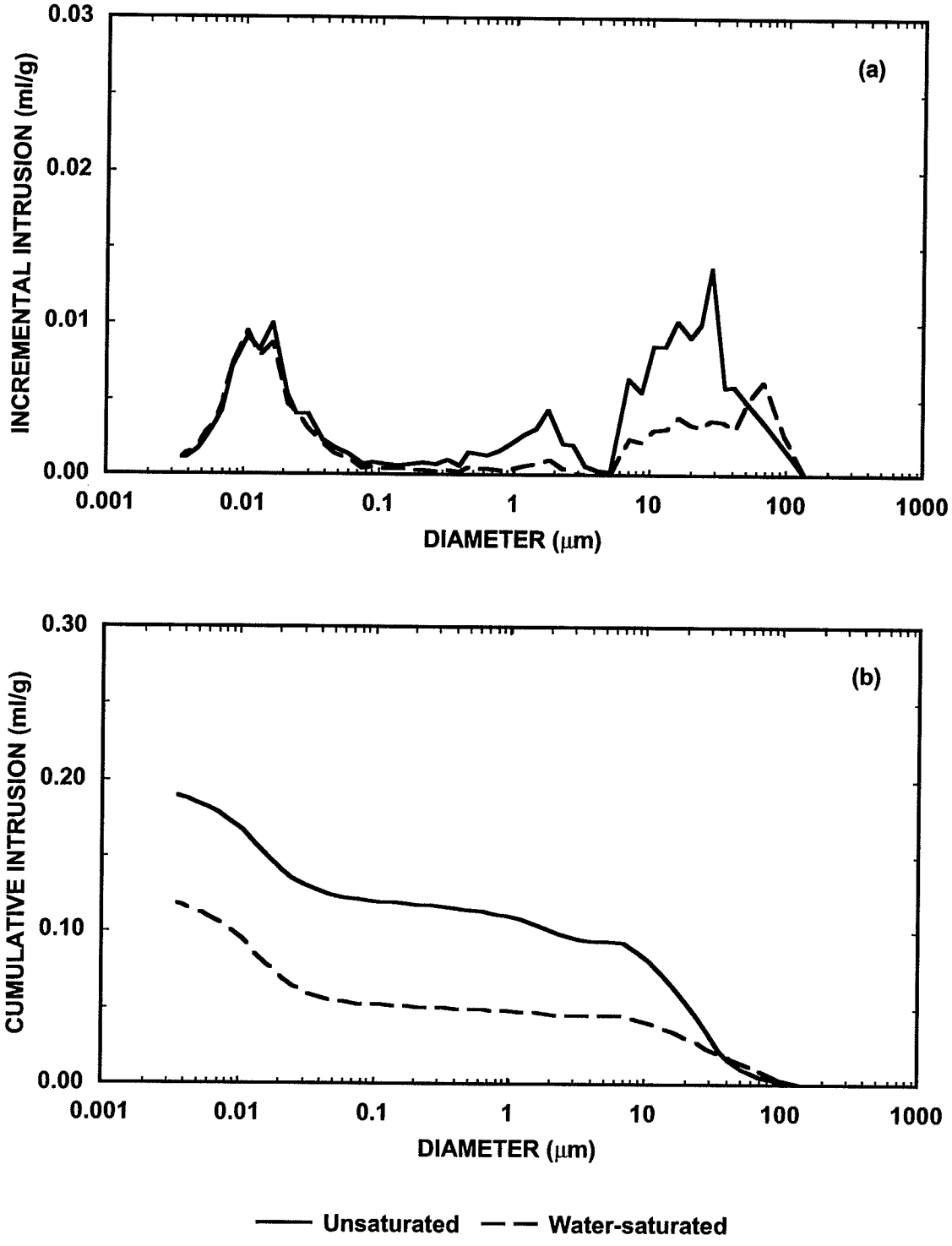

Figure 7.13 Comparison of pore size distributions in sand-bentonite specimens formed to different degrees of saturation.

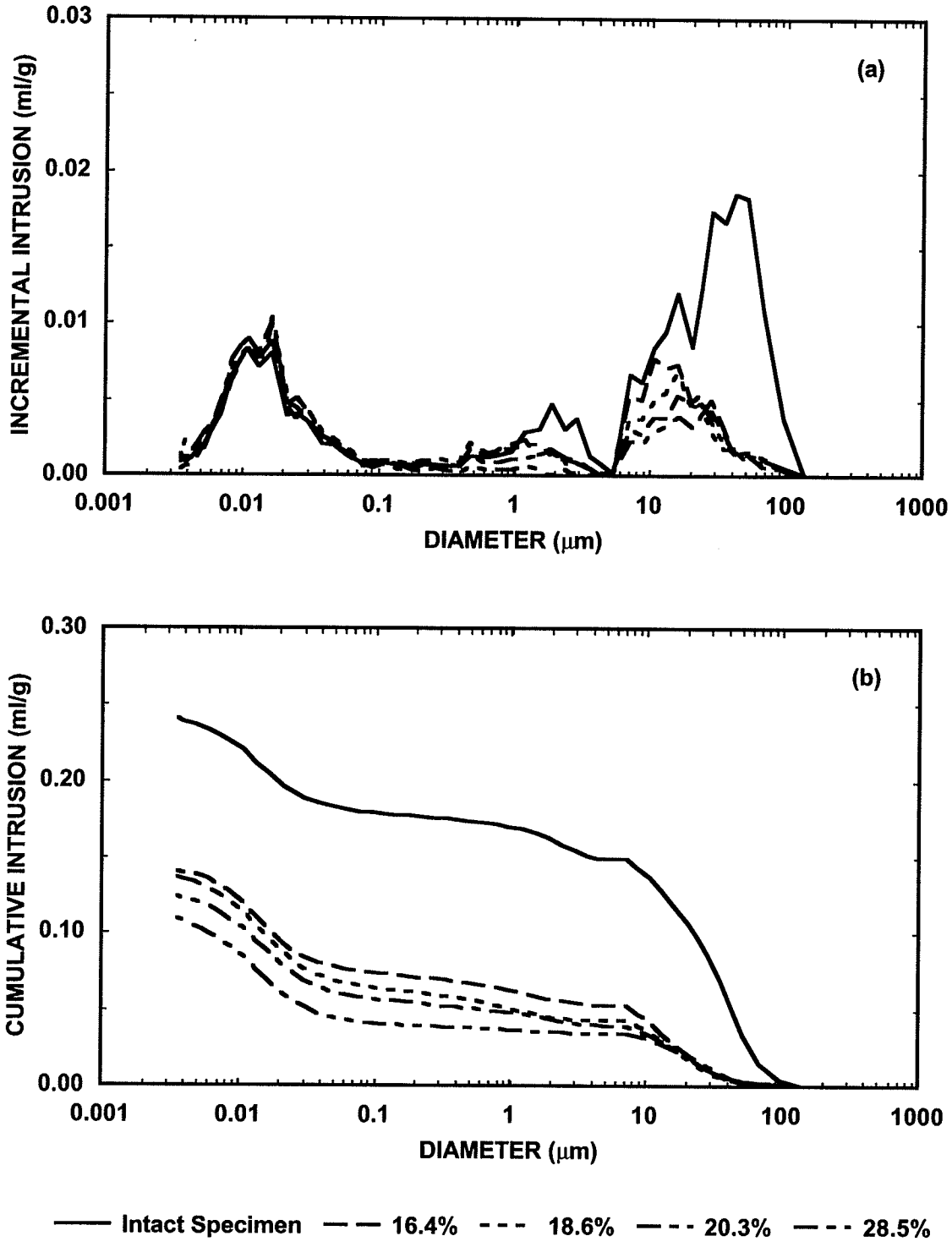

Figure 7.14 Comparison of pore size distributions in isotropically compressed sand-bentonite specimens formed at γ_d = 1.40 to 1.45 Mg/m^3 to specified water contents.

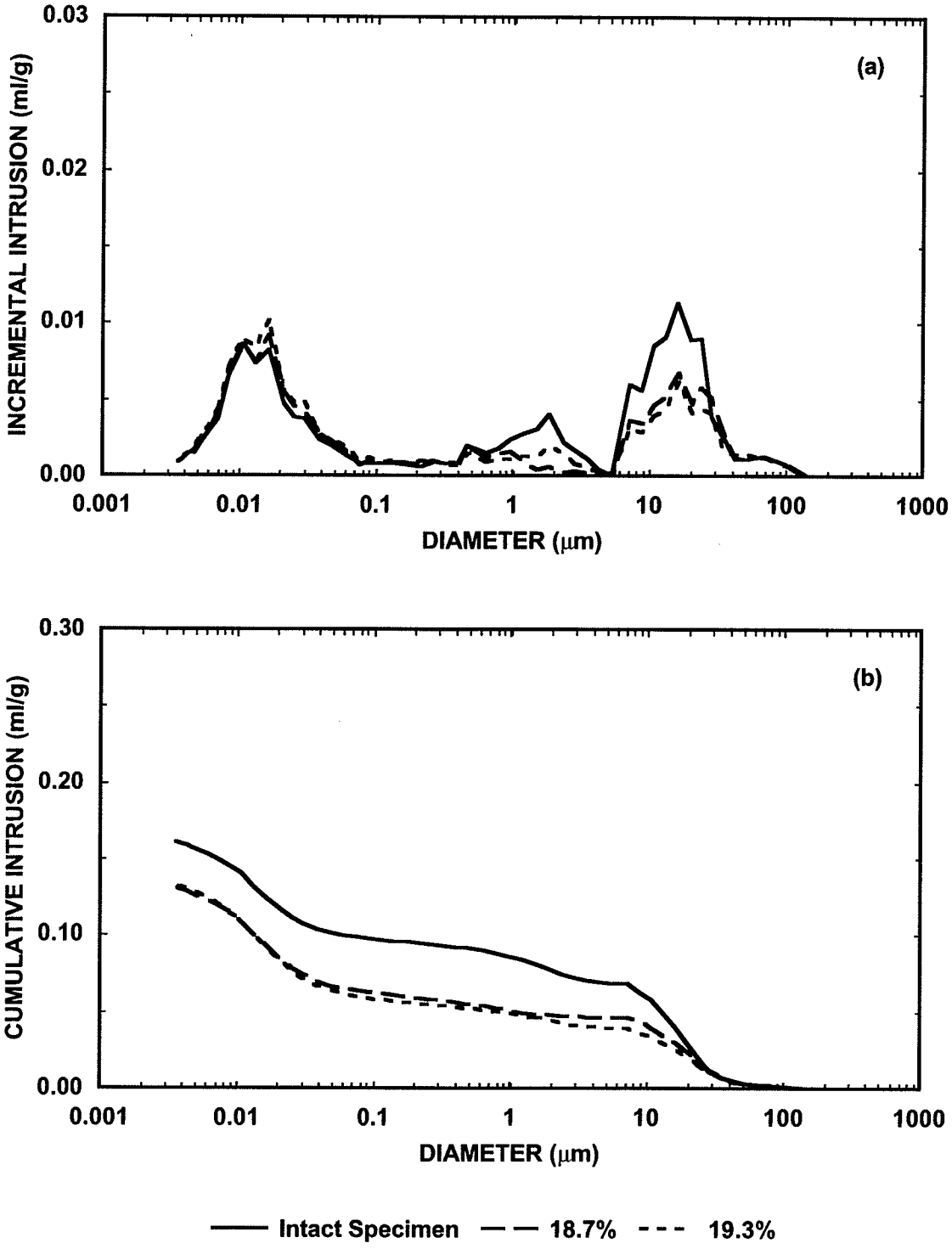

Figure 7.15 Comparison of pore size distributions in isotropically compressed sand-bentonite specimens formed at γ_d = 1.66 Mg/m^3 to specified water contents.

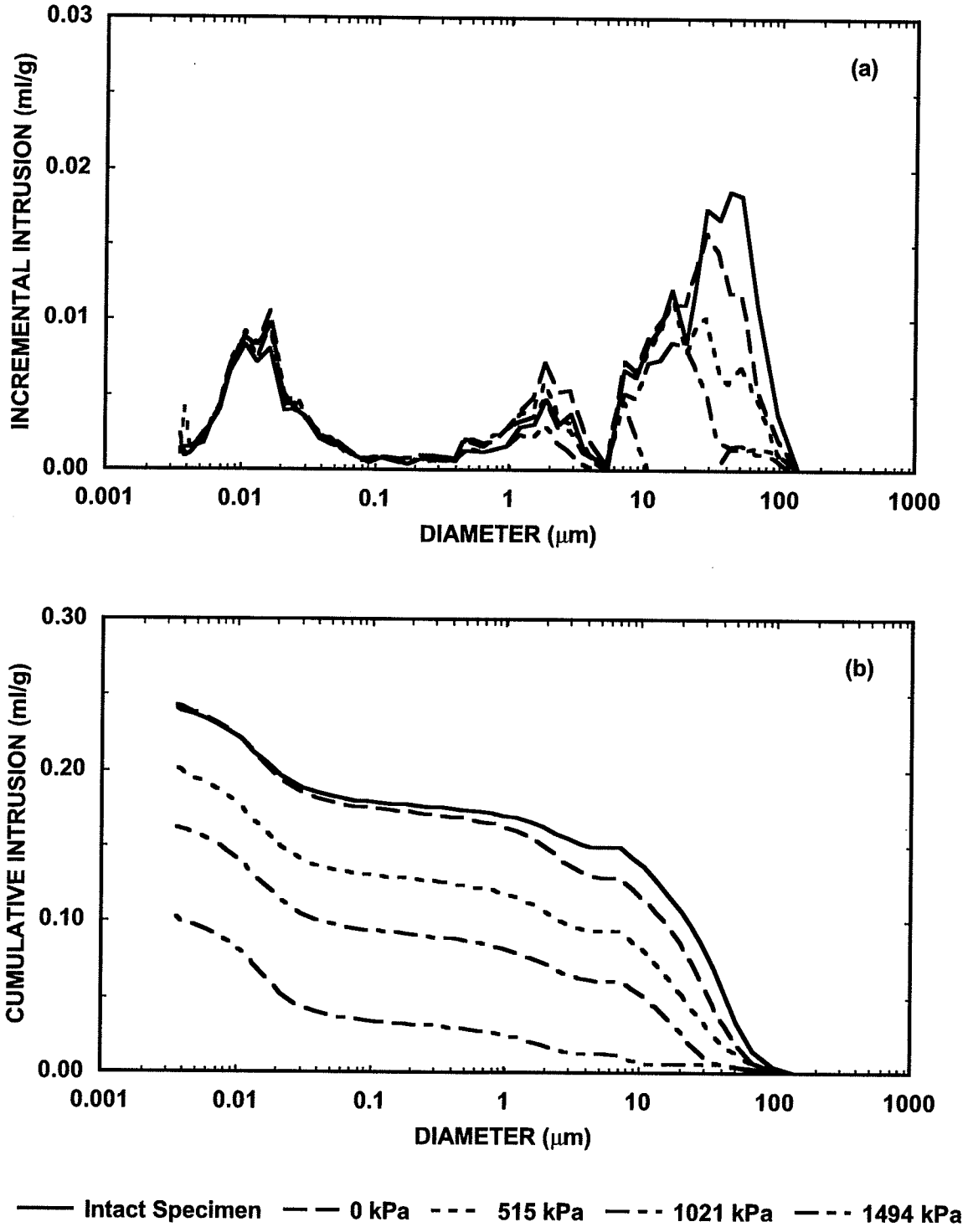

Figure 7.16 Comparison of pore size distributions in sheared sand-bentonite specimens formed at initial γ_d = 1.40 Mg/m^3 to 1.43 Mg/m^3 to w = 18.1% to 19.0%, tested at specified confining pressures.

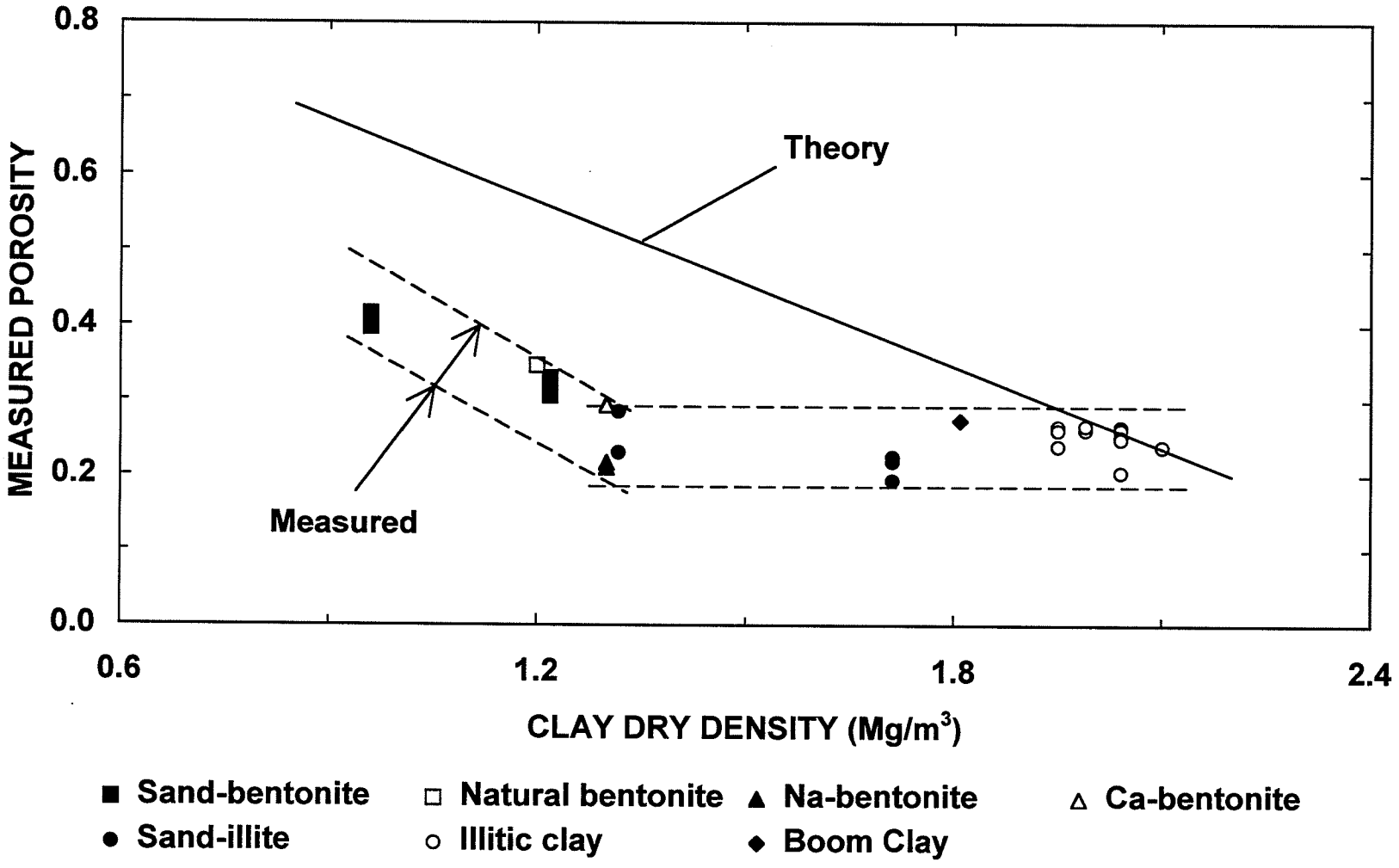

Figure 7.17 Comparison between measured and theoretical porosities in compacted clays.

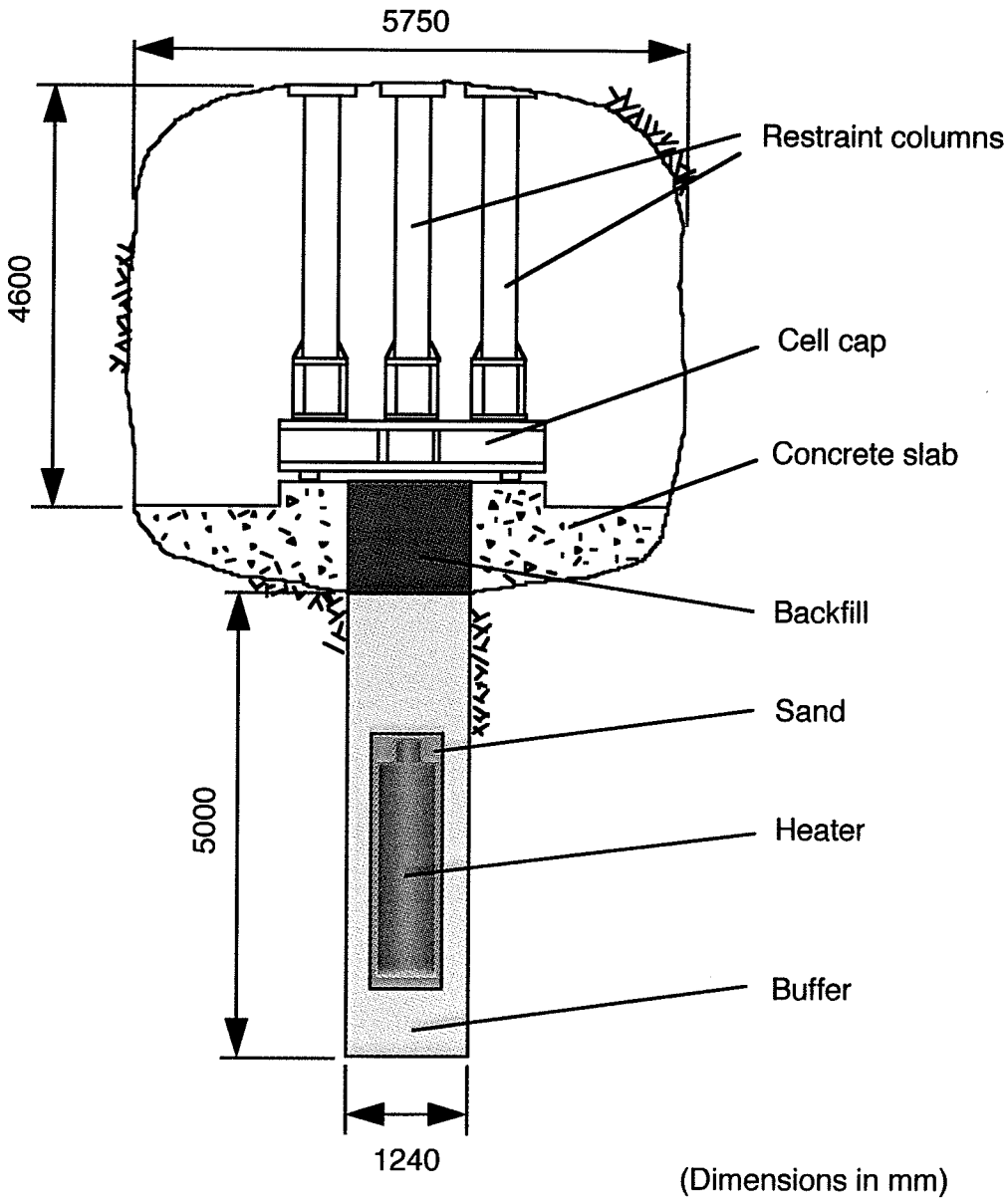

Figure 8.1 Buffer/Container Experiment.

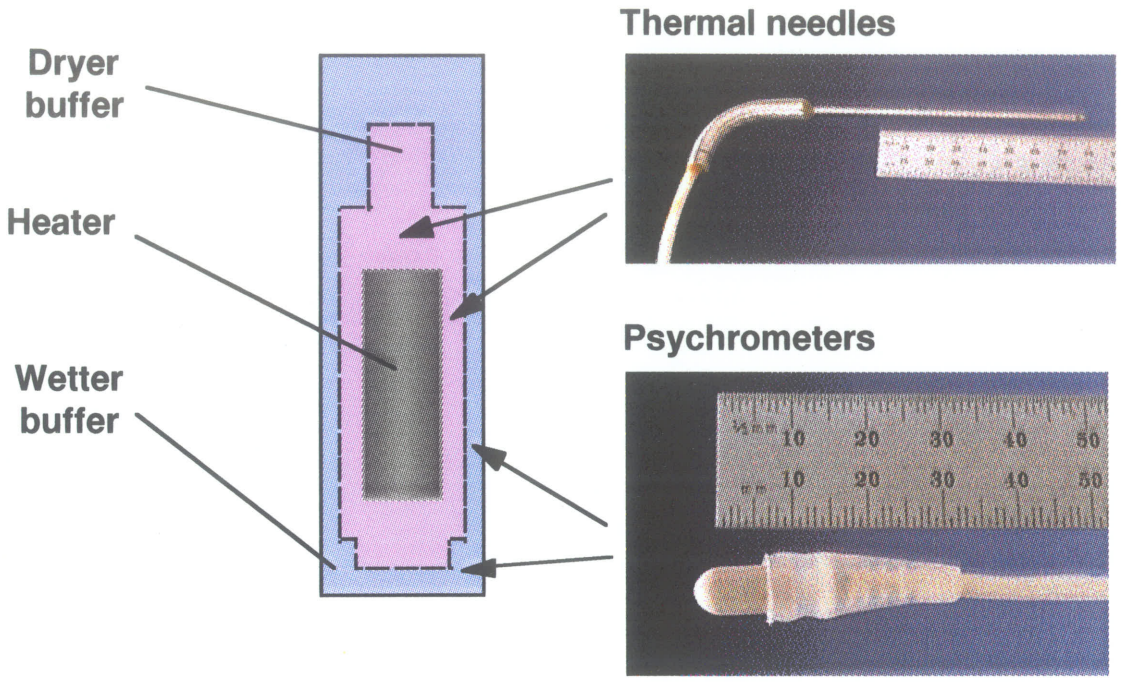

Figure 8.2 Moisture sensor scheme in the Buffer/Container Experiment.

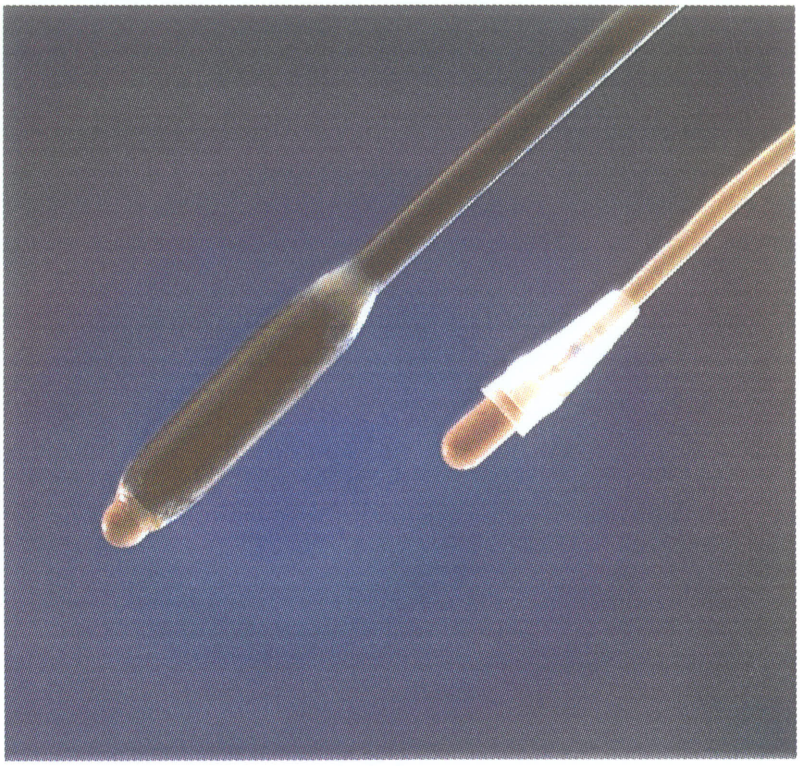

Modified Conventional

Figure 8.3 Modified and conventional Wescor psychrometers.

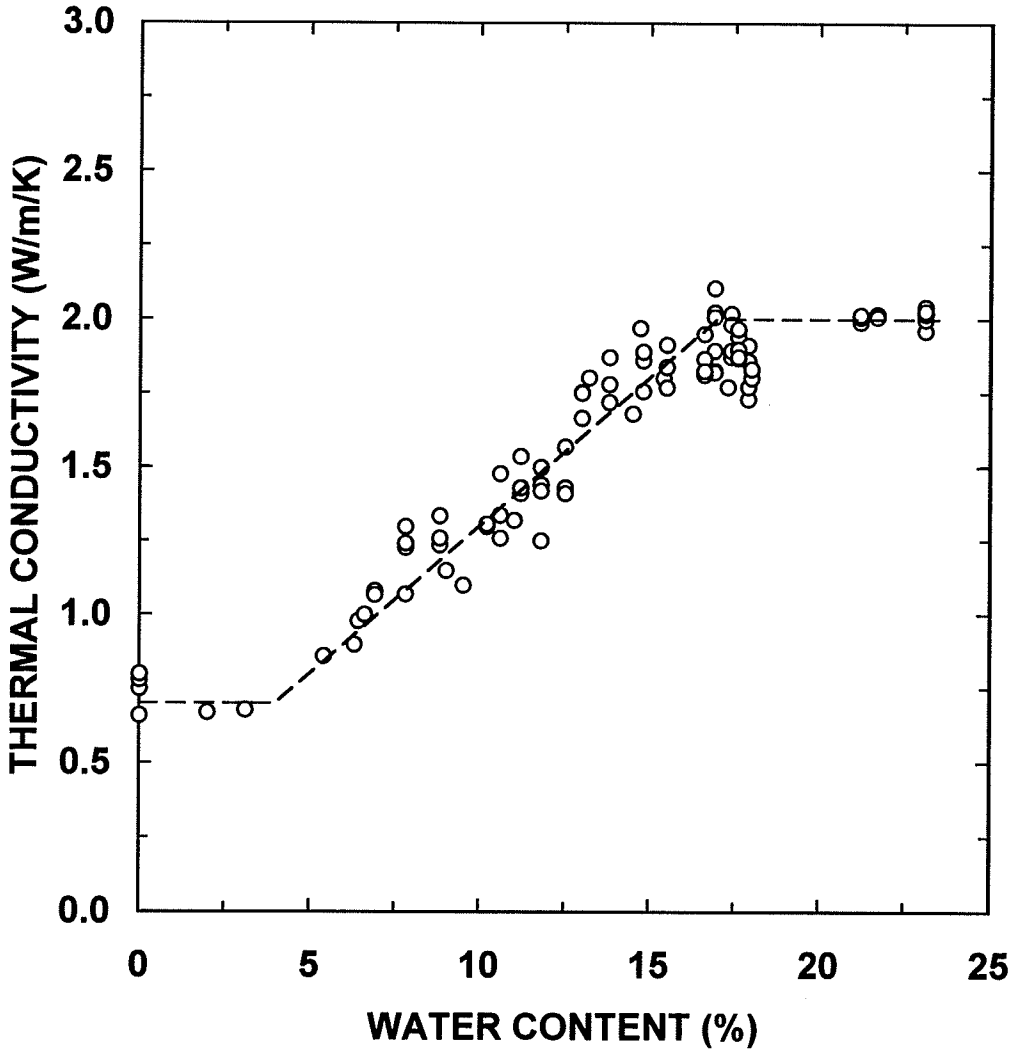

Figure 8.4 Thermal conductivity-water content relationship of unsaturated sand-bentonite material.

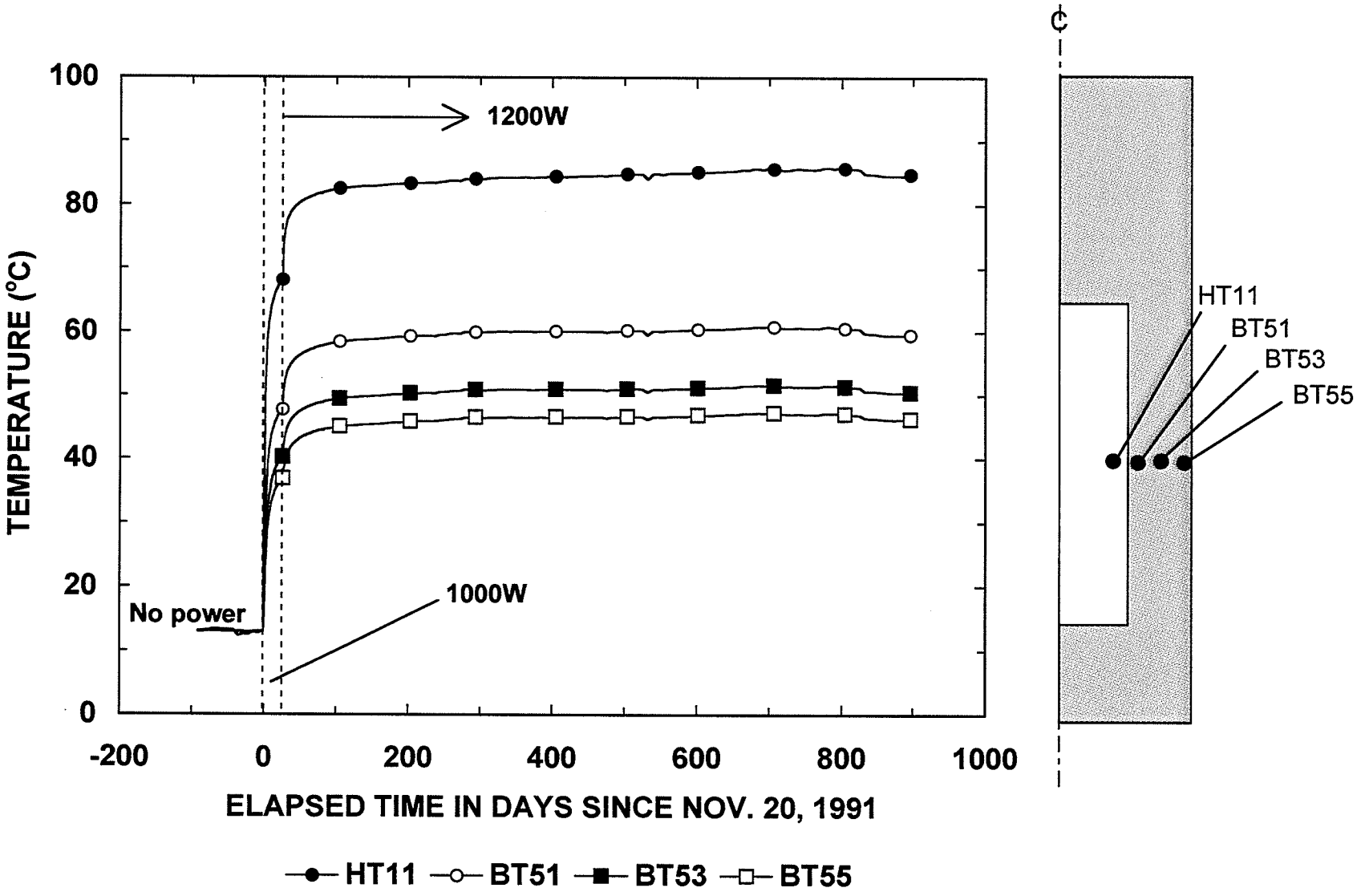

Figure 8.5 Evolution of temperature in the Buffer/Container Experiment.

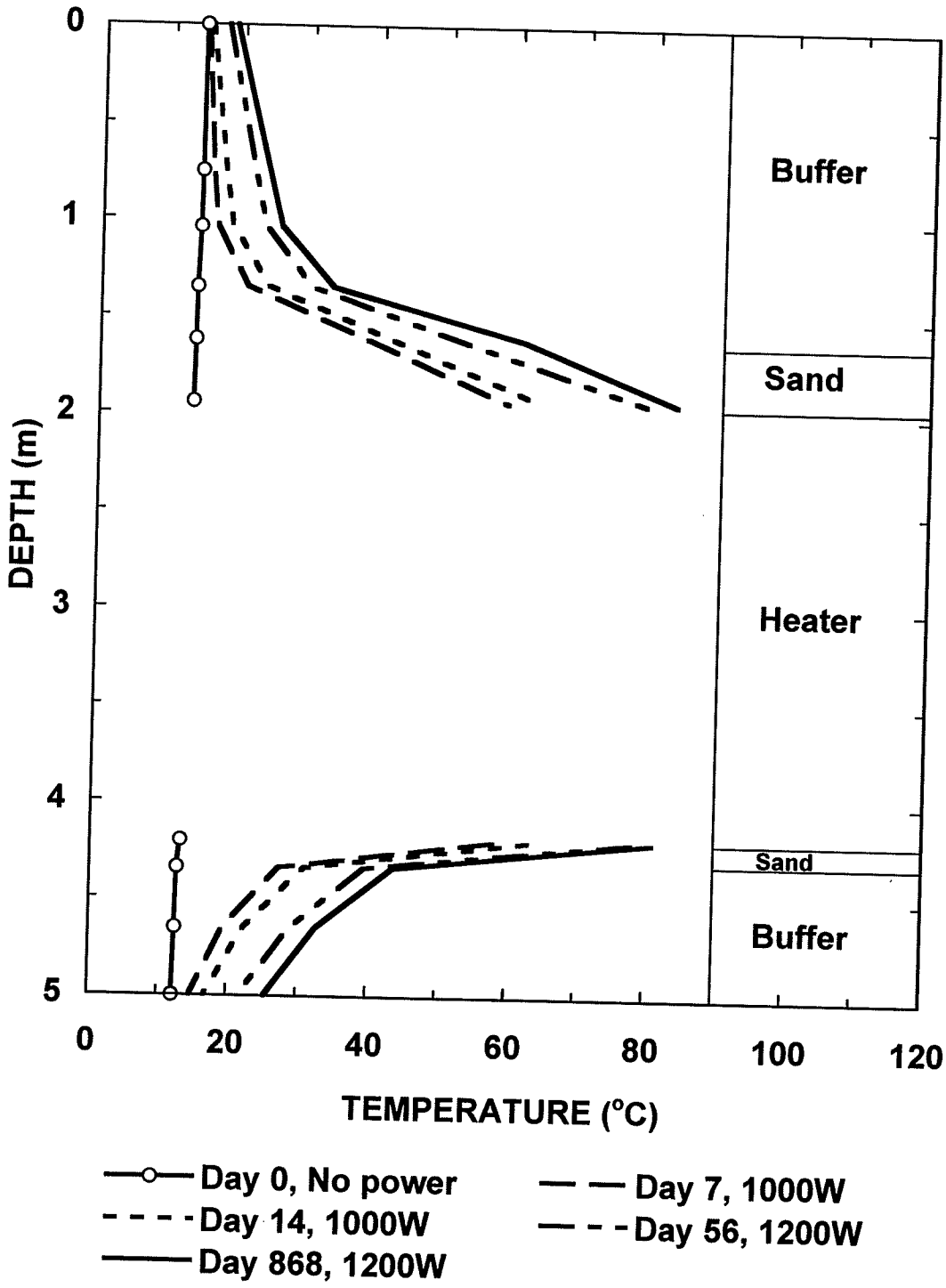

Figure 8.6 Temporal variations of temperature gradients in buffer and sand along the vertical axis of the Buffer/Container Experiment.

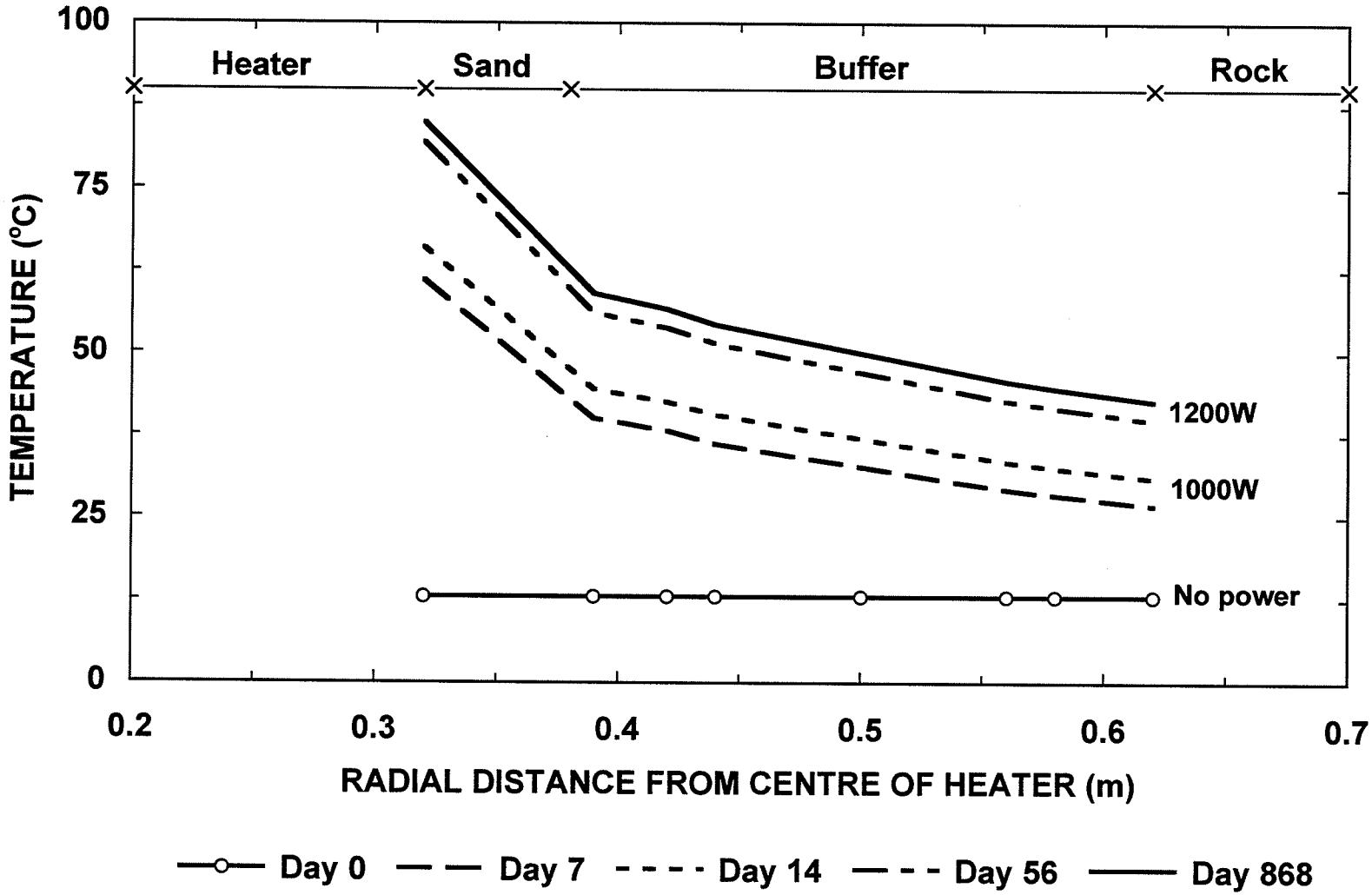

Figure 8.7 Temperature gradients in buffer and sand at the mid-height level of heater at specified times since heater activation.

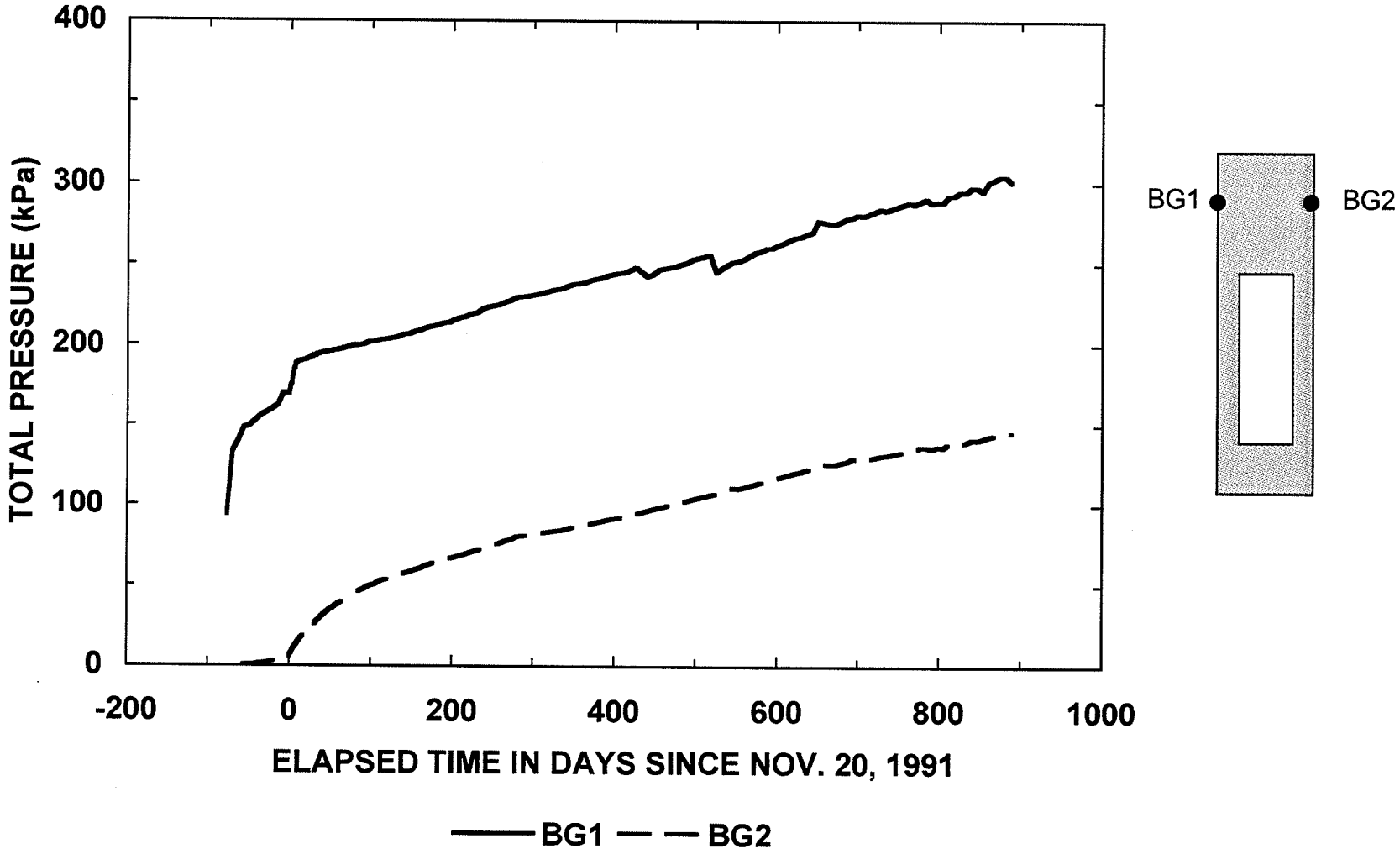

Figure 8.8 Total pressure responses in the Buffer/Container Experiment.

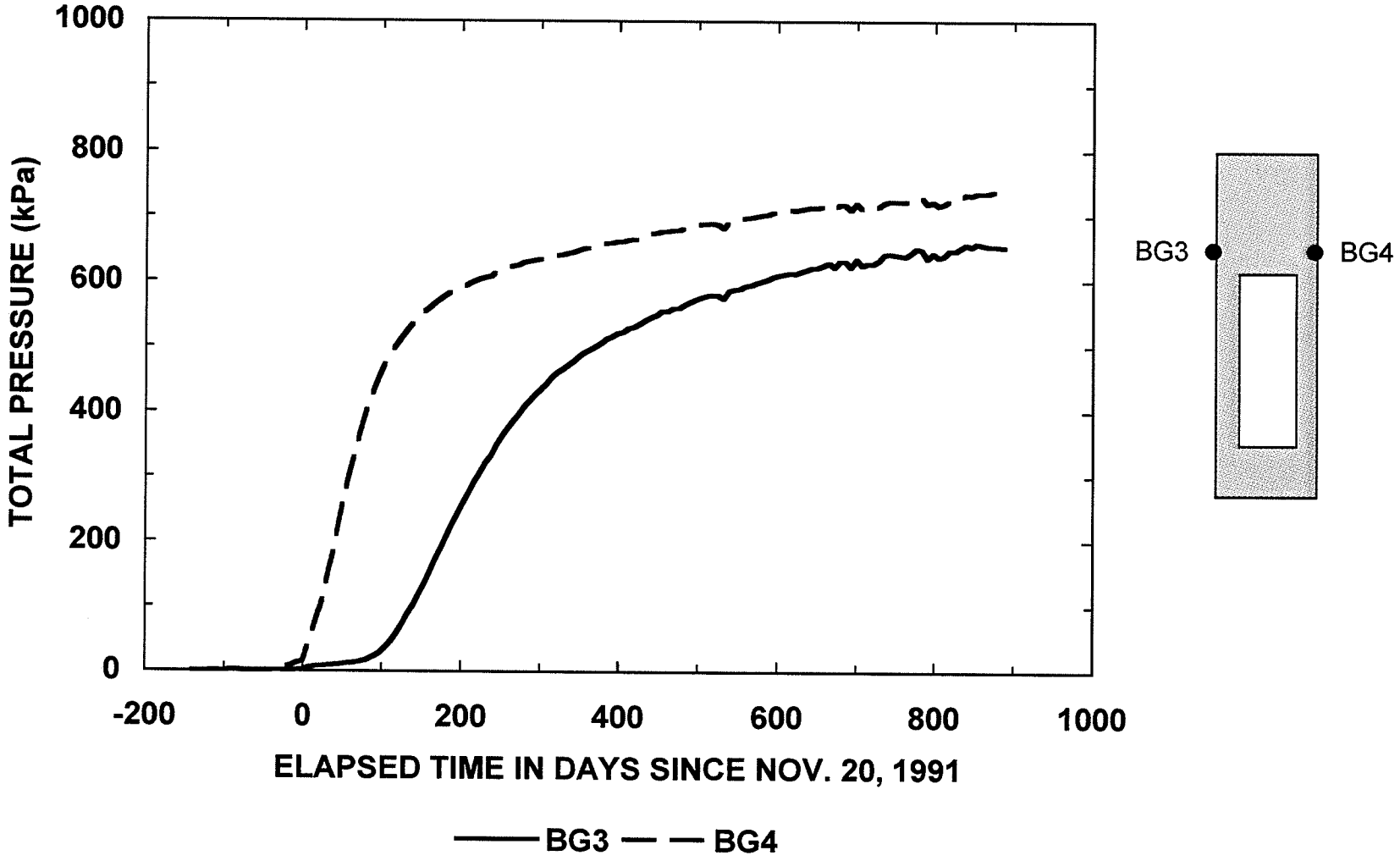

Figure 8.9 Total pressure responses in the Buffer/Container Experiment.

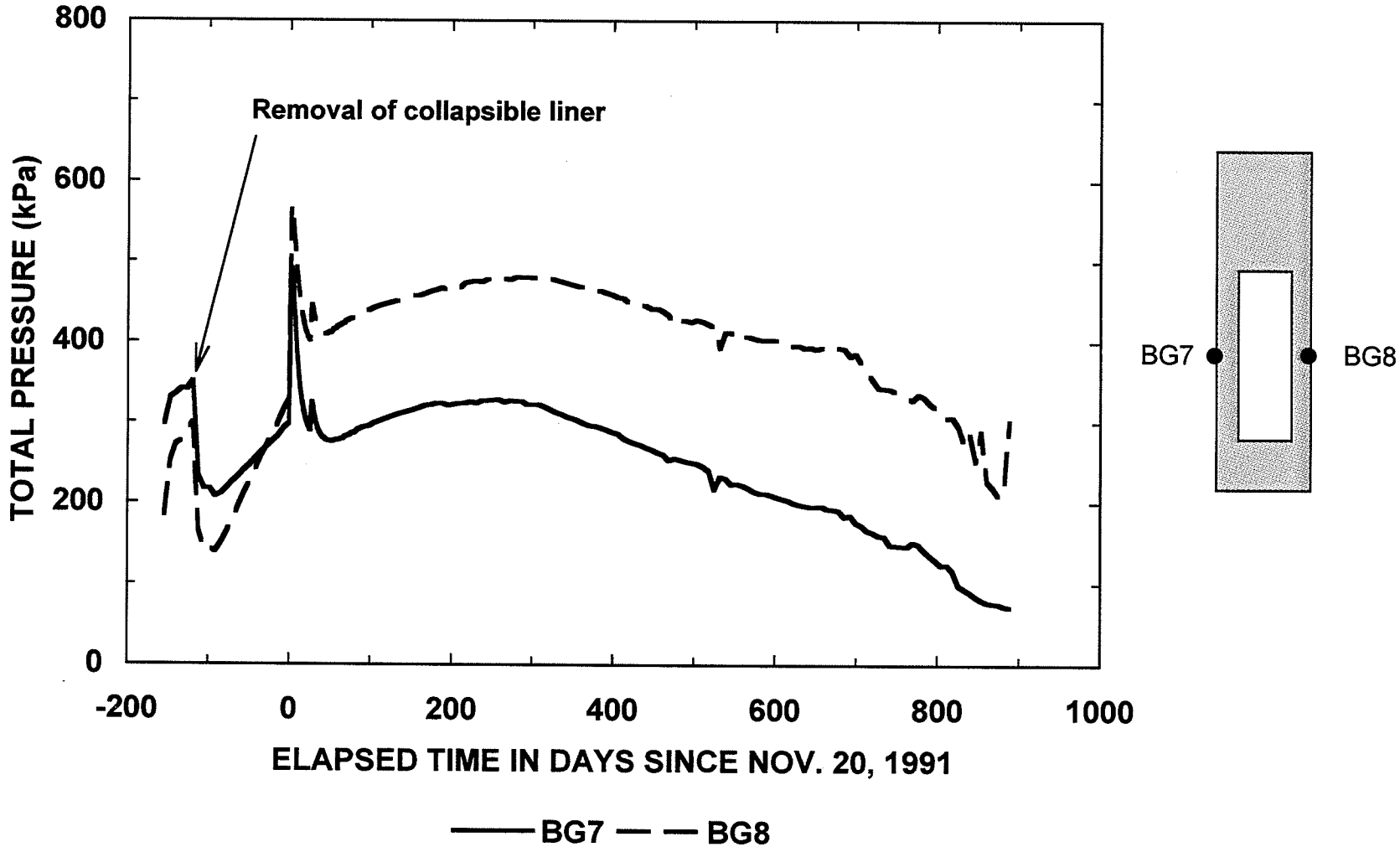

Figure 8.10 Total pressure responses in the Buffer/Container Experiment.

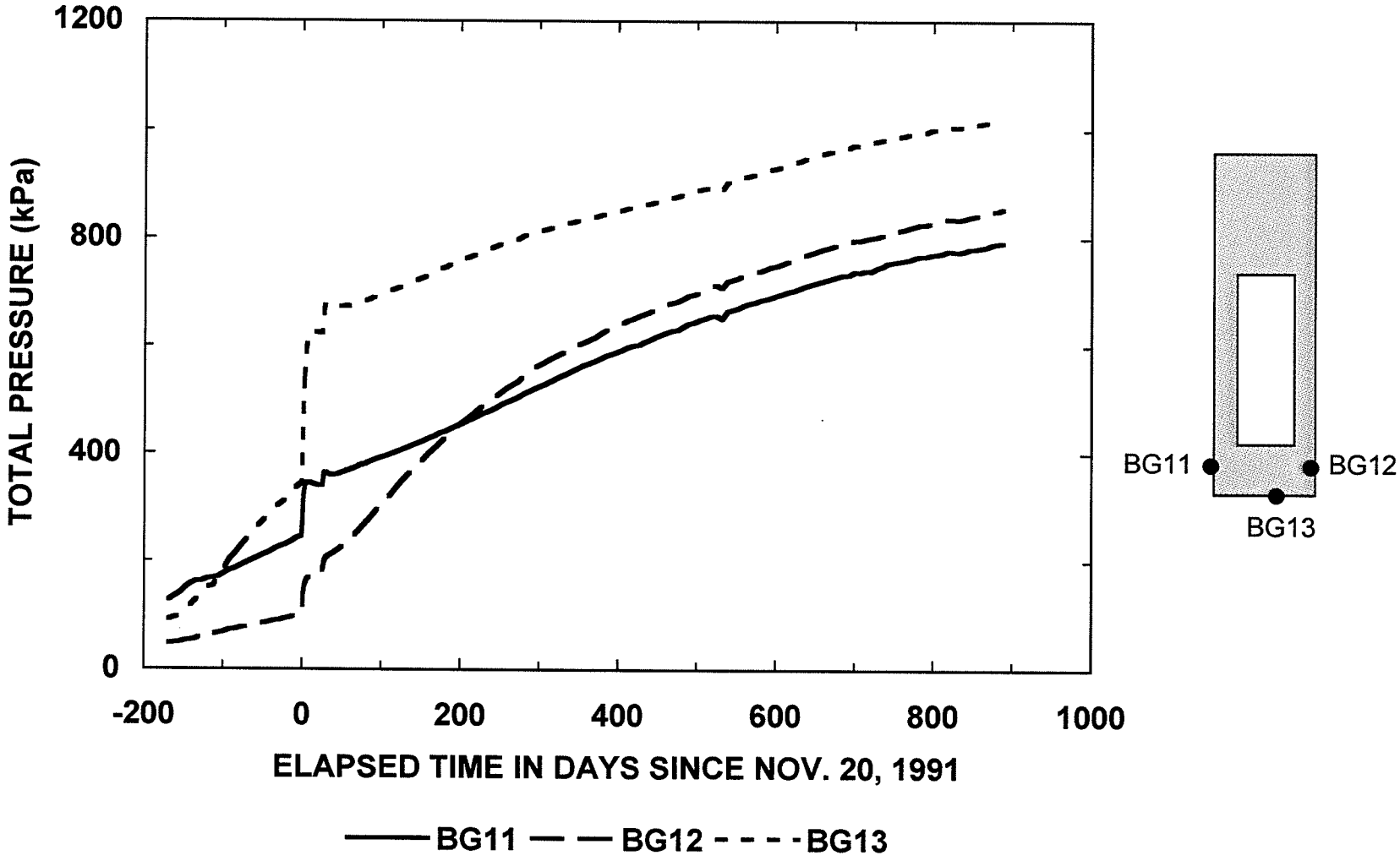

Figure 8.11 Total pressure responses in the Buffer/Container Experiment.

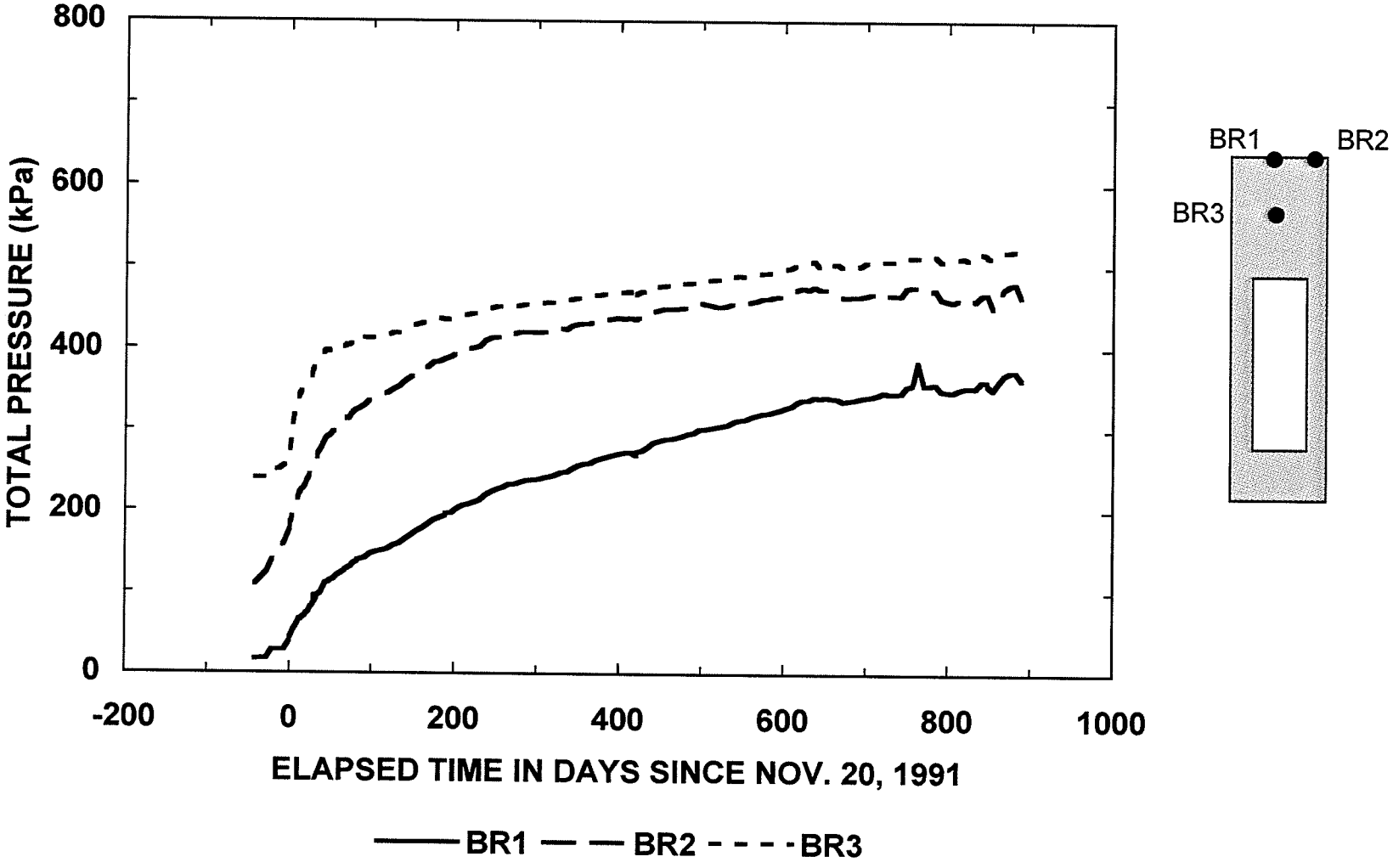

Figure 8.12 Total pressure responses in the Buffer/Container Experiment.

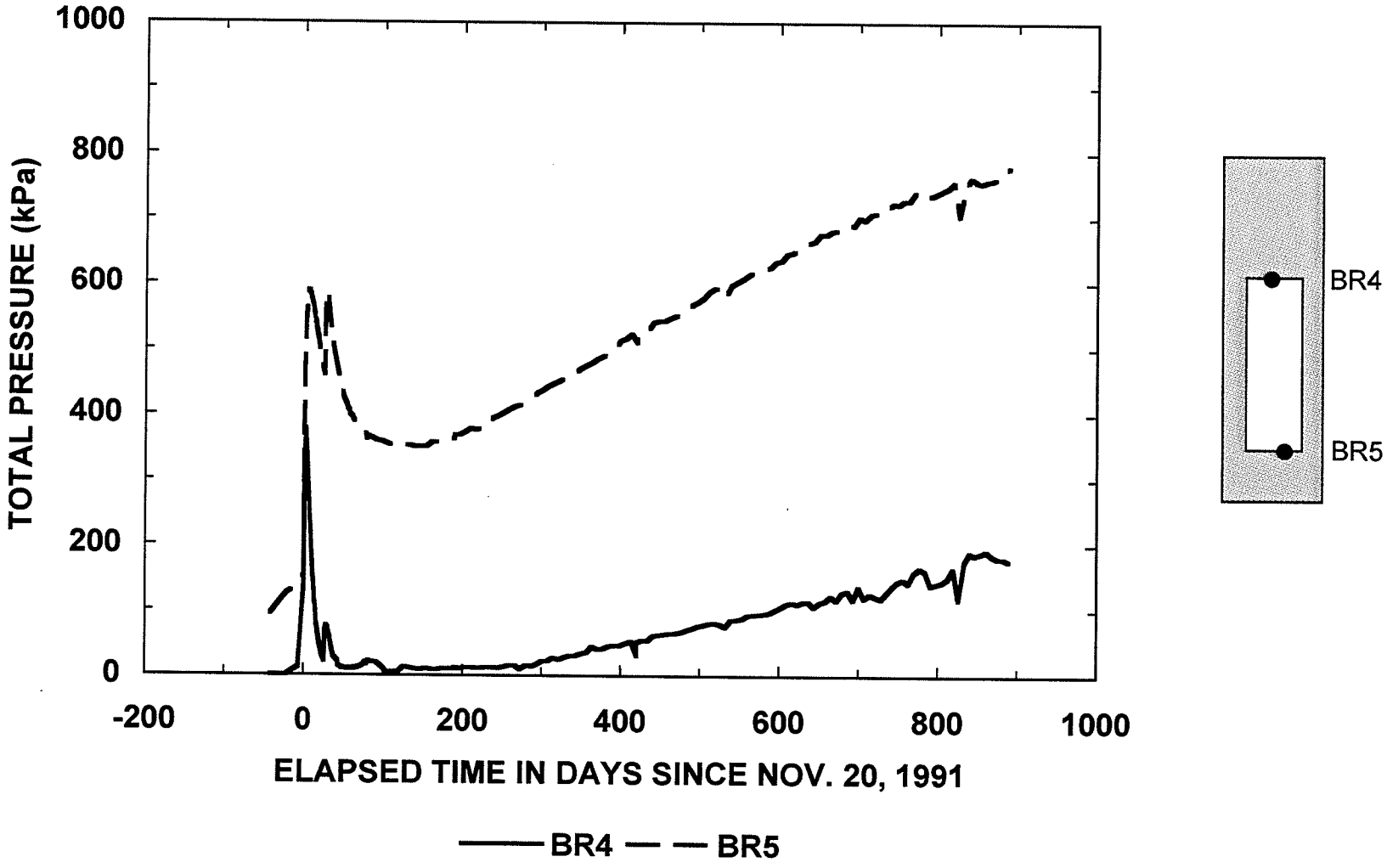

Figure 8.13 Total pressure responses in the Buffer/Container Experiment.

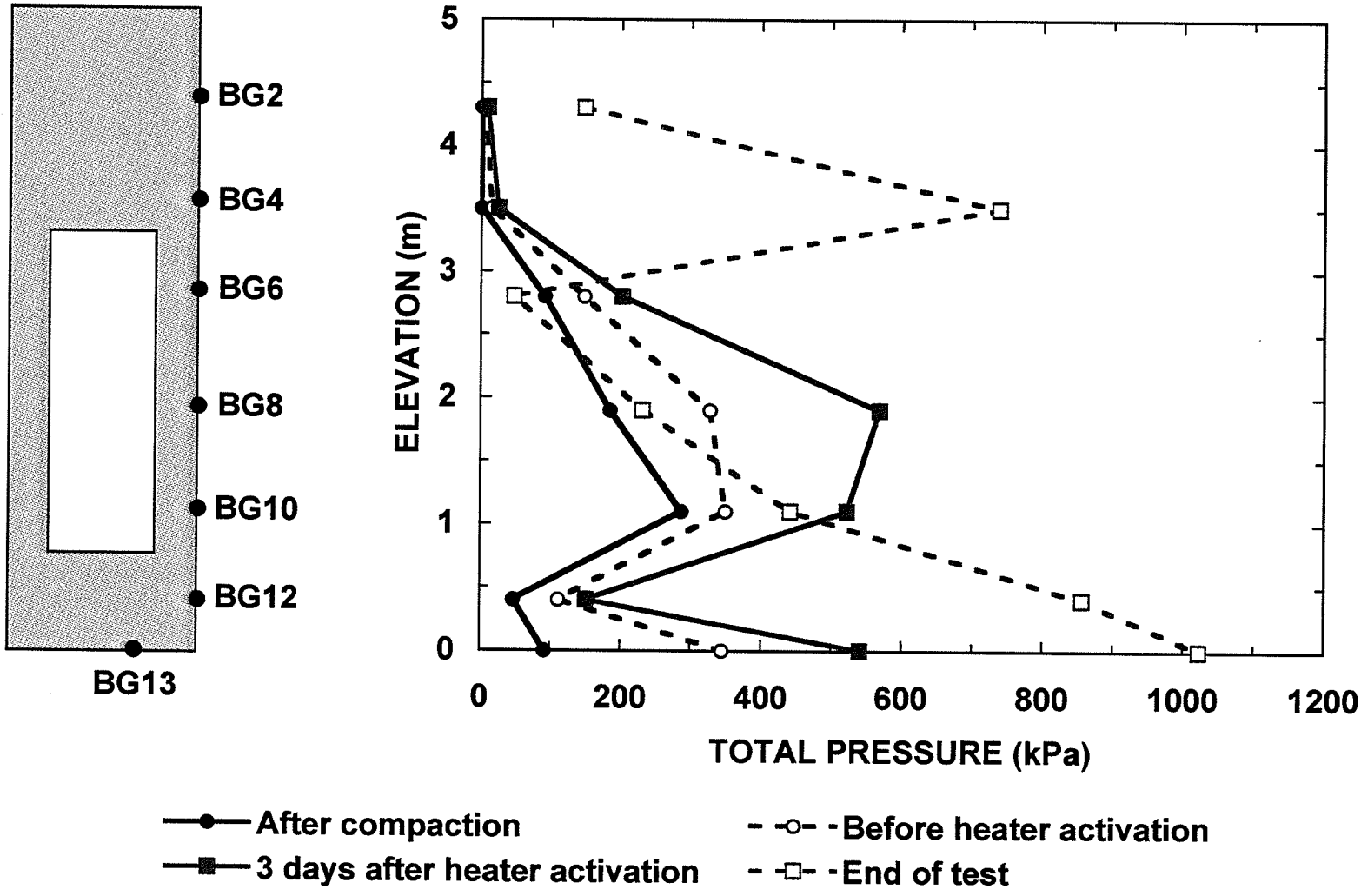

Figure 8.14 Total pressure distributions measured by Geonor total pressure cells along the buffer/rock interface.

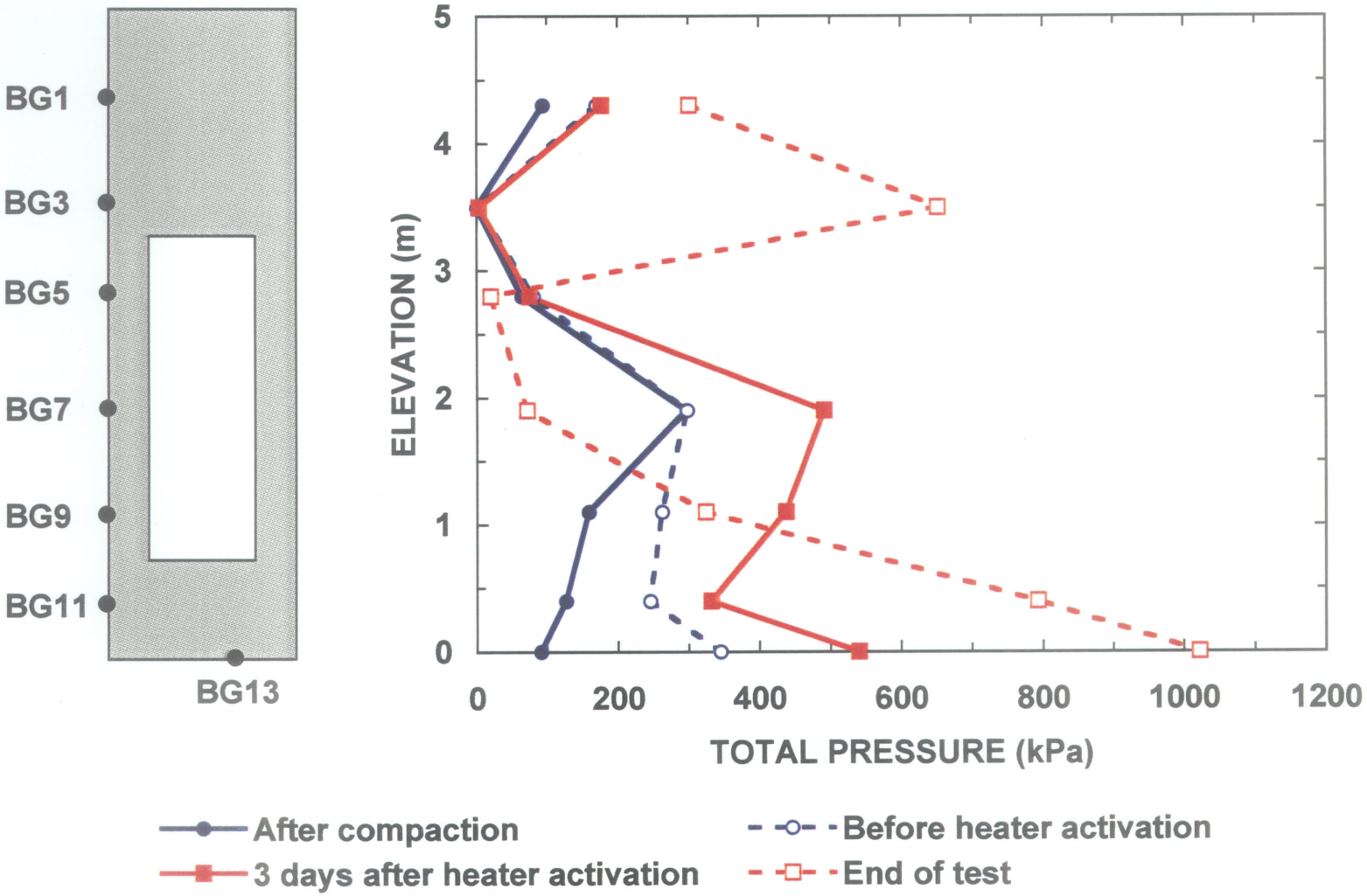

Figure 8.15 Total pressure distributions measured by Geonor total pressure cells along the buffer/rock interface.

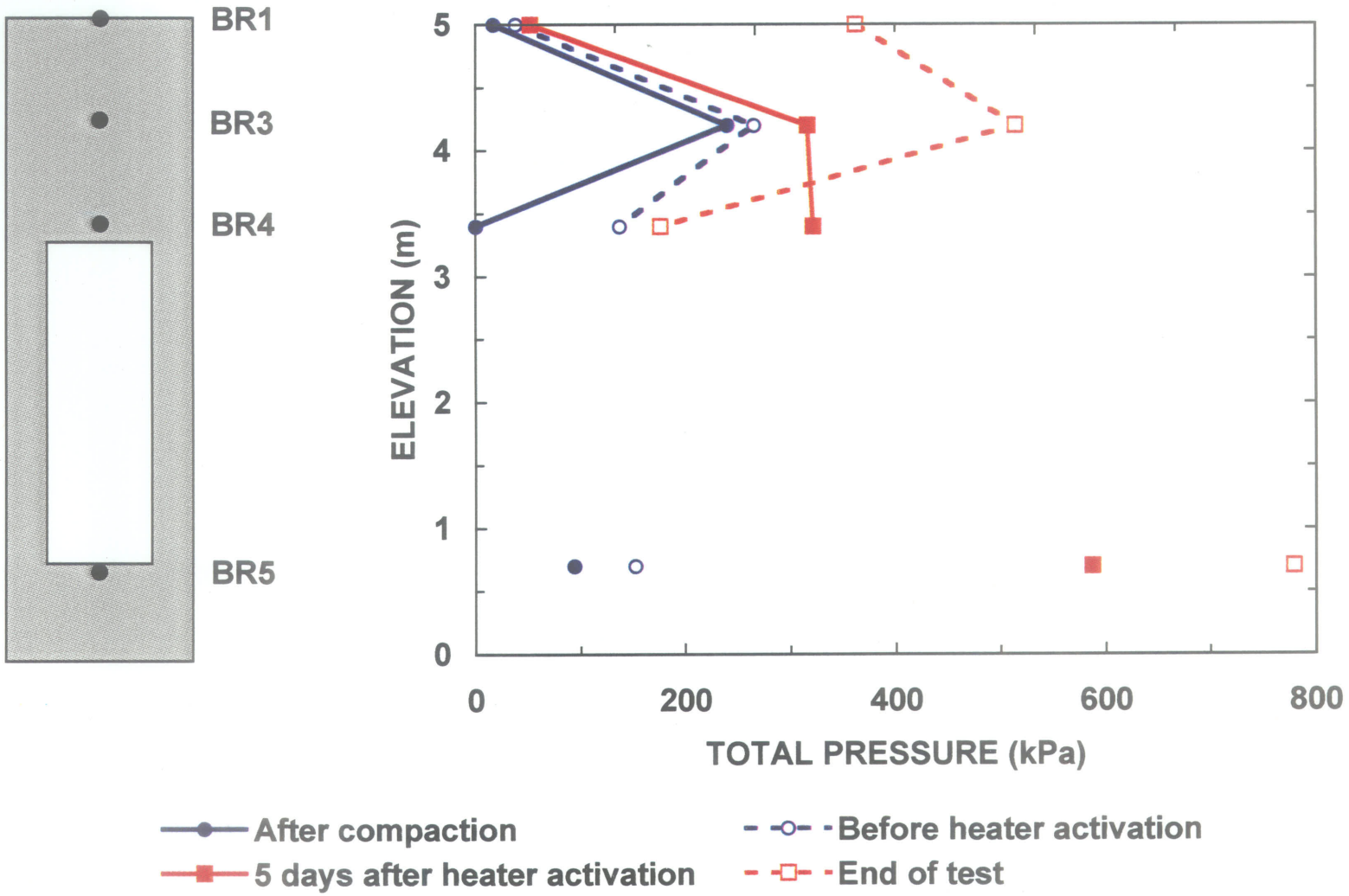

Figure 8.16 Total pressure distributions measured by Roctest pneumatic load cells along the vertical axis of the experiment.

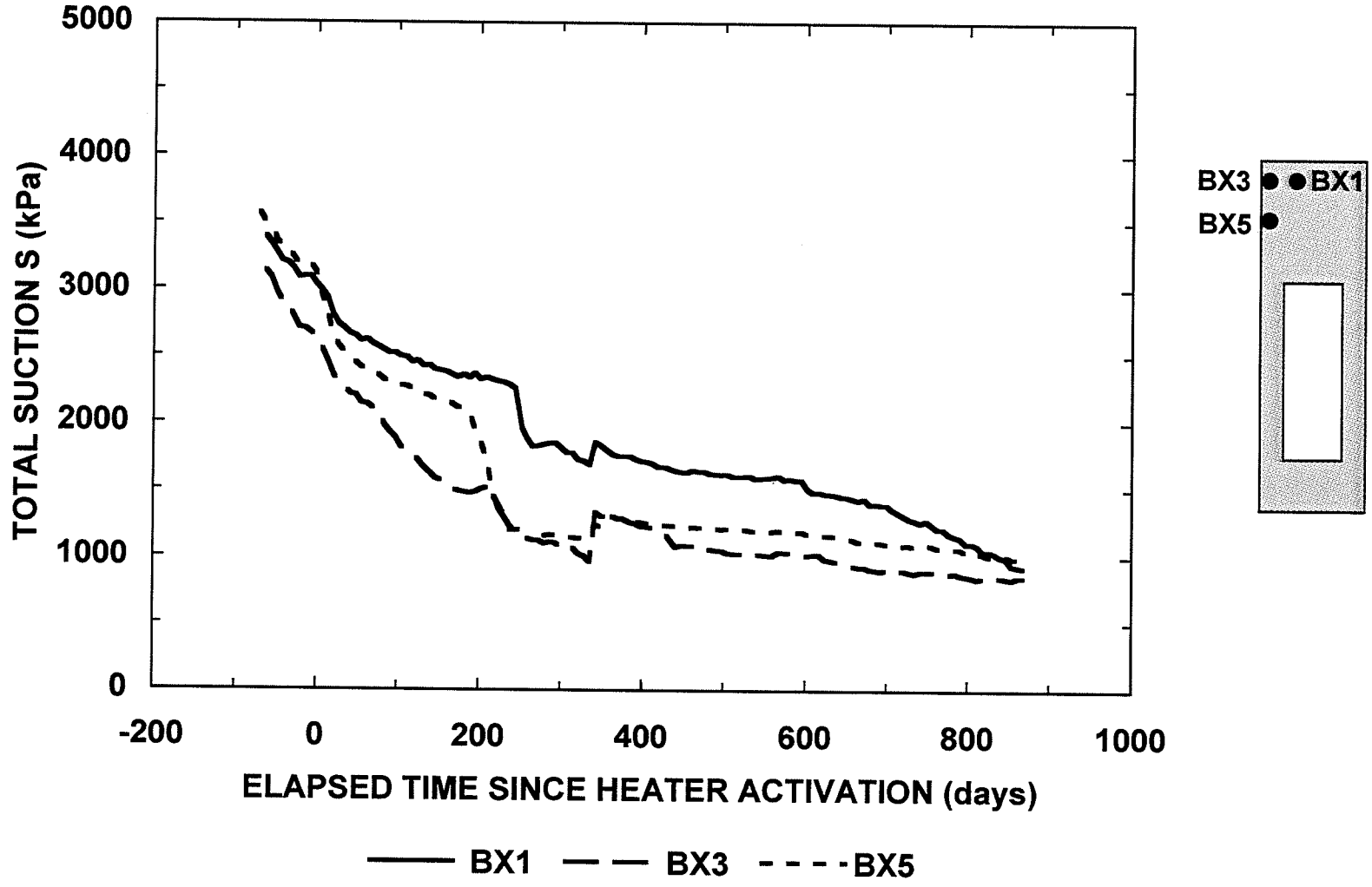

Figure 8.17 Total suction responses in the Buffer/Container Experiment.

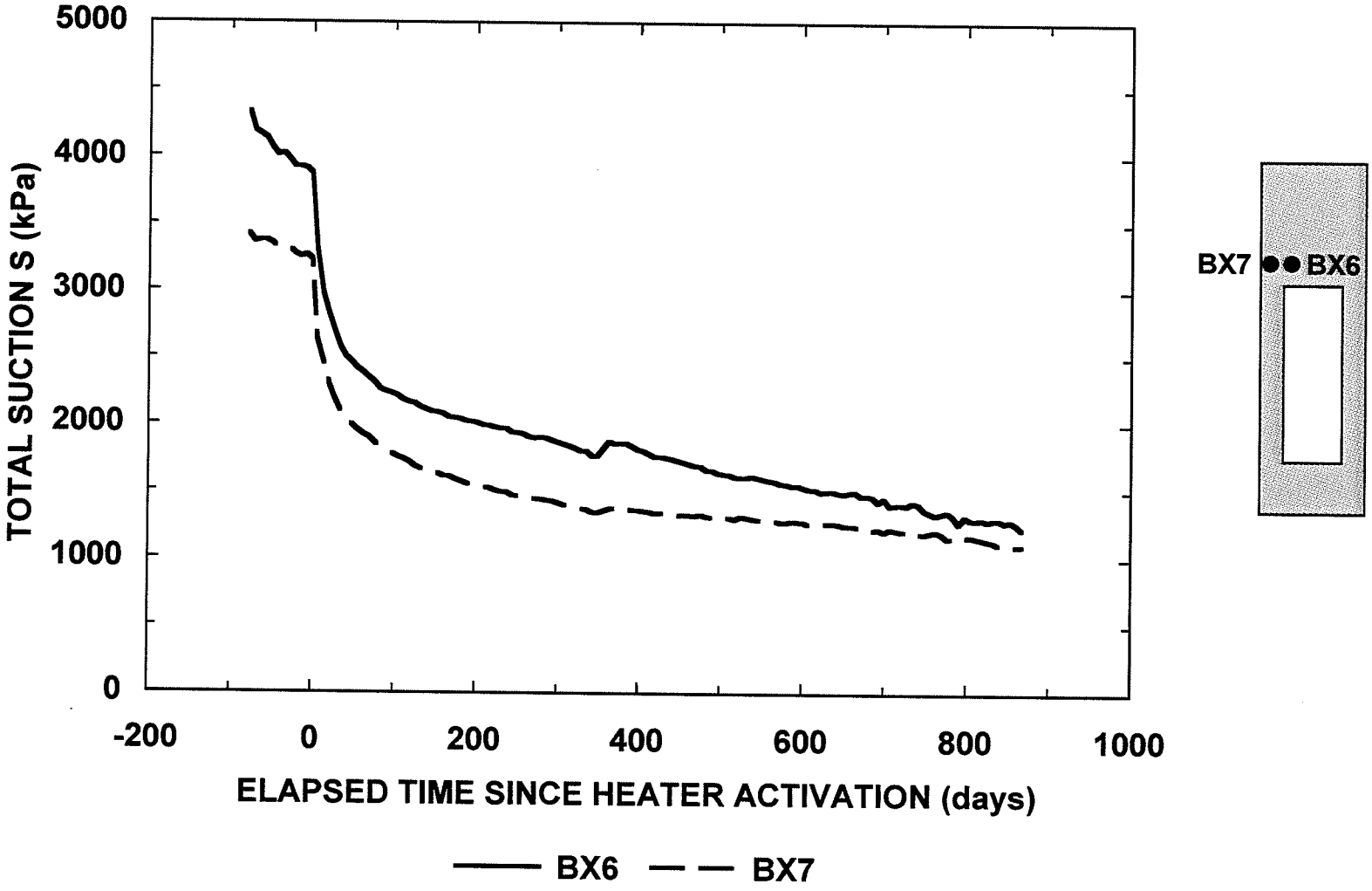

Figure 8.18 Total suction responses in the Buffer/Container Experiment.

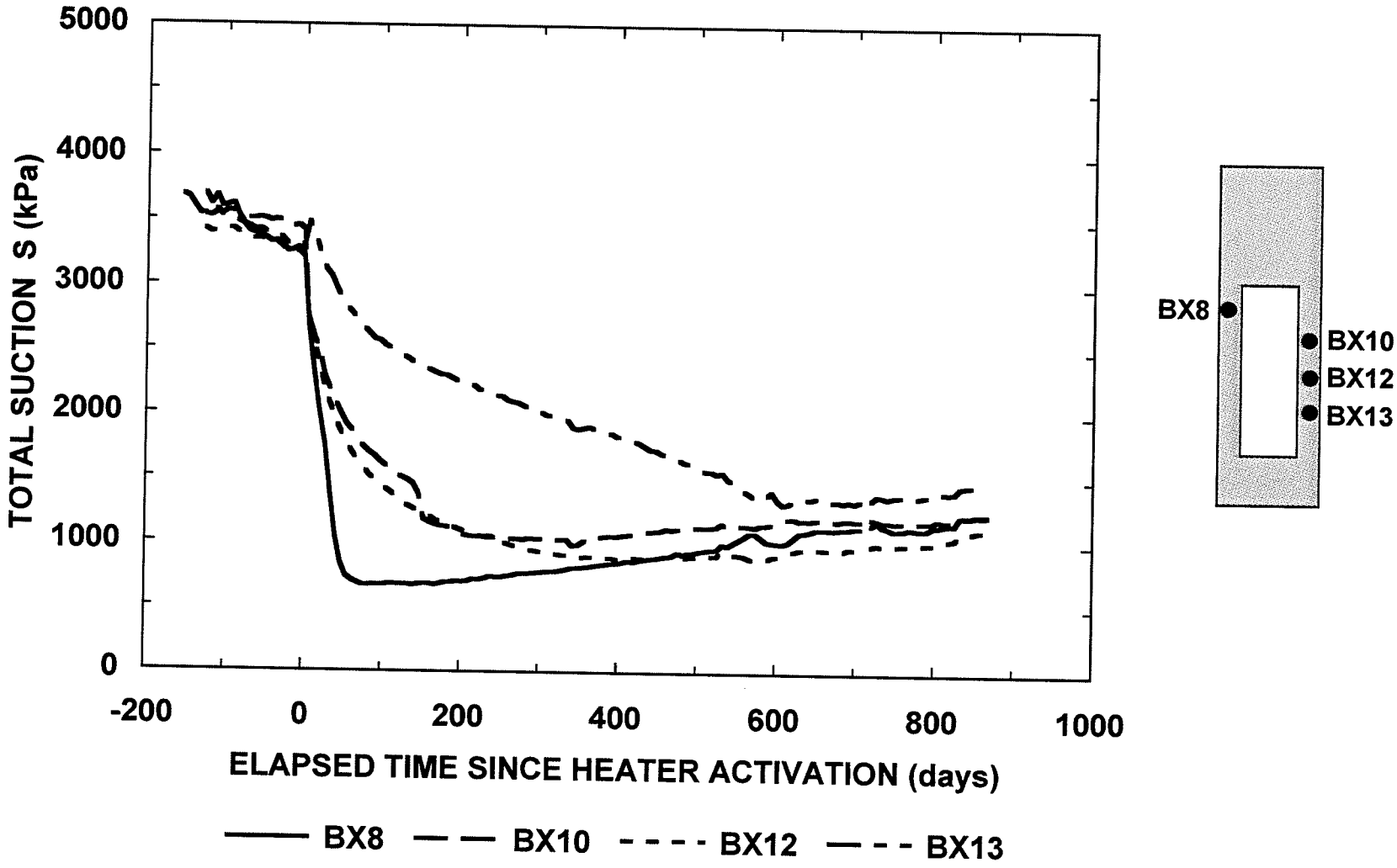

Figure 8.19 Total suction responses in the Buffer/Container Experiment.

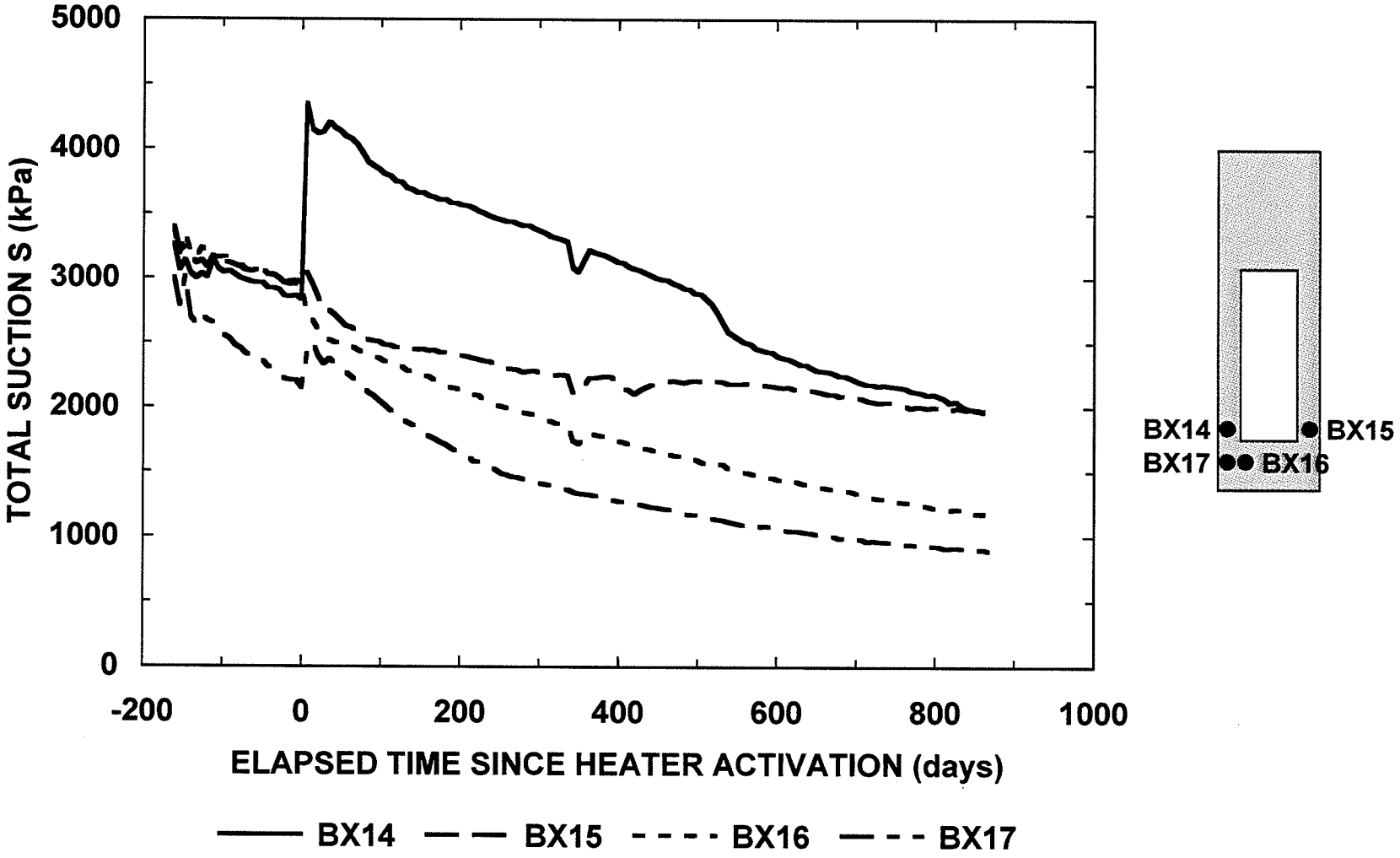

Figure 8.20 Total suction responses in the Buffer/Container Experiment.

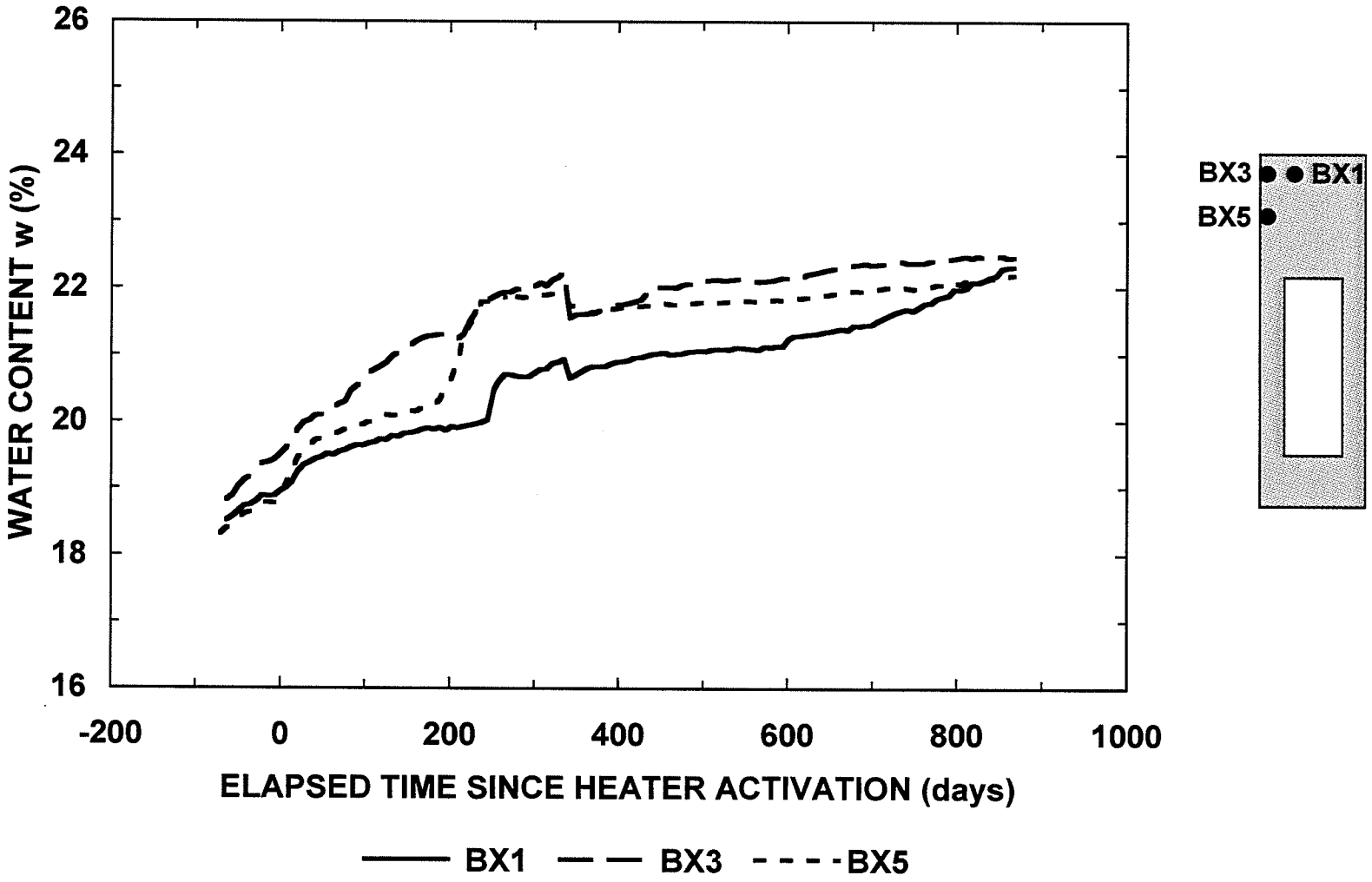

Figure 8.21 Water content-time relationships in the Buffer/Container Experiment determined from psychrometer outputs.

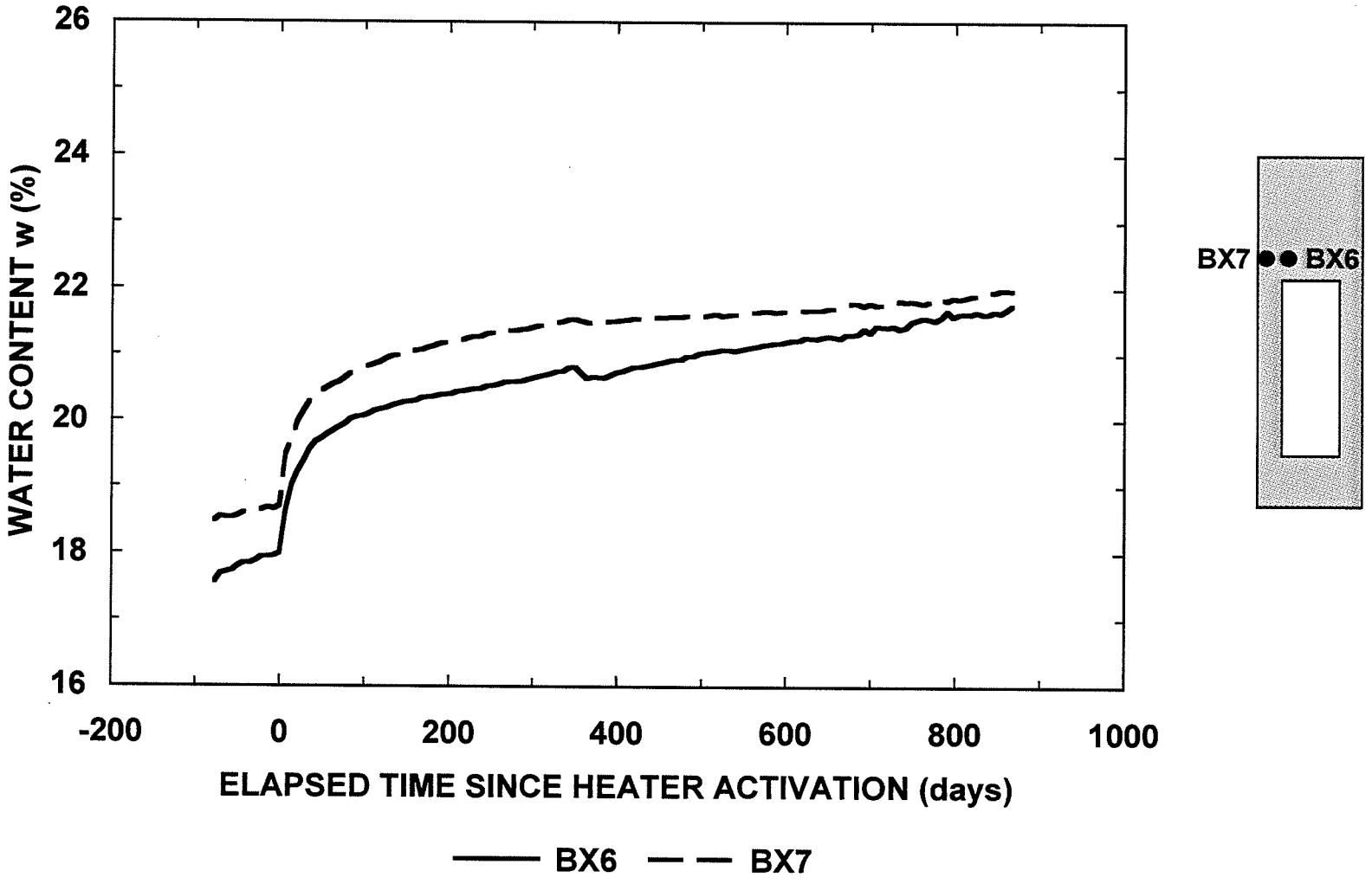

Figure 8.22 Water content-time relationships in the Buffer/Container Experiment determined from psychrometer outputs.

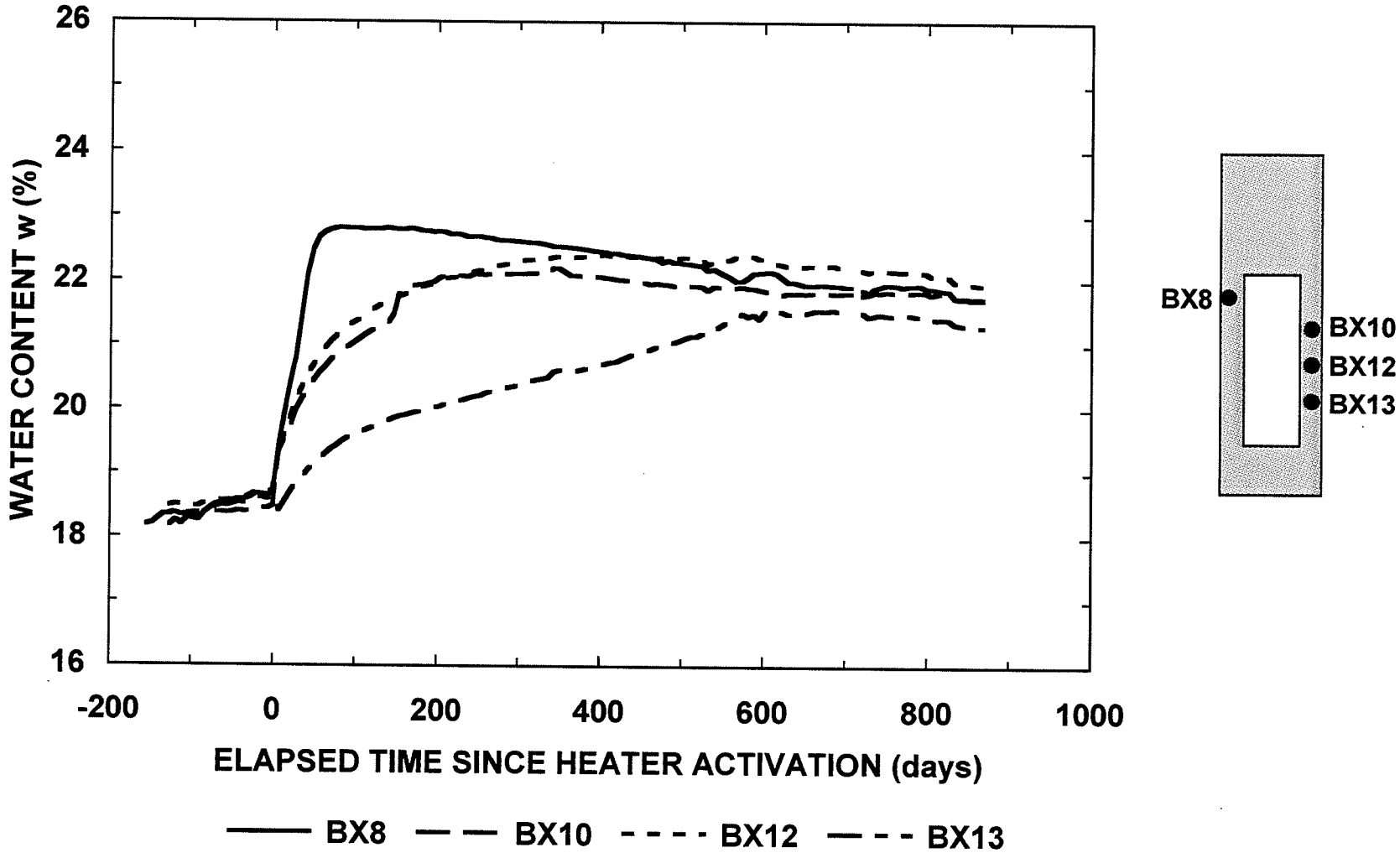

Figure 8.23 Water content-time relationships in the Buffer/Container Experiment determined from psychrometer outputs.

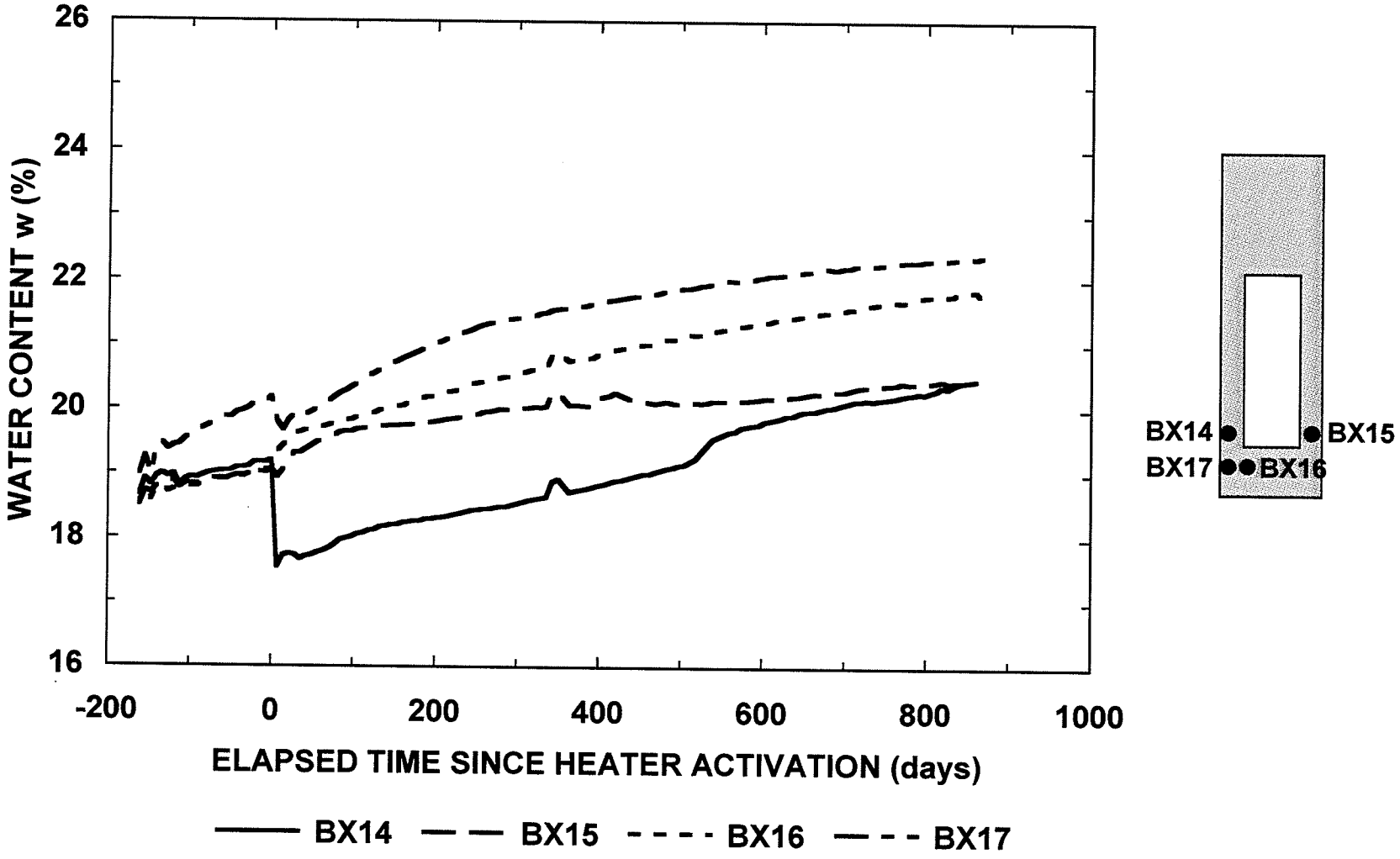

Figure 8.24 Water content-time relationships in the Buffer/Container Experiment determined from psychrometer outputs.

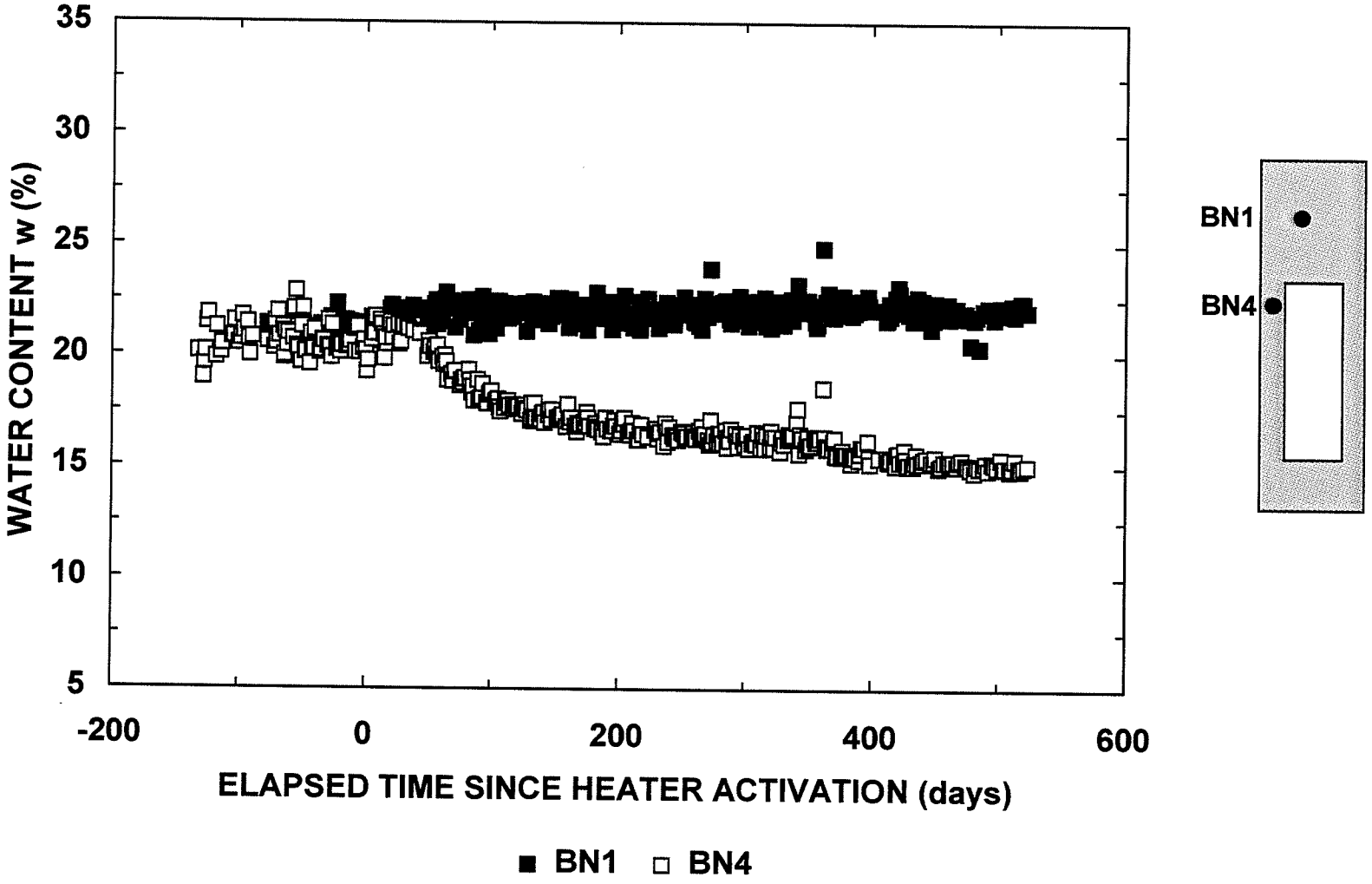

Figure 8.25 Water content-time relationships in the Buffer/Container Experiment measured using thermal needles.

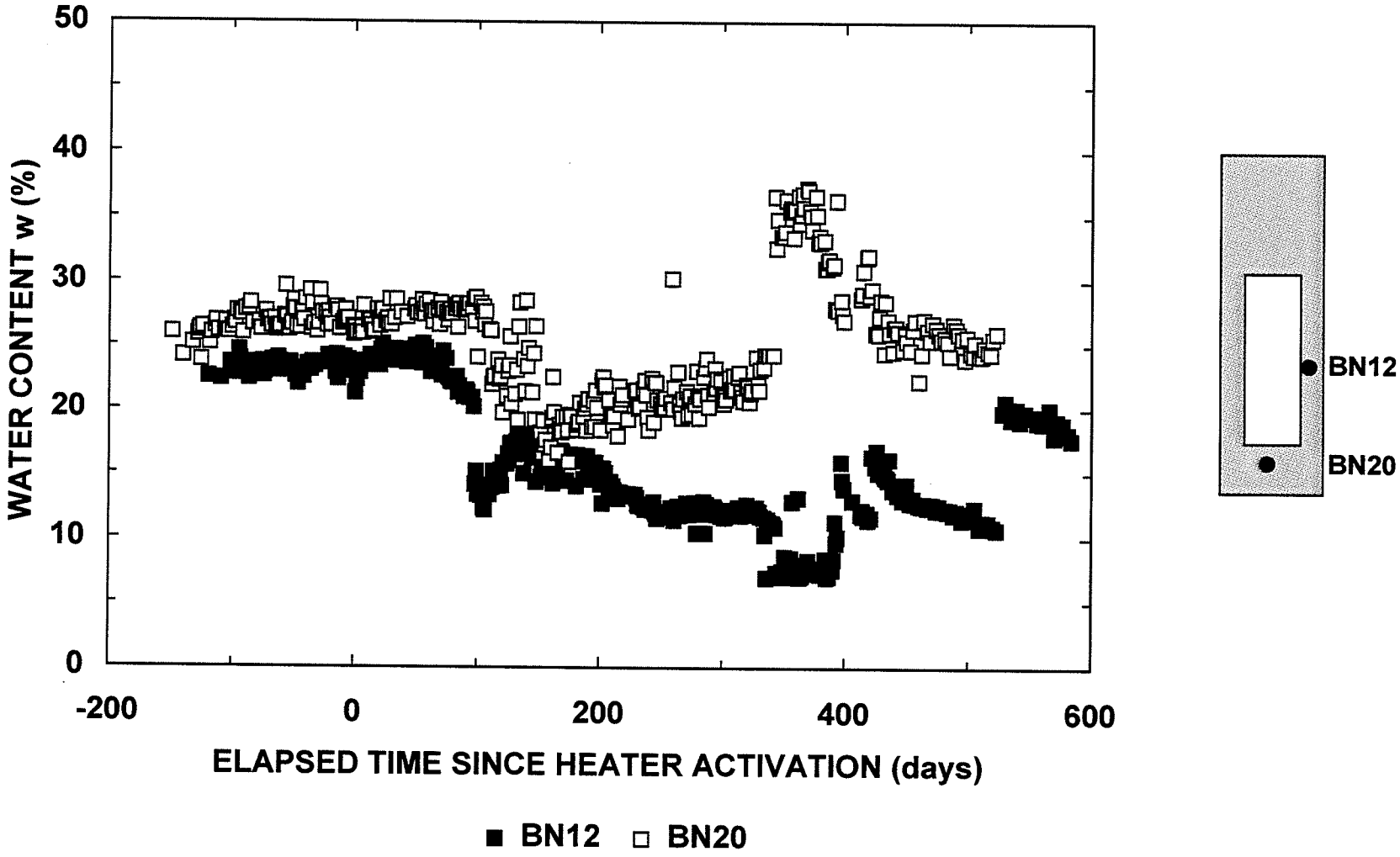

Figure 8.26 Water content-time relationships in the Buffer/Container Experiment measured using thermal needles.

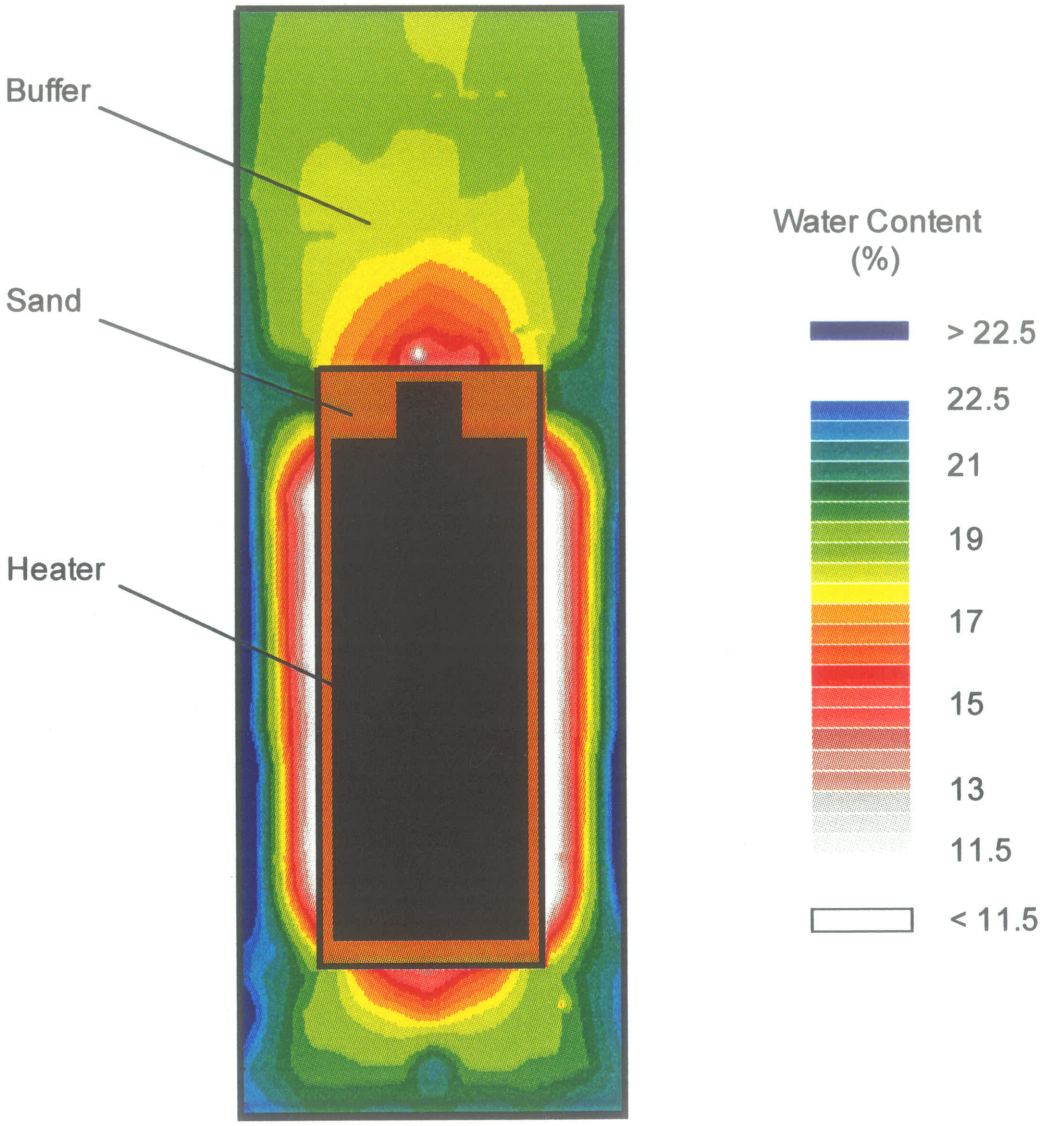

Figure 8.27 End-of-test water content distribution in the Buffer/Container Experiment.

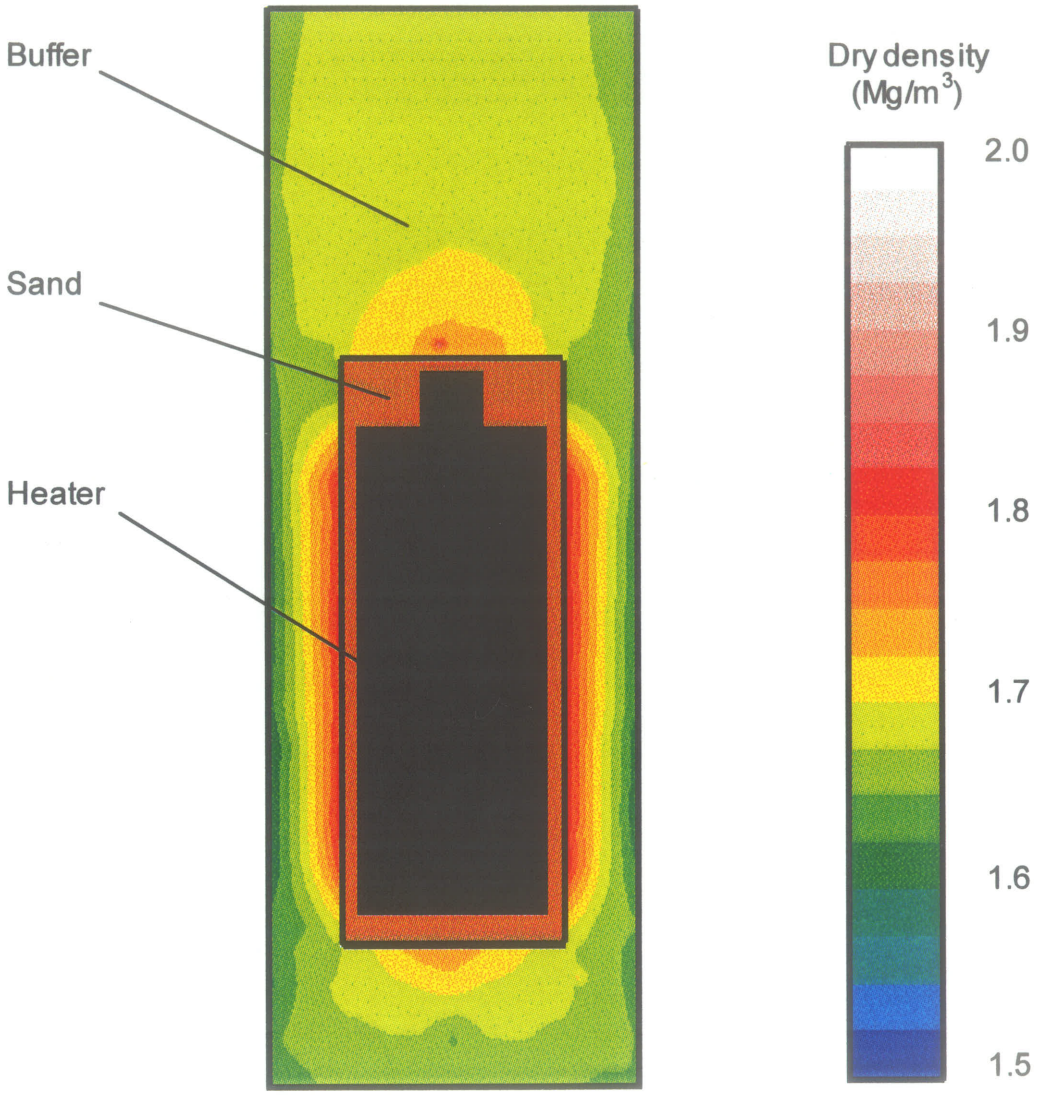

Figure 8.28 End-of-test dry density distribution in the Buffer/Container Experiment.

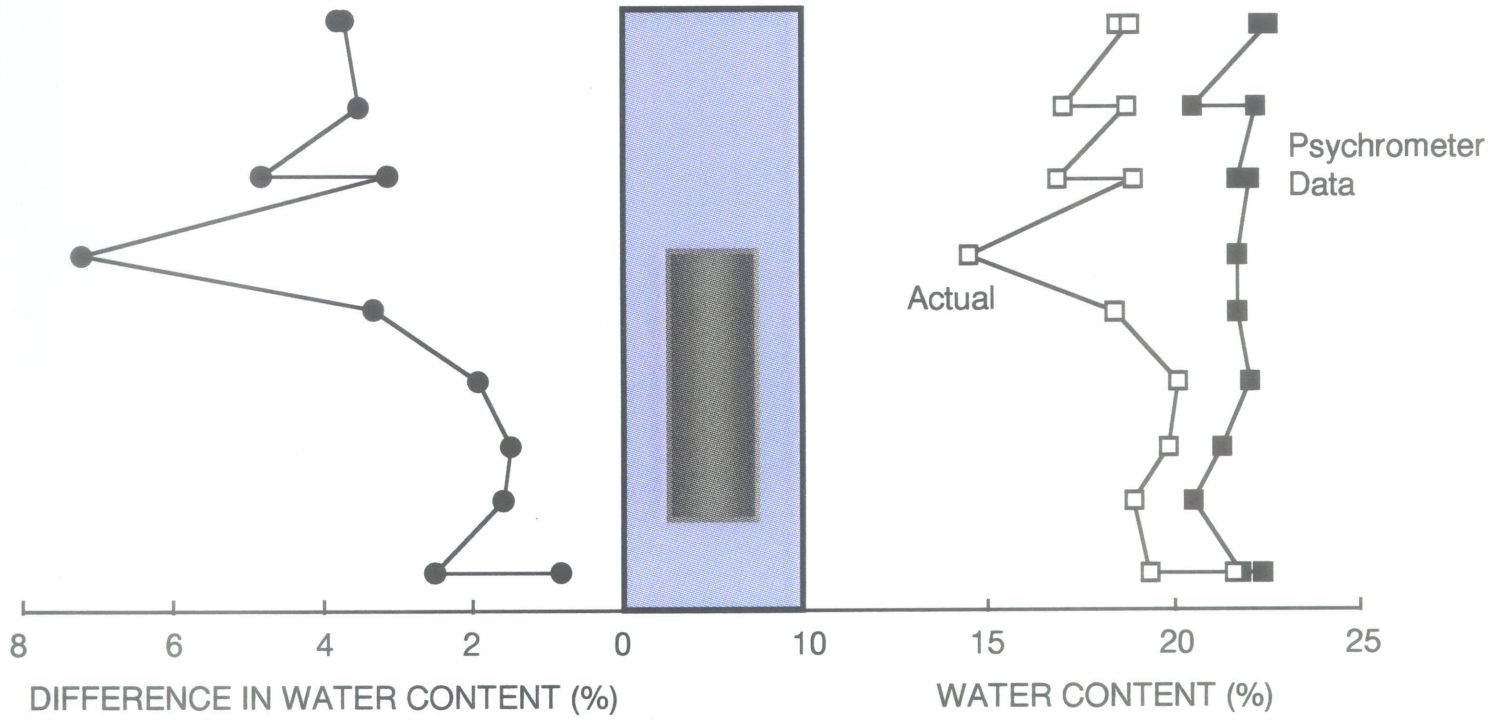

Figure 8.29 Comparison of water content measurements at the end of the Buffer/Container Experiment.

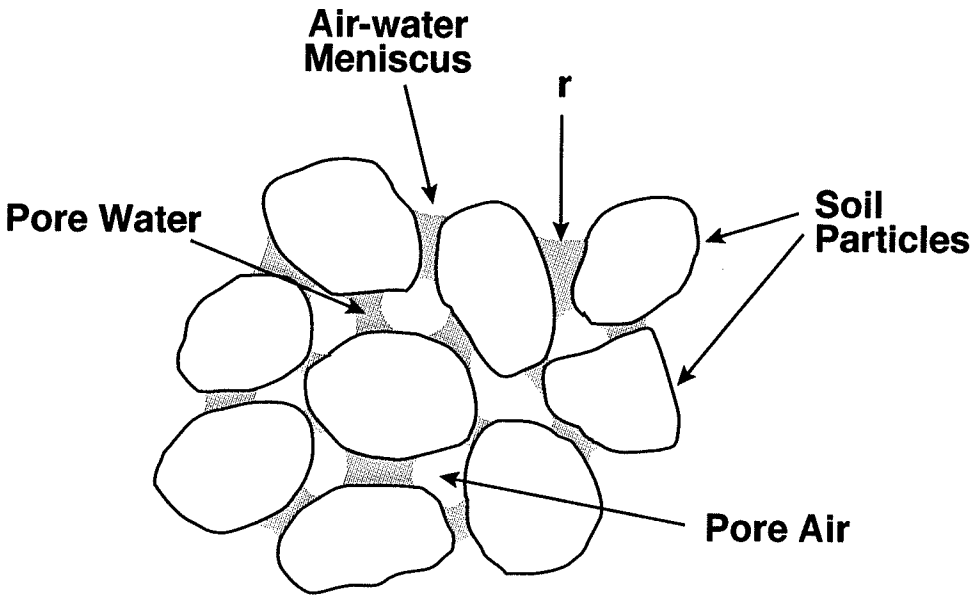

Figure 9.1 A simple unsaturated soil system.

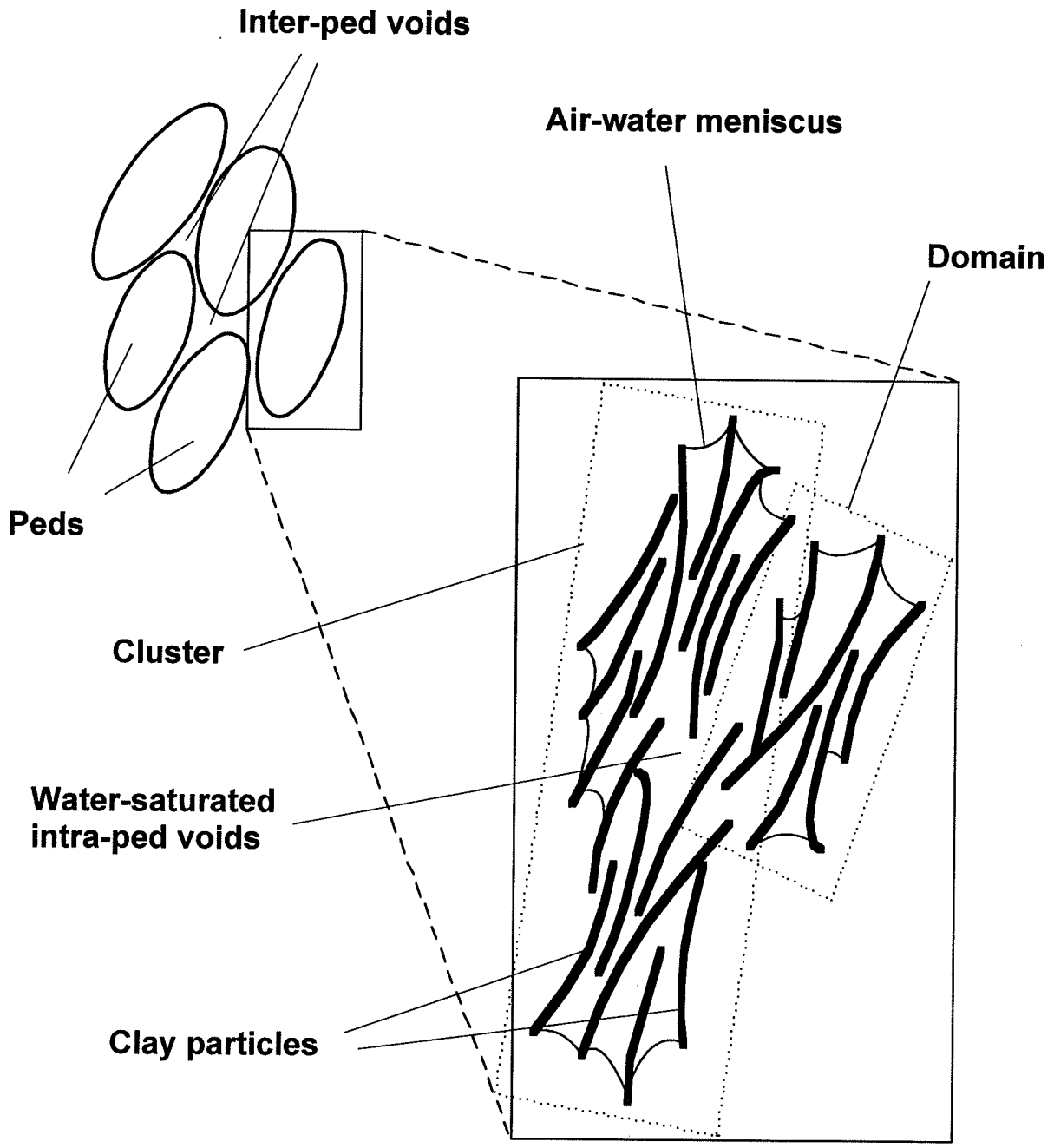

Figure 9.2 Soil structure in a compacted clay.

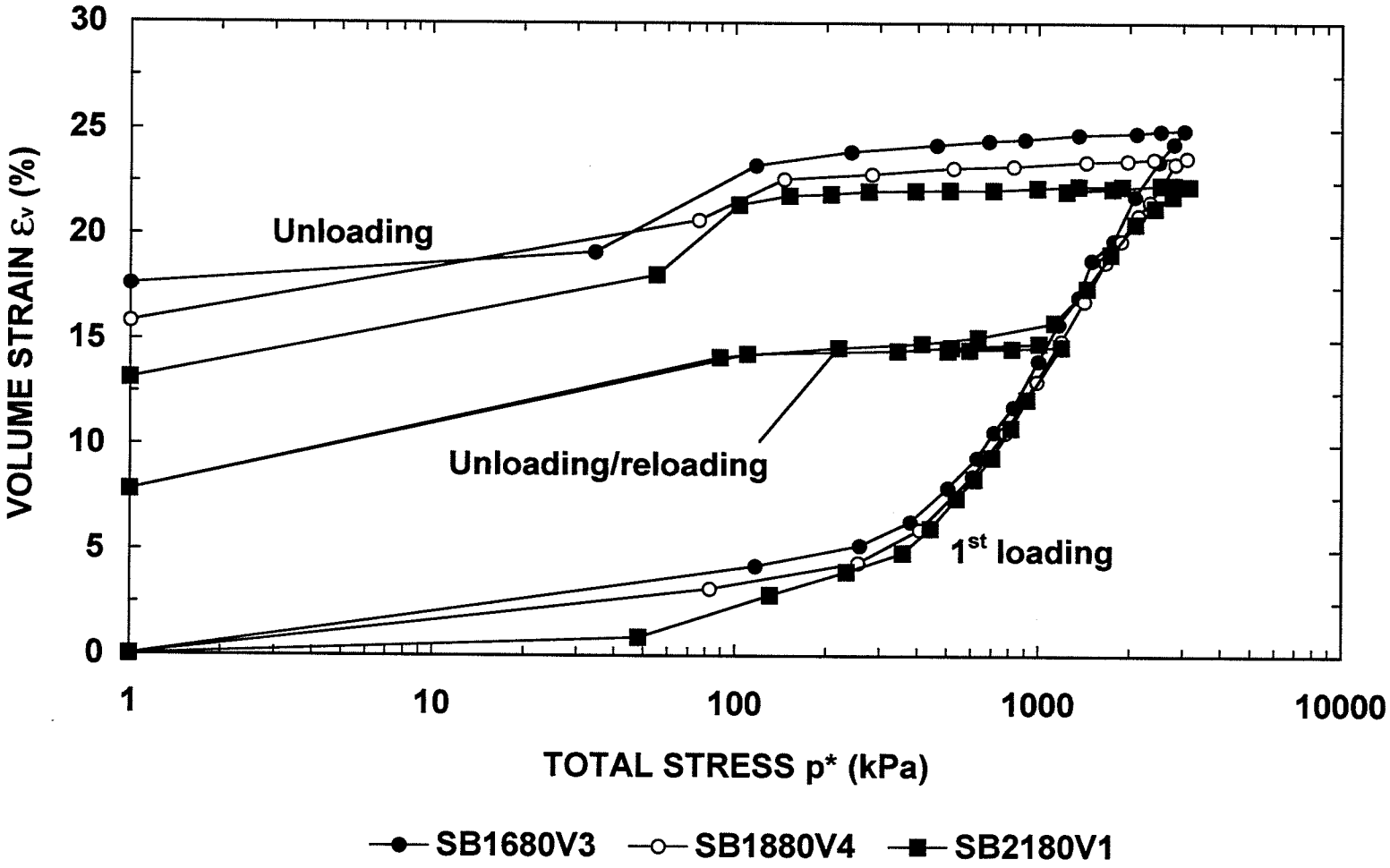

Figure 9.3 Volume strain-total stress relationships of unsaturated sand-bentonite material.

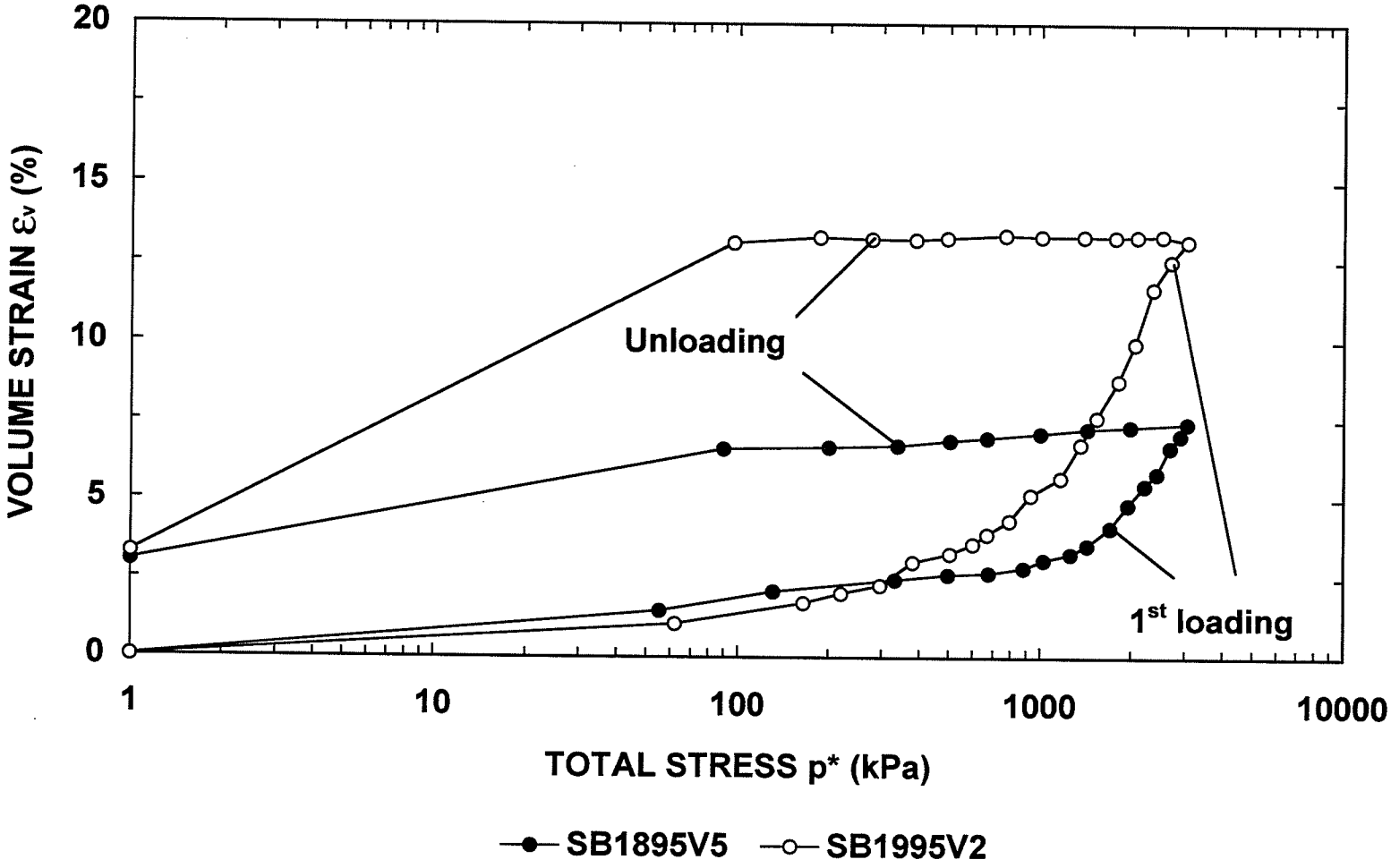

Figure 9.4 Volume strain-total stress relationships of unsaturated sand-bentonite material.

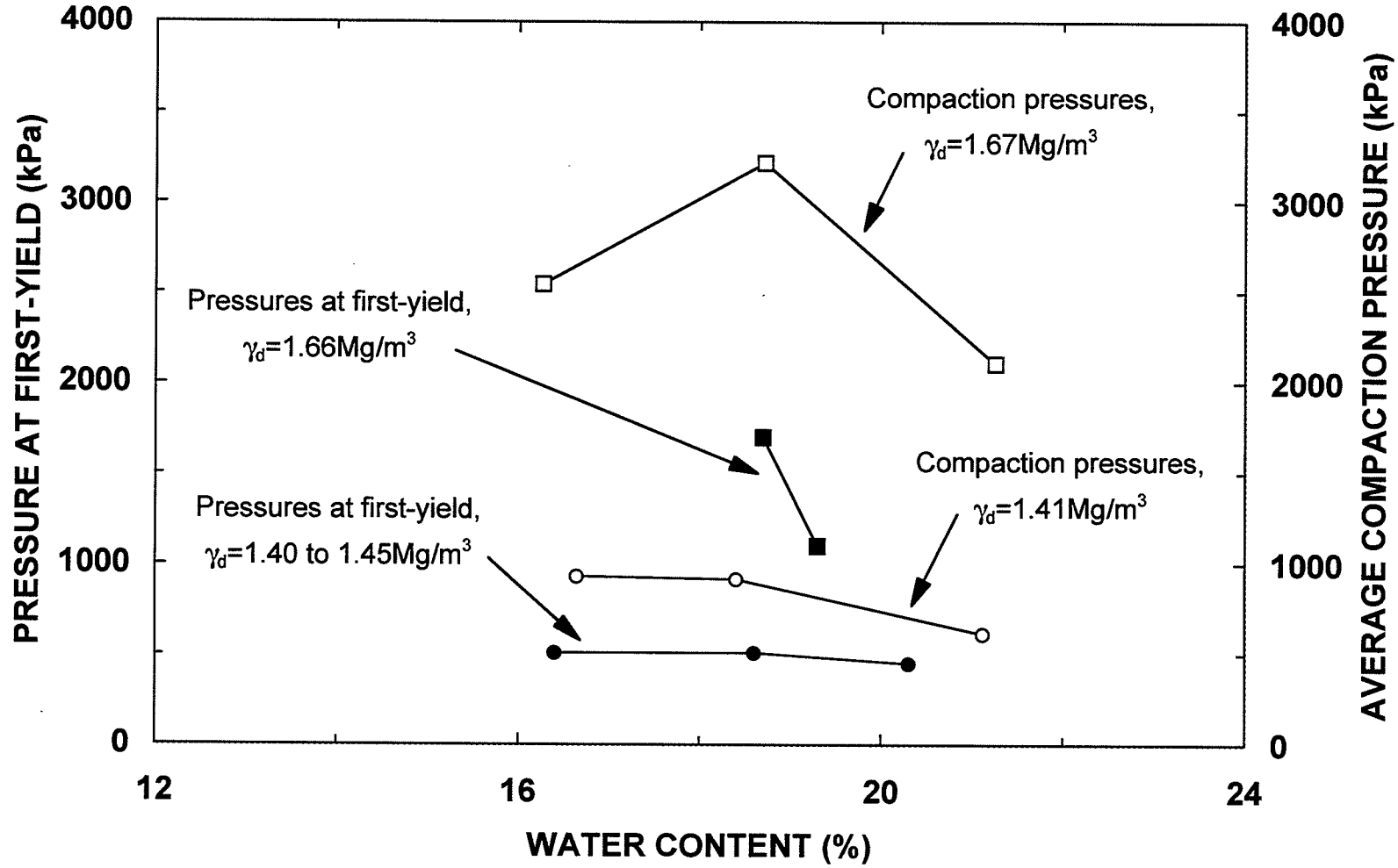

Figure 9.5 Relationship between pressure at first-yield and average compaction pressure in unsaturated sand-bentonite material.

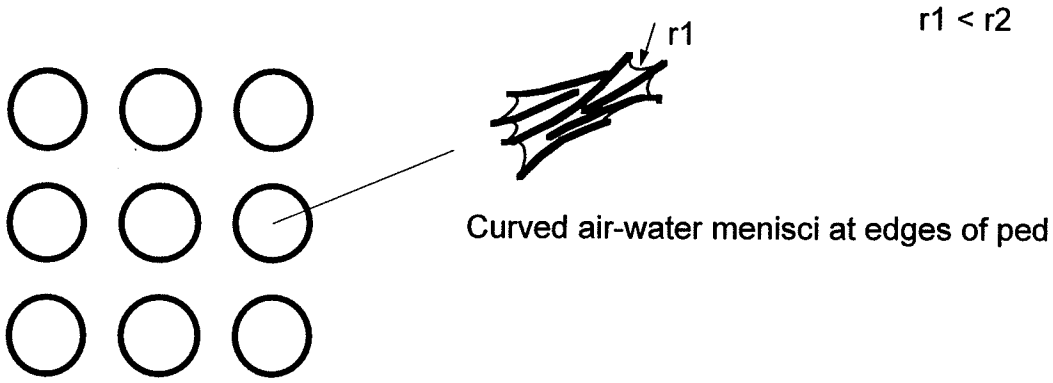

a) A stack of loosely organized sponge balls representing water saturated peds, with inter-ped voids.

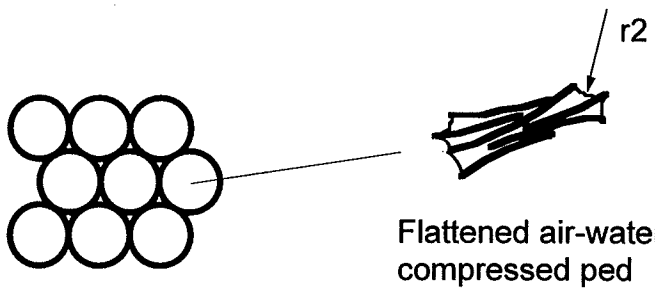

b) Tighter structure of re-organized compressed sponge balls: compressed peds and smaller inter-ped voids.

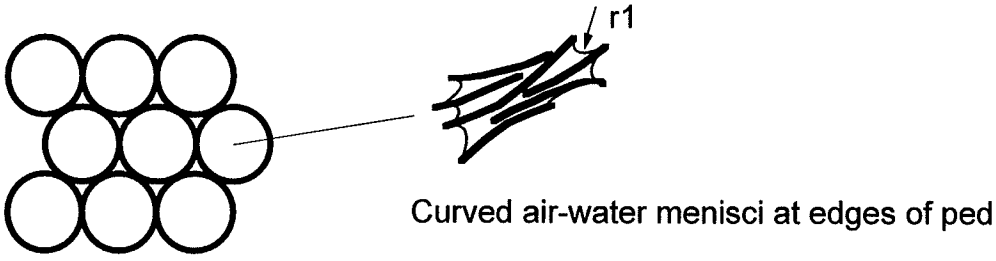

c) New structure of packed uncompressed sponge balls with smaller inter-ped voids.

Figure 9.6 Sponge-ball model to demonstrate the effect of compression on soil macro- and micro-structures.

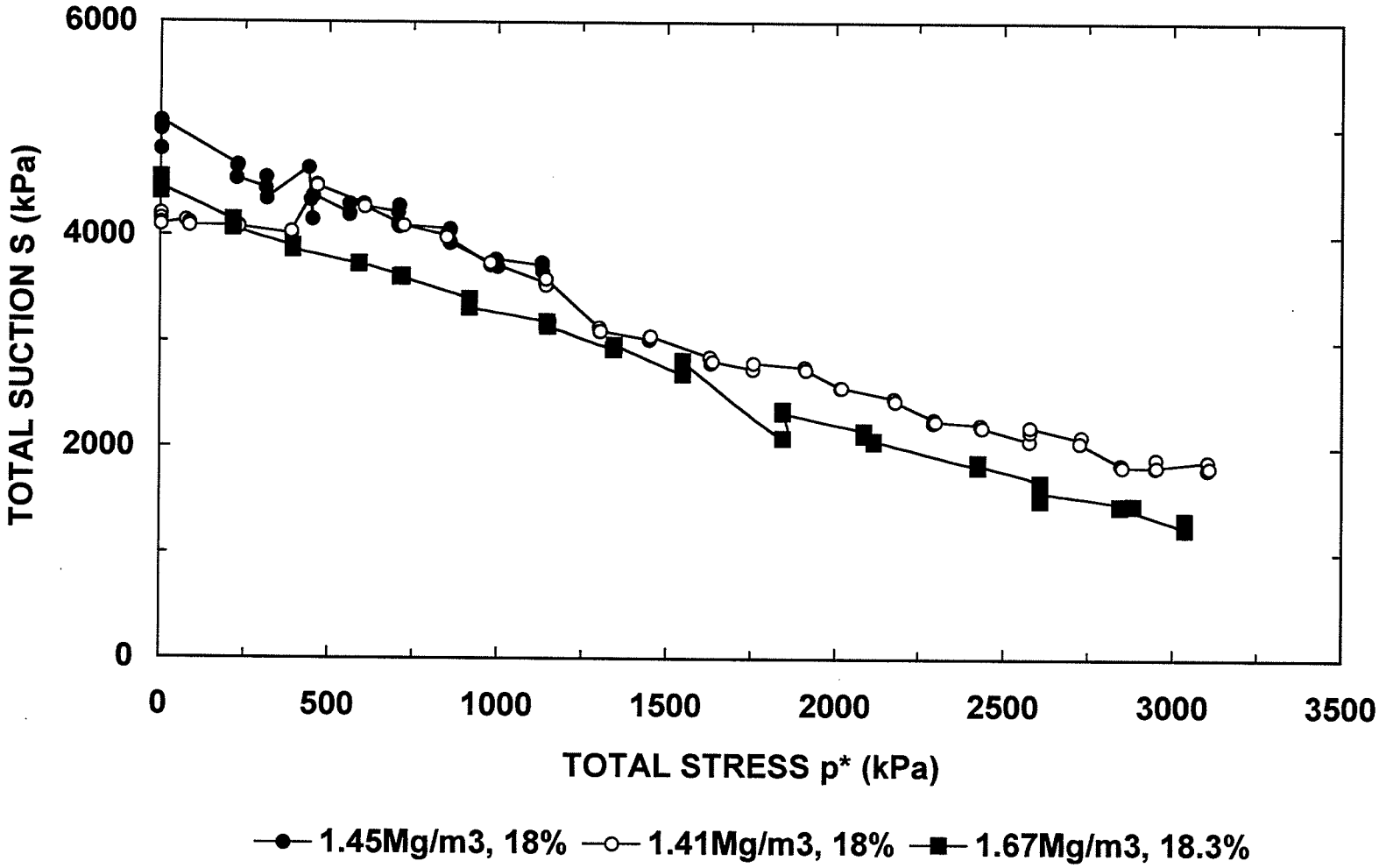

Figure 9.7 Comparison of total suction-total stress relationships of unsaturated sand-bentonite specimens formed to specified dry densities and water contents.

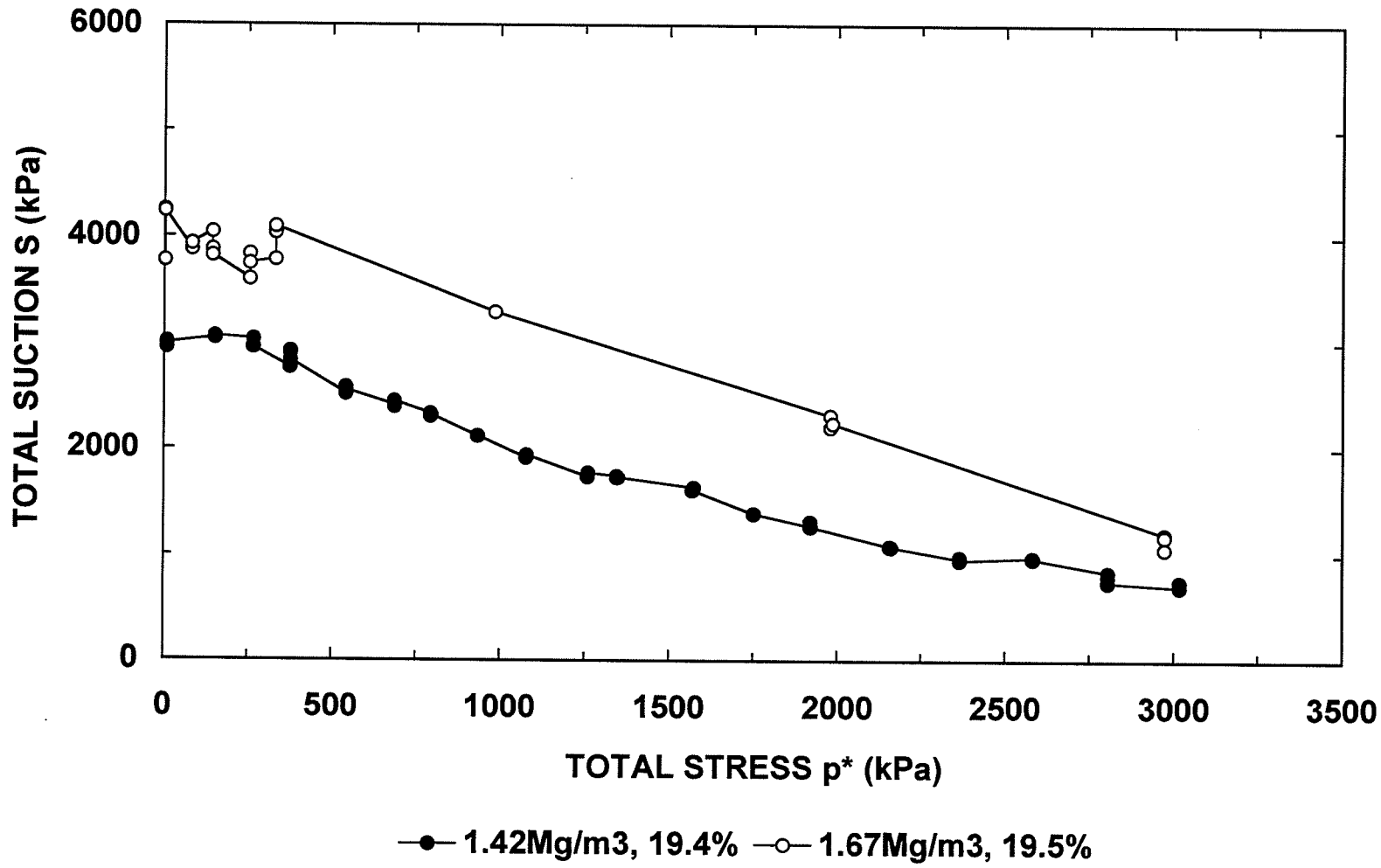

Figure 9.8 Comparison of total suction-total stress relationships of unsaturated sand-bentonite specimens formed to specified dry densities and water contents.

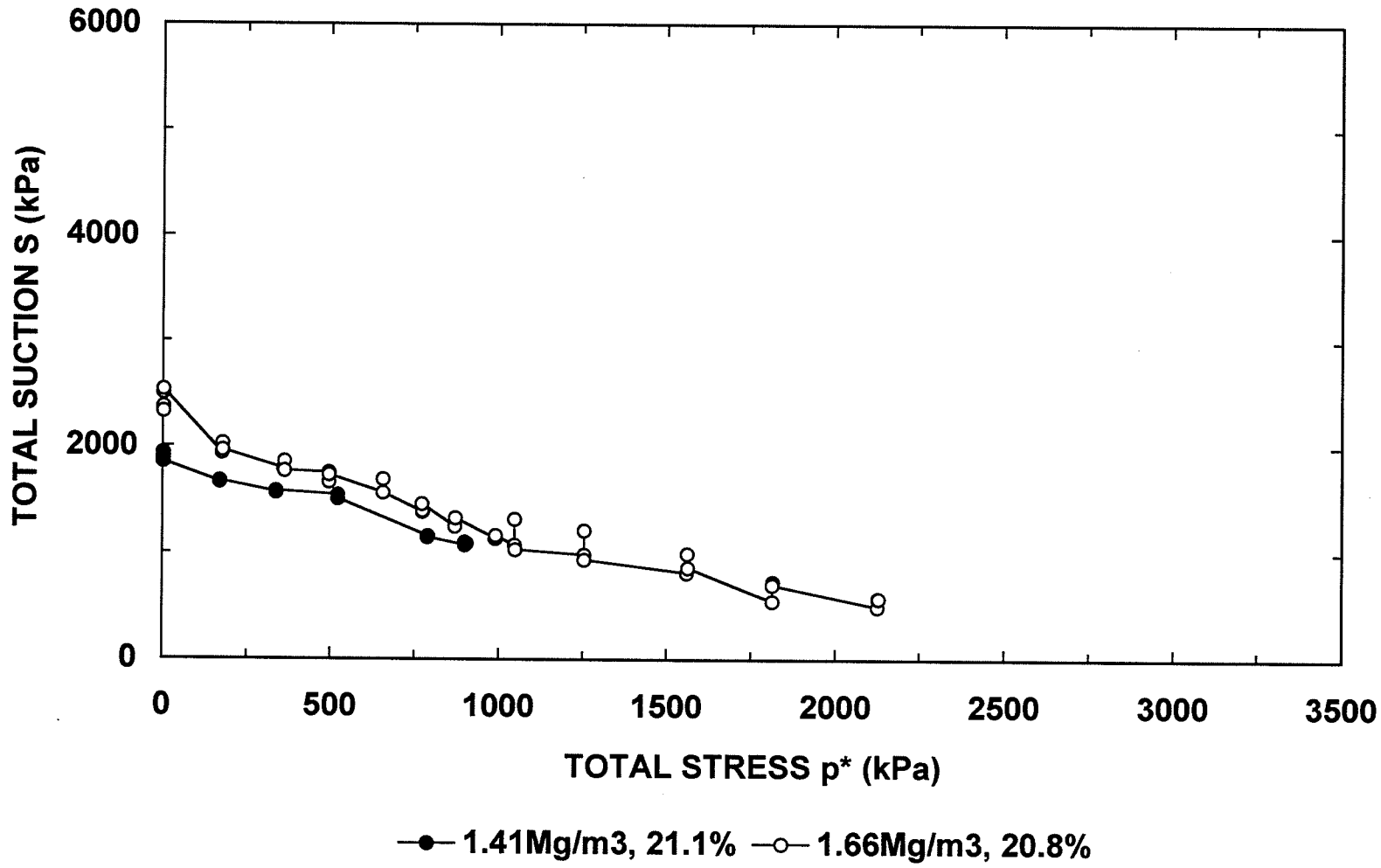

Figure 9.9 Comparison of total suction-total stress relationships of unsaturated sand-bentonite specimens formed to specified dry densities and water contents.

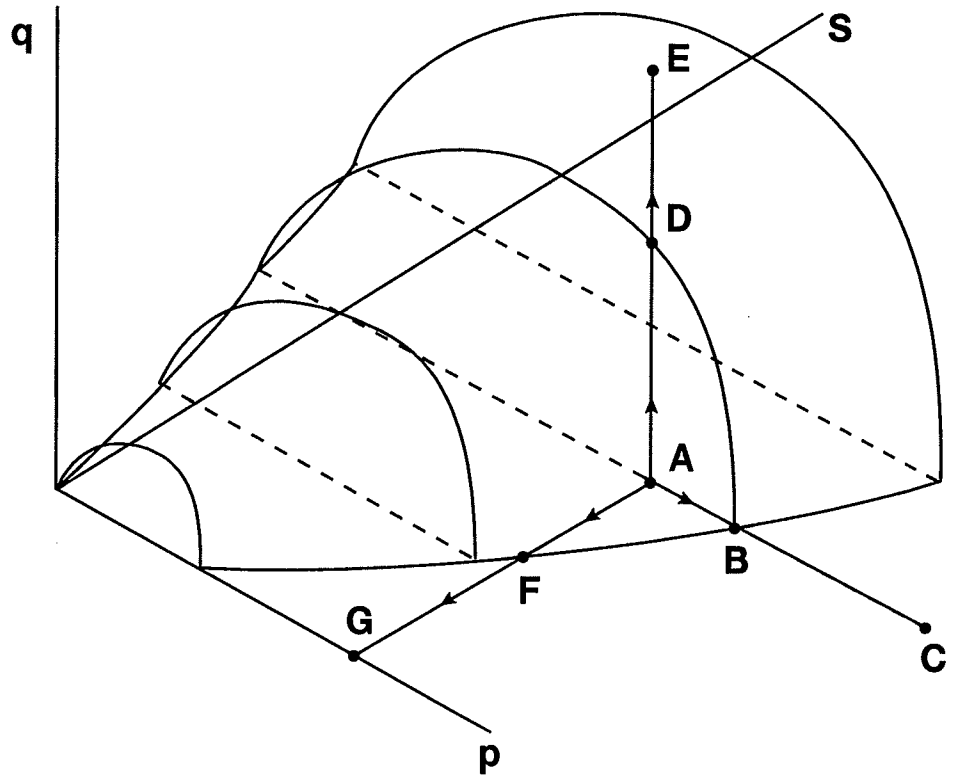

Figure 9.10 Yield surface for unsaturated soils (after Wheeler and Sivakumar, 1995). (Note: The yield surfaces on which points C, E, and G lie are omitted for clarity)

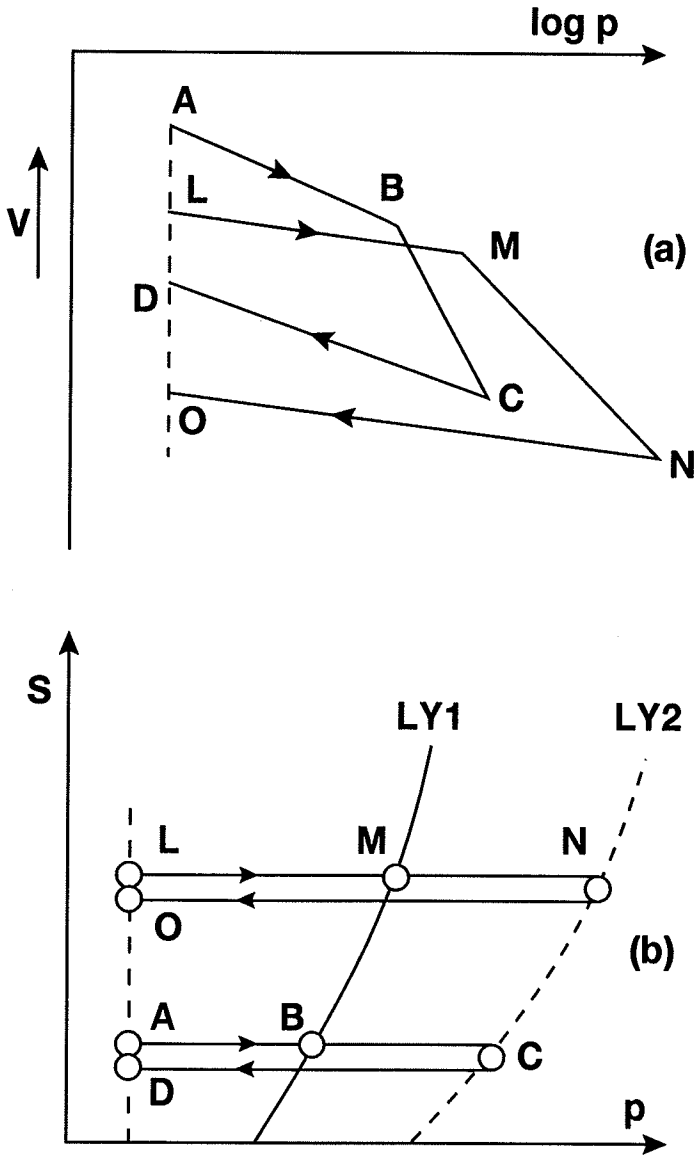

Figure 9.11 Schematic of load-induced yielding and development of a hardening surface (after Alonso et al., 1987).

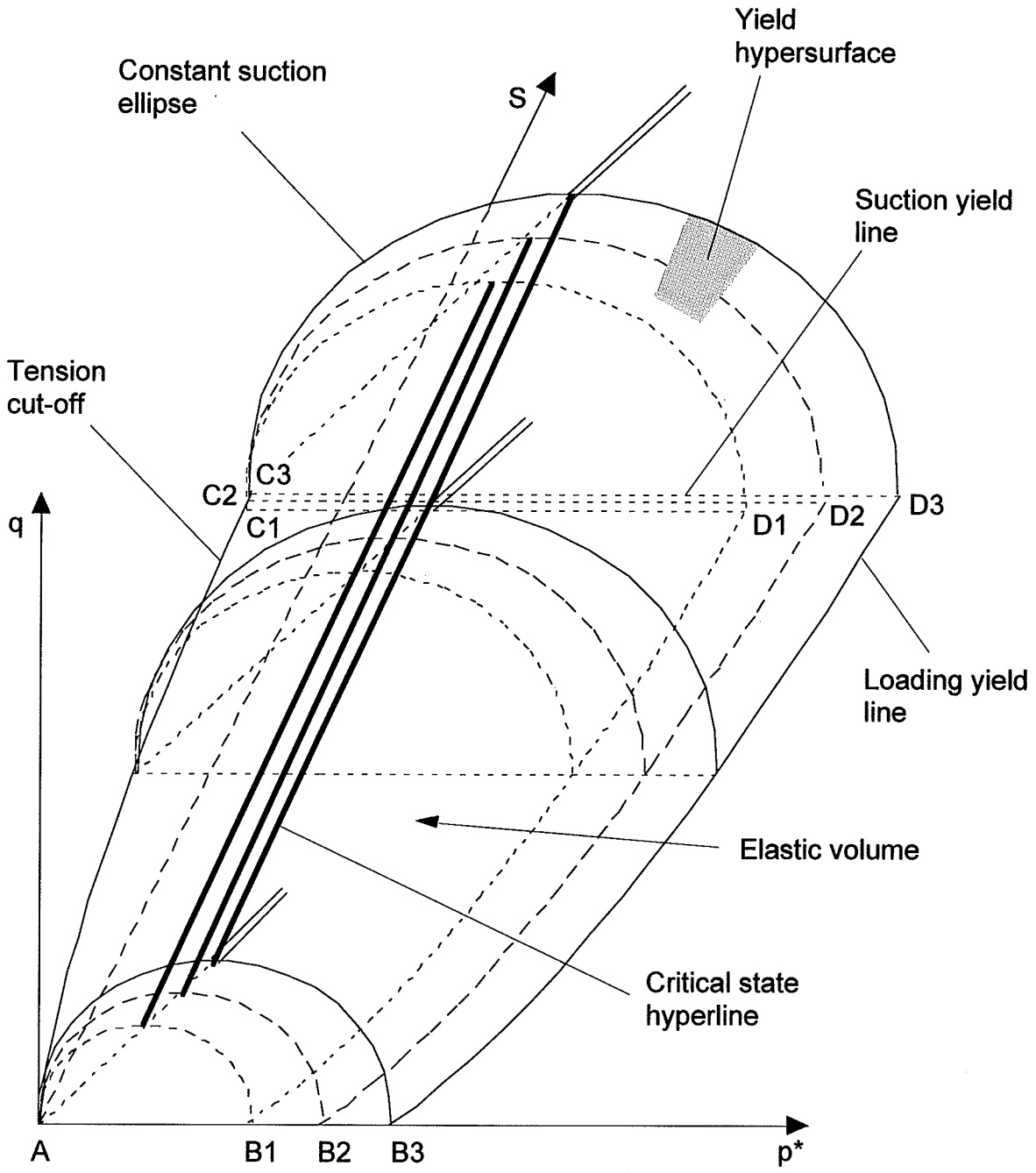

Figure 9.12 A conceptual model for unsaturated sand-bentonite material.

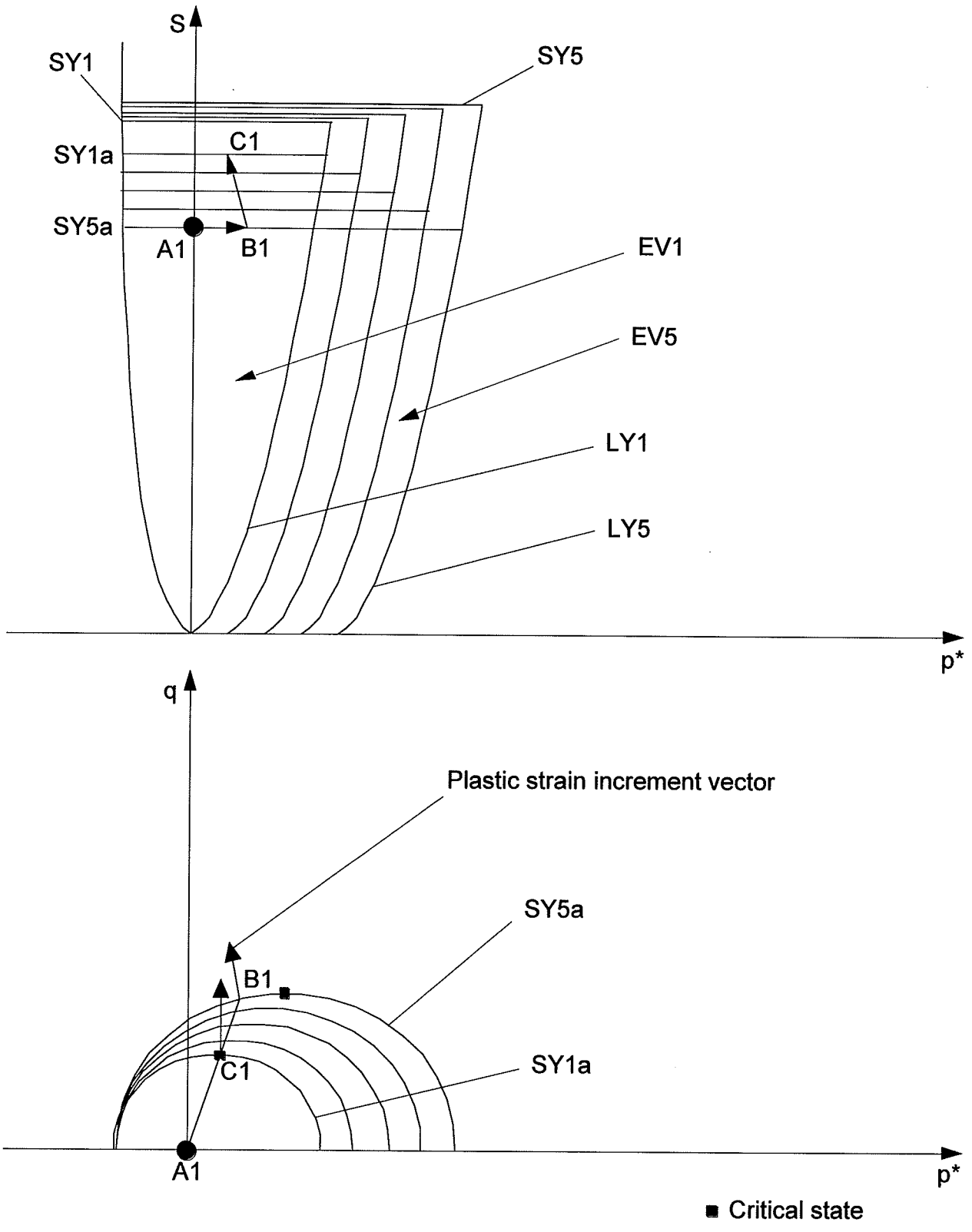

Figure 9.13 Stress path of Specimen SP1.

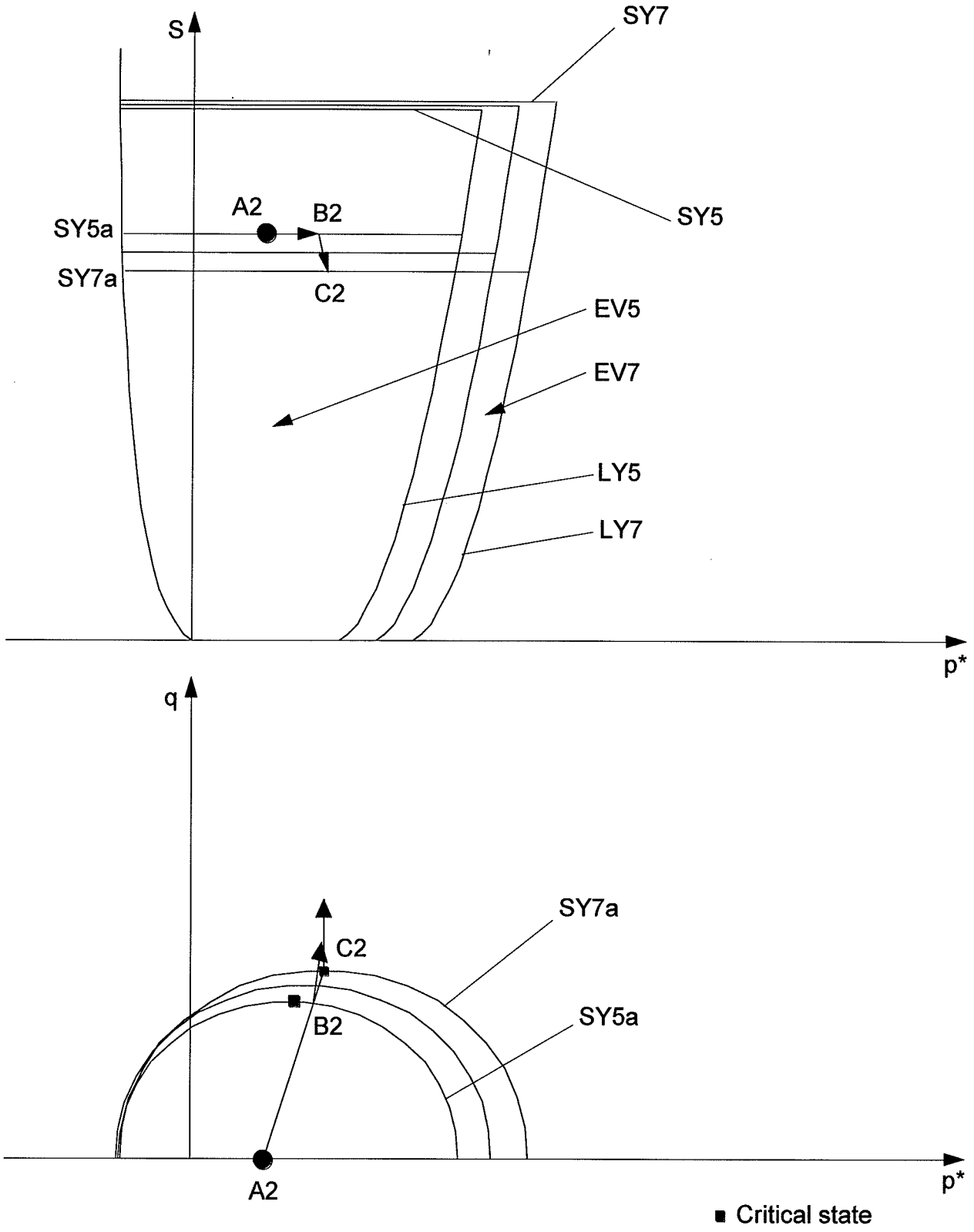

Figure 9.14 Stress path of Specimen SP2.

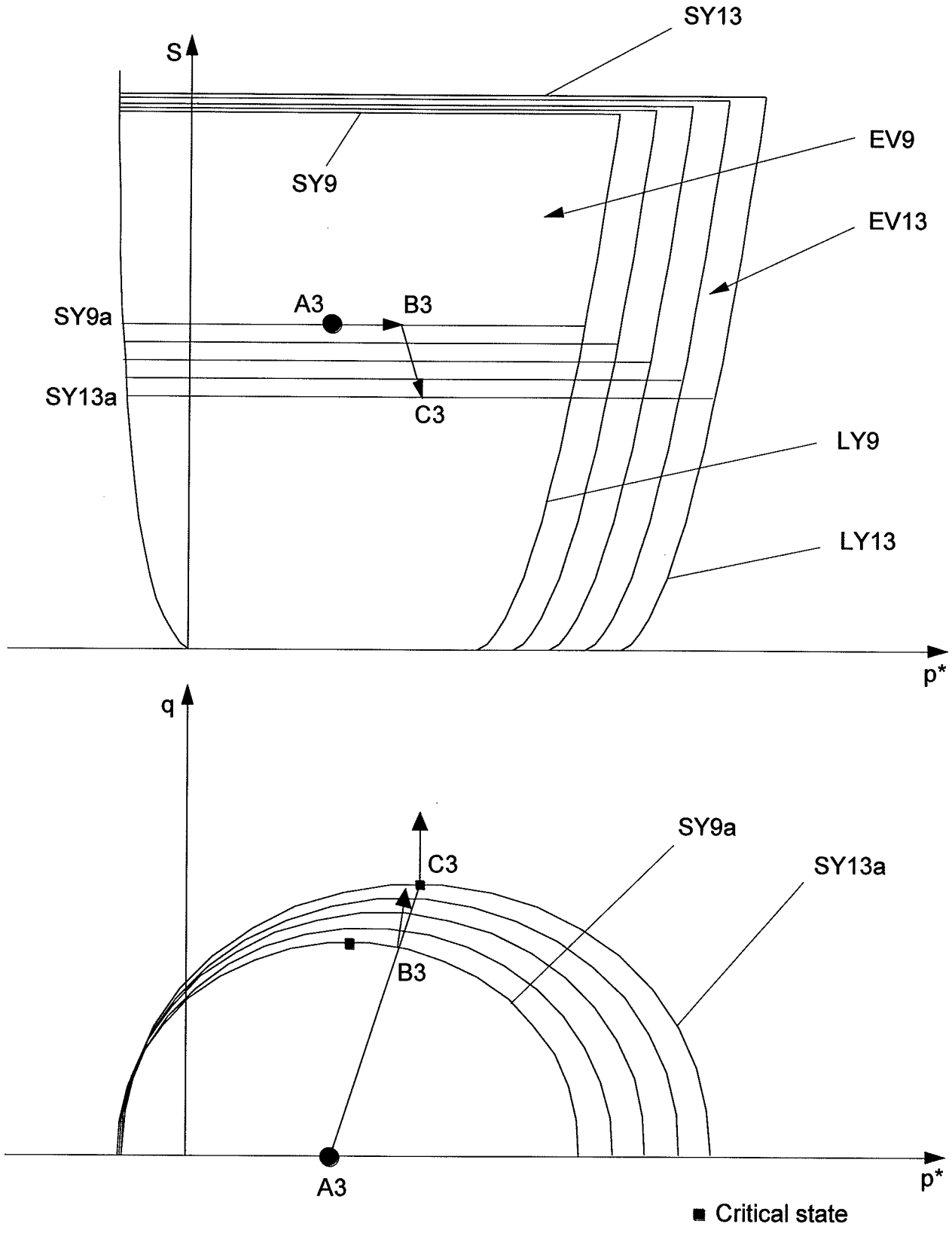

Figure 9.15 Stress path of SP3.

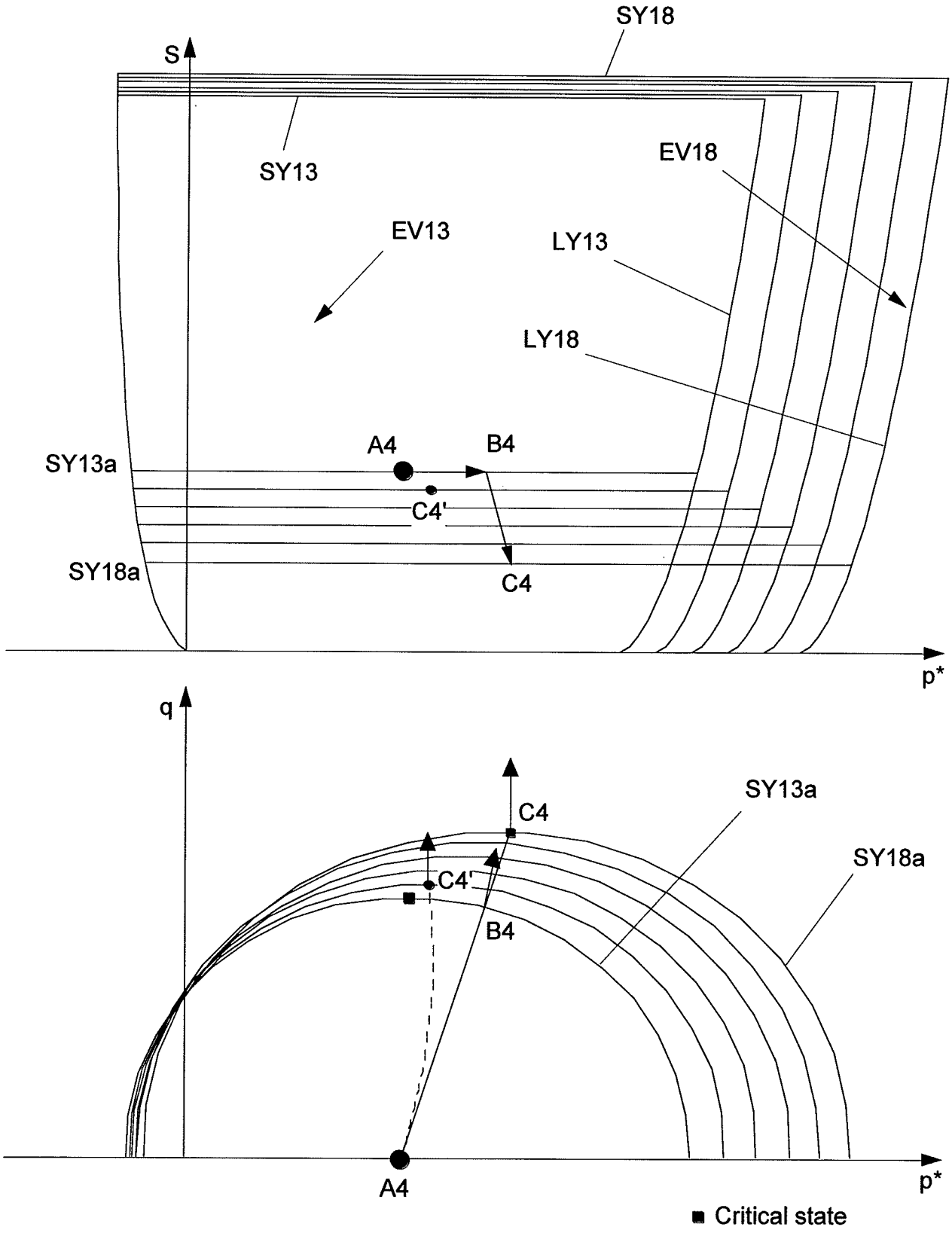

Figure 9.16 Stress path of SP4.

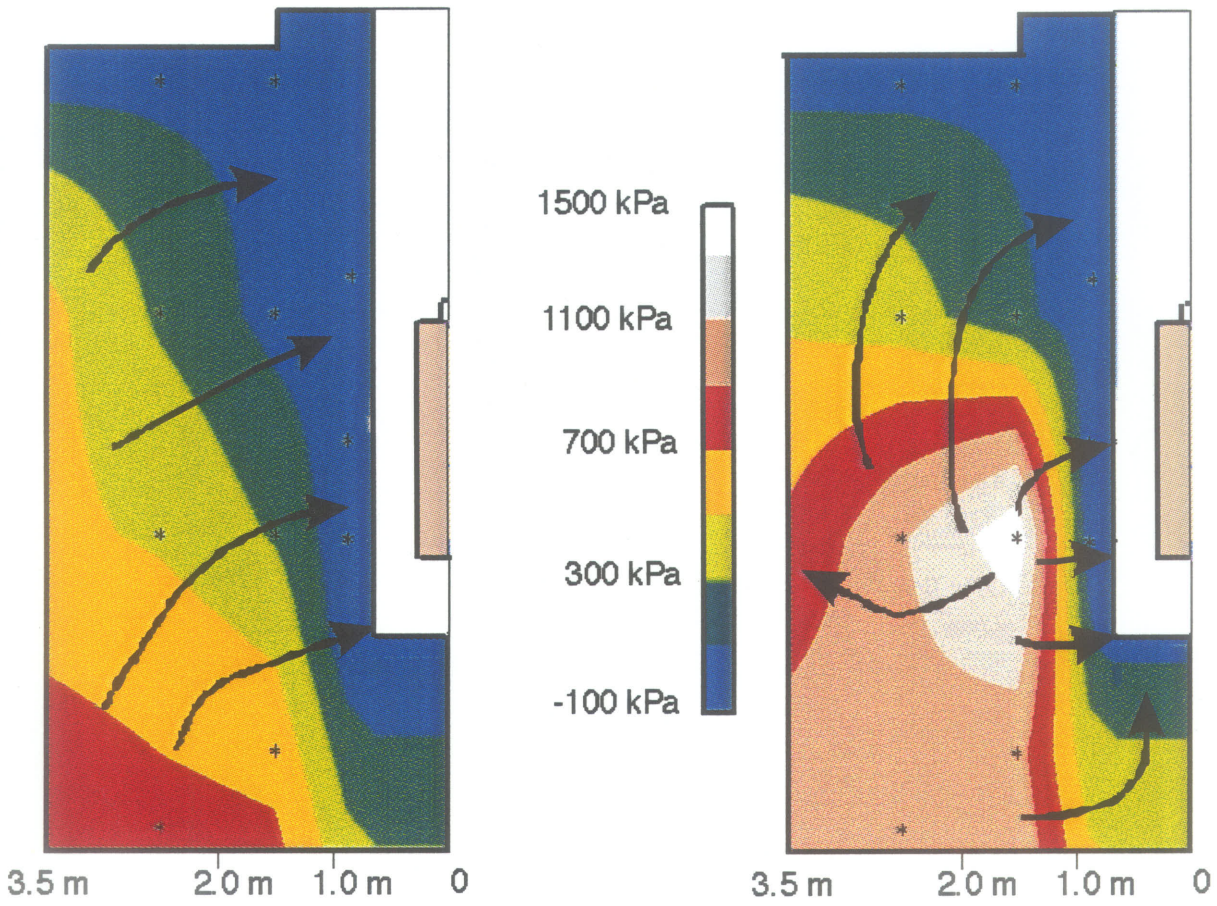

Before Heating - Day 0

After Heating - Day 896

Figure 9.17 Pore water potential contours and interpreted flow paths - zero head elevation at emplacment hole collar (after Graham et al. 1996).

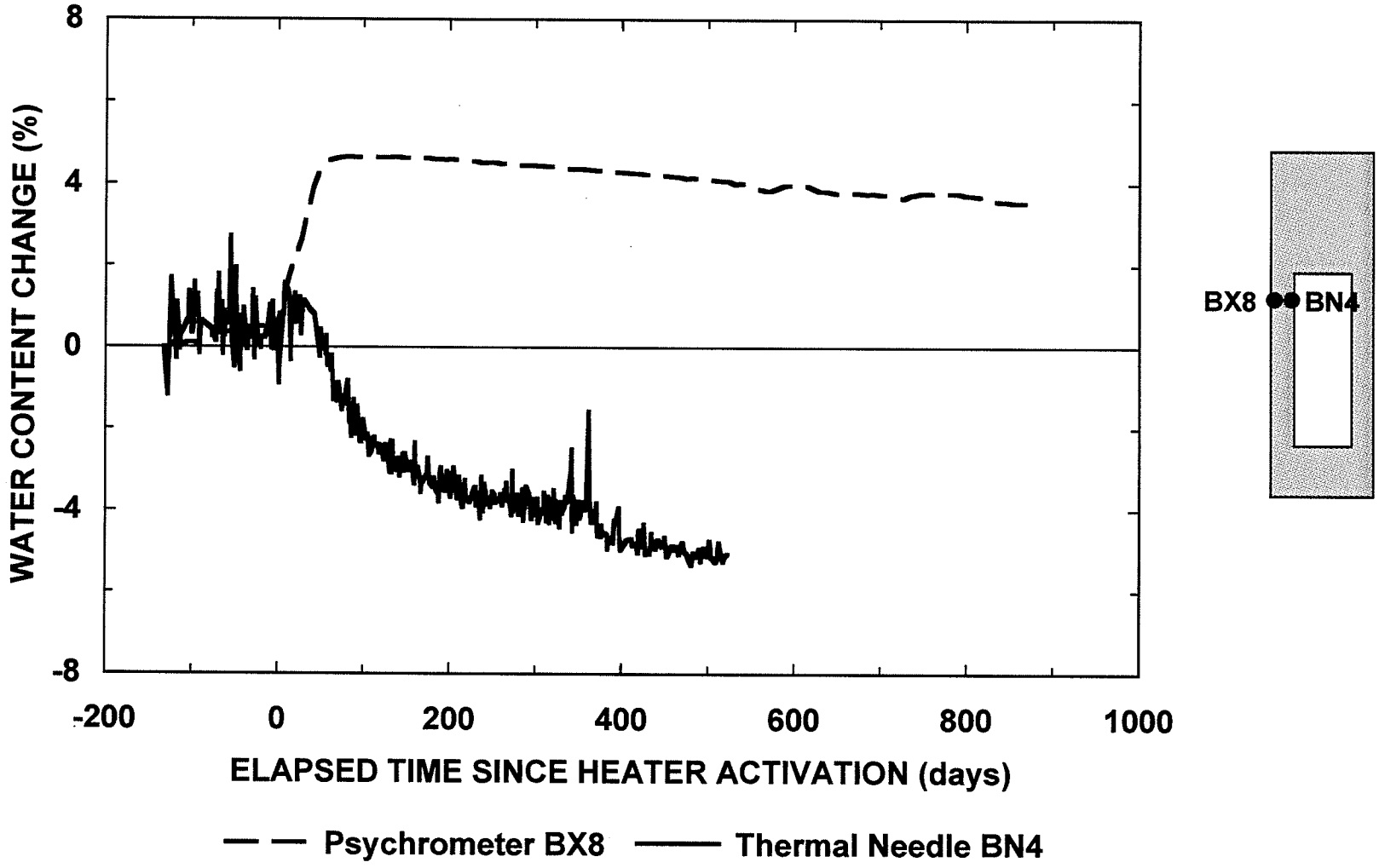

Figure 9.18 Comparison of water content change between psychrometer BX8 and thermal needle BN4.

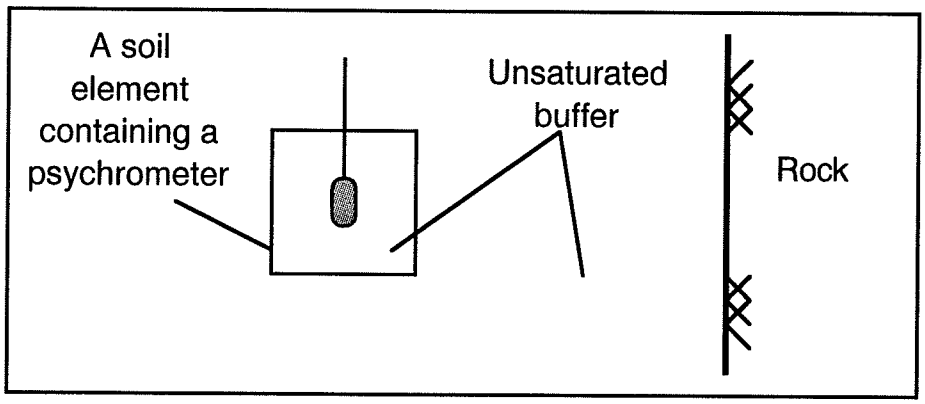

(a)

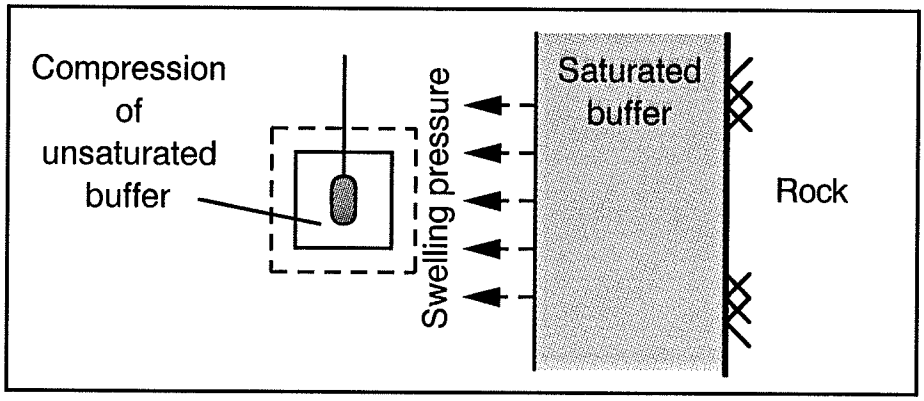

(b)

Figure 9.19 Swelling pressure development in saturated buffer and compression of unsaturated buffer.

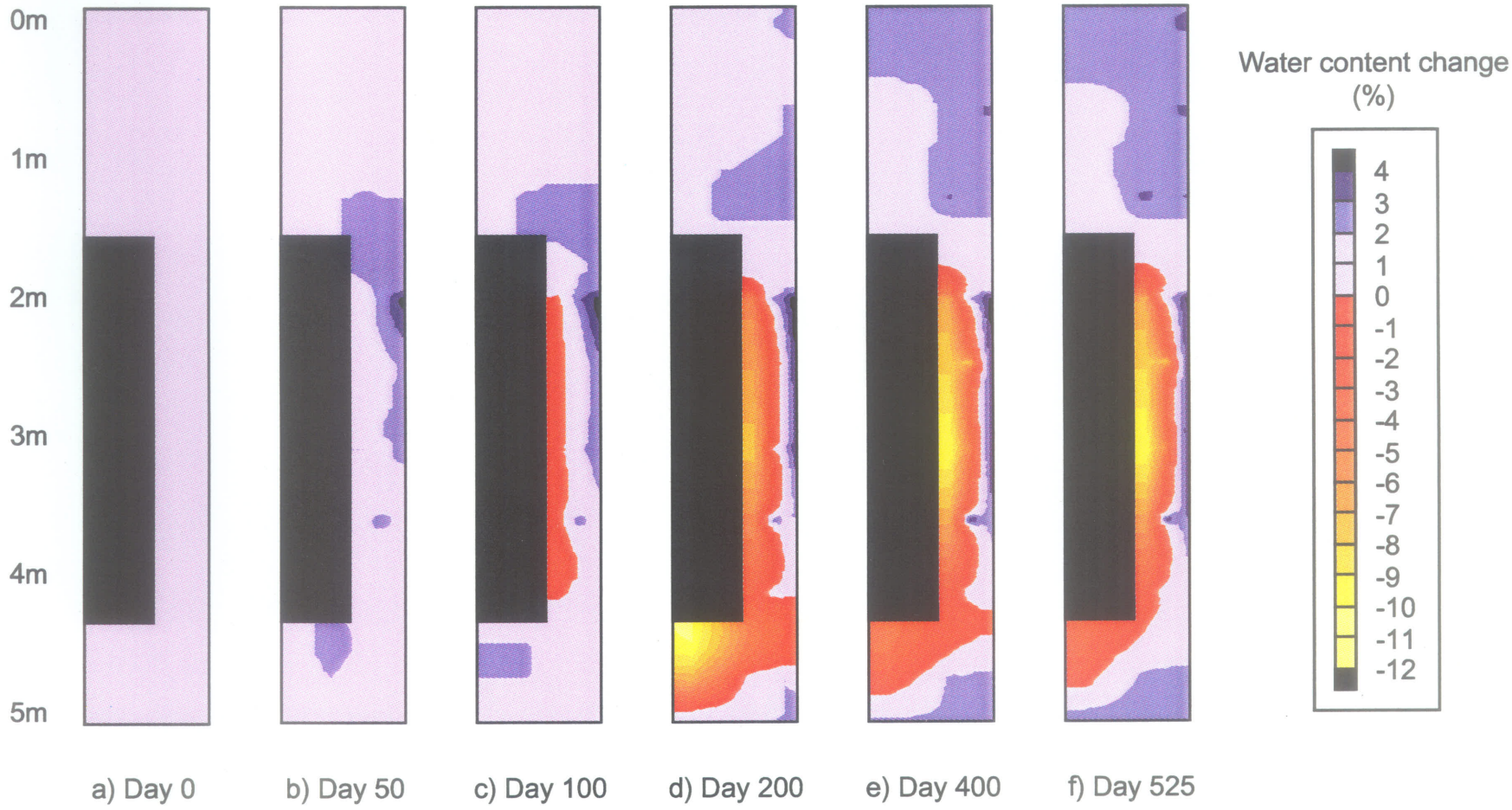

Figure 9.20 Interpretation of water content changes measured by psychrometers and thermal needles in the Buffer/Container Experiment at specified times since heater activation.

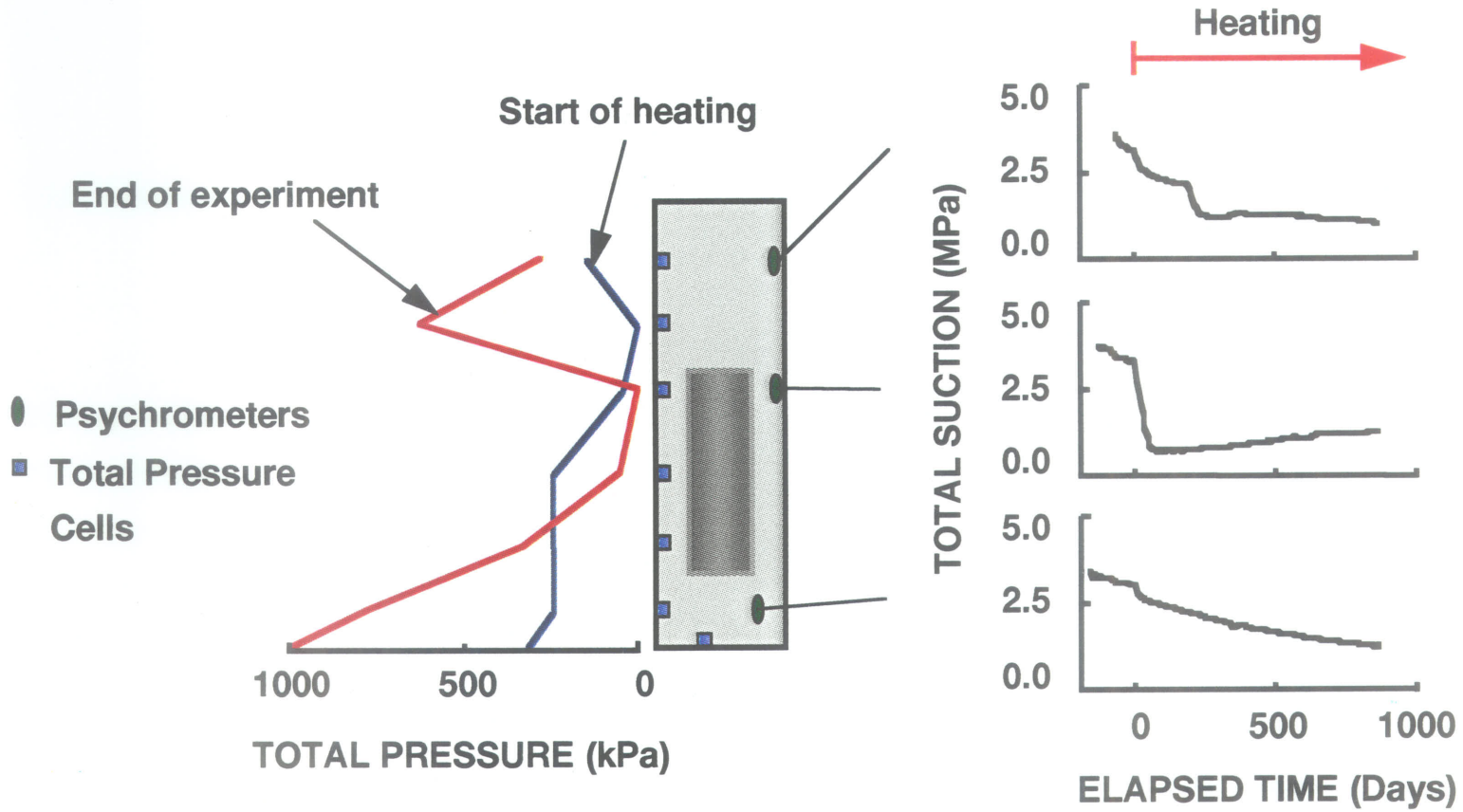

Figure 9.21 Total pressure and total suction responses in the Buffer/Container Experiment.